

# International Association of Geodesy Symposia

*Wolfgang Torge, Series Editor*

---

*Symposium 101:* Global and Regional Geodynamics

*Symposium 102:* Global Positioning System: An Overview

*Symposium 103:* Gravity, Gradiometry, and Gravimetry

*Symposium 104:* Sea Surface Topography and the Geoid

*Symposium 105:* Earth Rotation and Coordinate Reference Frames

*Symposium 106:* Determination of the Geoid: Present and Future

*Symposium 107:* Kinematic Systems in Geodesy, Surveying, and Remote Sensing

*Symposium 108:* Applications of Geodesy to Engineering

*Symposium 109:* Permanent Satellite Tracking Networks for Geodesy and Geodynamics

*Symposium 110:* From Mars to Greenland: Charting Gravity with Space and Airborne Instruments

*Symposium 111:* Recent Geodetic and Gravimetric Research in Latin America

*Symposium 112:* Geodesy and Physics of the Earth: Geodetic Contributions to Geodynamics

*Symposium 113:* Gravity and Geoid

*Symposium 114:* Geodetic Theory Today

# Geodetic Theory Today

Third Hotine-Marussi Symposium  
on Mathematical Geodesy

*Symposium No. 114*

L'Aquila, Italy, May 30 – June 3, 1994

Convened and Edited by  
Fernando Sansò



Springer

Fernando Sansò  
Politecnico di Milano  
Dipartimento di Ingegneria Idraulica,  
Ambientale e del Rilevamento  
Piazza Leonardo da Vinci 32  
I-20133 Milano, Italy

*Series Editor*  
Wolfgang Torge  
Institut für Erdmessung  
Universität Hannover  
Nienburger Straße 6  
D-30167 Hannover, Germany

**Library of Congress Cataloging-in-Publication Data**

Hotine-Marussi Symposium on Mathematical Geodesy (3rd : 1994 :  
L'Aquila, Italy)

Geodetic theory today : Third Hotine-Marussi Symposium on  
Mathematical Geodesy, L'Aquila, Italy, May 30-June 3, 1994 /  
convened and edited by Fernando Sansò.

p. cm. -- (International Association of Geodesy symposia ;  
symposium no. 114)

"The papers presented in this volume are the result of an IAG  
symposium held during the XX General Assembly of the International  
Union of Geodesy and Geophysics in Vienna, August 11-24, 1991"--T.p.  
verso.

Includes bibliographical references.

ISBN-13:978-3-540-59421-5(soft)

1. Geodesy--Mathematics--Congresses. I. Sansò, F. (Fernando),  
1945-. II. Title. III. Series: International Association of  
Geodesy symposia ; symposium 114.

QB283.H67 1994

526'.1--dc20

95-33018

CIP

For information regarding symposia volumes 101 and onward contact:  
Springer-Verlag GmbH & Co. KG  
Heidelberger Platz 3  
D-14197 Berlin, Germany

For earlier volumes contact:  
Bureau Central de l'Association Internationale de Géodésie  
2, Avenue Pasteur, F-94160 Saint-Mande, France

The papers presented in this volume are the result of the Third Hotine-Marussi Symposium on Mathematical Geodesy, held in L'Aquila, Italy, May 30–June 3, 1994, under the sponsorship of the IAG

ISBN-13:978-3-540-59421-5 e-ISBN-13:978-3-642-79824-5

DOI: 10.1007/978-3-642-79824-5

This work is subject to copyright. All rights are reserved, whether the whole or part of the material is concerned, specifically the rights of translation, reprinting, reuse of illustrations, recitation, broadcasting, reproduction on microfilms or in any other way, and storage in data banks. Duplication of this publication or parts thereof is permitted only under the provisions of the German Copyright Law of September 9, 1965, in its current version, and permission for use must always be obtained from Springer-Verlag. Violations are liable for prosecution under the German Copyright Law.

© Springer-Verlag Berlin Heidelberg 1995

The use of general descriptive names, registered names, trademarks, etc. in this publication does not imply, even in the absence of a specific statement, that such names are exempt from the relevant protective laws and regulations and therefore free for general use.

Product Liability: The publishers cannot guarantee the accuracy of any information about dosage and application contained in this book. In every individual case the user must check such information by consulting the relevant literature.

Typesetting: Camera ready by editor/authors

SPIN: 10492788 32/3136 - 5 4 3 2 1 0 - Printed on acid-free paper

## **FOREWORD**

The III Hotine-Marussi Symposium has been held in L'Aquila (Italy) from May 30 to June 3, 1994. It is the XI Hotine Symposium on Mathematical Geodesy, following the geodetic tradition. I think there is little doubt that all the main fields of fruitful research in theoretical geodesy have been touched upon during the Symposium.

Successful and new results have been presented in the field of relativistic geodesy, mapping, in all its mysterious and most fascinating advanced forms, approximation theory, random fields, boundary value problems, inverse gravimetric problem, spectral, Fourier and wavelets analysis, satellite geodesy, etc.

So the scientific "flow" has been intense and duly supported by the social events, facilitated by the perfect organization of the Local Committee, as well as by the warm hospitality of the Faculty of Engineering of the University of L'Aquila, also supported by the local STET School entitled to Guglielmo Reiss Romoli.

In spite of the very positive profile of the results certified by the present proceedings in the group of the elders of geodesy, to which I belong (not for scientific merits but just for my age), a doubt has become more and more evident; in the era of inflation of scientific symposia is it better to do like that, or it could be more useful to younger people to recover the original pioneering spirit of a full horizon discussion on theoretical problems? This is a challenging question for the future.

Fernando Sansò

## CONTENTS

### **Foreword**

Report on the III Hotine-Marussi Symposium (B. Benciolini)	1
---	---

### **Monday, May 30, 1994**

The Newton Form of the Geodesic Flow on $S^2_R$ and $E^2_{A,B}$ in Maupertuis Gauge (R.J. You, E. Grafarend)	3
The Lie Series Describing the Geodesic Flow on $S^2_R$ and $E^2_{A,B}$ (E.W. Grafarend, R. Syffus)	5
Conformal Structures and Reference Frames in the Post-Newtonian Approximation to General Relativity (D.S. Theiss)	6
3D Linear Similarity Coordinate Transformation Between a Global Geodetic System and a Local Geodetic System Without Local Ellipsoidal Heights (E. Grafarend, F.I. Okeke)	8
Application of Moebius Barycentric Coordinates (Natural Coordinates) for Geodetic Positioning (W. Pachelski, E.W. Grafarend)	9
DEM Generation with ERS-1 Interferometry (C. Prati, F. Rocca)	19
Fundamental GPS Network in Lithuania (K. Borre, P. Petroškevičius)	27
The Rotation of the Celestial Equatorial System With the So-called "Non-rotating Origin" (B. Richter)	32
On the GPS Double-difference Ambiguities and Their Partial Search Spaces (P.J.G. Teunissen)	39
The Exact Solution of the Nonlinear Equations of the 7-parameter Global Datum Transformation $C_7(3)$ (E. Grafarend, F. Krumm)	49

GPS - Spacetime Observables (V.S. Schwarze)	50
--	----

**Tuesday, May 31, 1994**

The Optimal Universal Transverse Mercator Projection (E. Grafarend)	51
The Generalized Mollweide Projection of the Biaxial Ellipsoid (E. Grafarend, A. Heidenreich)	52
The Hotine Oblique Mercator Projection of $E_{a,b}^2$ (J. Engels, E. Grafarend)	53
The Embedding of the Plumbline Manifold: Orthometric Heights (E. Grafarend, R.J. You)	54
Inverse Cartographic Problems (B. Marana, F. Sansò)	56
Accuracy of Orbit Computation for Geodetic Satellites: the Ordered and the Chaotic Case (A. Milani)	71
The Short-arc Approach to Laser Ranging Analysis (S. Usai, M. Carpino, A. Milani, G. Catastini, A. Rossi)	83
Orbital Injection Analysis for Twin LAGEOS Satellites in Supplementary Orbits and the Measurement of the Lense-Thirring Gravitomagnetic Effect (F. Vespe, L. Anselmo)	92
Determination of the Gravity Field from Satellite Gradiometry - A Simulation Study - (M. Belikov, M. van Gelderen, R. Koop)	102
New Wavelet Methods for Approximating Harmonic Functions (W. Freeden, M. Schreiner)	112
Satellite Gradiometry - A New Approach (W. Freeden, M. Schreiner)	122
Satellite Orbit Geometry Under Nonconservative Forces (E. Grafarend, R.J. You)	140
Spherical Cap Models of Laplacian Potentials and General Fields (A. De Santis, C. Falcone)	141
Solving the Inverse Gravimetric Problem: On the Benefit of Wavelets (L. Ballani)	151
Integrated Inverse Gravimetric Problems (R. Barzaghi)	162

**Wednesday, June 1, 1994**

Mathematical Statistics for Spatial Data; the Use of Geostatistics for Geodetic Purposes (A. Stein)	184
On the Reconstruction of Regular Grids from Incomplete, Filtered or Unevenly Sampled Band-limited Data (M.G. Sideris)	204
Non-parametric Statistics and Bootstrap Methods for Testing the Data Quality of a Geographic Information System (F. Crosilla, G. Pillirone)	214
The Effects of Fuzzy Weight Matrices on the Results of Least Squares Adjustments (H. Kutterer)	224
On Some Alternatives to Kalman Filtering (B. Schaffrin)	235
Chaotic Behaviour in Geodetic Sensors and Fractal Characteristics of Sensor Noise (Z. Li, K.-P. Schwarz)	246
Discriminant Analysis to Test Non-Nested Hypotheses (B. Betti, M. Crespi, F. Sansò, D. Sguerso)	259

**Thursday, June 2, 1994**

On Stochastic Boundary Conditions for Laplace Equation (Yu.A. Rozanov)	272
A Series Solution for Zagrebin's Problem (J. Otero, J. Capdevila)	280
Solution of the Geodetic Boundary Value Problem in Spectral Form (M.S. Petrovskaya)	294
Gravity Reductions Versus Approximate B.V.P.s (F. Sansò, G. Sona)	304
Classical Methods for Non-spherical Boundary Problems in Physical Geodesy (P. Holota)	315
On a Scalar Fixed Altimetry - Gravimetry Boundary Value Problem (W. Keller)	325
Non-linear Effects in the Geodetic Version of the Free Geodetic Boundary Value Problem Based on Higher Order Reference Fields (B. Heck, K. Seitz)	332

Perturbation Expansion for Solving the Fixed Gravimetric Boundary Value Problem (R. Klees)	340
Application of the Concept of Biorthogonal Series to a Simulation of a Gradiometric Mission (A. Albertella, F. Migliaccio, F. Sansò)	350
Local Geoid Accuracies from Different Kinds of Data (A. Albertella, F. Sacerdote)	362
On Calculating the Attraction of the Topographic-Isostatic Masses (H.A. Abd-Elmotaal)	372
The Fast Hartley Transform Applied to the Iberian Geoid Calculation (M.J. Sevilla, G. Rodriguez-Velasco)	381
The Impact of the Gravitational Potential of Topographic and Isostatically Adjusted Masses on the Geoid (J. Engels, E. Grafarend, P. Sorcik)	391
The Topographic Potential with Respect to the Reference Ellipsoid (M. Feistritzer)	392
 <b>Friday, June 3, 1994</b>	
On the Application of Wavelets in Geodesy (F. Barthelmes, L. Ballani, R. Klees)	394
Geodetic Applications of Wavelets: Proposals and Simple Numerical Experiments (L. Battha, B. Benciolini, P. Zatelli)	404
How Accurately Do We Know the Marine Geoid in Shallow Water Regions? (M. Metzner, S. Dick, E.W. Grafarend, M. Stawarz)	413
Rank Deficiency of Altimetry-Gravimetry SST Determination (R. Barzaghi, M.A. Brovelli, F. Sansò)	429
List of participants	441

Report on the:

**III HOTINE-MARUSSI SYMPOSIUM**  
on  
**MATHEMATICAL GEODESY**  
L'Aquila, Italy  
May 30 - June 3, 1994

The III Hotine-Marussi Symposium on Mathematical Geodesy was held in L'Aquila (Italy), from May 30 to June 3, 1994. It was organized by Prof. F. Sansò, president of IAG Sect. IV, with the cooperation of the local host Prof. B. Betti. The Symposium was sponsored by the International Association of Geodesy, the International Union of Geodesy and Geophysics, the University of L'Aquila and the CARISPAQ Foundation.

The symposium was attended by more than 70 participants from 15 countries; about 60 papers were presented, covering all the major aspects of mathematical geodesy and, in particular, the fields of celestial mechanics, boundary value problems, gravity field modelling, estimation theory, approximation theory, positioning and inverse problems.

The presented papers treated both classical subjects revisited in a modern way and topics which more recently entered into the field of interest of geodesy. Among this I want to mention the theory of chaotic systems, the theory of stochastic BVP and the use of wavelets in approximation theory.

Five invited relations were presented during the symposium.

T. Krarup presented a speech entitled "Is Geodesy Possible?", treating the dilemma of the reconstruction of continuous fields from discrete measurements. The final answer to the question of the title was affirmative, encouraging geodesists not to look for another job!

The other invited papers were: "SAR Interferometry" by F. Rocca and C. Prati, "Accuracy of Orbit Computation for Geodetic Satellites: the Ordered and the Chaotic Case" by A. Milani, "Mathematical Statistics for Spatial Data: the Use of Geostatistics for Geodetic Purposes" by A. Stein and "Boundary Problems for Random Fields" by Y. Rozanov.

It must be mentioned that the presence of specialists of disciplines

different from geodesy strongly enriched the works of the symposium and was appreciated by all the participants.

The scientific work was complemented by a social dinner and an interesting tour in the region surrounding L'Aquila.

The proceedings will be published by Springer-Verlag.

Battista Benciolini

# THE NEWTON FORM OF THE GEODESIC FLOW ON $S_R^2$ AND $E_{A,B}^2$ IN MAUPERTUIS GAUGE

**R. J. You and E. Grafarend**  
**Department of Geodetic Science**  
**Stuttgart University, Keplerstraße 11, D-70174 Stuttgart, Germany**

Geodesics, in particular minimal geodesics, are of focal geodetic interest. In the paper we apply the *Maupertuis variational principle of least action* in the Newton mechanics to transform the geodesic flow on the twodimensional sphere  $S_R^2$  with the radius  $R$  and on the biaxial ellipsoid  $E_{A,B}^2$  with the semi-major axis  $A$  and semi-minor axis  $B$  into the Newton form. A geodesic flow on a twodimensional Riemann manifold takes the form of the Newton law if two assumptions are met:

1. The twodimensional Riemann manifold is represented by *conformal coordinates* (isometric coordinates, isothermal coordinates),
2. The arc length  $s$  as the curve parameter of a geodesic flow is replaced by the *dynamic time*  $t$  according to the *Maupertuis gauge*

$$ds = \lambda^2(q^1, q^2) dt$$

where  $\lambda^2$  is the *factor of conformality* and  $q^1, q^2$  are the conformal coordinates which form a local chart of the twodimensional Riemann manifold.

If these two assumptions are satisfied, then the differential equations of a geodesic flow

$$\frac{d^2 q^k}{ds^2} + \left\{ \begin{array}{c} k \\ i j \end{array} \right\} \frac{dq^i}{ds} \frac{dq^j}{ds} = 0 , \quad i, j, k = 1, 2$$

on the sphere  $S_R^2$  and biaxial ellipsoid  $E_{A,B}^2$  take the equations of the simple Newton form (see fig. 1)

$$\frac{d^2 q^k}{dt^2} - \frac{1}{2} \frac{\partial \lambda^2}{\partial q^k} = 0 .$$

Here the “*conservative force field*” is produced by the *half* the gradient of the *factor of conformality*  $\lambda^2(q^1, q^2)$ .

*Maupertuis gauged geodesic flows* can be formulated for conformally flat differential manifolds of type sphere  $S_R^2$  and biaxial ellipsoid  $E_{A,B}^2$  both in the *Lagrange portray* as well as in the *Hamilton portray*. The numerical solutions and illustrations of the twodimensional *Maupertuis gauged geodesic flows* on the universal Mercator projection map, the universal polar stereographic projection map, the universal transverse Mercator projection map and

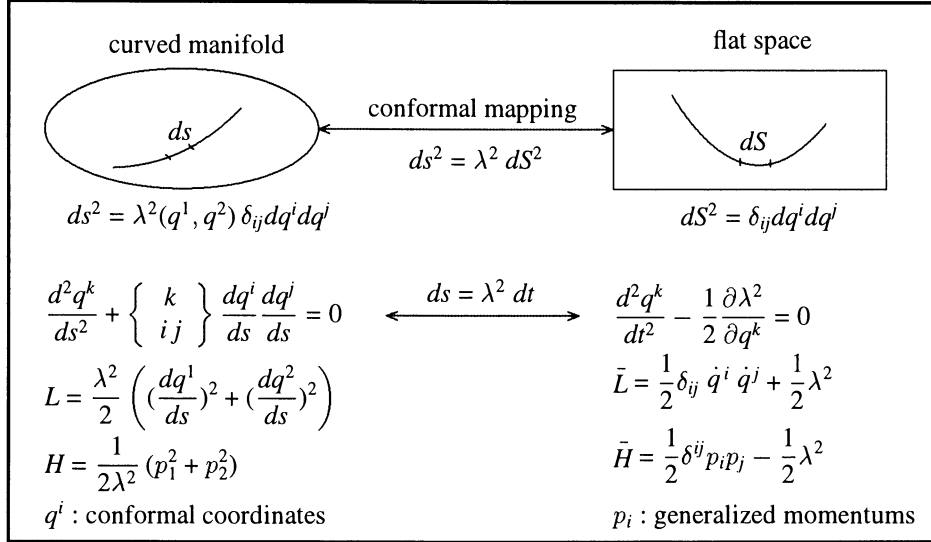


Figure 1

the universal Lambert projection map are given in a complete paper which is being published in *Zeitschrift für Vermessungswesen* (ZfV).

## REFERENCES

- Goenner, H., E. W. Grafarend and R. J. You: Newton mechanics as geodesic flow on Maupertuis' manifold: The local isometric embedding into flat spaces, *manuscripta geodaetica*(1994) in print.
- Grafarend, E.: Lecture Notes on map projections (Kartenprojektionen). Department of Geodetic Science, Stuttgart University, 1985.
- Grafarend, E. W. and R. J. You: The Newton form of a geodesic in Maupertuis gauge on the sphere and the biaxial ellipsoid: Part I and II. *Zeitschrift für Vermessungswesen*(1994) in print.
- de Maupertuis, P. L. M.: Accord de différentes lois de la Nature. Qui avoient jusqu'ici paru incompatibles. de l'Académie Royal des Sciences de Paris 1744. Reprinted in 1965 *Oeuvres* Band IV pp. 3-28, Georg Olms Verlagsbuchhandlung, Hildesheim.
- Snyder, P. (1987): Map projections — A working manual. U.S. geological survey professional paper 1395, U.S. Government Printing Office, Washington D.C.

# THE LIE SERIES DESCRIBING THE GEODESIC FLOW ON $S_R^2$ and $E_{A,B}^2$

E.W. Grafarend and R. Syffus

Department of Geodetic Science

Stuttgart University, Keplerstr. 11, D-70174 Stuttgart, Germany

Geodesics, in particular minimal geodesics, are of focal geodetic interest. The differential equations of a minimal geodesic can be written as a system of two second order ordinary differential equations, well known in the Lagrange portrait. Alternatively the system can be transformed by Legendre transformation into a system of four first order ordinary differential equations subject to the Hamilton portrait of a geodesic based on the generalized momenta. Assuming that the differentiable manifold  $\{ M, G_{\mu\nu} \}$  is partially covered by a set of orthogonal coordinates the cyclic coordinate  $P_1$  generates the conservation of angular momentum, Clairaut constant, for any surface of revolution. The Lie series method is then used as one possible tool to describe analytically the geodesic flow on the sphere  $S_R^2$  and on the ellipsoid of revolution  $E_{A,B}^2$ . The solution of the initial value problem is given, whereas higher order terms of the Lie series expansion are calculated by recurrence relations. The solution of the boundary value problem is given by a bivariate series inversion via *Riemann polar/normal coordinates*. In order to overcome the problem of singularity a change of chart will be performed, whereas the minimal atlas of  $\{ M, G_{\mu\nu} \}$  is established by two charts.

A more detailed description can be found in the paper *The oblique azimuthal projection of geodesic type for the biaxial ellipsoid: Riemann polar and normal coordinates* by E.W. Grafarend and R. Syffus which has been submitted to *scripta geodaetica*.

# CONFORMAL STRUCTURES AND REFERENCE FRAMES IN THE POST-NEWTONIAN APPROXIMATION TO GENERAL RELATIVITY

Dietmar S. Theiss

*Department of Geodetic Science  
University of Stuttgart  
Keplerstrasse 11  
D-70174 Stuttgart  
F.R. Germany*

According to general relativity, the gravitational field of a body is described by the metric tensor field  $g$  on the spacetime manifold. With respect to some given local chart  $(x^\mu) \equiv (x^0, x^1, x^2, x^3)$  of spacetime, the components ("potentials")  $g_{\mu\nu}$  of  $g$  contain ten independent elements in general. That is, in order to describe the *relativistic* gravitational field of the Earth, the knowledge of the multipole structure of each of these "potentials" is required. The gravitational field of the Earth, however, is weak so that the post-Newtonian approximation to general relativity can be used in this context. To be more specific, let  $U$  be the Newtonian potential in the vicinity of the Earth and  $c$  the velocity of light. Then one obtains  $U/c^2 \approx 10^{-10}$ ; which expresses essentially the weakness of the gravitational field.

In the post-Newtonian approximation, the number of independent relativistic "potentials" can be reduced to four, in a certain class of *quasi-inertial* coordinate charts (geocentric frames of reference). However, the multipole structure of the Earth is actually determined relative to a *rotating* (Earth-fixed) reference frame, in which the potential of gravity, and so the multipole moments, are just independent of *time*. In the classical, Newtonian, theory of gravitation, such a reference frame is well defined and can be constructed in a straightforward manner. An appropriate *general relativistic* treatment of the problem, however, requires some care. In what follows, we give a brief description of the corresponding geometrical methods involved by applying the post-Newtonian approximation scheme.

At each instant of time, one can define a three-dimensional (configuration) space  $\varphi_t$  in spacetime with each space possessing a (timelike) normal vector field  $N_t$ . Then, the metric tensor  $g$  can be represented in terms of  $N_t$  and the *induced* (intrinsic) metric  ${}^3g_t$  defined on  $\varphi_t$ . Furthermore, on each  $\varphi_t$ , we introduce the second fundamental form  $K_t$  to describe the *exterior* curvature of the 3-spaces (spacelike hypersurfaces)  $\varphi_t$  relative to the spacetime manifold. At the (first) post-Newtonian level, it then

turns out that, in a certain class of coordinate charts ("gauges"), only the *spatial* part of the exterior curvature contributes to  $K_t$ .

In order to describe the relations between the (intrinsic) 4-curvature of the underlying spacetime, the (exterior) 3-curvature  $K_t$  and the (intrinsic) curvature of the three-dimensional spaces  $\{\varphi_t\}$ , generalized Gauß-Codazzi-Ricci equations can be set up. An analysis of these equations shows that they contain an expression, the *Schouten tensor*, depending algebraically on the spatial projection of the *Einstein tensor*. The post-Newtonian (gravitational) field equations, however, just imply the *vanishing* of these terms. Thus, by applying the theorems of *Weyl* (1918) and *Schouten* (1921),\* it follows that the three-dimensional (configuration) spaces  $\{\varphi_t\}$  are *conformally flat* (i.e., at each instant of time) and can be related to each other, especially, via *conformal* transformations in three dimensions.

It can be shown, in addition, that this *simple* geometric structure of the three-spaces occurs within the whole class of post-Newtonian coordinate charts of spacetime. The relativistic Earth-fixed reference frame mentioned above can then be constructed by performing transformations of these charts, which, expressed in geometrical terms, show up as deformations of the three-dimensional conformally flat configuration spaces. From these, "transformed", spaces, the desired relativistic "potentials" of the Earth can be finally derived.

*A detailed version of the present contribution is intended to be submitted for publication.*

## Acknowledgments

I wish to thank Prof. E.W. Grafarend for stimulating discussions and his support. This work was supported by the Sonderforschungsbereich 228.

\* See, e.g., L.P. Eisenhart, *Riemannian Geometry*, (Princeton University Press, Princeton, 1960) and the corresponding references cited therein.

# **3D LINEAR SIMILARITY COORDINATE TRANSFORMATION BETWEEN A GLOBAL GEODETIC SYSTEM AND A LOCAL GEODETIC SYSTEM WITHOUT LOCAL ELLIPSOIDAL HEIGHTS**

**E.Grafarend and F.I.Okeke**  
**Geodätisches Institut, Universität Stuttgart**  
**Keplerstraße 11, D-70174 Stuttgart, Germany**

## **ABSTRACT**

In certain situations where there is need to transform coordinates from a local geodetic system to a global geodetic system and vice versa, information about local ellipsoidal height is not available. This problem arises where in the local geodetic system (i) the vertical and horizontal geodetic datums are separated, (ii) there are no gravity data for use in the reduction and adjustment of levelling networks, (iii) there is no information on the geoid undulation. This paper describes a model for the analysis and synthesis of linear similarity coordinate transformation parameters, in the absence of local ellipsoidal heights.

In the analysis stage, Taylor series expansions of the local longitude and latitude are taken with the expansion point at the point where the coordinates from the two systems are equal. By so doing the design matrix consists of global longitude, latitude and height. Again in the synthesis stage, Taylor series expansions of the global longitude and latitude are taken at the same expansion point. Analogous to the analysis stage, the coefficients of the transformation parameters in the synthesis stage consist of local longitude, latitude and height. But this time the height component is eliminated from these coefficients. It is observed that the elimination of the height component has little or no impact on the computed global coordinates. Numerical examples show RMS of residuals to be less than 0.1m in longitude and 0.05m in latitude.

# APPLICATION OF MOEBIUS BARYCENTRIC COORDINATES (NATURAL COORDINATES) FOR GEODETIC POSITIONING

W. Pacholski,  
Space Research Centre,  
Bartycka 18a,  
00-716 Warsaw, Poland

E.W. Grafarend,  
Department of Geodetic Science,  
Stuttgart University, Keplerstr. 11,  
70174 Stuttgart, Germany

## ABSTRACT

Moebius barycentric coordinates (also known as natural, area, triangular, simplex, etc., coordinates) are exposed in some geodetic applications such as the Ansermet's resection problem, GPS positioning, shape functions (in geodetic uses of the finite element method), and a photogrammetric problem. The exposition is preceded by some theoretical considerations which show, among other properties, also the one of their invariance with respect to linear transformations of the frame. In a 2-D space barycentric coordinates are recognized as an effective tool for expressing relative positions of points within a triangular reference frame.

## INTRODUCTION - THEORETICAL BACKGROUND

Any linearly independent  $(s+1)$  points belonging to the  $n$ -dimensional affine space  $\mathbb{R}^n$ ,  $s \leq n$ , span an affine subspace  $H$  of  $\mathbb{R}^n$  so that any new point  $P$  in  $H$  can be given through its position vector:

$$p = \lambda^0 p_0 + \lambda^1 p_1 + \dots + \lambda^s p_s \quad \text{or} \quad p = \lambda^i p_i \quad (1)$$

with:  $\lambda^0 + \lambda^1 + \dots + \lambda^s = 1$  or  $\delta_i \lambda^i = 1$  (2)

(Reinhardt and Soeder, 1974, p.241), and  $\lambda^i \in \mathbb{R}$ ,  $i = 0, \dots, s$ .

The points are by definition linearly independent if and only if the matrix:

$$A = \begin{pmatrix} x_0^1 & x_0^2 & \dots & x_0^n & 1 \\ x_1^1 & x_1^2 & \dots & x_1^n & 1 \\ \dots & \dots & \dots & \dots & \dots \\ x_s^1 & x_s^2 & \dots & x_s^n & 1 \end{pmatrix} \quad (3)$$

where each  $x_i^j$  is the  $j$ -th coordinate of the  $i$ -th point, is of full rank equal  $(s+1)$ ; (Wallace, 1957, p. 95).

Then, exactly  $(s+1)$  independent points in  $\mathbb{R}^n$ :

- define an  $s$ -dimensional affine subspace  $H$  in  $\mathbb{R}^n$ , and
- form a **reference frame** or a **base** for defining point positions within the subspace by means of the numbers  $\lambda^0, \lambda^1, \dots, \lambda^s$ , called the **barycentric coordinates**; the sum of the last ones must be always equal one.

Among the main properties of the barycentric coordinates there are:

- 1<sup>o</sup>- according to (1) they are coefficients (or weights) assigned to the base vectors, so they are **dimensionless** (which is a property of any not normalized frame);
- 2<sup>o</sup>- according to (2) there is no point in  $H$  with all  $\lambda$ 's equal 0, so they are **originless**;
- 3<sup>o</sup>- they are **invariant** with respect to linear transformations of the vector reference frame of  $\mathbb{R}^n$  (any multiplication of both  $p$  and  $p_i$  in (1) by a transformation matrix causes no change of  $\lambda$ 's);
- 4<sup>o</sup>- since coefficients in (1) do not depend on metric properties of the subspace **no vector representation** (including a position vector) is *per se* allowed, so the scalar product is undefined.

The Moebius barycentric coordinates can be simply derived in an **oblique reference frame**, which is translational invariant, but neither orthogonal nor normalized. In  $\mathbb{R}^2$ , for instance, we have the base  $\{p_1, p_2\}$  so that any point position vector is given through its contravariant components as (Fig. 1):

$$p = \lambda^1 p_1 + \lambda^2 p_2 \quad (4)$$

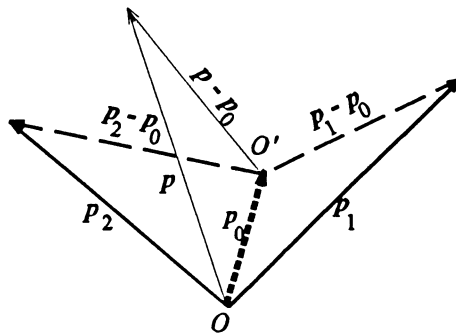


Fig. 1.

Now, if we move the frame origin from  $O$  to  $O'$  by the vector  $p_0$  then the new base becomes  $\{p_1 - p_0, p_2 - p_0\}$  and the new point position vector is:

$$p - p_0 = \lambda^1 (p_1 - p_0) + \lambda^2 (p_2 - p_0) \quad (5)$$

which immediately leads to:

$$p = \lambda^0 p_0 + \lambda^1 p_1 + \lambda^2 p_2, \quad \text{with} \quad \lambda^0 = 1 - (\lambda^1 + \lambda^2) \quad (6)$$

so that it corresponds to (1) and (2), and  $\lambda^0, \lambda^1, \lambda^2$  are barycentric coordinates.

Accordingly, a triangle  $P_1 P_2 P_3$  may define a barycentric planar reference frame in  $\mathbb{R}^3$  (Fig. 2) and the corresponding transformation:

$$\begin{pmatrix} x^1 \\ x^2 \\ x^3 \end{pmatrix} = \begin{pmatrix} x_1^1 & x_2^1 & x_3^1 \\ x_1^2 & x_2^2 & x_3^2 \\ x_1^3 & x_2^3 & x_3^3 \end{pmatrix} \times \begin{pmatrix} \lambda^1 \\ \lambda^2 \\ \lambda^3 \end{pmatrix} \quad \text{with } \lambda^1 + \lambda^2 + \lambda^3 = 1 \quad (7)$$

A similar barycentric planar frame in  $\mathbb{R}^2$  (i.e. spanning the whole  $\mathbb{R}^2$ , Fig. 3) can be:

$$\begin{pmatrix} x \\ y \end{pmatrix} = \begin{pmatrix} x_1 & x_2 & x_3 \\ y_1 & y_2 & y_3 \end{pmatrix} \times \begin{pmatrix} \lambda^1 \\ \lambda^2 \\ \lambda^3 \end{pmatrix} \quad \text{with } \lambda^1 + \lambda^2 + \lambda^3 = 1 \quad (8)$$

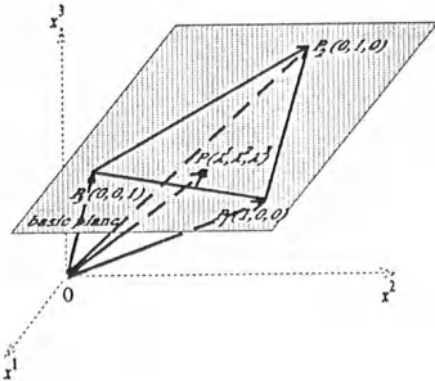


Fig. 2.

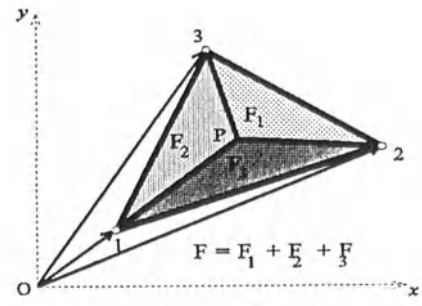


Fig. 3.

When solving (8) with respect to  $\lambda^1, \lambda^2, \lambda^3$  by means of the Cramer's rules we can easily find:

$$\lambda^1 = F_1/F, \quad \lambda^2 = F_2/F, \quad \lambda^3 = F_3/F \quad (9)$$

where all  $F$ 's are the areas of the corresponding triangles ( $F = F_1 + F_2 + F_3$ ). This motivates one of the other names of the coordinates, the area coordinates (Burnett, 1987).

## RELATION TO OBLIQUE COORDINATES

In order to allow for vector operations in the barycentric frame, including scalar product, we can easily recognize, acc. to (6) and Fig. 4, two of three barycentric coordinates as coordinates in the oblique covariant base  $\{g_1, g_2\}$  with  $g_1 = p_1 - p_3, g_2 = p_2 - p_3$ . The point position vector in that base is then:

$$l = \lambda^1 g_1 + \lambda^2 g_2 \quad (10)$$

with  $\lambda^1, \lambda^2$  as contravariant vector components, the point coordinates. In the local Cartesian frame  $\{e_1, e_2\}$  the covariant base vectors and the matrix of the covariant metric coefficients are:

$$\begin{aligned} g_1 &= g_1 \cdot e_1 + 0 \cdot e_2, \\ g_2 &= g_2 \cos \gamma_{12} \cdot e_1 + g_2 \sin \gamma_{12} \cdot e_2, \end{aligned} \quad (g_{ij}) = \begin{pmatrix} g_1 g_1 & g_1 g_2 \cos \gamma_{12} \\ g_2 g_1 \cos \gamma_{12} & g_2 g_2 \end{pmatrix} \quad (11)$$

while the contravariant base vectors and the matrix of the contravariant metric coefficients are:

$$\begin{aligned} \mathbf{g}^1 &= 1/g_1 \cdot \mathbf{e}_1 - 1/(g_1 \tan \gamma_{12}) \cdot \mathbf{e}_2 \\ \mathbf{g}^2 &= 0 \cdot \mathbf{e}_1 + 1/(g_2 \sin \gamma_{12}) \cdot \mathbf{e}_2 \end{aligned}, \quad (\mathbf{g}^i) = 1/(g_1 g_2 \sin^2 \gamma_{12}) \cdot \begin{pmatrix} g_2/g_1 & -\cos \gamma_{12} \\ -\cos \gamma_{12} & g_1/g_2 \end{pmatrix} \quad (12)$$

So, if we are given two points in barycentric coordinates:  $L(\lambda^1, \lambda^2, \lambda^3), M(\mu^1, \mu^2, \mu^3)$ , then in the oblique frame the vector connecting them is:

$$\mathbf{a} = \overline{LM} = (\mu^i - \lambda^i) \mathbf{g}_i = (\mu_i - \lambda_i) \mathbf{g}^i = \mathbf{a}^i \mathbf{g}_i = \mathbf{a}_i \mathbf{g}^i, \quad i = 1, 2 \quad (13)$$

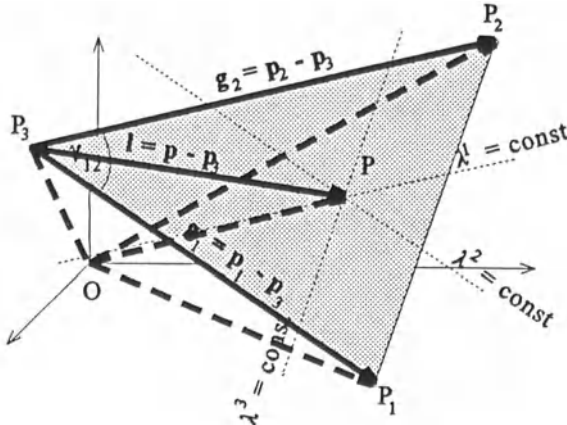


Fig. 4.

Thus, the vector calculus is fully possible, e.g. (Klingbeil, 1966):

$$\mathbf{a} + \mathbf{b} = (\mathbf{a}^i + \mathbf{b}^i) \cdot \mathbf{g}_i = (\mathbf{a}_i + \mathbf{b}_i) \cdot \mathbf{g}^i, \quad \mathbf{a} \cdot \mathbf{b} = g_{ij} \mathbf{a}^i \mathbf{b}^j = g^{ij} \mathbf{a}_i \mathbf{b}_j = \mathbf{a}^i \mathbf{b}_i = \mathbf{a}_i \mathbf{b}^i \quad (14)$$

The transition backwards, i.e. from oblique contravariant to barycentric coordinates, only requires using the obvious relation:  $\lambda^3 = 1 - (\lambda^1 + \lambda^2)$ .

Concluding, the barycentric coordinates give **relative positions** of points, in which:

- **nonmetric relations** between points and other geometric constructs, which require no scalar product (e.g. a link between points), **are involved**, but in which
- **no information on metric relations** between them, such as distances, angles, scale, shape, etc., requiring scalar product, **is contained**.

The simple transition to oblique coordinates (if metric characteristics of the space are known) defines the scalar product, so that the use of the **covariant/contravariant metric coefficients**:

- **separates non-metric and metric relations** between the space elements;
- **allows for vector operations**; and
- **saves the invariance and relativity properties** of the barycentric coordinates.

## RESECTION PROBLEM ACCORDING TO ANSERMET

The geodetic resection problem consists in determining the position of a new point from the measured angles to three old points of known positions, the new point being their vertex.

We refer here to the solution of the planar resection problem given by Ansermet (1910), see also (Allan, 1962) and Fig. 5. If  $A, B, C$  are given points in the Cartesian frame, then coordinates of any new point  $P$  can be computed from:

$$x_P = \frac{g_A x_A + g_B x_B + g_C x_C}{g_A + g_B + g_C}, \quad y_P = \frac{g_A y_A + g_B y_B + g_C y_C}{g_A + g_B + g_C} \quad (15)$$

The quantities  $g_A, g_B, g_C$ , the "barycentric coordinates" in Ansermet's formulation, are given as:

$$g_A = 1 / (\cot A - \cot \alpha), \quad g_B = 1 / (\cot B - \cot \beta), \quad g_C = 1 / (\cot C - \cot \gamma) \quad (16)$$

where  $A, B, C$  are the given angles of the base triangle (not to be confused with the corresponding triangle vertices) and  $\alpha, \beta, \gamma$  are the measured angles at  $P$ .

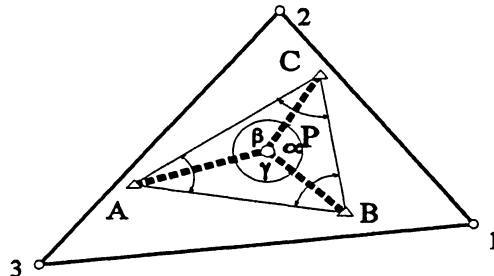


Fig. 5.

Once, instead of Cartesian coordinates, the barycentric coordinates of the given points are known, it is easy to show that the barycentric coordinates of the new point are:

$$\begin{aligned} \lambda_P^1 &= \lambda_A^1 p_A + \lambda_B^1 p_B + \lambda_C^1 p_C \\ \lambda_P^2 &= \lambda_A^2 p_A + \lambda_B^2 p_B + \lambda_C^2 p_C \\ \lambda_P^3 &= \lambda_A^3 p_A + \lambda_B^3 p_B + \lambda_C^3 p_C \end{aligned} \quad (17)$$

were:  $p_A = g_A / (g_A + g_B + g_C)$ ,  $p_B = g_B / (g_A + g_B + g_C)$ ,  $p_C = g_C / (g_A + g_B + g_C)$ . As a matter of fact, (17) is the transformation formula of barycentric coordinates between different reference frames: the  $p$ -frame  $A-B-C$  and the  $\lambda$ -frame 1-2-3.

## STATION POSITIONS FROM GPS PSEUDORANGES

The single station GPS pseudorange observational equation is formulated in the Cartesian system as:

$$p' = \sqrt{(x - x')^2 + (y - y')^2 + (z - z')^2 + c \Delta t} \quad (18)$$

with the measured station-to-satellite pseudoranges  $\rho^s$  and the bias  $c.\Delta t$  due to the unknown clock offset. At least four pseudoranges are needed to determine the station position and the clock offset (Grafarend, 1992).

The known four satellite positions can be recognized as vertices of the tetrahedron forming a 3-D base of barycentric coordinates, to which an oblique system with the covariant base vectors  $\mathbf{g}_1, \mathbf{g}_2, \mathbf{g}_3$  can be affiliated (Fig. 6). In the following we employ that particular system and make use of its close relations to barycentric coordinates, as shown earlier.

Each station-to-satellite vector  $\mathbf{l}^s$  can be expressed in that system as:

$$\mathbf{l}^s = (\lambda^i - \lambda^{is}) \cdot \mathbf{g}_i, \quad i = 1, 2, 3, \quad s = 1, \dots, 4 \quad (19)$$

where  $\lambda^i$  are the unknown contravariant coordinates of the new point and  $\lambda^{is}$  are the known contravariant coordinates of the satellite positions;  $\lambda^{is} = \delta^{is}$  for  $s \leq 3$  and  $\lambda^{is} = 0$  for  $s = 4$ .

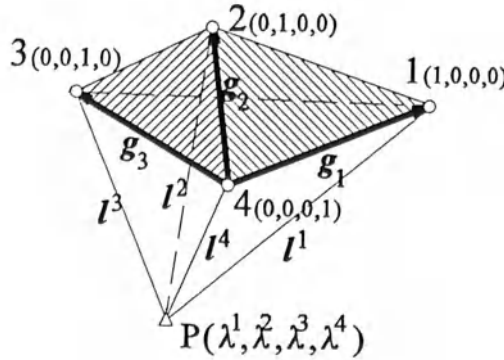


Fig. 6.

Then, the satellite-to-station path length can be expressed as (Klingbeil, 1966):

$$(\mathbf{l}^s)^2 = \mathbf{l}^s \cdot \mathbf{l}^s = g_{ij} (\lambda^i - \lambda^{is}) (\lambda^j - \lambda^{is}) \quad (20)$$

where  $g_{ij}$  are covariant metric coefficients. By linearizing  $\mathbf{l}^s$  and inserting it into (18) we get four linear equations to be solved for  $\Delta\lambda^s$  and  $\Delta t$ :

$$\begin{cases} \frac{1}{l^s} (\lambda_j - \lambda_j^s) \Delta \lambda^j + c \Delta t = \rho^{so} - \rho^{sc}, & \text{for } s = 1, 2, 3, 4 \\ \delta_j^s \Delta \lambda^j = 0 \end{cases} \quad (21)$$

with:

$$\lambda_j = g_{ij} \lambda^i$$

$$\lambda_j^s = g_{js} \quad \text{for } s = 1, 2, 3$$

$$\lambda_j^s = 0 \quad \text{for } s = 4$$

where  $\rho^{so}$  and  $\rho^{sc}$  mean "observed" and "calculated" values of the pseudoranges.

Although numerically (21) is much alike its Cartesian counterpart, the linearized form of (18), it represents quite different strategy. While (18) is usually solved in a global geocentric Cartesian reference system provided by the  $x, y, z$ -coordinates of the given satellite positions, the solution based on (21), once the satellite positions have been used to define the purely local and autonomous reference frame of barycentric coordinates, is completely closed within that frame.

## SHAPE FUNCTIONS IN THE METHOD OF FINITE ELEMENTS

In the geodetic practice there are often given some measured discrete values of a continuous function  $F(x,y)$ , such as, e.g., vertical displacements, at nodes of a network composed of triangular *elements*. The problem is to find out an approximation model function  $u(x,y)$  of  $F$  subjected to a number of constraints such as (Schwarz, 1991):

- 1) preserving the form of  $u(x,y)$  with linear transformations of coordinates, which means the **geometrical isotropy** of the function;
- 2) the elements should be **conformal**, which reflects the continuity of  $u(x,y)$  (and possibly of its derivatives) with passing from one element to another;
- 3) it should be  $u(x,y) = F(x,y)$  at nodal points (the element vertices), and possibly also for the derivatives, which is the boundary value problem;
- 4) the differences  $u(x,y) - F(x,y)$  should satisfy the least squares principle in the given continuous domain, etc.

Among the functions satisfying the first constraint usually complete polynomials up to a given order are chosen, e.g.:

$$u(x,y) = c_1 + c_2x + c_3y + c_4x^2 + c_5xy + c_6y^2 \quad (22)$$

The other constraints, however, demand for an **interpolation within separate elements** rather than for an approximation of all given data by a single model function. Such an approximation would corrupt the given physical data by an artificial model. We replace then the ineffective form (22) by the equivalent linear combination of the so-called nodal variables, so within any given element we get:

$$u^{(e)}(x,y) = \sum_{i=1}^p u_i^{(e)} N_i^{(e)}(x,y) \quad \text{with the property} \quad N_i^{(e)}(x_j^{(e)}, y_j^{(e)}) = \begin{cases} 1 & \text{for } j=i \\ 0 & \text{for } j \neq i \end{cases} \quad (23)$$

Here,  $N_i^{(e)}(x,y)$  are the so-called **shape functions**, which are specific for the particular model function type used. They are local carriers of nodal variable  $u_i^{(e)}$  contributions to the value of  $u^{(e)}(x,y)$  being looked for within each element.

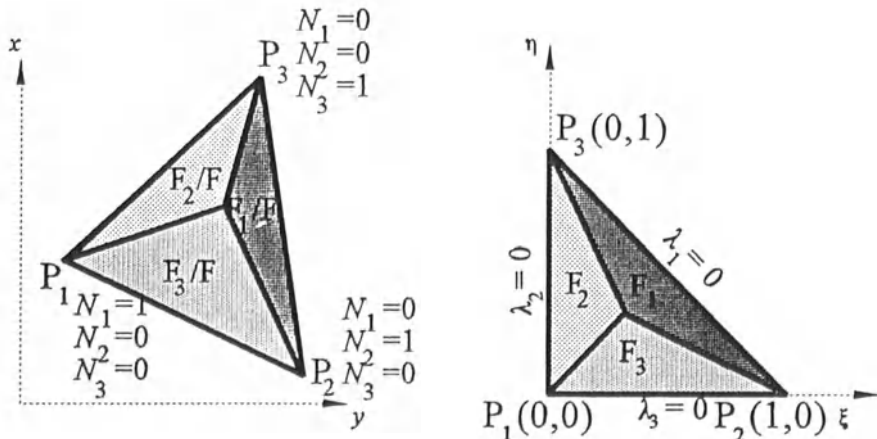


Fig. 7.

It results from (23) that each  $N_i(x,y)$  depends on some relative dimensionless measures of the given point location within the element rather than on its absolute coordinates. This inspires the transformation of the given triangular element into the unit triangle as shown on Fig. 7. Then we get for the linear model function  $u(x,y) = c_1 + c_2x + c_3y$  in the  $(\xi,\eta)$ -system:  
 $u(\xi, \eta) = \alpha_1 + \alpha_2 \xi + \alpha_3 \eta$ . The last relation should satisfy (23), so that from given  $u_i$  at nodal points we get:

$$u(\xi, \eta) = u_1(1 - \xi - \eta) + u_2 \xi + u_3 \eta \quad (24)$$

then the shape functions are given through barycentric coordinates as:

$$N_1(\xi, \eta) = \lambda_1, \quad N_2(\xi, \eta) = \lambda_2, \quad N_3(\xi, \eta) = \lambda_3 \quad (25)$$

A plot of  $N_1(\xi, \eta)$  is shown on Fig. 8.

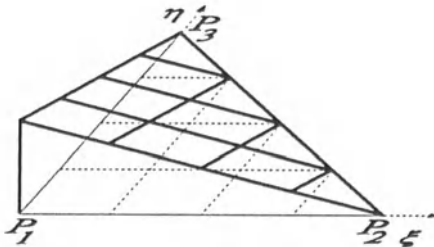


Fig. 8.

Similarly, for the quadratic model function (22) we get in the  $(\xi,\eta)$ -system:

$$u(\xi, \eta) = \alpha_1 + \alpha_2 \xi + \alpha_3 \eta + \alpha_4 \xi^2 + \alpha_5 \xi \eta + \alpha_6 \eta^2 \quad \text{and} \quad u(\xi, \eta) = \sum_{i=1}^6 u_i N_i(\xi, \eta) \quad (26)$$

There are six model coefficients  $\alpha_i$ , six nodal variables  $u_i$  and six shape functions, so we need three additional nodal point data. If we have chosen the function values at three additional nodal points as central points of the element sides, then the shape functions and the plots of  $N_1$  and  $N_6$  are:

$$\begin{aligned} N_1(\xi, \eta) &= \lambda_1(2\lambda_1 - 1) & N_4(\xi, \eta) &= 4\lambda_1\lambda_2 \\ N_2(\xi, \eta) &= \lambda_2(2\lambda_2 - 1) & N_5(\xi, \eta) &= 4\lambda_2\lambda_3 \\ N_3(\xi, \eta) &= \lambda_3(2\lambda_3 - 1) & N_6(\xi, \eta) &= 4\lambda_3\lambda_1 \end{aligned} \quad (27)$$

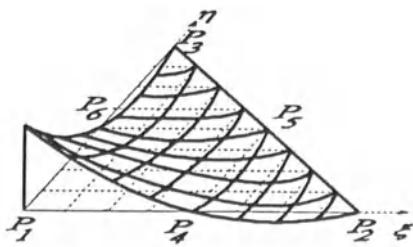


Fig. 9.

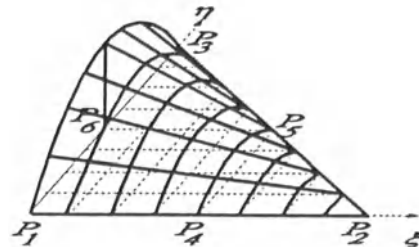


Fig. 10.

## A PHOTOGRAMMETRIC PROBLEM

In a 3-D Cartesian frame  $(x,y,z)$  there are given the ground points  $1, 2$  and  $3$ , and also the camera positions  $O'$  and  $O''$  (Fig. 11). The points, together with the new ground point  $P$ , are projected onto the photoplates as the points  $1', 2', 3', P'$ , and  $1'', 2'', 3'', P''$ , and then measured in the plate Cartesian systems  $(\xi', \eta')$ ,  $(\xi'', \eta'')$  of both photoplates, respectively. The problem is to determine the coordinates  $(x,y,z)$  of the new point  $P$ .

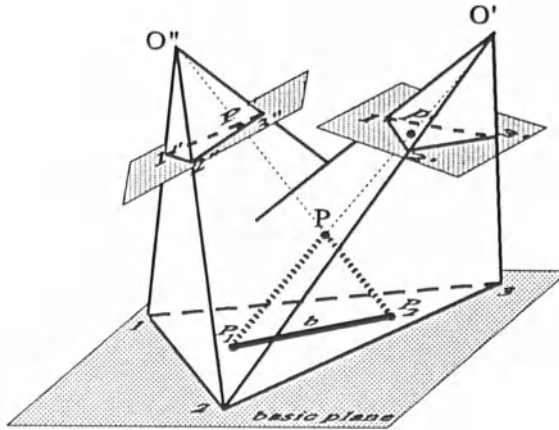


Fig. 11.

The problem can be solved through a series of barycentric frames and successive transformations of corresponding points:

- 1) Transform  $P'(\xi', \eta')$  into  $P'(\mu^1, \mu^2, \mu^3)$  in the 2-D barycentric frame  $1'-2'-3'$ , and also  $P''(\xi'', \eta'')$  into  $P''(\nu^1, \nu^2, \nu^3)$  in the frame  $1''-2''-3''$ .
- 2) The transformation between the frames  $1'-2'-3'$  and  $1-2-3$ , and also between  $1''-2''-3''$  and  $1-2-3$  is linear, so due to the invariance property the barycentric coordinates of corresponding points are equal, then:

$$P'(\mu^1, \mu^2, \mu^3)_{[1'-2'-3']} = P_1(\mu^1, \mu^2, \mu^3)_{[1-2-3]}, \quad P''(\nu^1, \nu^2, \nu^3)_{[1''-2''-3'']} = P_1(\nu^1, \nu^2, \nu^3)_{[1-2-3]}$$

- 3) In the 3-D barycentric frame  $1-2-3-O'$  the points  $P_1$  and  $P_2$  belong to the plane  $\lambda^4=0$ , then we have also another identity of coordinates:

$$P_1(\mu^1, \mu^2, \mu^3, 0)_{[1-2-3-O']} \text{ and } P_2(\nu^1, \nu^2, \nu^3, 0)_{[1-2-3-O']}$$

while the camera coordinates are:  $O'(0, 0, 0, 1)$  and  $O''(\lambda_{O''}^1, \lambda_{O''}^2, \lambda_{O''}^3, \lambda_{O''}^4)$ , the last ones to be computed from the given Cartesian coordinates.

- 4) Now, we have to solve the intersection problem (through solving the triangle  $P-P_1-P_2$ ) in the barycentric frame  $1-2-3-O'$  to determine the point  $P(\lambda^1, \lambda^2, \lambda^3, \lambda^4)$ .
- 5) Finally, we transform  $P(\lambda^1, \lambda^2, \lambda^3, \lambda^4)$  into the Cartesian frame to determine  $P(x^1, x^2, x^3)$ .

## CONCLUSIONS

1. Barycentric coordinates are a useful tool for expressing **relative positions** of points within a triangular or tetrahedral **local reference frame**.
2. Their basic property consists in their **invariance with respect to linear transformations of the frame**.
3. They involve by themselves only **nonmetric characteristics of interpoint relations**, which require no scalar product (e.g. a link between points), while metric characteristics are implied in the frame through the given shape and scale of the base triangle and are not expressed by barycentric coordinates.
4. Barycentric coordinates have **neither dimensions nor origin** (within the reference frame); therefore **no vector operations** are *per se* defined and available.
5. There is a simple relation between the triangular (or tetrahedral) base of barycentric coordinates and vector base of **oblique coordinates**. The last ones allow for **metric characteristics of interpoint relations**, e.g. scale, distances and angles, through defining metric coefficients. Thus, consequently, the scalar product and vector operations become available.
6. In this way a linear transformation of the barycentric base changes metric coefficients only, while it leaves the coordinates themselves unchanged; in this way we have a separation between coordinates and nonmetric relations on one side, and metric coefficients and metric relations on the other side.
7. Finally, barycentric coordinates, with the help of the associated oblique coordinates and metric coefficients, can be used for effective performing standard, as well as non-standard, geodetic operations in a purely local reference frame.

## ACKNOWLEDGEMENT

The presented here work was performed in 1994 at the Geodetic Institute of the University of Stuttgart within the financial means of the project SFB 228 *High Precision Navigation*. This support of the SFB 228 is herewith highly appreciated.

## REFERENCES

- Allan, A.L. (1962). The Tienstra Method of Resection. *Int. Hydr. Rev.*, No.2, pp. 71 - 76.  
Burnett, D.S. (1987). *Finite Element Analysis*. Addison-Wesley Publ. Comp.  
Ansermet, A. (1910). Eine Auflösung des Rückwärtseinschneidens. *Zeit. d. Vereins Schweiz. Konkordatsgeometer*, Jahrgang VIII, pp. 81 - 91.  
Farin, G. (1988). *Curves and surfaces for computer aided geometric design*. Academic Press, New York.  
Grafarend, E.W. (1992). The modelling of free satellite networks in spacetime. *Proc. Int. Workshop on "Global Positioning Systems in Geosciences"*, 8-10 June, 1992, ed. S.P. Mertikas. Techn. Univ. of Crete, Chania, Greece.  
Klingbeil, E. (1966). *Tensorrechnung für Ingenieure*. Bibl. Inst. Mannheim/Wien/Zürich.  
Preparata, F. and Shamos, M.I (1985). *Computational geometry*. Springer Verlag, Berlin.  
Reinhardt, F. and Soeder, H. (1980). *dtv-Atlas zur Mathematik; Band I: Grundlagen, Algebra und Geometrie*. Deutschen Taschenbuch Verlag.  
Schwarz, H.R. (1991). *Methode der finiten Elemente*. B.G. Teubner Stuttgart.  
Stoffi, J. (1991). *Oriented projective geometry*. Springer Verlag, Berlin.  
Wallace, A.H. (1957). *An Introduction to Algebraic Topology*. Pergamon Press.

# DEM GENERATION WITH ERS-1 INTERFEROMETRY \*

C. Prati, F. Rocca

Dipartimento di Elettronica e Informazione - Politecnico di Milano

Piazza L. da Vinci, 32 - 20133 Milano - Italy

Ph.: +39 2 2399 3585 - Fax: +39 2 2399 3413 - e.mail: prati@ipmel2.elet.polimi.it

May 17, 1995

## Abstract

*SAR interferometry can be usefully exploited for generating elevation maps. A problem derives from the image deformation due to SAR geometry. As the terrain slope along range approaches the off-nadir angle (foreshortening areas), no elevation information can be extracted. However, if ascending and descending passes are considered, terrain coverage is increased. Those areas affected by foreshortening in one image are well covered (if not in shadow) in the other image.*

## 1 Introduction

Ascending and descending orbits combination is essential for slopes coverage in SAR interferometry. As an example, the different curves of figure 1 identify terrain slopes  $\alpha$  recoverable from ERS-1 as a function of their azimuth orientation (see the lower part of figure 1). Thick and thin lines refer to ascending and descending passes respectively (here a baseline of 100 meters has been assumed both for ascending and descending passes). If just ascending passes are used, slopes that can be recovered from ERS-1 (at the equator in this example) are contained in the white area. To understand how that plot has been generated, let us consider a 9 degrees azimuth orientation (i.e. the orbit orientation) and let us consider slopes ranging from  $-90$  to  $+90$  degrees (i.e. from the lower to the upper limits of the plot). It is clear that, if we consider an incidence angle of 23 degrees for flat terrain, slopes from  $-90$  to  $-67$  degrees will not be observed since in shadow (lower shaded areas). On the other hand, slopes from 20 to 26 degrees will not be observable since the interferometric images are uncorrelated (Gatelli, 1994; Prati, 1993) (this is the region between the two thick lines). Finally, slopes from 26 to 90 degrees are in layover (upper gray and shaded area). These simple considerations can be repeated for every azimuth orientation and for descending ERS-1 orbits. Then, if both ascending and descending passes are used, the unrecoverable areas are represented by the shaded areas only. This point is clear if one consider that those areas affected by foreshortening and layover in one image are well covered (if not in shadow) in the other image. Finally, if layover areas could be

---

\*This paper has been presented at IGARSS'94

separated from the rest of the image (a not always possible operation), the irrecoverable slopes are further reduced to the small black areas shown in the figure 1.

## 2 An experiment with ERS-1 data

An elevation map of Vesuvius (the big volcano close to Naples in Italy) has been generated with the combination of interferograms taken from ascending and descending passes of ERS-1. Detected images are shown in figures 2 and 3. The first estimate of the baselines has been obtained from the ancillary data. Then, the coastline (in the lower left part of the images) has been exploited to improve the accuracy of the estimates. Fringes of the ascending and descending images are shown in figures 4 and 5 (baselines are approximately 54 and 192 meters for ascending and descending pairs respectively).

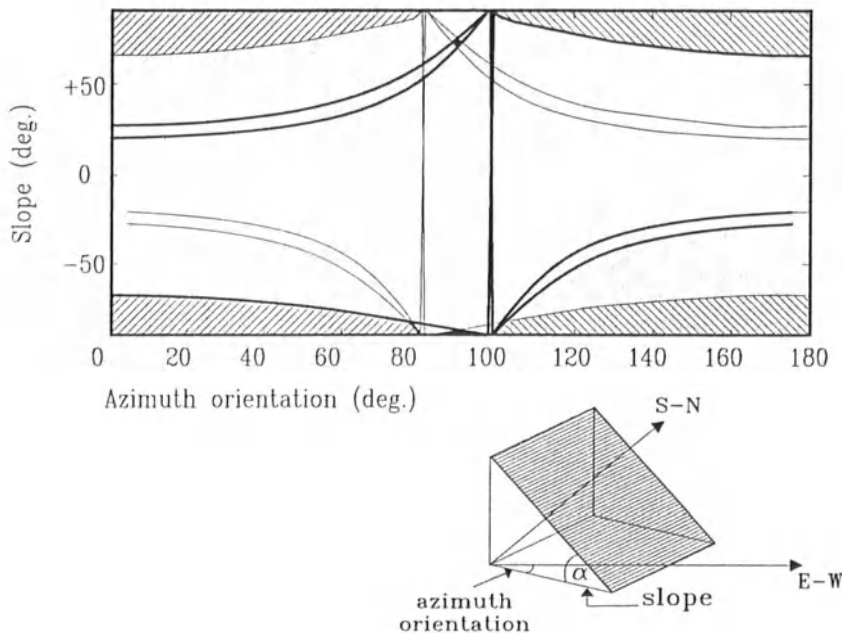


**Figure 1:** Combinations of slope and azimuth orientation that cannot be recovered from ERS-1 data. With ascending orbits (gray and shaded areas). With both ascending and descending orbits (shaded areas only). With layover separation (black areas).

After phase unwrapping (Rocca, 1994; Prati, 1994) and phase to elevation scaling, elevation maps have been rectified (from slant to ground range). They are shown in figures 6 and 7. Terrain elevation ranges from 0 to about 1200 meters. Please notice that foreshortening areas (e.g. just above the top of Vesuvius in the descending pairs and below in the ascending ones) look very smooth since they have been obtained with a linear interpolation from elevation maps in slant range. Finally, elevation maps derived from ascending and descending passes have been resampled on a common grid (by exploiting again the coast line as a common reference) and combined as a coherence weighted average (Prati, 1992; Rocca, 1992). In other words, wherever coherences of ascending and descending pairs was

comparable, the elevation has been computed as the average. Otherwise, just one map (that with higher coherence, of course) has been exploited. The result is shown in figure 8. It can be noted that linearly interpolated areas have been eliminated and that the spatial resolution of both sides of Vesuvius is now comparable.

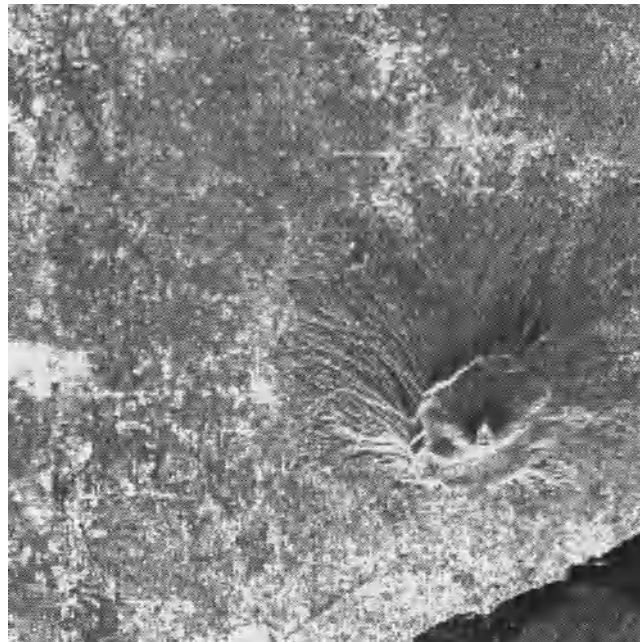


**Figure 2:** ERS-1 detected image of Vesuvius: ascending passes.



**Figure 3:** ERS-1 detected image of Vesuvius: descending passes.

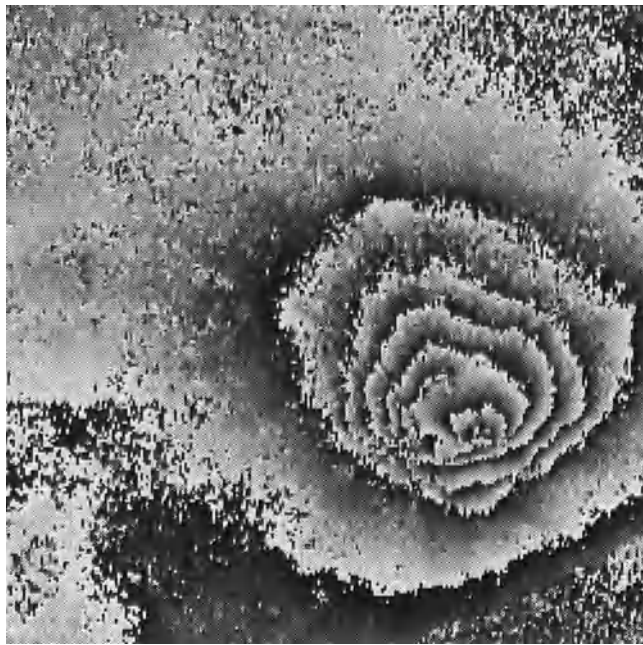


**Figure 4:** ERS-1 fringes image of Vesuvius: ascending passes.



**Figure 5:** ERS-1 fringes image of Vesuvius: descending passes.

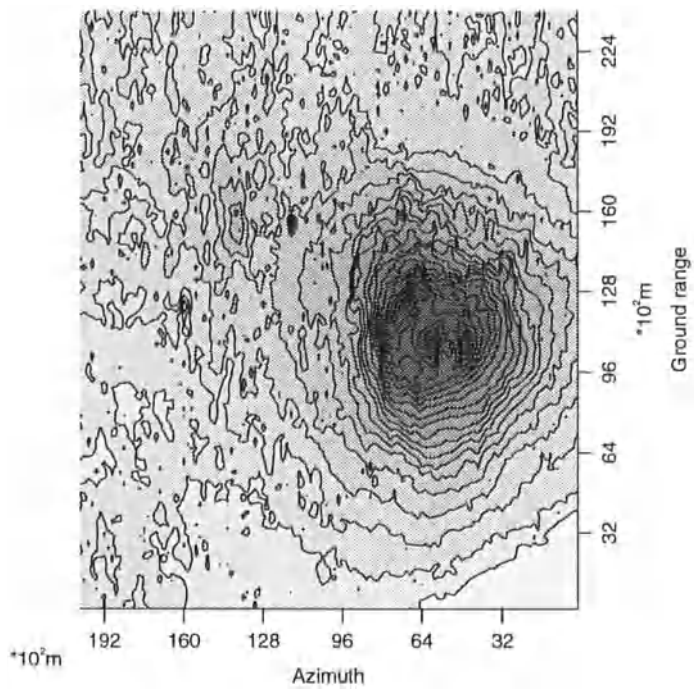


**Figure 6:** Rectified elevation maps of Vesuvius. Ascending passes.

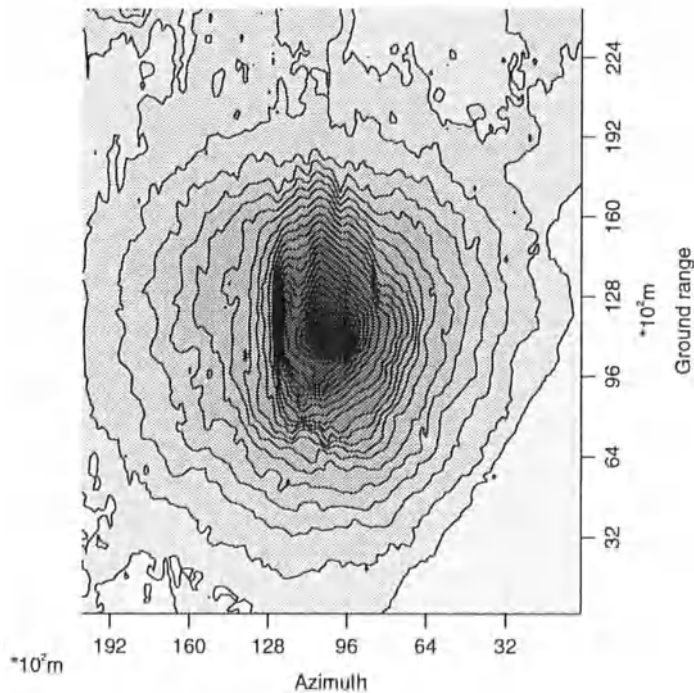


**Figure 7:** Rectified elevation maps of Vesuvius. Descending passes.

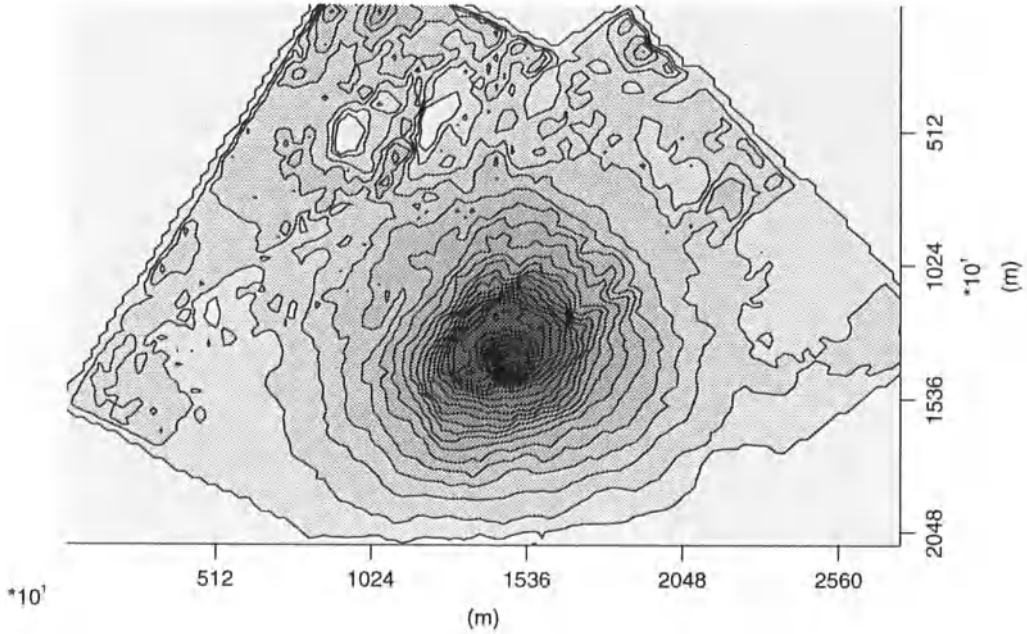


**Figure 8:** Rectified elevation maps of Vesuvius. Combination of ascending and descending passes.

### 3 Analysis of results

Since no existing DEM was available to us, other than a 1:25000 map, the consistency of the results have been checked by considering elevation differences in high coherence areas of both ascending and descending images. The map of elevation differences from white ( $-40\text{m}$ ) to black ( $+40\text{m}$ ) is shown in figure 9. By comparing figures 8 and 9, it can be noted a large systematic error proportional to the estimated elevation. This effect depends on the estimation error of geometric parameters probably due to the inaccuracy of the used ground control points. On the other hand the measured inconsistency could be used as an information to get a better estimate of the unknown parameters. As a final result, figure 10 shows the combination of the detected images after geometric rectification and reflectivity compensation. By a comparison with figures 2 and 3, it can be noted how, as expected, the image intensity is now less dependent on terrain slopes (Ulander, 1993; Werner, 1993).

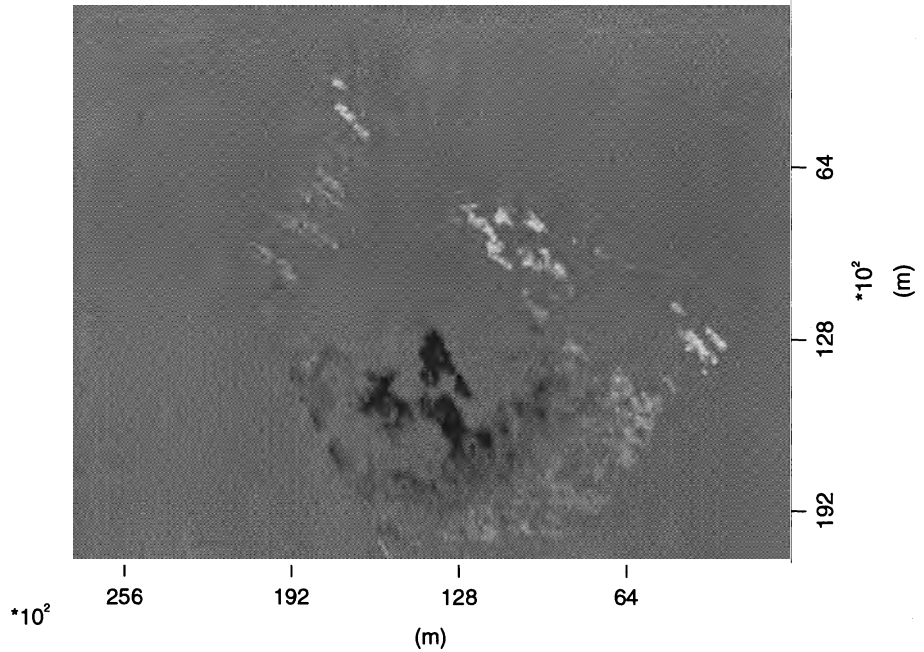


**Figure 9:** Elevation differences in high coherence areas between ascending and descending images (Black=40m, White=−40m).

#### 4 Conclusions

The need of both ascending and descending satellite passes for DEM generation have been demonstrated. Results from a difficult area as that of Vesuvius show that in order to avoid systematic errors, a few ground control points should be available. For this sake, monuments visible from both ascending and descending satellite passes are needed. In this framework investigations on the suitability of vertical corner reflectors should be carried out. Moreover, elevation differences among ascending and descending maps (i.e. not necessarily two pairs only) could be exploited as "floating" ground control points to solve the inverse problem: from data to parameters of the forward model.

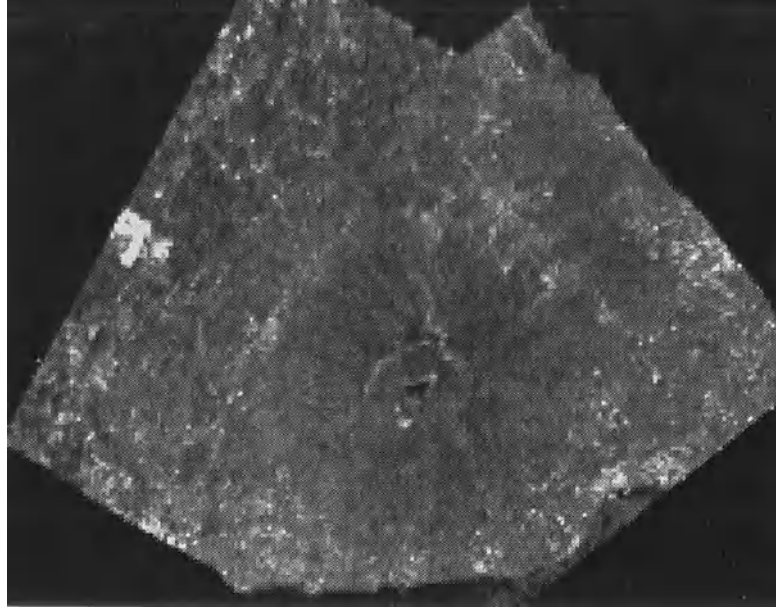


**Figure 10:** Combination of the detected images after geometric rectification and reflectivity compensation.

## References

- [1] F. Gatelli, A. Monti Guarnieri, F. Parizzi, P. Pasquali, C. Prati, F. Rocca, "The wavenumber shift in SAR interferometry", to appear in *IEEE Transactions on GARS*, Aug. 1994.
- [2] C. Prati, F. Rocca, "Improving slant range resolution of stationary objects with multiple SAR surveys", *IEEE Transactions on AES*, Vol. 29, No.1, 1993, pp.135-144.
- [3] Prati C., Rocca F., Monti Guarnieri A., "Measuring Volumetric Scattering Effects With SAR Interferometry", Proceedings of PIERS'94, 1994.
- [4] Prati C., Rocca F., Monti Guarnieri A., "SAR interferometry experiments with ERS-1, Proceedings of the First ERS-1 Symposium, Cannes, 4-6 November 1992, pp. 211-218.
- [5] Rocca F., Prati C., "Innovative applications of repeated satellite SAR surveys, ISY Conference, Munchen, April 1992, pp.193-198.
- [6] Rocca F., Prati C., Monti Guarnieri A., "ERS-1 SAR Interferometry techniques and applications", ESA report n.3-7439/92/HGE-I, 1994.
- [7] Ulander L., Hagberg J., "Use of InSAR for Radiometric Calibration over Sloping Terrain", SAR Calibration Workshop, ESTEC - Noordwijk, 1993, pp.147-159.
- [8] Werner C., Rosen P., "Topographic Slope form the SAR Interferometric Phase Gradient", Proceedings of PIERS'93, Pasadena - CA, 1993, p. 922.

# FUNDAMENTAL GPS NETWORK IN LITHUANIA

**Kai Borre**  
**Aalborg University**  
**Fibigerstræde 11, DK-9220 Aalborg Ø, Denmark**  
and  
**Petras Petroškevičius**  
**Institute of Geodesy**  
**Vilnius Technical University, Saulėtekio al. 11, 2054 Vilnius, Lithuania**

## Organizational Circumstances

In the spring of 1991 the first author conceived the plan of establishing a fundamental network in Lithuania by means of GPS. In July 1992 the financial support for the plan was provided. The Danish Government payed for GPS receivers, personal computers, and other materials needed while the Lithuanian Government agreed to subsidize the renovation of the survey ground marks, the observational campaign, and calculations.

All planning and actual observations and calculations were undertaken under the responsibility of the Lithuanian partners. The superior job was managed by the State Department of Surveying and Mapping while the observational and calculational tasks were performed by staff from Vilnius Technical University, Institute of Geodesy. Consequently the scientific responsibility of the project lies at the Institute of Geodesy.

Dr Kai Borre has been responsible for the project, and the daily administration has been attended to Dr Petras Petroškevičius. The computational procedure and the pertinent calculations are all due to Dr Eimuntas Kazimieras Paršeliūnas.

## The Existing Lithuanian Network

The existing Lithuanian first order triangulation network was created in 1926–1940. It was established by the Department of Topography at the Ministry of Defence, cf. Ratautas (1937), Kodatis (1937), Šleževičius (1937). The network made a part of the Baltic triangulation work conducted by the Baltic Geodetic Commission. The Lithuanian part of the network consisted of 84 points. Three short baselines were measured with an accuracy of 0.3 ppm, and from it were observed and calculated three baselines with an accuracy of 2.5 ppm. The standard deviation of an observed angle was about 0.5".

After World War II the network was augmented by the triangulation network of the Vilnius area. The augmented network comprised 110 points. An earlier used ellipsoid was aban-

doned in favour of the Krassovsky ellipsoid and the Russian 1942 coordinate system. Today about 90% of these points still are in existing.

## **Planning and Preparations Prior to the Observations**

With view to future users of geodetic information it was decided to establish a fundamental GPS network including 40–50 points. These points will be carriers of the new Lithuanian coordinate system which shall be the basis for all future geodetic works. Four network points within Lithuania and two points in Latvia already were coordinated during the EUREF BAL GPS campaign in August–September 1992, cf. Madsen & Madsen (1993). The over all accuracy was planned to be better than 1 ppm. The newly determined coordinates may be used to establish transformation formulas between the Russian 1942 coordinate system and the new one.

The planning of the network was started in 1992 by geodesists from the Vilnius Technical University, Institute of Geodesy. Here an analysis of the existing network was carried through with reference to involve as many old points as possible. The points were selected with due regard to safe location, stable construction, and suitability for GPS observations.

Furthermore, the geomorphologic, geologic, and tectonic properties at the various areas were taken into consideration. Consequently, a sub-surface point at the Ignalina Power Plant was included into the network. The final network includes 54 points.

The average length of vector is approximately 40 km, the shortest one being 9 km (322–522) and the longest one being 126 km (116–407).

New ground marks were erected at 12 places. 45 points are identical to old triangulation points and even two are identical to points in the Baltic triangulation network and finally 7 points are identical with points in the Vilnius area triangulation.

All points of the network are documented by a sketch, a shadow diagram, a drawing of the survey mark, a short description of the site and a small map for identification.

## **The Observations**

Despite some bureaucracy it was possible to start the observations in May 1993. The 12 channel dual frequency Ashtech receivers observe C/A and P codes on L1 and P code on L2.

The observations were performed during the days 141, 142, 146, 148–150, 152–155, 161–164, 173–177, 181–186, 201–203, 206, 208–210, 258, and 292. Each session was planned as a period of 12 hours. The recording interval is 20 s, except for days 161–164 where 30 s intervals were dictated by the participation in the Baltic Sea Level campaign. The elevation angle for cutoff is 10°. The antenna heights were observed four times before and after the sessions. Meteorology was observed every second hour but otherwise not used in the subsequent processing.

## Processing of Observations

The procedure used may be described by the following four steps:

1. preliminary session-wise processing
2. vector-wise processing
3. quality control
4. testing and subsequent further “corrections”

*ad 1.* The sessions were processed by means of the commercial software GPPS using the wide lane combination of observations for determination of ambiguity unknowns and the mean of the wide and the narrow lane observables ( $\lambda = 0.484436 \text{ m}$ ) for the fixed double difference solution for the vector components. The elevation angle for cutoff was set to  $20^\circ$ . Satellites were omitted according to Notice Advisory for Navigation Users.

In the ‘project’ file the antenna height was entered as well as preliminary coordinates (‘known = 2’) provided from an interim adjustment.

This calculation yields a preliminary solution indicating the best reference satellite. By study of the plot file the best period of contiguous observations were selected. The goal was to select a period of approximately 800 epochs, but any number in the range 300–1100 was accepted. Simultaneously it was decided which satellites to omit in the following calculation. The satellites were omitted if their observational periods contain less than 100 epochs, or if there are too many interruptions in the signal or if the residuals change more than 0.5 wavelength between consecutive epochs.

In some cases no double difference solution was obtained at all. Then the situation was analysed by means of FILETOOL. The problems often were connected with registration of bad epoch intervals (Remedy: use ‘Thin a bedata file to selected epoch intervals’) or a gab in the data (Remedy: use ‘Look at a bedata file’).

*ad 2.* The preliminary processing was followed by a processing of the *individual vectors*. The following values in ‘Run-Time Parameters’ were changed: The first and last epoch were entered according to the information obtained in the previous step, the elevation angle for cutoff was still  $20^\circ$ ; possible satellites to be omitted was listed by their numbers.

*ad 3.* The *quality of the single vectors* should be so that the integer search ratio was larger than 100% and the standard deviation of the length less than 15 mm.

If these two requirements were fulfilled (if not, see below under ad 4.) we accepted the solution if furthermore the following tests were passed:

The change in any vector component between the float and fixed double difference solutions must be less than 20 mm, the fit of ambiguities must be less than 0.25, the standard deviation of the ambiguities must be less than 0.1, and finally the decimal part of the ambiguity number must lie in the intervals .000–.2 or .8–.999. The latter three conditions strongly depend on the number of epochs. A combination of studying the plot file and changes of the epoch numbers led to the final solution.

When all vectors of a given session had passed this test they were adjusted by means of the FILLNET programme. We glanced over the normalized residuals to try to identify the

outliers. The criteria for an acceptable solution were the following: All corrections to vector components must be less than 25 mm, the standard error of unit weight  $\hat{\sigma}_0 < 0.1$  and the length component better than 0.1 ppm. Sometimes the float solution was accepted in stead of the fixed one and thereby violating the demand that we want to use a solution which is freed of the ionospheric influence.

*ad 4.* If the two above-mentioned requirements were not fulfilled we tried to obtain a more accurate vector by manipulating the choice of reference satellite. This conduct should reveal which satellite is really bad. Also the selection of another interval of epochs and thus another combination of satellites was used in this step.

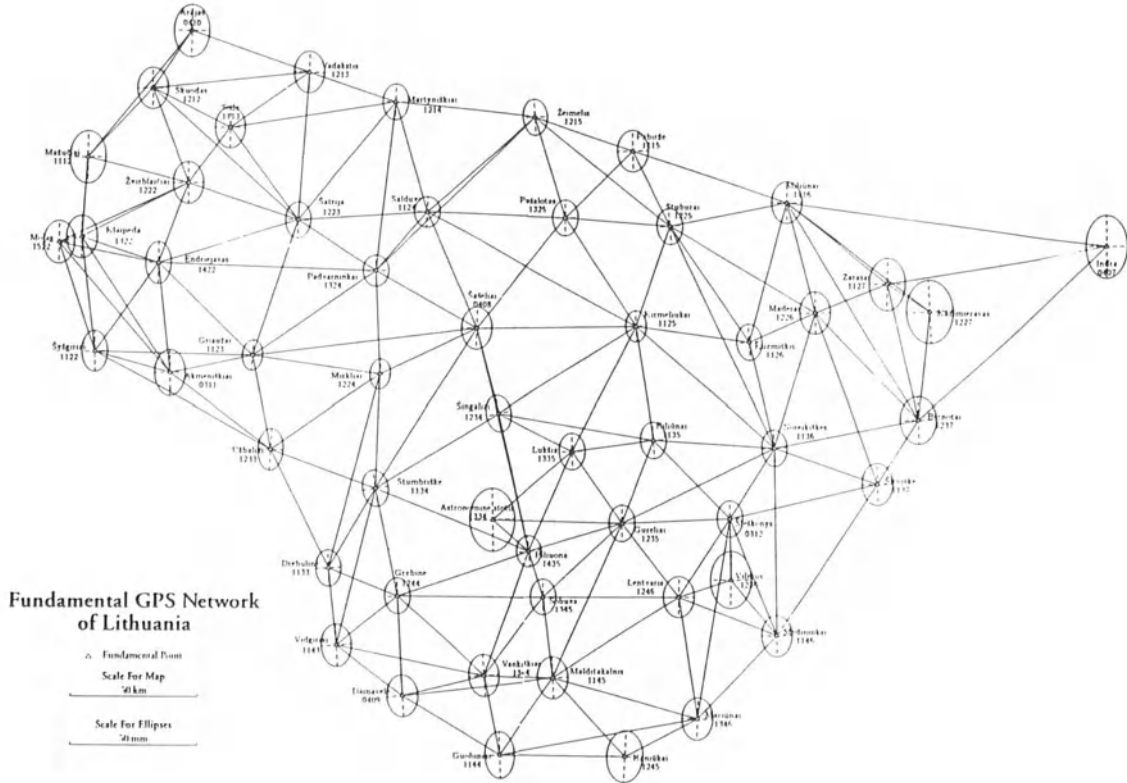


**Fig. 1.** Minimally constrained adjustment of the Fundamental GPS Network of Lithuania

## The Adjustment

The final adjustment was done by TURBO-NET and includes 193 vectors. It is terminated after 2 iterations. In a minimally constrained adjustment the weighted sum of squares is  $r^T Cr = 3653$ , and the number of degrees of freedom is  $df = m - n = 579 - 159 = 420$ , cf. figure 1. Consequently the *a posteriori* standard deviation of unit weight equals

$$\hat{\sigma}_0 = \sqrt{\frac{r^T Cr}{df}} = 2.9.$$

In the final adjustment 6 points are kept fixed with the coordinate values as postulated in the Baltic GPS campaign in August–September 1992, cf. Madsen and Madsen (1993), cf. figure 2. The above values now are changed to  $r^T C r = 5728$ ,  $df = m - n = 579 - 144 = 435$ , and  $\hat{\sigma}_0 = 3.6$ .

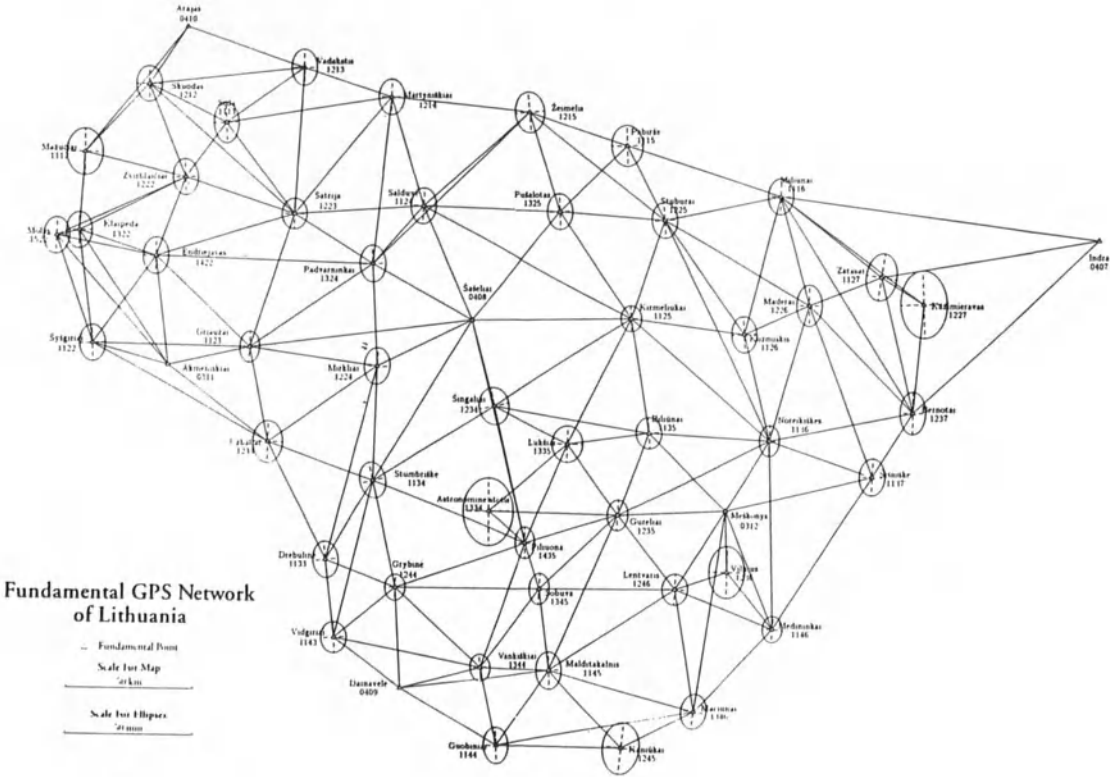


**Fig. 2.** Fixed adjustment of the Fundamental GPS Network of Lithuania

## REFERENCES

- Ratautas, M. (1937). *Lietuvos trianguliacija*. Kariuomenės štabo Karo topografijos skyriaus Metraštis, It., II<sup>o</sup>d., Kaunas.
- Kodatis, B. (1937). *Lietuvos astronominė observatorija*. Kariuomenės štabo Karo topografijos skyriaus Metraštis, It., Id., Kaunas.
- Šleževičius, K. (1937). *Svorio jėgos greitėjimas Lietuvoje*. Kariuomenės štabo Karo topografijos skyriaus Metraštis, It., Id., Kaunas.
- Madsen, Frede & Finn Bo Madsen (1993). *A new GPS-network in the Baltic countries*. National Survey and Cadastre, Denmark.

# THE ROTATION OF THE CELESTIAL EQUATORIAL SYSTEM WITH THE SO-CALLED "NON-ROTATING ORIGIN"

Burghard Richter

Deutsches Geodätisches Forschungsinstitut, Dept. I  
Marstallplatz 8, D-80539 München, Germany

## ABSTRACT

*Guinot* suggested in 1979 to replace the vernal equinox by the so-called "non-rotating origin" as the first axis of the celestial equatorial system. This paper derives the analytical relation between the traditional and the alternative equatorial systems by means of their rotation vectors. Under the assumption of a regular precession of the mean celestial pole, the motions of the rotation vector and the first axis of the alternative mean equatorial system with respect to a space-fixed ecliptical system are investigated and illustrated.

## 1. INTRODUCTION

The celestial equatorial system plays an important role as an intermediate system between a space-fixed system and an earth-fixed one. Its third axis is directed towards the celestial ephemeris pole. It has the motions of precession and nutation. Thus also the equatorial plane, to which the celestial ephemeris pole is perpendicular, changes its orientation in space.

This paper deals with the first axis within the equator. Its traditional definition as the vernal equinox has certain disadvantages: The equator is defined by the rotational motion of the earth, which geodetic space observations are very sensitive to. The ecliptic, however, is defined by the translational motion of the earth, which geodetic observations are almost insensitive to. The equinox, being the intersection of the equator with the ecliptic, is therefore not directly observable, and its realization is rather inaccurate.

Furthermore, the motion of the equinox on the celestial sphere with respect to a space-fixed system has not only a component perpendicular to the equator (which is inevitable because of the precession and nutation of the celestial pole), but also an – even larger – component parallel to the equator. So the rotation of the traditional equatorial system is much larger than it would be necessary. And that is why the derivative of sidereal time (the hour angle of the vernal equinox) with respect to time is different from the magnitude of the rotation vector of the earth.

These facts made *Guinot* (1979) propose a new definition of the first axis of the equatorial system. The concept of the so-called "non-rotating origin" (of right ascensions) was later on in some details discussed by several authors (*Aoki, Kinoshita*, 1983; *Capitaine, Guinot*,

*Souchay, 1986; Aoki, 1988; Yan, Grotens, 1992, and others).* Although it has not gained general acceptance, it is still recommended by a number of scientists.

## 2. ANALYTICAL REPRESENTATION

At an initial epoch  $t_0$ , the "non-rotating origin" is chosen arbitrarily on the equator, for instance coinciding with the vernal equinox. For all subsequent times it is defined such that it never has a motion along the instantaneous equator. This means that the rotation vector of the alternative equatorial system, the first axis of which is the "non-rotating origin", relative to a space-fixed reference system has no component around its own third axis, because such a rotation component would move the first axis along the equator, what shall not be allowed.

Let

$$\underline{\mathbf{e}} = \begin{bmatrix} e_1 \\ e_2 \\ e_3 \end{bmatrix}, \quad \underline{\mathbf{f}} = \begin{bmatrix} f_1 \\ f_2 \\ f_3 \end{bmatrix}, \quad \underline{\mathbf{g}} = \begin{bmatrix} g_1 \\ g_2 \\ g_3 \end{bmatrix} \quad (1)$$

be the orthonormal basis vectors of a space-fixed reference system, of the celestial equatorial system in the traditional definition (its first axis  $f_1$  being directed towards the vernal equinox) and of the celestial equatorial system in the alternative definition (its first axis  $g_1$  being directed towards the "non-rotating origin"), respectively.

The transformation from the space-fixed system to the traditional equatorial system is

$$\underline{\mathbf{f}} = \mathbf{R}_f \underline{\mathbf{e}}, \quad (2)$$

where the time-depending rotation matrix

$$\mathbf{R}_f = \mathbf{R}(\zeta, \theta, z, \Delta\psi, \Delta\varepsilon) \quad (3)$$

is a function of the precession parameters  $\zeta, \theta, z$  and the nutation parameters  $\Delta\psi, \Delta\varepsilon$ .

The traditional and the alternative equatorial systems differ only by a rotation around their common third axis:

$$\underline{\mathbf{g}} = \mathbf{R}_3(q) \underline{\mathbf{f}}. \quad (4)$$

The antisymmetric matrix

$$\dot{\mathbf{R}}_f \mathbf{R}_f^T = \begin{bmatrix} 0 & \omega_3 & -\omega_2 \\ -\omega_3 & 0 & \omega_1 \\ \omega_2 & -\omega_1 & 0 \end{bmatrix} \quad (5)$$

yields the rotation vector  $\omega_f$  of the traditional equatorial system  $\underline{\mathbf{f}}$  relative to the space-fixed system  $\underline{\mathbf{e}}$ :

$$\underline{\omega}_f = \begin{bmatrix} \omega_1 \\ \omega_2 \\ \omega_3 \end{bmatrix}^T \underline{\mathbf{f}}. \quad (6)$$

The rotation vector  $\underline{\omega}_g$  of the alternative equatorial system  $\underline{\mathbf{g}}$  relative to the space-fixed system  $\underline{\mathbf{e}}$  has the same equatorial components as  $\underline{\omega}_f$ , but its third component with respect to the equatorial system has to be zero. Therefore, the angle  $q$  must, at any time  $t$ , compensate the third component of the rotation vector  $\underline{\omega}_f$  of  $\underline{\mathbf{f}}$ :

$$q = - \int_{\tau=t_0}^t \omega_3 d\tau. \quad (7)$$

According to (5) and (3),  $\omega_3$  depends on the orientation parameters  $\zeta, \theta, z, \Delta\psi, \Delta\epsilon$  and their derivatives with respect to time. However, the differential

$$-dq = \omega_3 dt = a_1 d\zeta + a_2 d\theta + a_3 dz + a_4 d\Delta\psi + a_5 d\Delta\epsilon \quad (8)$$

is in general anholonomic, since the coefficients  $a_i$  don't fulfill the integrability conditions. This is why the direction of the "non-rotating origin" is not a function of the instantaneous position of the pole; but it depends on the whole path the pole has covered on the celestial sphere since the initial epoch  $t_0$ . Therefore, an integration over time according to (7) has to be performed.

As far as the precession and the nutation of the celestial ephemeris pole are known as functions of time by an appropriate model, the integration can be done within this model. Since the precession parameters  $\zeta, \theta, z$  are expressed in power series and the nutation parameters  $\Delta\psi, \Delta\epsilon$  are expressed in periodic series, the resulting representation of  $q$  is very complicated and lengthy. A series representation containing only the most dominant terms was given by *Capitaine, Guinot, Souchay* (1986).

### 3. THE ROTATION VECTOR OF THE EQUATORIAL SYSTEM IN A SIMPLIFIED MODEL

In order to analyse the rotation of the alternative equatorial system, let us make some simplifications: We neglect the nutation of the celestial pole and assume its precession to be a regular motion on a circular cone around a fixed ecliptic normal.

Let  $\underline{\mathbf{e}}$  now be an ecliptical system with three space-fixed axes,  $e_3$  being directed towards the northern ecliptical pole. The matrix  $\mathbf{R}_f$  transforming from  $\underline{\mathbf{e}}$  to the traditional equatorial system  $\underline{\mathbf{f}}$  is now

$$\mathbf{R}_f = \mathbf{R}_1(-\epsilon) \mathbf{R}_3(-p) = \begin{bmatrix} \cos p & -\sin p & 0 \\ \sin p \cos \epsilon & \cos p \cos \epsilon & -\sin \epsilon \\ \sin p \sin \epsilon & \cos p \sin \epsilon & \cos \epsilon \end{bmatrix}. \quad (9)$$

The precessional angle  $p$  is a linear function of time, performing one revolution of  $360^\circ$  within one Platonic year (p.y.)  $\approx 25800$  years, and the obliquity of the ecliptic  $\epsilon \approx 23^\circ 26'$  is constant.

From (9) we find

$$\dot{\mathbf{R}}_f \mathbf{R}_f^T = \begin{bmatrix} 0 & -\cos \varepsilon \dot{p} & -\sin \varepsilon \dot{p} \\ \cos \varepsilon \dot{p} & 0 & 0 \\ \sin \varepsilon \dot{p} & 0 & 0 \end{bmatrix},$$

and hence

$$\underline{\omega}_f = \begin{bmatrix} 0 \\ \sin \varepsilon \dot{p} \\ -\cos \varepsilon \dot{p} \end{bmatrix}^T \quad \underline{\mathbf{f}} = \begin{bmatrix} 0 \\ 0 \\ -\dot{p} \end{bmatrix}^T \quad \underline{\mathbf{e}}. \quad (10)$$

So, the rotation vector  $\underline{\omega}_f$  of the traditional equatorial system  $\underline{\mathbf{f}}$  is constant, and it is directed towards the southern ecliptical pole.

From

$$\omega_3 = -\cos \varepsilon \dot{p} \quad (11)$$

we find, according to (7),

$$q = \cos \varepsilon p. \quad (12)$$

As the precessional angle  $p$  is a linear function of time,  $q$  is a linear function of time, too. According to (2) and (4) in connection with (9), the composed transformation from  $\underline{\mathbf{e}}$  to the alternative equatorial system  $\underline{\mathbf{g}}$  is

$$\underline{\mathbf{g}} = \mathbf{R}_g \underline{\mathbf{e}} \quad (13)$$

with

$$\mathbf{R}_g = \mathbf{R}_3(q) \mathbf{R}_f = \mathbf{R}_3(q) \mathbf{R}_1(-\varepsilon) \mathbf{R}_3(-p) \quad (14)$$

$$= \begin{bmatrix} \sin p \cos \varepsilon \sin q + \cos p \cos q & \cos p \cos \varepsilon \sin q - \sin p \cos q & -\sin \varepsilon \sin q \\ \sin p \cos \varepsilon \cos q - \cos p \sin q & \cos p \cos \varepsilon \cos q + \sin p \sin q & -\sin \varepsilon \cos q \\ \sin p \sin \varepsilon & \cos p \sin \varepsilon & \cos \varepsilon \end{bmatrix}$$

From this we find

$$\dot{\mathbf{R}}_g \mathbf{R}_g^T = \begin{bmatrix} 0 & 0 & -\sin \varepsilon \cos q \dot{p} \\ 0 & 0 & \sin \varepsilon \sin q \dot{p} \\ \sin \varepsilon \cos q \dot{p} & -\sin \varepsilon \sin q \dot{p} & 0 \end{bmatrix},$$

and hence

$$\underline{\omega}_g = \begin{bmatrix} \sin \varepsilon \sin q \dot{p} \\ \sin \varepsilon \cos q \dot{p} \\ 0 \end{bmatrix}^T \quad \underline{\mathbf{g}} = \begin{bmatrix} 0 \\ \sin \varepsilon \dot{p} \\ 0 \end{bmatrix}^T \quad \underline{\mathbf{f}} = \begin{bmatrix} \sin p \sin \varepsilon \cos \varepsilon \dot{p} \\ \cos p \sin \varepsilon \cos \varepsilon \dot{p} \\ -\sin^2 \varepsilon \dot{p} \end{bmatrix}^T \quad \underline{\mathbf{e}}. \quad (15)$$

A comparison of (15) with (10) reveals that the rotation vector  $\underline{\omega}_g$  of the alternative equatorial system  $\underline{\mathbf{g}}$  is quite different from the rotation vector  $\underline{\omega}_f$  of the traditional equatorial system  $\underline{\mathbf{f}}$ . Its magnitude is by the factor  $\sin \varepsilon \approx 0.4$  smaller, and its direction differs by the angle  $90^\circ - \varepsilon$ .

With respect to the system  $\underline{\mathbf{g}}$ , the rotation vector  $\omega_g$  has the constant latitude 0 (as expected) and the linearly decreasing longitude  $90^\circ - q$ . So it is revolving in the equator with the constant angular velocity

$$\dot{q} = \cos \epsilon \dot{p}. \quad (16)$$

The polhodial cone is the equatorial plane with a semi-vertical angle of  $90^\circ$ :

With respect to the ecliptical system  $\underline{\mathbf{e}}$ , the rotation vector  $\omega_g$  has the constant latitude  $-\epsilon$  and the linearly decreasing longitude  $90^\circ - p$ . So it is revolving on a herpolhodial cone which opens towards the southern ecliptical pole with a semi-vertical angle of  $90^\circ - \epsilon$ . As the longitude is decreasing with the constant rate  $\dot{p}$ , the period of revolution is exactly 1 p.y.

Since  $\dot{q}$  is smaller than  $\dot{p}$  by the factor  $\cos \epsilon$ , one revolution of the rotation vector  $\omega_g$  on the equator lasts a little longer than 1 p.y., namely  $1 \text{ p.y.}/\cos \epsilon = 1.09 \text{ p.y.}$  This can easily be visualized by the idea that the polhodial cone (the equator) rolls on the herpolhodial cone. The instantaneous rotation vector  $\omega_g$ , along which the two cones are always tangent to one another, has the same angular velocity on both cones rolling upon each other. But the circumference of the great circle in which the polhodial plane intersects the unit sphere is longer than the circumference of the small circle in which the herpolhodial cone intersects the unit sphere. So after 1 p.y., when the rotation vector has accomplished one revolution on the herpolhodial cone, it has not yet finished one revolution on the polhodial plane.

#### 4. THE FIRST AXIS OF THE EQUATORIAL SYSTEM IN A SIMPLIFIED MODEL

Let us continue to assume the simple model of a regular precession without nutation introduced in the last section.

The first axis  $\underline{\mathbf{f}}_1$  of the traditional equatorial system  $\mathbf{f}$  is the vernal equinox revolving regularly along the ecliptic within 1 p.y. The ecliptical coordinates of the first basis vector  $\underline{\mathbf{g}}_1$  of the alternative equatorial system  $\underline{\mathbf{g}}$  are the entries in the first row of the rotation matrix  $\mathbf{R}_g$  (14):

$$\underline{\mathbf{g}}_1 = \begin{bmatrix} \sin p \cos \epsilon \sin q + \cos p \cos q \\ \cos p \cos \epsilon \sin q - \sin p \cos q \\ -\sin \epsilon \sin q \end{bmatrix}^T \underline{\mathbf{e}}. \quad (17)$$

The derivative with respect to time relative to the system  $\underline{\mathbf{e}}$  is, with consideration of (12),

$$\dot{\underline{\mathbf{g}}}_1 = \begin{bmatrix} -\sin p \sin^2 \epsilon \cos q \dot{p} \\ -\cos p \sin^2 \epsilon \cos q \dot{p} \\ -\sin \epsilon \cos \epsilon \cos q \dot{p} \end{bmatrix}^T \underline{\mathbf{e}} = \begin{bmatrix} 0 \\ 0 \\ -\sin \epsilon \cos q \dot{p} \end{bmatrix}^T \underline{\mathbf{g}}. \quad (18)$$

As expected, the motion of the first axis  $\underline{\mathbf{g}}_1$  relative to the space-fixed ecliptical system  $\underline{\mathbf{e}}$  is always in the direction of  $\underline{\mathbf{g}}_3$ , that is perpendicular to the equator.

The first axis  $\underline{\mathbf{g}}_1$  has with respect to the ecliptical system  $\underline{\mathbf{e}}$  the latitude  $\phi$  and the longitude  $\lambda$ :

$$\tan\varphi = \frac{-\sin\epsilon \sin q}{\sqrt{\cos^2\epsilon \sin^2q + \cos^2q}},$$

$$\tan\lambda = \frac{\cos p \cos\epsilon \sin q - \sin p \cos q}{\sin p \cos\epsilon \sin q + \cos p \cos q} \quad (19)$$

or decomposed as

$$\lambda = q - p - \xi \quad (20)$$

with

$$\tan\xi = \frac{(1-\cos\epsilon) \sin q \cos q}{\cos\epsilon \sin^2q + \cos^2q}. \quad (21)$$

$\varphi$  is a periodical function of time with the amplitude  $\epsilon \approx 23^\circ 26'$  and the period of  $q$ , namely 1 p.y./cos  $\epsilon \approx 1.09$  p.y.  $\lambda$  consists of a linear part  $q-p = -(1-\cos\epsilon)p$ , decreasing by  $29^\circ 71'$  within 1 p.y. or  $360^\circ$  within 12.12 p.y., and a periodical part  $-\xi$ , which has an amplitude smaller than  $2.5^\circ$  and half the period of  $q$ , namely 1 p.y. /  $2 \cos\epsilon \approx 0.545$  p.y.

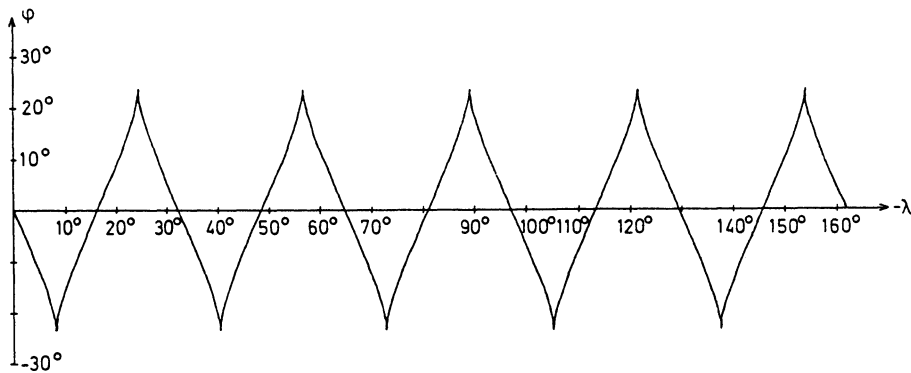


Fig. 1. The path of the so-called "non-rotating origin" on the celestial sphere

Figure 1 visualizes the path of the first axis  $g_1$ , the so-called "non-rotating origin", with respect to the space-fixed ecliptical system on the celestial sphere. At the vertices for  $q = 90^\circ, 270^\circ, 450^\circ, \dots$ , the motion has singularities, where both derivatives  $\dot{\varphi}, \dot{\lambda}$  are equal to zero.

The path is indeed permanently perpendicular to the instantaneous equator. So the "non-rotating origin" has, in a differential term, no motion along the equator. After one Platonic year, the equator has the same orientation in space as before; but the first axis  $g_1$  has not the same direction as before, with respect to the space-fixed ecliptical system. Both directions of  $g_1$  lie in the same equatorial plane, and they include an angle of  $(1-\cos\epsilon) \cdot 360^\circ$ . So, in the long term, the "non-rotating origin" has a secular motion relative to the space-fixed ecliptical system even along the equator. Its angular velocity has the absolute value

$$(1-\cos\epsilon) \cdot 360^\circ/1 \text{ p.y.} = (1-\cos\epsilon) \dot{p} = 29^\circ 71/1 \text{ p.y.} = 360^\circ/12.12 \text{ p.y.}$$

This secular motion, which does not exist in the differential term, corresponds to the secular mean motion of the "non-rotating origin" along the ecliptic, disregarding its periodic oscillation above and below the ecliptic. It is, however, considerably smaller than the differentially defined angular velocity of the equinox along the ecliptic ( $\dot{p}$ ) or its component along the equator (cose  $\dot{p}$ ).

## 5. REAL CONDITIONS

In reality,  $\epsilon$  is not strictly constant,  $p$  is not a strictly linear function of time, and the ecliptical system, to which these two parameters refer, is not perfectly fixed in space. Therefore the real motion of the "non-rotating origin" of the mean equatorial system will slightly deviate from the motion analysed in the last section for an ideally regular precession.

For the nutation components, which are superposed on the precession, the situation is similar. Each nutation component is a small elliptical motion of the pole. If it is nearly circular, the corresponding motion of the "non-rotating origin", due to just this singular component of nutation, is similar to its motion due to regular precession, only in a different scale of time and angular extension.

The superposition of precession and all the nutation components results in a rather complex rotation of the alternative true equatorial system. But nevertheless, the polhodial cone is still the equatorial plane, whereas the herpolhodial cone is no longer a circular cone with a smooth surface. It can rather be imagined as a cone with a grooved surface, in such a way that, when the equator is rolling on it, the axis  $g_3$  of the celestial pole describes on the celestial sphere its undulated curve of precession and nutation around the ecliptical pole.

As the motion of the "non-rotating origin" in the case of regular precession comprises besides its periodic components also a secular component, it will be similar for nearly circular nutation components. So nutation, although being defined as the purely periodic part of the motion of the celestial pole, will still cause a secular component of the rotation of the alternative equatorial system.

## REFERENCES

- Aoki, Shinko (1988): Relation between the celestial reference system and the terrestrial reference system of a rigid earth. *Celestial Mechanics* **42**, 309-353.
- Aoki, Shinko; Kinoshita, Hiroshi (1983): Note on the relation between the equinox and Guinot's non-rotating origin. *Celestial Mechanics* **29**, 335-360.
- Capitaine, N.; Guinot, B.; Souchay, J. (1986): A non-rotating origin on the instantaneous equator: Definition, properties and use. *Celestial Mechanics* **39**, 283-307.
- Guinot, Bernard (1979): Basic problems in the kinematics of the rotation of the earth. In: McCarthy, D.D.; Pilkington, J.D. (eds.): *Time and the Earth's Rotation*, I.A.U., 7-18.
- Yan, H.J.; Groten, E. (1992): Discussion on the origin of right ascension. *Manuscripta geodaetica* **17**, 65-86.

# **ON THE GPS DOUBLE-DIFFERENCE AMBIGUITIES AND THEIR PARTIAL SEARCH SPACES**

**P.J.G. Teunissen**

**Delft Geodetic Computing Centre (LGR)**

**Faculty of Geodetic Engineering**

**Delft University of Technology**

**Thijsseweg 11, 2629 JA Delft**

**The Netherlands**

## **ABSTRACT**

The search for the integer least-squares estimates of the double-difference ambiguities usually suffers from inefficiency when short observational time spans are used based on carrier phase data only. In the present contribution the cause for this inefficiency will be discussed on the basis of the partial search spaces of the double-difference ambiguities. In particular some of the characteristics of the spectrum of conditional variances of the double-difference ambiguities will be stressed. These characteristics are typical for the GPS double-difference ambiguities and they are directly related to the structure of the carrier phase model of observation equations. As a result the least-squares estimators of the GPS double-difference ambiguities are highly correlated and their confidence ellipsoid extremely elongated. It will be shown how the LAMBDA-method, of which the principles were introduced in [8], allows one to overcome the drawbacks that are connected to the use of the double-difference ambiguities. The method is based on an integer approximation of the conditional least-squares transformation and it replaces the original double-difference ambiguities by new ambiguities that show a dramatic decrease in correlation and improvement in precision.

## **1. INTRODUCTION**

The computation of the integer least-squares estimates of the GPS double-difference ambiguities is a non-trivial problem if one aims at numerical efficiency. This is particularly true in case of very short observational time spans and in the absence of precise P-code data. The topic of ambiguity fixing has therefore been a rich source of GPS-research over the last decade or so, see e.g. [1-7]. For different applications, the research resulted in effective search algorithms and provided important insights into the various intricacies of the ambiguity fixing problem. Nevertheless, at present times, it is still expedient to seek ways of improving the efficiency of the various search methods.

This is in particular true for real-time or near real-time applications of GPS. In [8] the author introduced a new method that allows for such a very fast integer least-squares estimation of the ambiguities. The method makes use of an ambiguity transformation that enables one to reformulate the original ambiguity estimation problem as a new problem that is much easier to solve. First numerical results of the method were presented in [9] and [10].

In the present contribution some of the typical characteristics of the GPS double-difference ambiguities that can be seen as the cause for the inefficiency in the search, will be highlighted and discussed. Ofcourse, it is well known since the relative positions of the GPS satellites change only very little with respect to the receiver over short observational time spans, that in such cases the least-squares double-difference ambiguities are generally of a very poor precision. But as it will be shown, it is in particular the shape of the spectrum of conditional variances of the double-difference ambiguities that prohibits one from executing an efficient search for these ambiguities. This shape, which is so typical for GPS, at the same time however allows one through a reparametrization of the ambiguities, to overcome the inefficiency in the search.

## 2. THE DOUBLE-DIFFERENCE AMBIGUITY SEARCH SPACE

As our point of departure we consider the integer least-squares problem

$$\min_a. (\hat{a} - a)^* Q_{\hat{a}}^{-1} (\hat{a} - a) , \quad a \in Z^n , \quad (1)$$

in which  $\hat{a}$  denotes the  $n$ -vector of real-valued least-squares estimates of the double-difference ambiguities and  $Q_{\hat{a}}$  the corresponding variance-covariance matrix. Due to the presence of the integer-constraint  $a \in Z^n$  in (1), there are unfortunately in general no standard techniques available for solving this least-squares problem as they are available for solving ordinary least-squares problems. As a consequence one has to resort to methods that in one way or another make use of a discrete search strategy for finding the integer least-squares solution. The idea is to first restrict the solution space by replacing the space of integers,  $Z^n$ , by a smaller subset that can be enumerated. This smaller subset is referred to as the double-difference ambiguity search space or simply, ambiguity search space. The ambiguity search space is defined as the set of all  $a \in Z^n$  that satisfy the ellipsoidal inequality

$$(\hat{a} - a)^* Q_{\hat{a}}^{-1} (\hat{a} - a) \leq \chi^2 , \quad (2)$$

in which  $\chi^2$  is a suitably chosen positive constant. This ellipsoidal region is centred at  $\hat{a} \in R^n$  and its orientation and elongation are governed by the ambiguity variance-covariance matrix  $Q_{\hat{a}}$ . The size of the search space can be controlled through the choice of the positive constant  $\chi^2$ . It will be assumed that  $\chi^2$  has been chosen such that the search space at least contains the sought for integer least-squares solution.

In order to set up a search strategy that makes use of sharp bounds, the quadratic form of (2) is first written as a sum of squares. In order to do so the *sequential conditional least-*

*squares* principle is applied. It follows [8], if we denote the least-squares estimate of  $a_i$ , conditioned on the first  $(i-1)$ -number of ambiguities as  $\hat{a}_{i|I}$  and its variance as  $\sigma_{\hat{a}_{i|I,i|I}}$ , that the ellipsoidal inequality (2) can also be written as

$$\sum_{i=1}^n (\hat{a}_{i|I} - a_i)^2 / \sigma_{\hat{a}_{i|I,i|I}} \leq \chi^2 . \quad (3)$$

The sum-of-squares structure in this inequality now allows us to come up with a set of  $n$  scalar inequalities that also can be used to characterize the ambiguity search space. This set of inequalities is given by

$$\left\{ \begin{array}{l} (\hat{a}_1 - a_1)^2 \leq \sigma_{\hat{a}_{(1,1)}} \chi^2 \\ (\hat{a}_{2|1} - a_2)^2 \leq \sigma_{\hat{a}_{(2|1,2|1)}} [\chi^2 - (\hat{a}_1 - a_1)^2 / \sigma_{\hat{a}_{(1,1)}}] \\ \vdots \\ (\hat{a}_{n|N} - a_n)^2 \leq \sigma_{\hat{a}_{(n|N,n|N)}} [\chi^2 - \sum_{j=1}^{n-1} (\hat{a}_{j|J} - a_j)^2 / \sigma_{\hat{a}_{(j|J,j|J)}}] . \end{array} \right. \quad (4)$$

Note that this set of inequalities consists of scalar bounds on the *individual* ambiguities. Hence, it can be used to formulate a search strategy for obtaining the sought for integer least-squares solution [8].

### 3. ON PARTIAL SEARCH SPACES AND THEIR NUMBER OF INTEGER CANDIDATES

The complete set of  $n$  scalar inequalities of (4) characterizes the ambiguity search space for all the  $n$ -number of ambiguities. But, each one of the first  $j$ -number of inequalities of (4), with  $j$  varying from 1 up to and including  $n$ , may also be seen as characterizing a search space. In this case however, they can be interpreted as characterizing a partial search space. In order to see this consider the following.

If we relax the constraints of (1) by replacing  $a \in Z^n$  by the constraints  $a_i \in Z$  for  $i = 1, \dots, j$  and  $a \in R$  for  $i = j+1, \dots, n$ , then the integer least-squares problem (1) clearly reduces to

$$\min_{a_{(j)}} (\hat{a}_{(j)} - a_{(j)})^* Q_{\hat{a}_{(j)}}^{-1} (\hat{a}_{(j)} - a_{(j)}) , \quad a_{(j)} \in Z^j , \quad (5)$$

in which  $\hat{a}_{(j)}$  stands for the  $j$ -vector  $\hat{a}_{(j)} = (\hat{a}_1, \hat{a}_2, \dots, \hat{a}_j)^*$  and  $Q_{\hat{a}_{(j)}}$  stands for its variance-covariance matrix. Hence, instead of solving for the integer least-squares estimates of all the ambiguities we are now solving for the integer least-squares estimates of only the first  $j$ -number of ambiguities. It now follows from the sequential conditional least-squares principle that we again can make use of the bounds of (4) to solve for the partial integer least-squares problem (5). That is, the set of bounds consisting of the first  $j$ -number of bounds of (4) characterizes the partial ambiguity search space

$$(\hat{a}_{(j)} - a_{(j)})^* Q_{\hat{a}_{(j)}}^{-1} (\hat{a}_{(j)} - a_{(j)}) \leq \chi^2 . \quad (6)$$

Thus, a search based on these first  $j$ -number of bounds will allow us to solve for the partial integer least-squares problem (5).

Now that we have defined the concept of the partial ambiguity search space, it is for the purpose of this contribution of interest to count the number of integer ambiguity vectors (or number of integer candidates) that are contained in these  $n$ -number of partial ambiguity search spaces. The relevance of knowing how the number of candidates behaves as function of the level  $j$ , with  $j$  running from 1 up to and including  $n$ , is that it gives an indication on how well the search for the integer least-squares solution will perform. For instance, a decreasing function shows that the number of candidates decreases with an increase in level. This implies then, that for a number of integer candidates  $a_{(j)} = (a_1, a_2, \dots, a_j)^*$  of level  $j$ , no integer  $a_{j+1}$  can be found such that  $a_{(j+1)} = (a_{(j)}, a_{j+1})^*$  is an integer candidate of level  $j+1$ . As a result, the search will exhibit the property of halting [8]. And the likelihood that the search halts will be more pronounced the steeper the decrease in function value is.

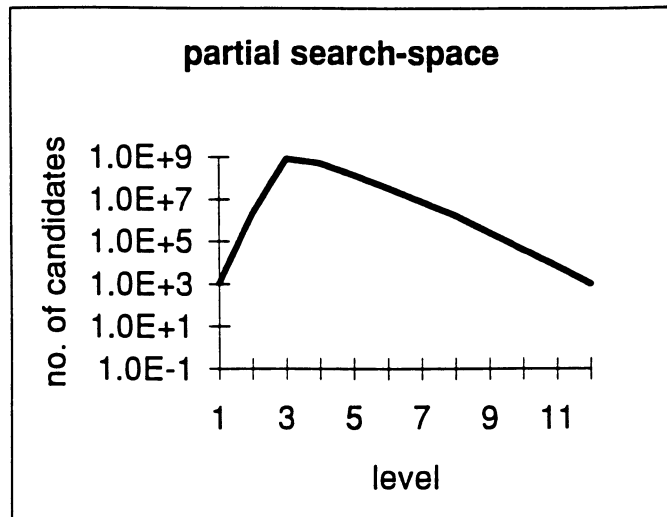


Figure 1: The number of candidates  $a_{(j)} = (a_1, a_2, \dots, a_j)^*$  per partial search space  $j = 1, 2, \dots, 12$ .

Figure 1 shows a representative plot of the number of candidates as function of the level  $j$ , with  $j$  running from 1 up to and including  $n = 12$ . Note the logarithmic vertical scaling. The plot is based on dual-frequency data for a single baseline using carrier-phases only, observing 7 satellites over an observational time span of 1 second, with the a priori standard deviation of the  $L_1$  and  $L_2$  data chosen as  $\sigma = 3\text{mm}$  and the  $\chi^2$  set at the value of 100. We observe that the function increases from level 1, that it reaches its maximum at level 3 and that it from then on strictly decreases. This behaviour of the function is very typical for the GPS double-difference ambiguities. The fact that the function reaches its maximum at level 3 is because only a single three dimensional baseline is solved for. Due to the sharp decrease in function value when going from level 3 to level 4, the search for the integer least-squares solution of the double-difference ambiguities will unfortunately suffer from a high likelihood of halting. As a result, one will experience in practice that

the computational efficiency of finding the integer least-squares estimates of the double-difference ambiguities will be rather poor.

#### 4. WHY IS THE SEARCH FOR THE DOUBLE-DIFFERENCE AMBIGUITIES SO INEFFICIENT?

In the previous section it was shown that in case of GPS the halting problem of the search for the integer least-squares ambiguities is indeed a very serious one. This is particularly true, when the double-difference ambiguity estimates are based on carrier phase data only, collected over a short observational time span. The inefficiency of the search was illustrated by means of the typical behaviour of the function describing the number of integer candidates per partial search space.

Now in order to understand the reason for the inefficiency of the search, we need to understand why the function shown in figure 1 exhibits this typical behaviour. Consider therefore again the scalar inequalities of (4). It will be clear that each one of these inequalities will admit less integer candidates the smaller their respective bounds are. It follows from (4) that these bounds depend on the chosen constant  $\chi^2$ , on the conditional least-squares estimates  $\hat{a}_{i|I}$ , on their conditional variances  $\sigma_{\hat{a}_{i|I}}$  and on the previously chosen integer candidates. Since the general behaviour of the function shown in figure 1 is typical for all GPS single-baseline solutions, this general behaviour cannot be data-driven but has to be model-driven. Hence, the typical behaviour of the function shown in figure 1 has to be due to the characteristics of the conditional variances  $\sigma_{\hat{a}_{i|I}}$ ,  $i = 1, \dots, n$ . And indeed, this can be clearly recognized when one considers the spectrum of the conditional variances of the double-difference ambiguities.

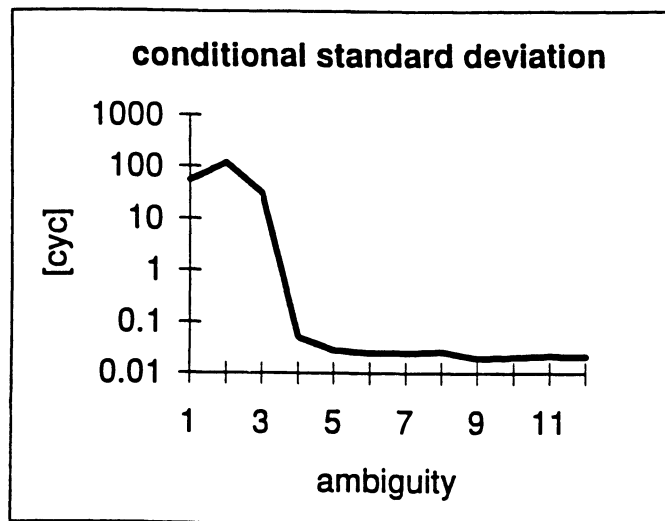


Figure 2: The spectrum of conditional standard deviations of the double-difference ambiguities.

For the same configuration as used in figure 1, figure 2 shows the spectrum of conditional standard deviations of the twelve double-difference ambiguities. The standard deviations

are expressed in cycles. Again note the logarithmic scaling along the vertical axis. The figure clearly shows a tremendous drop in value when passing from the third to the fourth standard deviation. There are three large conditional standard deviations and nine extremely small ones. The first three bounds of (4) will therefore be rather loose, while the remaining bounds will be very tight due to the discontinuity in the spectrum. As a consequence the potential of halting will indeed be significant when one passes from the third bound to the fourth bound.

The discontinuity shown in the above spectrum of conditional standard deviations is typical for the GPS *double-difference* ambiguities. It is intrinsically related to the structure of the GPS carrier phase model of observation equations and the chosen parametrization in terms of the double-difference ambiguities.

## 5. THE LAMBDA-METHOD

In the previous section it was explained why the search for the integer least-squares estimates of the double-difference ambiguities performs so poorly. The method introduced in [8] of the Least-squares AMBiguity Decorrelation Adjustment (LAMBDA), allows for a dramatic improvement in the computational efficiency of estimating the integer ambiguities. In this section the underlying principles of the method are briefly discussed and some numerical results illustrating its performance are presented.

As indicated in the previous section, it is the large discontinuity in the spectrum of conditional variances that prohibits an efficient search for the integer least-squares estimates. The search would therefore improve considerably in efficiency if we would be able to eliminate the discontinuity in the spectrum and lower the values of the large conditional variances. One trivial way of flattening the spectrum would of course be to include more information in the model. This can be reached either through the use of a longer observational time span or through the use of additional GPS observables such as the code observations. It will be shown however, that also without the use of any additional data, a very significant improvement in the spectrum can be reached.

The basic idea that lies at the root of the method is, that integer least-squares estimation of the ambiguities becomes trivial once all the least-squares ambiguities are fully decorrelated. In case of GPS however, the least-squares ambiguities are usually highly correlated and their ambiguity search space is usually extremely elongated. This is particularly true in case of short observational time spans and in the absence of precise *P*-code data. As a consequence the spectrum of conditional standard deviations of the double-difference ambiguities will exhibit a large discontinuity as illustrated in figure 2. The essence of the LAMBDA-method is therefore to aim at a *decorrelation* of the least-squares ambiguities such that the large discontinuity of the spectrum is removed. As a result the original integer least-squares problem is reparametrized such that an equivalent formulation is obtained, but one that is much easier to solve.

In order to explain the underlying principles of the method, we first need to know the

admissible class of ambiguity transformations. This is an important issue, since it must be guaranteed with each and any of the reparametrizations applied, that the integerness of the ambiguities remains preserved. In [11] the class of admissible ambiguity transformations was identified. It was shown that ambiguity transformations are admissible if and only if they are *volume preserving* and have entries which all are *integer*.

With the admissible ambiguity transformations identified, we can concentrate on the property of decorrelation. Consider therefore the two-dimensional ambiguity search space as shown in figure 3. The search space is elongated and its principal axes are not aligned with the grid axes. A full decorrelation of the two ambiguities can be reached if we replace the second ambiguity estimate  $\hat{a}_2$  by the conditional least-squares estimate  $\hat{a}_{2|1}$ . Geometrically this can be realized, if we push the two horizontal tangents of the ellipse from their original level inwards to the  $\pm(\sigma_{\hat{a}_{2|1}, 2})^{\frac{1}{2}}$  level. While doing this, we keep the area of the ellipse constant and also the location of the two vertical tangents constant. The ellipse so obtained is less elongated and it has its principal axes aligned to the grid axes.

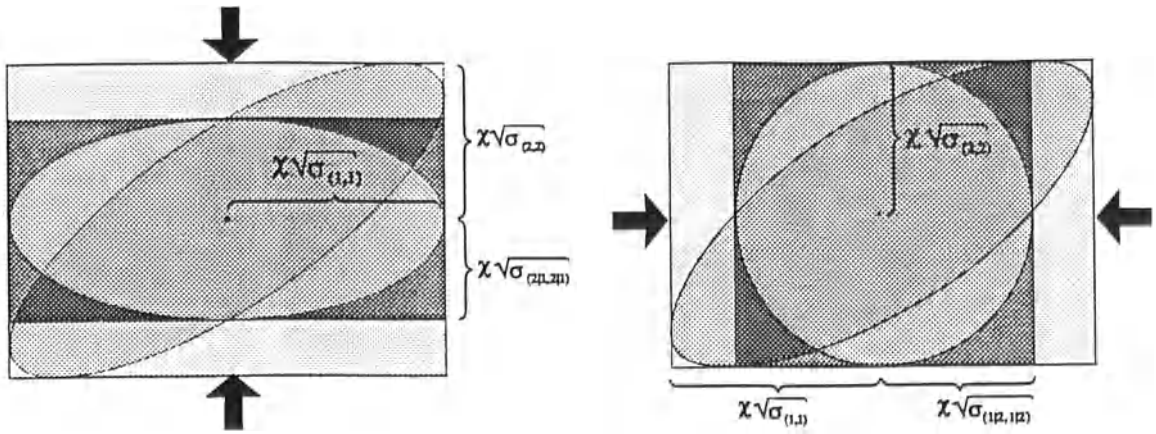


Figure 3: Decorrelating ambiguities by pushing tangents

Although the above transformation guarantees a full decorrelation, it is unfortunately not admissible. The estimate  $\hat{a}_{2|1}$  can namely not be interpreted as an unbiased estimate of an integer. Fortunately we can repair this situation quite easily. The idea is therefore to use, as an admissible transformation, the *integer approximation* of the above fully decorrelating transformation. The price we have to pay for the guarantee of integerness is of course that the full decorrelation property is not retained anymore. But although a full decorrelation is now out of the question, one can proof that a significant decrease in correlation can still be achieved [8]. This is possible through the use of a sequence of the above transformation in which each time the role of the two ambiguities is interchanged.

When the above principles are generalized to the  $n$ -dimensional case, the decorrelation of the least-squares ambiguities results in a transformation from the original ambiguity vector  $\hat{a}$  and its variance-covariance matrix  $Q_a$  to the new ambiguity vector  $\hat{z}$  and its variance-covariance matrix  $Q_z$ . The transformed ambiguities will then be much less correlated and the variance-covariance matrix  $Q_z$  will be much closer to diagonality than the original variance-covariance matrix  $Q_a$ . And as a consequence of the volume-preserving property together with the decrease in correlation, the spectrum of conditional variances of the transformed ambiguities will be largely flattened.

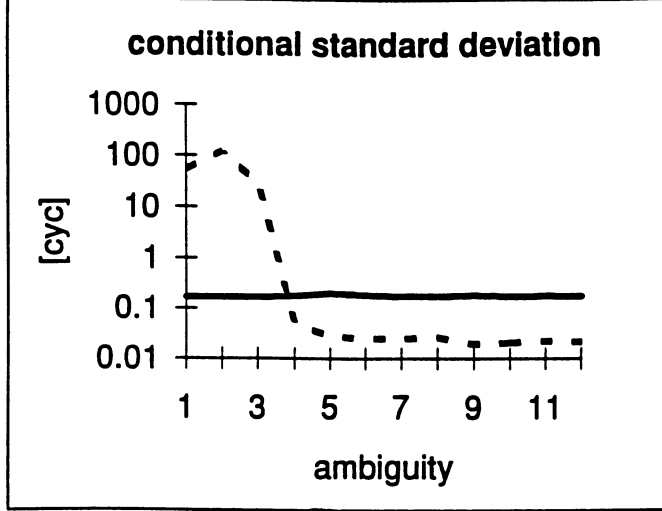


Figure 4: The original and transformed spectrum of conditional standard deviations.

Based on the same data as used before, figure 4 shows both the original and the transformed spectrum of conditional standard deviations. The dramatic improvement in the spectrum is clearly shown. The large discontinuity has been removed and the transformed conditional standard deviations are all of about the same small order.

Now that the original ambiguity vector  $\hat{a}$  has been transformed to the new ambiguity vector  $\hat{z}$ , we can again apply the principle of sequential conditional least-squares estimation and parametrize the ellipsoidal inequality (3) in terms of the transformed ambiguities as

$$\sum_{i=1}^n (\hat{z}_{i|I} - z_i)^2 / \sigma_{\hat{z}_{i|I|I}} \leq \chi^2 . \quad (7)$$

The corresponding set of  $n$  scalar inequalities which is used for the search reads then

$$\left\{ \begin{array}{l} (\hat{z}_1 - z_1)^2 \leq \sigma_{\hat{z}_{(1,1)}} \chi^2 \\ (\hat{z}_{2|1} - z_2)^2 \leq \sigma_{\hat{z}_{(2|1,2|1)}} [\chi^2 - (\hat{z}_1 - z_1)^2 / \sigma_{\hat{z}_{(1,1)}}] \\ \vdots \\ (\hat{z}_{n|N} - z_n)^2 \leq \sigma_{\hat{z}_{(n|N,n|N)}} [\chi^2 - \sum_{j=1}^{n-1} (\hat{z}_{j|J} - z_j)^2 / \sigma_{\hat{z}_{(j|J,J|J)}}] . \end{array} \right. \quad (8)$$

Due to the lowered and flattened spectrum of conditional variances, the search for the integer least-squares solution based on (8) can now be executed in a highly efficient manner. To illustrate how the method has succeeded in reducing the halting problem and thereby improving the efficiency of the search, the number of transformed integer candidates are shown in figure 5 as function of the level  $j$ . The corresponding numerical values are given in table 1.

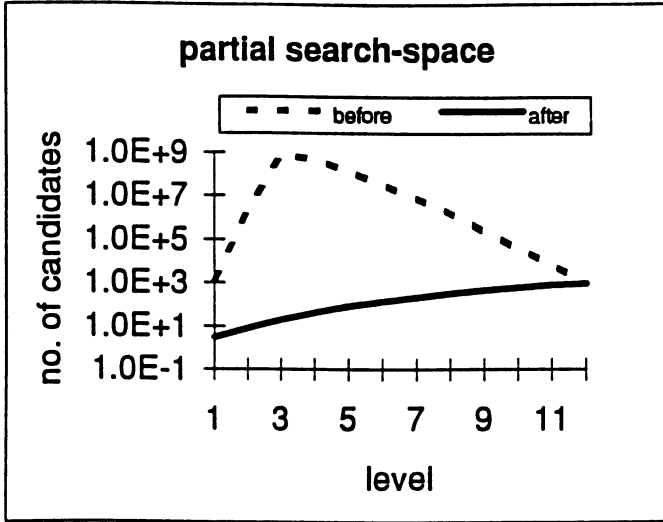


Figure 5: The number of transformed integer candidates  $z_j = (z_1, z_2, \dots, z_j)^*$  per partial search space  $j = 1, 2, \dots, 12$  (solid line).

level $j$	# candidates $a_j$	# candidates $z_j$
1	1082	3
2	1984219	8
3	$8.23 * 10^8$	19
4	$4.77 * 10^8$	43
5	$1.4 * 10^8$	84
6	33376533	146
7	7516578	223
8	1674159	331
9	261118	469
10	40999	616
11	6641	803
12	966	966

Table 1: The number of integer candidates in the original and transformed partial search spaces.

Based on these results, the following observations can be made. First we note that the original and transformed ambiguity search spaces both have an identical number of integer candidates, namely 966. This is as it should be and is a consequence of the volume preserving property of the ambiguity transformation. Secondly, we observe that for the first eleven levels the numbers of integer candidates in the transformed partial search spaces are very much smaller than the corresponding numbers of integer candidates in the original partial search spaces. For instance, at the first level we only have 3 integer candidates for  $z_1$ , as opposed to the 1082 integer candidates for  $a_1$ . This is due to the lowering of the

spectrum of conditional variances which results in a drastic improvement in precision of the ambiguities. And finally we note that the number of transformed integer candidates is strictly increasing as function of the level. This is due to the removal of the discontinuity from the original spectrum of conditional variances. As a result of the above properties, the search for the transformed integer least-squares ambiguities commences with tight bounds and is largely freed from the potential problem of halting, thus assuring that the solution can indeed be found in a highly efficient manner.

## REFERENCES

- [1] Counselman, C.C., S.A. Gourevitch (1981): Miniature Interferometer Terminals for Earth Surveying: Ambiguity and Multipath with Global Positioning System. *IEEE Transactions on Geoscience and Remote Sensing*, Vol. GE-19, No. 4, pp. 244-252.
- [2] Remondi, B. W. (1986): Performing Centimeter-Level Surveys in Seconds with GPS Carrier Phase: Initial Results. *Journal of Navigation*, Volume III, The Institute of Navigation.
- [3] Blewitt, G. (1989): Carrier Phase Ambiguity Resolution for the Global Positioning System Applied to Geodetic Baselines up to 2000 km. *Journal of Geophysical Research*, Vol. 94, No. B8, pp. 10.187-10.203.
- [4] Seeber, G., G. Wübbena (1989): Kinematic Positioning with Carrier Phases and "On the Way" Ambiguity Solution. Proceedings *5th Int. Geod. Symp. on Satellite Positioning*. Las Cruces, New Mexico, March 1989.
- [5] Hatch, R. (1989): Ambiguity Resolution in the Fast Lane. Proceedings *ION GPS-89*, Colorado Springs, CO, 27-29 September, pp. 45-50.
- [6] Frei, E., G. Beutler (1990): Rapid Static Positioning Based on the Fast Ambiguity Resolution Approach FARA: Theory and First Results. *Manuscripta Geodaetica*, Vol. 15, No. 6, 1990.
- [7] Goad, C. (1992): Robust Techniques for Determining GPS Phase Ambiguities. Proceedings *6th Int. Geod. Symp. on Satellite Positioning*. Columbus, Ohio, 17-20 March 1992.
- [8] Teunissen P.J.G. (1993): Least-Squares Estimation of the Integer GPS Ambiguities. In: *LGR-Series No.6*, pp. 59-74. Also as invited lecture, Section IV Theory and Methodology, IAG General Meeting, Beijing, China, August 1993.
- [9] Teunissen P.J.G. (1994): A New Method for Fast Carrier Phase Ambiguity Estimation. Proceedings *IEEE Position Location and Navigation Symposium PLANS'94*. pp. 562-573.
- [10] Jonge de P.J., C.C.J.M. Tiberius (1994): A New GPS Ambiguity Estimation Method based on Integer Least-Squares. Proceedings *DSNS'94*, Vol. II, paper no.73, pp.9.
- [11] Teunissen P.J.G. (1993): *The Invertible GPS Ambiguity Transformations*. Accepted for publication in *Manuscripta Geodaetica*.

# THE EXACT SOLUTION OF THE NONLINEAR EQUATIONS OF THE 7-PARAMETER GLOBAL DATUM TRANSFORMATION $C_7(3)$

E.Graffarend and F.Krumm  
Geodätisches Institut, Universität Stuttgart  
Keplerstraße 11, D-70174 Stuttgart, Germany

## ABSTRACT

In geodetic datum transformation problems two sets of threedimensional Cartesian coordinates, which are both given with respect to two different geodetic datums A and B, are usually related to each other by a system of nonlinear equations of the form  $Y_B = \lambda RY_A + t$  including as unknown parameters – the geodetic datum parameters – a common scale factor  $\lambda$ , an orthonormal matrix  $R$  of three different rotations and a vector  $t$  of three translations. The given cartesian coordinates are collected in the  $3 \times n$  arrays  $Y_A$  and  $Y_B$ . The basic nonlinear model for the subsequent determination of the seven datum parameters is derived using the Schut decomposition (or normalized quaternions) of the orthonormal matrix  $R = (I_3 - S)^{-1}(I_3 + S)$  where  $S$  denotes a skew symmetric matrix the elements of which represent the linearly independent three rotation angles. Given  $R$  we can easily compute  $S$  and vice versa (except for certain pathological cases which are not treated here). After premultiplying our basic nonlinear model equation by  $(I_3 - S)$  we can rearrange all term such that  $Y_B = SY_B + \lambda Y_A + \lambda SY_A + ue_n^T$ ,  $u := (I_3 - S)t$ ,  $e_n := n \times 1$  summation vector. Using the Kronecker-Zehfuss product this matrix equation is mapped into the equivalent vector equation  $\text{vec}Y_B = [(Y_B^T \otimes I_3)K, \text{vec}Y_A, e_n \otimes I_3]w + \lambda(Y_A^T \otimes I_3)Ks$  where  $w := (s^T, \lambda, u^T)^T$  and  $s := (a, b, c)^T = K\text{vec}S$  for a certain matrix K. The part which is still nonlinear in the unknowns is eliminated by premultiplication with a suitable matrix  $D_A$  having as entries the coordinates of system A. Compared to existing methods no linearization and no approximate values for the unknown parameters are needed. The solution of the resulting linear model is tackled by means of a least squares approach. The design matrix of size  $n \times 7$  is of full column rank such that exactly seven points in 3-D space are necessary and sufficient to determine the transformation parameters. However, a sensitivity analysis of the design matrix shows that especially in the case of small rotational parameters a two step procedure should be implemented. Starting from the linear model  $D_A \text{vec}Y_B = D_A[(Y_B^T \otimes I_3)K, \text{vec}Y_A, e_n \otimes I_3]w$  (which has been derived analytically from the nonlinear one) a sufficiently stable estimate for the scale factor can be computed in the first step. Subsequently this estimate is used as input for the nonlinear model in order to derive the remaining unknown parameters. Numerical calculations show that this approach is superior to the ordinary procedure to determine approximate values by iterative methods and a linearization of the nonlinear system equations. Numerical results are presented.

# GPS - Spacetime Observables

Volker S. Schwarze  
Geodätisches Institut, Universität Stuttgart  
Keplerstraße 11, D-70174 Stuttgart, Germany

## ABSTRACT

Modern Satellite Positioning Systems have to be modelled in the framework of General Relativity which affects the high precision orbit computation, the propagation of electromagnetic waves and the behaviour of clocks (oscillators), moving in the gravitational field of the celestial bodies. This has to be combined to obtain observation equations in satellite geodesy.

The starting point is the definition of an observable on a pseudo-riemannian manifold which consists of two steps. The first step is the description of electromagnetic wave propagation within the framework of general relativity. As it has been shown in (*V.S. Schwarze et al. 1993*) the electromagnetic wave follows a geodesic line in the vacuum, refractive and dispersive case with respect to the corresponding space-time metric. For verification see also the reference mentioned above. The second step considers the fact that an observer moving on a pseudo-riemannian manifold refers his measurements to a pseudo-orthonormal (anholonomic) frame, whereas the required quantities refer to a coordinate induced (holonomic) frame which is in general not pseudo-orthogonal. The relations between these two reference frames can be given by applying a proper normalization technique and a sequence of spatial and timelike rotations which will be published elsewhere.

These two steps are combined to derive observation equations for the time-difference and phase-difference technique. The relativistic model can be separated in orbit, propagation and oscillator terms. Numerical investigations have shown that the contribution of the relativistic medium terms (refractive, dispersive) is below the measurement accuracy. Only the kinematical influence of the Earth's rotation and the monopole part of the Earth's gravitational field have to be taken into account for the relativistic propagation model. In most cases it is sufficient to describe the relativistic oscillator model by the monopole and quadrupole part of the Earth's gravitational field. By using a geocentric chart the influence of the other planets can be neglected in the case of satellite positioning whereas they have to be considered for the definition of high accuracy time standards.

## References:

Schwarze, V.S., T. Hartmann, M. Leins and M.H. Soffel (1993): Relativistic Effects in Satellite Positioning, *manuscripta geodaetica*, 18, 306-316

# THE OPTIMAL UNIVERSAL TRANSVERSE MERCATOR PROJECTION

E.Graffarend  
Geodätisches Institut, Universität Stuttgart  
Keplerstraße 11, D-70174 Stuttgart, Germany

## ABSTRACT

The *Korn-Lichtenstein* partial differential equations subject to an integrability condition of *Laplace-Beltrami* type which govern conformal mapping are reviewed. They are completed by an extensive review of deformation measures (Cauchy-Green deformation tensor, Euler-Lagrange deformation tensor, simultaneous diagonalization of a pair of symmetric matrices) extending the *Tissot* deformation portrait. W.r.t. one system of *isometric parameters* which cover a surface (oriented two-dimensional Riemann manifold) the d'Alembert-Euler equations (*Cauchy-Riemann* equations) subject to an integrability condition of *Laplace-Beltrami* type are solved in *real analysis* by various systems of functions (fundamental solution: 2d-polynomial, separation of variables) *plus* a properly chosen boundary value problem, namely the equidistant mapping of one parameter line. Finally the optimal transverse Mercator projection is outlined by solving a boundary value problem of the *d'Alembert-Euler* equations (*Cauchy-Riemann* equations) of a biaxial ellipsoid (ellipsoid of revolution) where a dilatation factor of a central meridian is to be determined. It is proven that for a non-symmetric and a symmetric UTM strip the total areal distortion approaches zero once the total departure from an isometry is minimized. According to the "Geodetic Reference System 1980" for a strip  $[-l_E, +l_E] \times [B_S, B_N] = [-3.5^\circ, +3.5^\circ] \times [80^\circ S, 84^\circ N]$  - the standard UTM strip - an optimal dilatation factor is  $\rho = 0.999,578$ , while for a strip  $[-2^\circ, +2^\circ] \times [80^\circ S, 84^\circ N]$  - the standard *Gauß-Krüger* strip - an optimal dilatation factor is  $\rho = 0.999,864$ . The paper is being published in *manuscripta geodaetica*.

# THE GENERALIZED MOLLWEIDE PROJECTION OF THE BIAXIAL ELLIPSOID

E.Graffarend and A. Heidenreich  
Geodätisches Institut, Universität Stuttgart  
Keplerstraße 11, D-70174 Stuttgart, Germany

## ABSTRACT

The standard Mollweide projection of the sphere  $S_R^2$  which is of type pseudocylindrical - equiareal is generalized to the biaxial ellipsoid  $E_{A,B}^2$ . Within the class of pseudocylindrical mapping equations of  $E_{A,B}^2$  (semimajor axis A, semiminor axis B) it is shown by solving the general eigenvalue problem (Tissot analysis) that only equiareal mappings, no conformal mappings exist. The mapping equations which generalize those from  $S_R^2$  to  $E_{A,B}^2$  lead under the equiareal postulate to a generalized Kepler equation which is solved by Newton iteration, for instance. Two variants of the ellipsoidal Mollweide projection are presented which guarantee that parallel circles (coordinate lines of constant ellipsoidal latitude) are mapped onto straight lines in the plane while meridians (coordinate lines of constant ellipsoidal longitude) are mapped onto ellipses of variable axes. The theorem collects the basic results. Six computer graphics examples illustrate the first pseudocylindrical map projection of  $E_{A,B}^2$  of generalized Mollweide type. The paper is being published in *manuscripta geodaetica*.

# The Hotine oblique Mercator projection of $\mathbb{E}_{a,b}^2$

J. Engels and E. Grafarend

While the standard *Mercator projection / transverse Mercator projection* maps the equator / the transverse metaequator equivalent to the meridian of reference *equidistantly*, the *oblique Mercator projection* aims at a *conformal* mapping of the ellipsoid of revolution constraint to an *equidistant mapping of an oblique metaequator*. *Obliqueness* is determined by the extension of the area to be mapped, e.g. determined by the inclination of satellite orbits: Satellite cameras map the area just under the orbit geometry. Here we derive the *mapping equations* of the *oblique Mercator projection* being characterized to be *conformal* and *equidistant on the oblique metaequator* extending results of *M. Hotine* (1946, 1947). The paper is submitted for publication in *manuscripta geodaetica*.

# THE EMBEDDING OF THE PLUMBLINE MANIFOLD: ORTHOMETRIC HEIGHTS

E. Grafarend and R. J. You

Department of Geodetic Science

Stuttgart University, Keplerstraße 11, D-70174 Stuttgart, Germany

The first question the paper attacks is the question whether the *plumline* (orthogonal trajectory, field line of the terrestrial gravity field) can be interpreted as a *geodesic*: ( $\alpha$ ) If the differential equation  $x' = \text{grad } W / \|\text{grad } W\|$  of a plumline ( $W$  indicates the gravity potential,  $\text{grad } W$  the gravity vector of Euclidean length  $\|\text{grad } W\|$ ) is gauged instead of arc length  $s$  to A. Marussi time  $t$  by means of  $ds/dt = \|\text{grad } W\|$  (A. Marussi, 1985, p132) the differential equation of a plumline reads  $\ddot{x}^\mu - \frac{1}{2} \partial_\mu \|\text{grad } W\|^2 = 0$  as a *geodesic in Newton form*. ( $\mu = 1, 2, 3$ ). ( $\beta$ ) If the differential equation  $x' = \text{grad } W / \|\text{grad } W\|$  of a plumline is gauged instead of arc length  $s$  to M. Hotine time  $\tau$  by means of  $ds/d\tau = \|\text{grad } W\| \cdot f(W)$  for an arbitrary function  $f(W)$  (M. Hotine, 1966, p131-132) the differential equation of a plumline reads  $\ddot{x}^\mu - \frac{1}{2} \partial_\mu (\|\text{grad } W\|^2 \cdot f^2(W)) = 0$  as a *geodesic in Newton form*. ( $\mu = 1, 2, 3$ ). Note the arc length

$$(\alpha) \quad ds_{\text{plumb}}^2 = \|\text{grad } W\|^2 (dx^2 + dy^2 + dz^2)$$

$$(\beta) \quad ds_{\text{plumb}}^2 = \|\text{grad } W\|^2 \cdot f^2(W) (dx^2 + dy^2 + dz^2)$$

of the *plumline manifold*: The threedimensional Riemann manifold is *conformally flat* with a factor of *conformality* ( $\alpha$ )  $\|\text{grad } W\|^2$ , ( $\beta$ )  $\|\text{grad } W\|^2 \cdot f^2(W)$ , respectively. The threedimensional *plumline manifold* which carries the plumline as a geodesic can be embedded in a five dimensional (pseudo-) Euclidean space by means of *Brinkmann's Embedding Theorem*. In case of an isotropic gravity field inside and outside the Earth, e.g

$$w(r) = \begin{cases} \frac{1}{2} \frac{gm}{R} \left( 3 - \frac{r^2}{R^2} \right) & \text{for all } 0 \leq r \leq R \text{ (inside)} \\ \frac{gm}{r} & \text{for all } R \leq r \leq \infty \text{ (outside)} \end{cases}$$

the 3 differential equations of geodesic type are solved with respect to the *Marussi gauge* in spherical coordinates (longitude  $\lambda$ , latitude  $\phi$ , radius  $r$ ) to amount to

$$\lambda = \text{const}, \quad \phi = \text{const}, \quad r = \begin{cases} r_0 \exp(gm(t - t_0)/R^3) & \text{for } R \geq r \\ \sqrt[3]{r_0^3 + 3gm(t - t_0)} & \text{for } R \leq r \end{cases}$$

leading to the *normal orthometric height*

$$r(w_0) - r(w) = \frac{1}{\sqrt{\gamma\gamma_0}} (w_0 - w)$$

for the modulus of normal gravity  $\|grad w_0\| = \gamma_0$  at normal geoid level and  $\|grad w\| = \gamma$  at topocentric level.  $\sqrt{\gamma\gamma_0}$  accounts for *the geometric mean* of gravity and  $w_0 - w$  for voltage against Earth (normal geoid). The paper is submitted for publication in *manuscripta geodaetica*.

## REFERENCES:

- Goenner, H., E. W. Grafarend and R. J. You: Newton mechanics as geodesic flow on Maupertuis' manifold: The local isometric embedding into flat spaces, *manuscripta geodaetica*(1994) in print.
- Hotine, M. : Geodetic applications of conformal transformations, *Bulletin Geodesique* 80(1966) 123-140.
- Marussi, A.: Intrinsic geodesy, Springer Verlag, Berlin 1985.
- Moritz, H.: The Hamiltonian structure of refraction and of the gravity field, *manuscripta geodaetica* (1994) in print.

## **INVERSE CARTOGRAPHIC PROBLEMS**

**B. Marana, F. Sanso'**  
**D.I.I.A.R.**  
**Politecnico di Milano - Italy**

### **Abstract**

This work is an approach to the solution of inverse cartographic problems, arising when we want to compare or to merge two maps, one of known mathematical form and one which is not well known, even if we assume they are of the same kind, for instance both conformal or both equivalent. So we tried to estimate the unknown transformation function starting from the knowledge of a certain number of points on both maps and taking advantage of their known analytical properties. This problem has been solved through the analysis of variational problems and of suitable potentials. To get the interpolation function, we imposed constraints at points known on both maps; these constraints are sharp or just statistically imposed depending on the hypothesis of the absence or presence of measurement errors. The formulas have been tested with numerical examples giving satisfactory results for conformal maps. We are now working to develop a proper software for equivalent maps so as to realize practical simulations.

### **1 Introduction**

Working on practical items connected with territory study and management, can create the problem of comparing maps of well known mathematical form, for example in Italy the official maps provided by the Istituto Geografico Militare, with maps which are not perfectly known though we assume that they satisfy some constraint.

So we tried to solve the problem of matching two maps realized with different representations, while we are supposing they are of the same kind, for instance both conformal or both equivalent.

So we want to get the transformation law between two selected maps assuming to know only some points on both of them. Naturally such a problem is basically undetermined, very much in the same way as in field estimation problems; so we are pushed to apply some regularization criterion, using the type of the maps a suitable mathematical constraint.

Let us explain our solution for the two different kinds of maps we have considered.

## 2 Conformal maps

Conformal maps exploit analytic-function rules because the projection or the transformation functions are analytic.

Moreover, we can work on the complex plane and get all the properties these functions are provided with.

We can think about using two cartesian reference systems:  $(x,y)$  on the known map and  $(r,s)$  on the unknown one.

Let us speak about points  $z = x+iy$  on the first map and points  $t = r+is$  on the second, let also  $t = f(z)$  be the transformation between them where ' $f$ ' is an analytic function.

Moreover we require that the relation  $t_i = f(z_i)$  to be straightly satisfied - assuming the hypothesis of errorless measurements of  $t_i$  and  $z_i$  - for a certain selected number of points on both maps.

Searching an estimate for  $f(z)$ , we have introduced an optimality criterion, requesting that the difference between coordinates of points on both maps is little. This implies that the situation we are actually describing is one in which the unknown part of the transformation (deformation) is small.

Therefore we introduced a function  $g(z) = z - f(z)$  and we chose, agreeing the above mentioned optimality criterion, to minimize a suitable norm just obtained from the function ' $g$ '.

Let us see how we can define this norm using for ' $g$ ' all the analytic function properties.

So let us start including all the selected points in a circular domain with center at the origin; we can then write the Cauchy's formula:

$$g(z) = \frac{1}{2\pi i} \oint \frac{g(\zeta)}{\zeta - z} d\zeta \quad (1)$$

where the integral is extended on the boundary of the circular domain.

One could observe that this operation could wrongfully widen the analyticity domain; moreover we're helped in that by Runge's theorem.

In fact this theorem roughly maintains that an analytic function, holomorphic on a certain domain, can be approximated, but for arbitrary little errors, by an analytic function defined over a wider domain.

Using Cauchy's formula we can, by proper steps, express  $g(z)$  by the integral of only its real part  $u(\vartheta)$  on the boundary of the domain and by a so called 'reproducing kernel'  $Q$ ; apart from an arbitrary imaginary constant.

In fact we have:

$$g(z) = \frac{1}{2\pi} \int_0^{2\pi} u(\vartheta) \frac{\operatorname{Re}^{i\vartheta} + z}{\operatorname{Re}^{i\vartheta} - z} d\vartheta \quad (2)$$

and we define

$$Q(z, \vartheta) = \frac{1}{2\pi} \frac{\operatorname{Re}^{i\vartheta} + z}{\operatorname{Re}^{i\vartheta} - z} \quad (3)$$

We also know that  $u(x,y) = \Re g(z)$  is harmonic in the circle  $C_R$  with its center at the origin and radius  $R$ .

Now we know that - due to the maximum principle - harmonic functions get their maximum value on the boundary of the considered domain, where they are not so regular as in the interior; then we have considered as suitable norm, to be controlled, the simple  $L^2$  norm, i.e.

$$\int_0^{2\pi} u^2(\vartheta) d\vartheta \quad (4)$$

defined using the values of  $u(\vartheta)$  over the circumference of radius  $R$ .

So our problem is now to find a function  $\hat{g}$ , obtained by the minimization of the above defined norm imposing on the same time constraints over the known points on both the selected maps:

$$g(z_i) = w_i = z_i - t_i$$

Thus we can use the Lagrange multipliers method and minimize the functional:

$$\phi(u) = \frac{1}{2} \int_0^{2\pi} u^2(\vartheta) d\vartheta + \Re \left( \sum_{i=1}^N \lambda_i \int_0^{2\pi} u(\vartheta) Q(z_i, \vartheta) d\vartheta \right) \quad (5)$$

To find the estimate which minimizes  $\phi$ , we impose the relation

$$\frac{d}{d\tau} \Phi(u + \tau \delta u) \Big|_{\tau=0} = 0 \quad (6)$$

to be satisfied  $\forall \delta u$

So we get

$$\hat{u}(\vartheta) = - \sum_{i=1}^N \Re(\lambda_i Q_i(\vartheta)) \quad (7)$$

where  $Q_i(\vartheta) = Q(z_i, \vartheta)$

Since  $\lambda_i$  are complex parameters and also the kernel  $Q$  is complex, we can develop this expression as

$$\hat{u}(\vartheta) = - \sum_{i=1}^N \Re(\lambda_i Q_i(\vartheta)) = - \frac{1}{2} \sum_{i=1}^N (\lambda_i Q_i(\vartheta) + \bar{\lambda}_i \bar{Q}_i(\vartheta)) \quad (8)$$

Using this estimate inside (2) we get the normal system:

$$\hat{g}(z) = - \frac{1}{2} \sum_{i=1}^N (\lambda_i \int_0^{2\pi} Q_i(\vartheta) Q(z, \vartheta) d\vartheta + \bar{\lambda}_i \int_0^{2\pi} \bar{Q}_i(\vartheta) Q(z, \vartheta) d\vartheta) \quad (9)$$

In particular, using (9) at points  $z_j$ , we will find:

$$g(z_j) = - \frac{1}{2} \sum_{i=1}^N (\lambda_i \int_0^{2\pi} Q_i(\vartheta) Q_j(\vartheta) d\vartheta + \bar{\lambda}_i \int_0^{2\pi} \bar{Q}_i(\vartheta) Q_j(\vartheta) d\vartheta) \quad (10)$$

So we need to solve a problem with  $N$  complex unknowns and we have obtained a suitable system of  $N$  complex equations to perform the task; the same system can also be written in real form going to real and imaginary parts.

We can notice that the integrals can be solved explicitly by the theory of residuals :

$$\begin{aligned}
\int_0^{2\pi} Q_i(\vartheta) Q_j(\vartheta) d\vartheta &= \frac{1}{4\pi^2} \int_0^{2\pi} \frac{Re^{i\vartheta} + z_i}{Re^{i\vartheta} - z_i} \frac{Re^{i\vartheta} + z_j}{Re^{i\vartheta} - z_j} d\vartheta = \\
&= \frac{1}{4\pi^2 i} \oint \frac{z+z_i}{z-z_i} \frac{z+z_j}{z-z_j} \frac{dz}{z} = \frac{1}{4\pi^2 i} 2\pi i (\text{Res}(0) + \text{Res}(z_i) + \text{Res}(z_j)) = \frac{1}{2\pi}
\end{aligned} \tag{11}$$

$$\begin{aligned}
\int_0^{2\pi} \bar{Q}_i(\vartheta) Q_j(\vartheta) d\vartheta &= \frac{1}{4\pi^2} \int_0^{2\pi} \frac{\bar{Re^{-i\vartheta}} + \bar{z_i}}{\bar{Re^{-i\vartheta}} - \bar{z_i}} \frac{\bar{Re^{i\vartheta}} + \bar{z_j}}{\bar{Re^{i\vartheta}} - \bar{z_j}} d\vartheta = \\
&= \frac{1}{4\pi^2 i} \oint \frac{\bar{R^2 + z_i z_j}}{\bar{R^2 - z_i z_j}} \frac{z+z_i}{z-z_i} \frac{dz}{z} = \frac{1}{4\pi^2 i} 2\pi i (\text{Res}(0) + \text{Res}(z_j)) = \frac{1}{2\pi} (-1 + 2 \frac{\bar{R^2 + z_j z_i}}{\bar{R^2 - z_j z_i}})
\end{aligned} \tag{12}$$

Once we have found the N unknowns  $\lambda_i$  we can put them into the expression (9) and then at last get the sought interpolation function.

### A simple test

Before applying this solution to practical problems, we have performed some simulations. We describe now one of them.

First of all we selected an area centered on a latitude of  $45^\circ$ :  $0.2^\circ$  in latitude (22.2 Km) and  $0.32^\circ$  in longitude (25.2 Km) wide. We analyzed two kinds of conformal maps: one Mercator projection and one Gauss map at a scale 1:25000.

The points selected as reference points of known coordinates on both maps are fourteen. They are positioned on three parallels at  $44.9^\circ$ ,  $45.0^\circ$ ,  $45.1^\circ$  and on five meridians at the same distance from  $0.84^\circ$  to  $1.16^\circ$  (east from the central meridian).

Moreover we selected some other points to check our interpolation theory : they are fortytwo and placed on a grid over six values of latitude, three north and three south from the central value of  $45^\circ$ , far from this one of  $0.025^\circ$ ,  $0.050^\circ$ ,  $0.075^\circ$  and over seven longitude values from  $0.85^\circ$  to  $1.15^\circ$ , one far from the other of  $0.05^\circ$ .

See figure 1.

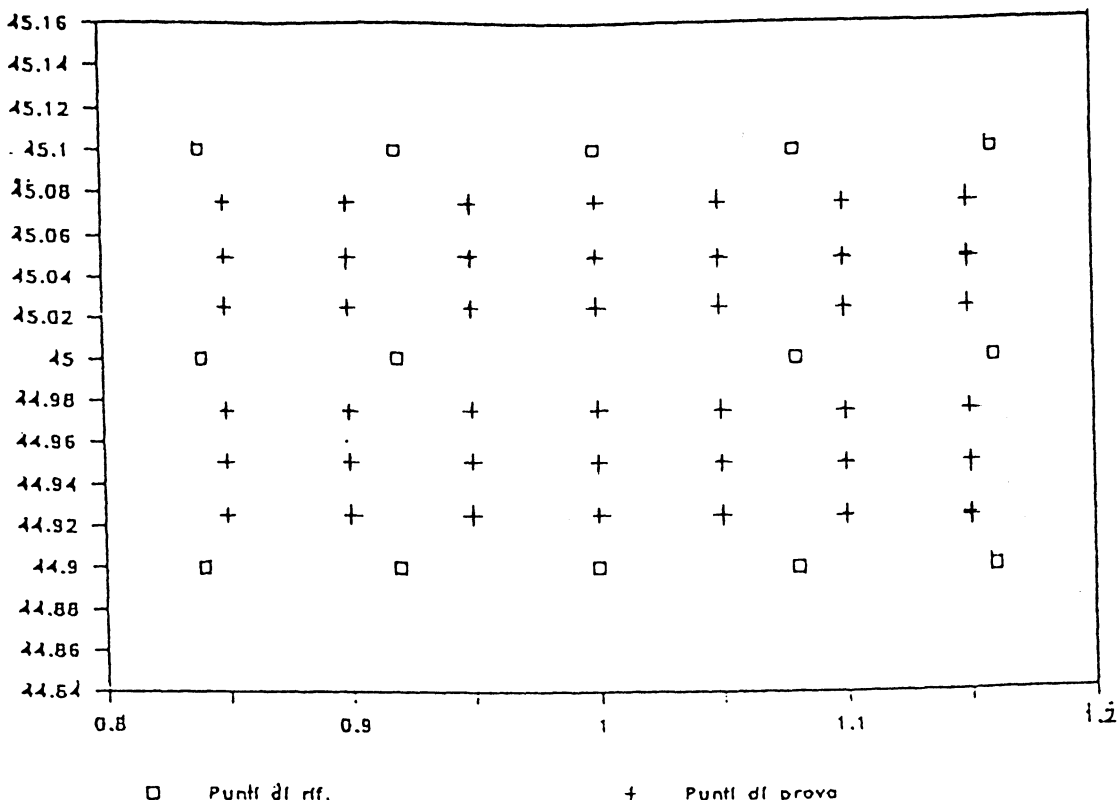


Fig. 1 - Location of reference and computation points in simulation.

The difference between the coordinates of these points, directly calculated by using their projection formulas, have been compared to values obtained using the interpolation approach previously described.

The errors of interpolation in these fortytwo selected points (see table 1) are all well under the error of graphicism ( $10^{-2}$  cm).

It is also possible to analyze our results through contour lines (fig.2) and 3D plot (fig.3) of discrepancies listed in table 1.

The results found from this simulation have been so encouraging that we further applied it to some practical case with satisfactory results (Sanso', Marana, Sacerdote 1993).

		0.85	0.90	0.95	1.00	1.05	1.10	1.15
45.075		$3.23 \times 10^{-3}$	$5.40 \times 10^{-4}$	$1.66 \times 10^{-4}$	$8.03 \times 10^{-5}$	$7.04 \times 10^{-5}$	$3.90 \times 10^{-5}$	$1.42 \times 10^{-3}$
		$1.56 \times 10^{-3}$	$-2.05 \times 10^{-4}$	$-9.43 \times 10^{-5}$	$-6.74 \times 10^{-5}$	$-1.06 \times 10^{-4}$	$-2.82 \times 10^{-4}$	$-8.02 \times 10^{-4}$
45.050		$2.30 \times 10^{-4}$	$2.79 \times 10^{-4}$	$1.39 \times 10^{-4}$	$7.74 \times 10^{-5}$	$3.33 \times 10^{-5}$	$8.81 \times 10^{-5}$	$4.14 \times 10^{-4}$
		$1.75 \times 10^{-3}$	$2.35 \times 10^{-4}$	$-6.13 \times 10^{-6}$	$-4.44 \times 10^{-5}$	$-7.06 \times 10^{-5}$	$-9.36 \times 10^{-5}$	$4.20 \times 10^{-4}$
45.025		$7.03 \times 10^{-4}$	$9.73 \times 10^{-6}$	$7.85 \times 10^{-5}$	$6.17 \times 10^{-5}$	$2.16 \times 10^{-5}$	$3.13 \times 10^{-5}$	$9.93 \times 10^{-5}$
		$1.44 \times 10^{-4}$	$1.65 \times 10^{-4}$	$2.16 \times 10^{-5}$	$-1.80 \times 10^{-5}$	$-3.03 \times 10^{-5}$	$-6.06 \times 10^{-6}$	$1.21 \times 10^{-4}$
44.975		$6.99 \times 10^{-4}$	$8.07 \times 10^{-6}$	$7.83 \times 10^{-5}$	$6.15 \times 10^{-5}$	$2.17 \times 10^{-5}$	$3.10 \times 10^{-5}$	$9.79 \times 10^{-5}$
		$-1.53 \times 10^{-4}$	$-1.64 \times 10^{-4}$	$-2.11 \times 10^{-5}$	$1.79 \times 10^{-5}$	$3.01 \times 10^{-5}$	$6.29 \times 10^{-6}$	$-1.21 \times 10^{-4}$
44.950		$2.05 \times 10^{-4}$	$2.79 \times 10^{-4}$	$1.38 \times 10^{-4}$	$7.67 \times 10^{-5}$	$3.33 \times 10^{-5}$	$8.64 \times 10^{-5}$	$4.15 \times 10^{-4}$
		$-1.74 \times 10^{-3}$	$-2.31 \times 10^{-4}$	$6.76 \times 10^{-6}$	$4.41 \times 10^{-5}$	$6.98 \times 10^{-5}$	$9.32 \times 10^{-5}$	$-4.13 \times 10^{-4}$
44.925		$3.22 \times 10^{-3}$	$5.31 \times 10^{-4}$	$1.64 \times 10^{-4}$	$7.93 \times 10^{-5}$	$6.97 \times 10^{-5}$	$4.00 \times 10^{-5}$	$1.39 \times 10^{-3}$
		$-1.50 \times 10^{-3}$	$2.07 \times 10^{-4}$	$9.38 \times 10^{-5}$	$6.66 \times 10^{-5}$	$1.04 \times 10^{-4}$	$2.77 \times 10^{-4}$	$8.06 \times 10^{-4}$

Table 1. Discrepancies (in cm) between measured and interpolated coordinate differences – Rigid-constraint case (the upper number in each couple is the component along meridian, the lower one along parallel)

Fig.2 – Contour lines of discrepancies listed in Tab.1

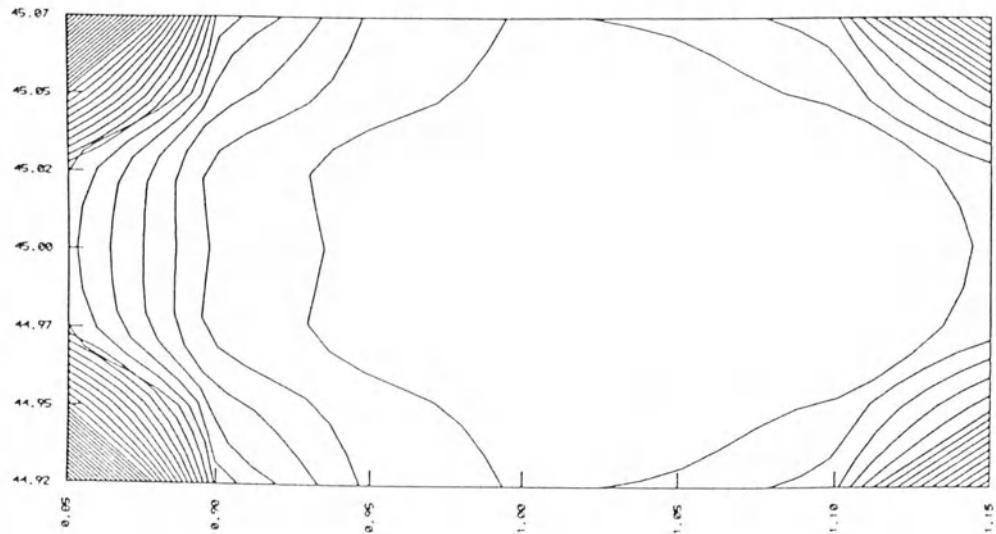
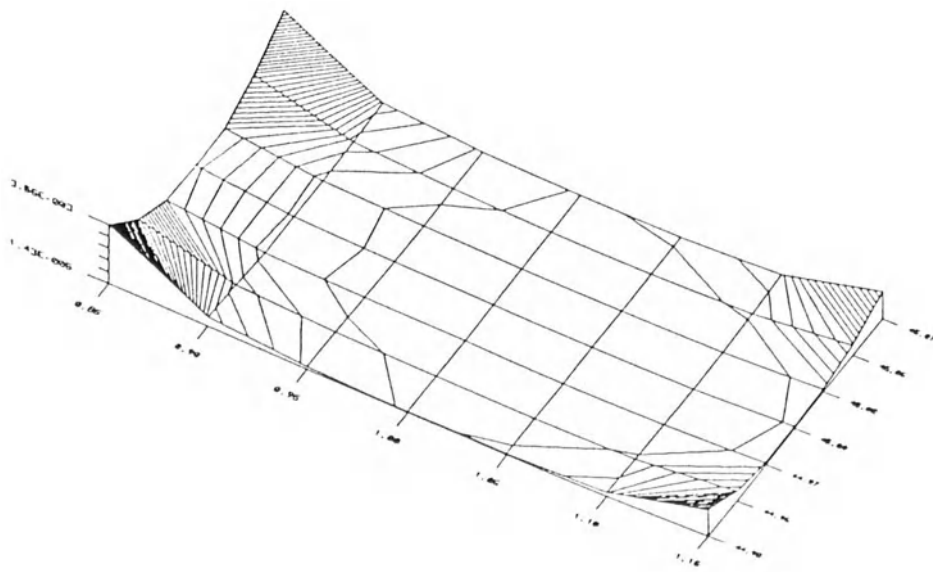


Fig.3 – 3D plot of discrepancies listed in Tab.1



**Remark 1**

A deeper analysis should be done about the choice of the radius R of the selected domain; in fact if R is too great, the reference points are enclosed in a little region near the central part of the map and this produces an ill-conditioned system (9); on the other hand if the radius is too small we can come too close to the boundary with the known points giving rise to numerical problems due to the singularity of the kernel Q.

**Remark 2**

The case when the 'observations' contain a measurement noise as well has been also developed by a suitable hybrid norm principle, based on the minimization of

$$\psi(u) = \frac{1}{2} \int_0^{2\pi} u^2(\vartheta) d\vartheta + \frac{1}{2} \lambda \sum_i |g(z_i) - w_i|^2 \quad (13)$$

**3 Equivalent maps**

Let us define an inverse problem for this kind of maps too. First of all we can think of the same part of ellipsoid being represented on two equivalent maps - with two coordinate systems  $(x,y)$  and  $(\xi,\eta)$  - through the following functions:

$$\underline{r}(P) = [x(P), y(P)] \quad , \quad \underline{\rho}(P) = [\xi(P), \eta(P)] \quad (1)$$

We can also require  $\underline{r}$  and  $\underline{\rho}$  to be linked by the relation  $\underline{r}(\underline{\rho}) = \underline{\rho} + \sigma(\underline{\rho})$  where  $\sigma$  is an infinitesimal quantity of the first order, since the 'large' part of the transformation from  $\underline{\rho}$  to  $\underline{r}$  is assumed to be known.

Componentwise we can write:

$$\begin{cases} x = \xi + u(\xi, \eta) \\ y = \eta + v(\xi, \eta) \end{cases} \quad (2)$$

Let us also assume 'u' and 'v' the unknowns to be infinitesimal and that transformation (2) must be equivalent .

Moreover we know N points  $P_i$  ( $i = 1, \dots, N$ ) on both maps, so we also know

$$U_i = u(P_i) , \quad V_i = v(P_i) \quad (3)$$

Then we want to determine the couple of functions  $(u, v)$  by satisfying the equivalence condition, relation (3) and a regularity criterion for  $(u, v)$ . The equivalence condition can be represented in this way: let us think of a little area  $dS$  on the plane  $(\xi, \eta)$ ; this must be the same of the corresponding  $dS'$  on the plane  $(x, y)$ . Since:

$$\frac{dS'}{dS} = \left| \frac{\partial(x, y)}{\partial(\xi, \eta)} \right| \quad (4)$$

then the equivalence condition is:

$$\frac{\partial(x, y)}{\partial(\xi, \eta)} = \det \begin{pmatrix} 1+u_\xi & u_\eta \\ v_\xi & 1+v_\eta \end{pmatrix} = 1+u_\xi + v_\eta + u_\xi v_\eta - u_\eta v_\xi = 1 \quad (5)$$

and omitting second order terms:

$$u_\xi + v_\eta = 0 \quad (6)$$

This relation can be identically satisfied by using a potential  $\Psi$  and setting:

$$\begin{cases} u = \frac{\partial \Psi}{\partial \eta} \\ v = -\frac{\partial \Psi}{\partial \xi} \end{cases} \quad (7)$$

So our problem is now to find  $\Psi$  satisfying

$$\begin{cases} U_i = \frac{\partial \Psi}{\partial \eta}(P_i) \\ V_i = -\frac{\partial \Psi}{\partial \xi}(P_i) \end{cases} \quad (8)$$

and also some proper regularity conditions.

We can then write our target function assuming that now we are analizing only the case without rigid constraints (remark 2):

$$\Phi(\Psi) = \int_{\Omega} |\nabla \Delta \Psi|^2 d\Omega + \lambda \sum_j (U_j - \Psi_{\eta}(P_j))^2 + \lambda \sum_j (V_j + \Psi_{\xi}(P_j))^2 \quad (9)$$

which is a combination of two terms: a sum of squares of differences arising from the fact that equations (8) are assumed to be verified only with errors, and a Tychonov functional. This functional must be such as to guarantee the regularity of  $\Psi$  and the continuity of (7); this why, using a theorem on the embedding of Sobolev spaces, we have decided to consider functions with square integrable third derivatives

$$\int_{\Omega} |\nabla \Delta \Psi|^2 d\Omega < +\infty \quad (10)$$

which implies continuity of first derivatives.

The parameter  $\lambda$  which appears in (9) is balancing the relative weight of the noise and of the pseudonorm of  $\Psi$ . Now we are going to describe one way to achieve and solve the normal system. By using the variation of (9) we derive the following relations, where  $C$  is the boundary of  $\Omega$ :

$$\Delta^3 \Psi = \lambda \sum_j [\lambda_j \partial_{\eta} \delta(P - P_j) - \mu_j \partial_{\xi} \delta(P - P_j)] \quad (11)$$

and also:

$$\begin{cases} \frac{\partial}{\partial n} \Delta \Psi \Big|_C = 0 \\ \Delta^2 \Psi \Big|_C = 0 \\ \frac{\partial}{\partial n} \Delta^2 \Psi \Big|_C = 0 \end{cases} \quad (12)$$

and where  $\lambda_j$  and  $\mu_j$  are :

$$\lambda_j = U_j - \Psi_{\eta}(P_j) \quad , \quad \mu_j = V_j + \Psi_{\xi}(P_j) \quad (13)$$

Now we need to find a solution for this problem; noticing that

$$G(r) = \frac{1}{64} r^4 (\log r - \frac{3}{2}) \quad (14)$$

is a fundamental solution of  $\Delta^3$  (i.e. it fulfils  $\Delta^3 G = \delta(\xi) \delta(\eta)$ ,  $r^2 = \xi^2 + \eta^2$ ), we can prove that the functions:

$$F = \frac{r^2}{16} (\log r - \frac{5}{4}) \eta \quad , \quad H = \frac{r^2}{16} (\log r - \frac{5}{4}) \xi \quad (15)$$

fulfil the following system

$$\begin{cases} \Delta^3 F(P - P_j) = \delta(\xi - \xi_j) \delta'(\eta - \eta_j) \\ \Delta^3 H(P - P_j) = \delta'(\xi - \xi_j) \delta(\eta - \eta_j) \end{cases} \quad (16)$$

consequently a particular integral of (11) is:

$$\bar{\Psi} = \lambda \sum_j [\lambda_j F(P - P_j) - \mu_j H(P - P_j)] \quad (17)$$

while the general integral will be

$$\Psi = \bar{\Psi} + \chi \quad (18)$$

with  $\chi$  satisfying

$$\begin{cases} \Delta^3 \chi = 0 \\ \frac{\partial}{\partial n} \Delta \chi \Big|_C = -\frac{\partial}{\partial n} \Delta \bar{\Psi} \Big|_C \\ \Delta^2 \chi \Big|_C = -\Delta^2 \bar{\Psi} \Big|_C \\ \frac{\partial}{\partial n} \Delta^2 \chi \Big|_C = -\frac{\partial}{\partial n} \Delta^2 \bar{\Psi} \Big|_C \end{cases} \quad (19)$$

Now let us assume that  $C$  is a circumference; we can then solve problem (19) by separation of the variables in polar coordinates. In particular we introduce two sequences of functions  $f_j$  and  $h_j$  both satisfying boundary value problems of the type (19) with  $F(P - P_j)$  instead of  $\bar{\Psi}$  for  $f_j$  and  $H(P - P_j)$  instead of  $\bar{\Psi}$  for  $h_j$ . Consequently, taking account of (17), we express the solution of (19) in the form

$$\chi = \lambda \sum_j (\lambda_j f_j(P) - \mu_j h_j(P)) \quad (20)$$

and then

$$\Psi = \bar{\Psi} + \chi = \lambda \sum_j \{ \lambda_j [F(P - P_j) + f_j(P)] - \mu_j [H(P - P_j) + h_j(P)] \} \quad (21)$$

The last step consists in the determination of  $\lambda_j$  and  $\mu_j$ ; this can be done through relations (13) :

$$\begin{aligned} \lambda_k &= U_k - \Psi_\eta(P_k) = \\ &= U_k - \lambda \sum_j \{ \lambda_j [F_\eta(P_k - P_j) + f_{j\eta}(P_k)] - \mu_j [H_\eta(P_k - P_j) + h_{j\eta}(P_k)] \} \end{aligned} \quad (22)$$

$$\begin{aligned} \mu_k &= V_k + \Psi_\xi(P_k) = \\ &= V_k - \lambda \sum_j \{ \lambda_j [F_\xi(P_k - P_j) + f_{j\xi}(P_k)] - \mu_k [H_\xi(P_k - P_j) + h_{j\xi}(P_k)] \} \end{aligned}$$

which give rise to a kind of normal system in our unknowns.

Once we know  $\lambda_j$  and  $\mu_j$  from (22), we can put them into (21) and then we are able to find the map deformation through

$$\begin{aligned} u &= \frac{\partial \Psi}{\partial \eta} \\ v &= -\frac{\partial \Psi}{\partial \xi} \end{aligned}$$

### Remark 1

The solution we showed above represents a first solution of our problem. Applying this method, we realize that the most heavy part of it lies in the determination of the two functions  $f_j$  and  $h_j$ . We can overcome this situation if we define implicitly, by means of a

reproducing kernel, the norm of the space where we want to find the best  $\Psi$ . This can be done with a statistical interpretation of the reproducing kernel as a covariance function of the process  $\Psi$ .

### Reproducing kernel approach

Let us assume  $\Psi$  to be a homogeneous and isotropic process with covariance

$$G(|P - Q|) = E\{\Psi(P)\Psi(Q)\} \quad (23)$$

it is easy to understand that

$$\begin{aligned} C_{UU}(|P - Q|) + C_{VV}(|P - Q|) &= E\{\Psi_\eta(P)\Psi_\eta(Q)\} + E\{\Psi_\xi(P)\Psi_\xi(Q)\} = \\ &= -G''(|P - Q|) - \frac{1}{r}G'(|P - Q|) \end{aligned} \quad (24)$$

where

$$G' = \frac{\partial G(r)}{\partial r}$$

$$G'' = \frac{\partial^2 G(r)}{\partial r^2}$$

Since we can estimate  $C_{UU}$  and  $C_{VV}$  by  $U_j$  and  $V_j$ , we can use (24) to estimate  $G$ .

Once we know  $G$  or even a rough estimate of it, we can use  $G$  as a reproducing kernel of the space to which  $\Psi$  belongs so that we can minimize now the following functional:

$$\Phi(\Psi) = \|\Psi\|_G^2 + \lambda \sum_i [(U_i - \partial_{\eta_i} \Psi)^2 + (V_i + \partial_{\xi_i} \Psi)^2] \quad (25)$$

here we use the easy notation

$$\begin{aligned} \partial_{\eta_i} F &= \partial_{\eta(P_i)} F[P_i, P_k, \dots] = \partial_{\eta_i} F[\eta_i, \xi_i, \eta_k, \xi_k, \dots] \\ \partial_{\xi_i} F &= \partial_{\xi(P_i)} F[P_i, P_k, \dots] = \partial_{\xi_i} F[\eta_i, \xi_i, \eta_k, \xi_k, \dots] \end{aligned} \quad (26)$$

to denote partial derivatives of a multipoint function  $F$ .

Then, applying the variational method and the properties of a reproducing kernel, we get

$$\Psi(Q) = \lambda \sum_i [\lambda_i \partial_{\eta_i} G(|P_i - Q|) - \mu_i \partial_{\xi_i} G(|P_i - Q|)] \quad (27)$$

where:  $\partial_{\eta_k} \Psi = U_k - \lambda_k$  ,  $\partial_{\xi_k} \Psi = \mu_k - V_k$

Then from (27) we get the normal system:

$$\begin{cases} U_k - \lambda_k = \lambda \sum_i \lambda_i \partial_{\eta_k} \partial_{\eta_i} G(|P_i - P_k|) - \mu_i \partial_{\eta_k} \partial_{\xi_i} G(|P_i - P_k|) \\ -V_k + \mu_k = \lambda \sum_i \lambda_i \partial_{\xi_k} \partial_{\eta_i} G(|P_i - P_k|) - \mu_i \partial_{\xi_k} \partial_{\xi_i} G(|P_i - P_k|) \end{cases} \quad (28)$$

from which we can obtain  $\lambda_i$  and  $\mu_i$ . Once we know them, we can finally obtain  $\Psi$  from (27) and then also  $(u, v)$ .

As we explained before, this way to find  $(u, v)$  is nearly the same as the one described previously, even if now we can avoid a heavy numerical work; on the other hand, we must pay the price of estimating the covariance function, i.e. the reproducing kernel  $G$ .

## References

Marana B., Vagliansindi B. *Problemi inversi in cartografia*. Degree Thesis, 1991.

Sacerdote F. *Un problema inverso per le rappresentazioni cartografiche conformi*. SIFET bulletin n. 4, 1992.

Sanso' F. *Statistical methods in physical geodesy*. Lecture Notes in Earth Sciences, vol.7, Mathematical and Numerical Techniques in Physical Geodesy, Ed. by Sunkel; Springer-Verlag, Berlin Heidelberg, 1986.

Sanso' F., Marana B., Sacerdote F. *Inverse cartographic problems arising in the transport of information from one cartographic basis to another*. European Conference and exhibition on geographical information systems - Genova, Italia, 29 march - 1 april 1993.

# Accuracy of orbit computation for geodetic satellites: the ordered and the chaotic case

A. Milani

Gruppo di Meccanica Spaziale, Dipartimento di Matematica, via Buonarroti 2,  
56127 Pisa, Italy

**Abstract.** *The choice of the orbital arc length for geodetic satellites depends upon the achievable accuracy in the orbit computation; the errors accumulate in a very different way in the ordered case (polynomial increase with time) and in the chaotic case (exponential accumulation). In the ordered case, the quadratic effects due to average along track non gravitational perturbations are the limiting factor. In the chaotic case, the orbit needs to be split into arcs whose size is controlled by the Lyapounov time. The exponential expansion in some directions in the phase space does not allow to accumulate geodetic information at the same rate; numerical problems arise at the bad conditioning horizon (about 20 Lyapounov times).*

## 1. Statement of the problem: accuracy and arc length

The purpose of satellite geodesy is to solve for geodetic parameters (e.g., station positions and velocities) and geophysical parameters (e.g. geopotential coefficients) by observing the orbit of a satellite. However, the orbit of the satellite has to be solved for in the process. Given the extreme accuracy of the measurements used in contemporary satellite geodesy (e.g. errors of a few centimetres in the station to satellite distance), the determination of the parameters of interest is degraded if the orbit is not computed with accuracy comparable to the observational error. This is not always possible; to achieve the required accuracy we need to split the orbit into *arcs*, each one with supposedly independent initial conditions, with a duration in time controlled by the accuracy requirements.

In this paper I briefly discuss which are the limiting factors in the accuracy of the orbit computation, and therefore the limiting factors to the duration of the orbital arcs to be employed in satellite geodesy. Two very different cases have to be discussed separately: ordered and chaotic orbits; the definition of the two cases are given in section 2. In the ordered case the limiting factor is the quadratic accumulation of errors due to imperfect modelling of non gravitational perturbations, which can be described as averaged along track acceleration (section

3). In the chaotic case the error grows exponentially, and the limiting time span needs to be computed as a multiple of the characteristic time scale of exponential divergence, the *Lyapounov time* (section 4). The exponential growth of the error cannot be exploited to increase sensitivity to the solve for parameters (section 5 and 6).

## 2. Order and chaos

A dynamical system can be either *discrete* or *continuous*. In the discrete case a dynamical system is defined by a map  $\Theta : M \rightarrow M$  which is a diffeomorphism (differentiable, with a differentiable inverse) of some differentiable manifold  $M$ . Then the *orbit* of a point  $P$  is the set of points  $\Theta^n(P)$ , for all integer  $n$ . Discrete dynamical systems are mostly used as convenient model problems; they can also be obtained from the continuous case by observing the state of the system in a discontinuous way, either at discrete times  $t_n = nh$  or whenever a given cross section is crossed (Poincaré map). In the continuous case a dynamical system is defined by a flow  $F^t : M \rightarrow M$  defined for every time  $t$ ; then the *orbit* of  $P$  is  $F^t(P)$  for all real  $t$ . Continuous dynamical systems occur naturally as solutions of ordinary differential equations, such as the ones describing the orbit of some object in outer space.

There are two main classes of behaviour for the orbits of a dynamical system: ordered and chaotic. An *ordered orbit* is such that the error in computing the orbit grows polynomially with time (for a discrete system, we use  $t_n = nh$  with some  $h > 0$  as discrete time) both  $t \rightarrow +\infty$  and for  $t \rightarrow -\infty$ . In most cases encountered in practice, the error grows like  $ct^2 + dt$ , where  $c, d$  are numbers depending upon both the orbit and the method used to compute it. A *chaotic orbit* is such that the error in computing it grows exponentially with time, again both for  $t \rightarrow +\infty$  and for  $t \rightarrow -\infty$ . Thus for a chaotic orbit there is a positive number  $\chi$  such that the principal part of the error is  $c \exp(\chi t)$ , with  $c$  depending upon the computational method. The number  $\chi$  is called the *maximum Lyapounov exponent*, the inverse  $T_L = 1/\chi$ , which has the dimension of a time, is called the *Lyapounov time*; in intuitive terms,  $T_L$  is the time over which the error grows by a factor  $\exp(1)$ .

To understand correctly these definitions we need to stress that the source of the error does not matter. The error in computing an orbit includes the effects of the error in estimating the initial conditions, the error in the physical model (e.g. having neglected some exotic radiation pressure effect, see section 3), the error in the estimation of the model parameters appearing in the differential equations of motion (such as the geopotential coefficients, the moments of inertia of a spinning body, etc.), the error in the computational procedure itself (such as the truncation, or discretisation, error of numerical integration algorithms, and the rounding off error due to the finite mantissa of the representation of real numbers in a digital computer), and possibly others. In the end, all errors, regardless of their source,

behave in the same way. This can be understood by reducing all sources of error to errors in initial conditions: once a portion of the orbit has been computed, say from time  $t_0$  to time  $t_1$ , as a result of the error accumulated so far the follow up integration is an attempt to compute an orbit whose initial conditions at time  $t_1$  are not the same; they indeed correspond to some other orbit, whose initial conditions at  $t_0$  were also different. Thus, if the error due to imperfect estimation of the initial conditions grows exponentially, the same property is shared by the accumulation of any other error from whatever source. This is a loose statement, but a rigorous one could be given and proven.

A *conservative* dynamical system is such that the flow preserves volume (e.g. an hamiltonian flow is conservative by Liouville theorem). In a conservative system, the existence of a positive Lyapounov exponent implies the existence of a negative one; thus exponential growth of the error occurs both for  $t \rightarrow +\infty$  and for  $t \rightarrow -\infty$ . In a hamiltonian system for each positive Lyapounov exponent  $\chi$ , the opposite  $-\chi$  is also a Lyapounov exponent, thus exponential divergence of the errors occurs at the same rate in both directions. The dynamical system describing the motion of an artificial satellite is not hamiltonian, because of non gravitational perturbations, but generally it does differ from a hamiltonian system only by small dissipative perturbations, thus its behaviour does not differ qualitatively from that of a conservative system, at least for the kind of time spans usually encountered in satellite geodesy.

Most conservative dynamical systems contain both ordered and chaotic orbits. There are indeed examples of the contrary, like the integrable (Arnold–Jost) systems for which all the orbits are ordered, and the completely hyperbolic (Anosov) systems for which all orbits are chaotic. However, most systems to be used in practice to model the dynamics of celestial bodies contain some ordered and some chaotic orbits. Actually in the hamiltonian systems obtained by a perturbation of an integrable system the ordered and the chaotic orbits are intermingled together in a very complicated way, forming a “fractal” shape. In practice, the quantity which needs to be measured is the Lyapounov time: if it is much shorter than the time interval over which the orbit needs to be computed, the chaotic behaviour cannot be ignored; if on the contrary the time span of the observations is either shorter or of the same order of the Lyapounov time, the chaotic nature of the orbit can be ignored.

### 3. Outer space is not empty

For small celestial bodies, such as all the artificial satellites and space probes, and for time spans of the order of a few years, the main source of error in the computation of the orbit are the non gravitational perturbations. These arise from the fact that outer space is not perfectly empty; it is on the contrary full of both particles and photons. For the area to mass ratios typical of today’s

artificial satellites, the interaction of both particles and photons with the spacecraft surface results in an exchange of linear momentum which is small, but by no means negligible. Here I would like only to list the most important effects of this class (for a general discussion of this subject, see Milani et al., 1987).

Neutral gas particles impart upon the spacecraft a drag, which is a deceleration proportional to the gas density, to the area to mass ratio, and to the square of the relative velocity. Geodetic satellites are by design launched to orbit at altitudes well above the bulk of the neutral atmosphere, therefore this effect was believed to be small, e.g. for the LAGEOS class of satellites, with altitudes of  $\simeq 6,000 \text{ Km}$ . The magnetosphere of the Earth is filled with charged particles, whose density strongly depends upon the altitude, the latitude, the solar and geomagnetic activity. This density is anyway small, to the point that the resulting drag would appear negligible if the same formula of the neutral particle drag was used. However the interaction of a charged particle with a spacecraft is controlled by a very different physics. First, the charged particles are moving faster than the spacecraft, and the exchange of linear momentum occurs in all directions, with a non zero resultant. Second, the satellite itself picks up some negative charge by impacting preferentially the free electrons (which have an higher average speed than the positive ions), thus it attracts and significantly deflects ions passing by at a distance several times larger than the size of the spacecraft. By these effects, the overall drag-like deceleration is larger by more than an order of magnitude than the effect of the same density of neutral gas (Afonso et al., 1980, 1985)

Direct radiation pressure from the Sun is significant (e.g. it acts upon LAGEOS with an acceleration of  $\simeq 3 \times 10^{-7} \text{ cm/s}^2$ ), but for a simple shape spacecraft the effects on the orbit do not accumulate quadratically with time, because the along track acceleration averages to zero over one orbit. This is not the case if the satellite enters the Earth's shadow (also the Moon's shadow). A more complex model, which takes into account of the refraction of the Earth's atmosphere when the satellite experiences sunset, has been published recently by Vokroulický et al. (1994); penumbra and refraction effects are also significant at a few centimetres level. The most important effect of radiation pressure which can accumulate quadratically with time (up to a few  $10^{-10} \text{ cm/s}^2$  of average along track acceleration) is due to earthshine, that is to the light reflected form the Earth. This so called "albedo" effect averages to zero for diffusive earthshine, but accumulates along track for mirror-like reflections on the surface of the oceans; thus the actual intensity of this effect depends, at any given time, upon the degree of cloud cover over the sea surface which happens to be located in the appropriate position, with respect to the LAGEOS orbit, to send the "spade of the sun" towards the satellite (Anselmo et al., 1983; Barlier et al., 1986; Vokroulický et al., 1993). Therefore no modelling of this effect is possible without accessing actual meteorological data on a global scale; prediction is as impossible as long term metereological prediction is known to be (and this is also due to chaotic effects).

A third group of non gravitational effects on the orbit of geodetic satellites is due to the momentum carried by infrared photons. The spacecraft behaves very much like a small planet; there is a summer emisphere which is hotter than the winter one, and therefore radiates more in the termal infrared; this effect would also average to zero over one orbit, but for the presence of the Earth. Non zero average occurs because the Earth contributes with its infrared emission to the seasonal cycle on the spacecraft (Rubincam 1987), and also introduces strong transients in the termal state whenever the satellite enters the shadow (Barlier et al., 1986; Afonso et al., 1989). These effects depend also upon the orientation of the rotation axis of the satellite, which is poorly known (because it can be changed after the launch by the interactions with the Earth's magnetic field), and are also of the order of  $10^{-10} \text{ cm/s}^2$  of average along track deceleration for LAGEOS.

A few more effects could be mentioned, but the list above should be enough to understand the main point. The non gravitational perturbations on geodetic satellites depend upon so many physically different phenomena, all relevant at the  $10^{-11} - 10^{-10} \text{ cm/s}^2$  level for LAGEOS, which contain so many unknown parameters (the solar activity, the cloud cover, the thermal properties of the satellite, the orientation and velocity of the satellite rotation, etc.), that a priori modelling with the accuracy needed to predict LAGEOS observations at a few *cm* level is impossible. A posteriori parameter fitting is possible (as it always is), but it would be a very serious mistake to think that either a "reflectivity coefficient" or a "spin axis orientation parameter" derived from these fits can be interpreted as a true physical quantity, rather than just a fit coefficient, which cannot have predictive value. Indeed, the first reports on orbit determination for LAGEOS II indicate that predictions based upon the models previously used for LAGEOS I have failed to give the same accuracy.

The conclusion has to be that orbit computations for geodetic satellites over long arcs (e.g. a few months, or more) is not possible at a level of accuracy comparable to the observational accuracy, at least not for LAGEOS-class satellites (however, similar conclusion would apply to GPS-class satellites). The only way out is either to fit a large number of parameters to accomodate unknown perturbations, or to use a short arc approach (as outlined by Usai et al., these proceedings). In the end, the number of parameters used to absorb the unmodellable effects turns out to be very similar in these two approaches, which can both be very effective not only in reducing the observational residuals to level comparable to the expected observational errors, but also in allowing very accurate geodetic and geophysical parameter estimations (Milani et al., 1994).

#### **4. Parameter estimation for chaotic systems**

First I would like to stress that strongly chaotic systems do occur in a geophysical and geodetical context. The satellite of a regularly shaped, nearly spherical body

has a regular orbit (unless it is near the boundary of the planetary sphere of influence, as the retrograde satellites of Jupiter). However, the satellite of an irregularly shaped body may well have a strongly chaotic orbit. Only one case of a natural satellite of an asteroid has been observed (Dattylos, the satellite of asteroid 243 Ida; Chapman 1994); unfortunately in this case the orbit cannot be accurately computed. In the near future a number of artificial satellites will be launched in orbits around small and irregular bodies: e.g. the NASA mission NEAR will orbit around the asteroid 433 Eros, and the ESA mission ROSETTA will orbit around a short periodic comet. The problem will then arise, to determine the gravity field of these small bodies; for this purpose, the spacecraft must orbit very close and for a comparatively long time (taking into account that the orbital periods can be several days). The orbits around such irregularly shaped bodies are chaotic when the distance of the satellite is only a few radii (Chavineau et al., 1993). Thus we need to investigate the behaviour of the parameter estimation process under chaotic dynamical conditions.

As another example, a strongly asymmetric planetary body can be forced by external torques to rotate in a chaotic way. The Saturn's satellite Hyperion, has a very irregular shape (probably as the result of a partial collisional shattering; Farinella et al., 1993). As pointed out by Peale and Wisdom (1984), the rotation state of Hyperion cannot remain close to the usual synchronous rotation state (as it occurs for our Moon), because such a state is dynamically unstable; large scale chaotic wandering of the rotation state must occur for a wide range of values of the (unknown) moments of inertia. Wisdom (1987) pointed out that this could be an opportunity to solve for the principal moments of inertia, by using only the groundbased observations (light curve). He wrote:

*In fact because of the exponential variety of trajectories which exists, the rotation state at the midpoint of the interval covered by the observations, and the principal moments of inertia, are determined with exponential accuracy. Thus the knowledge gained from measurements on a chaotic dynamical system grows exponentially with the timespan covered by the observations.*

I found this a very surprising statement; not only the presence of a chaotic dynamical state would not impair our capability to extract information from the system, but it would result in an accumulation of information growing exponentially with the observation time span, a unique phenomenon in science. Therefore I set out to test this statement, first by performing a simple numerical experiment, then by looking for rigorous results.

## 5. Chaotic determination: a simple test case

The simplest example of a conservative dynamical system which has both chaotic and ordered orbits can be built by means of an area preserving map of a two

dimensional manifold. The *standard map* is such an example: it is defined by

$$\Theta = \begin{cases} X_{n+1} = X_n + Y_n \\ Y_{n+1} = Y_n - \mu \sin(X_{n+1}) \end{cases}$$

The perturbation parameter parameter is  $\mu$ , that is the system has more regular orbit for small  $\mu$ , and more chaotic orbits for large  $\mu$ . I choose some intermediate value of  $\mu$ , e.g.  $\mu = 0.5$ , in such a way that ordered and chaotic orbits are both present, and intermingled in the phase space in a complicated way; figure 1 shows the situation, with e.g. the orbit starting at  $X_0 = 2.8, Y_0 = 0$  ostensibly regular, the orbit with  $X_0 = 2.9, Y_0 = 0$  still regular but locked in an high order resonance, and the orbit with  $X_0 = 3, Y_0 = 0$  strongly chaotic.

The advantage of such a simple example is that the least square parameter estimation process can be performed with an explicit formula: I first compute the linearized map:

$$D\Theta = \begin{pmatrix} 1 & h \\ -\mu \cos(X_{n+1}) & 1 - \mu \cos(X_{n+1}) \end{pmatrix}$$

and from this the linearized state transition matrix, which is the solution of the variational equation (for infinitesimal displacements in the initial conditions):

$$A_n = \frac{\partial(X_n, Y_n)}{\partial(X_0, Y_0)} \quad ; \quad A_{n+1} = D\Theta A_n$$

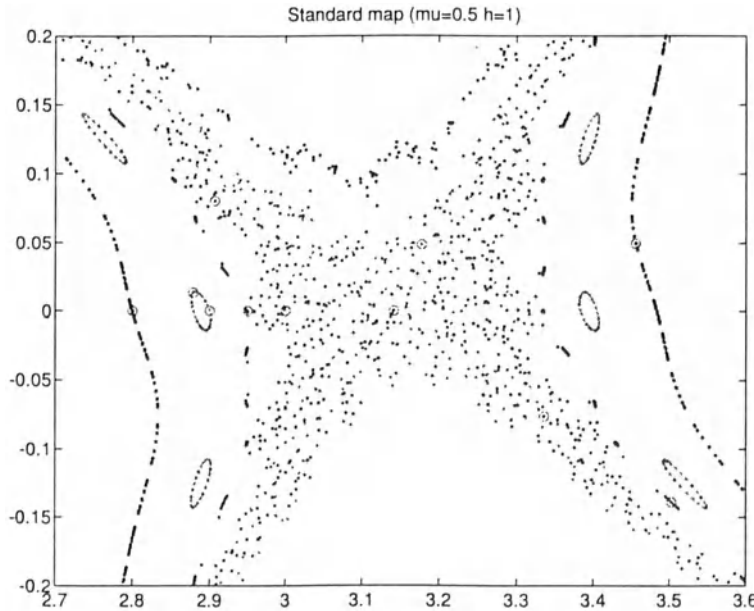


**Figure 1:** Some orbits of the standard map for the perturbation parameter  $\mu = 0.5$ . This is a blow up of the central region around the hyperbolic fixed point, showing the strongly chaotic region and a few regular orbits on both sides.

The variational equation for the derivatives with respect to the model parameter  $\mu$  is:

$$\frac{\partial(X_{n+1}, Y_{n+1})}{\partial\mu} = D\Theta \frac{\partial(X_n, Y_n)}{\partial\mu} + \begin{pmatrix} 0 \\ -\sin(X_{n+1}) \end{pmatrix}$$

Then I set up an observation process, in which both coordinates  $X$  and  $Y$  are observed at each iteration (this is of course the best possible observations): the residuals of these observations are

$$\begin{cases} \xi_{2i-1} = X_i(\mu_0) - X_i(\mu) \\ \xi_{2i} = Y_i(\mu_0) - Y_i(\mu) \end{cases}$$

(where  $\mu_0$  is the “true” value,  $\mu$  the current guess). Then the least squares fit is obtained from the normal equations:

$$G = \sum_{i=1}^n B_i^T B_i \quad ; \quad D = - \sum_{i=1}^n B_i^T \begin{pmatrix} \xi_{2i-1} \\ \xi_{2i} \end{pmatrix}$$

$$B_i = \frac{\partial(\xi_{2i-1}, \xi_{2i})}{\partial(X_0, Y_0, \mu)} = -(A_i | \frac{\partial(X_i, Y_i)}{\partial\mu})$$

The least squares solution for both the solve for parameter  $\mu$  and the initial conditions is then:

$$\begin{pmatrix} \delta X_0 \\ \delta Y_0 \\ \delta \mu \end{pmatrix} = \Gamma D \quad ; \quad \Gamma = G^{-1}$$

with  $\Gamma$  the variance-covariance matrix of the result.

As pointed out correctly by Wisdom, the experiment requires to be performed with the initial condition in the middle of the observations interval, otherwise the initial conditions would be essentially undetermined along the stable manifold of the initial conditions. Therefore the experiment was performed by allowing  $n$  to range from  $-300$  to  $300$ ; for the initial condition at  $X_0 = 3, Y_0 = 0 = 0$  the Lyapounov exponent was about  $0.1$  (thus the experiment was performed for about  $30$  Lyapounov times). The results are summarized in figures 2–4.

In figure 2 we see the exponential divergence of the eigenvalues of the state transition matrix  $A_n$ ; at about  $\pm 20 T_L$ , the maximum and the minimum eigenvalue are so widely apart, that a “bad conditioning horizon” is reached, and the computation of the state transition matrix  $A_n$  becomes numerically impossible ( $\det(A_n)$  should be 1). In figure 3 we see that the derivative of the residuals with respect to the solve for parameters are indeed growing exponentially, and this appears to confirm Wisdom’s argument. However, determination of  $\mu$  is not possible without simultaneous determination of the initial conditions; figure 4 shows the overall results of the full 3-parameter fit. The initial conditions are indeed determined with exponentially growing accuracy: the upper curve shows (in a logarithmic scale) the

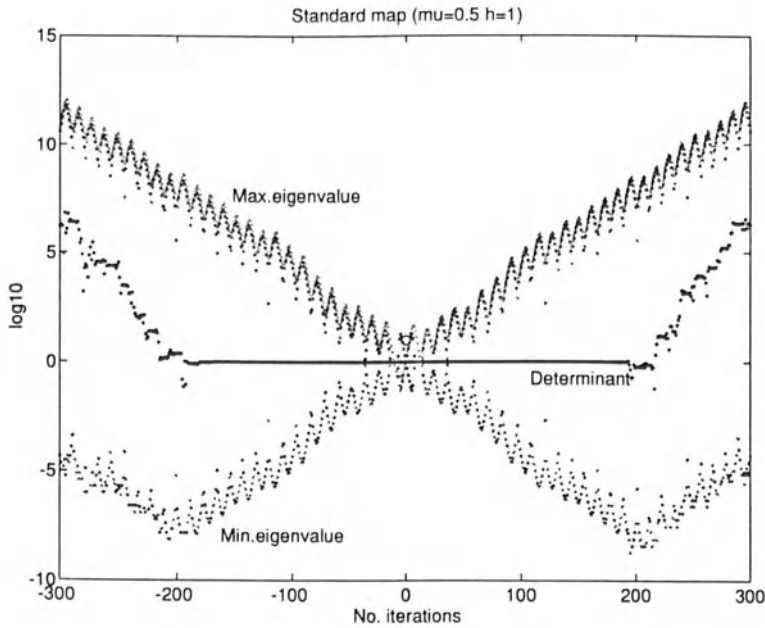


**Figure 2:** The eigenvalues of the state transition matrix  $A_n$  in a semilogarithmic scale, as a function of the iteration number  $n$ . The product of the two eigenvalues would be 1 in exact arithmetic. When the condition number of the matrix becomes larger than the inverse of the machine rounding off error, the computation of the matrix becomes numerically impossible. The initial conditions for this and the following figures was  $X_0 = 3, Y_0 = 0$ , in the strongly chaotic region; the slope of the eigenvalues curves indicates Lyapounov exponents of  $\pm 0.1$  per iteration.

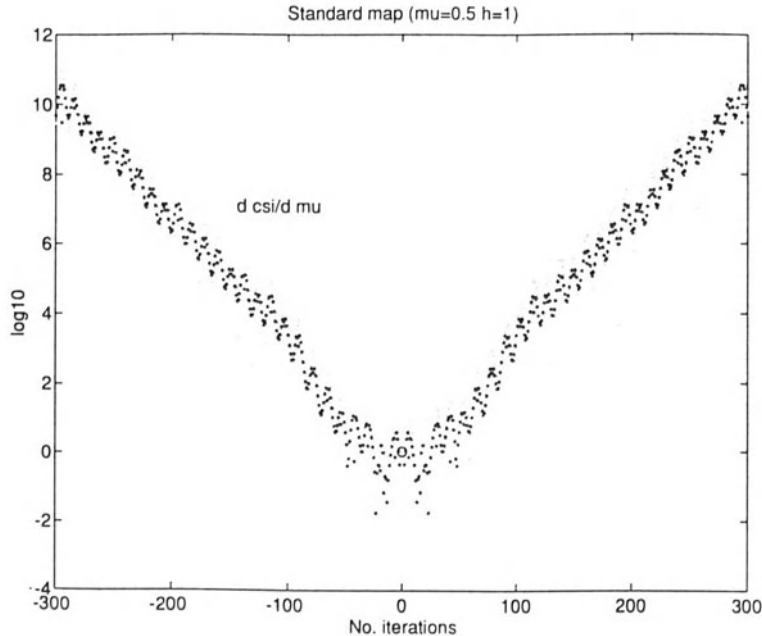


**Figure 3:** The partial derivatives of the observations (and of the residuals) with respect to the perturbation parameter  $\mu$ , as a function of the iteration number, in a semilogarithmic scale: derivatives of the  $X$  coordinate (black points) and of the  $Y$  coordinate (grey points). The exponential increase is slower than the ones of figure 2, but still quite pronounced.

inverse of the RMS accuracy of the initial conditions solution, as a function of  $N$ , for a solution based upon the observation of all the points for  $|n| \leq N$  with RMS error in each observation normalized to 1. However, the formal accuracy of the determination of  $\mu$  does not grow exponentially at all; moreover, beyond the bad conditioning horizon the iterative solution of the nonlinear least squares problem is divergent, and the results are actually much more inaccurate than the formal accuracy would imply.

To understand these experimental results is not difficult, if we compute the condition number of the normal system matrix  $G$  (as a function of  $N$ ). The condition number grows exponentially, until the very computation of the normal system becomes impossible at about  $25 T_L$ . On the contrary the  $2 \times 2$  portion  $C$  of the normal system which refers to the initial conditions only is well conditioned, and this is why the initial conditions can be determined.

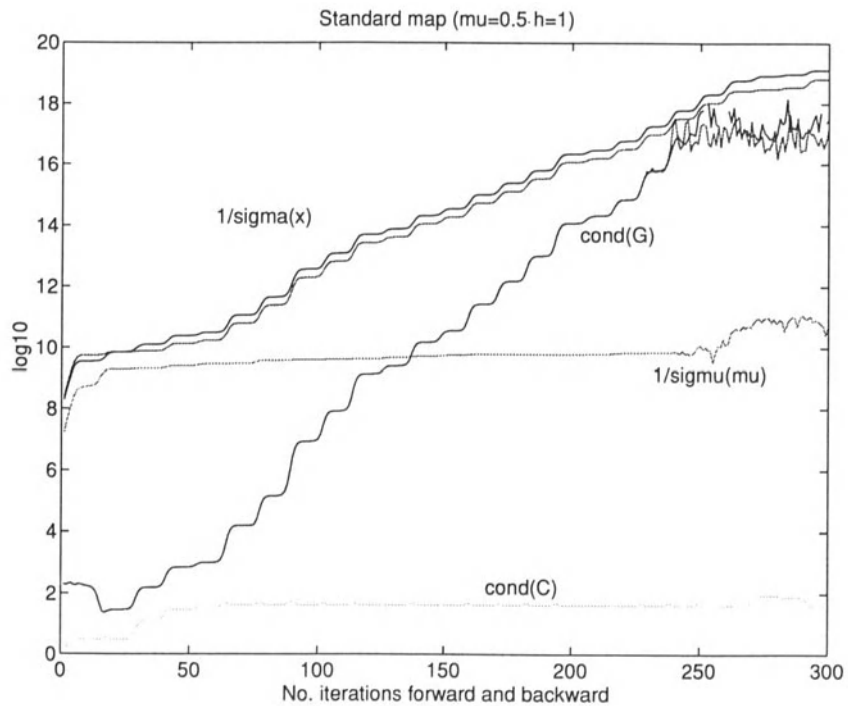


**Figure 4:** The formal accuracy of the solution of the least squares fit for initial conditions and the parameter  $\mu$ . The two upper curves give the logarithm of the inverse of the formal RMS of the two coordinates of the initial condition. The lowest curve gives the same quantity for the parameter  $\mu$ ; it is apparent that no exponential improvement of the accuracy occurs. The two other curves give the logarithm of the condition number of the normal system solving for the three variables  $X_0, Y_0$  and  $\mu$  ('cond( $G$ )'), showing the occurrence of the bad conditioning horizon, and the logarithm of the condition number for the reduced normal system solving for  $X_0, Y_0$  only ('cond( $C$ )'), with no exponential increase of the condition number.

The row of the normal system which refers to  $\mu$  becomes very large, but it also becomes more and more close to be linearly dependent from the other two rows. The residuals are indeed strongly dependent upon  $\mu$ , in an exponentially growing way, but they also are exponentially dependent upon the position of the initial condition upon the unstable manifold, and the two effects are more and more difficult to disentangle.

Of course when a non chaotic initial condition is chosen, the bad conditioning horizon does not occur and the accuracy of the parameter and initial condition solving process improves with time in the usual way. There is no evidence whatsoever for an anomalous behaviour, by which chaos would result in increased knowledge.

It is possible to give a formal proof that the results of this experiment are generally applicable, at least when the initial conditions are on an hyperbolic set with local product structure; this will be discussed in a forthcoming paper.

## 6. Chaotic determination: conclusions

Wisdom's conjecture on parameter estimation in chaotic systems is false. If the only solve-for parameters are the initial conditions, then they can be estimated with accuracy decreasing exponentially with time provided they are at the center of the observed interval, and only until the bad conditioning horizon is reached (at about 20 Lyapounov times for today's processors). However, the convergence domain of the differential corrections is also decreasing in size exponentially with time, and the usual iterative least square fit diverges; may be an adaptive algorithm can be used. On the contrary, simultaneous estimation of initial conditions and of parameters appearing in the dynamical equations does not result into exponentially decreasing accuracy, until the bad conditioning horizon is reached. After that, the formal standard deviation of the dynamical parameter estimation appears to decrease exponentially, but this is only the result of the inaccurate computations resulting from bad conditioning of the state transition matrix, while the differential correction algorithm is divergent for every initial guess. In practice, all the parameter estimations for chaotic dynamical system need to use a multi arc algorithm, with arc length not longer than about 10 Lyapounov times on both sides of the initial conditions, that is limited by the predictability horizon. In realistic systems, since there are always unknown parameters, even the determination of initial conditions is very dangerous and becomes unreliable as soon as the predictability horizon is reached, and even earlier unless the orbit computation is performed with special care and with the use of very accurate and very stable numerical methods. In conclusion, to study the dynamical parameters of a system which has both chaotic and ordered orbits –depending upon the initial conditions– it is wiser to chose an initial condition leading to an ordered solution.

**Acknowledgment.** This research program has been sponsored by the Italian Space Agency (ASI) under research contract ASI-92-RS-120.

## References

- Afonso G., Barlier F., Berger C. and Mignard F. (1980): Effet du freinage atmosphérique et de la traînée électrique sur la trajectoire du satellite LAGEOS, *C. R. Acad. Sci. Paris* **290**, B 445–448
- Afonso G., Barlier F., Berger C., Mignard F. and Walch J.J. (1985): Reassessment of the charge and neutral drag of LAGEOS and its geophysical implications, *J. Geophys. Res.* **90B**, 9381–9398
- Afonso G., Barlier F., Carpino M., Farinella P., Mignard F., Milani A. and Nobili A.M. (1989): Orbital effects of LAGEOS seasons and eclipses, *Annales Geophysicae* **7**, 501–514
- Anselmo L., Farinella P., Milani A. and Nobili A.M. (1983): Effects of the Earth-reflected sunlight on the orbit of LAGEOS satellite, *Astron. Astrophys.* **117**, 3–8
- Barlier F., Carpino M., Farinella P., Mignard F., Milani A. and Nobili A.M. (1986): Non-gravitational perturbations on the semimajor axis of LAGEOS, *Annales Geophysicae* **4**, 193–210
- Chapman, C (1994): in *Asteroids, Comets, Meteors 1993* (A. Milani, M. Di Martino & A. Cellino, eds.), Proc. IAU Symp. 160, pp. 357–366, Kluwer, Dordrecht
- B. Chauvineau, P. Farinella and F. Mignard (1993): Planar orbits about a triaxial body: Application to asteroidal satellites, *Icarus* **105**, 370–384
- P. Farinella, P. Paolicchi, R.G. Strom, J.S. Kargel and V. Zappalà (1990): The fate of Hyperion's fragments, *Icarus* **83**, 186–204
- Milani A., Carpino M., Rossi A., Catastini G. and Usai S. (1994): Local geodesy by satellite laser ranging: a European solution, *Manuscripta Geodaetica*, in press
- Peale, S. and Wisdom, J. (1984): *Bull. Am. Astron. Soc.* **16**, 707
- Rubincam D.P. (1987): LAGEOS orbit decay due to infrared radiation from Earth, *J. Geophys. Res.* **92B**, 1287–1294
- Vokrouhlický D., Farinella P. and Lucchesi D. (1993): Long-periodic albedo perturbations on LAGEOS, *Astron. Astrophys.* **280**, 282–294
- D. Vokrouhlický, P. Farinella and F. Mignard (1994): Solar radiation pressure perturbations for Earth satellites, II: An approximate method to model penumbra transitions and their long-term orbital effects on LAGEOS, *Astronomy and Astrophysics* **285**, 333–343
- Wisdom, J. (1987): *Icarus* **72**, 241

# The short-arc approach to laser ranging analysis

S. Usai<sup>1,2</sup>, M. Carpino<sup>1</sup>, A. Milani<sup>3</sup>, G. Catastini<sup>3</sup>, A. Rossi<sup>4</sup>

<sup>1</sup> Osservatorio Astronomico di Brera, via Brera 28, 20121 Milano, Italy

<sup>2</sup> Telespazio S.p.A., via Tiburtina 965, 00156 Roma, Italy

<sup>3</sup> Gruppo di Meccanica Spaziale, Dipartimento di Matematica, via Buonarroti 2, 56127 Pisa, Italy

<sup>4</sup> CNUCE, CNR, via S.Maria 37, 56126 Pisa, Italy

**Abstract.** *We present the scientific motivations and the first results obtained with an alternative method for the analysis of laser ranging data for the determination of the coordinates of ground stations and their temporal variations. The method makes use of very short orbital arcs (lasting less than two hours for LAGEOS) observed almost simultaneously by at least three stations and is particularly addressed to the solution of “local” networks (of continental or sub-continental scale). The method is very robust with respect to errors in the force model and can attain centimetric accuracy in the determination of station positions even with a simplified dynamics, as it is shown by a test campaign involving six European stations for a duration of seven years. We propose a modification of the method which should reduce its sensitivity to large systematic errors in the observations and improve the stochastic model.*

## 1. The need for a short-arc approach

During the past years (from 1986 up to present) our group has been working on the definition and implementation of an alternative method for the analysis of satellite laser ranging data with the purpose of determining the positions and the relative displacements of the ground stations with the best possible accuracy. The main features of the method are the use of very short orbital arcs (lasting less than one orbital revolution of the satellite) and the application to a *local* network: the ground stations are distributed over a region having a limited extension, so that they can track the satellite almost simultaneously. After a period of initial tests, these concepts led to the development of a software package for orbital analysis (ORBIT10) which is now fully operational.

The idea of using a short arc approach was suggested by the study we were conducting on the non-gravitational perturbations on LAGEOS satellite. When LAGEOS was launched in 1976, its main purpose was to provide “*a very stable bench mark from which geophysicists can accurately determine the geodynamical motions of the Earth*” (Johnson *et al.*, 1976); therefore its orbit, shape and physical properties were designed in such a way as to minimize every source of uncertainty in the force model and to allow the most precise orbital determination. Soon after the launch, however, it became apparent that non-gravitational perturbations on the satellite were significantly larger than expected. In particular, the average value of the along-track acceleration  $T \simeq -3 \cdot 10^{-10} \text{ cm s}^{-2}$  (producing a secular semimajor axis decrease  $\dot{a} \simeq 2T/n \simeq -1 \text{ mm d}^{-1}$ ) was found to be much larger than the drag that could be computed on the basis of any reasonable estimate of the particle density at the height of LAGEOS. Although the precision of laser range measurements was then much lower than today, the secular effect of the perturbation on the satellite longitude  $\lambda$

$$a\ddot{\lambda} \simeq -\frac{3}{2} n\dot{a} \simeq -3T \simeq 7 \text{ cm d}^{-2} \quad (1)$$

(where  $a = 12270 \text{ km}$  is the satellite semimajor axis and  $n = 4.65 \cdot 10^{-4} \text{ rad s}^{-1}$  its mean motion) was large enough to represent a serious limitation on the accuracy achievable over orbital arcs lasting more than few orbital revolutions.

The “anomalous” orbital decay was the subject of investigation by several authors, and different physical mechanisms were invoked to explain it: charged particle drag (Afonso *et al.*, 1980, 1985; Rubincam, 1982), Earth reflected radiation pressure (Anselmo *et al.*, 1983; Vokrouhlický *et al.*, 1993a and 1994b), anisotropic thermal emission from the satellite surface (*thermal thrust*) produced by direct solar heating (Barlier *et al.*, 1986, Afonso *et al.*, 1989) or by infrared emission from the Earth (Rubincam, 1987), eclipses and penumbra effects (Vokrouhlický *et al.*, 1993b and 1994a). Although these studies were successful in pointing out the physical causes of the perturbation and in explaining its order of magnitude and (sometimes) its main spectral characteristics, they were not able to construct a quantitative model of the force acting on the satellite precise enough to be useful for the sake of orbital prediction. This is not surprising, since the involved mechanisms depend upon properties of the space environment (plasma density and temperature), of the Earth (geographical distributions of albedo and reflectivity, including their meteorological variations; atmospheric refraction and absorption) and of the satellite (thermal and optical model, spin state) which are poorly known. Therefore orbital solutions for LAGEOS routinely included among the *solve-for* parameters monthly or fortnightly average values of the along-track acceleration with the purpose of absorbing the combined effect of unmodelled perturbations of non-gravitational origin and reducing the fit residuals. A similar reduction of the orbital error could be obtained also by reducing the duration of orbital arcs; in this case the rôle of introducing in the solution additional degrees of freedom is

played by independent sets of initial conditions rather than by the time variations of an unconstrained along-track acceleration.

We think that, in this respect, the situation has not changed substantially over the last decade, although the comprehension of the physical mechanisms at work has made progress. Even when more refined models of non-gravitational effects are adopted, the parameters on which they depend usually are not constrained by independent observations but are solved for in the orbital fit, absorbing also the contributions from different physical mechanisms which are not included in the model but have similar spectral behaviour<sup>(1)</sup>. Therefore the determined quantities have not a definite physical meaning, although they are useful in reducing the residual rms error.

How short should be a *short arc*? We like to take as a “natural” measure of the arc length the relative importance of orbital with respect to instrumental errors, and therefore define as “short” a time interval for which the uncertainty in the dynamical model is negligible with respect to the accuracy of the measurements. Equation (1) shows that, if an accuracy of the order of one centimeter in the satellite position is required without including in the force model “exotic” non-gravitational effects, the maximum integration timespan is inferior to one day (of course an accurate computation of direct solar radiation pressure, producing an acceleration on LAGEOS of  $3.2 \cdot 10^{-7} \text{ cm s}^{-2}$ , is required anyway). Moreover, if the arc length is much shorter than one day, also the accuracy required in the definition of the terrestrial reference system is much decreased and the Earth orientation parameters can be assumed to be known with sufficient precision and do not need to be solved for. These considerations naturally push towards the minimum-scale approach of a *local geodetic network*: coordinates are determined only for stations belonging to a limited area of the Earth surface, distributed in such a way that they can observe the satellite almost simultaneously (for LAGEOS, such a network can have continental extent, due to the height of the satellite). The orbit of the satellite is determined only for the duration of the transit over the network, assigning independent initial conditions to each transit (namely, each transit corresponds to a separate *orbital arc*); the initial conditions of the satellite are determined using only the observations collected by the stations of the local network. Throughout the rest of the paper, we shall use the term “short arc” according to this restricted meaning: the duration of a short arc is therefore below half orbital period of the satellite (for LAGEOS, it is typically of the order of one or two hours).

---

<sup>(1)</sup> all the physical effects listed above are sensitive to the position of the Sun with respect to the orbit of the satellite and therefore have significant spectral content at frequencies resulting from linear combinations of the derivatives of the longitude of the Sun  $\lambda_{\odot}$  and of the ascending node of LAGEOS’ orbit  $\Omega$ , in particular at  $\dot{\lambda}_{\odot} - \dot{\Omega} = 2\pi/560 \text{ d}$  and  $2(\dot{\lambda}_{\odot} - \dot{\Omega}) = 2\pi/280 \text{ d}$

Another kind of considerations that led us towards a short arc approach was the concern for the correctness of the stochastic model of measurement errors and of the procedure adopted for the formation of normal points. The range residuals after a least-squares adjustment of the orbit (either for a short- or a long-arc technique) contain both a white noise component, which is mostly representative of accidental instrumental errors, and a correlated signal, produced by time variations in the calibration constants, changes in propagation delay and orbital errors (Betti *et al.*, 1987). The correlated part of the error is by no means small, but it is usually neglected in orbital solutions based on a long-arc approach, with the consequence that the formal covariance matrix supplied by the least-squares fit for the adjusted parameters (including station coordinates) grossly underestimates real error bars and often is not even representative of their order of magnitude. In fact, to handle correctly such correlations would mean to compute the inverse of a  $N \times N$  covariance matrix, where  $N$  is the number of range measurements included in the fit and therefore (even using normal points) is of the order of several thousands per month. On the contrary, when the arc duration is decreased, the number  $N$  of observations per arc is reduced so that the use of a full  $N \times N$  weight matrix becomes feasible. For this reason, ORBIT10 included from the beginning the capability of handling correlated observations; this required the development of dedicated software for the compression of raw data, since normal points distributed by NASA do not contain any information on correlations.

## 2. Peculiarities of the short-arc approach

From a mathematical point of view, a short-arc orbital solution is not different from a long-arc one: in both cases, the position of the satellite is integrated numerically for the duration of the selected orbital arc, together with its partial derivatives with respect to the parameters to be adjusted; a linearized system of normal equations is set up and its solution is computed; then the procedure is iterated until convergence is reached. From a practical point of view, however, there are particular problems which present very different aspects in either cases, and require different solutions.

A problem that needs to be reconsidered when the length of the orbital arc is reduced to less than one orbital revolution of the satellite is the singling out of *approximate rank deficiencies*, namely of parameters (or combinations thereof) that cannot be solved for in the least squares fit, because they would produce an almost singular normal matrix and make the solution unstable (for a more precise definition of approximate rank deficiency, see Milani and Melchioni, 1989). The list of these singular cases includes all the dynamical parameters which do not affect in a significant way the orbit of the satellite on the short arc: this is of course the consequence of the insensitivity of the method to the details of the dynamical model. In general, the short-arc approach is not suitable for studying the dynamics of the

satellite; presently, we do not need to determine any of the parameters appearing in the force model, which are all kept fixed at some “standard” value (derived from preliminary medium-arc solutions or from published sources). An extensive series of *robustness tests* has been performed in order to guarantee that this procedure is appropriate, namely that the uncertainties affecting the parameters do not introduce any significant error in the solution (Milani *et al.*, 1994).

A more delicate point is to understand which are the minimum requirements allowing the determination of the initial conditions of the satellite for each arc. Numerical simulations (Milani and Melchioni, 1989) show that, in general, it is necessary that the satellite be observed by at least three stations: observations collected during transits of the satellite which are observed only by one or two stations must be discarded. As a consequence, the short-arc approach can be applied more easily to regions where the density of laser ranging stations is high, like northern America or Europe, and to stations with a high number of observed passes. As an example, we have not been able to include in our European solution any mobile station, because for them the number of passes observed in coincidence with other stations is too low.

There is also another class of *geometric* degeneracies, which lead to a singular normal matrix if the coordinates of all the stations are determined simultaneously. In the long-arc approach, this is a consequence of the ambiguity in the definition of the terrestrial reference system, which can be rotated in an arbitrary way on the Earth surface; such ambiguity therefore corresponds to an arbitrary choice of three rotation parameters (e.g., Euler angles) and is usually resolved by constraining three station coordinates (latitude and longitude of one station, plus only the longitude of another station). In the short-arc approach, however, the ambiguity involves four degrees of freedom, and can be suitably resolved by constraining: a) the position of the center of the local network on the Earth surface (2 degrees of freedom); b) the distance of the center of the local network from the center of the Earth (one degree of freedom); c) the rotation of the local network around the axis connecting the center of the Earth with the center of the network itself (one degree of freedom). While a) and c) correspond to the classical constraint on the orientation of the terrestrial frame, b) is peculiar to the short-arc solution, which is highly insensitive to a change in the average height of all the stations, which can be almost compensated by a corresponding change in the height of the satellite (for a more extensive treatment of symmetries and rank deficiencies in a short-arc solution, see Milani and Melchioni, 1989).

### **3. Results, problems and perspectives**

The concepts explained in the previous sections have been applied to a test campaign: seven years of data from LAGEOS satellite have been used to obtain the coordinates of six fixed laser ranging stations distributed over Europe. While the details of the solution are published elsewhere (Milani *et al.*, 1994), we want to stress here the principal results and problems.

The European campaign has shown that the short-arc method is capable of attaining centimetric precision in the determination of the relative position of ground stations. The residual rms error ranges from less than 1 cm for stations equipped with most recent laser devices to more than 7 cm for older hardware. The accuracy of the determined station coordinates has been estimated by dividing the available orbital arcs into two non-intersecting lists, computing an independent solution for each of them and comparing the results; since systematic errors affect in a different way the two solutions (due to different arc geometries and dates), their comparison gives information not only about random errors but also about observational biases and calibration problems, and therefore can give a more realistic estimate of the total error than the formal covariance matrix of the fit. The errors in the baseline rates estimated with this procedure range from 2 to 5 mm  $y^{-1}$ ; within these error bars, the station velocities agree with solutions published by other authors (Smith *et al.*, 1990; Zerbini, 1993).

One of the main characteristics of the short-arc method is its marked tendency to absorb systematic effects into the initial conditions of each arc, without affecting too much the fit residuals. In the case of orbital errors, this mechanism improves the determination of the relative position of the satellite with respect to the ranging stations, decreasing the sensitivity of the solution with respect to errors in the dynamical model. On the contrary, systematic effects on the observed range (errors in calibration, tropospheric delay etc.) cannot be eliminated by a simple readjustment of the satellite position, and produce also a distortion of the station coordinates; we think that this is the principal source of error affecting our present short-arc solutions. Also in this case, however, a substantial fraction of the error is absorbed by a change of the initial conditions: as a consequence, a reliable description of the observation errors cannot be extracted in a simple way from a statistical analysis of fit residuals. This situation prevents further improvement of the fit accuracy, especially in two fields:

- 1) *passage editing*: we refer here to identification and removal of sets of observations having particularly large errors. On a single-observation basis, this task is performed in ORBIT10 at the stage of normal point production, by comparing each raw range measurement with nearby observations. In this way obviously it is not possible to detect systematic errors affecting whole passages,

which can be produced, for instance, by particular meteorological situations or failures in the calibration procedure;

- 2) *stochastic model of observation errors*: a realistic covariance matrix for observation errors should include estimates of three separate components: a) accidental (uncorrelated) instrumental error; b) orbital error; c) observation biases. In ORBIT10, the first component is estimated at the compression stage: raw range measurements are interpolated with a polynomial of sufficiently high degree, leaving a residual that generally is pure white noise; normal points are defined by the value of the interpolating polynomial at selected points, where the density of raw measurements is particularly high; the covariance matrix of the normal points is then computed with the usual law of linear covariance propagation. In a short-arc approach, the second component is negligible, as discussed before. The third component, although important, cannot be computed from the orbital residuals: as an example, the autocovariance function of the residuals of a short-arc fit grossly underestimate the real correlation over timescales longer than half an hour.

In order to overcome these difficulties, we are presently exploring the possibility of using also information coming from *medium-arc* solutions (spanning few days) and therefore attempting a *mixed* approach, in which medium arcs are used for the recognition of outliers and the estimation of covariance matrix, but the final determination of station coordinates is performed with a short-arc technique. The proposed approach should therefore consist of the following steps:

- 1) preparation of normal points for the medium arc solution. The network used should include 20 or 30 high-precision stations with a good worldwide distribution; at this stage all the passes observed by the selected stations can be used, without the constraint of almost-simultaneity. The procedure for the production of normal points is the polynomial interpolation described in Milani *et al.* (1994); as an alternative, also normal points distributed by NASA-DIS could be used;
- 2) orbit adjustment, using arcs of duration of 3 to 15 days; the purpose of this step is only to obtain a good reference orbit (RMS smaller than 10 cm); therefore station coordinates and Earth orientation parameters need to be solved for only if it is required in order to attain a better solution;
- 3) selection of passes to be included in the short-arc solution (as explained above) and generation of *pseudo-observations* (obtained from the medium-arc solution) for each of them, namely values of the station-satellite range computed from the reference orbit at a constant periodicity (e.g., every 60 s);
- 4) production of the normal points to be used in the short-arc solution, according to a modified algorithm which uses medium-arc pseudo-observations for the first stage of outlier rejection (raw data points which are too far away from the polynomial passing through pseudo-observations are discarded);

- 5) short-arc solution, solving for the initial conditions of satellite arcs and the coordinates of the stations belonging to the local network (in our example, the six European stations).

In a similar way, it would be possible to obtain from the residuals of medium-arc solution some information on the statistics of systematic errors, to be included in the covariance matrix of normal points to be used in the short-arc solution; however, this is a much more delicate point, since orbital errors in the two cases are very different.

**Acknowledgment.** This research program has been sponsored by the Italian Space Agency (ASI) under research contract ASI-293-GGS.

## References

- Afonso G., Barlier F., Berger C. and Mignard F. (1980): Effet du freinage atmosphérique et de la traînée électrique sur la trajectoire du satellite LAGEOS, *C. R. Acad. Sci. Paris* **290**, B 445–448
- Afonso G., Barlier F., Berger C., Mignard F. and Walch J.J. (1985): Reassessment of the charge and neutral drag of LAGEOS and its geophysical implications, *J. Geophys. Res.* **90B**, 9381–9398
- Afonso G., Barlier F., Carpino M., Farinella P., Mignard F., Milani A. and Nobili A.M. (1989): Orbital effects of LAGEOS seasons and eclipses, *Annales Geophysicae* **7**, 501–514
- Anselmo L., Farinella P., Milani A. and Nobili A.M. (1983): Effects of the Earth-reflected sunlight on the orbit of LAGEOS satellite, *Astron. Astrophys.* **117**, 3–8
- Barlier F., Carpino M., Farinella P., Mignard F., Milani A. and Nobili A.M. (1986): Non-gravitational perturbations on the semimajor axis of LAGEOS, *Annales Geophysicae* **4**, 193–210
- Betti B., Carpino M., Migliaccio F. and Sansò F. (1987): Signal and noise in SLR data, *Bull. Geod.* **61**, 235–260
- Johnson C.W., Lundquist C.A. and Zurasky J.L. (1976): The LAGEOS satellite, *XXVIIth Congr. Int. Astronaut. Fed.*, Anaheim, California
- Milani A. and Melchioni E. (1989): Determination of a local geodetic network by multi-arc processing of satellite laser ranges, in *F. Sansò and R. Rummel (eds.), Theory of Satellite Geodesy and Gravity Field Determination*, Springer-Verlag, 417–445

- Milani A., Carpino M., Rossi A., Catastini G. and Usai S. (1994): Local geodesy by satellite laser ranging: a European solution, *Manuscripta Geodaetica*, in press
- Rubincam D.P. (1982): On the secular decrease in the semimajor axis of LAGEOS' orbit, *Cel. Mech.* **26**, 361–382
- Rubincam D.P. (1987): LAGEOS orbit decay due to infrared radiation from Earth, *J. Geophys. Res.* **92B**, 1287–1294
- Smith D.E., Kolenkiewicz R., Dunn P.J., Torrence M.H., Klosko S.M., Williamson R., Pavlis E.C., Douglas N.R. and Fricke S.K. (1990): Tectonic motion and deformation from satellite laser ranging to LAGEOS, *J. Geophys. Res.* **95B**, 22013–22041
- Vokrouhlický D., Farinella P. and Lucchesi D. (1993a): Long-periodic albedo perturbations on LAGEOS, *Astron. Astrophys.* **280**, 282–294
- Vokrouhlický D., Farinella P. and Mignard, F. (1993b): Solar radiation pressure perturbations for Earth satellites. I. A complete theory including penumbra transitions, *Astron. Astrophys.* **280**, 295–312
- Vokrouhlický D., Farinella P. and Mignard, F. (1994a): Solar radiation pressure perturbations for Earth satellites. II. An approximate method to model penumbra transitions in their long-term orbital effects on LAGEOS, *Astron. Astrophys.* **285**, 333–343
- Vokrouhlický D., Farinella P. and Mignard, F. (1994b): Solar radiation pressure perturbations for Earth satellites. III. Global atmospheric phenomena and the albedo effect, *Astron. Astrophys.* **290**, 324–334
- Zerbini S. (1993): Crustal motions from short-arc analysis of LAGEOS data, *Space Geodesy*, AGU, Washington D. C., in press

***Orbital Injection Analysis  
for Twin LAGEOS Satellites in Supplementary Orbits  
and the Measurement of the  
Lense-Thirring Gravitomagnetic Effect***

**Francesco Vespe**  
Agenzia Spaziale Italiana  
Centro di Geodesia Spaziale  
Matera (Italy)

**Luciano Anselmo**  
Istituto CNUCE/CNR  
Via S. Maria, 36  
Pisa (Italy)

## **ABSTRACT**

In 1984 it was proposed to measure the gravitomagnetic field using two non-polar laser ranged satellites, of LAGEOS type, with supplementary inclination (butterfly configuration). The LAGEOS gravitomagnetic, Lense-Thirring, nodal precession is equal to 31 milliarcsec/year.

The orbital injection errors are among the list of potential error sources which could affect the measurement. A joint NASA-ASI scientific working group estimated an error budget considering orbits of supplementary inclination to LAGEOS I.

The present work will perform a new computation of the uncertainties due to orbital injection errors, having adopted JGM-2 as gravity model. The improvement of the precision is of a factor 4, if compared with the previous computation performed by using the GEM-T1 model [1][2].

Furthermore it is investigated the possibility to use LAGEOS II as twin satellite in the "butterfly" configuration. The conclusion is that the accuracy in the measurement of the Gravitomagnetic effect is worsened.

Finally the improvements in the knowledge of the Earth's gravity models makes wider the opportunities of using launchers less precise than DELTA-2 with a non-dramatic worsening of the error-budget. Therefore features of some candidates launchers and the impact of their associated orbit injection uncertainties on the measurement are discussed in the present paper.

Error Source	1993 (JGM-2) (% of L-T)	1989(GEM-T1) (% of L-T)
Geopotential And Tides	2	5
Earth radiation pressure	1	1
Uncertainty in other relativistic effects	1	1
Thermal Forces	1-3	3
Even zonals (0.1° Inclination injection errors)	1	3
Random and stochastic Errors	2	5
<b>Total Error Budget</b>	<b>3-4%</b>	<b>8%</b>

Table 1.  
The Estimated (3- $\sigma$ ) Error Budget for Lense-Thirring Experiment  
revised using the JGM-2 gravity model as in [7].

## INTRODUCTION

The measurement of the Lense-Thirring Gravitomagnetic effect, as proposed by Ciufolini [3][4], using two non-polar satellites placed in supplementary orbits, exploits the dependence on the cosine of the inclination of the even zonal terms of Earth's Gravity potential. As a matter of fact the bisector between the nodal lines of the satellites behaves as a gyroscope [5] because the classical nodal precession and its uncertainties cancel out. The motion of such a gyroscope is ruled only by the Gravitomagnetic dragging which doesn't depend on the cosine of inclination.

In 1988 a joint study between NASA and ASI was performed in order to prove the feasibility of the experiment. All the effects which are no correlated with the cosine of the inclination and contribute significantly to the node precession were investigated in order to define the errors able to affect the measurement. The Lense-Thirring dragging of the nodes for LAGEOS is of about 31 mas/yr.

In the joint study three classes of effects were investigated: gravitational (tides, odd zonal terms of the gravity field and orbit injection errors), surface (Earth's albedo, Charged and Neutral Particle Drag) and thermal forces (Yarkovsky-Schach and Rubincam effect). The results achieved by the joint study group were very satisfying with an overall error budget associated to the experiment of only 8% considering an injection error of 0.1° in the inclination [6][7].

At that time, however, GEM-T1 was the gravity model adopted for the computations. In 1993 the computations were repeated [7] but using the JGM-2 gravity model. In this second computation the overall error affecting the measure was dramatically reduced of a factor 2. The results are shown and compared with the previous computations as in [7], in Table 1.

After the first computation of 1989 other new effects such as the anisotropic optical properties of LAGEOS [8] and Penumbra [9][10], together with a better assessment of Earth's albedo [11][12], have been investigated to achieve a more refined modelling of LAGEOS Along Track and Normal residuals.

The present work will show how much the JGM-2 gravity model reduces the orbital injection errors. Furthermore it will investigate if such errors are reduced using LAGEOS II as partner of the third. Finally it will perform an investigation to assess if launchers less precise than DELTA II are suitable to assure a positive outcome of the mission. As a matter of fact, the very refined JGM-2 gravity model makes less critical the orbital injection errors..

## ORBITAL INJECTION ERRORS WITH JGM-2

The uncertainties on the orbital parameters for an Earth's satellite like LAGEOS depend on the errors concerning the Gravity field harmonics (in our case the even zonal terms which give a secular node precession) and how much precise it is the orbit injection [2]. In the case of the node precession:

$$1) \quad \Delta\dot{\Omega}_{cl} = \sum_{i=1,3} \sqrt{\left[ \frac{\partial^2 \dot{\Omega}}{\partial p_i \partial J} \right] C_{2J} \left[ \frac{\partial^2 \dot{\Omega}}{\partial p_i \partial J} \right]^T} \delta p_i$$

where  $C_{2J}$  is the Variance-Covariance Matrix of the Even Geopotential coefficients, and  $\delta p = (\Delta a, \Delta e, \Delta I)$ , the error on semimajor axis, eccentricity and inclination, respectively. The second order partial derivatives in 1) is an outcome of the geometrical property of the butterfly configuration between two satellites:

$$\partial\dot{\Omega}_{class} = \Omega_I(a, e, I, J_{2n}) + \Omega_{III}(a + \Delta a, e + \Delta e, 180 - I + \Delta I, J_{2n})$$

i.e. having:  $\dot{\Omega}_{cl}^I(a, e, I) = -\dot{\Omega}_{cl}^{III}(a, e, \pi - I)$  we obtain:

$$2) \quad \partial\dot{\Omega} = \frac{\partial\dot{\Omega}}{\partial a} \Delta a + \frac{\partial\dot{\Omega}}{\partial e} \Delta e + \frac{\partial\dot{\Omega}}{\partial I} \Delta I + 2\dot{\Omega}_{L-T}$$

The expression of the classical nodal rate is in [2].

Taking into account also the uncertainties of the gravity field (on even zonals) and the covariances between the harmonics, we obtain the equation 1). In Table 2 are shown the second partial derivatives of the nodal rate both of LAGEOS I and II.

The JGM-2 solution for the gravity model has been achieved by a joint effort among the NASA/GSFC, the University of Texas and CNES [13]. They have incorporated Laser, Doppler and Optical tracking data of 33 Satellites in addition to the available data of TOPEX/POSEIDON. Regarding this last satellite, for the recovery of the gravity field, orbit solutions on arcs 10 days long were used, computed both by a SLR network of 31 stations, and a DORIS-DOPPLER network of 46 stations.

Furthermore, altimeter data (GEOS-3, GEOSAT and SEASAT) and surface gravity data have been included in the solution. The use of T/P data makes the JGM-2 solution very strong for satellites with inclinations close to 50°.

Till now it has been never seriously investigating the hypothesis to use LAGEOS II as twin satellite to the Third.

	$\frac{\partial^2 \dot{\Omega}}{\partial J_{2n} \partial a}$ (mas/yr km)		$\frac{\partial^2 \dot{\Omega}}{\partial J_{2n} \partial I}$ (mas/yr rad)		$\frac{\partial^2 \dot{\Omega}}{\partial J_{2n} \partial e}$ (mas/yr)	
	LAGEOS I	LAGEOS II	I	II	I	II
J <sub>2</sub>	2.67146E+8	-4.95328E+8	-2.5731E+12	-2.2427E+12	-1.4985E+10	9.43235E+10
J <sub>4</sub>	2.07477E+8	-7.29278E+7	-3.1686E+11	2.47597E+12	-2.0366E+10	2.42998E+10
J <sub>6</sub>	7.15942E+7	1.12519E+8	5.41833E+11	8.53552E+11	-1.0307E+10	-5.4970E+10
J <sub>8</sub>	6.80845E+6	3.50094E+7	3.80506E+11	-3.5082E+11	-1.30137E+9	-2.2698E+10
J <sub>10</sub>	-6.38867E+6	-1.01018E+7	1.31003E+11	-1.8957E+11	1.52669E+9	8.18283E+9
J <sub>12</sub>	-4.23464E+6	-6.38732E+6	2.01626E+10	1.58625E+10	1.21598E+9	6.21218E+9
J <sub>14</sub>	-1.42572E+6	104203.	-5.15414E+9	2.59647E+10	4.78393E+8	-1.1831E+8
J <sub>16</sub>	-249614.	741323.	-4.80435E+9	2.43467E+9	9.58697E+7	-9.62303E+8
J <sub>18</sub>	26116.3	112685.	-1.80844E+9	-2.45069E+9	-1.13001E+7	-1.64573E+8
J <sub>20</sub>	37508.8	-58779.7	-3.8454E+8	-6.52217E+8	-1.80548E+7	9.53599E+7
J <sub>22</sub>	15240.5	-20994.3	-5.43127E+6	1.46143E+8	-8.07818E+6	3.74438E+7
J <sub>24</sub>	3590.06	2430.83	3.41448E+7	8.82525E+7	-2.07779E+6	-4.72536E+6
J <sub>26</sub>	252.754	2424.98	1.63815E+7	-316838.	-158599.	-5.10079E+6
J <sub>28</sub>	-210.893	153.132	4.4239E+6	-8.51115E+6	142606.	-346375.
J <sub>30</sub>	-119.153	-203.771	547526.	-1.30121E+6	86374.9	492992.

Table 2.  
Second Partial Derivatives of Nodal Precession Rate for LAGEOS I and II.

	Lageos			Lageos II		
	JGM-2	JGM-3	GEM-T1	JGM-2	JGM-3	GEM-T1
$\Delta a$ (Km)	108.89	171.383	26.98	56.29	105.205	15.37
$\Delta e$	0.803	1.352	0.188	0.217	0.289	0.08
$\Delta I$ ( $^{\circ}$ )	0.421	0.934	0.121	0.11	0.251	0.07

Table 3.

The tolerable orbit injection errors (at  $1-\sigma$  level) computed with the method of equal influences on each of three parameters. Three different gravity models are used: GEM-T1 (1988), JGM-2 (1993) and JGM-3 (1994). The last model has been prepared by the University of Texas incorporating their own informations and LAGEOS II data [15].

Therefore Table 2 shows the values of the second order partial derivatives of the nodal rate also for LAGEOS II which is worthwhile to be discussed in more details.

Table 3. shows the bounds of the injection orbit errors in the case of an overall error of the 3% of Lense-Thirring (1 mas/yr) equally divided among the three orbital parameters as in the method of equal influences [2].

The formula adopted as a consequence of the application of equal influences is:

$$3) \quad \Delta p_i = \frac{2\sigma_{\dot{\Omega}}}{\sqrt{3 \left[ \frac{\partial^2 \dot{\Omega}}{\partial J \partial p_i} \right] C_{J_{2n}} \left[ \frac{\partial^2 \dot{\Omega}}{\partial J \partial p_i} \right]^T}} \quad \text{where } p_i \text{ are respectively } a, e \text{ and } I$$

while  $\sigma_{\dot{\Omega}}$  is the overall error on the rate of the mean node.

The outcome shows how the sensible improvement of the gravity field has dramatically reduced of a factor 4 the uncertainties.

## THE LAUNCHERS

In 1990 MDSSC performed a vehicle mission analysis for LAGEOS III [13] with both the hypotheses of short (1.5 hours) and long (20-24 hours) flight plan. In Table 4 we show the results of such a study. The case of short flight plan is more than enough to assure the success of the LAGEOS III mission. From the comparison between the Tables 3 and 4 we can infer that eccentricity is not a dramatic parameter and, therefore, the overall error can be divided only between the inclination and the semi-major axis.

	LFP		SFP	
	Min	Max	Min	Max
$\Delta a$ (Km)	-8.0	7.8	$\pm 15$	
$\Delta e$	.000	.0012	=	
$\Delta I$ ( $^{\circ}$ )		$\pm .027$		$\pm .1$

Table 4.  
*Results of the LAGEOS III mission analysis using MDSSC Delta II rocket. All uncertainties are at 3- $\sigma$  level*

So the values of Table 3 for the Inclination and the Semimajor axis have to be multiplied by a factor  $\sqrt{3/2}$  to have more realistic (and favourable) constraints.

In October 1992, the LAGEOS II satellite, a Joint NASA/ASI space mission, was injected in orbit around the Earth by the IRIS (Italian Research Interim Stage) and an AKM (Apogee-Kick-Motor) deployed during the Space Shuttle mission STS-52.

IRIS is a rocket completely developed in Italy. Our goal is to check if a Shuttle assisted launch of LAGEOS III could allow a successfull outcome of the mission, notwithstanding the big orbital injection errors if compared to a DELTA II launch.

Of course the STS/IRIS system is not able to inject LAGEOS-3 in the desired 70 degrees orbit from a standard 28.5 degrees STS parking orbit. But the Space Shuttle uses occasionally even higher inclination orbits: 62° for classified DoD missions; 57° for civilian remote-sensing or Spacelab missions; 52° for the planned flights to Space Station Mir. In such cases the LAGEOS-3 mission could be accomplished, at least from a dynamical point of view.

Three options have been preliminarily considered, corresponding to the following three STS parking orbits:

- 1) STS parking orbit inclination = 46.5 deg
- 2) STS parking orbit inclination = 52.0 deg
- 3) STS parking orbit inclination = 57.0 deg

Option 1 would allow to use for the mission the same configuration used for LAGEOS-2. In the other cases the Delta-V requirements are significantly lower:

Option 2	Perigee Delta-V = 1680 m/sec Apogee Delta-V = 1220 m/sec
----------	---

Option 3	Perigee Delta-V = 1400 m/sec
	Apogee Delta-V = 1100 m/sec

Such requirements would violate the off-loading constraints of the IRIS stage unless an appropriate amount of ballast could be placed on it. While the technical feasibility of this approach should be verified, some preliminary estimations of the injection errors in the final orbit have been made taking into account the additional data available for IRIS and comparable solid propellant rocket motors.

The values provided in Table 5 are just the result of a very rough estimate and have been summarized assuming both an "optimistic" and a "pessimistic" guess (3-sigma confidence level), corresponding to different estimates of the IRIS thrust error (1.4% or 2.4%):

These estimations are based on very conservative assumptions. Therefore a detailed engineering analysis (too time consuming at this preliminary stage) could find significantly better results.

In any case, the LAGEOS-3 mission, with the new, relaxed, requirements, seems no more out of reach of the STS/IRIS launch system: with injection errors equal to those obtained for LAGEOS-2, the measure of the Lense-Thirring effect as proposed by Ciufolini could be accurate at the 5% level (1-sigma)!

The Values of the last column are the equivalent error percentages computed on Lense-Thirring precession.

An orbit supplementary to that of LAGEOS II has not be considered because the supplementary angle to its inclination is of 127.5°, i.e. a retrograde orbit, which is out of reach for a shuttle-launched IRIS.

STS parking orbit inclination	Error on Semi-major axis	Error on Inclination	Error on Eccentricity	$\%(\dot{\Omega}_{L-T})$
46.5 deg	opt 420 km	0.80 deg	0.030	12
	pes 560 km	1.20 deg	0.040	16.5
52.0 deg	opt 353 km	0.67 deg	0.025	10.1
	pes 470 km	1.01 deg	0.034	12.1
57.0 deg	opt. 305 km	0.58 deg	0.021	8.73
	pes. 406 km	0.87 deg	0.029	11.9

Table 5.  
*Summary of some launch hypothesis using the STS-IRIS system. The uncertainties on the orbital parameters are at 3- $\sigma$  level*

Rocket	Height	$\Delta a$	$\Delta e$	$\Delta I$	$\%(\dot{\Omega}_{L-T})$
CYCLON	1500 Km	$\pm 25$ Km	=	$\pm 0.083^\circ$	0.83
	5900 Km	$\pm 75$ Km	=	$\approx 0.1^\circ$	1.93
ZENITH	GTO	$\pm 300$ Km	0.0075	$\pm 0.7^\circ$	9.0
	5900 Km	$\pm 300$ Km *	0.0075 *	$\pm 0.7^\circ$	9.0

\* The values are conservative because only the data for Geostationary Transfer Orbits (GTO) are currently available

TABLE 6.  
3- $\sigma$  *Orbit injection errors for Russian rockets.*

Finally a preliminary investigation about ex-USSR rockets suitable for the LAGEOS III mission has been performed. In particular we have circumscribed our research only to liquid propellant rockets. In Table 6 we summarize the main features of the Cyclon and Zenith launchers:

## CONCLUSIONS

Since the original proposal by I. Ciufolini to detect the Lense-Thirring effect by using a LAGEOS satellite (LAGEOS-3) with inclination supplementary to that of LAGEOS-1 or II, several error sources have been dramatically reduced. We have analyzed in the present paper the consequences of the improvement of the gravity field on the orbital injection errors.

In particular the improvements of the gravity field, from GEM-T1 to JGM-2 model, have reduced by a factor 4 the uncertainties.

However, the investigation should take into account also the time variation of the gravity field ( $j_2, j_4, \dots$ ), mainly due to the tides. Their contribution, as a matter of fact, may exceed the uncertainties in the constant part of the gravity model [15]. Therefore they have to be taken into account to perform a more complete analysis.

The results we get also for LAGEOS II, considered as twin satellite to the third, emphasize a significant worsening of the errors budget on each of the 3 Keplerian variables of factors ranging from 2 to 4 as in Table 3.

These outcomes are mainly due to the fact we don't have several years of LAGEOS II data available for the solutions of the gravity models. We have performed another computation using JGM-3 model where LAGEOS II data have been incorporated. In Table 3 we have summarized also the tolerable errors achieved using JGM-3.

The improvement we obtain is of a factor 2 for LAGEOS II. Also for LAGEOS I there are significant improvements of the tolerable uncertainties. Such improvements, however, could be optimistic in the sense that they are due only to the particular values of the covariant terms in the errors matrix without a real improvement of the variances [15].

Of particular interest it is the discussion of the tolerable errors on inclination. Focusing only on the quadrupole term of the node, its derivative, depending on the sine of inclination, is slightly higher for LAGEOS I than for the II. But extending the analysis to the octupole momentum ( $J_4$ ) we have for LAGEOS II a much higher value of derivative (See Table 2) which dramatically increases the uncertainties. This evidence remarks how the measurement of the Lense-Thirring effect is intrinsically less precise using LAGEOS II as twin satellite. Furthermore the third satellite supplementary to the second should be retrograde ( $127.5^\circ$  of inclination) and a very high energy consumption is required to inject in orbit it.

Looking at the Tables 4, 5 and 6, the sensitiveness of the orbital injection errors to the eccentricity is very low. So we can restrict the source of errors only to the semimajor-axis and Inclination. In such a way the tolerable uncertainties for these parameters, as in Table 3, have to be multiplied by a factor  $\sqrt{3/2}$  according to the method of equal influences [2].

The use of more refined gravity models has made much more favourable the tolerable errors on the orbital parameters. We have shown that less precise launchers other than DELTA II, are able to assure a good success of the mission. Also the use of the Shuttle-assisted IRIS solid propellant rocket could assure a measurement of the Lense-Thirring effect with an uncertainty, in the worst case, of about 20% at the 3-sigma level. The ex-USSR launchers could be in any case a good alternative to DELTA II and able to guarantee the measurement of L-T with an uncertainty of about 10%. For these reasons it would be very important to perform a LAGEOS III mission analysis including also these launchers.

**Acknowledgement.** We are grateful to S. Nerem (GSFC/NASA), J. Ries and R. Eanes (University of Texas) for having provided us with the even zonals variance-covariance matrix of JGM-2 and JGM-3 gravity models. We appreciated very much the discussions and the helpful suggestions we had with J. Ries.

#### References:

- [1] S. Casotto, I. Ciufolini, F. Vespe, G. Bianco; "Earth Satellites and Gravitomagnetic Field", Nuovo Cimento, Vol. 105 B, N.5, (1990)
- [2] S. Casotto; "Orbit Injection Error Analysis for the Proposed LAGEOS III Mission", Celestial Mechanics, Vol 56 No. 3, July (1993)
- [3] I. Ciufolini, "Measurement of the Lense-Thirring Drag on High-Altitude, Laser-Ranged Artificial Satellites", Phys. Rev. Lett. **56**, 278-281, (1986)
- [4] I. Ciufolini, "A Comprehensive Introduction to the LAGEOS Gravitomagnetic Experiment: from the Imprtance of the Gravitomagnetic Field in Physics to Preliminary Error Analysis and Error Budget", Int. J. Mod. Phys. 4, 3083-3145, (1989)

- [5] B. Bertotti, I. Ciufolini, "*Measurement of the Gravitomagnetic Field Using a Pair of LASER Ranged Satellites*", ASI Final Report about LAGEOS III,(1989)
- [6] B. D. Tapley; I. Ciufolini, J. Ries, R. Eanes, M. Watkins, B. Bertotti, G. Bianco, M. Carpino, M. Dobrowolny, P. Farinella, L. Iess, A. Nobili, S. Rabbia, F. Vespe;"*LAGEOS III Joint NASA/ASI: final report*" Presented at the LAGEOS III Science Advisory Group Meeting, Lanham ,Md, May 22-23, (1989)
- [7] J.Ries, R.J. Eanes, B.D. Tapley, M. Watkins;"*LAGEOS III Mission Analysis*", Presented at LAGEOS II Science Working Team Meeting, ASI Matera (Italy), May 10-12 (1993)
- [8] R. Scharroo, K.F. Wakker, B. Ambrosius, R. Noomen;"*On the Along Track Acceleration of the LAGEOS Satellite* ",J. Geophys. Res. B, 96, 729, (1991)
- [9] Inversi P., Vespe F.;"*Direct and Indirect Solar Radiation Effect Acting on LAGEOS Satellite: Some Refinements*", presented at 29<sup>th</sup> COSPAR Plenary Meeting, Aug-Sept (1992)
- [10]D. Vockroulicky, P. Farinella, F. Mignard; "*Solar Radiation Pressure Perturbations for Earth Satellites*"Astron. & Astrophys., 285, 333-343, (1994)
- [11]D. Lucchesi, P. Farinella;"*Optical properties of the Earth Surface and Long Term Perturbations of LAGEOS orbit*", J.Geophys.Res. B, 97, 7121 (1992)
- [12]D. Vockroulicky, P. Farinella, D. Lucchesi; "*Long Periodic Albedo Perturbation on LAGEOS*", Astron. & Astrophys., 280, 282-294, (1993)
- [13]Lerch F.J., Nerem R.S., Marshall J.C., Putney B.H., Pavlis E. C., Klosko S. M., Luthcke S.B., Patel G.B., Pavlis N.K., Williamson R.G., Chan J.C., Tapley B.D., Shum C.K., Ries J.C., Eanes R.J., Watkins M.M., Schutz B.E., Biancal R., Nouel F.;"*Gravity Model Development for TOPEX/POSEIDON*", Presented at AGU 1993 Spring Meeting, Baltimore, May 24, (1993)
- [14]G. Ousley;"*LAGEOS III Delta Launch Vehicle Support*"; Presented at the LAGEOS III ASI meeting, Rome, 20 June (1991)
- [15]J. Ries;Private communications, University of Texas, (1994)

# DETERMINATION OF THE GRAVITY FIELD FROM SATELLITE GRADIOMETRY

– A Simulation Study –

Michael Belikov\*    Martin van Gelderen    Radboud Koop  
Faculty of Geodetic Engineering, Delft University of Technology, NL

## INTRODUCTION

For the analysis of the yield of a satellite gradiometry mission, different methods can be employed, see e.g. (Koop, 1993) or (Rummel et al., 1993). Most studies carried out so far rely on *covariance propagation*. In the present study full *simulations* are used to evaluate future missions like STEP. This gives the opportunity to investigate several effects in more detail than before.

The three methods of analysis we discriminate are summarized in table 1. The most simple one is degree variance propagation. It is essentially covariance propagation but with some strong assumptions on the linear model. This makes a very simple and straightforward covariance propagation in the spectral domain possible. The second method is covariance propagation with an adequate linear model. This model still contains approximations but is accurate enough for realistic covariance propagation (and can also serve as model for the actual analysis of the future data). The most advanced method, however, is a full simulation. Problems like modelling errors, instability etc., which cannot be evaluated very well by means of covariance propagation, can now be studied in detail.

In this paper only some results are shown of simulation studies carried out with gradiometric data from a STEP-like mission. The use of the orbital geometry, e.g. from GPS data, other components of the gravity tensor etc. can also be incorporated in our adjustment model, but are omitted here.

The following assumptions underlie our linear model:

- Closed orbit ( $e$  and  $i$  fixed,  $\Omega$  and  $\omega$  drift linearly).
- Accurate orbit available at a fixed altitude.
- Regular along-track data sampling.

If the potential is developed in a series of inclination functions also non-polar orbits can be accommodated. The solution is found with a least-squares adjustment. With the assumptions above, the normal matrix is block-diagonal: each order and parity

---

\*Now at The Russian Academy of Sciences, St. Petersburg

Table 1. The possibilities of the three methods of analysis. (●: feasible; ○: limited feasibility)

	Altitude	Noise level	Component	Orbit	Coloured noise	Instability	Model errors	Sampling error	Non-perfect repeat
Degree variances	●	●	○						
Covariance propagation	●	●	●	●	●	●	○		
Simulation	●	●	●	●	●	●	●	●	●

of degree can be solved independently. The accuracy is improved by means of an iterative procedure. For more details see (Rummel et al., 1993).

Furthermore it can be remarked that the processing time is proportional to  $L_{max} \cdot N_{obs}$  (the maximum degree times the number of observations). So even for high degree and order solutions the computation time remains fairly reasonable.

## RESULTS

In this paper only one mission scenario is presented. Its parameters are derived from the specifications of the possible future STEP mission, be it with a reduced mission time in order to limit the computational effort. It is summarized in table 2. As true input field serves OSU91A, complete up to degree and order 360. The approximate values for the unknowns are taken from GRS80.

The results obtained are presented here in several ways: relative errors for individual potential coefficients, global RMS errors for geoid heights and gravity anomalies and  $1^\circ \times 1^\circ$  block mean value errors of geoid heights. To illustrate some general trends degree variances are used.

### Errors in Potential Coefficients

The errors in potential coefficients recovered from the simulated observations, are presented as relative errors with respect to the true field. They are computed as:

$$\Delta \hat{C}_{lm} = \frac{|\hat{C}_{lm} - C_{lm}|}{c_{lm}}, \quad \Delta \hat{S}_{lm} = \frac{|\hat{S}_{lm} - S_{lm}|}{c_{lm}},$$

with  $C_{lm}$  and  $S_{lm}$  the potential coefficients ("^" for estimated) and  $c_{lm}$  the root of the signal-degree-order variances of the true field.

Table 2. Mission characteristics.

Geopotential model	OSU91A
Mean altitude	342380 m
Inclination	97°565
Mean eccentricity	0.0014
Groundtrack repeat period	33 siderial days
Duration	2852060 seconds
Closure	< 14 km
Number of observations	190137
Sampling interval	15 seconds
Number of revolutions	520
Equatorial separation between tracks	0°33
Observed component	Cross-track

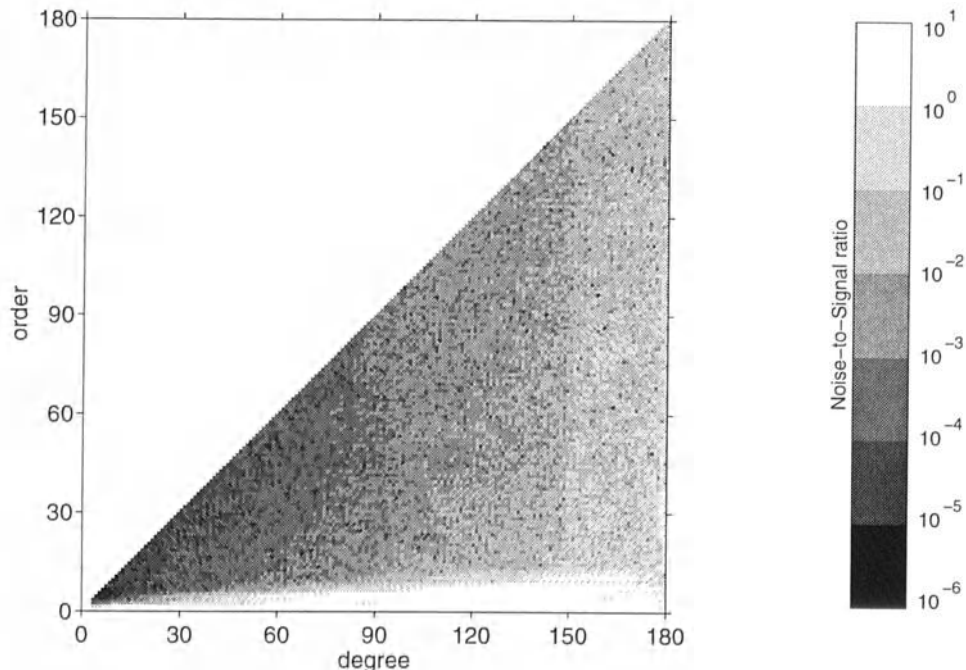


Fig. 1. Errors of the potential coefficients recovered after three iterations.

After the software was tested with noise-free and un-aliased data (i.e. the maximum degree of the true input field was reduced) the first test was made with the orbit of table 2. No noise was added to the observations. The results are shown in figure 1. The scale of the figure is logarithmic; the dark areas indicate a good (high) signal-to-noise ratio, the light areas a low ratio. The coefficients in the white region suffer

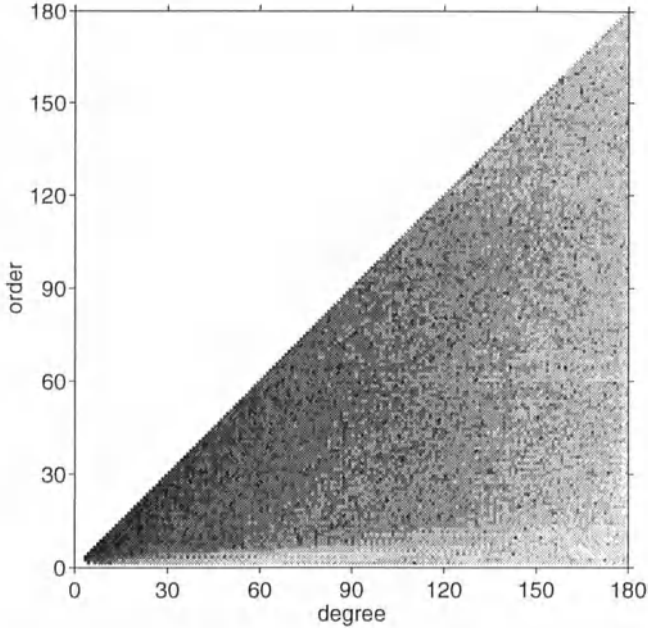


Fig. 2. Errors of the potential coefficients recovered after three iterations (stabilized solution)

from a signal-to-noise ratio lower than one and can not be recovered properly. The grayscale of the following figures is the same. Comparison with the results obtained from a polar orbit (not shown here) and inspection of the condition number of the sub-blocks of the normal matrix clearly indicate that the coefficients of low order suffer from instability due to the polar gaps.

The instability can be overcome by means of adding a weight to the diagonal elements of the normal matrix. In these studies the degree variance model of Tscherning and Rapp was used as a-priori information. Although the estimation is no longer unbiased, see e.g. (Xu and Rummel, 1992), the errors for the low orders are reduced dramatically: almost all coefficients (below degree and order 180) can be recovered (figure 2). The accuracy of the coefficients of high order remains almost unchanged. Only some effect of the stabilization is visible because its result is not exactly identical for each sub-block due to different condition numbers.

As a last step, noise is added to the data (figure 3). This mainly influences the accuracy of the high degrees; the high orders profit from the fact that the second derivative in the cross-track direction was observed. Surprisingly, the low orders even get a little better with respect to the situation without noise.

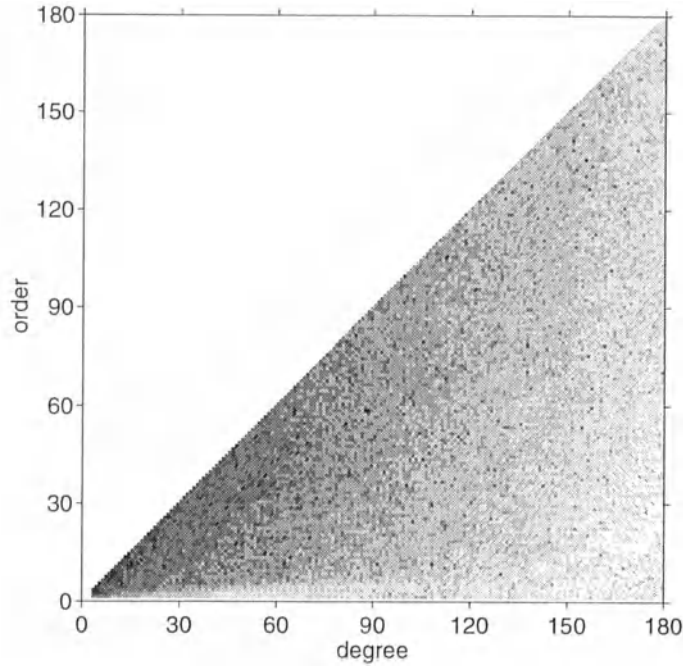


Fig. 3. Errors of the potential coefficients recovered after three iterations (stabilized solution, noise  $\sigma = 10^{-4}$  E).

Table 3. The RMS errors of the stabilized solutions ( $\sigma = 10^{-4}$  E). The omission error is from the maximum degree  $L$  up to 360.

Gravity anomalies (mGal)				Geoid undulations (m)				Domain	
$L = 120$		$L = 180$		$L = 120$		$L = 180$			
comm.	omiss.	comm.	omiss.	comm.	omiss.	comm.	omiss.		
0.9	10.2	4.1	5.7	8.3	41.2	17.6	16.8	$0^\circ \leq \vartheta \leq 180^\circ$	
0.3	10.2	3.9	5.7	2.0	41.0	15.4	16.8	$10^\circ \leq \vartheta \leq 170^\circ$	
0.3	10.0	3.9	5.6	2.0	40.4	15.4	16.5	$20^\circ \leq \vartheta \leq 160^\circ$	

### Geoid and Gravity Error

Although this study was mainly intended to investigate the performance of the iterative solution and of the effects of e.g. polar gaps, it can be interesting to see how the results translate into geoid and gravity errors. World-wide  $1^\circ \times 1^\circ$  block mean values were computed, from the true field and from the solution of figure 3. The differences are plotted in figure 4. The RMS-values are listed in table 3. From the figure it can be seen that the error in the geoid heights is reasonably homogeneous, with an except for the polar regions. When the domain for the global RMS is limited to  $10^\circ \leq \vartheta \leq 170^\circ$ ,

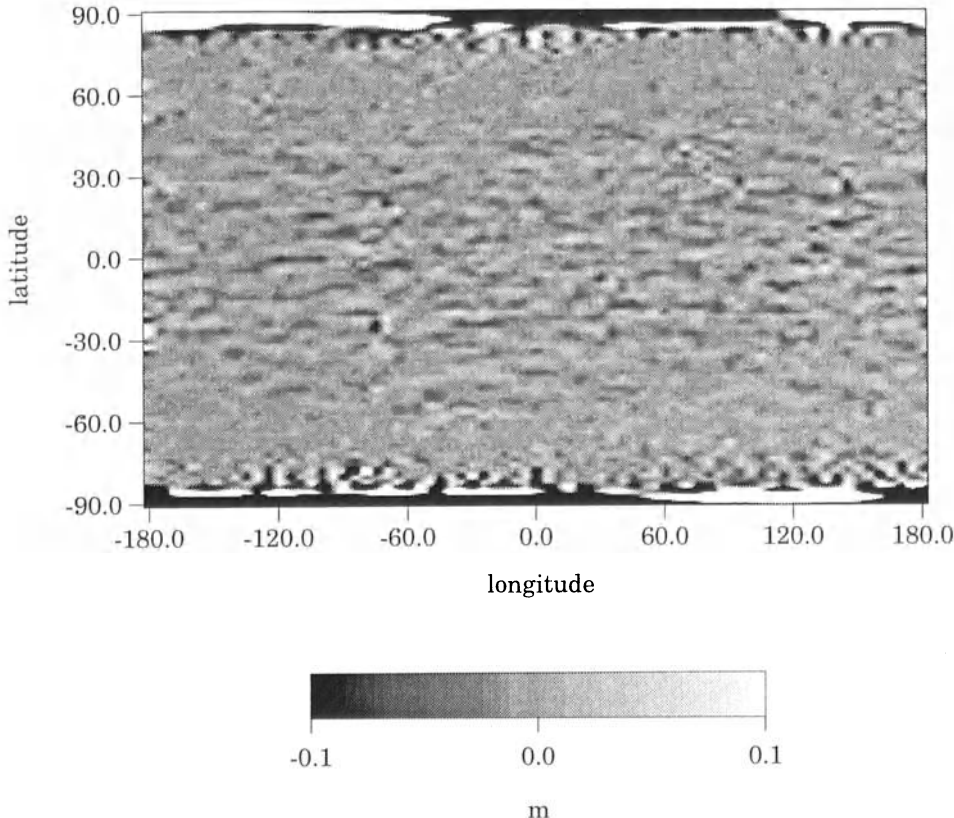


Fig. 4. Errors in geoid undulations (stabilized solution,  $\sigma = 10^{-4}$  E)

a *total* geoid error of only 23 cm results. However, we have to keep in mind when interpreting this number that the true field used has a maximum degree of 360. To obtain a more realistic error, the omission error above degree 360 should be added (about 3 cm).

### Error-Degree Variances

From the solution of figure 3 the error degree variances are computed. Together with the true signal from OSU91A they are shown in figure 5. By excluding some lower orders from the degree variances it can be seen that the characteristic bulge which is always found for a non-polar orbit can be attributed to the weak estimability of the low orders.

In the next figure (6) the error degree variances are plotted from three successive iterations. The gain in accuracy is easily visible; especially for the low degrees (they suffer relatively more from the polar gaps) and the high degrees which are initially more affected by aliasing.

The three methods of analysis discussed in the introduction are compared in fig-

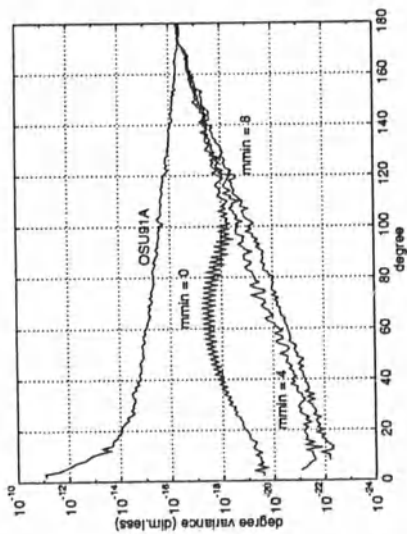


Fig. 5. Degree error variances for varying  $m_{min}$  (stabilized solution) and OSU91A.

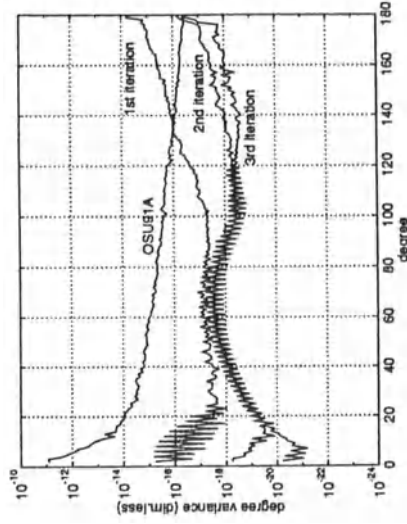


Fig. 6. The iteration process illustrated by degree variances (stabilized solution, no noise) and OSU91A.

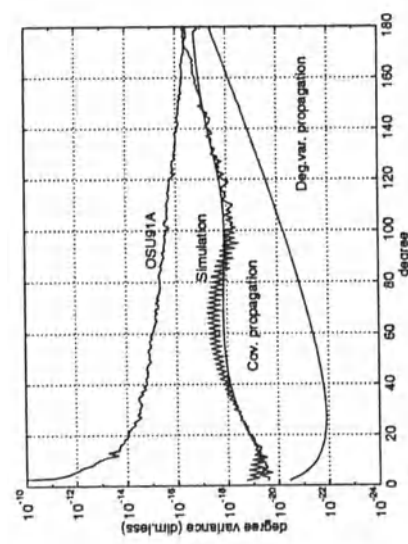


Fig. 7. The different methods of analysis compared (stabilized solution) and OSU91A.

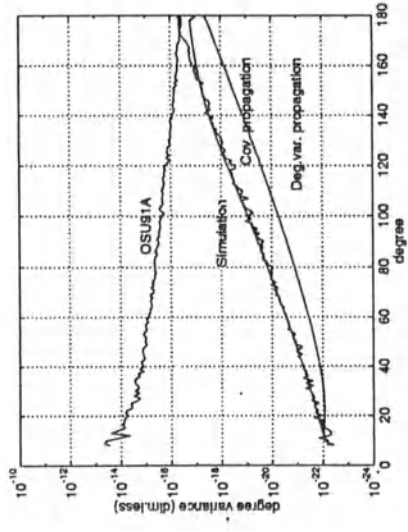


Fig. 8. The different methods of analysis compared for  $m_{min} = 8$  (stabilized solution) and OSU91A.

ure 7. Since for the degree variance propagation only a polar orbit can be studied, its results deviate significantly from the other two. Moreover, the cross-track component can only be implemented into this approach by scaling the spectrum obtained from the radial component; see (Rummel & Van Gelderen, 1992). The results of the covariance propagation are in reasonable agreement with the simulation results, although deviations are still clearly visible.

As the main effect of the polar gaps is concentrated in the lower degrees we make the same comparison of the three methods but now with the lower eight orders removed from the predicted error-degree variances. This is shown in figure 8. Now the three lines are much closer. Only the degree variance study is too optimistic still because of the assumption of global data distribution. This again shows that the effect of the polar gaps, which is completely absent from the degree variance propagation, is mainly concentrated in the lower orders. Also in the space domain the deterioration of the result due to the polar gaps is limited, as can be concluded from figure 4 and table 3. The (global) error of geoid heights predicted by degree variances is very close to the result of the simulation study if we consider the domain  $10^\circ \leq \theta \leq 170^\circ$ .

This means that even the very simple method of degree variance propagation gives reliable results for many situations.

## GENERAL TRENDS

The general pattern of the relative error of the potential coefficients shown in the figures 1 to 3, can be attributed to four main sources:

- Signal decreases with  $1/n^2$ .
- Altitude attenuation with  $(r/R)^n$ .
- Noise decreases with  $m^2$  (cross-track component observed).
- Polar gaps yield bias and instability for the low orders

The first three are easily modeled and shown in figure 9. For this figure the above three rules-of-the-thumb where programmed and multiplied to get the relative error. Apart from the lower orders and some individual coefficients, this picture does not deviate significantly from the results obtained from the simulation (figure 3).

The effect of the polar gaps is studied separately. It is not intended to give an estimate of the actual error, since this depends highly on the linear model, stabilization method etc., but to try to see which coefficients may be sensitive for the polar gaps.

With global continuous data we have for the potential coefficient

$$C_{lm} = \frac{1}{2} \int_0^\pi a_m(\theta) \bar{P}_{lm}(\cos \theta) \sin \theta d\theta, \quad a_m(\theta) = \frac{1}{2\pi} \int_0^{2\pi} V(\theta, \lambda) \cos \lambda d\lambda.$$

In case of polar caps of radius  $\theta_0$  this might be replaced by

$$\hat{C}_{lm} = \frac{1}{2} \int_{\theta_0}^{\pi-\theta_0} a_m(\theta) \bar{P}_{lm}(\cos \theta) \sin \theta d\theta.$$

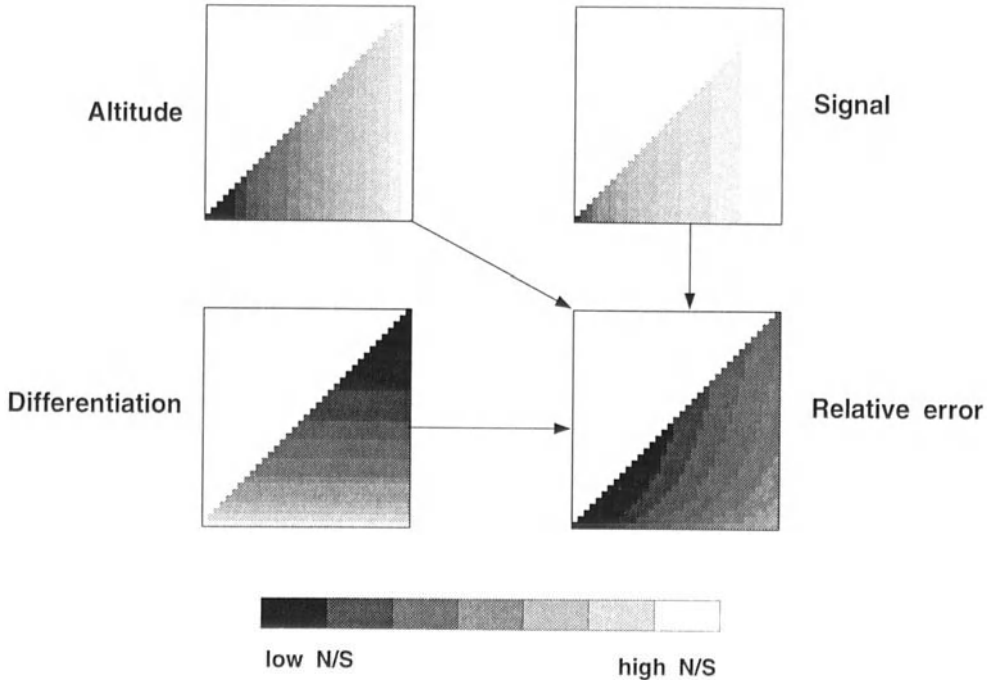


Fig. 9. The three general trends in the relative error (N/S ratio).

For the relative error caused by the polar gaps  $\varepsilon_{lm} = \frac{\hat{C}_{lm} - C_{lm}}{C_{lm}}$  we derive

$$M\{\varepsilon_{lm}^2\} \approx 1 - \frac{1}{2} \int_{\theta_0}^{\pi - \theta_0} \bar{P}_{lm}^2(\cos \theta) \sin \theta d\theta,$$

which is simply the loss of power of the Legendre functions due to the limitation of the domain. Although direct quadrature is not applied in the simulation studies here, it was expected that for reasonably dense data sets the effects are not very different. Indeed, the general picture obtained (figure 10) is quite the same as in figure 1 if we look at which potential coefficients are affected. Most coefficients are not affected at all, the same as was concluded from the simulations. Only in a very sharply defined, wig-shaped spectral area the effect of the polar gaps is apparent but still quite small.

By numerically experimenting with different  $\theta_0$  it was shown that for the maximum order  $m$  affected by the polar gaps the following rule of the thumb holds:

$$m_{max} \approx \theta_0 \cdot l = \left| \frac{\pi}{2} - I \right| \cdot l$$

with  $\theta_0$  and  $I$  (the inclination of the orbit) in radians.

## CONCLUSIONS

From this study the following conclusions can be drawn:

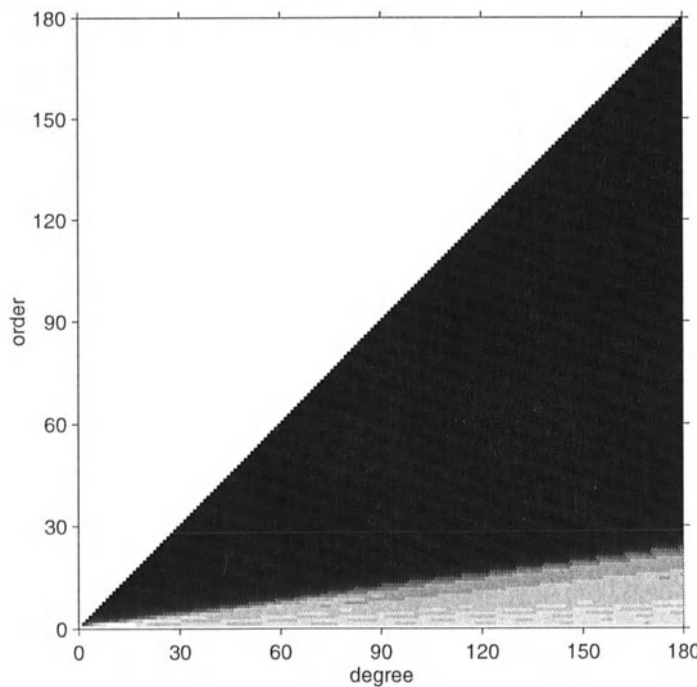


Fig. 10. Percentage power loss of the Legendre functions due to the exclusion of the polar domains of  $\theta_0 = 7^\circ 5$  (black areas: 0% ; white areas: 6%)

- With the method proposed the analysis of all realistic gradiometric missions can be handled.
- The results are in good agreement with the degree variance and the covariance analysis.
- An almost complete geopotential model up to degree 180 can be derived from a STEP-like gradiometry mission.
- The total geoid error is about 23 cm (RMS) for  $1^\circ \times 1^\circ$  block mean values.
- Polar gaps have only limited influence on the quality of the solution.

## REFERENCES

- Koop, R. (1993), Global gravity field modelling using satellite gravity gradiometry, *Netherlands Geodetic Commission, New Series*, **38**, Delft, Netherlands.
- Rummel, R., M. van Gelderen, R. Koop, E. Schrama, F. Sansò, M. Brovelli, F. Migliaccio, F. Sacerdote (1993), Spherical harmonic analysis of satellite gradiometry, *Netherlands Geodetic Commission, New Series*, **39**, Delft, Netherlands.
- Rummel, R., M. van Gelderen (1992), Spectral analysis of the full gravity tensor, *Geophys. J. Int.*, **111**, 159-169
- Xu P.L., R. Rummel (1992), The value of minimum norm estimation of geopotential fields, *Geophys. J. Int.*, **111**, 170-178.

# NEW WAVELET METHODS FOR APPROXIMATING HARMONIC FUNCTIONS

Willi Freeden and Michael Schreiner

University of Kaiserslautern

Laboratory of Technomathematics, Geomathematics Group

P.O.-Box 3049, 67653 Kaiserslautern, Germany

Some new approximation methods are described for harmonic functions corresponding to boundary values on the (unit) sphere. Starting from the usual Fourier (orthogonal) series approach, we propose here nonorthogonal expansions, i.e. series expansions in terms of "overcomplete" systems consisting of "localizing" functions. In detail, we are concerned with the so-called Gabor, Toeplitz, and wavelet expansions. Essential tools are modulations, rotations, and dilations of a "mother wavelet". The Abel-Poisson kernel turns out to be the appropriate "mother wavelet" in approximation of harmonic functions from potential values on a spherical boundary.

## FOURIER EXPANSION

It is well known that while spline functions have been used very successfully for analysing both exact and noisy data, the technique of Fourier transformation is the standard tool for studying the corresponding spectral behaviour. Indeed, in many applications, some incoming information, available for a function  $F$  is given as a discrete table of numbers rather than its original form. The base functions, of course, can be chosen in such a way that the countable family forms an orthonormal basis of a Hilbert space. Best known in all geosciences are the ( $\mathcal{L}^2$ - orthonormal) spherical harmonics  $Y_{n,j}$ ,  $n = 0, 1, \dots$ ,  $j = 1, \dots, 2n + 1$ , in the Hilbert space  $\mathcal{L}^2(\Omega)$  of square-integrable functions on the unit sphere  $\Omega$  in  $\mathbb{R}^3$ . Clearly, in this case, the "spherical Fourier transform"  $F \mapsto (\text{FT})(F)$ , may be formulated in analogy to its counterpart in Euclidean spaces as follows

$$((\text{FT})(F))_{n,j} = F_{n,j} = (F, Y_{n,j})_{\mathcal{L}^2(\Omega)} = \int_{\Omega} F(\eta) Y_{n,j}(\eta) d\omega(\eta), \quad F \in \mathcal{L}^2(\Omega), \quad (1)$$

( $d\omega$  is the surface element on  $\Omega$ ). As required above, the function  $F$  is characterized by the values  $((\text{FT})(F))_{n,j}$ . The recovery of  $F \in \mathcal{L}^2(\Omega)$  by means of spherical harmonics is then quite straightforward by taking the Fourier series (i.e. orthogonal expansion):

$$F = \sum_{n=0}^{\infty} \sum_{j=1}^{2n+1} F_{n,j} Y_{n,j} = \sum_{n=0}^{\infty} \sum_{j=1}^{2n+1} ((\text{FT})(F))_{n,j} Y_{n,j}. \quad (2)$$

More explicitly, for every  $F \in \mathcal{L}^2(\Omega)$ ,

$$\lim_{N \rightarrow \infty} \|F - \sum_{n=0}^N \sum_{j=1}^{2n+1} F_{n,j} Y_{n,j}\|_{\mathcal{L}^2(\Omega)} = 0. \quad (3)$$

In other words, when  $N$  is large, the  $N$ -th truncation of the Fourier expansion of  $F \in \mathcal{L}^2(\Omega)$  in terms of spherical harmonics  $Y_{n,j}$

$$\sum_{n=0}^N \sum_{j=1}^{2n+1} F_{n,j} Y_{n,j}(\xi), \quad \xi \in \Omega$$

represents an approximation of  $F$ , and the sum

$$\sum_{n=0}^N F_{n,j} h^n Y_{n,j}(\xi), \quad x = h\xi, h = |x|, h < 1, \quad \xi \in \Omega$$

resp.

$$\sum_{n=0}^N F_{n,j} h^{-(n+1)} Y_{n,j}(\xi), \quad x = h\xi, h = |x|, h > 1, \quad \xi \in \Omega$$

is the uniquely determined solution of the inner resp. outer Dirichlet problem corresponding to this  $N$ -th truncated Fourier sum on  $\Omega$ . However, although Fourier expansion techniques are very powerful, there are some serious deficiencies of this approach, namely: the orthonormalization process and the recovery of the function are in many instances of very undesirable computational complexity, local changes of the function  $F$  will affect the whole table of orthogonal coefficients  $F_{n,j}$ . This shortcoming was already observed by (Gabor, 1946) who introduced the Gaussian kernel to "window" the Fourier integral.

## GABOR EXPANSION

In what follows we first derive an analogue to Gabor's technique, viz. spherical Gabor transform by use of the Abel-Poisson kernel, which will enable us to keep local changes of a function  $F$  on the unit sphere  $\Omega$  under control.

Let  $Q_h : [-1, +1] \rightarrow \mathbb{R}$ ,  $h \in (0, 1)$ , denote the Abel-Poisson kernel

$$Q_h(t) = \frac{1}{4\pi} \frac{1-h^2}{(1+h^2-2ht)^{3/2}} = \sum_{n=0}^{\infty} \frac{2n+1}{4\pi} h^n P_n(t), \quad (4)$$

where  $P_n$  is the Legendre-polynomial of degree  $n$ .  $Q_h$  is a nonnegative kernel satisfying

$$\int_{\Omega} Q_h(\xi \cdot \zeta) Q_{h'}(\eta \cdot \zeta) d\omega(\zeta) = Q_{hh'}(\xi \cdot \eta) \quad (5)$$

for all  $(\xi, \eta) \in \Omega \times \Omega$  and  $0 < h, h' < 1$ . Furthermore  $Q_h$  fulfils the "localization property"

$$\lim_{\substack{h \rightarrow 1 \\ h < 1}} \int_{-1}^{\delta} Q_h(t) dt = 0, \quad \delta \in (-1, +1). \quad (6)$$

Thus  $Q_h$  may be taken as a "cutoff function". Chopping up the function amounts to multiplying  $F \in \mathcal{L}^2(\Omega)$  by axisymmetric kernels  $Q_{h_0}(\xi \cdot \cdot) : \eta \mapsto Q_{h_0}(\xi \cdot \eta), \eta \in \Omega, h_0 \in (0, 1)$  around the axes  $\xi \in \Omega$ . In other words, we have to compute the "Gabor coefficients" of  $F$

$$(F, Q_{h_0}(\xi \cdot \cdot)Y_{n,j})_{\mathcal{L}^2(\Omega)} = \int_{\Omega} F(\eta)Q_{h_0}(\xi \cdot \eta)Y_{n,j}(\eta)d\omega(\eta), \xi \in \Omega, \quad (7)$$

using "rotations"  $R_\xi : Q_{h_0}(\eta \cdot \cdot) \mapsto R_\xi Q_{h_0}(\eta \cdot \cdot) = Q_{h_0}(\eta \cdot \xi)$  and "modulations"  $M_{n,j} : Q_{h_0}(\eta \cdot \cdot) \mapsto M_{n,j}Q_{h_0}(\eta \cdot \cdot) = Q_{h_0}(\eta \cdot \cdot)Y_{n,j}$ . The function  $F \in \mathcal{L}^2(\Omega)$  then is completely characterized by the Gabor coefficients and can be recovered by the *Gabor expansion* relative to the "mother wavelet"  $Q_{h_0}, h_0 \in (0, 1)$ , in the sense that

$$\lim_{N \rightarrow \infty} \|F - \sum_{n=0}^N \sum_{j=1}^{2n+1} \frac{1}{Q_{h_0^2}(1)} \int_{\Omega} \int_{\Omega} F(\zeta)Q_{h_0}(\eta \cdot \zeta)Y_{n,j}(\zeta)d\omega(\zeta)Q_{h_0}(\eta \cdot \cdot)d\omega(\eta)Y_{n,j}\|_{\mathcal{L}^2(\Omega)} = 0.$$

The spherical Gabor series works by first dividing a "signal"  $F \in \mathcal{L}^2(\Omega)$  into short consecutive segments (i.e. spherical caps) of fixed size and then computing the "expansion coefficients" of each segment. Therefore the spherical Gabor transform  $F \mapsto (\text{GT})(F)$  given by

$$((\text{GT})(F))_{n,j;\xi} = \frac{1}{\sqrt{Q_{h_0^2}(1)}} \int_{\Omega} F(\eta)Q_{h_0}(\eta \cdot \xi)Y_{n,j}(\eta)d\omega(\eta), F \in \mathcal{L}^2(\Omega), \xi \in \Omega, \quad (8)$$

is constructed in close orientation to its counterpart in Euclidean spaces which is known as the "Weyl-Heisenberg wavelet transform" (cf. e.g. (Heil and Walnut, 1989)). One problem with such a method is that much effort must be done to resolve phenomena shorter than the "window" (determined by the parameter  $h_0$ ). For a "moderate window" high modulations are required to increase the resolution especially if the "short-frequency phenomena" being investigated do not occur very often. That is one of the reasons why we are interested in alternate techniques.

## TOEPLITZ EXPANSION

Another technique of finding an approximation and its harmonic counterpart inside resp. outside  $\Omega$  may be based on the convolution of the Abel-Poisson kernel against the function  $F \in \mathcal{L}^2(\Omega)$  (cf. (Freedon and Schreiner, 1993)). More explicitly, from singular integral theory we are able to deduce that

$$\lim_{\substack{h \rightarrow 1 \\ h < 1}} \left\| \int_{\Omega} F(\zeta)Q_h(\zeta \cdot \cdot)d\omega(\zeta) - F \right\|_{\mathcal{L}^2(\Omega)} = 0 \quad (9)$$

and

$$\lim_{\substack{h \rightarrow 1 \\ h < 1}} \left\| \int_{\Omega} \int_{\Omega} F(\zeta)Q_h(\zeta \cdot \eta)d\omega(\zeta)Q_h(\eta \cdot \cdot)d\omega(\eta) - F \right\|_{\mathcal{L}^2(\Omega)} = 0. \quad (10)$$

Thus we see that the singular integrals are close to the function  $F$  provided that the value  $h$  is close to 1. Note that the function

$$\xi \mapsto \int_{\Omega} F(\zeta)Q_h(\xi \cdot \zeta)d\omega(\zeta), h = |x|, h < 1, \xi \in \Omega, \quad (11)$$

is the uniquely determined solution of the (inner) Dirichlet problem corresponding to the (continuous) boundary values  $F$  on  $\Omega$ . A similar result holds for the outer case. The right choice of the parameter  $h$  to find a good candidate for approximation by singular integrals, however, depends on a priori information about the function  $F$  which is usually not available. Consequently there is a practical need to develop "zooming in" techniques, although such an automatic approximation process probably leads to more computational complexity.

A first step are summability methods based on the concept of Toeplitz (cf. (Hardy, 1949)): let  $\{h_n\}, h_n \in (0, 1), n = 1, 2, \dots$  be a sequence converging to the limit 1 (for example,  $h_n = 1 - (\frac{1}{2})^n, n = 1, 2, \dots$ ). Furthermore, suppose that the elements  $t_{Tn}$  ( $1 \leq n \leq T$ ) of an infinite triangle matrix  $(t_{Tn})$  satisfy the following conditions:

$$t_{Tn} \rightarrow 0 \quad \text{as } T \rightarrow \infty \quad \text{for each } n$$

and

$$\begin{aligned} t_{Tn} &\geq 0 \quad \text{for all } T, 1 \leq n \leq T, \\ \sum_{n=1}^T t_{Tn} &= 1 \quad \text{for all } T. \end{aligned}$$

Then it follows easily that

$$\lim_{T \rightarrow \infty} \left\| \sum_{n=1}^T t_{Tn} \int_{\Omega} F(\zeta) Q_{h_n}(\zeta \cdot) d\omega(\zeta) - F \right\|_{L^2(\Omega)} = 0 \quad (12)$$

and

$$\lim_{T \rightarrow \infty} \left\| \sum_{n=1}^T t_{Tn} \int_{\Omega} \int_{\Omega} F(\zeta) Q_{h_n}(\zeta \cdot \eta) d\omega(\zeta) Q_{h_n}(\eta \cdot) d\omega(\eta) - F \right\|_{L^2(\Omega)} = 0 \quad (13)$$

hold for each  $F \in L^2(\Omega)$ .

The following examples for Toeplitz summation are of particular significance:

(i) arithmetical summation (Cauchy's example)

$$t_{Tn} = \frac{1}{T}, n = 1, \dots, T$$

(ii) binomial summation

$$(\alpha) \quad t_{Tn} = \frac{\binom{T-1}{n-1} z^{n-1}}{(1+z)^T}, n = 1, \dots, T, z > 0,$$

$$(\beta) \quad t_{Tn} = \frac{\binom{T-1}{n-1} z^{T-n}}{(1+z)^T}, n = 1, \dots, T, z > 0$$

(iii) Cesaro summation

$$t_{Tn} = \frac{\binom{T-n+k-2}{T-n-1}}{\binom{T-1-k}{T-1}}, n = 1, \dots, T, k \geq 1. \quad (14)$$

The Toeplitz singular integral transform  $F \mapsto (\text{TT})(F)$  given by

$$((\text{TT})(F))_{n;\xi} = \sqrt{t_{Tn}} \int_{\Omega} F(\eta) Q_{h_n}(\xi \cdot \eta) d\omega(\eta), \quad F \in \mathcal{L}^2(\Omega), \xi \in \Omega, h_n \in (0, 1), \quad (15)$$

acts as a localization procedure in the the following way. Roughly speaking, if  $n$  is large, then  $Q_{h_n}(\xi \cdot \zeta)$  seen as an axisymmetric function in the variable  $\zeta$  around the axis  $\xi$  is highly concentrated around the point  $\xi$ . As  $h_n$  approaches the value 1,  $Q_{h_n}(\xi \cdot \cdot)$  becomes more and more concentrated around  $\xi$ , so that  $F \in \mathcal{L}^2(\Omega)$  can be recovered in the following way

$$\lim_{T \rightarrow \infty} \|F - \sum_{n=1}^T \int_{\Omega} ((\text{TT})(F))_{n;\xi} \sqrt{t_{Tn}} Q_{h_n}(\xi \cdot \cdot) d\omega(\xi)\|_{\mathcal{L}^2(\Omega)} = 0.$$

Note that

$$\int_{\Omega} Q_{h_n}(\xi \cdot \zeta) d\omega(\zeta) = 1, \quad h_n \in (0, 1),$$

holds for all  $n$  and all  $\xi \in \Omega$ . Thus it behaves like a "small wave", and so the terminology "wavelet" has come into play in connection with the Abel-Poisson kernel. The Toeplitz singular integral transform displays the information of  $F$  at various levels of resolution (*multilevel method*). This means that the Toeplitz singular integral transform gives sharper and sharper resolution as  $h_n$  approaches the value 1. Obviously, the Toeplitz singular integral transform is generated from the "mother wavelet"  $Q_{h_0}$  by "dilations"  $D_n : Q_{h_0}(\xi) \mapsto D_n Q_{h_0}(\xi \cdot \cdot) = Q_{h_n}(\xi \cdot \cdot)$  and "rotations"  $R_\xi : Q_{h_0}(\eta \cdot \cdot) \mapsto Q_{h_0}(\eta \cdot \xi), \xi \in \Omega$ . The price to be paid for this multilevel method is a (somehow artificial) summation process, namely Toeplitz summation. On the other hand, as numerical experiences have shown for a large class of test examples (cf. (Brand, 1994)), Toeplitz summation causes a convergence acceleration compared with the original sequence of singular integral values.

## TOEPLITZ-GABOR EXPANSION

Of more theoretical concern than practical use is a combination of both the Toeplitz singular integral transform and the Gabor transform: given  $F \in \mathcal{L}^2(\Omega)$  and a sequence  $\{h_n\}$ ,  $h_n \in (0, 1)$ , converging to the limit 1 as  $n \rightarrow \infty$ , then  $F$  is representable (in the  $\mathcal{L}^2$ -sense) by the *Toeplitz-Gabor expansion*

$$\lim_{N \rightarrow \infty} \sum_{n=1}^T t_{Tn} \sum_{p=0}^N \sum_{q=1}^{2p+1} \frac{1}{Q_{h_n^2}(1)} \int_{\Omega} \int_{\Omega} F(\zeta) Q_{h_n}(\eta \cdot \zeta) Y_{p,q}(\zeta) d\omega(\zeta) Q_{h_n}(\eta \cdot \cdot) d\omega(\eta) Y_{p,q}.$$

The Toeplitz-Gabor transform  $F \mapsto (\text{TGT})(F)$  given by

$$((\text{TGT})(F))_{n;p,q;\xi} = \sqrt{\frac{t_{Tn}}{Q_{h_n^2}(1)}} \int_{\Omega} F(\eta) Y_{p,q}(\eta) Q_{h_n}(\eta \cdot \xi) d\omega(\eta), \quad \xi \in \Omega, \quad (16)$$

includes "rotations"  $R_\xi : Q_{h_0}(\eta \cdot \cdot) \mapsto Q_{h_0}(\eta \cdot \xi)$ , "modulations"  $M_{p,q} : Q_{h_0}(\eta \cdot \cdot) \mapsto Q_{h_0}(\eta \cdot \cdot) Y_{p,q}$ , and "dilations"  $D_n : Q_{h_0}(\eta \cdot \cdot) \mapsto Q_{h_n}(\eta \cdot \cdot)$ .

Obviously,

$$\lim_{\substack{T \rightarrow \infty \\ N \rightarrow \infty}} \left\| \sum_{n=1}^T \sqrt{\frac{t_{Tn}}{Q_{h_n^2}(1)}} \sum_{p=0}^N \sum_{q=1}^{2p+1} \int ((\text{TGT})(F))_{n;p,q;\xi} Q_{h_n}(\xi \cdot) d\omega(\xi) Y_{p,q} - F \right\|_{L^2(\Omega)} = 0,$$

so that the Toeplitz-Gabor series has the capability of "zooming in" on high frequency phenomena. From numerical point of view, however, the computational complexity is a serious deficiency.

## WAVELET EXPANSION

Finally we derive an approximation method by decomposing  $L^2(\Omega)$  by a nested sequence of approximating subspaces (*multiresolution analysis*). A more detailed approach to spherical wavelets can be found in (Freeden and Windheuser, 1995b). We want to show how some of the main ideas of the wavelet theory in Euclidean spaces carry over to the spherical case. The main difficulty is to implement "spherical dilations" as efficient as possible (quite similarly to techniques known from onedimensional wavelet theory). We start again from singular integral theory by considering

$$A_\rho(F)(\xi) = \int_{\Omega} B_\rho(\xi \cdot \eta) F(\eta) d\omega(\eta), \quad F \in L^2(\Omega), \quad (17)$$

where, by definition, we let

$$B_\rho(\xi \cdot \eta) = Q_{e^{-\rho}}(\xi \cdot \eta), \quad (\xi, \eta) \in \Omega^2, \quad \rho > 0.$$

The set  $\{A_\rho\}$ ,  $\rho > 0$ , forms a semigroup of contraction operators on  $L^2(\Omega)$  in the sense that (cf. (Pawelke, 1969))

- for each  $\rho \in (0, \infty)$ ,  $A_\rho$  is a linear bounded operator mapping  $L^2(\Omega)$  into itself ( $A_0 = I$  is the identity operator)
- for all  $0 < \rho_1, \rho_2 < \infty$

$$A_{\rho_1 + \rho_2} = A_{\rho_1} A_{\rho_2}$$

- for all  $F \in L^2(\Omega)$

$$\lim_{\substack{\rho \rightarrow \infty \\ \rho > 0}} \|A_\rho(F) - F\|_{L^2(\Omega)} = 0$$

- for all  $\rho \in (0, \infty)$  and  $F \in L^2(\Omega)$

$$\|A_\rho(F)\|_{L^2(\Omega)} \leq \|F\|_{L^2(\Omega)}.$$

In what follows the dyadic sequence

$$\rho_n = 2^{-n}, \quad n = 0, 1, \dots$$

and the functions

$$\begin{aligned} R_{\rho_{n-1}}(\xi \cdot \eta) &= B_{\rho_n}(\xi \cdot \eta) - B_{\rho_{n-1}}(\xi \cdot \eta), (\xi, \eta) \in \Omega^2, \\ S_{\rho_{n-1}}(\xi \cdot \eta) &= B_{\rho_n}(\xi \cdot \eta) + B_{\rho_{n-1}}(\xi \cdot \eta), (\xi, \eta) \in \Omega^2 \end{aligned}$$

play an important role. In fact it is not hard to see that the *scaling relations*

$$\int_{\Omega} B_{\rho_n}(\xi \cdot \zeta) B_{\rho_n}(\eta \cdot \zeta) d\omega(\zeta) = B_{2\rho_n}(\xi \cdot \eta) = B_{\rho_{n-1}}(\xi \cdot \eta), \quad (18)$$

$$\int_{\Omega} R_{\rho_n}(\xi \cdot \zeta) S_{\rho_n}(\eta \cdot \zeta) d\omega(\zeta) = R_{\rho_{n-1}}(\xi \cdot \eta) \quad (19)$$

hold for all  $(\xi, \eta) \in \Omega^2$ . Furthermore, by using these facts, it can be readily seen that

$$\begin{aligned} &\int_{\Omega} F(\zeta) B_{\rho_n}(\xi \cdot \zeta) d\omega(\zeta) \\ &= \int_{\Omega} F(\zeta) B_{\rho_0}(\xi \cdot \zeta) d\omega(\zeta) + \sum_{l=0}^{n-1} \int_{\Omega} F(\zeta) R_{\rho_l}(\xi \cdot \zeta) d\omega(\zeta), \xi \in \Omega. \end{aligned}$$

But this implies that (see also (Freeden and Windheuser, 1995a))

$$F = \int_{\Omega} F(\zeta) B_{\rho_0}(\zeta) d\omega(\zeta) + \sum_{l=0}^{\infty} \int_{\Omega} F(\zeta) R_{\rho_l}(\zeta) d\omega(\zeta) \quad (20)$$

(in the sense of  $\|\cdot\|_{L^2(\Omega)}$ ). The *wavelet transform*  $F \mapsto (\text{WT})(F)$  is defined by

$$((\text{WT})(F))_{0;\xi} = \int_{\Omega} F(\zeta) (R_{\rho_0}(\xi \cdot \zeta) + B_{\rho_0}(\xi \cdot \zeta)) d\omega(\zeta) \quad (21)$$

$$((\text{WT})(F))_{n;\xi} = \int_{\Omega} F(\zeta) R_{\rho_n}(\xi \cdot \zeta) d\omega(\zeta), n \geq 1. \quad (22)$$

Again,  $F$  is characterized by these values and can be recovered (in  $L^2(\Omega)$ -sense) by its "wavelet expansion"

$$F = \int_{\Omega} ((\text{WT})(F))_{0;\xi} (S_{\rho_0}(\xi) - B_{\rho_0}(\xi)) d\omega(\xi) + \sum_{n=1}^{\infty} \int_{\Omega} ((\text{WT})(F))_{n;\xi} S_{\rho_n}(\xi) d\omega(\xi).$$

Indeed, in analogy to the wavelet theory in Euclidean spaces,  $B_{\rho_k}$ ,  $R_{\rho_k}$ , and  $S_{\rho_k}$  may be interpreted as "scaling function", "decomposition wavelet" and "reconstruction wavelet", respectively. Apart from the starting term the wavelet transform is characterized by dilations and rotations of the "mother wavelet"  $R_{\rho_0}$ .

All kernels  $\{B_{\rho_k}\}$ ,  $\{R_{\rho_k}\}$ , and  $\{S_{\rho_k}\}$  possess the localization property mentioned above. The wavelet series has the capability of "zooming in" on "short lived high frequency phenomena" and "zooming out" in low frequency environment. Here it should be noted that

$$\int_{\Omega} B_{\rho_k}(\xi \cdot \eta) d\omega(\eta) = 1, \quad (23)$$

$$\int_{\Omega} R_{\rho_k}(\xi \cdot \eta) d\omega(\eta) = 0 \quad (24)$$

for all nonnegative  $k$  and all  $\xi \in \Omega$ . In other words, although the Abel-Poisson kernel is of constant area for all nonnegative  $k$ , the wavelet series automatically narrows its "window" when  $k$  increases. Moreover, the wavelets  $R_{\rho_k}$  act as frequency localization since only a finite number of significant orders occurs when localization in frequency space is characterized in terms of spherical harmonics. This is exactly what is needed to study irregularities in the reconstruction of a function (signal)  $F \in \mathcal{L}^2(\Omega)$ .

Finally it should be mentioned that our approach enables us to develop a multiresolution analysis (MRA) so that both a sequence of nested subspaces and the "complementary subspaces", respectively, are generated from a single function, viz. the Abel-Poisson kernel. More explicitly,

$$V_k = \{H * B_{\rho_{k-1}} \mid H \in \mathcal{L}^2(\Omega)\}$$

and

$$W_k = \{H * R_{\rho_{k-1}} \mid H \in \mathcal{L}^2(\Omega)\}$$

satisfy the following properties:

$$\begin{aligned} V_0 &\subset \dots \subset V_{k-1} \subset V_k \subset V_{k+1} \subset \dots \subset \mathcal{L}^2(\Omega), \\ \overline{\bigcup_{k=0}^{\infty} V_k}^{\|\cdot\|_{\mathcal{L}^2(\Omega)}} &= \mathcal{L}^2(\Omega), \\ \bigcap_{k=0}^{\infty} V_k &= V_0. \end{aligned}$$

It is easily seen that

$$V_{k+1} = V_k + W_k, \quad (25)$$

where the sum decomposition is neither orthogonal nor direct. From our construction it can be readily deduced that

$$\begin{aligned} V_k &= \left\{ \int_{\Omega} (H, B_{\rho_k}(\xi \cdot))_{\mathcal{L}^2(\Omega)} B_{\rho_k}(\xi \cdot) | H \in \mathcal{L}^2(\Omega) \right\} \end{aligned} \quad (26)$$

$$\begin{aligned} &= \left\{ \int_{\Omega} G(\xi) B_{\rho_k}(\xi \cdot) d\omega(\xi) | G \in V_{k+1} \right\} \end{aligned} \quad (27)$$

and

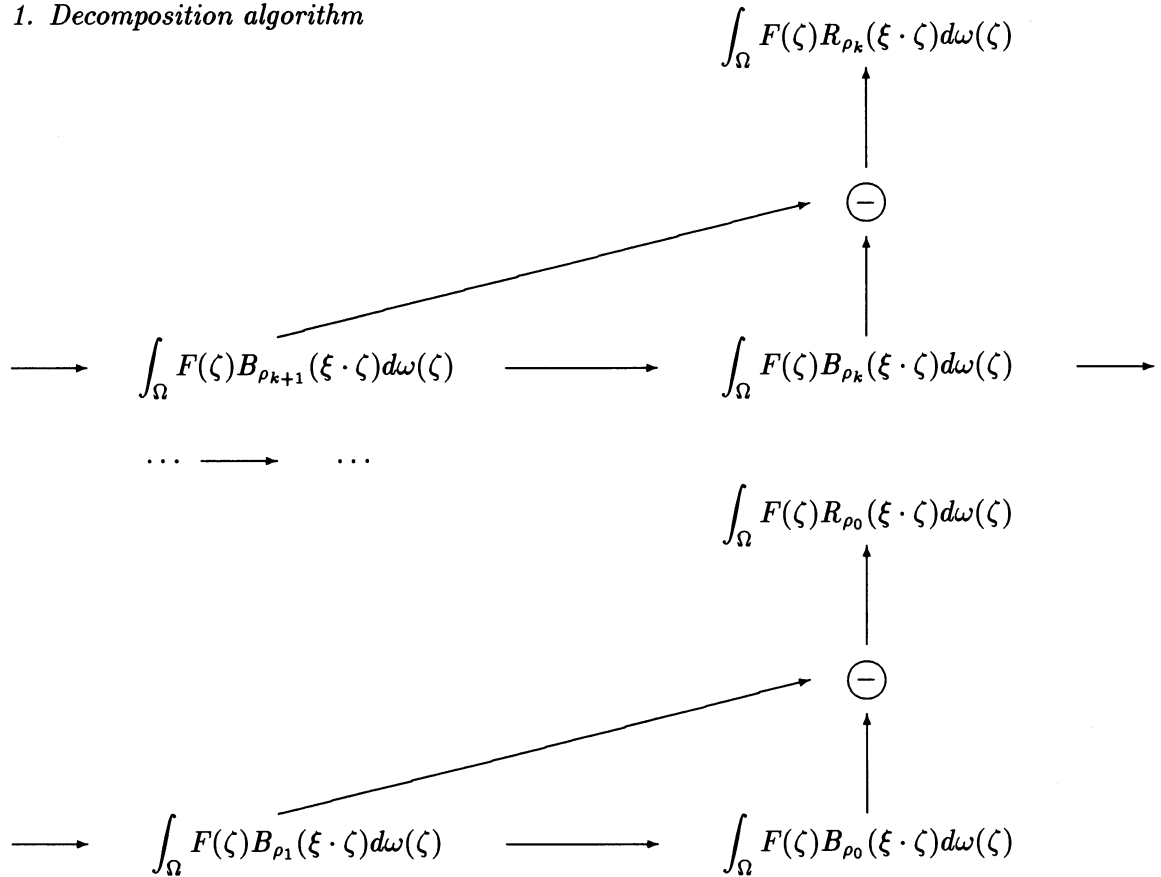
$$\begin{aligned} W_k &= \left\{ \int_{\Omega} (H, R_{\rho_k}(\xi \cdot))_{\mathcal{L}^2(\Omega)} S_{\rho_k}(\xi \cdot) d\omega(\xi) | H \in \mathcal{L}^2(\Omega) \right\} \end{aligned} \quad (28)$$

$$\begin{aligned} &= \left\{ \int_{\Omega} G(\xi) S_{\rho_k}(\xi \cdot) d\omega(\xi) | G \in V_{k+1} \right\}. \end{aligned}$$

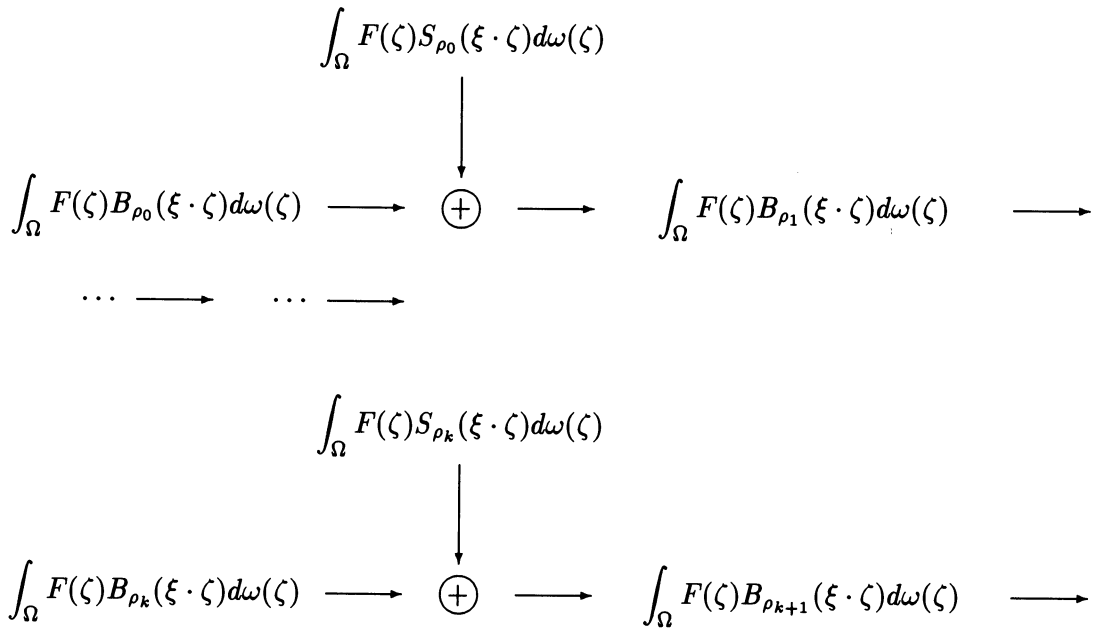
For numerical purposes it is of importance that a decomposition algorithm resp. reconstruction algorithm can be formulated according to the well-known Mallat-scheme. Seen in comparison to the classical Mallat-scheme, however, the filters are level dependent.

Since all our approximation methods developed above are based on the Abel-Poisson kernel, it is straightforward to determine the uniquely determined harmonic function inside (outside)  $\Omega$  having (a continuous approximation of)  $F$  as "boundary function" on  $\Omega$ . In other words, our methods enable us to derive at the same time both a continuous approximation of an  $L^2$ -function on the (unit) sphere and the solution of the Dirichlet problem corresponding to this approximation on the spherical boundary.

### 1. Decomposition algorithm



## 2. Reconstruction algorithm



## REFERENCES

- Brand, R. (1994). Approximation Using Spherical Singular Integrals and Its Application to Digital Terrain Modelling, *Diploma Thesis*, University of Kaiserslautern, Geomathematics Group
- Freedon, W. and Schreiner, M. (1993). Nonorthogonal Expansions on the Sphere, *AGTM-Report 97*, University of Kaiserslautern, Geomathematics Group, Math. Meth. in the Appl. Sci. (accepted for publication)
- Freedon, W. and Windheuser, U. (1995a). Earth's Gravitational Potential and It's MRA Approximation by Harmonic Singular Integrals, *ZAMM 75*, S633–S634
- Freedon, W. and Windheuser, U. (1995b). Spherical Wavelet Transform and Its Dicretization, *AGTM-Report 125*, University of Kaiserslautern, Laboratory of Technomathematics, Geomathematics Group
- Gabor, D. (1946). Theory of Communications, *J. Inst. Elec. Eng. (London) 93*, 429–457
- Hardy, G.H. (1949). *Divergent Series*, Oxford, Clarendon Press
- Pawelke, S. (1969). Saturation and Approximation bei Reihen mehrdimensionaler Kugelfunktionen, *PhD-thesis*, RWTH Aachen
- Heil, C.E. and Walnut, D.F. (1989). Continuous and Discrete Wavelet Transforms, *SIAM Review, 31*, No. 4, 628–666

# SATELLITE GRADIOMETRY — A NEW APPROACH

Willi Freeden and Michael Schreiner

University of Kaiserslautern

Laboratory of Technomathematics, Geomathematics Group

P.O.-Box 3049, 67653 Kaiserslautern, Germany

## INTRODUCTION

The determination of the gravitational field of the earth by satellite gradiometry has been investigated in many publications (cf. e.g. (Rummel, 1986; Rummel et al., 1993) and the literature cited therein). These contributions mostly deal with the gravitational field as finite series in terms of spherical harmonics and assume that the data are given in discrete points. In this paper, we study two different aspects of satellite gradiometry. At first, we consider the data to be given as continuous function on a surface in the harmonicity domain of the potential. This enables us to classify which types of data guarantee the uniqueness of the solution. Needless to say that those investigations turn also out to be of importance for the discrete problem. Then we propose a method for the determination of the gravitational field by use of locally supported trial functions in satellite gradiometry. We expect that such methods will significantly improve the knowledge of the microstructure of the earth's gravitational field in the future.

## PRELIMINARIES

We start with introducing some abbreviations used in this contribution.

For  $R > 0$ , let  $\Omega_R$  be the sphere around the origin with radius  $R$  in  $\mathbb{R}^3$  with surface measure  $d\omega_R$  and let  $\Omega_R^{\text{ext}}$  denote its outer space, i.e.  $\Omega_R^{\text{ext}} = \{x \in \mathbb{R}^3 \mid |x| > R\}$ . If  $R = 1$ , we simply write  $\Omega = \Omega_1$  and  $d\omega = d\omega_1$ . Points on the unit sphere  $\Omega$  are usually denoted by greek letters.  $\otimes$  means the dyadic or tensor product for vectors in  $\mathbb{R}^3$ , while the inner product in  $\mathbb{R}^3$  and in  $\mathbb{R}^3 \otimes \mathbb{R}^3$  is designated by  $\cdot$ .

In what follows, we are concerned with functions  $F : \Omega_R \rightarrow \mathbb{R}$ , vector fields  $f : \Omega_R \rightarrow \mathbb{R}^3$ , and tensor fields  $\mathbf{f} : \Omega_R \rightarrow \mathbb{R}^3 \otimes \mathbb{R}^3$ , defined on the sphere  $\Omega_R$ . If possible, we use capital letters to denote scalar quantities and small resp. small boldface letters to indicate vector resp. tensor valued quantities. We consider the spaces  $C^{(\infty)}(\Omega_R)$  ( $c^{(\infty)}(\Omega_R)$ , resp.  $\mathbf{c}^{(\infty)}(\Omega_R)$ ) of infinitely often differentiable functions (vector fields resp. tensor fields) on the sphere  $\Omega_R$ . The space of square-integrable functions (vector fields resp. tensor fields) is denoted by  $\mathcal{L}^2(\Omega_R)$  ( $l^2(\Omega_R)$  resp.  $\mathbf{l}^2(\Omega_R)$ ). They are Hilbert spaces with respect to the usual inner products  $(\cdot, \cdot)_{\mathcal{L}^2(\Omega_R)}$  ( $(\cdot, \cdot)_{l^2(\Omega_R)}$  resp.  $(\cdot, \cdot)_{\mathbf{l}^2(\Omega_R)}$ ). We shall also make use of the space

$\mathcal{C}^{(\infty)}(\Omega_R^{\text{ext}})$  consisting of infinitely often differentiable functions in  $\Omega_R^{\text{ext}}$ , and  $\mathcal{C}^{(0)}(\overline{\Omega_R^{\text{ext}}})$ , the space of continuous functions in  $\overline{\Omega_R^{\text{ext}}}$ .

The set of spherical harmonics of order  $n$  defined on  $\Omega$  is denoted by  $\text{Harm}_n$ . We assume that  $\{Y_{n,j}\}_{n=0,1,\dots, j=1,\dots,2n+1}$  forms a complete  $L^2(\Omega)$ -orthonormal system of spherical harmonics.

When dealing with tangential tensor fields on the sphere, it turns out that a decomposition with respect to certain differential operators makes the calculations easy. In order to define these operators, the use of the Riemannian structure of the sphere is of advantage. For the convenience of the reader, we therefore give a short review on these topics. More information can be found e.g. in (Spivak, 1975).

Let  $x^1, x^2$  be local coordinates of a coordinate patch around  $\xi \in \Omega$ . The *tangential space*  $T_\xi\Omega$  of  $\Omega$  at the point  $\xi$  is spanned by the basis  $\frac{\partial}{\partial x^1}(\xi), \frac{\partial}{\partial x^2}(\xi)$ , i.e. we have  $T_\xi\Omega = \text{span}\left(\frac{\partial}{\partial x^1}(\xi), \frac{\partial}{\partial x^2}(\xi)\right)$ . Its dual, the co-tangential space at the point  $\xi$ , is denoted by  $T_\xi^*\Omega$ . Of course, we have  $T_\xi^*\Omega = \text{span}(dx^1(\xi), dx^2(\xi))$ . The tangential bundle  $T\Omega$  and the co-tangential bundle  $T^*\Omega$  are defined as usual by the disjoint union of the tangential spaces or the co-tangential spaces, respectively. Loosely speaking, we attach at each point  $\xi \in \Omega$  the corresponding tangential space or co-tangential space on the unit sphere  $\Omega$ . The  $(p,q)$ -*tensor bundle* (i.e.  $p$  contravariant and  $q$  covariant components) is denoted by  $\bigotimes^p T\Omega \otimes \bigotimes^q T^*\Omega$ , ( $p, q \geq 0$ ). For convenience, we set  $\bigotimes^0 T\Omega = \mathcal{C}^{(\infty)}(\Omega)$ . Using local coordinates, we have for  $\mathbf{f} \in \bigotimes^p T\Omega \otimes \bigotimes^q T^*\Omega$ , the usual expression

$$\mathbf{f}(\xi) = \sum_{\alpha_1 \dots \alpha_p} \sum_{\beta_1 \dots \beta_q} F_{\beta_1 \dots \beta_q}^{\alpha_1 \dots \alpha_p}(\xi) \frac{\partial}{\partial x^{\alpha_1}}(\xi) \otimes \dots \otimes \frac{\partial}{\partial x^{\alpha_p}}(\xi) \otimes dx^{\beta_1}(\xi) \otimes \dots \otimes dx^{\beta_q}(\xi) \quad (1)$$

with functions  $F_{\beta_1 \dots \beta_q}^{\alpha_1 \dots \alpha_p} \in \mathcal{C}^{(\infty)}(\Omega)$ .

The induced Riemannian metric is the covariant tensor  $\mathbf{g}$ , which in local coordinates is given by  $\mathbf{g}(\xi) = \sum_{i,k=1}^2 G_{ik}(\xi) dx^i(\xi) \otimes dx^k(\xi)$ , where  $G_{ik}(\xi) = \frac{\partial}{\partial x^i}(\xi) \cdot \frac{\partial}{\partial x^k}(\xi)$ . The inverse of the matrix  $G_{ik}(\xi)$  is denoted by  $G^{ik}(\xi)$ ,  $\xi \in \Omega$ . If no confusion is likely to arise, we omit the argument  $\xi$  in the following.

The Riemannian metric defines the canonical isomorphism between  $T_\xi\Omega$  and its dual  $T_\xi^*\Omega$ , and hence between  $T\Omega$  and  $T^*\Omega$ . So we do not have to distinguish between co- and contravariant tensors. We just have co- or contravariant representations of tensor components.

Contractions  $c_{i,k}$ ,  $i = 1, \dots, p$ ,  $k = 1, \dots, q$  are linear maps

$$c_{i,k} : \bigotimes^p T\Omega \otimes \bigotimes^q T^*\Omega \longrightarrow \bigotimes^{p-1} T\Omega \otimes \bigotimes^{q-1} T^*\Omega,$$

defined as follows: let  $\mathbf{f} \in \bigotimes^p T\Omega \otimes \bigotimes^q T^*\Omega$  be of the form (1). Then we define as usual

$$\begin{aligned}
c_{i,k} \mathbf{f} = & \sum_{k=1}^2 \sum_{\alpha_1, \dots, \alpha_{i-1}, \alpha_{i+1}, \dots, \alpha_p} \sum_{\beta_1, \dots, \beta_{k-1}, \beta_{k+1}, \dots, \beta_q} F_{\beta_1 \dots k \dots \beta_q}^{\alpha_1 \dots k \dots \alpha_p} \\
& \frac{\partial}{\partial x^{\alpha_1}} \otimes \dots \otimes \frac{\partial}{\partial x^{\alpha_{i-1}}} \otimes \frac{\partial}{\partial x^{\alpha_{i+1}}} \otimes \dots \otimes \frac{\partial}{\partial x^{\alpha_p}} \otimes \\
& dx^{\beta_1} \otimes \dots \otimes dx^{\beta_{k-1}} \otimes dx^{\beta_{k+1}} \otimes \dots \otimes dx^{\beta_q}.
\end{aligned}$$

Since we look at the co- and contravariant components of a tensor as different representations of the same object, we can use the contraction operator also for the contraction of two covariant or contravariant components. In doing so, the Riemannian metric has to be taken into account what in literature is often called the raising and lowering of indices.

Besides the surface identity tensor  $\mathbf{i}_{\text{tan}} = \mathbf{g}$  the surface rotation tensor  $\mathbf{j}_{\text{tan}}$  which in Riemannian geometry is usually called  $\varepsilon$ -tensor is of importance in the following considerations. For completeness we give its coordinate expression. We have

$$\mathbf{j}_{\text{tan}} = \pm \sqrt{\det(G_{ik})} (dx^1 \otimes dx^2 - dx^2 \otimes dx^1), \quad (2)$$

where we assume that the sign is chosen in such a way that for a vector field  $v \in T\Omega$ , we have

$$c_{2,3} \mathbf{j}_{\text{tan}}(\xi) \otimes v(\xi) = \xi \times v(\xi), \quad \xi \in \Omega. \quad (3)$$

The sign of this equality is, of course, defined by the orientation of the basis  $x^1, x^2$ .

Let  $u \in T\Omega$  be a vector field. Then the derivative of a function  $F \in C^{(\infty)}(\Omega)$  at the point  $\xi$  in direction  $u(\xi)$  is given by

$$dF(u)(\xi) = \sum_{i=1}^2 U^i(\xi) \frac{\partial}{\partial x^i} F(\xi),$$

where the representation of  $u$  in local coordinates is  $u(\xi) = \sum U^i(\xi) \frac{\partial}{\partial x^i}(\xi)$ . By linearity it is clear, that  $dF \in T^*\Omega$ .

The natural generalization for the derivation of vector fields is the *covariant derivative*. If  $v \in T\Omega$  is another vector field given in local coordinates by  $v(\xi) = \sum_i V^i(\xi) \frac{\partial}{\partial x^i}(\xi)$ , then the covariant derivative of  $v$  in direction  $u$  reads

$$\nabla_u^* v = \sum_i \left( \sum_j U^j \frac{\partial V^i}{\partial x^j} + \sum_{j,k} \Gamma_{jk}^i U^j V^k \right) \frac{\partial}{\partial x^i},$$

where the functions  $\Gamma_{jk}^i$  are defined by the relation

$$\nabla_{\frac{\partial}{\partial x^j}}^* \frac{\partial}{\partial x^k} = \sum_i \Gamma_{jk}^i \frac{\partial}{\partial x^i}.$$

The functions  $\Gamma_{jk}^i$  are the *Christoffel symbols*. They are given by (cf. e.g. (Spivak, 1975))

$$\Gamma_{jk}^i = \frac{1}{2} \sum_l G^{il} \left( \frac{\partial}{\partial x^j} G_{kl} + \frac{\partial}{\partial x^k} G_{lj} - \frac{\partial}{\partial x^l} G_{jk} \right).$$

It follows that the covariant derivative is a mapping

$$\nabla^* : T\Omega \longrightarrow T^*\Omega \otimes T\Omega,$$

or, by the isomorphism described before,

$$\nabla^* : T\Omega \longrightarrow \bigotimes^2 T\Omega.$$

The definition of  $\nabla^*$  can be extended to tensors of rank  $\geq 2$  by the *product rule*. For any tensors  $\mathbf{f}$  and  $\mathbf{h}$  and any vector field  $u \in T\Omega$  we have by definition

$$\nabla_u^* (\mathbf{f} \otimes \mathbf{h}) = \nabla_u^* \mathbf{f} \otimes \mathbf{h} + \mathbf{f} \otimes \nabla_u^* \mathbf{h}. \quad (4)$$

In the following, we also use the symbol  $\nabla^*$  for the differential of a function, i.e., for  $F \in C^{(\infty)}(\Omega)$  we set  $\nabla^* F = dF$ , so that the symbol  $\nabla^*$  is defined for functions, vector fields and tensor fields of any rank.

The combination of covariant derivation together with rotation will become important later on. We introduce the operator  $L^*$  by

$$L^* = c_{2,3} j_{tan} \otimes \nabla^*.$$

Roughly speaking, the operator  $L^*$  first applies the covariant derivative and rotates then the first tensor component with respect to  $j_{tan}$ . In the same way as  $\nabla^*$ , the operator  $L^*$  can be applied to functions, vector fields, and tensors of any rank.

*It is of basic importance, that all these definitions are independent of any choice of spherical coordinates.* Thus, no problems from singularities appear. However, for the convenience of the reader, we state the representations of our definitions using the local spherical coordinates

$$\begin{aligned} (-1, 1) \times (0, 2\pi) &\longrightarrow \mathbb{R}^3 \\ (t, \varphi) &\longmapsto \begin{pmatrix} \sqrt{1-t^2} \cos \varphi \\ \sqrt{1-t^2} \sin \varphi \\ t \end{pmatrix}. \end{aligned} \quad (5)$$

We will perform all calculations with respect to the covariant basis. One easily obtains for the modulus of  $dt$  and  $d\varphi$ , respectively,

$$|dt| = \sqrt{1-t^2}, \quad |d\varphi| = \frac{1}{\sqrt{1-t^2}}. \quad (6)$$

Thus, the expressions of  $i_{tan}$  and  $j_{tan}$  are (in pure covariant form)

$$i_{tan}(t, \varphi) = \frac{1}{1-t^2} dt \otimes dt + (1-t^2) d\varphi \otimes d\varphi, \quad j_{tan}(t, \varphi) = d\varphi \otimes dt - dt \otimes d\varphi.$$

Since  $dt$  and  $d\varphi$  are orthogonal, we get the contractions

$$\mathbf{c}_{1,2}(d\varphi \otimes dt) = \mathbf{c}_{1,2}(dt \otimes d\varphi) = 0.$$

Furthermore, it follows from (6) that

$$\begin{aligned}\mathbf{c}_{1,2}(dt \otimes dt) &= 1 - t^2 \\ \mathbf{c}_{1,2}(d\varphi \otimes d\varphi) &= \frac{1}{1 - t^2}.\end{aligned}$$

As it is well-known, the differential  $\nabla^* F$  (i.e. the surface gradient in covariant form) of a function  $F \in C^{(\infty)}(\Omega)$  is

$$\nabla^* F(t, \varphi) = \frac{\partial}{\partial t} F(t, \varphi) dt + \frac{\partial}{\partial \varphi} F(t, \varphi) d\varphi.$$

Thus, we obtain for  $L^* F$

$$\begin{aligned}L^* F(t, \varphi) &= \mathbf{c}_{2,3} \mathbf{j}_{\tan} \otimes \nabla^* F(t, \varphi) \\ &= \mathbf{c}_{2,3} \left( \frac{\partial}{\partial t} F(t, \varphi) (d\varphi \otimes dt \otimes dt - dt \otimes d\varphi \otimes dt) \right. \\ &\quad \left. + \frac{\partial}{\partial \varphi} F(t, \varphi) (d\varphi \otimes dt \otimes d\varphi - dt \otimes d\varphi \otimes d\varphi) \right) \\ &= \frac{\partial}{\partial t} F(t, \varphi) (\mathbf{c}_{2,3} (d\varphi \otimes dt \otimes dt) - \mathbf{c}_{2,3} (dt \otimes d\varphi \otimes dt)) \\ &\quad + \frac{\partial}{\partial \varphi} F(t, \varphi) (\mathbf{c}_{2,3} (d\varphi \otimes dt \otimes d\varphi) - \mathbf{c}_{2,3} (dt \otimes d\varphi \otimes d\varphi)) \\ &= \left( \frac{\partial}{\partial t} F(t, \varphi) \right) (1 - t^2) d\varphi - \left( \frac{\partial}{\partial \varphi} F(t, \varphi) \right) \frac{1}{1 - t^2} d\varphi \\ &= -\frac{1}{1 - t^2} \frac{\partial}{\partial \varphi} F(t, \varphi) dt + (1 - t^2) \frac{\partial}{\partial t} F(t, \varphi) d\varphi.\end{aligned}$$

The application of  $\nabla^*$  and  $L^*$  for tangential vector fields can be easily performed using the Christoffel symbols defined by the Riemannian metric. If the vector field  $f \in C^{(\infty)}(\Omega)$  is of the form  $f(t, \varphi) = F_t(t, \varphi)dt + F_\varphi(t, \varphi)d\varphi$  for  $t \in (-1, 1)$  and  $\varphi \in (0, 2\pi)$  it follows that

$$\begin{aligned}\nabla^* f(t, \varphi) &= \left( \frac{\partial}{\partial t} F_t(t, \varphi) - \frac{t}{1 - t^2} F_t(t, \varphi) \right) dt \otimes dt \\ &\quad + \left( \frac{\partial}{\partial t} F_\varphi(t, \varphi) + \frac{t}{1 - t^2} F_\varphi(t, \varphi) \right) dt \otimes d\varphi \\ &\quad + \left( \frac{\partial}{\partial \varphi} F_t(t, \varphi) + \frac{t}{1 - t^2} F_\varphi(t, \varphi) \right) d\varphi \otimes dt \\ &\quad + \left( \frac{\partial}{\partial \varphi} F_\varphi(t, \varphi) - t(1 - t^2) F_t(t, \varphi) \right) d\varphi \otimes d\varphi\end{aligned}$$

and

$$\begin{aligned}
\mathsf{L}^* f(t, \varphi) = & \left( -\frac{1}{1-t^2} \frac{\partial}{\partial \varphi} F_t(t, \varphi) - \frac{t}{1-t^2} F_\varphi(t, \varphi) \right) dt \otimes dt \\
& + \left( -\frac{1}{1-t^2} \frac{\partial}{\partial \varphi} F_\varphi(t, \varphi) + t F_t(t, \varphi) \right) dt \otimes d\varphi \\
& + \left( (1-t^2) \frac{\partial}{\partial t} F_t(t, \varphi) - t F_t(t, \varphi) \right) d\varphi \otimes dt \\
& + \left( (1-t^2) \frac{\partial}{\partial t} F_\varphi(t, \varphi) + t F_\varphi(t, \varphi) \right) d\varphi \otimes d\varphi.
\end{aligned}$$

## SATELLITE GRADIOMETRY AS A CONTINUOUS PROBLEM

The study of a continuous satellite gradiometry problem is not only of mathematical interest but also gives valuable information for the situation with discrete measurements. We shall show in this section, that the measurements of second order directional derivatives (as it is the case in the planned STEP experiment) do in general not ensure the uniqueness of the solution. Thus, in these cases, there are subspaces of harmonic functions which cannot be observed by data of this type. And this is, in particular, true for the discrete case.

Let us develop the problem in a simple geometric setting: let  $\Omega_R$ ,  $0 < R < 1$  denote the surface of the spherical earth, and assume that the gradiometer measurements are given on  $\Omega$ . (This scaling simplifies the forthcoming notations.) A reasonable formulation could read as follows:

let  $\mu \in c^{(\infty)}(\Omega)$  be a smooth vector field on  $\Omega$  with  $|\mu(\xi)| = 1$ ,  $\xi \in \Omega$ . Determine a function  $U \in \mathcal{C}^{(\infty)}(\Omega_R^{\text{ext}}) \cap \mathcal{C}^{(0)}(\bar{\Omega}_R^{\text{ext}})$  satisfying  $\Delta U = 0$  in  $\Omega_R^{\text{ext}}$  and  $|U(x)| = O(1/|x|)$  as  $|x| \rightarrow \infty$ , uniformly with respect to all directions, from the prescribed values

$$\mu^T(\xi) \mathbf{Hess} U(\xi) \mu(\xi), \quad \xi \in \Omega.$$

The question is now whether the function  $U$  is uniquely determined by this condition or not.

It can be shown that the answer of this question is “yes” if  $\mu(\xi) = \xi$  for all  $\xi \in \Omega$ , i.e. the second order radial derivatives are given. But this must be regarded as a special case, since the uniqueness of the solution cannot be established in the case of a general vector field. In order to verify this, suppose that  $U \in \mathcal{C}^{(\infty)}(\Omega_R^{\text{ext}})$  is an arbitrarily given harmonic function. The tensor  $\mathbf{Hess} U(\xi)$  is a real symmetric matrix for every  $\xi \in \Omega$ . Thus, for every  $\xi \in \Omega$  there exists an orthogonal matrix  $A(\xi) \in \mathbb{R}^3 \otimes \mathbb{R}^3$  such that

$$A^T(\xi) \mathbf{Hess} U(\xi) A(\xi) = \text{diag}(\lambda_1(\xi), \lambda_2(\xi), \lambda_3(\xi)),$$

where  $\lambda_1(\xi), \lambda_2(\xi), \lambda_3(\xi)$  are the eigenvalues of  $\mathbf{Hess} U(\xi)$ . From the harmonicity of  $U$  it is clear that  $\text{trace } \mathbf{Hess} U(\xi) = 0$  or, equivalently,  $\lambda_1(\xi) + \lambda_2(\xi) + \lambda_3(\xi) = 0$  for all  $\xi \in \Omega$ .

Let  $\mu_0 = 3^{-1/2}(1, 1, 1)^T$ . We define the vector field  $\mu : \Omega \rightarrow \mathbb{R}$  by  $\mu(\xi) = A(\xi)\mu_0$ ,  $\xi \in \Omega$ . Then it holds

$$\begin{aligned}
\mu^T(\xi) \mathbf{Hess} U(\xi) \mu(\xi) &= \mu_0^T A^T(\xi) \mathbf{Hess} U(\xi) A(\xi) \mu_0 \\
&= \mu_0^T \text{diag}(\lambda_1(\xi), \lambda_2(\xi), \lambda_3(\xi)) \mu_0 \\
&= \frac{1}{3} (\lambda_1(\xi) + \lambda_2(\xi) + \lambda_3(\xi)) \\
&= 0.
\end{aligned}$$

Hence we have constructed a vector field  $\mu$  such that the second order directional derivative of  $U$  in the direction of  $\mu(\xi)$  is zero for every point  $\xi \in \Omega$ . It can be easily seen that for a given  $U$  there exist many vector fields leading to the same uniqueness problems as the vector field  $\mu$ . Observing these arguments we are led to the conclusion that the function  $U$  is undetectable from the directional derivatives corresponding to  $\mu$ . So this approach is not appropriate.

It is, however, good news that we are not lost here. As a matter of fact there do exist conditions under which only one quantity of the Hesse matrix yields a unique solution (at least up to low order spherical harmonics). In order to formulate these results, a certain decomposition of the Hesse tensor is necessary, which strongly depends on the separability of the Laplace operator with respect to polar coordinates.

We define operators  $\mathbf{o}^{(i,k)} : \mathcal{C}^{(\infty)}(\Omega) \rightarrow \mathbf{c}^{(\infty)}(\Omega)$ ,  $i, k = 1, 2, 3$ , transforming functions into tensor fields by

$$\begin{aligned}
\mathbf{o}^{(1,1)}F(\xi) &= \xi \otimes \xi F(\xi) & \mathbf{o}^{(2,2)}F(\xi) &= \mathbf{i}_{\tan}(\xi)F(\xi) \\
\mathbf{o}^{(1,2)}F(\xi) &= \xi \otimes \nabla^*F(\xi) & \mathbf{o}^{(2,3)}F(\xi) &= (\nabla^*\nabla^* - \mathbf{L}^*\mathbf{L}^*)F(\xi) \\
\mathbf{o}^{(1,3)}F(\xi) &= \xi \otimes \mathbf{L}^*F(\xi) & \mathbf{o}^{(3,2)}F(\xi) &= (\nabla^*\mathbf{L}^* + \mathbf{L}^*\nabla^*)F(\xi) \\
\mathbf{o}^{(2,1)}F(\xi) &= \nabla^*F(\xi) \otimes \xi & \mathbf{o}^{(3,3)}F(\xi) &= \mathbf{j}_{\tan}(\xi)F(\xi).
\end{aligned}$$

For the definition of the tangential operators see also (Backus, 1966; Backus, 1967), where related decomposition problems have been considered.

Again, we illustrate these coordinate-free definitions using the same local coordinates as before. We obtain

$$\begin{aligned}
\mathbf{o}^{(1,1)}F(t, \varphi) &= F(t, \varphi)\xi \otimes \xi \\
\mathbf{o}^{(1,2)}F(t, \varphi) &= \frac{\partial}{\partial t}F(t, \varphi)\xi \otimes dt + \frac{\partial}{\partial \varphi}F(t, \varphi)\xi \otimes d\varphi \\
\mathbf{o}^{(1,3)}F(t, \varphi) &= -\frac{1}{1-t^2}\frac{\partial}{\partial t'\varphi}F(t, \varphi)\xi \otimes dt + (1-t^2)\frac{\partial}{\partial t}F(t, \varphi)\xi \otimes d\varphi \\
\mathbf{o}^{(2,1)}F(t, \varphi) &= \frac{\partial}{\partial t}F(t, \varphi)dt \otimes \xi + \frac{\partial}{\partial \varphi}F(t, \varphi)d\varphi \otimes \xi \\
\mathbf{o}^{(3,1)}F(t, \varphi) &= -\frac{1}{1-t^2}\frac{\partial}{\partial t'\varphi}F(t, \varphi)dt \otimes \xi + (1-t^2)\frac{\partial}{\partial t}F(t, \varphi)d\varphi \otimes \xi
\end{aligned}$$

$$\begin{aligned}
\bullet^{(2,2)} F(t, \varphi) &= \frac{1}{1-t^2} F(t, \varphi) dt \otimes dt + (1-t^2) F(t, \varphi) d\varphi \otimes d\varphi \\
\bullet^{(2,3)} F(t, \varphi) &= \left( \frac{\partial^2}{\partial t^2} F(t, \varphi) - \frac{1}{(1-t^2)^2} \frac{\partial^2}{\partial \varphi^2} F(t, \varphi) \right) dt \otimes dt \\
&\quad + 2 \left( \frac{\partial^2}{\partial t \partial \varphi} F(t, \varphi) + \frac{t}{1-t^2} \frac{\partial}{\partial \varphi} \right) (dt \otimes d\varphi + d\varphi \otimes dt) \\
&\quad + \left( -(1-t^2)^2 \frac{\partial^2}{\partial t^2} F(t, \varphi) + \frac{\partial^2}{\partial \varphi^2} F(t, \varphi) \right) d\varphi \otimes d\varphi \\
\bullet^{(3,2)} F(t, \varphi) &= -2 \left( \frac{1}{1-t^2} \frac{\partial^2}{\partial t \partial \varphi} F(t, \varphi) + \frac{t}{(1-t^2)^2} \frac{\partial}{\partial \varphi} F(t, \varphi) \right) dt \otimes dt \\
&\quad + \left( \frac{\partial^2}{\partial t^2} F(t, \varphi) - \frac{1}{(1-t^2)^2} \frac{\partial^2}{\partial \varphi^2} F(t, \varphi) \right) (dt \otimes d\varphi + d\varphi \otimes dt) \\
&\quad + 2 \left( (1-t^2) \frac{\partial^2}{\partial t \partial \varphi} F(t, \varphi) + t \frac{\partial}{\partial \varphi} F(t, \varphi) \right) d\varphi \otimes d\varphi \\
\bullet^{(3,3)} F(t, \varphi) &= F(t, \varphi) d\varphi \otimes dt - F(t, \varphi) dt \otimes d\varphi
\end{aligned}$$

Assume now, that at the point  $\xi \in \Omega$  there is a local orthonormal triad  $\{\varepsilon_x, \varepsilon_y, \varepsilon_z\}$  with  $\varepsilon_z$  pointing to the zenith,  $\varepsilon_x$  pointing north and  $\varepsilon_y$  pointing east, i.e.

$$\begin{aligned}
\varepsilon_x &= \frac{1}{\sqrt{1-t^2}} dt \\
\varepsilon_y &= -\sqrt{1-t^2} d\varphi \\
\varepsilon_x &= \xi.
\end{aligned}$$

Then, using the identification  $\xi = (t, \varphi)$  via the relation (5), we obtain easily the following expressions:

$$\begin{aligned}
\bullet^{(1,1)} F(\xi) &= F(t, \varphi) \varepsilon_z \otimes \varepsilon_z \\
\bullet^{(1,2)} F(\xi) &= \sqrt{1-t^2} \frac{\partial}{\partial t} F(t, \varphi) \varepsilon_z \otimes \varepsilon_x - \frac{1}{\sqrt{1-t^2}} \frac{\partial}{\partial \varphi} F(t, \varphi) \varepsilon_z \otimes \varepsilon_y \\
\bullet^{(1,3)} F(\xi) &= -\frac{1}{\sqrt{1-t^2}} \frac{\partial}{\partial \varphi} F(t, \varphi) \varepsilon_z \otimes \varepsilon_x - \sqrt{1-t^2} \frac{\partial}{\partial t} F(t, \varphi) \varepsilon_z \otimes \varepsilon_y \\
\bullet^{(2,1)} F(\xi) &= \sqrt{1-t^2} \frac{\partial}{\partial t} F(t, \varphi) \varepsilon_x \otimes \varepsilon_z - \frac{1}{\sqrt{1-t^2}} \frac{\partial}{\partial \varphi} F(t, \varphi) \varepsilon_y \otimes \varepsilon_z \\
\bullet^{(3,1)} F(\xi) &= -\frac{1}{\sqrt{1-t^2}} \frac{\partial}{\partial t' \varphi} F(t, \varphi) \varepsilon_x \otimes \varepsilon_z - \sqrt{1-t^2} \frac{\partial}{\partial t} F(t, \varphi) \varepsilon_y \otimes \varepsilon_z \\
\bullet^{(2,2)} F(\xi) &= F(t, \varphi) \varepsilon_x \otimes \varepsilon_x + F(t, \varphi) \varepsilon_y \otimes \varepsilon_y \\
\bullet^{(2,3)} F(\xi) &= \left( (1-t^2) \frac{\partial^2}{\partial t^2} F(t, \varphi) - \frac{1}{(1-t^2)} \frac{\partial^2}{\partial \varphi^2} F(t, \varphi) \right) \varepsilon_x \otimes \varepsilon_x \\
&\quad - 2 \left( \frac{\partial^2}{\partial t \partial \varphi} F(t, \varphi) + \frac{t}{1-t^2} \frac{\partial}{\partial \varphi} \right) (\varepsilon_x \otimes \varepsilon_y + \varepsilon_y \otimes \varepsilon_x) \\
&\quad + \left( -(1-t^2) \frac{\partial^2}{\partial t^2} F(t, \varphi) + \frac{1}{1-t^2} \frac{\partial^2}{\partial \varphi^2} F(t, \varphi) \right) \varepsilon_y \otimes \varepsilon_y
\end{aligned}$$

$$\begin{aligned}
\mathbf{o}^{(3,2)}F(\xi) &= -2 \left( \frac{\partial^2}{\partial t \partial \varphi} F(t, \varphi) + \frac{t}{1-t^2} \frac{\partial}{\partial \varphi} F(t, \varphi) \right) \varepsilon_x \otimes \varepsilon_x \\
&\quad - \left( \frac{\partial^2}{\partial t^2} F(t, \varphi) - \frac{1}{(1-t^2)^2} \frac{\partial^2}{\partial \varphi^2} F(t, \varphi) \right) (\varepsilon_x \otimes \varepsilon_y + \varepsilon_y \otimes \varepsilon_x) \\
&\quad + 2 \left( \frac{\partial^2}{\partial t \partial \varphi} F(t, \varphi) + \frac{t}{1-t^2} \frac{\partial}{\partial \varphi} F(t, \varphi) \right) \varepsilon_y \otimes \varepsilon_y \\
\mathbf{o}^{(3,3)}F(\xi) &= F(t, \varphi) \varepsilon_x \otimes \varepsilon_y - F(t, \varphi) \varepsilon_y \otimes \varepsilon_x.
\end{aligned}$$

The following orthogonality property is important: if  $F, G \in \mathcal{C}^{(\infty)}(\Omega)$ , then

$$(\mathbf{o}^{(i,k)}F, \mathbf{o}^{(i',k')}G)_{L^2(\Omega)} = 0 \text{ if } (i, k) \neq (i', k').$$

The adjoint operators  $\mathbf{O}^{(i,k)}$ ,  $i, k = 1, 2, 3$ , transforming tensor fields into scalar valued functions are defined by the condition

$$(\mathbf{O}^{(i,k)}\mathbf{f}, F)_{L^2(\Omega)} = (\mathbf{f}, \mathbf{o}^{(i,k)}F)_{L^2(\Omega)}$$

for all  $F \in \mathcal{C}^{(\infty)}(\Omega)$  and  $\mathbf{f} \in \mathbf{c}^{(\infty)}(\Omega)$ . They allow the definition of the spaces

$$\mathbf{c}_{(i,k)}^{(\infty)}(\Omega) = \left\{ \mathbf{f} \in \mathbf{c}^{(\infty)}(\Omega) \mid \mathbf{O}^{(i',k')}\mathbf{f} = 0 \text{ for all } (i', k') \neq (i, k) \right\},$$

yielding an orthogonal decomposition of the space  $\mathbf{c}^{(\infty)}(\Omega)$  of the form

$$\mathbf{c}^{(\infty)}(\Omega) = \bigoplus_{i,k=1}^3 \mathbf{c}_{(i,k)}^{(\infty)}(\Omega). \quad (7)$$

As it is proved in (Freeden et al, 1993), this decomposition can be established in a constructive way. In particular we have:

**Theorem 1.** Let  $\mathbf{f} \in \mathbf{c}^{(2)}(\Omega)$ . Then there exist uniquely defined functions  $F_{i,k} \in \mathcal{C}^{(2)}(\Omega)$ ,  $(i, k) \in \{(1,1), (1,2), \dots, (3,3)\}$  with

$$\begin{aligned}
F_{i,k} &\perp \text{Harm}_0 \text{ for } (i, k) \in \{(1,2), (1,3), (2,1), (2,3), (3,1), (3,2)\} \\
F_{i,k} &\perp \text{Harm}_1 \text{ for } (i, k) \in \{(2,3), (3,2),
\end{aligned}$$

such that

$$\mathbf{f} = \sum_{i,k=1}^3 \mathbf{o}^{(i,k)} F_{i,k},$$

and the functions  $F_{i,k}$  are given by:

$$F_{1,1} = \mathbf{O}^{(1,1)}\mathbf{f}, \quad F_{2,2} = \frac{1}{2}\mathbf{O}^{(2,2)}\mathbf{f}, \quad F_{3,3} = \frac{1}{2}\mathbf{O}^{(3,3)}\mathbf{f}.$$

For  $(i, k) \in \{(1,2), (1,3), (2,1), (3,1)\}$

$$F_{i,k}(\xi) = - \int_{\Omega} G(\Delta^*; \xi, \eta) \mathbf{O}_{\eta}^{(i,k)} \mathbf{f}(\eta) d\omega(\eta),$$

while for  $(i, k) \in \{(2, 3), (3, 2)\}$

$$F_{i,k}(\xi) = \int_{\Omega} G(\Delta^*(\Delta^* + 2); \xi, \eta) O_{\eta}^{(i,k)} \mathbf{f}(\eta) d\omega(\eta).$$

Thereby,  $(G(\Delta^*; \cdot, \cdot)$  and  $G(\Delta^*(\Delta^* + 2); \cdot, \cdot)$  denote the spherical Green's functions with respect to the Beltrami operator  $\Delta^*$  and its iteration  $\Delta^*(\Delta^* + 2)$ , respectively (cf. (Freeden, 1978)).

Of fundamental importance for the following results is the decomposition of the Hesse tensor of a harmonic function according to this decomposition. Let therefore  $Y_n \in \text{Harm}_n$  be a spherical harmonic of order  $n$ . Then we easily get

$$\begin{aligned} \text{Hess } \frac{1}{r^{n+1}} Y_n(\xi) &= (n+1)(n+2) \frac{1}{r^{n+3}} \mathbf{o}^{(1,1)} Y_n(\xi) \\ &\quad - (n+2) \frac{1}{r^{n+3}} (\mathbf{o}^{(1,2)} Y_n(\xi) + \mathbf{o}^{(2,1)} Y_n(\xi)) \\ &\quad - \frac{(n+1)(n+2)}{2} \frac{1}{r^{n+3}} \mathbf{o}^{(2,2)} Y_n(\xi) + \frac{1}{2} \frac{1}{r^{n+3}} \mathbf{o}^{(2,3)} Y_n(\xi). \end{aligned}$$

Thus, it follows that

$$\begin{aligned} \text{Hess } \frac{1}{r^{n+1}} Y_n(\xi)|_{r=1} &= (n+1)(n+2) \mathbf{o}^{(1,1)} Y_n(\xi) \\ &\quad - (n+2) (\mathbf{o}^{(1,2)} Y_n(\xi) + \mathbf{o}^{(2,1)} Y_n(\xi)) \\ &\quad - \frac{(n+1)(n+2)}{2} \mathbf{o}^{(2,2)} Y_n(\xi) + \frac{1}{2} \mathbf{o}^{(2,3)} Y_n(\xi). \end{aligned}$$

If we use the projection operators  $\mathbf{P}_{(i,k)}$  corresponding to the decomposition (7) we finally obtain the following

**Theorem 2.** *Let  $U \in \mathcal{C}^{(\infty)}(\Omega_R^{\text{ext}}) \cap \mathcal{C}^{(0)}(\overline{\Omega_R^{\text{ext}}})$  be a harmonic function in  $\Omega_R^{\text{ext}}$  with  $|U(x)| = O(1/|x|)$  as  $|x| \rightarrow \infty$ , uniformly with respect to all directions. Then the following statements are valid:*

1.  $\mathbf{P}_{(i,k)} \text{Hess } U(\xi) = 0$  if  $(i, k) \in \{(1, 3), (3, 1), (3, 2), (3, 3)\}$
2.  $\mathbf{P}_{(i,k)} \text{Hess } U(\xi) = 0$  for  $(i, k) \in \{(1, 1), (2, 2)\}$  if and only if  $U = 0$ .
3.  $\mathbf{P}_{(i,k)} \text{Hess } U(\xi) = 0$  for  $(i, k) \in \{(1, 2), (2, 1)\}$  if and only if  $U|_{\Omega} \in \text{Harm}_0$ .
4.  $\mathbf{P}_{(2,3)} \text{Hess } U(\xi) = 0$  if and only if  $U|_{\Omega} \in \text{Harm}_0 \cup \text{Harm}_1$ .

The meaning of this theorem is as follows: the gravitational potential in the exterior of the earth is uniquely defined by prescribing the  $\mathbf{P}_{(1,1)}$ - or  $\mathbf{P}_{(2,2)}$ -component of its Hesse matrix. It can be uniquely recovered up to the 0th order coefficient of its series expansion using the  $\mathbf{P}_{(1,2)}$ - or  $\mathbf{P}_{(2,1)}$ -component, while the  $\mathbf{P}_{(2,3)}$ -component guarantees the uniqueness up to the 0th and 1st order spherical harmonics. Thus, sufficient conditions for uniqueness are established.

## LOCALLY SUPPORTED SPLINES IN SATELLITE GRADIOMETRY

The approximation of the earth's gravitational potential by the use of a truncated series in terms of spherical harmonics has a long tradition in all geosciences. Though this approach has many nice properties, it has the drawback that the high frequency parts of the gravitational potential have to be approximated by globally supported functions showing high oscillations. On the other hand there is a strong need for models with a fine spatial resolution. Hence, harmonic trial functions with a localizing property are very promising as alternative for modern approximations of the gravitational field of the earth.

In this section, we propose the use of locally supported spline functions for the determination of the gravitational field from satellite gradiometry data. In view of the results given in the last section, we consider the following model problem: determine a function  $U \in \mathcal{C}^{(\infty)}(\Omega_R^{\text{ext}}) \cap \mathcal{C}^{(0)}(\Omega_R^{\text{ext}})$  with  $\Delta U = 0$  in  $\Omega_R^{\text{ext}}$  and  $|U(x)| = O(1/|x|)$  as  $|x| \rightarrow \infty$ , uniformly with respect to all directions, from discretely given data  $(\eta_i, y_i) \in \Omega \times \mathbb{R}$ ,  $i = 1, \dots, N$ , such that the second order radial derivatives of  $U$  at the points  $\eta_i$  are equal to  $y_i$ , i.e.

$$\eta_i^T \mathbf{Hess} U(\eta_i) \eta_i = y_i, \quad i = 1, \dots, N.$$

The spline techniques we have in mind are based on results described e.g. in (Freeden, 1981; Freeden, 1990; Freeden et al., 1994). However, a direct application of the available method for this problem is not possible because of the following reason: suppose there are given trial functions for spline interpolation which are harmonic outside the spherical earth. Then it is clear from potential theory that the restrictions of such functions to a surface that lies in the interior of the domain of harmonicity (as it is the case in satellite gradiometry) cannot have a local support. The same fact is true for the second order derivatives of those functions. On the other hand, a direct application of spline interpolation techniques with globally supported trial functions would lead to systems of linear equations with a fully sized system matrix. Since the number of unknowns is as large as the number of the given data points, this method would be unacceptable in view of the huge amount of measurements generated in satellite gradiometry.

A viable way to overcome this difficulty will be outlined by the following four steps:

*Spline interpolation of the given data.* Assume that  $\mathcal{H}$  is a Hilbert space of functions defined on  $\Omega$  which has a reproducing kernel  $K_{\mathcal{H}} : \Omega \times \Omega \rightarrow \mathbb{R}$ , i.e.

$$(K_{\mathcal{H}}(\xi, \cdot), F(\cdot))_{\mathcal{H}} = F(\xi) \text{ for all } \xi \in \Omega.$$

Then it is a well-known fact of spline theory that the problem “minimize  $\|F\|_{\mathcal{H}}$  among all functions  $F \in \mathcal{H}$  with  $F(\eta_i) = y_i$ ,  $i = 1, \dots, N$ ” has a unique solution. As it is well-known, this interpolating spline  $S_N$  can be represented by

$$S_N(\xi) = \sum_{i=1}^N a_i K_{\mathcal{H}}(\xi, \eta_i), \quad \xi \in \Omega,$$

where the  $a_i$  are given by the solution of the linear equations

$$\sum_{j=1}^N K_{\mathcal{H}}(\eta_i, \eta_j) a_j = y_i, \quad i = 1, \dots, N.$$

In order to be confronted with a manageable numerical effort, the underlying system matrix has to be sparse, what corresponds to the fact that the kernel  $K_{\mathcal{H}}$  has a local support. We shall describe below how an appropriate Hilbert space with a locally supported reproducing kernel  $K_{\mathcal{H}}$  can be constructed, such that  $K_{\mathcal{H}}(\xi, \eta)$  depends only on the inner product of  $\xi$  and  $\eta$ , i.e.  $K_{\mathcal{H}}$  is an axisymmetric function. This symmetry will become important in the following.

*Transformation of the second order derivative into potential data.* It can be seen e.g. from (Svensson, 1983) that the transformation of  $U|_{\Omega}$  into  $\xi \mapsto \xi^T \text{Hess } U(\xi)\xi$ ,  $\xi \in \Omega$ , can be described by a pseudodifferential operator  $\Lambda$  with spherical symbol  $\{\Lambda^{\wedge}(n)\}_{n=0,1,\dots}$ , where  $\Lambda^{\wedge}(n) = (n+1)(n+2)$ ,  $n = 0, 1, \dots$ . Thus, the function

$$\Lambda_{\xi}^{-1} S_N(\xi) = \sum_{i=1}^N a_i \Lambda_{\xi}^{-1} K_{\mathcal{H}}(\xi, \eta_i), \quad \xi \in \Omega$$

is an approximation of  $U|_{\Omega}$ . Since the series expansion of  $K_{\mathcal{H}}$  is known, the application of  $\Lambda^{-1}$  is by no means difficult.

*Representation in the frequency domain.* The kernels we are interested in admit a series expansion in terms of the Legendre polynomials  $P_n$  of the form

$$K_{\mathcal{H}}(\xi, \eta) = \sum_{n=0}^{\infty} \frac{2n+1}{4\pi} K_{\mathcal{H}}^{\wedge}(n) P_n(\xi \cdot \eta).$$

Thus,  $\Lambda^{-1} S_N$  can be represented by

$$\Lambda^{-1} S_N(\xi) = \sum_{i=1}^N \sum_{n=0}^{\infty} a_i \frac{2n+1}{4\pi} \frac{K_{\mathcal{H}}^{\wedge}(n)}{\Lambda^{\wedge}(n)} P_n(\xi \cdot \eta_i), \quad \xi \in \Omega. \quad (8)$$

*Numerical filtering.* Formula (8) would lead to the approximation of the gravitational potential  $U$  by the series

$$x \mapsto \sum_{i=1}^N \sum_{n=0}^{\infty} a_i \frac{2n+1}{4\pi} \frac{K_{\mathcal{H}}^{\wedge}(n)}{\Lambda^{\wedge}(n)} \frac{1}{|x|^{n+1}} P_n\left(\eta_i \cdot \frac{x}{|x|}\right)$$

for  $|x| \geq R$ . However, this series converges in general only for  $|x| \geq 1$  but not for  $R \leq |x| < 1$ . Hence, some filtering technique is necessary. The simplest approach is the truncation of the infinite series. Thus, the final solution of the described procedure can be easily expressed (using the addition theorem) by a finite series of spherical harmonics. In doing so, the existing programs for e.g. synthesis or orbit determination can still be applied in the usual way. However, one should be aware of aliasing effects.

Next, we study the choice of the Hilbert space  $\mathcal{H}$ . Starting point is the definition of a function  $B_h : [-1, 1] \rightarrow \mathbb{R}$ , which is for fixed  $h \in (0, 1)$  defined by

$$B_h(t) = \begin{cases} 0 & \text{for } -1 \leq t \leq h \\ (t-h)/(1-h) & \text{for } h < t \leq 1 \end{cases}.$$

Other possible types of trial functions have been proposed in (Freeden and Schreiner, 1993). The function  $\xi \mapsto B_h(\xi \cdot \eta)$ ,  $\xi \in \Omega$ , is for fixed  $\eta \in \Omega$  an axisymmetric Lipschitz–continuous function. The support of  $B_h(\eta \cdot \cdot)$  is

$$\text{supp } B_h(\eta \cdot \cdot) = \{\xi \in \Omega \mid h \leq \xi \cdot \eta \leq 1\}.$$

$B_h$  admits a series expansion of the form

$$B_h(\xi \cdot \eta) = \sum_{n=0}^{\infty} \frac{2n+1}{4\pi} B_h^{(n)}(\eta) P_n(\xi \cdot \eta), \quad \xi \in \Omega.$$

The coefficients  $B_h^{(n)}$  can be calculated by a recursion formula (cf. (Freeden and Schreiner, 1993)).

We define the iteration of this kernel by

$$B_h^{(2)}(\xi \cdot \eta) = \int_{\Omega} B_h(\xi \cdot \zeta) B_h(\zeta \cdot \eta) d\omega(\zeta), \quad \xi, \eta \in \Omega.$$

The function  $B_h^{(2)}(\eta \cdot \cdot)$  has the support  $\text{supp } B_h^{(2)}(\eta \cdot \cdot) = \{\xi \in \Omega \mid -1 + 2h^2 \leq \xi \cdot \eta \leq 1\}$ . It follows from the Funk–Hecke formula, that  $B_h^{(2)}$  has the series expansion

$$B_h^{(2)}(t) = \sum_{n=0}^{\infty} \frac{2n+1}{4\pi} B_h^{(2)}(n) P_n(t), \quad t \in [-1, 1], \quad (9)$$

where  $B_h^{(2)}(n) = (B_h^{(n)})^2 > 0$ . The positivity of these coefficients imply (cf. (Freeden et al., 1994)) that the function  $(\xi, \eta) \mapsto B_h^{(2)}(\xi \cdot \eta)$  is the reproducing kernel of a Hilbert subspace of  $\mathcal{C}(\Omega)$ , here denoted by  $\mathcal{H}_h$ .

Thus, the underlying Hilbert space structure is found. Moreover, under these assumptions, convergence results for spline interpolation can be proved. This will be done elsewhere.

The following figures illustrate computational results based on the method described above. We show isolines of the potential and its approximations measured in  $1m^2/s^2$ . As reference data, the OSU91A model was chosen, using the coefficients up to degree and order 180 and starting from the order 3. The second order radial derivatives of this potential at the height 200 km were calculated in 41164 points on 181 circles of latitude including the North Pole and the South Pole, and used for the spline interpolation. In particular, the points were generated by the following method:

choose a parameter  $\gamma \in \mathbb{N}$ , set  $\Delta\vartheta = \pi/\gamma$ , and define

$$\begin{aligned} \vartheta_0 &= \frac{\pi}{2}, \quad \varphi_{00} = 0 \quad (\text{North Pole}) \\ \vartheta_i &= \vartheta_0 - i\Delta\vartheta, \quad 1 \leq i \leq \gamma - 1 \\ \gamma_i &= \left[ 2\pi / \arccos \left( \left( \cos \Delta\vartheta - \cos^2 \vartheta_i \right) / \sin^2 \vartheta_i \right) \right], \quad 1 \leq i \leq \gamma - 1 \\ \varphi_{ij} &= j \frac{2\pi}{\gamma_i}, \quad 0 \leq j \leq \gamma_i - 1 \\ \vartheta_\gamma &= -\frac{\pi}{2}, \quad \varphi_{\gamma 0} = 0 \quad (\text{South Pole}) \end{aligned}$$

The data points are then located at the points given in the local coordinates (5) by  $(\arccos \vartheta_i, \varphi_{ij})$ ,  $0 \leq i \leq \gamma$ ,  $0 \leq j \leq \gamma_i - 1$ , hence  $N$  is controlled by  $\gamma$ . The Figures 1 and 2 illustrate the defined pointsets for different values of  $\gamma$ .

The parameter  $h$  which determines the support of the function  $B_h^{(2)}$ , and hence the underlying Hilbert space, was chosen to  $h = 0.999$ .

The Figures 3 and 4 show the reference potential at height 200 km and the result of the spline interpolation. The corresponding result at the height 0 km is shown in the Figures 5 and 6. As filtering, we used the truncation of the series (9) at  $n = 240$ . It can be seen that instability phenomena arise from the downward continuation of the solution since it corresponds to an integral equation of the first kind. In order to stabilize this process, the spline interpolation should be substituted by smoothing using splines, i.e. a minimization procedure in  $\mathcal{H}_h$  with respect to a functional of type

$$\sum_{i=1}^N \left( \frac{y_i - S_N(\eta_i)}{\beta_i^2} \right)^2 + \delta \|S_N\|_{\mathcal{H}_h}$$

with suitably chosen  $\beta_i, \delta > 0$ . A final result using this smoothing procedure with  $\beta_i = 1$ ,  $i = 1, \dots, N$  and  $\delta/B_h^{(2)}(1) = 0.05$  is shown in Figure 7.

Thus we have demonstrated how locally supported splines can be successfully applied for the determination of the earth's gravitational potential in satellite gradiometry. Since the downward continuation has to be regularized the use of filtering and smoothing techniques is indispensable.

Fig. 1. Pointset with  $\gamma = 20$ ,  $N = 501$ .

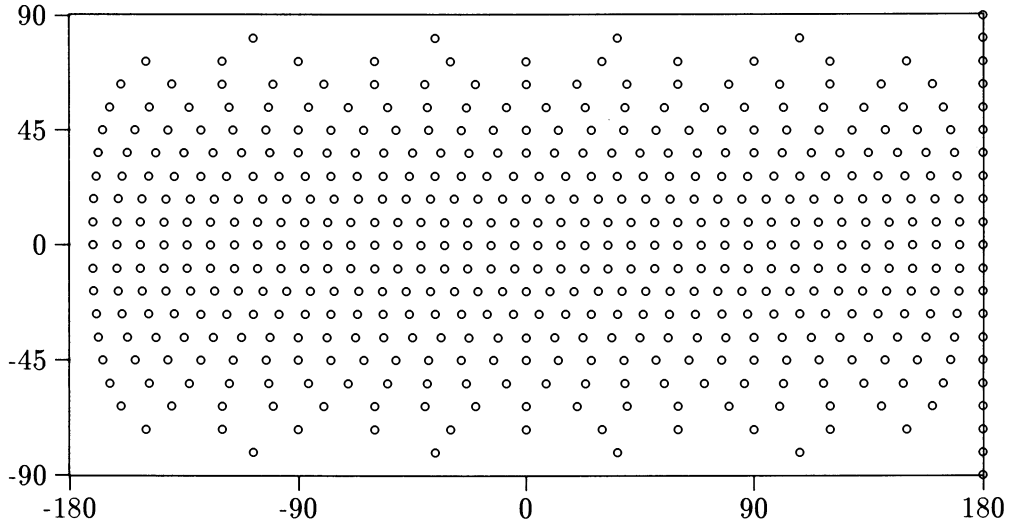


Fig. 2. Pointset with  $\gamma = 40$ ,  $N = 2013$ .

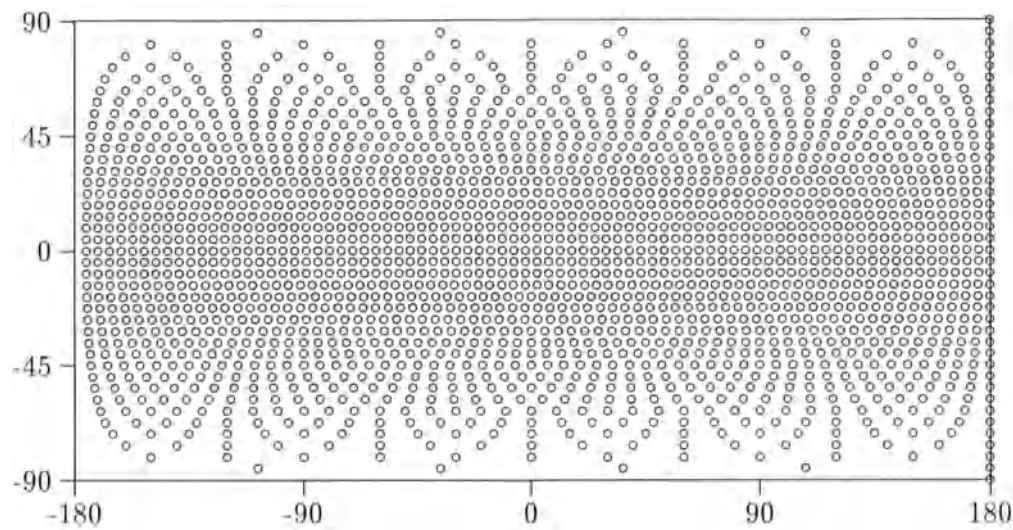
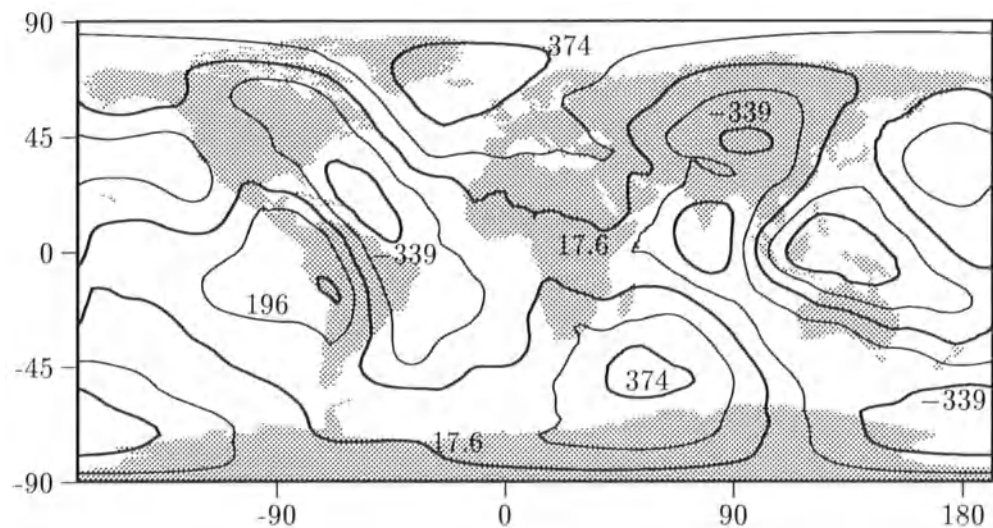
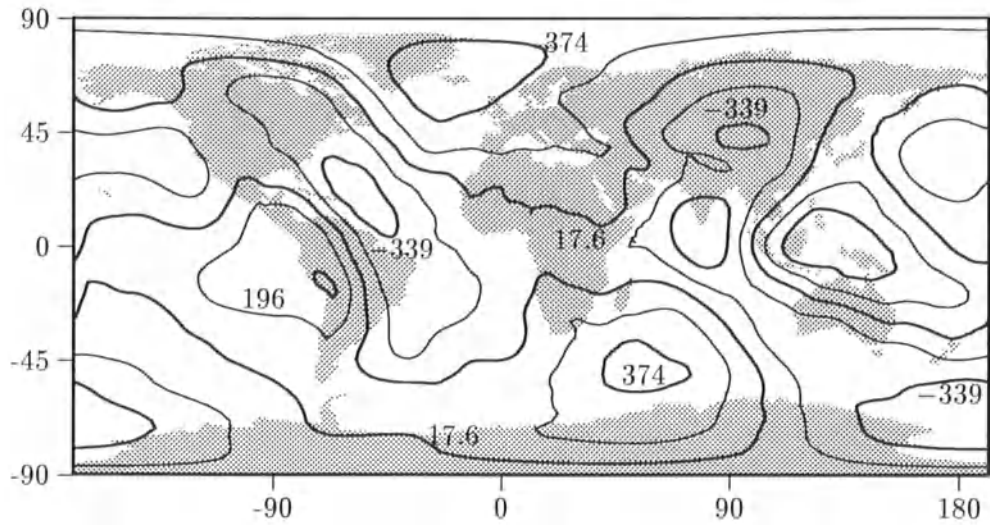


Fig 3. Reference data at height 200 km.



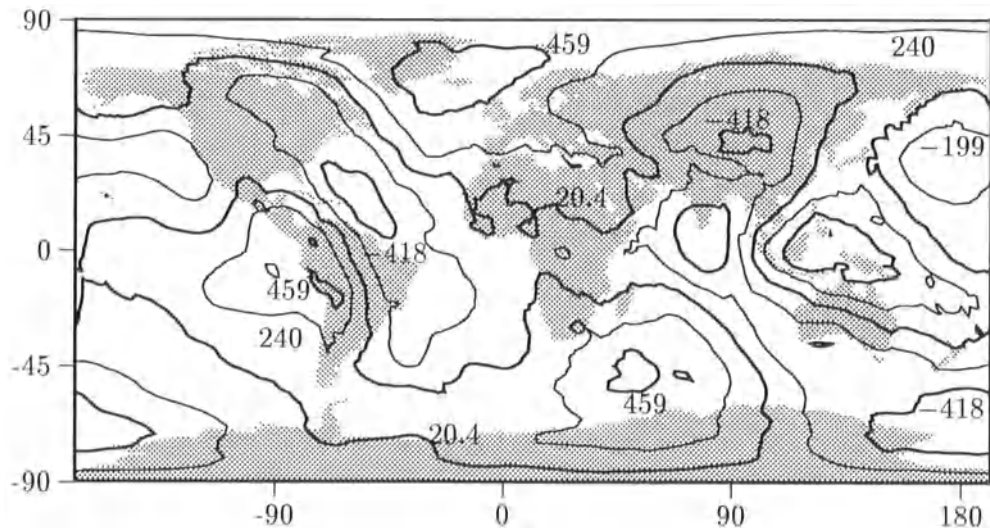
Isolines at  $-339, -161, 17.6, 196, 374$ .

Fig. 4. Computational result using spline interpolation at height 200 km.



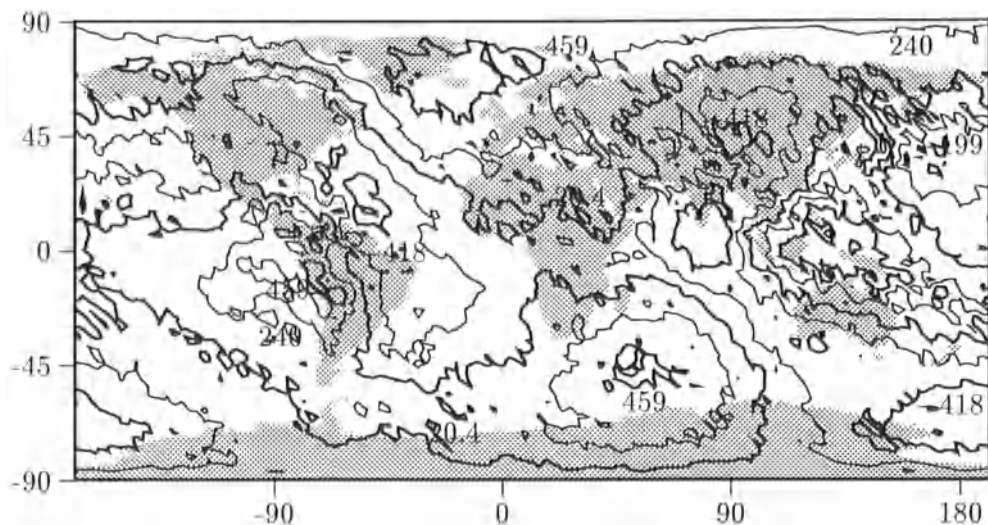
Isolines at  $-339, -161, 17.6, 196, 374$ .

Fig 5. Reference data at height 0 km.



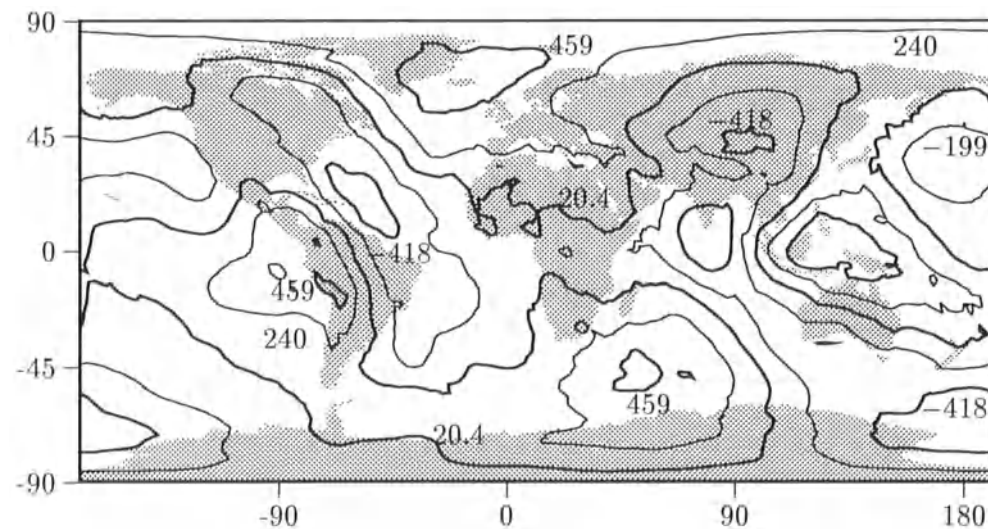
Isolines at  $-418, -199, 20.4, 240, 459$ .

Fig. 6. Computational result using spline interpolation at height 0 km.



Isolines at  $-418, -199, 20.4, 240, 459$ .

Fig. 7. Computational result using spline smoothing at height 0 km.



Isolines at  $-418, -199, 20.4, 240, 459$ .

## REFERENCES

- Backus, G.E. (1966). Potentials for Tangent Tensor Fields on Spheroids, *Arch. Rational Mech. Anal.* **22**, 210–252
- Backus, G.E. (1967). Converting Vector and Tensor Equations to Scalar Equations in Spherical Coordinates, *Geophys. J.R. Astr. Soc.* **13**, 71–101
- Freedon, W. (1978). Eine Klasse von Integralformeln der Mathematischen Geodäsie, *Veröff. Geod. Inst. RWTH Aachen* **27**
- Freedon, W. (1981). On Spherical Spline Interpolation and Approximation, *Math. Meth. in the Appl. Sci.* **3**, 551–575
- Freedon, W. (1990). Spherical Spline Approximation and its Application in Physical Geodesy, *Geophysical Data Inversion Methods and Applications*, A. Vogel et al. (eds), Vieweg, Braunschweig, 79–104
- Freedon, W., Gervens, T., Schreiner, M. (1994). Tensor Spherical Harmonics and Tensor Spherical Splines, *Manuscr. Geod.* **19**, 70–100
- Freedon, W. and Schreiner, M. (1993). Nonorthogonal Expansions on the Sphere, *AGTM-Report* **97**, University of Kaiserslautern, Geomathematics Group, accepted for publication in *Math. Meth. in the Appl. Sci.*
- Rummel, R. (1986). Satellite Gradiometry, *Mathematical and Numerical Techniques in Physical Geodesy*, Lecture Notes in Earth Sciences **7**, H. Sünkel (ed.), Springer, Berlin, 318–363
- Rummel, R., van Gelderen, M., Koop, R., Schrama, E., Sansò, F., Brovelli, M., Miggliaccio, F., Sacerdote, F. (1993). Spherical Harmonic Analysis of Satellite Gradiometry, *Publications on Geodesy, New Series* **39**, Delft
- Schreiner, M. (1994). Tensor Spherical Harmonics and Their Application in Satellite Gradiometry, *PhD-Thesis*, University of Kaiserslautern, Geomathematics Group, Kaiserslautern
- Spivak, M. (1975). A Comprehensive Introduction to Differential Geometry, Vols. I–III, Publish or Perish, Boston
- Svensson, S.L. (1983). Pseudodifferential Operators — a New Approach to the Boundary Value Problems of Physical Geodesy, *Manuscr. Geod.* **8**, 1–40

# SATELLITE ORBIT GEOMETRY UNDER NONCONSERVATIVE FORCES

E. Grafarend and R. J. You

Department of Geodetic Science

Stuttgart University, Keplerstraße 11, D-70174 Stuttgart, Germany

## ABSTRACT

The motions of satellite can be interpreted as the geodesic flows according to the object of connexion. The different objects of connexion define the different spaces. In the conservative force fields the motions of satellite can be treated as the geodesic flows on a *Riemann* manifold with respect to the *Maupertuis metric* which defines a metric and symmetric object of connexion, while in the nonconservative force fields the motions can be also explained as geodesic flows in *Weyl* space with respect to a *semimetric* and symmetric object of connexion. As a example the motion of charged satellite, e.g. LAGEOS, in the gravitational and geomagnetic field is investigated. The geomagnetic field produces a *Lorentz* force field which causes the classical *Zeeman effect* in the computation of the satellite's orbital motion. Consequently, the frequency of orbital motion is split into three components: the first one is equal to the mean orbital motion and the other two is equal to the frequency of the mean orbital motion plus/minus a *Larmor frequency* which relates to the charge of satellite, the mass of satellite and the magnitude of geomagnetic field.

# Spherical cap models of Laplacian potentials and general fields

De Santis A., Falcone C.

Istituto Nazionale di Geofisica, Rome, Italy.

**keywords:** Harmonic analysis, regional modelling

## Abstract

A rather new technique was introduced by Haines in 1985 to derive regional models of the geomagnetic field. Some implementations and derivations have been successively proposed. The basic concepts of the original method and of the late developments are here described, together with the main and possible limitations.

## 1. Introduction

A new technique was introduced by Haines (1985a) to derive regional models of the geomagnetic potential which satisfy the physics of the problem, i.e. the Laplace's equation (we show briefly this well-known partial differential equation simply to introduce the symbols we are going to mention):

$$\nabla^2 V = 0, \quad V(r, \theta, \lambda) = \sum_{k,m} c_k^m \rho_k(r) Y_{n_k}^m(\theta, \lambda),$$

the orders  $m$  and degrees  $n_k$  ( $k$  is a simple index, as we will soon show) are the separation constants used to split the equation in three ordinary differential equations dependent separately on  $r$ ,  $\theta$ ,  $\lambda$ .

This technique, called Spherical Cap Harmonic Analysis (SCHA) is based on the expansion of the potential  $V$  in terms of particular solutions  $Y_{n_k}^m$  of Laplace's equation. These harmonics have been named *spherical cap harmonics* (the adjective "spherical" should be attributed more to "cap" than to "harmonics" because these new functions are not physically acceptable all over the sphere, since they have a singular point at the south pole) because the values of their degrees  $\{n_k\}$  are determined by specific boundary conditions imposed at the edge of the cap. The  $\{n_k\}$  are in general noninteger (they *must* be integer in the global analysis!) and dependent on the order  $m$  of the harmonic expansion.

If the potential is expressed in terms of internal ( $V_i$ ) and external ( $V_e$ ) contributions with respect to a reference sphere of radius  $R$ , (in practice we will suppose a spherical Earth with mean radius  $R=6371.2$  km) i.e.

$$V = V_i + V_e$$

then, in spherical (cap) coordinates ( $\theta$ = colatitude,  $\lambda$ =longitude and  $r$ =radial distance from the Earth's centre), for example, the internal part has the following form:

$$V_i(r, \theta, \lambda) = R \sum_{k=0}^{K_{max}} \sum_{m=0}^k (R/r)^{n_k(m)+1} c_k^m Y_{n_k(m)}^m(\theta, \lambda) =$$

$$R \sum_{k=0}^{K_{max}} \sum_{m=0}^k (R/r)^{n_k(m)+1} (g_k^m \cos m\lambda + h_k^m \sin m\lambda) \cdot P_{n_k(m)}^m(\cos \theta) \quad (1)$$

$V_e$  is similar to  $V_i$  but the function in  $r$  is expanded in terms of  $(r/R)^{n_k(m)}$ .  $P_{n_k}^m$  are the generalized Legendre functions,  $c_k^m$  are the spherical (cap) harmonic coefficients, which become  $g_k^m$  and  $h_k^m$ , in the sin and cos notation; these coefficients characterize the spherical cap model. We focused our attention to  $V_i$  because in geomagnetism generally it is the *internal* potential which is considered significant. The components of the magnetic field  $\mathbf{B}$  are simply the components of the negative gradient of  $V$ . This is said because, being the field  $\mathbf{B}$  the quantity which is observable (and not the potential), to find the coefficients  $\{g_k^m, h_k^m\}$  it is a common procedure to minimize the residuals between the observed magnetic components (along a local Cartesian reference system) of  $\mathbf{B}$  (i.e.,  $X, Y$  and  $Z$ ) and their expressions in terms of the components of the negative gradient of  $V$ . A thing which is usually forgotten is that the corresponding expressions of the magnetic components are not necessarily formed by orthogonal functions (this is the case of  $X$  and  $Y$ ). However the contemporary use of  $X, Y$  and  $Z$  together (i.e. the complete knowledge of  $\mathbf{B}$ ) guarantees an orthogonal expansion (see e.g. De Santis et al., 1994).

The main difference from SHA is in the  $\theta$ -dependent functions (i.e. the Legendre functions,  $P_n^m$ ). The values of degree  $n_k$  of the Legendre functions of (1) are chosen in order to satisfy the following boundary conditions (Haines, 1985a):

$$\frac{dP_{n_k}^m(\theta)}{d\theta}|_{\theta_0} = 0, \quad \text{for } k - m = \text{even}; \quad (2)$$

$$P_{n_k}^m(\theta = \theta_0) = 0, \quad \text{for } k - m = \text{odd}; \quad (3)$$

where  $\theta_0$  is the cap half-angle, and  $k$  is used to index (in ascending order) the roots  $n_k$  of (2) and (3) at a given value of  $m$ . These two conditions permit to define two orthogonal (over the cap) sets of functions, as we shall see in the next section. As anticipated by De Santis (1991), these boundary conditions can be heuristically explained by comparing the case of the largest possible cap, i.e. one hemisphere ( $\theta_0 = 90^\circ$ ), for which the conventional Legendre polynomials (i.e. with integer degree  $n$ ) form two orthogonal sets, characterized at the boundary (the equator) by functions with alternately zero  $\theta$ -derivative or zero value. Therefore "conditions (2) and (3) represent the local extension of the equatorial features of the functions to the edge of any cap" (De Santis, 1991). Since expression (1) is a solution of Laplace's equation, the technique has the powerful theoretical aspect to be easily extended to model any zero curl and divergence field that can be expressed by a potential, for example the regional gravity field. In addition, equation (1) represents for  $r=R$  the appropriate expansion theorem of any general field which is defined in a restricted region of the Earth's surface (Haines, 1988). This fact has been already considered applying SCHA also to model, for example, the behaviour of the critical frequency of the F2 ionospheric layer (De Santis et al., 1991).

In the context of regional modelling, SCHA preserves (apparently; see end section 3) the advantages of the more conventional Spherical Harmonic Analysis (SHA), such as physical background, altitude continuation, and it *orthogonalizes* its basis functions within the region of validity (the spherical cap).

The basic concepts and the further developments will be here described. In particular, section 2 gives the analytical justification for the specific boundary conditions (2) and (3); section 3 describes some properties of the spherical cap harmonics, like symmetry or antisymmetry, wavelength content, and orthogonality, while section 4 shows some limits which are typical of SCHA; section 5 presents also other spherical cap models; finally section 6 presents some final remarks. This short note is not exhaustive, being an introduction to the subject for the Geodesy community, with the hope to be of some help for its members.

## 2. Boundary conditions

From Sturm-Liouville theory we will see that boundary conditions (2) and (3) can be imposed to the solutions of Laplace's equation in order to obtain an orthogonal set of functions.

The main difference between regional and global analysis is in the space of interest: in terms of spherical coordinates this means that while  $\lambda$  and  $r$  are still ranging in the space  $[0, 2\pi]$ ,  $[R, \infty]$ , in the cap analysis colatitude is now ranging in the space  $[0, \theta_0]$ , instead of  $[0, \pi]$ . Let's see the  $\theta$ -dependent part of Laplace's equation (associated Legendre's equation) that, for a given integer  $m$ , is:

$$\left( \frac{d}{dx} \left[ (1 - x^2) \frac{d}{dx} \right] - \frac{m^2}{1 - x^2} \right) P_n^m(x) = -n(n + 1) P_n^m(x), \quad (4)$$

where  $x = \cos \theta$ .

Sturm-Liouville theory (e.g. Arfken, 1985) teaches us to treat this differential equation as an eigenvalue problem, i.e.:

$$L_m P_n^m(x) = \mu_n P_n^m(x).$$

$L_m$  is the so-called Legendre operator, the  $P_n^m$  are its eigenfunctions (the Legendre functions), and  $\mu_n = -n(n + 1)$  are their associated eigenvalues. The Legendre operator has the form:

$$L_m = \frac{d}{dx} \left[ (1 - x^2) \frac{d}{dx} \right] - \frac{m^2}{1 - x^2}$$

In the following notations, when not necessary, we will not use the suffix  $m$  associated to the operator  $L_m$  and to the Legendre functions.

From the general theory of mathematics, it is well known (and easy to demonstrate) that if an operator is self-adjoint (Hermitian) in the space  $S$ , then its eigenvalues (eigenfunctions) constitute an orthogonal basis in  $S$ .

To be  $L$  self-adjoint in  $S$ , it should be:

$$(Lu, v)_S = (u, Lv)_S, \quad (5)$$

where  $(f, g)_S$  is the scalar product between functions  $f$  and  $g$  defined in the space  $S$ ; the extended expression of the scalar product in  $S = [x_1, x_2]$  is

$$(f, g)_{[x_1, x_2]} = \int_{x_1}^{x_2} f \cdot g \, dx.$$

where obviously  $x_1 = \cos \theta_1$  and  $x_2 = \cos \theta_2$ . Applying the Legendre operator in a scalar product of the kind  $(LP_i, P_j)_S$ , we have:

$$(LP_i, P_j)_S = (P_i, LP_j)_S + [(1 - x^2)(P'_i P_j - P_i P'_j)]_{x_1}^{x_2}$$

where  $P'(x) = dP/dx$ . It is evident that L is Hermitian (i.e. condition (5) is satisfied) if:

$$[(1 - x^2)(P'_i P_j - P_i P'_j)]_{x_1}^{x_2} = 0,$$

which is automatically satisfied in the global case ( $S = [-1, 1]$ ) with the only condition for the functions  $P_i, P_j$  to be regular in  $S$  (condition satisfied by those solutions of the Legendre equation associated with integer  $n$ ); in the regional (spherical cap) space  $S = [0, \cos \theta_0]$  the term  $(1 - x^2)$  does not eliminate in  $\theta = \theta_0$ , so we need to impose conditions (2) or (3) to both  $P_i, P_j$  to obtain:

$$[P'_i P_j - P_i P'_j]_{\theta_0} = 0,$$

thus getting *two* orthogonal sets.

Generally  $i$  and  $j$  are not integer, which is typical of the SCHA. The boundary conditions allow us to find those basis functions (practically those Legendre functions) that we can put in equation (1) to represent the potential field.

### 3. Some properties of the spherical cap harmonic solutions

Legendre functions are calculated searching for a Taylor expansion in  $x = \cos \theta$  of the solution of the differential equation (Legendre equation) obtained from (4) (associated Legendre equation) in the case  $m = 0$  (Frobenius method, e.g. Arfken, 1975); we give here directly the general expression, noting that in the case  $m = 0$  the term that multiplies the Taylor's sum is simply 1 (it is much simpler in this case!):

$$P_n^m(x) = (1 - x^2)^{m/2} \sum_k a_k(m, n)(x - x_0)^k.$$

Normally  $x_0$  is chosen to be 0, the expansion is with respect to the equator: this approach gives both the solutions of the second order differential equation (in the space  $S \subset [-1, 1]$ , which is the only one we need to study). They have opposite parity with respect to the equator, being them expressed with only odd or even terms ( $a_{2h+1} = 0$  for the even solution and  $a_{2h} = 0$  for the odd one), the relation between two successive coefficients being:

$$a_{k+2}(m, n) = a_k(m, n) \cdot \frac{(k+m)(k+m+1) - n(n+1)}{(k+1)(k+2)};$$

choosing the starting value  $a_0$  according to the used normalization (e.g. the Schmidt *quasi-normalization* in geomagnetism; Chapman and Bartels, 1940). The dependence in  $m$  can be easily evaluated considering Rodrigues' relation between simple ( $m = 0$ ) and associated Legendre functions (e.g. Arfken, 1985):

$$P_n^m(x) = (1 - x^2)^{m/2} \frac{d^m}{dx^m} P_n^0(x).$$

In the case of integer  $n$  (say  $n$  even) only one of the two solutions is regular at the poles (singular points of Legendre's equation), being the one with its same parity (the polynomial  $P_n^m(x)$ , symmetric), while the second solution ( $Q_n^m(x)$ , antisymmetric) goes to infinite when  $x = \pm 1$  (e.g. Hobson, 1931; section 54). However both go to infinite at the poles for noninteger degree. It can be easily seen observing that the term  $a_{k+2}$  vanishes if  $k + m = n$  (so reducing the sum to a polynomial), and noting that, in the case the sum has infinite terms, it converges to finite values only if  $|x| < 1$ .

Applying Frobenius method to find the cap harmonics, i. e. expanding about the north pole ( $x_0 = 1$ ), it does not give both the solutions, but just one of them, given by (Haines, 1985a):

$$P_n^m(x) = (1 - x^2)^{m/2} \sum_{j=0}^{\infty} A_j(m, n) \left(\frac{1-x}{2}\right)^j;$$

$A_0$  will depend on the specific chosen normalisation. In the particular case of integer  $n$ , the above expression reduces to a Legendre polynomial. For noninteger degree, the solution is none of those found with the expansion about the equator: simply, it is a linear combination of the two 'conventional' solutions; it goes to infinite at the south pole, i.e. well outside the spherical cap, and behaves in different way being up or down the equator; in simple words, it has no longer any symmetry about it.

As in the SHA, the meaning of  $n_k$  is the number of wavelengths in a great meridian circle, i.e. the minimum wavelength is given by  $2\pi R/n_k$  (Bullard, 1967; Haines, 1988): analogously to the global case where, being  $n = 1, 2, \dots$  the wavelengths range from the great -circle length down trough its integer-ratios, the values of  $n_k$  found imposing conditions (2), (3) are such that the wavelengths used in this analysis are comparable with the linear size of the cap. As example Fig.1 shows the first few  $P_{n_k}^m$  associated to a  $35^\circ$  cap. The values of  $n$  listed in the figure correspond to those that satisfy (2) and (3).

#### 4. Limits of SCHA

A characteristic of the spherical cap harmonics is the fact that they do not form an orthogonal set, but two orthogonal sets. The conditions (2) or (3) determine the construction of two sets of basis (Legendre) functions, with which we expand the magnetic potential  $V$  within the spherical cap. We have shown that these functions are mutually orthogonal in each set, but a function of a set is not orthogonal with respect to one of the other set (Haines, 1985a). A consequence is that, in comparison with SHA, for SCHA it is not possible to introduce an integral method to find the spherical cap harmonic coefficients. However, this can be done if we expand the potential or a general function in the cap with those basis functions which satisfy just the boundary condition (2), i.e. those with zero  $\theta$ -derivatives (for a potential, this means to impose null *north*-component  $X$  of the Laplacian field at the edge of the cap-like region). An example of this application is described by Haines (1985b). Otherwise, when considering both sets of basis functions,  $\{g_k^m, h_k^m\}$  coefficients are commonly found by least-squares regression of the experimental data.

Actually, at expenses of the real completeness of the set of basis functions, a simple trick could allow us to introduce an integral method. In practice, taking advantage of

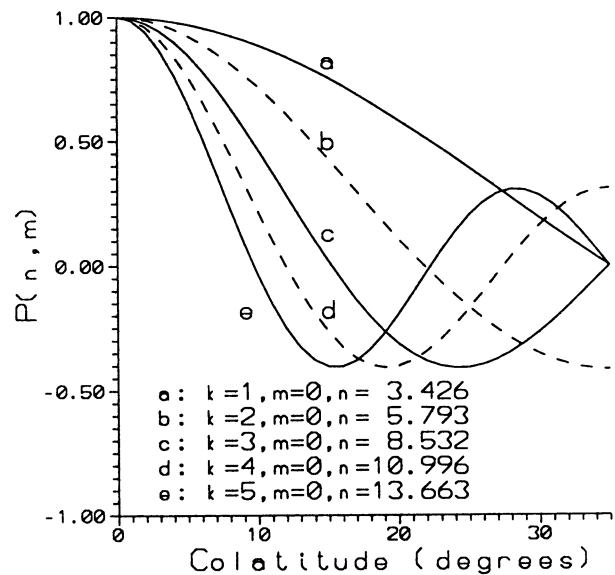


FIG 1

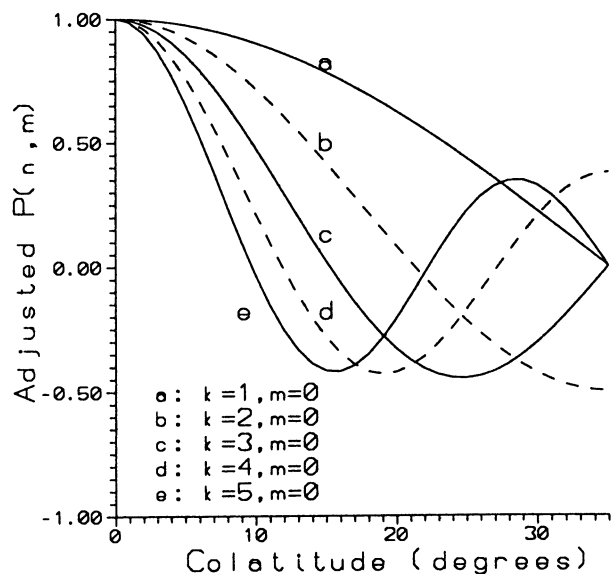


FIG 3

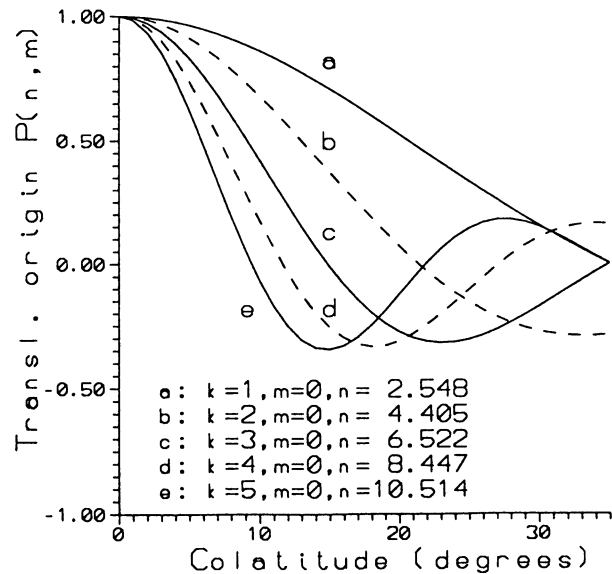


FIG 2

the orthogonality of the trigonometric functions in longitude, it could be possible to use only one set of orthogonal functions (with same  $k\text{-}m$  parity) at the time for each  $m$  (for example,  $m = 0, 1, 2, \dots$  and, say,  $k$  always even)

The SCHA applies to phenomena whose spectral content is defined within the space interval of data definition. When studying fields with longer wavelengths some trouble can arise, since the fitting criterion practically constrains the method to work in any case, but any physical meaning of the expansion coefficients is lost.

Another point which has not been deeply investigated (however see Lowes and Haines, 1993) is the fact that, although the space defining  $r$  does not change ( $r \in [R, \infty]$ ) between global and regional case, the form of the radial dependence changes from  $(R/r)^{n+1}$  with  $n = 1, 2, \dots \infty$  to  $(R/r)^{n_k+1}$  with non integer values of  $n_k$ , which depends on the cap size (for example,  $n_k = 0, 3.4, 5.8, 8.5, 11.0, \dots \infty$  for a  $35^\circ$  half-angle cap, and  $m = 0$ ). implicitly, Haines (1985a) has hence derived a sort of expansion theorem in the radial function of the following form:

$$f(r) = \sum_{k=0}^{\infty} \sum_{m=0}^k a_k^m \left(\frac{R}{r}\right)^{n_k(m)+1} = \sum_{n=0}^{\infty} a'_n \left(\frac{R}{r}\right)^{n+1} \quad (6)$$

where  $a_k^m$  and  $a'_n$  are appropriate expansion coefficients. These expressions come simply from considering the expansions of SHA and SCHA at fixed colatitude and longitude, but varying  $r$ . The real problems might arise in the *truncated* version of this relation, especially when the field to be fitted has contributions of low integer degree harmonics for which a few radial components of integer degree can be expressed by (6) only using many noninteger degree components. This is the mirror image of the case of conventional expansion when to represent a typical short-wavelength field as the crustal one we would need a huge number of harmonics of integer degree; this is much more valid in case of an isolated anomaly which can be considered an approximated Dirac's delta function for which the spectral distribution is essentially spread all over the spectrum. This point is rather delicate and needs more study because has direct consequence to the internal-external separation of the fields, which is of fundamental importance in geomagnetism. An example for all has been described by Torta et al. (1992). The case consisted of the synthesis of field values over a 16-degree cap of a dipole placed at the centre of the Earth. The use of SCHA with both internal and external basis functions improved the fit with respect to the only use of internal contributions alone, in evident contradiction with the original dipolar data.

## 5. Other spherical cap models: TOSCA and ASHA

To introduce TOSCA (Translated Origin Spherical Cap harmonic Analysis) let us follow the words by De Santis, 1991. "The main idea which lies behind TOSCA is that the best outside continuation from the cap is, *in mean*, a conventional global spherical harmonic model. It physically involves that, away from the considered source region, the potential  $V$  should decay toward the global background field associated to long-period wavelengths. This means that TOSCA should act as a sort of filter and should approximate the data in very fine detail (smaller wavelengths) in the central region but smooth them (longer wavelengths) going toward the borders of the cap, giving more weight to the global

global features of the field. The original aspect of TOSCA is the use of SCHA in a new reference system with a vertical translated origin, along the radius, from the centre of the Earth." TOSCA can be useful when the field under study requests a smoothing toward the periphery of the region of concern. This is typical in geomagnetism when studying aspects of geomagnetic anomalies. Along two cases in which TOSCA has been applied, it showed good results with an upward origin translation of around a thousand of kilometers (De Santis, 1991; Torta et al., 1993); however this value depends on the specific situation. Fig.2 describes the first few *translated origin*  $P_{n_k}^m$  for a  $35^\circ$  cap and a translation of 1565 km, corresponding to a translated cap of  $45^\circ$  (this is the reason for different values of  $n$ , with respect to those of Fig.1). The translated origin functions described in Fig.2, and improperly indicated with  $P(n,m)$ , actually depend also on the radial distance  $r'$  from the new translated origin, being at the Earth's surface:  $(1/r')^{n_k+1} \cdot P_{n_k}^m(\theta)$ , where the  $P_{n_k}^m(\theta)$  are the Legendre functions of noninteger degree in the translated cap.

The technique called Adjusted Spherical Harmonic Analysis (ASHA) was introduced by De Santis (1992) to describe a simple method to apply conventional spherical harmonics to magnetic vector data over a spherical cap. The basic concept is to *adjust* the original colatitudes  $\theta$  of the data to those  $\theta'$  of a fictitious hemisphere. Then, this artificial enlargement of the space of definition allows the direct use of the SHA with degree  $n$  coinciding with  $k$ . These adjusted spherical functions, which can be denoted as  $P_k^m(\theta')$  are simply conventional (integer degree) Legendre functions but expressed in the new colatitudes  $\theta'$ ; it can be proved that they are also approximated solution of Laplace's equation. Actually while the condition  $\text{rot}\mathbf{B}=0$  is preserved,  $\text{div}\mathbf{B}$  is not zero, although it assumes small values across the region of concern. In terms of modelling the geomagnetic field, this latter problem is not really significant because one fits  $\mathbf{B}$  instead of its derivatives (which form the expression of its divergence).

The main advantage with respect to SCHA is the use of conventional Legendre functions characterised by an integer harmonic degree. Another practical advantage is that these new *adjusted* basis functions are defined everywhere on the sphere, while the spherical cap harmonics possess a singular point at the antipodal (south) pole: hence any model based on the latter functions quickly deteriorates when extrapolated outside the cap, while an ASHA model is more stable.

Fig.3 shows the first few *adjusted*  $P_k^m$  for a  $35^\circ$  cap;  $n$  is not listed because in this case it coincides with  $k$ . Fig.1 and 3 are practically similar, while the basis functions of Fig.2 show the smoothing effect going far from the centre of the cap.

## 6. Concluding remarks

In this brief introduction, the central role is the consideration that the boundary condition problem associated to the Laplace's equation in a restricted region like a spherical cap, can be investigated in slightly different ways. Although the methods here described are all mathematical artifices, we can try to distinguish some properties of one with respect to the others, even with the risk to oversimplify. Hence, we could say that SCHA represents the most theoretical technique, say the *mathematical* one, defining a double set of orthogonal functions with a noninteger degree of the magnetic potential expansion. TOSCA considers also the specificity of some cases for which a better fit is obtained when

the origin is vertically translated. This is made without violating Laplace's equation. This fact could be explained with the tendency of the new origin, where we theoretically put all field sources, to be closer to the real sources; this is typical of the crustal anomaly field. For this reason, TOSCA can be considered a sort of *physical* method. Finally, ASHA represents an honest approximation of SCHA, giving the way to apply directly SHA, after an artificial scaling of the colatitudinal coordinates to those of a hemisphere. We could consider it a *practical* method. However all methods satisfy the boundary conditions imposed by the Haines (1985), and the use of one or another can be analysed case by case. Some caution should be taken considering that all methods are principally mathematical constructions, which are strictly valid in case of infinite expansions. In the real life, truncation is necessary, so some problems could emerge, mainly influenced by the spectral composition of the original field. A particular case is when one would like to represent a field with wavelengths longer than the data interval (e.g. secular variation and Sq magnetic fields may fall in this case, specially for cap half-angles smaller than 20-15°). In general, in addition to what stated by Haines (1985b; pag 2597) for which the method is potentially efficient at intermediate wavelengths, we add that better results can be obtained if the field under study does not possess spatial characteristic longer than the considered spherical cap. The usual subtraction of a global model can diminish the troubles, but does not completely remove them. None the less, the method has a *firm mathematical footing* (Haines, 1985b) and can be generally applied to many kinds of potential and general fields. The many advantages of the techniques here described and the very few possible drawbacks, give us some hopes to the possibility of extending the method to geodesy or gravimetry.

## Acknowledgements

The paper was presented at the III Hotine-Matussi Symposium on Mathematical Geodesy, L'Aquila, May 29 - June 3, 1994. We thank Gerry Haines and Fernando Sanso for their appropriate suggestions and comments.

## References

- Arfken, G., *Mathematical methods for physicists*, third ed., Academic Press, San Diego, pp. 985, 1985.
- Bullard E.C., The removal of trend from magnetic surveys, *Earth Plan. Sci. Let.*, 2, 293-300, 1967.
- Chapman, S. and J. Bartels, *Geomagnetism* (Oxford University Press, New York), Vol 2, 1940
- De Santis A., Translated origin spherical cap harmonic analysis, *Geophys. J. Int.*, 106, 253-263, 1991.
- De Santis A., Conventional spherical harmonic analysis for regional modelling of the geomagnetic field, 19, n.10, 1065-1067, 1992.
- De Santis A., De Franceschi G., Zolesi B., Cander Lj. R., Regional mapping of the critical frequency of the F2 layer by spherical cap harmonic expansion, *Ann. Geophys.*, 9, 401-406, 1991.

- De Santis A., Falcone C. and Lowes F.J., Remarks on the mean-square values of the geomagnetic field and its components, submitted to *Annali di Geofisica*, 1994.
- Haines, G.V., Spherical cap harmonic analysis, *J. Geoph. Res.*, **90**, 2583-2591, 1985a.
- Haines, G.V., Magsat vertical field anomalies above 40°N from spherical cap harmonic analysis, *J. Geoph. Res.*, **90**, 2593-2598, 1985b.
- Haines G.V., Computer programs for spherical cap harmonic analysis of potential and general fields, *Computers & Geosciences*, **14**, 4, 413-447, 1988.
- Hobson, E.W., *The theory of spherical and ellipsoidal harmonics*, pp. 500, Cambridge Press, 1931.
- Lowes F.J. and G.V. Haines, Some problems with spherical cap harmonic analysis,(abs.) *7<sup>th</sup> IAGA Scientific Assembly*, Part C, pag.413, 1993.
- Torta J.M., Garcia A., Curto J.J., De Santis A., New representation of geomagnetic secular variation over restricted regions by means of spherical cap harmonic analysis: application to the case of Spain, *Jour. Geomagn. Geoelectr.*, **74**, 209-217, 1992.
- Torta J.M., Garcia A., and De Santis A., A geomagnetic reference field for Spain at 1990, *Jour. Geomagn. Geoelectr.*, **45**, 573-588, 1993.

# SOLVING THE INVERSE GRAVIMETRIC PROBLEM: ON THE BENEFIT OF WAVELETS

Ludwig Ballani

GeoForschungsZentrum Potsdam (GFZ)

Department "Recent Kinematics and Dynamics of the Earth"

Telegrafenberg A17, D-14473 Potsdam

## INTRODUCTION

Inverse problems often consist in finding a physical quantity (density, diffusivity, conductivity) defined in a certain domain ('support'). The determination of a solution always requires a mathematical modelling of the corresponding (source or parameter) functions and domains involved. This process can be understood as a certain manner of probing or sounding. In this meaning 'sounding' can be directed to the approximation of one or several function values, e.g. by means of the known Backus-Gilbert method, but it is also done by the decomposition procedures to be considered here.

From both, the theoretical and numerical point of view there are different techniques to decompose the unknown physical quantity on its support: by systems of simple sources, by finite elements, or by suited function families (in general globally defined bases systems). However, in special situations (the study of inhomogeneities, of local effects, or of spectrally variable behaviour, also combined with irregularly spaced data) the ansatz of such function systems is useful which are orthogonal, living on scales being hierarchically ordered and having concentrated, (nearly) local supports, as well.

The wavelet functions, which were developed rapidly in the last years and are studied intensively further on, are function systems fulfilling these properties desired. Their effect can be compared with a 'mathematical microscope'. This function class is well adapted to describe the structure of matter (consisting of cells or grains with sizes on different scales, having inhomogeneous structures) and to account in a natural way for limited accuracy. Besides, there is rapid convergence in approximation processes, and the wavelet based algorithms are generally very fast. An introduction to this field can be found in (Daubechies 1992), (Jawerth and Sweldens 1993) or (Strichartz 1993) and related to geodesy (in these proceedings) in (Barthelmes et al 1994) and (Batha et al 1994) where further introductory literature is quoted.

Wavelet applications are not only restricted to image processing and data compression but have entered numerous functionalanalytic topics as an interesting numerical test area. The main objects decomposable by wavelets are operators and functions on

domains. Thus, the whole range of equations containing various types of operators (differential, integral etc.) have become the focus of attention. Of course, the inverse problems are involved here as well as the area of physical geodesy dealt with field modelling or approximation and the investigation of boundary value problems. But until now there exist only few papers on wavelet applications.

In the following section we sketch some fundamental points significant in applying wavelets to inverse problems taken from the literature. A further section is devoted to wavelets put into the inverse gravimetric problem as an example for a linear inverse source problem and is based on the theoretical frame given in (Ballani et al 1993a,b). Finally, a short outlook is added.

Of course, this paper is in no way able to treat the whole subject in detail, but will supply some ideas to the papers (Barthelmes et al 1994, Batha et al 1994, Freeden and Schreiner 1994) in accordance with the intentions of the Hotine-Marussi Symposium. Hopefully, it should be an impulse to start more detailed work.

## WAVELETS IN HANDLING INVERSE PROBLEMS

**Inverse problems** can be written in abstract form as operator equation

$$Au = v$$

with  $v$  as known function and the function  $u$  and/or the operator  $A$  as unknown(s) remembering an integral equation of the first kind. The mostly used and more detailed form is to choose, if possible, the representation by a differential operator:

$$\sum_{\alpha} a_{\alpha}(x) D^{\alpha} g(x) = f(x) \quad (1)$$

Then as usual a distinction can be made between an inverse coefficient problem or identification problem on the one hand (any function(s)  $a_{\alpha}(x)$  unknown) and a source problem or reconstruction problem on the other hand ( $f$  unknown) if information on  $g(x)$  is given (Anger 1990). The next section refers to a special source problem.

In the definition and notation of wavelet functions (**wavelets**) we follow those given in (Barthelmes et al 1994): If a function  $\psi(x)$  is defined on the whole real line  $\mathbb{R}$  and if the family

$$\left\{ \psi_{n,k}(x) = 2^{n/2} \psi(2^n x - k), \quad n, k \in \mathbb{Z} \right\} \quad (2)$$

forms a complete orthonormal system in  $L_2(\mathbb{R})$  then these functions  $\psi_{n,k}(x)$  are called (orthogonal) wavelets,  $\psi(x)$  itself is the Mother wavelet. The spans of single wavelet scales  $\{\psi_{n,k}(x), k \in \mathbb{Z}\}$  are orthogonal subspaces  $W_n$  whose orthogonal sums

$$\bigoplus_{-\infty}^{n-1} W_k = V_n \quad \left( \text{and} \quad \bigoplus_{-\infty}^{+\infty} W_k = L_2 \right)$$

form a sequence of nested subspaces  $V_n$  fulfilling some characteristic properties ('multiresolution analysis'). In addition, the concept of the Father function or scaling

function  $\phi(x)$  have to be mentioned: The set of its shiftings  $\{\phi(x - n), n \in \mathbb{Z}\}$  shall be a basis for  $V_0$ . Bases  $\{\phi_{n,k}\}$  for  $V_n$  can be generated after the scheme of (2).

What at all can be expected or happen if wavelets come into contact with inverse problems? A first insight can be gained - as one possible way - by looking at some mathematical objects and their properties coming into consideration:

**Functions** :  $x, f(x) \in \mathbb{R}^1, \mathbb{R}^2, \mathbb{R}^3$ , defined on bounded regions, having a certain degree of smoothness or belonging to special functionalanalytic spaces

**Operators** : defined between Hilbert or Banach spaces, linear or non-linear, bounded, compact (then the inverse operator is unbounded!), types: integral operators with different kernels, convolution operators, differential operators

In connection with **functions** in inverse problems thus the following features for wavelets are interesting and have to be discussed:

- dimensions higher than one
- definition on bounded intervals or bounded sets
- smoothness and approximation properties

The wavelet theory was originally developed for one dimension. Bases systems for **two dimensions** (or more) can be formed - as the simplest possibility - by collecting all products of the (one-dimensional) wavelets ('tensor product construction'). Thus the items of an orthogonal decomposition by means of this new wavelet basis combine mostly different scales in both directions (**rectangular wavelet decomposition**). If the father wavelets are included in forming the new (two-dimensional) basis elements a strongly scale-ordered two-dimensional wavelet decomposition (**square wavelet decomposition**) can be reached. (These approaches to multidimensional wavelet bases are presented more explicitly in (Batha et al 1994) in these proceedings). However, one remark should be added: It is a serious problem how to construct higher-dimensional wavelets which are not products of lower dimensional ones and are defined on more general regions not factorisable as a Cartesian product (Maaß 1992, Cohen and Daubechies 1993, Freeden and Schreiner 1994).

**Wavelets** are defined on the the whole real line  $\mathbb{R} = (-\infty, \infty)$ , but numerous inverse problems work mainly **on intervals or bounded sets**. The transition to such sets seems to be trivial, however, the actual aim consists in creating the full wavelet structures for them, too, i.e. completeness of the bases, multiresolution analysis with orthogonal subspaces. How can be found a construction providing a full valid wavelet theory living on the interval (or a bounded set) which avoids singularities and allows in addition to fulfill some boundary conditions?

There are at least three simple 'continuation' procedures to be applied to an 'interval function' making it to exist on the whole real axis: continuation by zero, periodical and 'reflected' periodical continuation (partly known from classical time series analysis). But their common disadvantage is to produce singularities for the new expanded  $\mathbb{R}$ -function or its first derivative repeating on all interval ends.

Two other proposals for bases constructions on the interval can be considered as more serious: In the first one all wavelet functions having a non-empty intersection

with the interesting interval are collected and their parts outside this interval are nullified. Then a new basis is simply generated by an orthogonalisation procedure for the function parts altogether existing on the interval. Now the crucial point is that by rigorous cutting off the remaining small wavelet parts near the interval boundaries can become weaker linearly independent and hence, the orthogonalisation procedure will not be very stable. This lack can be avoided by another procedure:

Only such near-boundary wavelet parts are considered which are results of the cutting-off process at the interval boundary: After exchanging these wavelet parts for monomials only these monomials are orthogonalised among themselves on the interval. The union of the unchanged wavelet subset and the replaced orthogonal function subset forms the new orthogonal basis. For bounded sets further constructions have been developed (hardly possible to describe in a short paper) (Auscher 1992, Jaffard and Laurençot 1992, Jawerth and Sweldens 1993).

The connection of **wavelets and smoothness** characterizes one of the recent highlights in approximation theory: Much more than with the well known Fourier series wavelets are linked with scales of functionalanalytic spaces (Hölder, Sobolev, Besov, Triebel-Lizorkin) because they reflect the local and global smoothness properties of the functions to be approximated. The following example limited to the one-dimensional case is a typical one:

Let be  $\Omega$  an open set in  $\mathbb{R}$ . For a function  $f$  and an integer  $l$ , non-negative,  $f^{(l)}$  shall denote the generalized (or weak)  $l$ -th derivative of  $f$ ,  $f^{(0)} \equiv f$ . Now the Sobolev space  $W_p^s(\Omega)$ ,  $s \geq 0$ , integer,  $1 \leq p < \infty$ , can be defined by (e.g. Adams 1975):

$$W_p^s(\Omega) := \left\{ f : f \in L_p(\Omega), f^{(l)} \in L_p(\Omega), 0 \leq l \leq s \right\} \quad (3)$$

For  $\Omega = \mathbb{R}$  the functions  $f$  belonging to the (Hilbert) space  $W_2^s(\mathbb{R})$  can be characterized by the summation condition for its wavelet coefficients  $d_{m,k} := (f, \psi_{m,k})$  (Jaffard and Laurençot 1992):

$$f \in W_2^s(\mathbb{R}) \iff \sum_{m \in \mathbf{Z}} \left( (1 + 2^{2m})^s \sum_{k \in \mathbf{Z}} |d_{m,k}|^2 \right) < \infty \quad (4)$$

This kind of summability statements exists for different types of Banach or Hilbert spaces, also for various degrees of regularity of the wavelets assumed as well as for (rectangular) bounded regions of  $\mathbb{R}^n$ , for  $\mathbb{R}^n$  itself and under the condition for the functions to fulfill given boundary values (e.g. Jaffard and Meyer 1989, Meyer 1992, Sickel 1991).

The favourable approximation capabilities combined with the structure of the multiresolution analysis lead to another point of interest in solving inverse problems: The nested orthogonal subspaces  $V_n$  are the base to construct efficient ‘wavelet-projection methods’ which are used to calculate regularised solutions for ill-posed operator equations, hence for inverse problems, too. Wavelet bases have also turned out to be an useful approximation tool for the moment problem, and thus, have opened a new look at the Backus-Gilbert technique (Maaß 1994, Louis 1993).

For the decomposition of operators by (one-dimensional) wavelets two types are known: **standard and non-standard form**, respectively. While the standard decomposition of an operator into an (infinite) matrix is identical to the usual way to decompose an operator by means of any basis, the non-standard form is especially related to integral operators by decomposing its kernel. Obviously, all operators appearing in physical geodesy can be handled in this way, e.g. the integral operators and the Laplacian, too (Beylkin et al 1991). For simple one-dimensional differential operators this decomposition process (requiring to solve a linear equation system at the end) was explicitly performed by Beylkin (1992). In more detail these decomposition principles are discussed in (Batha et al 1994).

Supplementary to these decomposing methods there is another one which generalizes the well known Singular Value Decomposition (SVD) used to solve operator equations of the form  $Af = g$ ,  $A$  (compact) :  $X \rightarrow Y$ ,  $X, Y$  Hilbert spaces.

The key role plays the so-called singular system  $\{u_n, v_n, \lambda_n^{1/2}\}$  for  $A$  defined by

$$A^*Av_n = \lambda_n v_n \quad u_n := \lambda_n^{-1/2}Av_n$$

The ‘solution’  $f$  can be written at least formally as

$$f = \sum_n \lambda_n^{-1/2}(g, u_n)v_n$$

Typically, the elements  $u_n, v_n$  are only adapted to the operator  $A$ , but not to the ‘object’  $f$  ! This deficiency can be overcome by the so-called **Wavelet-Vaguelette-Decomposition** which works in analogy to the SVD with a tripel  $\{\psi_{m,k}, \mathbf{v}_{\mathbf{m},k}, \kappa_{m,k}\}$  defined by the relations

$$A^*\mathbf{v}_{\mathbf{m},k} = \kappa_{m,k}\psi_{m,k}$$

and for a solution  $f^{appr}$  approximated by regularisation then holds

$$f^{appr} = \sum_{m \in M_{reg}} \sum_k \kappa_{m,k}^{-1}(g, \mathbf{v}_{\mathbf{m},k})_Y \psi_{m,k}$$

Here the **wavelets**  $\psi_{m,k}$  (compactly supported and equipped with a certain regularity) represent the ‘object’ function  $f$  with the corresponding regularity. The so-called **vaguelettes**  $\mathbf{v}_{\mathbf{m},k}$  carry the properties of the operator  $A$  and provide a kind of diagonalisation for it, but they themselves have no orthogonality. The numbers  $\kappa_{m,k}$  can be considered as ‘quasi singular values’.

This decomposition method can be applied to a wide class of operators in mathematical physics. Especially, convolution operators are well appropriated, which some mathematical assumptions have to be checked for (not specified here). Dicken (1994) has investigated some criteria in employing the Wavelet-Vaguelette-Decomposition to the solution of inverse problems, especially containing convolution operators. The benefit of this kind of ‘operator breaking’ consists in the possibility to use well-adapted wavelets and to profit numerically from their algorithmic advantages (hierarchical structures, recursive computation) (Donoho 1992, Maaß 1994).

## ASPECTS FOR THE INVERSE GRAVIMETRIC PROBLEM

The **inverse gravimetric problem** which is a right-hand side problem (or source problem) can be formulated in accordance to (1) in differential form by

$$-\frac{1}{4\pi k} \Delta u(x) = \begin{cases} f(x) & x \in \Omega \\ 0 & x \in \mathbb{R}^3 \setminus \Omega \end{cases} \quad \begin{array}{l} \text{(Poisson equation)} \\ \text{(Laplace equation)} \end{array}$$

with  $\Omega$  bounded,  $u(x), x \in \mathbb{R}^3 \setminus \Omega$  given (the gravitational potential outside the sources (masses) of the gravitational field) and the density  $f, f \in L_2(\Omega)$ , unknown.

The choice of the Hilbert space frame for such source problems as studied in (Ballani et al 1993a,b) has a lot of advantages, not only for the theory. A second formulation as an integral equation is represented by the formula for the Newtonian potential

$$u(x) = k \int_{\Omega} \frac{f(y)}{\|x - y\|_2} d\Omega \quad x \in \mathbb{R}^3 \setminus \Omega$$

Of course, both formulations can be interpreted as operator equations and the possibilities for the **operator decomposition** shown above can be applied.

For the **decomposition of (density) functions in 2 or 3 dimensions** by wavelets it is necessary to use geometrically simple regions (being Cartesian products: e.g. rectangle, sphere, cube, cuboid, torus) if the tensor product construction is used to form higher dimensional wavelet bases. (Another fundamental principle to build wavelet bases in  $L_2(\mathbb{R}^2)$  was studied in (Cohen and Daubechies 1993).)

**Example:** With the Haar wavelets  $H_{n,k}(x)$  defined on the interval  $[0,1]$  by

$$H_{n,k}(x) = 2^{n/2} H(2^n x - k) \quad \text{with} \quad H(x) = \chi_{[0,1/2)} - \chi_{[1/2,1]} \quad (\text{Haar mother wavelet})$$

the various tensor bases constructions for the space  $L_2(\Omega)$ ,  $\Omega = [0,1] \times [0,1]$ , can be illustrated easily: The rectangular decomposition is formed by the simple products

$$\{e_{i,k,j,l}(x, y) = H_{i,k}(x)H_{j,l}(y)\} \tag{5}$$

showing the mixture of all scales  $(i, j)$ .

By means of the basis functions  $\chi_{k,n}(x) = \chi(2^k x - n)$  derived from the characteristic function  $\chi_{[0,1]}(x)$  (the 'Father function') the scale-ordered ('k!') two-dimensional basis (square wavelet decomposition) is generated by three types of basis function products:

$$\{e_{k,n,m}(x, y) = \chi_{k,n}(x)H_{k,m}(y), H_{k,n}(x)\chi_{k,m}(y), H_{k,n}(x)H_{k,m}(y)\}$$

By the first principle also **mixed bases** can be constructed combining a wavelet basis in one dimension and another (globally defined) orthonormal basis for the second and third variable.

**Example:** Let be the unit sphere  $\Omega$  split up by  $\Omega = [0,1] \times \partial\Omega$ . If for the unit interval the Haar wavelets  $H_{i,k}$  are chosen and the surface of the sphere  $\partial\Omega$  is spanned

by the complete orthonormal system of the spherical surface harmonics  $Y_{l,m}(\vartheta, \varphi)$ ,  $l = 0, 1, \dots$ ,  $m = -l, \dots, l$ , then the set

$$\{e_{i,k,l,m}(r, \vartheta, \varphi) = H_{i,k}(r)Y_{l,m}(\vartheta, \varphi)\}$$

forms a complete basis (well adapted to the radially stratified Earth structure!) for the Hilbert space  $L_2(\Omega)$ , the density functions defined in a full spherical Earth ( $R_E = 1$ ).

Corresponding to this factorising scheme one could also think of finding wavelet bases defined on the surface of the sphere  $\partial\Omega$ . This could be realized at least formally by a parametric tensor product decomposition of the kind, e.g.

$$\{\psi_{p,q,r,s}(\vartheta, \varphi) = \Theta_{p,q}(\vartheta)\Phi_{r,s}(\varphi)\}$$

with the one-dimensional wavelet bases  $\{\Theta_{p,q}\}, \{\Phi_{r,s}\}$  resulting, however, in numerical difficulties and singularities well known.

In addition, geodesy needs the harmonicity (in the mass free outer space) for the continued surface bases functions (wavelets). Getting this property requires profunder construction principles as have already been proposed and developed in the papers (Freeden and Schreiner 1993, 1994) and (Freeden and Windheuser 1994). Although these developments aim at new possibilities for the approximation of the harmonic gravitational potential by wavelets (on the spherical Earth surface and in the outer space) they might also be important for the density approximation in the inverse gravimetric problem.

A favourable fact for the inverse gravimetric problem (and numerous other inverse source problems, too) is that the Hilbert space of (the unknown) **densities**  $L_2(\Omega)$  (in the following let be  $\Omega$  any three-dimensional bounded region) can be **orthogonally decomposed** into two subspaces having a clear mathematical characterization (Weck 1972, Ballani et al 1993a,b)

$$L_2(\Omega) = H \oplus G \quad (6)$$

with  $\mathbf{H} = N(\Delta)$  the kernel of the Laplacian (harmonic functions, ‘harmonic part’) which contains exactly the effective density functions generating the outer potential and  $\mathbf{G} = \Delta \overset{\circ}{W}_2^2$  the kernel of the Newtonian potential operator (‘anharmonic part’) which contains exactly the density functions with zero-potential in  $\mathbb{R}^3 \setminus \Omega$ .

(The Sobolev space  $\overset{\circ}{W}_2^2$  consists of those functions  $f \in W_2^2$  (defined in (3)) additionally fulfilling the boundary conditions

$$f|_{\partial\Omega} = 0 \quad \left. \frac{\partial f}{\partial n} \right|_{\partial\Omega} = 0 \quad .)$$

---

\*Most of these facts can be found in the article by Prof. A. MARUSSI “On the Density Distribution in Bodies of Assigned Outer Newtonian Attraction”, Boll. Geofis. Teor. Applic. XXII(1980) No.86, pp.83-94, reviewing various results of Italian scientists from the beginning of this century.

Thus, the task to decompose a  $L_2(\Omega)$ -density function by an orthogonal basis can also be moved to the two items  $H$  and  $G$ , separately.

With the recent results for the **approximation of harmonic functions** by wavelets the situation for the inverse gravimetric problem already appears a little more hopeful, too. It seems to be possible to construct new harmonic wavelet bases for  $N(\Delta)$ , e.g. in the sphere, corresponding to the remarks given above.

Considering, however, the item  $G$  in (6) the wavelet theory leads to interesting and completely new possibilities for the **description of ‘anharmonic’ densities**. This becomes clear comparing the structure of the zero-space  $\Delta \overset{\circ}{W}_2^2$  with the statements for wavelets related to Sobolev spaces  $W_2^s$  (see (3), (4)) for  $p = s = 2$ :

Let be  $f$  a zero-potential density,  $f \in \Delta \overset{\circ}{W}_2^2$ . Then there exists a function  $g$ ,  $g \in \overset{\circ}{W}_2^2$  with  $f = \Delta g$ . Analogous to (4) a summability condition for the wavelet coefficients  $(g, \psi_{m,k})$  of  $g$  is valid for a suitable wavelet basis  $\psi_{m,k}$  in  $L_2(\Omega)$  (Jaffard and Laurençot 1992, sections 2.2.4, 2.2.5, 4.2):

$$\sum_{m \in \mathbf{Z}} 2^{4m} \left( \sum_{k \in \mathbf{Z}} |(g, \psi_{m,k})|^2 \right) < \infty$$

The exchange of the wavelet basis  $\psi_{m,k}$  by means of  $\widetilde{\psi_{m,k}} = \Delta \widetilde{\psi_{m,k}}$  leads to the equivalent wavelet coefficient condition

$$\sum_{m \in \mathbf{Z}} 2^{4m} \left( \sum_{k \in \mathbf{Z}} |(f, \widetilde{\psi_{m,k}})|^2 \right) < \infty \quad (7)$$

now valid for the function  $f$  itself related to the exchanged wavelet basis  $\{\widetilde{\psi_{m,k}}\}$ . (However,  $\{\widetilde{\psi_{m,k}}\}$  will no longer be orthogonal, in general, but the supports are preserved!)

If for this process a wavelet basis for  $L_2(\mathbb{R}^3)$  is used, instead of  $L_2(\Omega)$  as demonstrated, then a changed  $(m, k)$ -summation is applied (which is limited to the interior of  $\Omega$  and proceeds in refining steps concerning the dyadic grid and the smoothness of the boundary of  $\Omega$  (Jaffard and Meyer 1989)).

**Simple example** for basis exchange: Using on the square  $[0, 1] \times [0, 1]$  the products of Haar wavelets as a basis  $\psi$  (see (5)) then the basis exchange leads to the new basis  $\widetilde{\psi}$  which consists of parts of simple quadratic polynomials with the same signs as the Haar wavelet products and unchanged supports.

From this possibility (to model a zero-potential density  $f$  and to approximate it by the wavelet basis  $\{\widetilde{\psi_{m,k}}\}$ ) by the summation condition (7) follows: The number of scales (= the range for the index  $m$  in (7)) can be drastically reduced (factor  $2^{4m}!$ ) if a well adapted wavelet basis is used. If  $m$  even can be restricted to a finite number, say  $M_0$ , then the zero-potential densities can be approximated by a truncated series including only a finite number of scales:

$$f \approx \sum_{m \leq M_0} \sum_k \beta_{m,k} \widetilde{\psi_{m,k}}$$

This corresponds directly to the **number of additional conditions** necessary to diminish the nonuniqueness of the inverse problem.

In view of this new variant for the **zero space decomposition** (G) it is interesting to compare it with the two other fundamental ones elaborated in (Ballani et al 1993a):

- With the relation  $G = L_2 \ominus H$  a basis  $\{g_k\}$  for G can be generated by projection if bases  $\{e_k\}, \{h_k\}$  are given for both spaces  $L_2$  and  $H$ , respectively.

$$g_k = e_k - \sum_i (e_k, h_i) h_i$$

- Using the equivalence (valid under very weak conditions)

$$u \in \Delta \overset{\circ}{W}_2^2 \iff u = S^2 f, f \in L_2 \quad \text{with } S(x) = 0, x \in \partial\Omega, \quad S \text{ and } \partial\Omega \text{ smooth enough}$$

a basis  $\{g_i\}$  (non-orthogonal in general) can be constructed with an orthogonal basis  $\{e_i\}$  by means of the identity  $g_i = \Delta(S^2 e_i)$ .

Comparing these principles under the wavelet aspect (e.g. let be  $e_i$  compactly supported wavelets) it becomes clear that in the first case the supports of the basis functions  $g_i$  are determined by the supports of the harmonic basis functions  $h_i$  which are global ones. But the second variant yields identically local supports for  $e_i$  and  $g_i$ .

Thus with the intention of producing **local approximations of zero-potential densities** the second variant has to be preferred.

The approach demonstrated briefly in this section above is an alternative one: One starts with a locally defined wavelet basis  $\psi_{m,k}$  in  $L_2(\Omega)$  or in  $L_2(\mathbb{R}^3)$ . Then the zero-potential densities taken from  $L_2(\Omega)$  can be characterized by the summation condition (7) for its wavelet coefficients (related to an ‘exchanged’ wavelet basis). Both approaches of local approximation have their own value and complement each other.

## ON SITUATION AND PROSPECTS

This article can only reflect very few moments of the rapidly developing wavelet theory and thus stays uncomplete depending on the period of time. Some aspects could be mentioned, some others not (e.g. the role of the wavelet transform for inverse problems). Wavelet theory already works successfully in different fields. But the mathematical wavelet community still has to overcome some serious insufficiencies (e.g. to construct applicable multidimensional wavelets in arbitrary regions). Further sophisticated analytical and numerical work will be necessary. The problem of harmonic wavelets geodetically relevant for the approximation of the Earth gravitational field has made some progress. As concerns the inverse gravimetric problem the efforts from different sides (solution structure, numerical modelling) seem to converge. The topic addressed here (construction of bases as mathematical structures adapted to the

structure of matter) can be seen as a logical continuation of the papers (Ballani et al 1993a,b and earlier ones cited there). Some aspects are related to physical geodesy.

The future work requires intensive efforts in doing numerical experiments for the new methods. Simultaneously, serious comparisons with traditional methods and procedures are needed. A permanent task will be the quick transfer of the new theoretical results for wavelets into the geodetic theory to be applied.

**Acknowledgements.** Writing this paper was only possible by the supply (above all with preprints or hints about references) and the intensive discussion with many persons. Especially, I thank Prof. P. Maaß, Dipl.-Math. V. Dicken and Dipl.-Math. M. Böhm (University of Potsdam), Prof. W. Freeden (University of Kaiserslautern), Dr. R. Hochmuth (Free University of Berlin) as well as my colleagues Dr. F. Barthelmes, Prof. R. Klees, and Dr. D. Stromeier. Some critical remarks and useful additions by an unknown reviewer are gratefully acknowledged, as well.

## REFERENCES

- Adams, R. A. (1975): Sobolev Spaces. Academic Press, New York
- Anger, G. (1990): Inverse Problems in Differential Equations. Akademie Verlag, Berlin, and Plenum Press, London
- Auscher, P. (1992): Wavelets with Boundary Conditions on the Interval. in: Wavelets - A Tutorial in Theory and Applications, Chui, C. K.(ed.), Academic Press, Boston, pp. 217-236
- Ballani, L., Stromeier, D. and Barthelmes, F. (1993a): Decomposition Principles for Linear Source Problems. in: Inverse Problems: Principles and Applications in Geophysics, Technology, and Medicine, Anger, G. et al (eds.), (Mathematical Research, Vol. 74), Akademie Verlag, Berlin, pp. 45-59
- Ballani, L., Engels, J. and Grafarend, E. (1993b): Global base functions for the mass density in the interior of a massive body (Earth). Manuscr. Geod., Vol. 18, pp. 99-114
- Barthelmes, F., Ballani, L. and Klees, R. (1994): On the Application of Wavelets in Geodesy. (these proceedings)
- Batha, L., Benciolini, B. and Zatelli, P. (1994): Geodetic applications of wavelets: proposals and simple numerical experiments. (these proceedings)
- Beylkin, G., Coifman, R. R. and Rokhlin, V. (1991): Fast Wavelet Transforms and Numerical Algorithms I. Comm. on Pure and Applied Math., Vol. 44, pp. 141-183
- Beylkin, G. (1992): On the Representation of Operators in Bases of Compactly Supported Wavelets. SIAM J. Numer. Anal., Vol. 6, pp. 1716-1740
- Chui, C. K.(ed.) (1992): Wavelets - A Tutorial in Theory and Applications. (Wavelet Analysis and Its Applications Series, Vol. 2), Academic Press, Boston
- Cohen, A. and Daubechies, I. (1993): Non-separable bidimensional wavelet bases. Revista Mat. Iberoamericana, Vol. 9, pp. 51-137
- Daubechies, I. (1992): Ten Lectures on Wavelets. (CBMS-NSF Regional Conference Series in Applied Mathematics, Vol. 61), SIAM Press, Philadelphia

- Dicken, V. (1994): Die Behandlung Inverser Probleme durch Wavelet-Zerlegungen.  
 Fachbereich Mathematik, Philipps-Universität Marburg, Diploma Theses
- Donoho, D. L. (1992): Nonlinear Solution of Linear Inverse Problems by Wavelet-Vaguelette Decomposition. Tech. Rep. 403, Stat. Dep., Stanford Univ., 46p.
- Freeden, W. and Schreiner, M. (1993): Nonorthogonal Expansions on the Sphere. Univ. of Kaiserslautern, (preprint, to appear in Math. Meth. in the Appl. Sci.)
- Freeden, W. and Schreiner, M. (1994): New Wavelet Methods for Approximating Harmonic Functions. (these proceedings)
- Freeden, W. and Windheuser, U. (1994): Earth's Gravitational Potential and It's MRA Approximation by Harmonic Singular Integrals. (to appear in Zeitschr. Angew. Math. Mech. (ZAMM))
- Jaffard, S. and Meyer, Y. (1989): Bases d'Ondelettes dans des Ouverts de  $\mathbb{R}^n$ . Journ. de Math. Pures et Appl. Vol. 68, pp. 95-108
- Jaffard, S. and Laurençot, P. (1992): Orthonormal Wavelets, Analysis of Operators, and Applications to Numerical Analysis. in: Wavelets - A Tutorial in Theory and Applications. Chui, C. K. (ed.), Academic Press, Boston, pp. 543-601
- Jawerth, B. and Sweldens, W. (1993): An Overview of Wavelet Based Multiresolution Analyses. (submitted to SIAM Review)
- Louis, A. K. (1993): A Wavelet Approach to Identification Problems. University of Saarbrücken (preprint)
- Maaß, P. (1992): Families of orthogonal 2D-wavelets with compact support. University of Saarbrücken (preprint)
- Maaß, P. (1994): Wavelet-projection methods for inverse problems. University of Potsdam (preprint)
- Meyer, Y. (1992): Wavelets and Operators. (Cambridge Studies in Advanced Mathematics, Vol. 37) Cambridge University Press, Cambridge
- Sickel, W. (1991): A remark on orthonormal bases of compactly supported wavelets in Triebel-Lizorkin spaces. The case  $0 < p, q < \infty$ . Arch. Math., Vol. 57, pp. 281-289
- Strichartz, R. S. (1993): How to make wavelets. Amer. Math. Monthly, Vol. 100, pp. 539-556
- Weck, N. (1972): Zwei inverse Probleme in der Potentialtheorie. Mitt. Inst. Theor. Geod. Univ. Bonn, Nr. 4, pp. 27-36

# INTEGRATED INVERSE GRAVIMETRIC PROBLEMS

Riccardo Barzaghi  
DIIAR - Politecnico di Milano  
Piazza Leonardo da Vinci 32, 20133 Milano - Italy

## 1. Introduction

Gravity observations are frequently used in solving inverse problems, i.e. in finding density and geometry of causative bodies, layer structures and so on.

Since the inverse gravimetric problem is an ill-posed problem, different regularization techniques are adopted to obtain physically relevant solutions (Tarantola, 1987; Sanso' et al., 1986).

Among the others, one possibility is to consider a priori information of geological or of seismic type to constrain the solution: in this paper, two different models of inverse gravimetric problems are solved using seismic/geological information.

In the first approach, the 3D inversion method based on collocation (Barzaghi et al., 1992) is extended to a three layers model and it is applied to estimate the depth variations  $\varepsilon_1, \varepsilon_2$  with respect to the mean depths  $H_1, H_2$ . Geological information are used to fix the mean density contrasts between layers, while the seismic profiles allow to estimate the mean depths  $H_1$  and  $H_2$  of the two separation surfaces and to compute the empirical auto and cross covariances of the depth variations  $\varepsilon_1$  and  $\varepsilon_2$ .

The second method refers to a profile, where seismic and gravity data are known. Suppose that the seismic data interpretation is given in terms of reflectors and velocity parameters and that we would like to integrate in a consistent way the gravity observations into the seismic model. Usually, to do so, one converts velocity into density (using some linear relationship) and performs a trial and error analysis, adjusting the shape and the density of the causative bodies to fit observed with computed gravity. In the proposed approach a more objective procedure to integrate gravity and seismic is introduced. A likelihood function is considered to account for discrepancies between the density/gravity model and the velocity/seismic one; the compatibility between the two models is then reached in a stochastic way.

## 2. A three layers model: the collocation approach

We consider a three layers structure model with two separation surfaces having mean depth  $H_1$  and  $H_2$  ( $0 < H_1 < H_2$ ), and we want to estimate the depth variations  $\varepsilon_1$  and  $\varepsilon_2$  with respect to  $H_1, H_2$  (see Fig. 1). Gravity data are given on a reference plane (that we assume to be  $z=0$ ) and stochastic properties are hypothesized for  $\varepsilon_1$  and  $\varepsilon_2$  in order to apply the collocation method (Barzaghi et al., 1992; Knudsen, 1993).

Furthermore, we suppose to know depth information along profiles, coming from seismic interpretation. These are useful to fix the mean depths  $H_1$  and  $H_2$  for the area under investigation and, together with geological information, to define the density contrasts  $\Delta\rho_{12}$  and  $\Delta\rho_{23}$ , between the first and the second layer and between the second and the third layer respectively. In addition, as it will be clear in the following, seismic informatiuon are also necessary to estimate the auto and cross covariance functions of  $\varepsilon_1$  and  $\varepsilon_2$ , which are needed to get the collocation solution of the problem. The observed gravity are related to  $H_1$ ,  $H_2$ ,  $\varepsilon_1$ ,  $\varepsilon_2$ ,  $\Delta\rho_{12}$  and  $\Delta\rho_{23}$  according to the linearized model

$$X(x, y) = \delta g(x, y) + n(x, y) = G\Delta\rho_{12} \int_{-\infty}^{+\infty} d\xi \int_{-\infty}^{+\infty} d\eta \frac{\varepsilon_1(\xi, \eta) H_1}{r_1^3} + \\ + G\Delta\rho_{23} \int_{-\infty}^{+\infty} d\xi \int_{-\infty}^{+\infty} d\eta \frac{\varepsilon_2(\xi, \eta) H_2}{r_2^3} + n(x, y) \quad (2.1)$$

with

$$\delta g(x, y) = g_{\text{obs}} - E(g_{\text{obs}})$$

$n(x, y)$  = white noise

$G$  = gravitational constant

$$r_1 = \sqrt{(x - \xi)^2 + (y - \eta)^2 + H_1^2}$$

$$r_2 = \sqrt{(x - \xi)^2 + (y - \eta)^2 + H_2^2}$$

In (2.1) the density contrasts  $\Delta\rho_{12}$ ,  $\Delta\rho_{23}$  and the mean depths  $H_1$ ,  $H_2$  are assumed to be fixed; that is, we suppose to estimate them, as previously pointed out, by means of geological/seismic information.

If we compute the Hankel spectrum of the covariance function of  $\delta g$  (Watson, 1948)

$$S_{\delta g \delta g}(k) = \int_0^{+\infty} dr_{PQ} r_{PQ} C_{\delta g \delta g}(r_{PQ}) J_0(kr_{PQ}) \quad (2.2)$$

where

$$C_{\delta g \delta g}(r_{PQ}) = E[\delta g(P) \delta g(Q)] = \text{auto covariance of } \delta g$$

$$r_{PQ} = \sqrt{(x_P - x_Q)^2 + (y_P - y_Q)^2}$$

we obtain (Barzaghi et al., 1992)

$$\begin{aligned} S_{\delta g \delta g}(k) = & (2\pi G \Delta \rho_{12})^2 e^{-2kH_1} S_{\varepsilon_1 \varepsilon_1}(k) + \\ & + 2 (2\pi G)^2 \Delta \rho_{12} \Delta \rho_{23} e^{-k(H_1+H_2)} S_{\varepsilon_1 \varepsilon_2}(k) + \\ & + (2\pi G \Delta \rho_{23})^2 e^{-2kH_2} S_{\varepsilon_2 \varepsilon_2}(k) \end{aligned} \quad (2.3)$$

$S_{\varepsilon_1 \varepsilon_1}(k)$  and  $S_{\varepsilon_2 \varepsilon_2}(k)$  are the Hankel spectra of the autocovariance functions of  $\varepsilon_1$  and  $\varepsilon_2$ , while  $S_{\varepsilon_1 \varepsilon_2}(k)$  is the Hankel spectrum of the crosscovariance  $C_{\varepsilon_1 \varepsilon_2}(r_{PQ})$ .

Similarly, we can introduce the Hankel spectrum of the crosscovariance function  $C_{\underline{\varepsilon} \delta g}(r_{PQ})$ , between  $\underline{\varepsilon} = [\varepsilon_1, \varepsilon_2]^t$  and  $\delta g$ , and express it as a function of  $S_{\varepsilon_1 \varepsilon_1}(k)$ ,  $S_{\varepsilon_2 \varepsilon_2}(k)$  and  $S_{\varepsilon_1 \varepsilon_2}(k)$

$$S_{\underline{\varepsilon} \delta g} = \begin{bmatrix} 2\pi G \Delta \rho_{12} e^{-kH_1} S_{\varepsilon_1 \varepsilon_1}(k) + 2\pi G \Delta \rho_{23} e^{-kH_2} S_{\varepsilon_1 \varepsilon_2}(k) \\ 2\pi G \Delta \rho_{12} e^{-kH_1} S_{\varepsilon_1 \varepsilon_2}(k) + 2\pi G \Delta \rho_{23} e^{-kH_2} S_{\varepsilon_2 \varepsilon_2}(k) \end{bmatrix} \quad (2.4)$$

The collocation estimate of  $\underline{\varepsilon}$  is

$$\hat{\underline{\varepsilon}}(P) = \sum_{i,j=1}^N C_{\underline{\varepsilon} \delta g}(r_{PP_i}) \left[ C_{\delta g \delta g}(r_{P_k P_l}) + \sigma_n^2 \delta_{kl} \right]_{i,j}^{-1} X(P_j) \quad (2.5)$$

$k, l = 1, \dots, N$

and, to compute it, we must have  $C_{\delta g \delta g}(r_{PQ})$  and  $C_{\underline{\varepsilon} \delta g}(r_{PQ})$ . If we have only gravity values, we can straightforwardly estimate  $C_{\delta g \delta g}(r_{PQ})$  but not  $C_{\underline{\varepsilon} \delta g}(r_{PQ})$  and, so, we cannot solve our problem. This is strictly related to the ambiguity of the three layers model and more generally to the inverse gravimetric problem; if we had only two layers (i.e. only  $\varepsilon_1$ ) we could obtain  $S_{\varepsilon_1 \varepsilon_1}(k)$  directly from  $S_{\delta g \delta g}(k)$  and compute  $S_{\varepsilon \delta g}(k)$ , which depends only from  $S_{\varepsilon_1 \varepsilon_1}(k)$  (Barzaghi et al., 1992). Obviously, this procedure cannot be adopted in the three layers case, because in (2.3) we have the sum of three terms which we are not able to discriminate only using gravity.

However, if we have, in the area under investigation, seismic profile information, we can try to estimate  $C_{\varepsilon_1 \varepsilon_1}(r_{PQ})$ ,  $C_{\varepsilon_2 \varepsilon_2}(r_{PQ})$  and  $C_{\varepsilon_1 \varepsilon_2}(r_{PQ})$  using seismic derived depths and use such estimates to solve for the ambiguity of formulae (2.3) and (2.4).

So, the procedure for computing the collocation estimates of  $\underline{\varepsilon}$  in (2.5) is the following:

- i) to estimate the covariance function  $C_{\delta g \delta g}(r_{PQ})$  from the gravity data;
- ii) to estimate the autocovariances  $C_{\varepsilon_1 \varepsilon_1}(r_{PQ})$ ,  $C_{\varepsilon_2 \varepsilon_2}(r_{PQ})$  and the crosscovariance  $C_{\varepsilon_1 \varepsilon_2}(r_{PQ})$  using seismic information along profiles;
- iii) to compare the Hankel spectra of these functions to check that they fit properly, verifying that the constraint given by formula (2.3) is satisfied;
- iv) to use such estimates to compute (2.4) and then (2.5).

Naturally, there are some weak points in this procedure. The main concern relates to step ii); if we use profile values to estimate the auto and the cross covariances of  $\varepsilon_1$  and  $\varepsilon_2$ , we cannot ensure that these estimates are properly computed. Seismic profiles can be placed in such a way that we are unable to recover from them the full covariance structure of the depth variation  $\varepsilon_1$  and  $\varepsilon_2$ . If this is the case, i.e. if the agreement between spectra in (2.3) is not reached, we must, in principle, stop the procedure and we cannot compute  $\hat{\varepsilon}$ .

### 3. A simulated test

To verify the procedure previously described, we performed a simulation. Two depth fields were computed in such a way that their stochastic properties were a priori fixed. Infact, if we consider a covariance function

$$C_{\varepsilon\varepsilon}(r_{PQ}) = A_\varepsilon J_0(\alpha r_{PQ}) \quad (3.1)$$

and a white noise  $v$

$$\begin{cases} E(v) = 0 \\ C_{vv} = I \end{cases} \quad (3.2)$$

the quantity

$$\begin{aligned} \varepsilon &= T^t v \\ T &= \text{Cholesky factor of the covariance matrix } C = [C_{\varepsilon\varepsilon}(r_{P_i P_j})] \end{aligned} \quad (3.3)$$

is a correlated signal with covariance function (3.1). So, we fixed a  $20 \times 20$  grid, with grid mesh  $\Delta x = \Delta y = 1\text{km}$ , and we computed, according to (3.3), two interfaces with the following covariance properties:

a) first separation surface

$$\begin{aligned} C_{\varepsilon_1 \varepsilon_1}(r_{PQ}) &= A_{\varepsilon_1} J_0(\alpha_1 r_{PQ}) \\ A_{\varepsilon_1} &= 0.4 \text{ km}^2 \quad \alpha_1 = 0.8 \text{ km}^{-1} \\ h_1(P_i) &= -[H_1 + \varepsilon_1(P_i)] \quad H_1 = 3 \text{ km} \end{aligned} \tag{3.4}$$

b) second separation surface

$$\begin{aligned} C_{\varepsilon_2 \varepsilon_2}(r_{PQ}) &= A_{\varepsilon_2} J_0(\alpha_2 r_{PQ}) \\ A_{\varepsilon_2} &= 0.2 \text{ km}^2 \quad \alpha_2 = 0.3 \text{ km}^{-1} \\ h_2(P_i) &= -[H_2 + \varepsilon_2(P_i)] \quad H_2 = 7 \text{ km} \end{aligned} \tag{3.5}$$

Furthermore, the crosscovariance between  $h_1(P)$  and  $h_2(P)$  was set to zero, i.e.  $C_{\varepsilon_1 \varepsilon_2}(r_{PQ}) = 0$ .

Since the autocovariances of  $\varepsilon_1$  and  $\varepsilon_2$  are zero order Bessel functions, their Hankel spectra are  $\delta$  functions (Watson, 1948); therefore, being the crosscovariance zero and using (2.3), we have that

$$\begin{aligned} C_{\delta g \delta g}(\alpha r_{PQ}) &= \int_0^{+\infty} dk k S_{\delta g \delta g}(k) J_0(kr_{PQ}) = \\ &= \int_0^{+\infty} dk k (2\pi G \Delta \rho_{12})^2 e^{-2kH_1} A_{\varepsilon_1} \frac{\delta(k/\alpha_1 - 1)}{\alpha_1^2} J_0(kr_{PQ}) + \\ &\quad + \int_0^{+\infty} dk k (2\pi G \Delta \rho_{23})^2 e^{-2kH_2} A_{\varepsilon_2} \frac{\delta(k/\alpha_2 - 1)}{\alpha_2^2} J_0(kr_{PQ}) = \\ &= (2\pi G \Delta \rho_{12})^2 e^{-2\alpha_1 H_1} A_{\varepsilon_1} J_0(\alpha_1 r_{PQ}) + (2\pi G \Delta \rho_{23})^2 e^{-2\alpha_2 H_2} A_{\varepsilon_2} J_0(\alpha_2 r_{PQ}) \end{aligned} \tag{3.6}$$

which is the model covariance function of the gravity data. The simulated  $\varepsilon_1$  and  $\varepsilon_2$  values are plotted in Fig. 2 and Fig. 3. As we mentioned before, data are computed on a regular grid and their a posteriori statistics are the following

	n	Average (km)	St. dev. (km)	Max. (km)	min (km)
$\varepsilon_1$	400	-0.023	0.716	2.086	-1.822
$\varepsilon_2$	400	-0.027	0.458	0.976	-0.813

Table 1 - Simulated values statistics

In Fig. 2 and Fig. 3 are also shown the seismic profiles along which we suppose to know globally 50 depth values for both separation surfaces.

The gravity effect due to the three layers structure has been obtained by imposing the two density contrasts

$$\begin{aligned}\Delta\rho_{12} &= \rho_1 - \rho_2 = -0.3 \frac{\text{g}}{\text{cm}^3} \\ \Delta\rho_{23} &= \rho_2 - \rho_3 = -0.5 \frac{\text{g}}{\text{cm}^3}\end{aligned}\tag{3.7}$$

and the gravity values are plotted in Fig. 4.

Following the procedure that we devised in the second paragraph we used the fifty  $\varepsilon_1$  and the fifty  $\varepsilon_2$  values along the profiles to estimate the autocovariances  $C_{\varepsilon_1\varepsilon_1}(r_{PQ})$  and  $C_{\varepsilon_2\varepsilon_2}(r_{PQ})$ . Furthermore, for checking purposes, we estimated these two empirical functions using the whole sets of 400  $\varepsilon_1$  and 400  $\varepsilon_2$  values. The empirical autocovariances estimated in such a way are plotted in Fig. 5 and Fig. 6 respectively, together with the models (3.4) and (3.5). As one can see, a good agreement is reached for the autocovariance of  $\varepsilon_1$  either using the entire data set or the fifty profile values, so that we can say that the seismic values are statistically representative of the global data set.

The same conclusion doesn't hold for the deeper separation surface; while the empirical covariance computed using the complete data set fits the model function (3.5), the one based on the fifty  $\varepsilon_2$  values displays evident distortions with respect to the model.

The four empirical covariances were then fitted with model covariance functions: the best fit models and the related parameters are summarized in Table 2.

Best fit covariance model	50 values	400 values
$C_{\varepsilon_1\varepsilon_1}(r) = \hat{A}_{\varepsilon_1} J_0(\hat{\alpha}_1 r)$	$\hat{A}_{\varepsilon_1} = 0.53 \text{ km}^2$ $\hat{\alpha}_{\varepsilon_1} = 0.79 \text{ km}^{-1}$	$\hat{A}_{\varepsilon_1} = 0.46 \text{ km}^2$ $\hat{\alpha}_{\varepsilon_1} = 0.78 \text{ km}^{-1}$
$C_{\varepsilon_2\varepsilon_2}(r) = \hat{A}_{\varepsilon_2} J_0(\hat{\alpha}_2 r)$	$\hat{A}_{\varepsilon_2} = 0.24 \text{ km}^2$ $\hat{\alpha}_{\varepsilon_2} = 0.36 \text{ km}^{-1}$	$\hat{A}_{\varepsilon_2} = 0.20 \text{ km}^2$ $\hat{\alpha}_{\varepsilon_2} = 0.29 \text{ km}^{-1}$

Table 2 - Covariance models and estimated parameters

The best fit models are in each case zero order Bessel functions but, as expected, the parameters estimated using the fifty values data set are less close to the model parameters (3.4) , (3.5) than the ones obtained using the global data sets.

Using the values of Table 2 and (3.6), we derived the two model covariances of gravity based on the fifty seismic depths and on the whole data set of  $\varepsilon_1$  and  $\varepsilon_2$ . In Fig. 7 these two functions are compared with the empirical covariance of  $\delta g$ ; its fitting with the model functions based on the global sets of  $\varepsilon_1$  and  $\varepsilon_2$  is satisfactory while it is quite poor if we consider the fifty values derived model covariance. So, following the remark at the end of the second paragraph, we are in a doubtful case, i.e. the seismic derived covariance doesn't fit properly the empirical covariance of gravity. This obviously implies distortions in the estimates of  $\varepsilon_1$  and  $\varepsilon_2$  which cannot be computed properly. To quantify such distortions, we performed two tests. In the former, test (A), we considered the model covariance of  $\delta g$  as derived from the whole data set of  $\varepsilon_1$  and  $\varepsilon_2$ ; this is consistency test, which is done to verify that the simulation is properly set. The latter, test (B), is based on the gravity model covariance obtained from the along profile depth values; this is the "real case" situation and we are hence mainly interested in it. Furthermore, test (A) represents a target for test (B) since it gives the measure of the reliability of the method in the best possible case.

The results of such tests are summarized in Table 3.

	n	Average (km)	St. dev. (km)	Max (km)	min (km)
<b>TEST (A)</b>					
$\delta\varepsilon_1 = \varepsilon_1 - \hat{\varepsilon}_1$	400	0.008	0.181	0.376	-0.554
$\delta\varepsilon_2 = \varepsilon_2 - \hat{\varepsilon}_2$	400	-0.009	0.211	0.731	-0.492
<b>TEST (B)</b>					
$\delta\varepsilon_1 = \varepsilon_1 - \hat{\varepsilon}_1$	400	-0.009	0.250	0.609	-0.735
$\delta\varepsilon_2 = \varepsilon_2 - \hat{\varepsilon}_2$	400	0.024	0.409	0.902	-0.790

Table 3 - Test (A) and test (B) statistics

The consistency test (A) gives, as expected, good results (see Fig. 8 and Fig. 9) while the  $\hat{\varepsilon}_1$  and  $\hat{\varepsilon}_2$  values estimated in test (B) are quite poor (especially  $\hat{\varepsilon}_2$ ). Nevertheless, if we consider that test (B) is performed using an ill conditioned covariance structure, we can conclude that the inverted values are still quite significant. This is also confirmed by the contour line plots of  $\hat{\varepsilon}_1$  and  $\hat{\varepsilon}_2$ , test (B), which are drawn in Fig. 10 and Fig. 11 respectively. Even though serious distortions are present in  $\hat{\varepsilon}_1$  and  $\hat{\varepsilon}_2$  , the main features of  $\varepsilon_1$  and  $\varepsilon_2$  are reconstructed, al least for what concerns the position of maxima and

minima (the same conclusion doesn't hold for amplitudes which are overestimated, especially in  $\hat{\varepsilon}_2$  ).

In conclusion, we can say that the collocation method applied to the three layers model is able to give sufficient results even in a critical situation, as it is the one presented in test (B).

#### 4. Integrating tomography and gravity

The second approach here proposed to integrate gravity data and seismic information refers to a 2D profile.

We hypothesize to measure gravity data along a seismic profile ( or to reduce them to it ) and that a tomographic investigation has been performed on seismic data.

The outcome of such an inversion is a discrete set of slowness values  $S_i$  ( $S_i = 1/V_i$  ;  $V_i$  = velocity) for each block of the resolving grid, together with the covariance matrix of the estimated values (Aki & Richards, 1980). Usually, at this point, if gravity data has been measured along the profile, a trial and error procedure is applied to test if the seismic/tomographic model is consistent with gravity. The tomographic derived  $S_i$  values are grouped in layers and anomalous bodies inside the layers are considered where sharp changes of  $S_i$  are present. A linear relationship is then assumed between  $S$  and the density  $\rho$  and the direct gravity effect of such a density field is computed and compared with the observed values. By adjusting densities and shapes of the causative bodies, the fitting is improved and the density model refined.

This trial and error procedure is in some respect unsatisfactory. The first simplificatory step (which defines layers) is indeed based on geological evidences but it seems to be too much subjective and it can be misleading. The second concern relates to the conversion of  $S$  into  $\rho$ ; the linear relationship between density and slowness doesn't hold in general and therefore serious biases can be induced in the computed gravity effect. Finally, the adjustment of densities and shapes of the causative bodies based on the forth and back procedure leads in most cases to quite poor improvements in the fit between model and observed gravity values. At the end, due to what we have pointed out, the gravimetric investigation performed in such a way is a gross consistency test which doesn't add to much to the seismic/tomographic interpretation.

A more rigorous approach to the comparison and integration between seismic/tomography and gravity can be given on the basis of the criticism previously expressed. In particular, the problems related to the simplification of the tomographic model and to the linear relationship between  $\rho$  and  $S$  can be tackled in a more appropriate way using stochastic concepts (Tarantola, 1987).

Suppose that you have already done a tomographic interpretation of your seismic profile, so that you have estimated a set of  $S_i^0$  values and their covariance matrix  $C_{SS}$ . As we told before, using some linear relationship

$$\rho_i^0 = a S_i^0 \quad i = 1, \dots, n \quad (4.1)$$

we can compute the model gravity in the  $P_k$  measuring points

$$g_k^0 = G_k(\rho_i^0) \quad i = 1, \dots, n \quad k = 1, \dots, m$$

$$G_k(\rho_i^0) = \sum_{i=1}^n -2G\rho_i^0 \iint_{A_i} d\xi d\zeta \frac{z_k - \zeta}{(x_k - \xi)^2 - (z_k - \zeta)^2} \quad (4.2)$$

$$G = \text{gravitational constant}; \quad P_k = (x_k, y_k)$$

and compare it with the  $g_k^{\text{obs}}$  observed values. We can then determine the gravity discrepancies

$$\delta g_k = g_k^{\text{obs}} - g_k^0 \quad (4.3)$$

which accounts for model errors in (4.1) and for possible distortions in the seismic interpretation.

Consider now the likelihood function

$$L(\delta g, \delta \rho, \delta S) \propto e^{-\frac{1}{2}[\delta g - G(\delta \rho)]^T C_{gg}^{-1} [\delta g - G(\delta \rho)]} \times e^{-\frac{1}{2}[\delta \rho - a \delta S]^T C_{mm}^{-1} [\delta \rho - a \delta S]} \times e^{-\frac{1}{2}[\delta S]^T C_{ss}^{-1} [\delta S]} \quad (4.4)$$

where

$$\delta \rho = \rho - \rho^0$$

$$\delta S = S - S^0$$

$C_{gg}$  = covariance matrix of gravity

$C_{mm}$  = covariance matrix of the model that we assume in order to link density and slowness

$C_{ss}$  = covariance matrix of slowness as derived from the tomographic interpretation

A priori assumptions are taken into account in  $C_{mm}$  and  $C_{ss}$ , while  $C_{gg}$  reflects the covariance structure of the data. Thus, we consider the seismic/tomographic interpretation

with its covariance  $C_{ss}$  as an a priori information concerning  $\rho$ . Similarly, the term containing  $C_{mm}$  is related to the a priori linear model which is assumed to exist between  $\rho$  and  $S$ . Since it is not errorless (Barton, 1986), we can introduce model errors by tuning the variances on the main diagonal of  $C_{mm}$ . Furthermore, we can consider layer information coming from the seismic/geological interpretation by mean of correlations between blocks which involve the extra diagonal terms of  $C_{mm}$ .

The main difference between this approach and the usual trial and error procedure is that we are now considering the relationship between  $\delta\rho$  and  $\delta S$  and the layer structures in a stochastic way, that is with a more flexible scheme. Obviously, the critical point is to fix the elements of the matrix  $C_{mm}$  in order to weight properly the information that we introduce in it. Once the structure of  $C_{mm}$  has been defined, we can estimate  $\delta\rho$  and  $\delta S$  by applying the maximum likelihood principle

$$\underset{(\delta\rho, \delta S)}{\text{Max}} \quad L(\delta g, \delta \rho, \delta S) \quad (4.5)$$

which leads to the resolving formulae

$$\hat{\delta\rho} = (G^t C_{gg}^{-1} G + C_{mm}^{-1} - a^2 C_{mm}^{-1} (a^2 C_{mm}^{-1} + C_{ss}^{-1})^{-1} C_{mm}^{-1})^{-1} G^t C_{mm}^{-1} \delta g \quad (4.6)$$

$$\hat{\delta S} = (a^2 C_{mm}^{-1} + C_{ss}^{-1})^{-1} a C_{mm}^{-1} \hat{\delta\rho} \quad (4.7)$$

Note that, if the errors in the a priori information tend to zero, (4.6) becomes simply the least squares estimator of  $\delta\rho$  having measured  $\delta g$  and (4.7) reduces to the linear relationship (4.1).

## 5. Conclusions

The two methods which we devised are suitable for integrating gravity data and seismic/geological information.

The first approach presented in the paper shows how we can consider seismic derived depths to constrain in a stochastic way the collocation inversion of gravity data in a three layers model. This method has been tested with a simulation which gave sufficient results even though the covariance structure of gravity, recovered from seismic, had relevant distortions. By virtue of this result, we can say that the collocation procedure can be extended quite straightforwardly to this more complex model (we recall that the collocation approach to gravity inversion has been originally proposed for a two layers structure).

The second method, based on the definition of a proper likelihood function, can be considered a stochastic generalization of the usual "trial and error" technique.

Heterogeneous information are merged together taking into account model errors in a probabilistic frame, a more flexible approach to such a problem.

## References

- Aki, K., Richards, P. G. (1980). Quantitative seismology; theory and methods. W.H. Freeman and Co., San Francisco.
- Barton, P. J. (1986). The relationship between seismic velocity and density in the crust; a useful constraint?. *Geophys. J. R. astr. Soc.*, 87, 195-208.
- Barzaghi, R., Gandino, A., Sanso', F. and Zenucchini C. (1992). The collocation approach to the inversion of gravity data. *Geophysical Prospecting* 40, 429-451.
- Knudsen, P. (1993). Optimal inversion of gravity data. Proceedings of the Interdisciplinary Inversion Workshop 2, Klaus Mosegaard (ed.), The Niels Bohr Institute for Astronomy, Physics and Geophysics, University of Copenhagen, ISBN 87-984767-1-8, 59-64.
- Sanso', F., Barzaghi, R. and Tscherning, C. C. (1986). Choice of norm for the density distribution of the Earth. *Geophys. J. R. astr. Soc.*, 87:1, 123-141
- Tarantola, A. (1987). Inverse Problem Theory. Elsevier.
- Watson, G. N. (1948). Theory of Bessel functions. 2nd Edition. Cambridge University Press

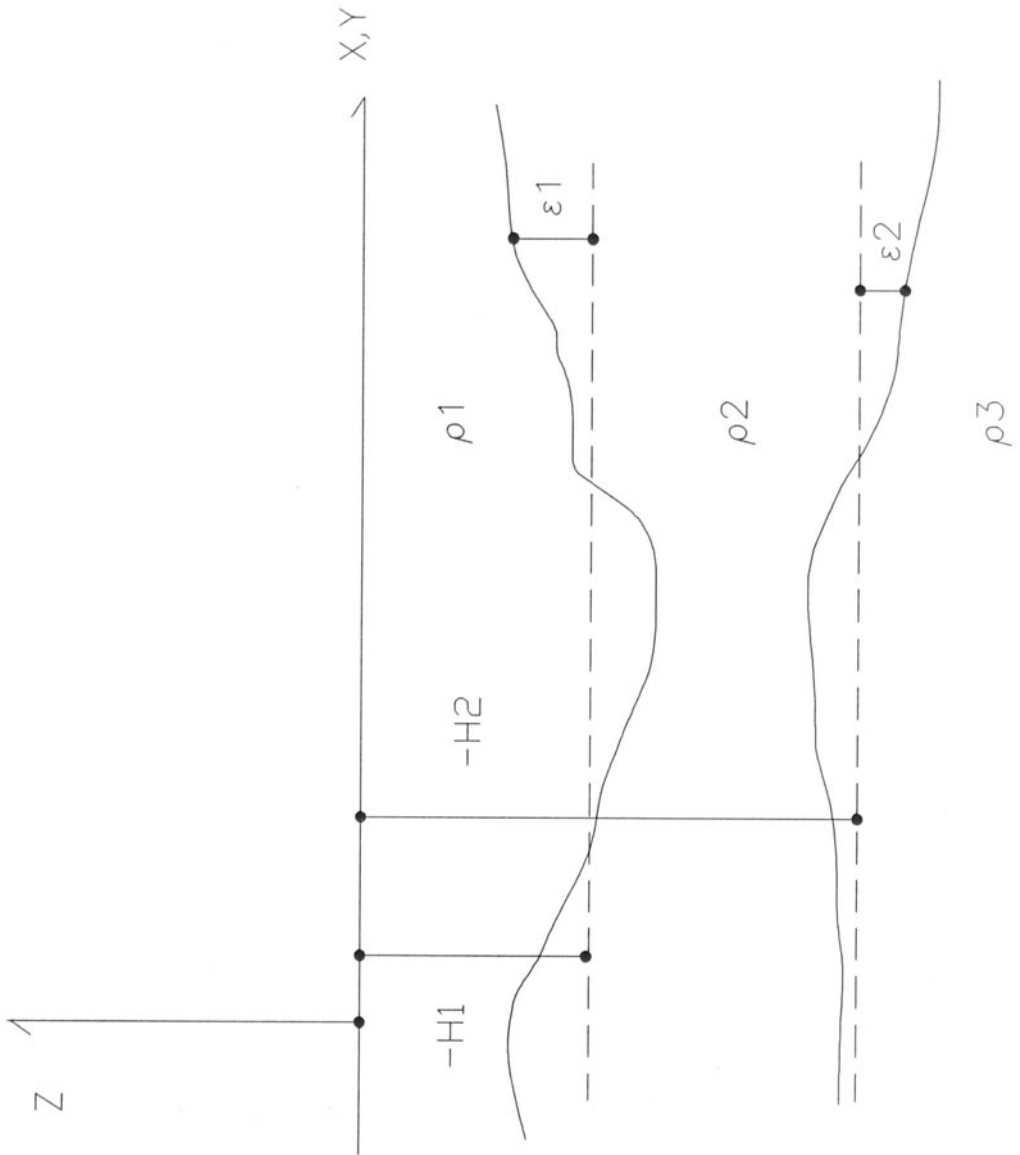


Fig. 1 - The three layers model

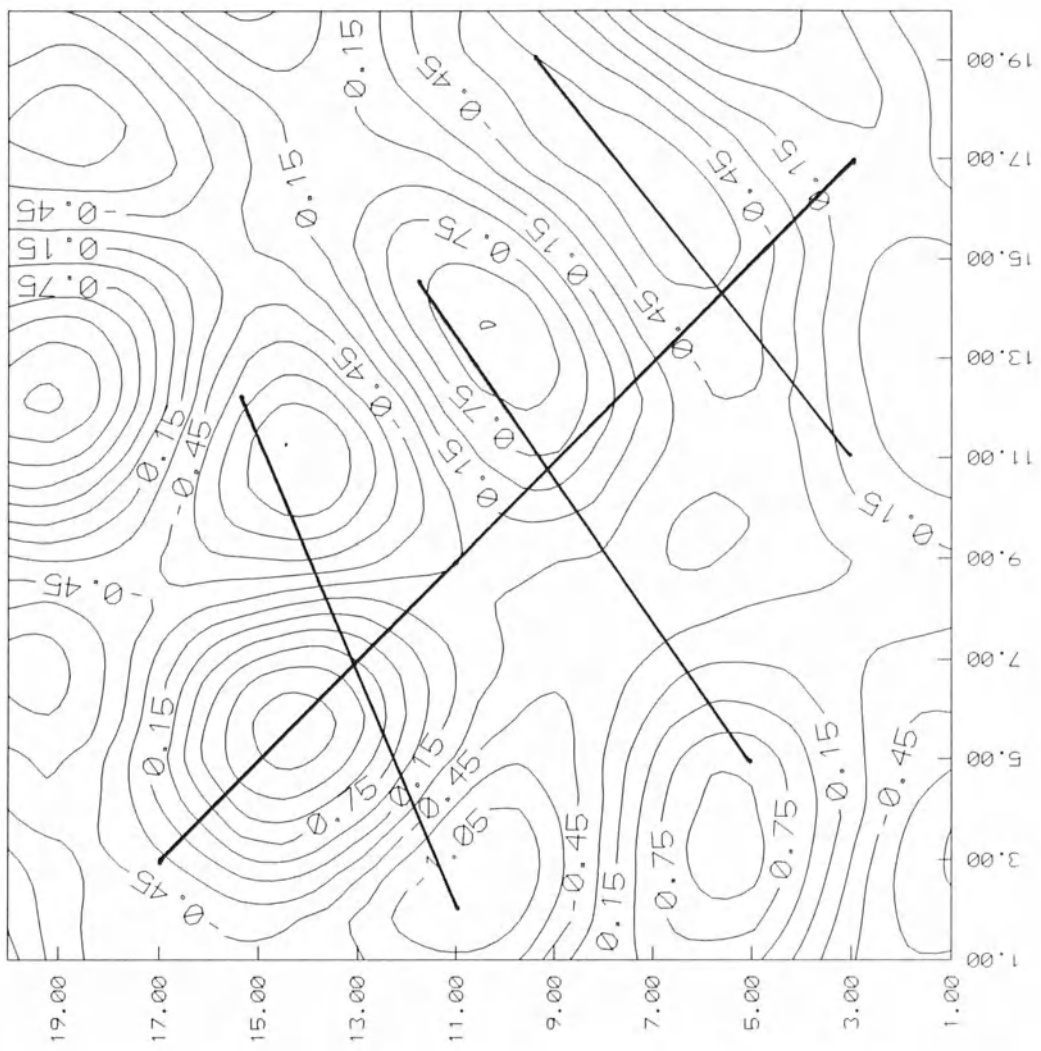


Fig. 2 -  $\varepsilon_1$  simulated values (km)

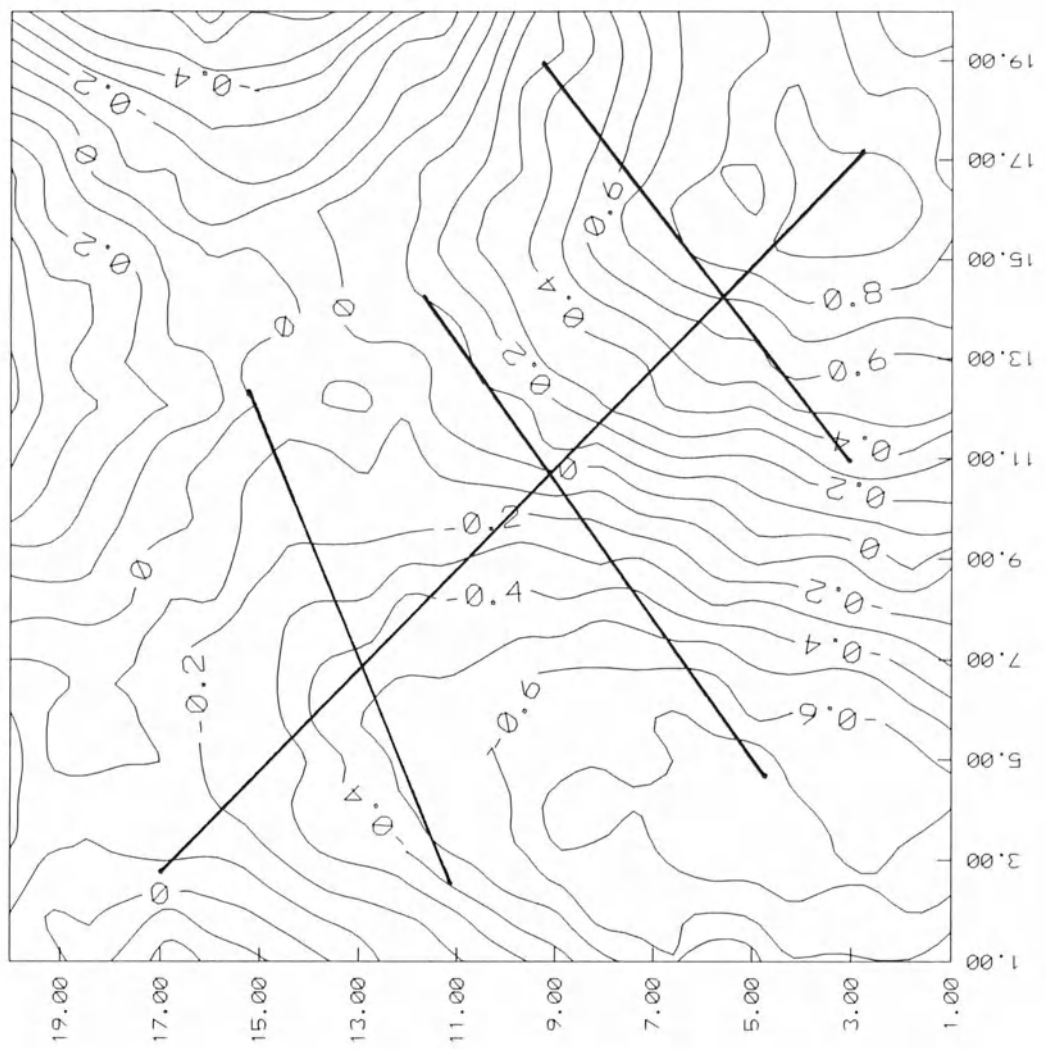


Fig. 3 -  $\varepsilon_2$  simulated values (km)

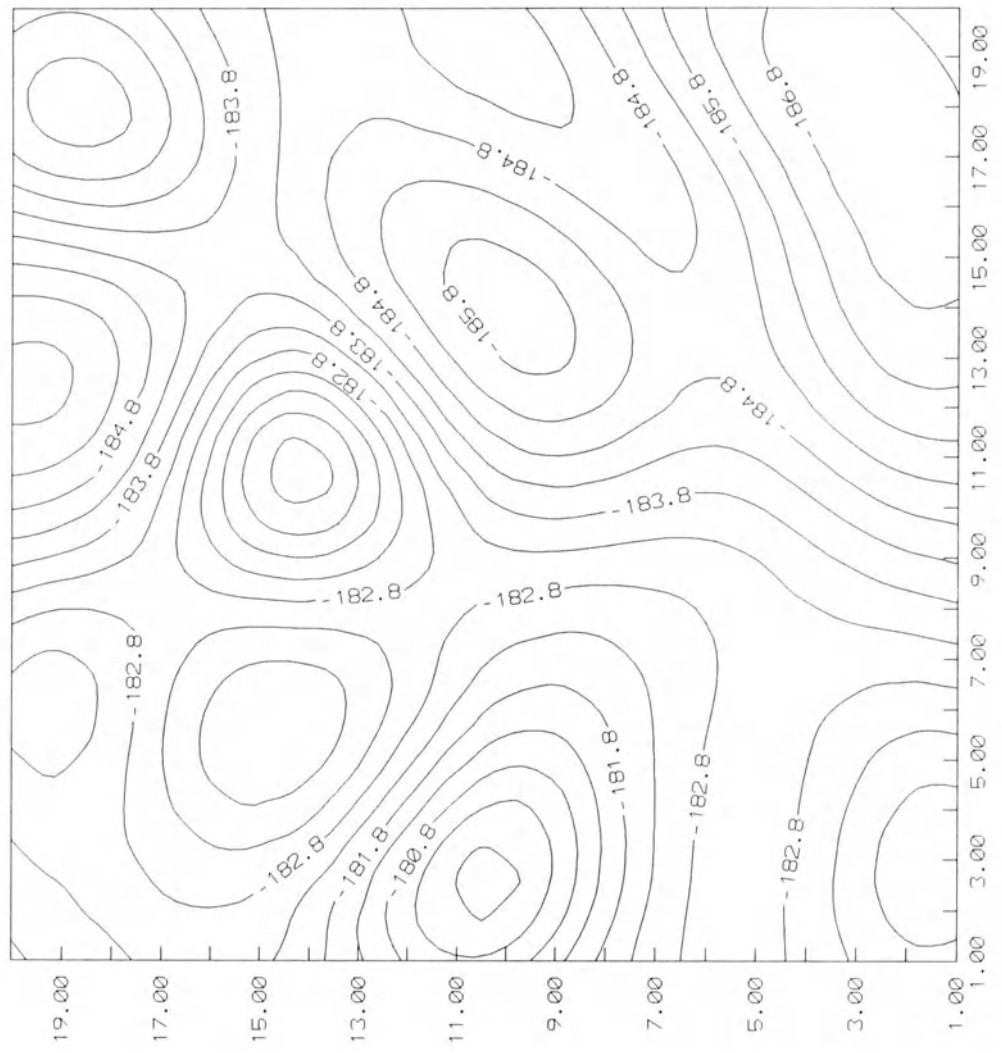


Fig. 4 -  $\delta g$  values implied by the simulated three layers model (mgal)

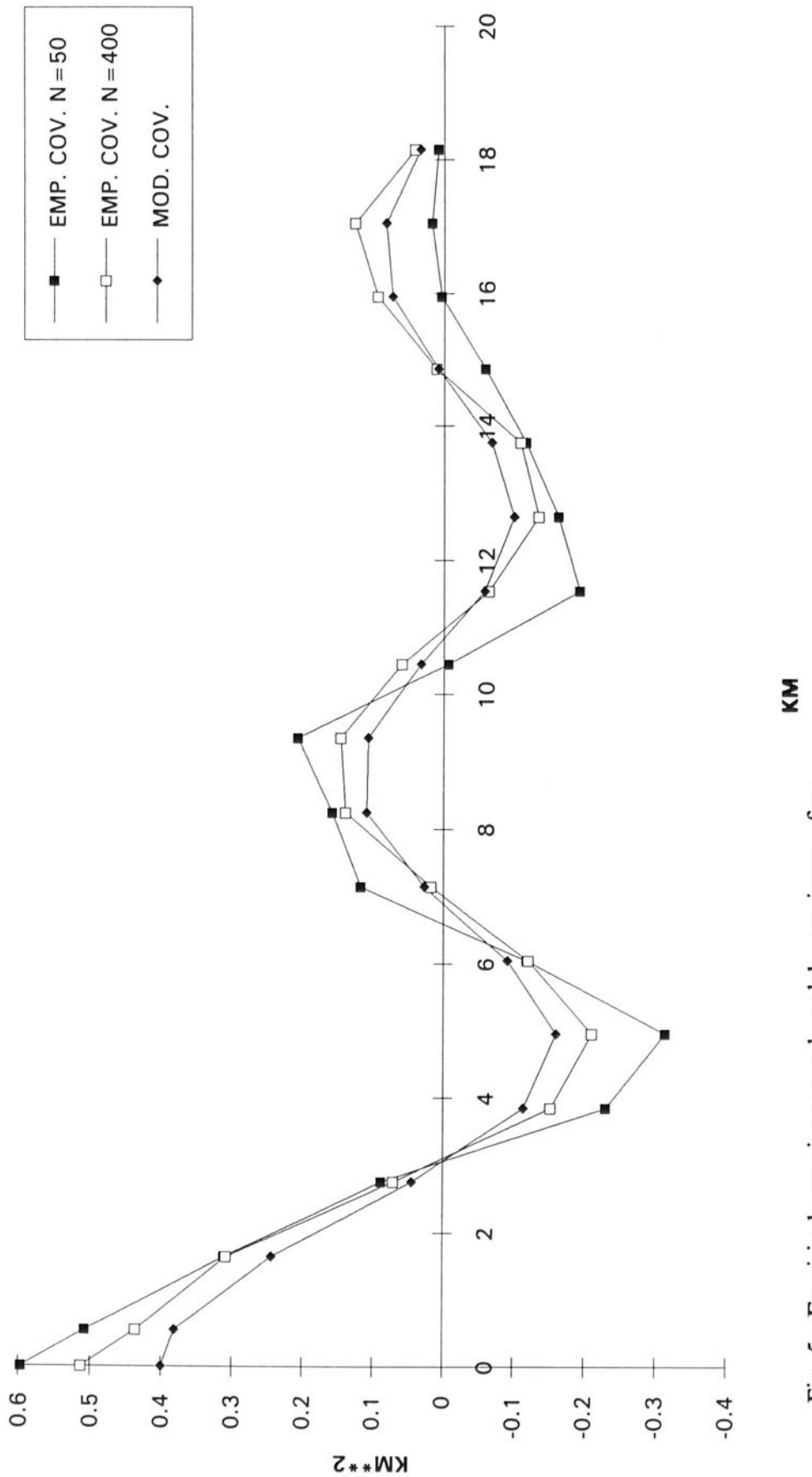


Fig. 5 - Empirical covariances and model covariance of  $\varepsilon_1$

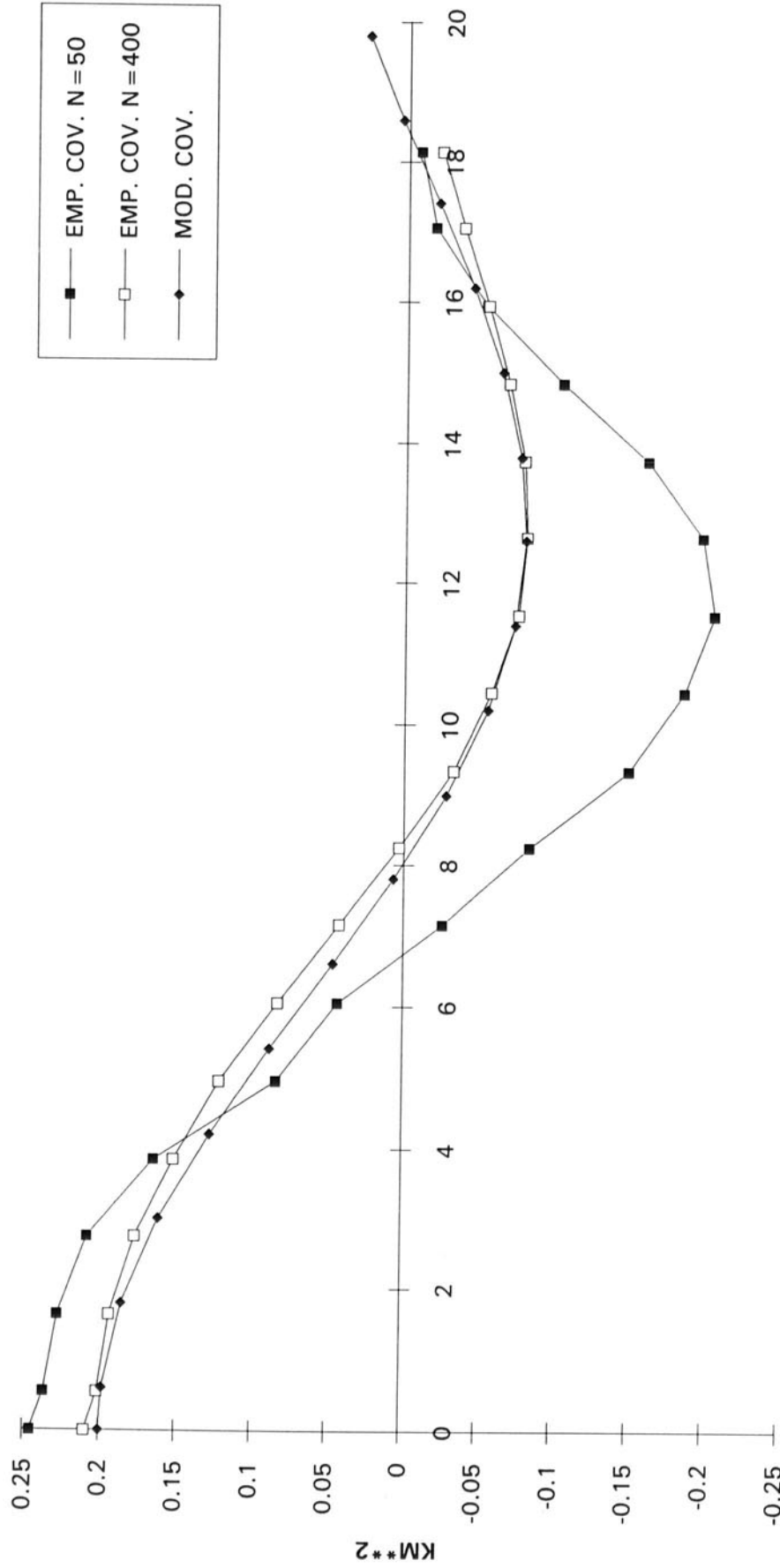


Fig. 6 - Empirical covariances and model covariance of  $\varepsilon_2$       **KM**

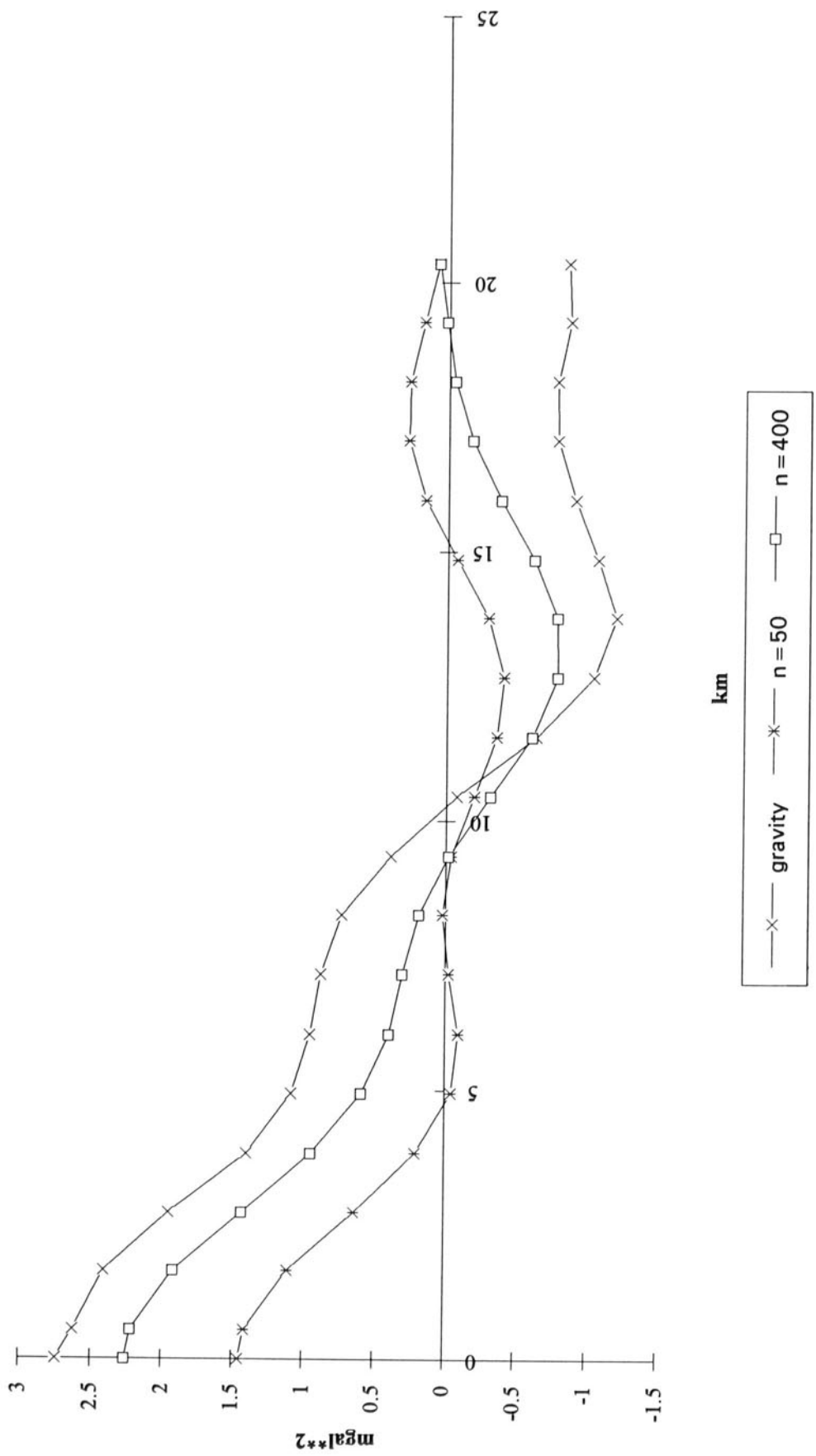


Fig. 7 - Empirical and model covariance of  $\delta g$

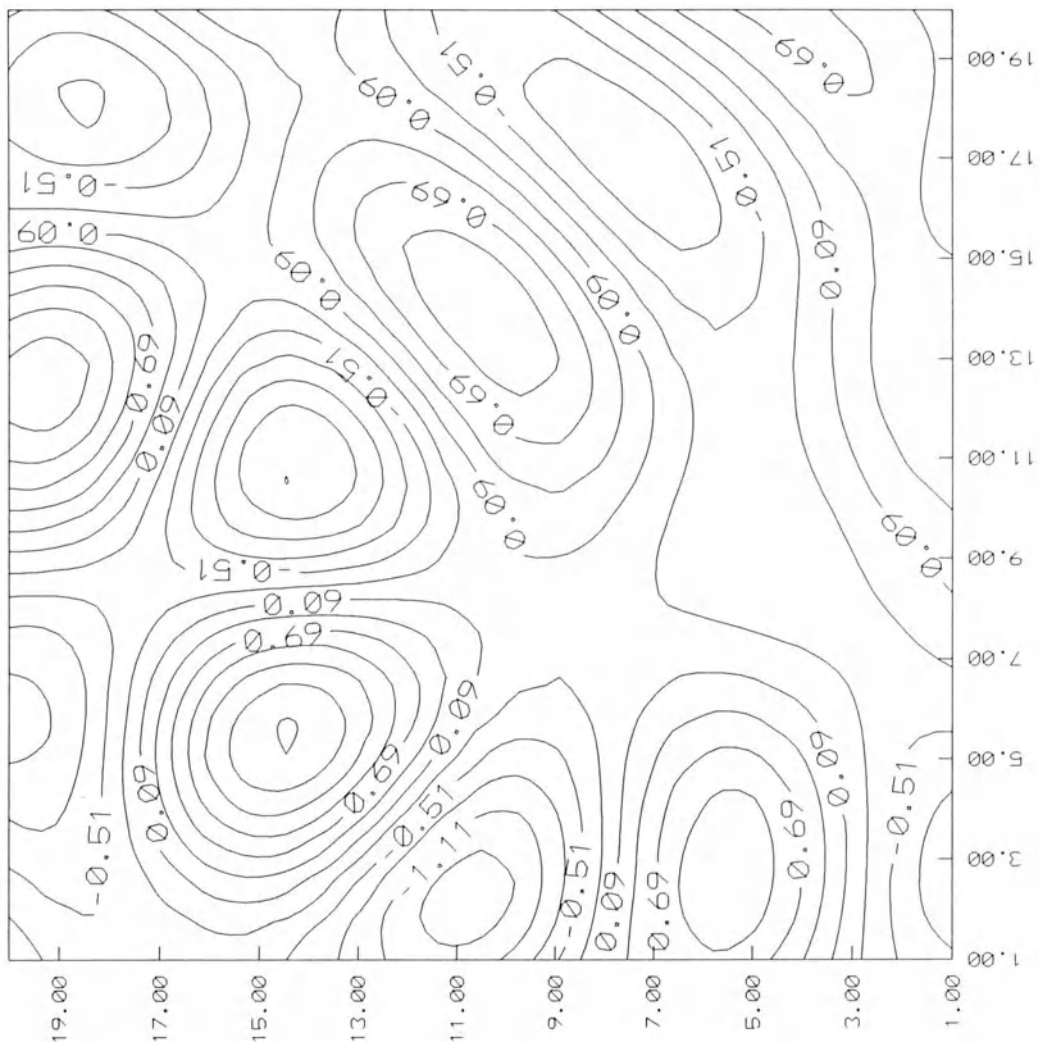


Fig. 8 - Test (A):  $\hat{\varepsilon}_1$  values (km)

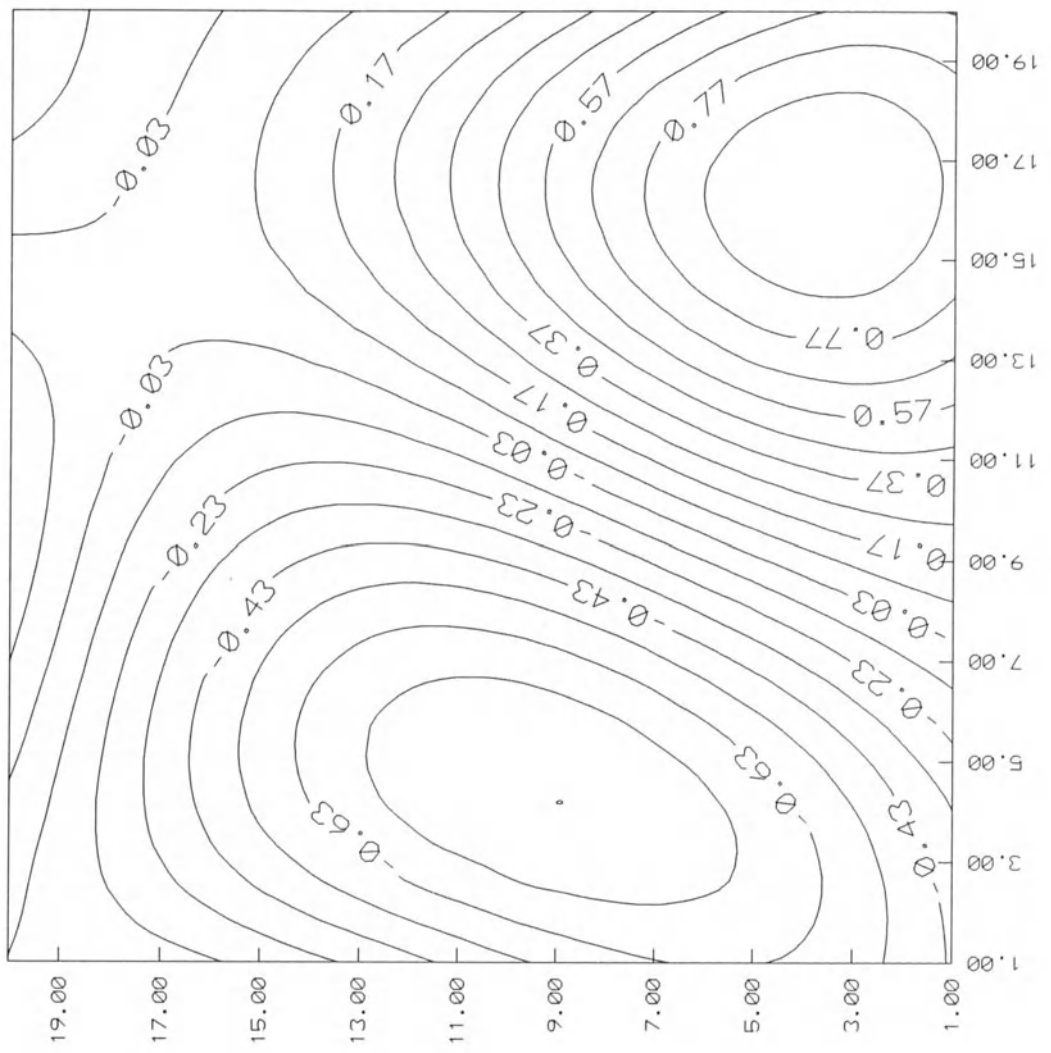


Fig. 9 - Test (A):  $\hat{\varepsilon}_2$  values (km)

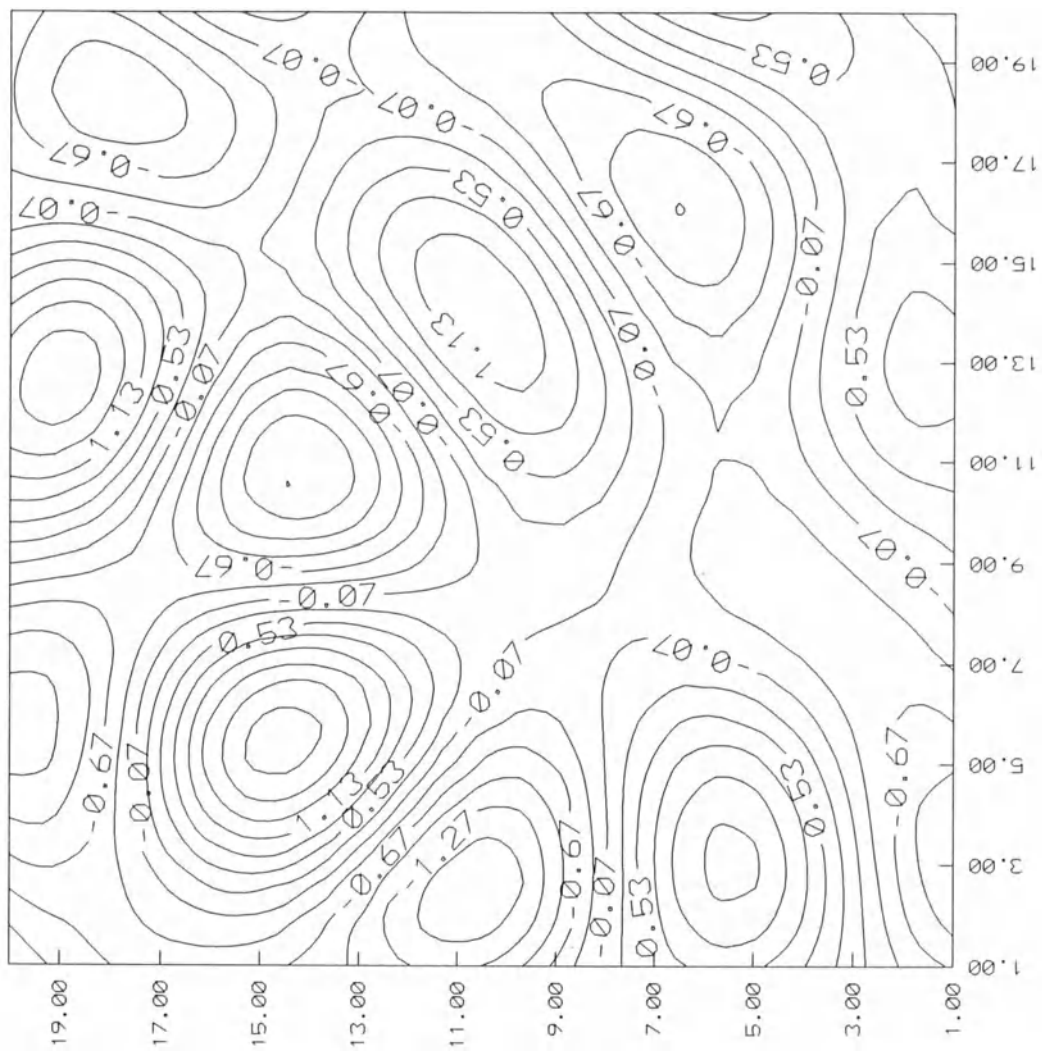


Fig. 10 - Test (B):  $\hat{\epsilon}_1$  values (km)

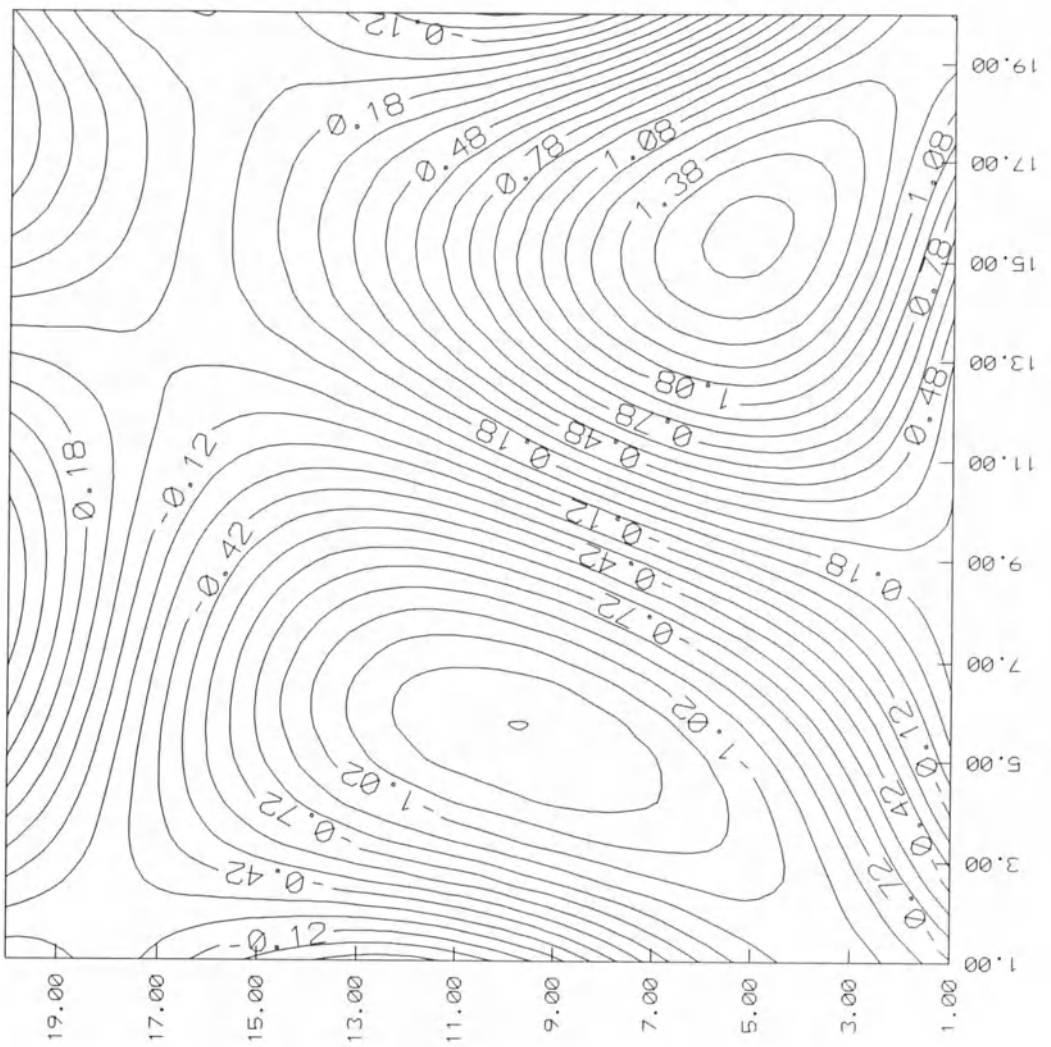


Fig. 11 - Test (B):  $\hat{\varepsilon}_2$  values (km)

# **MATHEMATICAL STATISTICS FOR SPATIAL DATA; THE USE OF GEOSTATISTICS FOR GEODETIC PURPOSES**

A. Stein

Dept. of Soil Science and Geology

Agricultural University, P.O. Box 37, 6700 AA Wageningen, The Netherlands

## **INTRODUCTION**

In geodesy long experience exists in using procedures to predict the earth's gravitational field at unvisited locations. A well known quantitative approach, least-squares collocation, has been proposed (Krarup, 1969) and has been used extensively in the past (see Moritz 1980a, which contains a detailed list of references). Least-squares collocation provides a linear unbiased predictor to predict e.g. the geoid on the basis of a number of observations on gravity anomalies. Fundamental aspects of Hilbert spaces and of approximation theory have been formulated (Meissl, 1976; Tscherning, 1978; Dermanis, 1977). Recent research has focused on application of the theory in many different areas (Haagmans and Van Gelderen, 1991) as well as on problems of taking the spherical shape of the earth into account (Schaffrin, 1992). Quite remarkably, a parallel rise may be observed in developing and using geostatistical theory, in particular inspired by the French work in the nineteen seventies. (Matheron, 1973; Delfiner, 1976; Journel and Huijbregts, 1978) and continuing in the nineties (Cressie, 1992). Geostatistics also provides a linear unbiased predictor of any spatial phenomenon, taking the spatial dependencies into account. A typical example is given on the land quality moisture deficit (Stein et al., 1991a), which is correlated with the mean highest groundwater level, leading to the use of universal cokriging as an appropriate prediction technique (Stein and Corsten, 1991). Modern approaches apply geostatistical procedures as well for geodetic purposes, using either generalized covariance functions (Blais, 1984) or anisotropy (Hansen, 1993).

During the past decade several attempts have been undertaken to highlight the many resemblances between the collocation and geostatistics (Blais, 1982; Dermanis, 1984; Hardy, 1984; Meier and Keller, 1990). Many correspondences exist, but differences are noted as well, in particular with respect to the use of the covariance function. In this presentation, the main focus will be on a mathematical statistical treatment of geostatistical procedures for geodetic purposes. A general lemma is proven, and universal kriging and cokriging are defined using multivariate random functions and multivariate increments. Attention will be given to stationarity of increments. The kriging and cokriging equations are derived without using Lagrange multipliers. The parameters of a polynomial generalized cross-covariance function, describing the covariances between increments, are estimated using Restricted Maximum Likelihood. The relation between collocation and kriging is established, and a practical example is included.

## SPATIAL PREDICTION.

In this section, an overview is given of spatial prediction procedures, based on the linear regression model. Attention will be focused first on a single spatial variables. In the second section, we will pay attention to the case of two spatial variables, of which the value of one has to be predicted at an unvisited location. Extension towards more variables is straightforward.

One of the important aspects to be stressed here is that we aim to estimate a stochastic variable, i.e. to predict a possible future observation, instead of to estimate a parameter, i.e. to estimate the expectation of an observation (Corsten, 1989). In ordinary linear regression theory with uncorrelated disturbances contained in the vector  $Z$ , all with the same variance, the two approaches differ only in their standard deviations. The best prediction and the estimate of its expectation for a new point with regressor values contained in the vector  $x_0$  will, admittedly, take the same value in this case, i.e. they are both equal to  $x_0'\beta$  with  $\beta$  defined as  $(X'X)^{-1}X'Z$ ,  $X$  being the matrix where each column contains the observations of a regressor. But the variance of the estimator of the expectation is the residual variance,  $\sigma^2$ , multiplied by  $x_0'(X'X)^{-1}x_0$ , while for the predictor the last factor must be replaced by  $1+x_0'(X'X)^{-1}x_0$ . Hence, another term  $\sigma^2$  should be added. The difference between these multiplication factors can be impressively large. Apart from numerical differences prediction of a random variable and estimation of its expectation are fundamentally different. From now on we deal mainly with the estimator of a stochastic effect, i.e. with prediction. As far as notation is concerned, we adopt the convention of indicating the transpose of a matrix or a column vector with a prime.

### Kriging

The prediction problem can be stated in the following way. We require a predictor  $t$  for the value  $Z_0$  of the predictand at a point  $s_0$  on the basis of the  $m$  observations at the points  $s_1, \dots, s_m$  which are contained in the stochastic  $m$ -vector  $Z$ . The expectation of each element of  $Z$  is supposed to be a polynomial in the one, two or three coordinates of the observation points  $s_i$  ( $i=1, \dots, m$ ) with respect to an arbitrary coordinate system, and so the expectations obey the structure:

$$E[Z] = X\beta. \quad (1)$$

Thus,  $E[Z]$  is a linear combinations of the regressor vectors with as yet unknown parameters  $\beta$ . The matrix  $X$  consists of  $m$  rows and  $r$  columns, where  $r$  depends on the degree ( $v$ ) of the polynomial expectation or trend of the variable and the dimension ( $dim$ ) of the region in which the observations are taken. It is easily shown that  $r$  equals

$$r = \frac{(dim+v)!}{dim!v!} = \binom{dim+v}{dim} \quad (2)$$

In a two-dimensional region and without trend,  $X$  is merely the vector  $1_m$ , consisting of ones

only. If the degree of the trend is equal to 1, each row of  $X$  consists of 1,  $\xi_1$  and  $\xi_2$ ,  $\xi_1$  and  $\xi_2$  representing the coordinates of an observation point of the predictand. If the trend is quadratic, each row of  $X$  consists of 1,  $\xi_1$ ,  $\xi_2$ ,  $\xi_1^2$ ,  $\xi_1\xi_2$ ,  $\xi_2^2$ . Obviously as well,  $E[Z_0] = x_0' \beta$ , in which the vector  $x_0'$  consists of one row of  $r$  monomial values of the coordinates of the point  $s_0$  where a prediction is required, similarly to the  $r$  regressors in  $X$ .

The observations in Kriging have a general dependence structure. This is modelled by means of the covariance between (actual and hypothetical) observation points or their disturbances with respect to expected values. The dependence structure of the vector  $(Z', Z_0)'$  is assumed to be given by the symmetric covariance matrix  $C^*$ , of order  $m+1$ . This matrix may be partitioned as

$$C^* = \begin{pmatrix} C & c_0 \\ c_0' & c_{00} \end{pmatrix} \quad (3)$$

where  $C$  is the covariance matrix of the elements of  $Z$  and  $c_0$  and  $c_{00}$  between  $Z_0$  and the elements of  $Z$  and  $Z_0$ . The matrix  $C^*$  must be positive definite in order that the variance of any linear predictor be non-negative. At present, we assume that each element of  $C$  and of  $c_0$  as well as  $c_{00}$  is known as an isotropic function  $c(|h|)$ , only of the distance  $|h|$  between the pair of observation points concerned, the so-called covariance function for the predictand. Further assumptions about the covariance functions are not required. To avoid complications we do not consider here the conditions which  $c(r)$ , must satisfy for  $C^*$  to be positive-definite (see Christakos, 1984). Below, problems of estimating covariance functions are addressed and attention is focused on generalized covariance functions, which are only to be applied to linear combinations of possible observations  $Z$  whose coefficient vector must obey certain linear restrictions. The semi-variogram, which is a special case of the opposite of such a generalized covariance function in particular in the absence of a trend, is considered below as well.

We have now the following linear model for actual observations  $Z$  and hypothetical observation  $Z_0$ :

$$\begin{pmatrix} Z \\ Z_0 \end{pmatrix} = \begin{pmatrix} X \\ x_0' \end{pmatrix} \beta + \eta; \quad E[\eta] = 0; \quad Cov[\eta] = C^*. \quad (4)$$

We require the best predictor  $t = \lambda' Z$  linear in the observations to satisfy the conditions

$$\begin{aligned} E(\lambda' Z - Z_0) &= 0 \\ Var(\lambda' Z - Z_0) &\text{ is minimal,} \end{aligned} \quad (5)$$

i.e. it is a *linear* predictor, *unbiased*, and with minimal variance of the prediction error. Expressed in terms of the prediction error, the expectation of the prediction error  $\lambda_1' Z_1 = \lambda' Z - Z_0$  is equal to 0, i.e.  $E[\lambda_1' Z_1] = 0$ , where  $\lambda_1$  is equal to  $\lambda$ , extended with the value -1, and  $Z_1$  is equal to  $Z$ , extended with  $Z_0$ . Its size, quantified by its mean squared error  $E[\lambda_1' Z_1]^2 = var[\lambda_1' Z_1]$  is minimal. The objective is to find the *best* linear unbiased predictor, i.e. the linear unbiased predictor with minimum mean squared error, the so called BLUP.

The procedure we adopt in this study is to improve a given linear unbiased predictor of  $Z_0$ . For example, the ordinary least squares predictor  $x_0'(X'X)^{-1}X'Z$  may be applied. The corresponding prediction error is denoted with  $\lambda_2'Z_1$ . The prediction error corresponding to any other linear unbiased predictor of  $Z_0$  is of the form  $(\lambda_2' - \delta_1')Z_1$ , where  $\delta_1 = (\delta' 0)'$ . The vector  $\delta$  is equal to the difference between the weights assigned to the elements of the finite restriction at the observation locations. Any  $\delta'Z$  is an unbiased predictor of 0, because the expectation of the difference of any two unbiased predictors is equal to 0. The collection of all vectors  $\delta_1$  is denoted with  $\Delta$ . It is noted, that the class  $\Delta$  is closed under addition. Further, since  $E[\delta'Z] = \delta'X\beta = 0$  for any  $\beta$ , it follows that  $\delta'X = 0$ .

A lemma is now formulated to obtain the best linear unbiased predictor of  $Z_0$ , by means of reducing the prediction error  $\lambda_2'Z_1$  of any linear unbiased predictor to the prediction error  $\lambda_1'Z_1$  of the best linear unbiased predictor. This is accomplished by means of a Gauss-Markov reduction. The lemma states that the prediction error with minimum variance, that is of the best predictor, has zero covariance with the prediction error of every unbiased predictor of 0. To obtain the BLUP, the vector  $\delta_1$  in  $\Delta$  is determined such that  $\lambda_1'Z_1 - \delta_1'Z_1$  has minimum length, where the inner product is defined in terms of the covariance. As a result, this procedure yields the prediction error  $\lambda_1'Z_1 = (\lambda_2' - \delta_1')Z_1$ , which is the orthogonal projection of  $\lambda_2'Z_1$  on the orthogonal complement of  $\Delta$ .

**Lemma** Let  $\lambda_2$  be given and let  $\lambda_1$  be such that  $\lambda_1 - \lambda_2$  is in  $\Delta$ . Then  $\lambda_1'Z_1$  has minimum variance iff.  $\text{cov}(\lambda_1'Z_1, \delta_1'Z_1) = 0$  for all  $\delta_1$  in  $\Delta$ .

**Proof.** Let  $\lambda_2$  be given and let  $\lambda_1$  be such that  $\lambda_1 - \lambda_2$  is in  $\Delta$ . Let  $\lambda_1'Z_1$  satisfy  $\text{cov}(\lambda_1'Z_1, \delta_1'Z_1) = 0$  for all  $\delta_1$  in  $\Delta$ . Choose a  $\delta_1$  in  $\Delta$ . Then  $(\lambda_2 - \lambda_1) - \delta_1$  is in  $\Delta$ , and

$$\begin{aligned}\text{Var}((\lambda_2 - \delta_1)'Z_1) &= \text{var}(\lambda_1'Z_1) + 2\text{cov}(\lambda_1'Z_1, ((\lambda_2 - \lambda_1) - \delta_1)'Z_1) + \text{var}(((\lambda_2 - \lambda_1) - \delta_1)'Z_1) \\ &= \text{var}(\lambda_1'Z_1) + \text{var}(((\lambda_2 - \lambda_1) - \delta_1)'Z_1) \\ &\geq \text{var}(\lambda_1'Z_1).\end{aligned}$$

Because this holds for any  $\delta_1$  in  $\Delta$ , the if part is proven.

Conversely, let  $\lambda_1$  be such that  $\lambda_1 - \lambda_2$  is in  $\Delta$  and that  $\lambda_1'Z_1$  has minimum variance. Let  $\delta_1$  be in  $\Delta$ . Then  $\omega = \lambda_1 - (\text{cov}(\lambda_1'Z_1, \delta_1'Z_1)/\text{var}(\delta_1'Z_1))\delta_1$  is such that  $\omega - \lambda_2$  is in  $\Delta$  too. Since  $\lambda_1'Z_1$  has minimum variance, obviously  $\text{var}(\omega'Z_1) \geq \text{var}(\lambda_1'Z_1)$ . On the other hand, the variance of  $\omega'Z_1$  equals  $\text{var}(\omega'Z_1) = \text{var}(\lambda_1'Z_1) - (\text{cov}(\lambda_1'Z_1, \delta_1'Z_1))^2/\text{var}(\delta_1'Z_1) \leq \text{var}(\lambda_1'Z_1)$  with equality holding if  $\text{cov}(\lambda_1'Z_1, \delta_1'Z_1) = 0$ , which completes the proof.

The linear combination  $\lambda_1'Z_1$  is a prediction error. The prediction error  $\lambda_1'Z_1$  with minimum variance satisfies the requirement of the lemma, which, in matrix form, is equal to  $\lambda_1'C^*\delta_1 = 0$  for all  $\delta_1 \in \Delta$ . This is equivalent to  $\delta'(C\lambda - c_0) = 0$  for all  $\delta$ . Since  $\delta'X = 0$ ,  $C\lambda - c_0$  is perpendicular to all  $\delta \in \langle X \rangle^\perp$ , i.e.  $C\lambda - c_0$  belongs to the column space of  $X$ . Hence, there exists a  $\tau$  such that  $C\lambda - c_0 = -X\tau$ . This equation and the equation  $\lambda'X - x_0 = 0$  are combined into the following partitioned matrix equation:

$$\begin{pmatrix} C & X \\ X' & 0 \end{pmatrix} \begin{pmatrix} \lambda \\ \tau \end{pmatrix} = \begin{pmatrix} c_0 \\ x_0 \end{pmatrix} \quad (6)$$

If  $\lambda$  satisfies this equation for a certain  $\tau$ , then  $\lambda_1'Z_1 = \lambda'Z - Z_0$  has minimum variance and therefore  $\lambda'Z$  is the BLUP of  $Z_0$ . Solving  $\lambda$  from the first equation for given  $\tau$  and inserting

it into the second equation, we obtain  $\tau = (X'C^{-1}X)^{-1}(X'C^{-1}c_0 - x_a)$ , which gives the solution for  $\lambda = C^{-1}c_0 - C^{-1}XVx_a$ , with  $V = (X'C^{-1}X)^{-1}$  and  $x_a = x_0 - c_0C^{-1}X$ . Thus the BLUP of  $Z_0$  is obtained as

$$t = x_0'\hat{\beta} + c_0'F, \quad (7)$$

where  $\hat{\beta}$  is defined as  $(X'C^{-1}X)^{-1}X'C^{-1}Z$  and  $F$  as  $C^{-1}(Z - X\hat{\beta})$ . Note that  $\hat{\beta}$  and  $F$  are completely determined by the observations and their locations and are independent of  $Z_0$ , i.e. of the observable at the prediction locations.

The first term of Eq. (7),  $x_0'\hat{\beta}$ , is itself a linear unbiased predictor of  $Z_0$ . It is of a polynomial form in the coordinates of the locations of  $Z$  and is obtained using generalized least squares for estimating the regression coefficients  $\hat{\beta}$ . The second term,  $c_0'F$ , improves  $x_0'\hat{\beta}$  as a predictor of  $Z_0$  by using a linear combination of the residuals  $Z - X\hat{\beta}$ . It is a linear combination of the observed residuals contained in  $Z - X\hat{\beta}$  with the best linear multivariate approximation of the predictand by all  $m+n$  observations as coefficients. Because  $t - x_0'\hat{\beta} = c_0'C^{-1}(Z - X\hat{\beta})$ , the procedure can be interpreted as regression of the residuals of  $T$  with respect to  $x_0'\hat{\beta}$  on the residuals of  $Z$  with respect to  $X\hat{\beta}$ .

The existence of a BLUP has been assured, so eq. (6) is always solvable. If  $C$  is singular, a large multiple of  $XX'$  is added to  $C$ , yielding a positive definite symmetric matrix, that shares the properties of  $C^*$ .

The mean square error of the BLUP is obtained as

$$\lambda_1' C^* \lambda_1 = c_{00} - c_0' C^{-1} c_0 + x_a' V x_a. \quad (8)$$

Eq. (8) defines the kriging variance, free of Lagrange multipliers, which is equal to the variance of the prediction error. It can be interpreted as follows:

$c_{00}$  is the variance of the variable under study;

$c_0' C^{-1} c_0$  is the reduction of that variance due to the best linear approximation by the other observations considered as  $m$  additional multivariate characteristics;

$x_a' V x_a = \text{Var}(x_a'\hat{\beta})$  is the variance of the sum of estimated expectations of predictand and covariate, however, not in the prediction location with regressors contained in  $x_0$ , but in a different but related point with regressors contained in  $x_a$ .

In fact the prediction error variance reflects the orthogonal decomposition of the prediction error into  $Z_0 - c_0' C^{-1} Z$  and  $x_a' \hat{\beta}$ , respectively.

The predictor  $t$  is an exact predictor: if a prediction is carried out at an observation point, the vector  $c_0$  is equal to the corresponding column of  $C$ , leading to the observation itself as the best prediction. Then, it turns out that the variance of the prediction error will vanish.

### Extension to multiple variables - cokriging

If, in addition, observations for a related covariate at  $n$  completely or partially different points  $s_{m+1}, \dots, s_{m+n}$  are available and are contained in the stochastic  $n$ -vector  $Z_2$ , the procedure just described is modified into the cokriging equations (Stein et al., 1991b).

Although in practice there will be shared measurement locations, which are in fact necessary to estimate the joint spatial structure function, there is no need to have those in the present prediction problem. The expectation of each element of  $Z_1$  and  $Z_2$  is supposed to be a polynomial in the one, two or three coordinates of the observation points  $s_i$  ( $i=1,\dots,m$ ) and  $s_j$  ( $j=m+1,\dots,m+n$ ), respectively, with respect to an arbitrary coordinate system, and so the expectations obey the structure:

$$\begin{aligned} E[Z_1] &= X_1 \beta_1 \\ E[Z_2] &= X_2 \beta_2. \end{aligned} \quad (9)$$

Both  $E[Z_1]$  and  $E[Z_2]$  are linear combinations of the regressor vectors with as yet unknown parameters  $\beta_1$  and  $\beta_2$ . The matrix  $X_1$  and  $X_2$  are similar to the matrix  $X$  considered before. Obviously again,  $E[Z_0] = x_0' \beta_1$ , in which the vector  $x_0'$  consists of one row of  $r$  monomial values of the coordinates of the point  $s_0$  where a prediction is required, similarly to the  $r$  regressors in  $X_1$ .

The dependence structure for cokriging is modelled by means of the covariance between (actual and hypothetical) observation points or their disturbances with respect to expected values. The dependence structure of the vector  $(Z_1', Z_2', Z_0)'$  is assumed to be given by the symmetric covariance matrix  $C^*$ , of order  $m+n+1$ . This matrix may be partitioned as

$$C^* = \begin{pmatrix} C_{11} & C_{12} & c_{01} \\ C_{21} & C_{22} & c_{02} \\ c_{01}' & c_{02}' & c_{00} \end{pmatrix} = \begin{pmatrix} C & c_0 \\ c_0' & c_{00} \end{pmatrix} \quad (10)$$

where  $C_{11}$  is the covariance matrix of the elements of  $Z_1$ ,  $C_{22}$  of the elements of  $Z_2$ ,  $C_{12}$  ( $= C_{21}$ ) between the elements of  $Z_1$  and those of  $Z_2$ , and  $c_{01}$ ,  $c_{02}$  and  $c_{00}$  between  $Z_0$  and the elements of  $Z_1$ ,  $Z_2$  and  $Z_0$ , respectively, while

$$C = \begin{pmatrix} C_{11} & C_{12} \\ C_{21} & C_{22} \end{pmatrix} \quad (11)$$

The matrix  $C^*$  must be positive definite in order that the variance of any linear predictor be non-negative. At present, we assume that each element of  $C_{11}$  and of  $c_{01}$  as well as  $c_{00}$  is known as an isotropic function  $c_1(|h|)$ , only of the distance  $|h|$  between the pair of observation points concerned, the so-called covariance function for the predictand. Likewise, each element of  $C_{22}$  is assumed to be known as an isotropic function  $c_2(|h|)$  of the distance  $|h|$  between the pair of observation points concerned, the covariance function for the co-variable, and each element of  $C_{12}$  and of  $c_{02}$  is assumed to be known as an isotropic function  $c_{12}(|h|)$  of the distance  $|h|$  between the pair of observation points concerned, the so-called cross-covariance function between predictand and co-variable. Further assumptions about the covariance functions are not required. To avoid complications we do not consider here the conditions which  $c_1(|h|)$ ,  $c_2(|h|)$ ,  $c_{12}(|h|)$  must satisfy for  $C^*$  to be positive-definite.

We have again the following linear model for actual observations  $Z$  and hypothetical

observation of the predictand  $Z_0$ :

$$\begin{pmatrix} Z \\ Z_0 \end{pmatrix} = \begin{pmatrix} X \\ x_0 \end{pmatrix} \beta + \eta; \quad E[\eta] = 0; \quad Cov[\eta] = C^*, \quad (12)$$

in which we now have introduced the abbreviations:

$$X = \begin{pmatrix} X_1 & 0 \\ 0 & X_2 \end{pmatrix}, \quad x_0 = \begin{pmatrix} x_0 \\ 0 \end{pmatrix}, \quad \beta = \begin{pmatrix} \beta_1 \\ \beta_2 \end{pmatrix} \quad (13)$$

Again, the best predictor  $t = \lambda'Z$  linear in the observations to should satisfy the conditions

$$E(\lambda'Z - Z_0) = 0 \quad (14)$$

*Var(\lambda'Z - Z\_0) is minimal.*

When the lemma defined above is applied to this particular situation, the BLUP of  $Z_0$  is obtained as

$$t = x_0' \hat{\beta} + c_0' F, \quad (15)$$

where  $\hat{\beta}$  is defined as  $(X'C^{-1}X)^{-1}X'C^{-1}Z$  and  $F$  as  $C^{-1}(Z-X\hat{\beta})$ . Note that  $\hat{\beta}$  and  $F$  are completely determined by the observations and their locations and are independent of  $Z_0$ , i.e. of the observable at the prediction locations. Considering the two variables that make up the vector  $Z$  separately, we notice that the predictor is the sum of the estimated local expectation of the predictand only, that is  $x_0'\hat{\beta} = x_0'\hat{\beta}_1$ . The mean square error of the BLUP is obtained as

$$\lambda_1' C^* \lambda_1 = c_{00} - c_0' C^{-1} c_0 + x_a' V x_a. \quad (16)$$

Eq. (16) defines the cokriging variance, also free of Lagrange multipliers, which is equal to the variance of the prediction error.

## RANDOM FUNCTIONS

In this section the aim is to provide a procedure to obtain generalized covariance functions and generalized cross-covariance functions from an available set of data. For this purpose, the main concepts of random functions and their increments will be given. First, the univariate and multivariate random functions are considered. Next, increments of order  $k$  and their stationarity are defined. Finally, the covariance structure between increments is defined. The theory was developed basically during the fifties (Ito, 1953) and has been given a strong mathematical foundation in the early sixties (Gel'fand and Vilenkin, 1964).

## Univariate random functions (URF)

Data collected in space may be considered as realizations of a regionalized variable, generated by a random function (Christakos, 1992). A univariate random function (URF) in a *dim*-dimensional region  $S$  will be denoted by  $Z(s)$  where the location in  $S$  is given by  $s$ . For example,  $Z(s)$  may be the earth's gravitational field and  $S$  a part of the earth surface (Haagmans and Van Gelderen, 1991), or  $Z(s)$  may be the moisture deficit for grassland and  $S$  an area in the eastern Netherlands. In both examples, *dim* is equal to 2. A random function can never be observed everywhere, but only at a finite number of locations. Hence, a finite restriction of  $Z(s)$  is defined as that function restricted to a finite number of  $m$  variables at locations  $s_i$  for  $i=1,\dots,m$ . The vector of  $m$  values  $Z(s_i)$  is denoted by  $Z$ .

A linear combination of a finite restriction is defined as

$$\lambda'Z = \sum_{i=1}^m \lambda_i Z(s_i), \quad (17)$$

where  $\lambda$  is a vector of  $m$  coefficients assigned to the variables at the locations of the finite restriction. A very special form of a linear combination is called an increment. An increment of order  $k+1$  is, for any  $k \geq 0$ , a finite linear combination  $\lambda'Z$  with the property that it eliminates polynomials of degree  $\leq k$ , i.e.  $\lambda'\pi = 0$  for all finite restrictions of polynomials  $\pi(s)$  of degree  $\leq k$  (Matheron, 1973; Delfiner, 1976). The class of increments of order  $k$  is denoted with  $\Lambda_k$ . For example, an increment of order 1 annihilates functions that are constant at the locations of the finite restriction. Since each polynomial is a linear combination of monomials up to  $k$ , such as 1,  $x_1$ ,  $x_2$ ,  $x_1^2$ ,  $x_2^2$ ,  $x_1x_2$ , an increment is a linear combination  $\lambda'Z$  with  $\lambda'X = 0$ , where  $X$  is the matrix consisting of the monomials up to the degree of the trend, evaluated at the observation locations. The class  $\Lambda_k$  is therefore equivalent to  $\langle X \rangle^\perp$ , i.e. the orthogonal complement to the space spanned by the columns of  $X$ . The elements of any basis of  $\Lambda_k$  can be arranged as rows of the matrix  $B$ . Any linear combination of the elements of the vector  $Y = BZ$  is an increment. Conversely, any increment of the observations can be expressed as a linear combination of the elements of the vector  $Y = BZ$  (Kitanidis, 1983). For example, the matrix

$$B = I - X(X'X)^{-1}X' \quad (18)$$

can be used. Obviously,  $BX = 0$ . The last  $r$  rows of  $X$  may be skipped, as the dimension of  $\langle X \rangle^\perp$  and hence the rank of  $B$ , equals  $N = m-r$ , yielding a matrix  $B$  of  $m-r$  rows and  $r$  columns, where  $r$  is defined by Eq. (2).

A URF  $Z(s)$  should have a consistent family of distributions for finite restrictions. If first and second moments of the family of distributions exist, the expectation function is defined as  $\mu(s) = E[Z(s)]$ . Also, for any two locations  $s$  and  $t$  the covariance function  $g(s,t)$  is defined as  $g(s,t) = \text{cov}(Z(s),Z(t))$ . The expectation and the variance of an arbitrary finite linear combination  $\lambda'Z$  are given by:

$$E[\lambda'Z] = \lambda'\mu = \sum_{i=1}^m \lambda_i \mu(s_i) \quad (19)$$

$$Var[\lambda' Z] = \lambda' G \lambda = \sum_{i=1}^m \sum_{j=1}^m \lambda_i g(s_i, s_j) \lambda_j \quad (20)$$

where  $\mu$  and  $G$  are the finite restrictions of  $\mu(s)$  and  $g(s,t)$ , respectively. Since negative variances are not allowed, eq. (14) should be positive for any linear combination  $\lambda' Z$ . Therefore, only a limited collection of functions  $g(s,t)$  may serve as covariance functions. These are called the generalized covariance functions.

### Multivariate random functions (MRF)

Next, we consider a collection of  $p$  univariate random functions. The variables will be denoted by  $Z_1(s)$  through  $Z_p(s)$ , where, as before, the location in  $S$  is indicated by  $s$ . This presentation will focus on  $p = 2$ , but the set-up of the theory will be quite general. Examples are i)  $Z_1(s)$  the geoid and  $Z_2(s)$  the gravity anomaly or the topographic height, and ii)  $Z_1(s)$  the moisture deficit for grassland and  $Z_2(s)$  the mean highest groundwater level. It is the simultaneous behavior of the  $p$  variables in terms of their spatial structure and their interrelationship that is of interest. A multivariate random function (MRF) is defined for every  $s \in S$  as a  $p$ -variate random variable  $Z(s) = (Z_1(s), \dots, Z_p(s))'$ . An MRF is used to describe simultaneously variables that may be mutually dependent. This distinguishes an MRF from  $p$  univariate functions. A finite restriction of an MRF consists of finite restrictions of each component to a finite number  $n_u$  of observations at locations  $s_{ui}$  for  $u=1, \dots, p$ . The vector of  $n=n_1+\dots+n_p$  values  $Z_u(s_{ui})$ ,  $u=1, \dots, p$ ,  $i=1, \dots, n_u$  is denoted by  $Z$ . Finite linear combinations of an MRF are defined as the sum of finite linear combinations of the URFs  $Z_u(s)$ :

$$\lambda' Z = \sum_{u=1}^p \lambda'_u Z_u = \sum_{u=1}^p \sum_{i=1}^{n_u} \lambda_{ui} Z_u(s_{ui}) \quad (21)$$

where  $\lambda$  is a vector of  $n$  unknown weights, partitioned in  $p$  sub-vectors  $\lambda_u$ , for  $u=1, \dots, p$ , of  $n_u$  elements. Analogous to an increment for a URF, an increment of order  $k+1$  for an MRF is defined as the finite linear combination  $\lambda' Z$  where each of its components is an increment of order  $k+1$ .

An MRF, just like a URF, should have a consistent family of distributions for finite restrictions of  $Z(s)$ . If first and second moments of the family of distributions exist, the  $p$ -variate expectation function is defined as  $\mu(s)=(\mu_1(s), \dots, \mu_p(s))'$ , where  $\mu_u(s) = E[Z_u(s)]$ ,  $u=1, \dots, p$ . Also, for any two locations  $s$  and  $t$  the  $p$ -variate covariance function  $G(s,t)$  is defined as the  $p \times p$  matrix  $\{g_{uv}(s,t)\}$  with the typical element  $g_{uv}(s,t) = \text{cov}(Z_u(s), Z_v(t))$ . The expectation and the variance of an arbitrary finite linear combination  $\lambda' Z$  are given by:

$$E[\lambda' Z] = \lambda' \mu = \sum_{u=1}^p \lambda'_u \mu_u = \sum_{u=1}^p \sum_{i=1}^{n_u} \lambda_{ui} \mu_u(s_{ui}) \quad (22)$$

$$Var[\lambda' Z] = \lambda' G \lambda = \sum_{u=1}^p \sum_{v=1}^p \lambda_u' g_{uv} \lambda_v \quad (23)$$

where  $\lambda$  and  $\lambda_u$  are defined before and  $\mu_u$ ,  $g_{uv}$ ,  $\mu$  and  $G$  are the finite restrictions of  $\mu_u(s)$ ,  $g_{uv}(s,t)$ ,  $\mu(s)$  and  $G(s,t)$ , respectively.

## Stationarity

Next, more general models to describe the randomness of a URF and an MRF will be considered. Assume that only expectations and covariances of increments of order  $k$  exist. Therefore, there exists a multivariate expectation function  $\mu(s)$  such that the expectation of an increment  $\lambda' Z$  can be calculated with eq. (22). The function  $\mu_u(s)$  is not an expectation in the ordinary sense anymore, because it is not unique: if  $\pi(s)$  is a polynomial of degree  $\leq k$ , then  $\mu(s) + \pi(s)$  may also serve as the expectation function. In fact, polynomials of degree  $\leq k$  are eliminated, because for  $Z = Z_1 + \pi$ , where  $\pi$  is the finite restriction of a polynomial of degree  $\leq k$  one has that  $\lambda' Z = \lambda' Z_1$ . Therefore, equivalence classes arise in MRFs, with respect to polynomials of degree  $k$ . For such increments, an extended class of generalized covariance functions is available. The function  $\mu(s)$  is therefore termed the generalized expectation. Also, there exists a multivariate matrix function  $G(s,t)$  such that the variance of an increment  $\lambda' Z$  can be calculated with eq. (23). The elements of  $G(s,t)$ , the functions  $g_{uv}(s,t)$ , are also not covariances in the ordinary sense: if  $\pi_i(s)$  are polynomials of degree  $\leq k$  for  $i=1,\dots,4$ , and  $f_1(s)$  and  $f_2(s)$  are any functions defined on  $S$ , then using  $G^*(s,t) = G(s,t) + \pi_1(s)f_1(t) + f_2(s)\pi_2(t) + \pi_3(s)\pi_4(t)$  is equivalent to using  $G(s,t)$ , as follows from the definition of increments. Therefore both  $G(s,t)$  and  $g_{uv}(s,t)$  are termed generalized covariance functions. Eq. (23) needs to be positive only for increments and not for any arbitrary linear combination. Expectation and variance of linear combinations that are not increments do not necessarily exist and if the variance exists it may be negative. Similar as for the univariate case, the collection  $\Lambda_k$  of  $\lambda$ s yielding positive definiteness for increments, the collection of permissible  $\lambda$ s (Christakos, 1984), forms a finite-dimensional linear space within the space of all  $\lambda$ s. The elements of any basis of  $\Lambda_k$  can be arranged as rows of the matrix  $B$ . For example, the matrix

$$B = \begin{pmatrix} B_1 & 0 & \dots & 0 \\ 0 & B_2 & \dots & 0 \\ \vdots & \ddots & \ddots & \vdots \\ 0 & 0 & \dots & B_p \end{pmatrix} = I - X(X'X)^{-1}X' \quad (24)$$

can be used, where  $X$  is a partitioned matrix with blocks  $X_{uv}$ , similar as in section 2. For  $u \neq v$  the blocks  $X_{uv}$  are equal to zero, whereas the blocks  $X_{uu}$  contain  $m$  monomials up to the degree of non-stationarity  $k$  of the coordinates of the  $n_u$  observation locations  $s_{ui}$ ,  $i=1,\dots,n_u$  of the  $u^{\text{th}}$  variable. The last  $r$  rows of  $X_{uu}$  may be skipped, as the rank of  $B_u$  equals  $n_u - r$ , yielding a matrix  $B$  of  $n - p \times r$  rows and  $n$  columns.

In order to treat stationarity of increments, attention will be paid first to stationarity of random functions. An MRF  $Z(s)$  which has the first and second order moments is called (weakly) stationary iff. both  $E[Z(s+h)]$  and  $\text{Var}[Z(s+h)]$  are independent on any translation vector  $h$ . Now consider a filtered random function, defined for any  $s \in S$  and any finite restriction defined by the locations  $s_i$  as  $Z_\lambda(s) = \sum \lambda_i Z(s_i+s)$ . A URF  $Z(s)$  is called stationary of order  $k$ , if  $Z_\lambda(s)$  is stationary for every increment  $\lambda'Z$  of order  $k$ . By means of this definition, the concept of stationarity is extended from univariate random functions to their increments, by taking a shift in the finite restrictions. Likewise, an MRF is called stationary of order  $k$ , if each of its components is stationary of order  $k$ . Such a URF and MRF are said to have  $k^{\text{th}}$  order stationary increments (Ito, 1953). Stationarity of increments corresponds to stationarity of random functions, and may be interpreted as non-changing expectation and variance with regard to translations. For example, the Wiener process  $Z(s)$  with  $E[Z(s+h)-Z(s)] = 0$  and  $\text{Var}[Z(s+h)-Z(s)] = |h|$  is stationary of order 1, whereas  $\text{Var}[Z(s)]$  does not necessarily exist. This agrees with (Gel'fand-Vilenkin, 1964, p. 264-265). Following (Matheron, 1973) one may call this process an intrinsic random function of order 0. An MRF  $Z(s)$ , stationary of order 1, has a generalized expectation and a generalized covariance function which are unique apart from polynomials of degree 0. For increments of order 0 or 1 the opposite of the semivariogram  $\gamma$ , defined by  $\gamma(s,t) = (1/2)*\text{Var}[Z(s) - Z(t)]$ , is equivalent to  $G(s,t)$ . For first order increments the variances of the constituting MRFs, do not necessarily exist. If they do exist, however, and are equal to  $G_0(s,t)$ , say, the well-known relation holds:

$$\gamma(s,t) = -\frac{1}{2}G_0(s,s) - \frac{1}{2}G_0(t,t) + G_0(s,t) \quad (25)$$

(Journel and Huijbregts, 1978). For increments stationary of order 1, one may define  $\gamma(h) = \gamma(s,s+h)$ , since the semivariogram depends upon the difference in place locations only.

Finally, an MRF  $Z(s)$  is called rotation invariant (or: isotropic) iff. for any  $u$  and any  $v$   $g_{uv}(s,t)$  depends on the length  $|h|$  of the distance vector  $h$  between  $s$  and  $t$  only, and not on its direction. In this case one may use  $g_{uv}(|h|)$  instead of  $g_{uv}(s,t)$ .

### Estimating the parameters of a linear generalized covariance function.

We will now pay attention towards modelling the generalized covariance functions and estimating of its parameters. It will be assumed throughout this section that the generalized covariance function is the sum of the functions  $g_{ii}(|h|)$  and  $g_{ij}(|h|)$ , each isotropic and linearly dependent on a vector of parameters,  $\gamma$ . The generalized covariance function of the  $i^{\text{th}}$  variable is denoted with  $g_{ii}(|h|)$  and the generalized cross-covariance function describing the spatial interaction between the  $i^{\text{th}}$  and the  $j^{\text{th}}$  variable with  $g_{ij}(|h|)$ :

$$g_{ij}(|h|) = \gamma_{ij,0} * \delta_K(|h|) + \gamma_{ij,1} * |h| + \gamma_{ij,2} * |h|^3 + \gamma_{ij,3} * |h|^5 \quad (26)$$

Here  $|h|$  is the distance between observation points and the Kronecker function,  $\delta_K(|h|)$ , equals 1 if  $|h| = 0$  and equals 0 if  $|h| \neq 0$ . The elements of the vector  $\gamma$  are denoted with  $\gamma_{ii,\alpha}$ , for  $i,j=1,\dots,p$  and  $\alpha = 1,\dots,k+2$ ,  $\alpha$  depending on the degree  $k$  of the polynomial trends:

$\gamma_{ii,2}|h|^3$  can be included only if  $k$  exceeds 0, and  $\gamma_{ii,3}|h|^5$  only if  $k$  exceeds 1, due to requirement of positive-definiteness (Delfiner, 1976).

The variance of increments of the observations,  $Q = \text{Var}[Y] = E[YY'|\gamma] = E[BZZ'B'|\gamma]$ ,  $= BE[ZZ'|\gamma]B'$  has a structure similar to Eq. (20), i.e.

$$Q = B \left( \sum_{i,j=1}^p \sum_{\alpha=1}^{k+2} \gamma_{ij,\alpha} G_{ij,\alpha} \right) B' = \sum_{i,j=1}^p \sum_{\alpha=1}^{k+2} \gamma_{ij,\alpha} Q_{ij,\alpha} \quad (27)$$

where the matrices  $Q_{ij,\alpha} = BG_{ij,\alpha}B'$  are of size  $N \times N$ . Elements of the matrix  $G_{ij,\alpha}$  are obtained from each of the constituting parts of Eq. (26). The number of terms in Eq. (27) is equal to  $\kappa = \frac{1}{2}p(p+1)*(k+2)$ .

The vector  $Y$  is assumed to have a Gaussian distribution with zero mean and variance matrix  $Q$ , which is linear in the parameter vector  $\gamma$ . As shown by standard methods the likelihood equations are

$$\text{Tr}(Q^{-1}Q_iQ^{-1}[Y_iY'_i - Q_i]) = 0 \quad (28)$$

for  $i=1, \dots, \kappa$ , where  $\text{Tr}(\cdot)$  denotes the trace of a square matrix. Eq. (28) is equivalent to the system of linear equations:

$$a = H\gamma \quad (29)$$

with  $\{a\}_i = \text{Tr}(Q^{-1}Q_iQ^{-1}Y_iY'_i)$ ,  $\{H\}_{ij} = \text{Tr}(Q^{-1}Q_iQ^{-1}Q_j)$  and  $\{\gamma\}_i = \gamma_i$ ,  $i, j = 1, \dots, \kappa$ . After a prior estimate of  $Q$ , these equations can be solved by determining the  $\gamma$ s and then calculating a new  $Q$ . This is repeated until convergence is achieved. The procedure, commonly known as restricted maximum likelihood (REML), maximizes the likelihood of the parameter  $\gamma$  for the observed increments.

A key statistic for distinguishing between various degrees of trends is Akaike's information criterion (Akaike, 1974), defined as:

$$AIC = -2*I(Y|\gamma) + 2*\kappa \quad (30)$$

where  $I(Y|\gamma)$  is the log-likelihood of the increments  $Y$  as a function of the vector  $\gamma$  of parameters. The degree of the trend which minimizes Eq. (30) is regarded as the appropriate degree of non-stationarity.

## MAIN RELATIONS BETWEEN KRIGING AND COLLOCATION

In order to establish the relation between kriging and collocation, first attention will be given to univariate collocation. Collocation is described at several places in the literature. For the purpose, we will pay attention to least-squares collocation as defined by Moritz (Moritz, 1973). The basic equation of least-squares collocation is:

$$x = AX + s + n \quad (31)$$

where  $x$  is the "measurement",  $s$  is the "signal" and  $n$  is the "noise". Usually, the measurement vector  $x$  is known, as well as the matrix  $A$ . This model closely corresponds to the model that was applied in the previous section. Given the measurements, the signal has to be predicted. To do so, the vector  $z$  is defined as  $z = x - AX$ . Next, the signal and the vector of residuals  $z$  are collected into one vector  $v$ :

$$v = [s_1 \dots s_p \ z_1 \dots z_q]' = [s' \ z']' \quad (32)$$

and the (partitioned) covariance matrix  $Q$  is determined:

$$Q = \begin{bmatrix} C_{ss} & C_{sx} \\ C_{xs} & C_{xx} \end{bmatrix} \quad (33)$$

where  $C_{ss} = \text{cov}(s, s) = E\{ss'\}$  contains the covariance between the signal,  $C_{xx} = \text{cov}(x, x) = E\{(x-AX)(x-AX)'\} = E\{zz'\}$  contains the covariances between the measurements, and  $C_{sx} = \text{cov}(s, x) = E\{s(x-AX)'\} = E\{sz'\}$  and  $C_{xs} = C_{sx}'$  contains the covariances between signal and measurements. Since the number of elements in the vector  $s$  is equal to  $p$ , a  $p$ -fold prediction is required. To do so, the prediction equation (7) is applied  $p$  times. We first realize that  $E[s]$  is equal to 0, and hence that  $\beta$  is equal to 0. Then the multivariate predictor consisting of  $p$  univariate predictors equals:

$$T = C_{sx}^{-1}(x-AX) \quad (34)$$

where the vector of predictors is denoted with  $T$ , and the matrix  $C_{sx}$  contains the covariances between the  $p$  locations where the signal is to be predicted and the  $q$  locations where  $x$  is observed.

The matrices  $C_{ss}$  and  $C_{sx}$  are in most practical studies filled on the basis of the so-called Tscherning-Rapp model (Tscherning and Rapp, 1974; Moritz, 1980a). This model describes the global covariance function of gravitational anomalies using a finite sum of Legendre polynomials as a function of the spherical angle between two points at the earth surface.

We now focus attention on bivariate MRF's. For example, both observations on gravity anomalies may be available as well as observations on the geoid. In order to predict a value at a single location, we apply eq. (15). This takes the following form:

$$t = c_0' \begin{pmatrix} C_{11} & C_{12} \\ C_{21} & C_{22} \end{pmatrix}^{-1} \left( \begin{pmatrix} Z_1 \\ Z_2 \end{pmatrix} - \begin{pmatrix} X_1 & 0 \\ 0 & X_2 \end{pmatrix} V^{-1} \begin{pmatrix} X_1' & 0 \\ 0 & X_2' \end{pmatrix} \begin{pmatrix} C_{11} & C_{12} \\ C_{21} & C_{22} \end{pmatrix}^{-1} \begin{pmatrix} Z_1 \\ Z_2 \end{pmatrix} \right) \quad (35)$$

with  $X_1$  and  $X_2$  as before,  $Z_1$  and  $Z_2$  containing the observations on the two variables, for instance the gravity anomalies (which we want to predict) and the geoid (which may improve the prediction) and  $V$  as before. The covariances and cross-covariances of the finite restrictions for the two variables are contained in the matrices  $C_{11}$  (for the first

variable),  $C_{22}$  (for the second variable) and in  $C_{12}$  (for their interaction). The vector  $c_0$  contains as its first  $q_1$ , say, elements the covariances between the single prediction location and the  $q_1$  measurement on the gravity anomalies, followed by  $q_2$  elements equal to the cross-covariances between the single prediction location and the  $q_2$  measurements of the second variable. If a multiple prediction is to be carried out, the multiple predictor  $T$  is formulated, with  $\beta$  equal to 0:

$$T = C_{sx} \begin{pmatrix} C_{11} & C_{12} \\ C_{21} & C_{22} \end{pmatrix}^{-1} \left( \begin{pmatrix} Z_1 \\ Z_2 \end{pmatrix} - \begin{pmatrix} X_1 & 0 \\ 0 & X_2 \end{pmatrix} V^{-1} \begin{pmatrix} X'_1 & 0 \\ 0 & X'_2 \end{pmatrix} \begin{pmatrix} C_{11} & C_{12} \\ C_{21} & C_{22} \end{pmatrix}^{-1} \begin{pmatrix} Z_1 \\ Z_2 \end{pmatrix} \right) \quad (36)$$

where the p-variate predictor is again denoted with  $T$  and the matrix  $C_{sx}$  equals the multivariate equivalent of  $c_0$ . In order to obtain the elements of the matrix  $C$ , the Tscherning-Rapp model is used in many practical studies. Also, the cross-covariances between gravity anomalies and, for example, the geoid are expressed as a finite sum of Legendre polynomials as a function of the spherical angle between two points at the earth surface.

### Remarks

1. One word should be mentioned to the similarities between the generalized covariance functions  $g(s)$  mentioned above and the covariance functions  $c(s)$  used in collocation. As long as first and second order moments exist, the two may be interchanged freely. The relation between the two is given by  $g(s) = c(s) - c(+0)$ , where  $c(+0)$  indicates the limiting value for  $s$  approaching 0 from the right. However, as illustrated above, several processes exist in which this is not the case, such as the Wiener process. Then, the covariance function is not stationary, because it depends both on the distance  $h$  and on the location vector  $x$ . Only generalized covariance functions may then be applied. The equations (34) - (37) do not change when generalized covariance functions are applied instead of ordinary covariance functions, neither do expressions for the kriging variance.
2. Considerable difficulties exist when estimating the covariance function for applying collocation techniques. In Moritz, 1980a, no satisfactory solution is given; it is stated (page 94): *the covariance function cannot be exactly determined empirically since [...] we should know the anomalous potential everywhere*. This problem is circumvented by applying kernel estimation procedures. However, it is well known that this approach may yield covariance functions that are different from the real covariance functions, and hence are not well-interpretable. As is shown by the first part of this presentation, estimation of the generalized covariance function does not cause substantial problems. The basic idea is to restrict oneself to a part of the space and hence filtering the existing trend.
3. Collocation techniques are in a certain sense more difficult, since the earth's surface is spherical, and not planar. In this presentation the problem is neglected. Interested readers are referred to Schaffrin, 1992, for a discussion concerning this topic.
4. In many treatments on collocation techniques, the deterministic aspect is stressed. Approaches that I encountered during the current study include a convolution type

approach and an approach using Lagrange multipliers. In the geostatistical literature it is nowadays recognized that one basically has a regression (prediction) problem with dependent observations. Hence the Gauss-Markov theorem on finding the best linear unbiased predictor is applicable.

5. Closely associated with the previous, the question may be posed as to what happens if the number of observations keeps increasing. Intuitively, the information becomes more and more detailed, therefore predictions are becoming increasingly precise. In geostatistical procedures, one is able to distinguish the *spatial* uncertainty from the *non-spatial* uncertainty. The spatial uncertainty diminishes when the sampling network is condensed; however, the non-spatial uncertainty can never be removed, since that is inherent to the measuring procedure.
6. In general, a multivariate prediction problem exists, with functional relations between the different variables that together contribute to describe the earth's gravitational field. Although no theoretical restriction appears to emerge, the most straightforward approach is to apply one group of models to describe the covariance structure. The generalized covariance functions may serve as an excellent tool for this purposes.

## PRACTICAL CASE STUDY

In order to show several of the concepts established in this study, attention will be paid to data collected in the past (Weber, 1984). We will pay attention only to predicting gravity anomalies. It will be indicated, however, how a multivariate approach may be applied as well. The data set contains free air gravity anomalies of Europe, including marine areas, collected on a  $3' \times 5'$  grid basis, expressed in mgal or  $10^{-5} \text{ m s}^{-2}$  with regard to a normal gravity model, the reference earth model GRS80 (Moritz, 1980b). The coordinates are geographical coordinates WGS84, with a lower left point equal to the latitude of  $45^\circ \text{ N}$  and the longitude of  $6^\circ \text{ W}$  and an upper right point equal to the latitude of  $59^\circ \text{ N}$  and the longitude of  $17^\circ \text{ E}$ . The grid mesh covers 276 blocks in the longitude direction and 280 blocks in the latitude direction. The anomalies range from  $-140.50 \times 10^{-5} \text{ m s}^{-2}$  to  $226.69 \times 10^{-5} \text{ m s}^{-2}$  with an average equal to  $6.26 \times 10^{-5} \text{ m s}^{-2}$  and standard deviation equal to  $24 \times 10^{-5} \text{ m s}^{-2}$ . A visual display, constructed with the GSLIB program (Deutsch and Journel, 1992), is given in figure 1.

Well recognizable are the Alps in the central south of the map, showing negative anomalies, in contrast to most of the map. Black parts of the map indicate small areas for which no data were available. On the basis of these gravity measurements, collocation is applied to predict the gravity anomalies at the areas where observations are missing.

Attention will be given first to analyze stationarity of the data and next to estimate the coefficients of the generalized covariance function describing the spatial variability.

The total set contains 77280 data, distributed evenly over the centers of grid cells. These values are derived from original measurements by means of different techniques, depending on the resolution of the original data, notably least squares prediction, digitizing of air anomaly maps, averaging point data within a grid cell and modification of Bouguer anomalies (Torge et al., 1983). Although these techniques may cause some smoothing of the data, for the subsequent analysis we have used the grid data.

## ***Gravity anomalies***

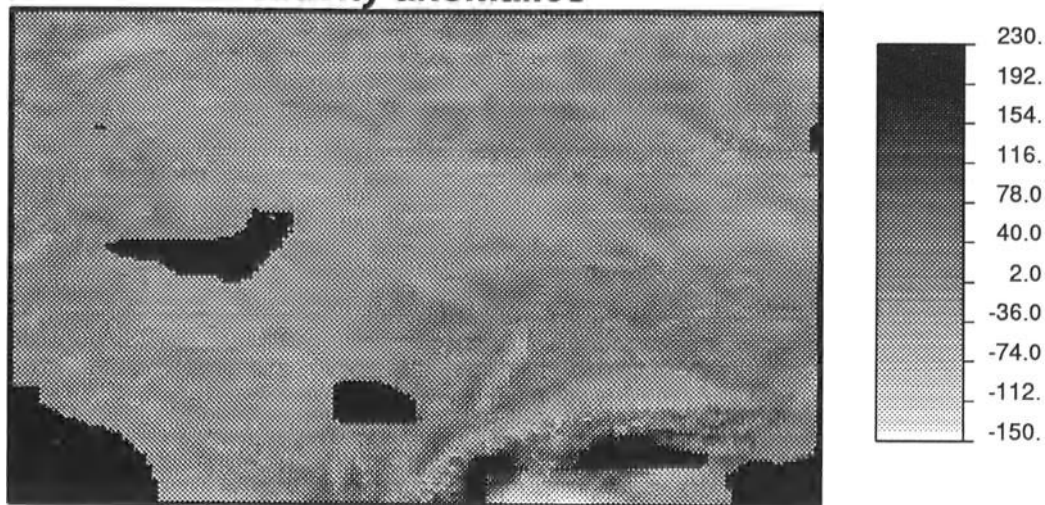


*Figure 1. Graphical display of gravity anomalies for north-western Europe.*

The total data set is too large to be used in its entirety to estimate the generalized covariance function. A basic way to overcome this difficulty is to select small subsets and to carry out the necessary computations on each of these subsets. The average values obtained of the subsets is then representative for the whole data set.

In order to calculate Akaike's Information Coefficient as a measure for non-stationarity, and the generalized covariance function, 35 data sets were selected at random, each of size 25 data from the whole data set. For each data set the degree of non-stationarity was determined as well as the coefficients  $\gamma_i$  of the generalized covariance function were estimated (Table 1)

*Table 1. Estimated coefficients of the polynomial generalized covariance function. Also included is Akaike's Information Criterion (AIC). The degree of non-stationarity ( $v$ ) that minimizes the AIC value is considered the most appropriate one.*

$v$	AIC	$\gamma_0$	$\gamma_1$	$\gamma_3$	$\gamma_5$
0	201.0	234.7	-89.3		
1	176.7	168.0	-149.7	0.301	
2	146.6	254.6	-168.9	5.546	-0.00598

### *Interpolated gravity anomalies*

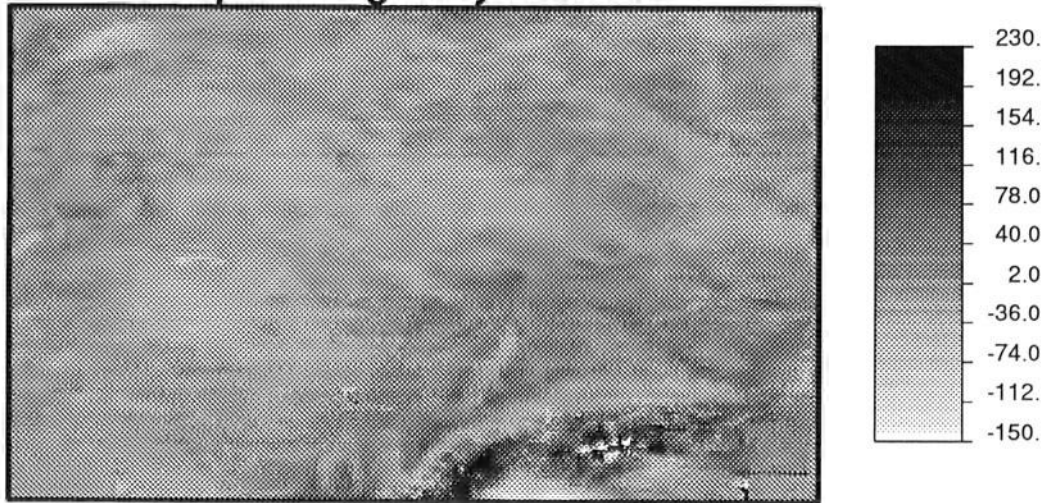


*Figure 2*    *Interpolated map of gravity anomalies. Clearly visible are the highly varying parts of the Alps, caused by high spatial heterogeneity of the anomalies in this region.*

### *Spatial uncertainty*



*Figure 3.*    *The uncertainty in the interpolated map. The uncertainty is zero for the larger part of the map, and increases with increasing distance from available observations.*

On the basis of the AIC it is judged that a second degree trend best fits the data. The coefficient  $\gamma_0$  is equal to 254.6, which corresponds to an non-spatial uncertainty equal to approximately 16 mgal in the measurements, due to measurement errors or to spatial variability at a much smaller scale than the scale at which observations were collected. The spatial uncertainty contributes to the total variance which increases for small distances linearly with a coefficient  $\gamma_1$  equal 150 mgal<sup>2</sup> for each degree distance between the points in the area. The spatial uncertainty increases according to a polynomial in the distance of degree 5 for larger distances, where the factors  $\alpha_3|h|^3$  and  $\alpha_5|h|^5$  give a substantial contribution,  $h$  being the (Euclidean) distance between two points, with coordinates expressed in degrees latitude and longitude. It is noted that this model is somewhat different from the model derived by Tscherning and Rapp (1974).

Next, collocation was applied (fig. 2) to predict the values of the gravity anomalies at those areas where data were missing. The generalized covariance function obtained above was used, with a degree of non-stationarity  $v$  equal to 2. Local neighborhoods consisting of the 21 closest points for each prediction location have been applied. One may notice, that a picture is obtained without the black spots as obtained previously. Some areas are interpolated in such a way, that a very natural picture emerges, for example the two larger areas in the center of the map. The highly heterogeneous area in the Alps, however, does show an interpolated surface that may lack any correspondence to actual anomalies. A highly varying picture is observed, with white (strongly negative) grid cells at short distances from dark (strongly positive) grid cells. Evidently, the data set may not be suitable for this type of spatial interpolation. Interesting as well are the uncertainties associated with this type of data (fig. 3). The uncertainties are relatively low close to the observations, with values well below 100 mgal<sup>2</sup>. However, they increase rapidly when extrapolation is involved to values well above 250 mgal<sup>2</sup>. The uncertainty thus obtained is a measure for the spatial uncertainty, and is as such different from the uncertainty that we noticed to emerge in the Alps.

*Acknowledgement.* I am very grateful to Prof. Teunissen from the Dept. of Geodesy of the Delft University of Technology, who gave many valuable contributions to improve this manuscript and who invited me to participate at the III Hotine-Marussi symposium. Also, the assistance of Ir. Haagmans from the same department is kindly acknowledged.

## REFERENCES

- Akaike, H. (1974). A new look at the statistical model identification, *IEEE Trans. Automat. Control*, **AC-19**, 716-723.
- Blais, J.A.R. (1982). Synthesis of kriging estimation methods. *Manuscripta Geodetica* **7**, 325-352.
- Blais, J.A.R. (1984). Generalized covariance functions and their applications in estimation, *Manuscripta geodetica* **9**, 307-322.
- Christakos, G. (1984). On the problem of permissible covariance and variogram models. *Water Resour. Res.* **20**, 251-265.

- Christakos, G. (1992). *Random field models for earth sciences*. Academic Press, New York.
- Corsten, L.C.A. (1989). Interpolation and optimal linear prediction. *Statistica Neerlandica* **43**, 69-84.
- Cressie, N.A.C. (1992). *Statistics for spatial data*. Wiley, New York.
- Delfiner, P. (1976). Linear estimation of nonstationary spatial phenomena, *Advanced Geostatistics in the Mining Industry*, M. Guarascio et al. (eds.), Reidel, Dordrecht, 49-68.
- Dermanis, A. (1977). Geodetic linear estimation techniques and the norm choice problem, *Manuscripta Geodetica* **2**, 15-97.
- Dermanis, A. (1984). Kriging and collocation - a comparison, *Manuscripta Geodetica* **9**, 159-167.
- Deutsch, C.V. and Journel, A.G. (1992). *GSLIB: Geostatistical Software Library and User's Guide*. Oxford University Press, New York.
- Gel'fand, I.M. and Vilenkin, N. (1964) *Generalized Functions 4*, Academic Press, New York.
- Haagmans, R.H.N., and Van Gelderen, M. (1991). Error-variances-covariances of GEM-T1: their characteristics and implications in geoid computations, *J. Geoph. Res.* **96**, 20011-20022.
- Hansen, R.O. (1993). Interpretive gridding by anisotropic kriging, *Geophysics* **58**, 1491-1497.
- Hardy, R.L. (1984). Kriging, collocation and biharmonic models for application in the earth sciences (what's the difference?) *Proceedings of the American Congress on Surveying and Mapping, 44th annual meeting*.
- Ito, K. (1953). Stationary random distributions, *Mem. Coll. Sci. Univ. Kyoto* **28**, 209-233.
- Journel, A.G. and Huijbregts, C.J. (1978). *Mining geostatistics*, Academic Press, London.
- Kitanidis, P.K. (1983). Statistical estimation of polynomial generalized covariance functions and hydrologic applications, *Water Resour. Res.* **19**, 901-921.
- Krarup, T. (1969). A contribution to the mathematical foundation of physical geodesy, *Publ. 44, Dan. Geod. Inst.*, Copenhagen.
- Matheron, G. (1973). The intrinsic random functions and their applications, *Adv. Appl. Prob.* **5**, 439-468.
- Meier, S. and Keller, W. (1990). *Geostatistik: Einführung in die Theorie der Zufallsprozesse*. Springer, Berlin.
- Meissl, H. (1976). Hilbert spaces and their application to geodetic least squares problems, *Boll. Geod. Sci. Affini* **35**, 49-80.
- Moritz, H. (1973). Least-squares collocation. *Publ. Deut. Geod. Komm.*, A, 75.
- Moritz, H. (1980a). *Advanced physical geodesy*. Herbert Wichmann Verlag, Karlsruhe.
- Moritz, H. (1980b). Geodetic Reference System 1980, *Bulletin Geodesique* **54**, 395-405.
- Schaffrin, B. (1992). Biased kriging on the sphere? *Geostatistics Tróia '92*, A. Soares (ed.), Kluwer, Dordrecht.
- Stein, A. and Corsten, L.C.A. (1991). Universal kriging and cokriging as a regression procedure, *Biometrics* **47**, 575-587.
- Stein, A., Staritsky, I.G., Bouma, J., Van Eijnsbergen, A.C., and Bregt, A.K. (1991a). Simulation of moisture deficits and interpolation by universal cokriging, *Water Resour. Res.* **27**, 1963-1973.

- Stein, A., Van Eijnsbergen, A.C., and Barendregt, L.G. (1991b). Cokriging non-stationary data, *Mathematical Geology* 23, 703-719.
- Torge, W., Weber, G., and Wenzel, H.G. (1983). 6' x 10' free air gravity anomalies of Europe including marine areas. *Paper presented to the XVIII IUGG general assembly, Hamburg, 15-27 August 1983.*
- Tscherning, C.C. (1978). Introduction to functional analysis with a view to its applications in approximation theory, *Approximation methods in geodesy*, H. Moritz and H. Sünkel (eds.), Herbert Wichmann Verlag, Karlsruhe.
- Tscherning, C.C., and Rapp, R.H. (1974). Closed covariance expressions for gravity anomalies, geoid undulations, and deflections of the vertical implied by anomaly degree variance models. *Rep. 208, Dep. of Geod. Sci.*, Ohio State Univ., Columbus.
- Weber, G. (1984). Hochauflösende mittlere Freiluftanomalien und gravimetrische Lotabweichungen für Europa, *Wissenschaftliche Arbeiten der Fachrichtung Vermessungswesen der Universität Hannover*, nr. 135.

# ON THE RECONSTRUCTION OF REGULAR GRIDS FROM INCOMPLETE, FILTERED OR UNEVENLY SAMPLED BAND-LIMITED DATA

Michael G. Sideris

Department of Geomatics Engineering, The University of Calgary  
2500 University Drive N.W., Calgary, Alberta, Canada T2N 1N4

## Abstract

This paper discusses some extensions and generalizations of Shannon's sampling theorem and points out possible applications in geodesy. More specifically, it shows that, for band-limited signals, missing data can be recovered from the remaining data on incomplete, filtered, rotated, scaled and/or transposed grids without the need of employing extra interpolation functions. In geodesy, such signals can be terrain-corrected gravity anomalies, geoid undulations from satellite altimetry, airborne gravity measurements, etc. These techniques are also applicable when irregularly distributed data are used directly to produce results on regular grids. Besides the recovery of the missing values, general schemes can be developed for interpolating at arbitrary locations employing only the remaining values, i.e., without the need to recover the missing data first. The sensitivity of these procedures to errors due to truncation, data noise, and jitter is also discussed briefly.

## 1. Introduction

As shown in Sideris (1994), it is possible to produce regular grids of, e.g., geoid undulations from irregular gravity measurements by using a hybrid method based on FFT or FHT combined with summation. The rationale for this approach is that the use of gridded data requires a preprocessing step which, in general, results in some loss of the original information. It would thus be advantageous if the irregular point measurements could be directly used in an efficient manner to compute the results on regular grids.

As an example, it will be shown how to compute geoid undulations on a grid with spacings  $\Delta x$ ,  $\Delta y$  by the planar Stokes formula using a set of  $n$  irregularly-distributed gravity anomalies at points  $(X_k, Y_k)$ ,  $k = 1, 2, \dots, n$ . Figure 1 shows a possible distribution of the gravity data with respect to the nodes of a regular grid. The contribution to all undulations on a grid of irregular gravity anomalies  $\Delta g$  with coordinates  $(X_k, Y_k)$  can be obtained by the following expression:

$$N(\vec{t}) = \frac{1}{2\pi\gamma} \mathbf{F}^{-I} \left\{ \sum_{k=1}^n \frac{1}{n_k} \Delta g(\vec{t}_k) e^{-2\pi i \vec{\omega}^T \vec{t}_k} \mathbf{F}\{S(\vec{t})\} \right\} = (2\pi\gamma)^{-1} \mathbf{F}^{-I} \{ \mathbf{F}\{\Delta g(\vec{t})\} \mathbf{F}\{S(\vec{t})\} \}, \quad (1)$$

where  $\vec{t} = (x, y)^T$ ,  $\vec{t}_k = (X_k, Y_k)^T$ ,  $i$  is the imaginary unit and  $\vec{\omega} = (u, v)^T$ , where  $u, v$  are the frequencies corresponding to  $x$  and  $y$ , respectively.  $S(\vec{t})$  is the planar Stokes kernel and  $n_k$  denotes the number of measurements that belong to the same grid element as  $\Delta g(\vec{t}_k)$  does; see Figure 1.  $\mathbf{F}$  and  $\mathbf{F}^{-I}$  denote the direct and inverse Fourier transform, respectively.

It is important to note that the summation term in eq. (1) gives the gravity anomaly spectrum  $\mathbf{F}\{\Delta g(\vec{t})\}$  computed from irregular point data. By applying the inverse Fourier transform to  $\mathbf{F}\{\Delta g(\vec{t})\}$ , gravity anomalies can also be obtained on a grid:

$$\Delta g(\vec{t}) = \mathbf{F}^{-I} \{ \mathbf{F}\{\Delta g(\vec{t})\} \} = \mathbf{F}^{-I} \left\{ \sum_{k=1}^n \frac{1}{n_k} \Delta g(\vec{t}_k) e^{-2\pi i \vec{\omega}^T \vec{t}_k} \right\}. \quad (2)$$

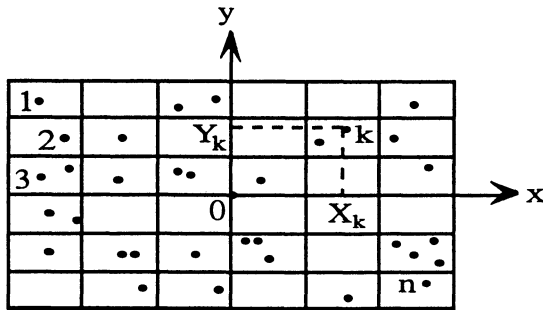


Figure 1. Distribution of irregular measurements with respect to a regular grid

The estimated grid of anomalies will naturally contain zeroes in the cells without any gravity data. The resulting grid of anomalies is thus incomplete. One way to fill it up is by frequency-domain interpolation; see, e.g., Mesc6, 1984; Vermeer, 1992. The  $\Delta g$ -spectrum in eqs. (1) and (2) should be modified by multiplying it by  $F\{w(\tilde{t})\}$ , where  $w(\tilde{t})$  is a specific interpolation function. Then, interpolated gravity anomalies will be obtained for all grid cells and improved geoid undulations will be obtained from the resulting  $\Delta g$ -grid without any empty cells. It was shown in Sideris (1994) that the use of even simple interpolation functions, such as linear, Gaussian, etc., results in a marked improvement of the accuracy of the predicted quantities.

The use of interpolation functions, however, alters the values of the given data by an amount that depends on the length of their support and special care must be taken in order to preserve the given values which, in addition, increases the time required for the computations. It would thus be advantageous to be able to fill the empty grid cells by just using the known grid values, without the use of extra interpolation functions. This, for example, would be helpful in the case that specific grid locations are empty because the values are missing, erased or contaminated by gross errors. This is indeed possible when the missing samples are taken from a band-limited, oversampled function (Marks II, 1983; Soumekh, 1988). In such a case, the missing values can be recovered even if the sampled values have been filtered or sampled on non-orthogonal grids. The procedure is based on generalizations of Shannon's sampling theorem.

## 2. Reconstruction in One Dimension

**Shannon's interpolation theorem and recovery of missing samples.** This section discusses Shannon's interpolation theorem which is the backbone of the interpolating schemes for the recovery of missing data. Assume that  $f(x)$  is a band-limited function with bandwidth  $B$ , i.e.,  $F(u) = 0$  if  $|u| > B$ , or  $F(u) = F(u)\Pi(u/2B)$ , where  $F(u)$  is the spectrum of  $f(x)$  and  $\Pi(u/2B)$  is the rectangle function with support  $2B$ . Shannon's theorem says that the continuous function  $f(x)$  can be reconstructed from its discrete samples  $f(n\Delta x)$  using the following cardinal series:

$$f(x) = \sum_{n=-\infty}^{\infty} f(n\Delta x) \text{sinc}(2Wx - n) = r \sum_{n=-\infty}^{\infty} f\left(\frac{n}{2W}\right) \text{sinc}(2Bx - rn), \quad W \geq B, \quad (3)$$

where  $\text{sinc} = \sin(\pi t)/(\pi t)$ ,  $\Delta x$  is the spacing of the samples and  $2W = 1/\Delta x$  is the sampling rate. The ratio  $r = B/W \leq 1$  is called the sampling rate parameter. Equivalently, the spectrum of  $f(x)$  can be reconstructed from the spectrum of the samples as follows:

$$F(u) = \frac{1}{2W} \sum_{n=-\infty}^{\infty} f\left(\frac{n}{2W}\right) e^{-j\pi nu/W} \Pi\left(\frac{u}{2W}\right) = \sum_{n=-\infty}^{\infty} F(u - 2nW) \Pi\left(\frac{u}{2W}\right). \quad (4)$$

The term  $F(u - 2nW)$  in the above equation indicates the well-known fact that sampling produces a replication of the spectrum of the continuous function. Consequently, as eq. (4) indicates, the function can be reconstructed by low-pass filtering of its samples.

(a)  $r = B/W = 1$ . In this case, the function is sampled at the minimum possible rate of sampling without aliasing, called the Nyquist rate ( $2W = 2B$ ) and its spectrum replications touch but do not overlap. Evaluating eq. (3) at  $x = m/2B$  yields

$$f\left(\frac{m}{2B}\right) = \sum_{n=-\infty}^{\infty} f(n\Delta x) \sin c(m - n) = \sum_{n=-\infty}^{\infty} f(n\Delta x) \delta[n - m] = f(m\Delta x), \quad (5)$$

where  $\delta[n]$  is the Kronecker delta. Since eq. (5) is an identity, samples taken at the Nyquist rate are independent. In other words, only the sample at  $x=m/2B$  contributes to the interpolation at that point while at a point other than the sample location  $f(x)$  is determined by all sample values. Consequently, in this case, it is not possible to recover missing samples from the remaining ones.

(b)  $r = B/W > 1$ . In this case, the function is undersampled, its spectrum replications overlap, and aliasing occurs. Thus, it is not possible to fully reconstruct  $f(x)$  from its samples.

(c)  $r = B/W < 1$ . In this case, the function is oversampled and there are regions of zeroes (e.g., the region  $B < |u| < 2W-B$ ) between the replications of its spectrum. Since  $F(W)$  is then zero, eq. (4) yields

$$F(W) = \sum_{n=-\infty}^{\infty} f\left(\frac{n}{2W}\right) e^{-j\pi n} = \sum_{n=-\infty}^{\infty} (-1)^n f\left(\frac{n}{2W}\right) = 0, \quad (6)$$

which indicates that the samples taken at a rate higher than the Nyquist are dependent. Thus, missing samples could be recovered from the remaining ones.

Assume that the total number of missing samples is  $M$  and let  $\mathcal{M}$  be the set of integers corresponding to the locations of these missing samples. Then, eq. (3) can be written as

$$f(x) = r \sum_{n \in \mathcal{M}} f\left(\frac{n}{2W}\right) \sin c(2Bx - m) + r \sum_{n \notin \mathcal{M}} f\left(\frac{n}{2W}\right) \sin c(2Bx - rn). \quad (7)$$

Evaluation of this expression at the missing points, i.e. at  $x = m/2W$ ,  $m \in \mathcal{M}$ , yields the following system of  $M$  equations and  $M$  unknowns:

$$\sum_{n \in \mathcal{M}} \{\delta[n - m] - r \sin c[r(n - m)]\} f\left(\frac{n}{2W}\right) = r \sum_{n \notin \mathcal{M}} f\left(\frac{n}{2W}\right) \sin c(2Bx - rn), \quad m \in \mathcal{M}. \quad (8)$$

The unknowns  $f(n/2W)$ ,  $n \in \mathcal{M}$ , can be determined from the solution of the above system if the matrix of their coefficients, say  $A$ , is non-singular. When  $r = 1$ ,  $A$  is singular. If there is no data noise, an arbitrarily large number of lost samples can be restored when  $r < 1$ . As  $M$  increases and  $r$  approaches 1, the restoration becomes more unstable.

After recovering all missing samples as described above,  $f(x)$  could be reconstructed from eq. (3). Alternately, it should also be possible to derive a scheme that interpolates the values of  $f(x)$  only from the remaining data, without first recovering the lost ones (Marks II, 1983 and 1991). If  $a_{kl}$  are the elements of the inverse of  $A$ , then the solution of system (8) is

$$f\left(\frac{\ell}{2W}\right) = r \sum_{n \in M} f\left(\frac{n}{2W}\right) \sum_{k \in M} a_{k\ell} \sin c[r(k-n)], \quad \ell \in M. \quad (9)$$

Substituting eq.(9) into eq. (7) gives the final formula for interpolating  $f(x)$  from only the remaining samples:

$$\begin{aligned} f(x) &= \sum_{n \notin M} f\left(\frac{n}{2W}\right) \sin c(2Wx - n) + \sum_{\ell \in M} f\left(\frac{\ell}{2W}\right) \sin c(2Wx - \ell) = \sum_{n \notin M} f\left(\frac{n}{2W}\right) h_n(2Wx), \\ h_n(x) &= \sin c(x - n) + r \sum_{k \in M} \sum_{\ell \in M} a_{k\ell} \sin c[r(n-k)] \sin c(x - \ell). \end{aligned} \quad (10)$$

Equation (10) can be viewed as a generalization of Shannon's interpolation theorem and  $h_n(x)$  can be considered as a generalized interpolation function. Such functions will be discussed in the following section.

**Generalized interpolation functions and reconstruction from filtered samples.** Often in geodesy we need to recover the disturbing potential from measurements of its functionals. Thus, in general, we need to recover a function  $f(x)$  from samples, taken at the Nyquist rate, of a linear functional of it defined by the convolution

$$g(x) = f(x) * h(x). \quad (11)$$

Expressing the spectrum of the filtering function as

$$H(u) = \frac{1}{2B} \Pi\left(\frac{u}{2B}\right) / D(u) \quad \text{or} \quad 2BD(u) = \Pi\left(\frac{u}{2B}\right) / H(u), \quad (12)$$

making use of the fact that  $f(x)$  is band-limited and using eq. (4) for  $g(x)$  with  $W = B$ , the spectrum of  $f(x)$ , when  $D(u)$  is bounded, takes the form

$$F(u) = \frac{G(u)}{H(u)} \Pi\left(\frac{u}{2B}\right) = 2BG(u)D(u)\Pi\left(\frac{u}{2B}\right) = \sum_{n=-\infty}^{\infty} g\left(\frac{n}{2B}\right) e^{-j\pi nu/B} \Pi\left(\frac{u}{2B}\right) \frac{1}{2BH(u)}. \quad (13)$$

The inverse Fourier transform applied to eq. (13) gives  $f(x)$  from the samples of  $g(x)$  by the following equation which is ill-posed when  $D(u)$  contains a pole (Marks II, 1991):

$$f(x) = \int_{-B}^{B} \sum_{n=-\infty}^{\infty} g\left(\frac{n}{2B}\right) e^{-j\pi nu/B} \Pi\left(\frac{u}{2B}\right) \frac{1}{2BH(u)} e^{j2\pi ux} du = \sum_{n=-\infty}^{\infty} g\left(\frac{n}{2B}\right) d\left(x - \frac{n}{2B}\right), \quad (14a)$$

$$d(x) = \frac{1}{2B} \int_{-B}^{B} \frac{1}{H(u)} e^{j2\pi ux} du = F^{-1}\{D(u)\}. \quad (14b)$$

Also important for geodesy is the case of reconstructing the signal from simultaneous or interlaced samples of it and its derivative. For example, sample velocity (speedometer) and distance (odometer) to determine position. This can have applications in AVL systems or kinematic positioning by GPS- and/or INS-based systems. In the case of simultaneous samples, they can even be taken at half the Nyquist rate without causing aliasing. In the case of simultaneous sampling, restoration becomes ill-posed (unstable) in the presence of noise. Details on this can be found in Marks II (1991), while the theory that generalizes Shannon's theorem to different types of sampling and sample data is given in Papoulis (1977).

**Error sources and their effects.** Noise can be introduced to the results of interpolation primarily due to three reasons: Imperfect data (data noise), model approximations (truncation error) and imperfect sampling procedures (jitter). These errors are usually present in sampled geodetic data; their modeling, however, is very difficult. To provide an idea about their role, these error sources and their individual effects are explained briefly in the sequel. For the more complex case where more than one of these effects occur simultaneously, see Marks II (1991).

**(a) Effect of data noise.** Assume that the data samples are affected by zero-mean stationary noise, e.g., white noise, with variance  $\sigma^2$  and call the variance of the interpolated values  $s^2$ . It can be shown (Marks II and Radbel, 1984) that, when no samples are missing,  $s^2$  and  $\sigma^2$  are related as follows:

$$s^2 = r\sigma^2 = BW^{-1}\sigma^2. \quad (15)$$

Thus, it is evident that (i) when sampling is done at the Nyquist rate ( $r = 1$ ), the error variance of the interpolated values is the same as the sample variance and (ii) oversampling ( $r < 1$ ) decreases the interpolation noise level. However, the noise level cannot be made arbitrarily small by oversampling since, eventually, adjacent samples will become correlated and the white noise assumption violated. More general, it can be shown that oversampling reduces the interpolation noise variance by suppressing the high-frequency noise components.

When the interpolation is performed in the case of missing samples, the ratio between  $s^2$  and  $\sigma^2$  increases. For example, when one sample is missing say at the origin, its error variance is

$$s^2(0) = r(1 - r)^{-1}\sigma^2. \quad (16)$$

Similar expressions can be derived when more than one samples are missing not only for the recovered missing values but for the values of the function interpolated at arbitrary locations. See Marks II (1991) for details.

**(b) Truncation error.** An infinite number of samples is required to recover a band-limited signal by the cardinal series of eq. (3). Since this is not possible in practice, a truncation error  $\varepsilon_N(x)$  occurs when the summation in eq. (3) is done from  $-N$  to  $N$  instead of  $-\infty$  to  $\infty$ . The square of  $\varepsilon_N(x)$  has an upper bound which is proportional to  $(E - E_N)$  for  $|x| < N/2B$ , where  $E$  is the energy of  $f(x)$  and  $E_N$  is the energy of  $f_N(x)$  computed from the truncated cardinal series by Parseval's theorem. Thus, the error bound tends to zero as  $N \rightarrow \infty$  and  $E_N \rightarrow E$ . It can also be shown (Marks II, 1991) that at the sample locations where  $|n| \leq N$ ,  $\varepsilon_N(n/2B) = 0$  and that the error bound is enveloped by the curve  $2N\pi^{-2}/(N^2 - x^2)$ .

**(c) Effect of jitter.** When samples are taken near to but not exactly at the desired sample locations, i.e. instead of the sample set  $\{f(n/2W), -\infty < n < \infty\}$  we have the sample set  $\{f(n/2W - e_n), -\infty < n < \infty\}$ , jitter occurs;  $e_n$  is the unknown jitter offset of the  $n$ -th sample. If  $e_n$  are identically-distributed random variables, cardinal series interpolation of jittered samples yields a biased estimate of the original signal. It is possible to design a filter to correct for this bias, however, the price to pay is an increase in the interpolation noise variance. Mathematical expressions and a detailed discussion on jitter can be found in Papoulis (1966) and Marks II (1991).

### 3. Reconstruction in Two Dimensions

**Generalized interpolation and recovery of missing samples.** Petersen and Middleton (1962) extended the sampling theorem to  $N$ -dimensions, while Clark et al. (1985) extended it further

for the cases of non-uniform sampling and non-band-limited functions. The following discussion is limited to two-dimensional (2D) signals, which occur more often in geodesy.

Let us assume that a continuous function  $f(x,y)$  is sampled on a grid which is rotated and/or scaled and/or transposed with respect to an orthogonal  $x$ - $y$  grid. An example of such a grid, defined by the  $\vec{q}_1$ ,  $\vec{q}_2$  vectors is given in Figure 2, where  $\vec{q}_1 = (B, 0)^T$ ,  $\vec{q}_2 = (-D\cos\theta, D\sin\theta)^T$ . It can represent shipborne or airborne gravity or seismic measurements, or, if we neglect jitter, ascending and descending tracks of satellite altimetry in a very local area. Using capital bold letters to denote matrices, we define:

$$\bar{\mathbf{t}} = \begin{pmatrix} x \\ y \end{pmatrix} = \begin{pmatrix} q_{11} & q_{12} \\ q_{21} & q_{22} \end{pmatrix} \begin{pmatrix} k \\ \ell \end{pmatrix} = (\vec{q}_1 \mid \vec{q}_2) \begin{pmatrix} k \\ \ell \end{pmatrix} = \mathbf{Q}\bar{n}, \quad (17)$$

where  $\bar{n} = (k, \ell)^T$  is an integer vector indicating the position of the sample points on the  $k$ - $\ell$  grid.  $\mathbf{Q}$  is called a sampling matrix and has non-zero determinant ( $\det \mathbf{Q} \neq 0$ ) when the sampling vectors  $\vec{q}_1 = (q_{11}, q_{21})^T$  and  $\vec{q}_2 = (q_{12}, q_{22})^T$  are linearly independent. The grid spacings are  $\Delta q_1 = |\vec{q}_1|$  and  $\Delta q_2 = |\vec{q}_2|$  and should be such that no aliasing is introduced in the spectrum of the sampled function.

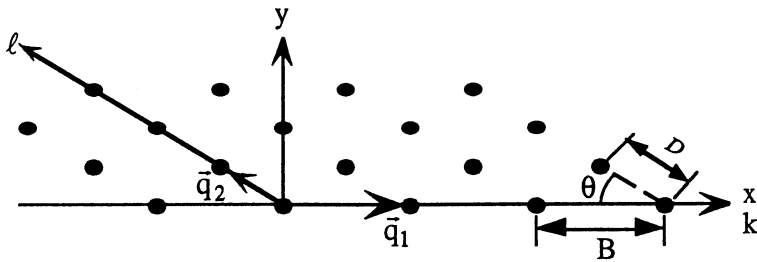


Figure 2. The geometry of sampling and transformation between grids

When  $\mathbf{Q}$  is an  $N \times N$  matrix, the sampling density, in samples per (unit length) $N$ , is  $1/|\det \mathbf{Q}|$ . The sampled signal and its spectrum are

$$f_s(\bar{\mathbf{t}}) = \sum_{\bar{n}} f(Q\bar{n}) \delta(\bar{\mathbf{t}} - Q\bar{n}), \quad F_s(\bar{\omega}) = \mathcal{F}\{f_s(\bar{\mathbf{t}})\} = \frac{1}{|\det \mathbf{Q}|} \sum_k F(\bar{\omega} - P\bar{k}), \quad (18)$$

where  $\delta(\bar{\mathbf{t}})$  is the 2D Dirac delta function.  $P$  is the Fourier periodicity matrix. It satisfies  $P^T \mathbf{Q} = \mathbf{I}$  and its column vectors dictate the geometry of the replication of  $F(\bar{\omega}) = \mathcal{F}\{f(\bar{\mathbf{t}})\}$  that is seen in eq. (18).

If  $F(\bar{\omega})$  is band-limited in a frequency area  $\mathcal{B}$  called the baseband, then  $F(\bar{\omega}) = 0$  outside  $\mathcal{B}$ . If  $\mathbf{Q}$  is such that there will be no aliasing when the spectrum of the function is computed from discrete data  $f(Q\bar{n})$ , i.e., there will be no overlapping as  $\mathcal{B}$  is periodically repeated in the frequency plane, then it is possible to regain  $F(\bar{\omega})$  from  $F_s(\bar{\omega})$  by low-pass filtering as follows:

$$F(\bar{\omega}) = F_s(\bar{\omega})G(\bar{\omega}), \quad G(\bar{\omega}) = \begin{cases} |\det \mathbf{Q}|, & \bar{\omega} \in \mathcal{W} \\ 0, & \bar{\omega} \notin \mathcal{W} \end{cases}, \quad (19)$$

where, similarly to the one-dimensional (1D) case,  $\mathcal{W}$  is an area completely enclosing  $\mathcal{B}$  which must not infringe into adjacent spectra and where  $F(\bar{\omega}) = 0$ ,  $\bar{\omega} \in (\mathcal{W}-\mathcal{B})$ . For a given  $\mathbf{Q}$ ,  $F_s(\bar{\omega})$  is separated into periods, where a period cell  $\mathcal{C}$  fills the entire  $\bar{\omega}$ -plane when replicated. In general, it is  $\mathcal{B} \leq \mathcal{W} \leq \mathcal{C}$ .

Then,  $f(\bar{t})$  is obtained as the convolution of  $f_s(\bar{t})$  and  $g(\bar{t})$  which yields the generalized sampling theorem (Dungeon and Mersereau, 1984) that allows for the reconstruction of the continuous function  $f(\bar{t})$  from its samples  $f(\mathbf{Q}\bar{n})$ :

$$\begin{aligned} f(\bar{t}) &= |\det \mathbf{Q}| \sum_{\bar{n}} \int_{\mathcal{W}} e^{2\pi i [\bar{\omega}^T (\bar{t} - \mathbf{Q}\bar{n})]} d\bar{\omega} = \sum_{\bar{n}} f(\mathbf{Q}\bar{n}) g(\bar{t} - \mathbf{Q}\bar{n}), \\ g(\bar{t}) &= |\det \mathbf{Q}| \int_{\mathcal{W}} e^{2\pi i \bar{\omega}^T \bar{t}} d\bar{\omega}, \end{aligned} \quad (20)$$

where  $g(\bar{t})$  is the interpolation function. It is easy to verify that when "orthogonal" sampling is performed along the  $x$  and  $y$  directions at  $\Delta x$ ,  $\Delta y$  intervals, respectively, the sampling vectors become  $\bar{q}_1 = (\Delta x, 0)^T$  and  $\bar{q}_2 = (0, \Delta y)^T$ ,  $\det \mathbf{Q} = \Delta x \Delta y$ , and eq. (20) for  $\mathcal{W} = \mathcal{B}$  reduces to the 2D Shannon sampling theorem:

$$\begin{aligned} f(x, y) &= \Delta x \Delta y \sum_k \sum_{\ell} f(k \Delta x, \ell \Delta y) \int_{-u_N}^{u_N} \int_{-v_N}^{v_N} e^{2\pi i [u(x - k \Delta x) + v(y - \ell \Delta y)]} du dv = \sum_k \sum_{\ell} f(k \Delta x, \ell \Delta y) \\ &\cdot \sin c[u_N(x - k \Delta x)] \sin c[v_N(y - \ell \Delta y)] = \sum_k \sum_{\ell} f(k \Delta x, \ell \Delta y) \sin c\left(\frac{x}{\Delta x} - k\right) \sin c\left(\frac{y}{\Delta y} - \ell\right), \end{aligned} \quad (21)$$

where now the baseband  $\mathcal{B}$  is defined by the Nyquist frequencies  $u_N$  and  $v_N$ , i.e.,  $\mathcal{B} = \{(u, v) : |u| < u_N, |v| < v_N\}$ .

It will now be shown how lost samples can be recovered. Figure 3 shows a grid where three samples are missing. Their location on the  $x$ - $y$  grid is  $\mathbf{Q}\bar{m}_k$ ,  $k=1, 2, 3$ , where  $\bar{q}_1 = (1, 1)^T$ ,  $\bar{q}_2 = (-1, 1)^T$  and their location on the  $k$ - $\ell$  grid is given by  $M = 3$  vectors  $\bar{m}_1 = (0, 0)^T$ ,  $\bar{m}_2 = (0, 1)^T$ ,  $\bar{m}_3 = (1, -2)^T$ . The set of lost samples is then defined as  $\mathcal{M} = \{\bar{m}_1, \bar{m}_2, \bar{m}_3\}$ . For this case, eq. (20) can be written (Marks II, 1991) as

$$f(\bar{t}) = \sum_{\bar{m} \in \mathcal{M}} f(\mathbf{Q}\bar{m}) g(\bar{t} - \mathbf{Q}\bar{m}) + \sum_{\bar{m} \in \mathcal{M}} f(\mathbf{Q}\bar{m}) g(\bar{t} - \mathbf{Q}\bar{m}), \quad (22)$$

This expression can be evaluated at  $M$  points. At these points, the missing grid values are the set  $\{f(\mathbf{Q}\bar{m}), \bar{m} \in \mathcal{M}\}$ . Denoting these  $M$  points by  $\bar{t} = \mathbf{Q}\bar{k}$ ,  $\bar{k} \in \mathcal{M}$ , eq. (22) yields

$$f(\mathbf{Q}\bar{k}) = \sum_{\bar{m} \in \mathcal{M}} f(\mathbf{Q}\bar{m}) g[\mathbf{Q}(\bar{k} - \bar{m})] + \sum_{\bar{m} \in \mathcal{M}} f(\mathbf{Q}\bar{m}) g[\mathbf{Q}(\bar{k} - \bar{m})], \quad \bar{k} \in \mathcal{M}, \quad (23)$$

which after rearranging gives

$$\sum_{\bar{m} \in \mathcal{M}} \{\delta[\bar{k} - \bar{m}] - g[\mathbf{Q}(\bar{k} - \bar{m})]\} f(\mathbf{Q}\bar{m}) = \sum_{\bar{m} \in \mathcal{M}} f(\mathbf{Q}\bar{m}) g[\mathbf{Q}(\bar{k} - \bar{m})], \quad \bar{k} \in \mathcal{M}, \quad (24)$$

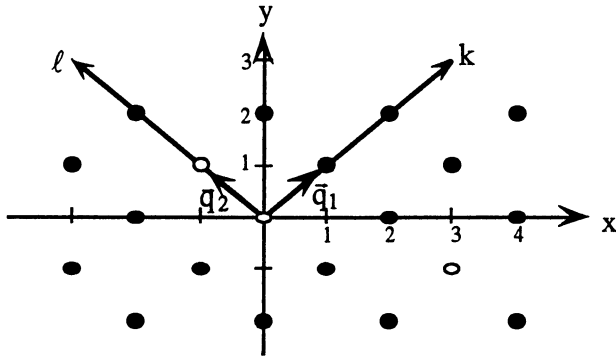


Figure 3. The geometry of a grid with three missing samples

The left hand side of eq. (24) contains the missing samples while the right hand side can be computed from the known values. Then, the solution of these  $M$  equations gives the values of the lost samples. Note that this system of equations is singular when the integration region  $\mathcal{W}$  is equal to the cell region  $\mathcal{C}$  (Marks II, 1986). Actually, restoration becomes more unstable as  $M$  increases and as the area  $\mathcal{W}$  increases with respect to that of  $\mathcal{C}$ .

Equations (9) and (10) for reconstructing the function from the existing samples without first recovering the missing ones can be extended to higher dimensions although the resulting formulas will be a lot more complicated. A simple example is given here for the case where only one sample is missing at the origin. If  $g(\vec{0}) \neq 1$ , eq. (24) for  $M = 1$  and  $\mathcal{M}$  containing only the origin gives

$$f(\vec{0}) = \frac{1}{1 - g(\vec{0})} \sum_{\vec{m} \neq \vec{0}} f(Q\vec{m})g(-Q\vec{m}), \quad (25)$$

which, when substituted into eq. (22) gives

$$f(\vec{t}) = \sum_{\vec{m} \neq \vec{0}} f(Q\vec{m})[g(\vec{t} - Q\vec{m}) + \frac{1}{1 - g(\vec{0})} g(-Q\vec{m})g(\vec{t})]. \quad (26)$$

**Noise sensitivity.** The error sources are the same as in the 1D case, however, their modeling is more complex. As an example, the effect of data noise when one sample is missing at the origin will be discussed here. Again, assume that the data noise is white with variance  $\sigma^2$  and call the variance of the interpolated values  $s^2$ . It can be shown (Marks II, 1986) that,  $s^2(\vec{0})$  and  $\sigma^2$  are related as follows:

$$s^2(\vec{0}) = g(\vec{0})[1 - g(\vec{0})]^{-1}\sigma^2 = (\mathcal{C}/\mathcal{W} - 1)^{-1}\sigma^2. \quad (27)$$

Thus, the restoration noise level depends on  $\mathcal{C}$  and is an increasing function of  $\beta$ . Consequently, for minimum restoration noise,  $\mathcal{W}$  must be chosen equal to  $\beta$ , which is its minimum allowable value. Also note that if the support has the shape of a cell, i.e.  $\beta = \mathcal{C}$ , restoration is not possible at the Nyquist rate and over-sampling is necessary.

#### 4. Reconstruction From Irregular Samples

The previous section discussed the reconstruction from samples unevenly spaced but in a regular fashion. A brief introduction will now be given on ways of reconstructing the function

$f(x)$  from samples taken at arbitrary locations  $x_n$ . Papoulis (1966) showed how to extend Shannon's theorem to sample sequences that were deviating slightly from a uniform sequence. We will follow here the more general extension by Clark et al. (1985) that treats an irregular sequence of samples as the result of a coordinate transformation of a uniform sample sequence.

**One-dimensional case.** If a one-to-one continuous mapping  $\mu(x)$  exists such that  $\tau = \mu(x)$  and  $x_0 + n\Delta x = \mu(x_n)$  for some arbitrary  $x_0$ , and if  $F\{h(\tau)\} = 0$  for  $|\tau| > B$ , where  $h(\tau) = f(\mu^{-1}(\tau))$ , the samples of the function  $h(\tau)$  will be uniformly spaced and so we can retrieve  $f(x)$  using the relationship  $f(x) = h(\mu(x))$ . Then, the following generalization of Shannon's theorem holds:

$$f(x) = \sum_{n=-\infty}^{\infty} f(x_n) \sin c[B(\mu(x) - n\Delta x)]. \quad (28)$$

The use of the above equation in practice requires the knowledge of  $\mu(x)$  at all points where we want to reconstruct  $f(x)$ . If an analytical expression is not available, then  $\mu(x)$  must be found by interpolation between the values of  $\mu(x)$  at the known points.

**Two-dimensional case.** Suppose that  $f(\vec{t})$  is sampled at points in the infinite set  $\{\vec{t}_s\}$ . If a one-to-one continuous mapping  $\vec{\mu}(\vec{t})$  exists such that  $\vec{\tau} = \vec{\mu}(\vec{t})$  and  $\vec{\tau}_s = \vec{\mu}(\vec{t}_s)$ , and if  $F\{h(\vec{\tau})\} = 0$  for  $\vec{\omega} \notin \mathcal{B}$ , where  $h(\vec{\tau}) = f(\vec{\mu}^{-1}(\vec{\tau}))$ , then, similarly to the 1D case, the following generalization of Shannon's theorem holds:

$$f(\vec{t}) = \sum_{\{\vec{t}_s\}} f(\vec{t}_s) g[\vec{\mu}(\vec{t}) - \vec{\mu}(\vec{t}_s)], \quad (29)$$

where  $g(\vec{t})$  is defined in eq. (20) for  $\mathcal{W} = \mathcal{B}$ . The determination of  $\vec{\mu}(\vec{t})$  can be done as in the 1D case. However, it is more complex due to the fact that there is no general scheme for ordering arbitrarily distributed points in two dimensions analogous to the sequential ordering available in one dimension, such that adjacency properties are preserved. An algorithm for this is given in Clark et al. (1985). Also, Soumekh (1988) gives similar algorithms for reconstruction when the spectrum of the function, instead of the function itself, has been unevenly sampled.

## 5. Concluding Remarks

It is now possible to compute grids of, e.g., gravity anomalies or geoid undulations from irregular gravity measurements by use of Fourier methods. When the irregular measurements do not cover all cells of the output grid, the resulting undulations will suffer some loss of accuracy while, when predicting gridded anomalies, zero values will result in the empty grid cells. These problems can be overcome by employing an interpolation function to fill up the empty grid cells. This, however, will alter the values in non-empty cells. To avoid this, two-dimensional adaptive filtering algorithms should be developed that take into account the existing empty cells.

Another way to avoid the above problem, is to try to recover the missing grid values from either the remaining ones or directly from the original irregular data. Using generalized versions of Shannon's sampling theorem for band-limited functions, reconstruction schemes were derived that recover the missing samples or can interpolate values at arbitrary locations directly from the remaining ones, even for the case that the function, or any functional of it, is sampled on non-orthogonal grids or arbitrarily at irregular locations. The usual remove-restore techniques produces band-limited data in geodesy, such as, e.g., reduced gravity anomalies

where the short wavelengths are removed by a terrain reduction. Data can also be band-limited due to the actual sampling process as is the case in, e.g., satellite altimetry or airborne gravimetry. In the absence of noise, an arbitrary large but finite number of missing samples can be regained from the remaining samples provided that the data are oversampled, i.e. not aliased and there are sections in the sampled signal's spectrum that are identically zero. For 2D signals, these conditions apply even at Nyquist densities while 1D signals can be recovered only when sampled at rates higher than the Nyquist. When the known samples are perturbed by additive noise, oversampling also results in a reduction of the restoration noise level.

Before closing, we must mention two important facts related to sampling. Firstly, that rectangular sampling is not the optimal way of sampling. Mersereau (1979) has shown that hexagonal sampling offers substantial savings in both storage and computational efficiency. It might thus be worth considering it for data-hungry applications such as airborne gravimetry. Secondly, that a signal can be reconstructed from its projections by the use of the Radon or other transform methods (Mersereau and Oppenheim, 1974). Some geodetic applications have already appeared for the processing of airborne geophysical data (Zhou, 1992) and satellite altimetry data (Hanssen, 1993), but further research is necessary to further explore the potential of this very promising technique.

## REFERENCES

- Clark, J.J., Palmer, M.R. and Lawrence, P.D., 1985, A transformation method for the reconstruction of functions from nonuniformly spaced samples, *IEEE Trans. on Acoustics, Speech, and Signal Processing* Vol. 33, No. 4, pp. 1151-1165.
- Dudgeon, D.E. and Mersereau, R.M., 1984, *Multidimensional Digital Signal Processing*, Prentice-Hall, Inc., Englewood Cliffs, New Jersey.
- Hanssen, R.H., 1993, The application of Radon transformation for the analysis of sparsely sampled data, TU Delft, Faculty of Geodetic Engineering Report No. 93.1, Delft.
- Marks II, R.J., 1983, Restoring lost samples from an oversampled band-limited signal, *IEEE Trans. on Acoustics, Speech, and Signal Processing* Vol. 31, No. 3, pp. 752-755.
- Marks II, R.J., 1986, Multidimensional-signal sample dependency at Nyquist densities, *Journal of the Optical Society of America A* Vol. 3, No. 2, pp. 268-273.
- Marks II, R.J., 1991, *Introduction to Shannon Sampling and Interpolation Theory*, Springer-Verlag, New York.
- Marks II, R.J. and Radbel, D., 1984, Error of linear estimation of lost samples in an oversampled band-limited signal, *IEEE Trans. on Acoustics, Speech, and Signal Processing* Vol. 32, No. 3, pp. 648-654.
- Mersereau, R.M., 1979, The processing of hexagonally sampled two-dimensional signals, *Proc. of the IEEE* Vol. 67, No. 6, pp. 930-949.
- Mersereau, R.M. and Oppenheim, A.V., 1974, Digital reconstruction of multidimensional signal from their projections, *Proc. of the IEEE* Vol. 62, No. 10, pp. 1319-1338.
- Meskó, A., 1984, *Digital Filtering: Applications in Geophysical Exploration for Oil*, Akadémiai Kiadó, Budapest.
- Papoulis, A., 1966, Error analysis in sampling theory, *Proc. of the IEEE* Vol. 54, No. 7, pp. 947-955.
- Papoulis, A., 1977, *Signal analysis*, McGraw-Hill, New York.
- Petersen D.P. and Middleton, D., 1962, Sampling and reconstruction of wave-number-limited functions in N-dimensional Euclidean spaces, *Information and Control* Vol. 6, pp. 279-323.
- Sideris, M.G., 1994, Fourier geoid determination with irregular data, Accepted for publication in *Manuscripta Geodaetica*.
- Soumekh, M., 1988, Band-limited interpolation from unevenly spaced sampled data, *IEEE Trans. on Acoustics, Speech, and Signal Processing* Vol. 36, No. 1, pp. 110-121.
- Vermeer, M., 1992, A frequency domain approach to optimal geophysical data gridding, *Manuscripta Geodaetica*, Vol. 17, pp. 141-154.
- Zhou, Y., 1992, Application of Radon transform to the processing of airborne geophysical data, Ph.D. dissertation, TU Delft, Delft.

# Non-parametric Statistics and Bootstrap Methods for Testing the Data Quality of a Geographic Information System

F. Crosilla

*Dipartimento di Ingegneria Civile*    *Dip. di Matematica e Informatica*  
*Università di Udine*                              *Università di Udine*

G. Pillirone

## Abstract

This paper presents a method for testing the data quality of a G.I.S. making use of the Wilcoxon test. Accuracy assessment procedures based on statistical hypothesis tests are considered first, then the Wilcoxon test is presented and a power formula is discussed. This expression needs the estimation of two parameters, obtained by the bootstrap. The advantages of the proposed procedure are that the hypothesis testing approach is preferable to the simple comparison of values, and that it minimizes control measurements, since the power expression allows to determine the optimal sample size.

## 1 Introduction

The quality requirements for G.I.S. data bases are usually imposed in technical specifications provided by public administrations, which are the main users of G.I.S. tools. In most cases metric accuracy and currency of the data base are considered, and data quality assessment is based on the comparison of a certain number of object attribute values contained in the Geographic Information System data file with the attribute values of the same objects alternatively obtained by survey methods which are known to give more precise results. The difference of values must be less than a tolerance value fixed a priori.

In agreement with the standard operational praxis of comparison of numerical data, a procedure for testing the quality of a G.I.S. data base, based on the application of a sequence of statistical tests, was proposed by Fritsch and Crosilla (1992) and Crosilla (1992), and is here taken as a starting point. The procedure is reinforced with some considerations which complete the theoretical bases and lead to some optimizations.

The procedure proposed by Crosilla (1992) regards the testing of the metric quality of a digital map and will be briefly recalled. Data quality is evaluated comparing the contents of the data base to be controlled with some high precision reference data obtained by field measurements. A statistical hypothesis test is applied to the differences between the two data sets to verify if the contents of the data base differ significantly from reference data.

In order to choose the appropriate statistical test, a preliminary analysis is computed, applying a goodness-of-fit test to the distribution of the least squares residuals of a block adjustment; in the ideal case this block adjustment should consider the introduction of a continuous model specifying the planimetric and altimetric form of the represented object. This operation permits to verify if the data follow a normal distribution or not.

In the affirmative case the well known tests based on the normal distribution can be used for the comparison of the point coordinates under control. Whenever the normal distribution of residuals is not verified the use of non parametric tests is suggested, such as the Wilcoxon test

(Lehmann, 1975). The choice falls on this test for its properties of efficiency and because it fits to the situation under study.

The aim of this work is to study in depth the Wilcoxon test applied to data quality control in Geographical Information Systems. From the analysis of available data sets it turns out that the hypothesis of normality is often rejected, and this is expected to be almost always true for non-metric attribute data. Non-parametric statistics can also be successfully applied in testing other quality parameters, as for instance currency (Crosilla, 1992), which consists in verifying that an available data base acquired at time  $t_0$ , is up-to-date at a later time. This kind of test, although seldom performed, is a matter of great importance and may lead to an economical advantage, since this verification (when carried out in a statistical way) needs only a random sample of limited size, rather than a complete new data acquisition.

The main result presented in this paper is the discussion of the power of the Wilcoxon test. The correct application of a statistical test requires, besides the significance level, the explicit consideration of the power. The power function also links two important "performance" parameters of the test: the size of the random sample and the obtained accuracy.

Statistical theory provides some power expressions for the Wilcoxon test (Lehmann, 1975), but their practical use needs particular assumptions to be made about the distribution shape of the data being tested. The non-parametric approach that inspires the whole procedure, nevertheless, dissuades from making such assumptions.

An attempt to the solution of these problems posed by non-parametric statistics can be given by the Bootstrap (Efron & Tibshirani, 1993), a statistical method based on the resampling of the data. The advantage of Bootstrap methods is that inferences come directly from the observed data and require no assumption about the underlying distribution.

## 2 Theoretical bases

### 2.1 Power evaluations

Coordinate values are the final result of a measurement process and must be considered random variables. In this kind of theoretical setup, any evaluation about coordinate values is carried out making use of the mathematical framework of statistics, and in particular of hypothesis testing.

The testing procedure consists of a statistical test which performs the comparison between two random variables. The null hypothesis  $H_0$  states the equality between the measurements to be tested and the reference measurements, and corresponds to a map having a good metric quality.

The correct application of a statistical test requires the consideration of several parameters: the probabilities of first kind and second kind error, the sample size, the alternative hypothesis.

The probability of first kind error, denoted with  $\alpha$ , is usually fixed at the conventional threshold of .05 or .025. As is well known this value is the probability that the test rejects the null hypothesis when it is true. The value of  $\alpha$  fixes the critical value of the test  $q_\alpha$ .

The probability of second kind error and the alternative hypothesis are strictly related. The alternative hypothesis  $H_a$  is considered true when the null one is rejected, and the second kind error takes place (with probability denoted with  $\beta$ ) when the test leads to acceptance of the null hypothesis and the alternative is true. As can be seen from Figure 1, a same  $q_\alpha$  gives a different  $\beta$  if a different alternative is considered, and can be made arbitrarily low if an alternative pushed far away from  $H_0$  is considered, but in real situations this can be of little sense: in the case of interest for our purposes, that is in the comparison of coordinate values, for example, the null hypothesis states that two sets of values have the same distribution, while the alternative states that there is a difference, measured by a position parameter  $\delta$ , in the centers of the two

distributions ( $\delta$  is a systematic error). We can make  $\beta$  small if we consider a bigger  $\delta$ , but it would not be quite interesting to know that we have a low probability of erroneously accepting the null hypothesis when the tested coordinates are extremely bad. The value of  $\delta$  measures the accuracy satisfied by the tested map: a test performed against a small  $\delta$  means to detect small differences.

The size of the random sample on which the test is based is another important aspect of the procedure, and it is related to the other ones. It is intuitively plausible that if the two populations to be compared are much different, that is  $H_0$  and  $H_a$  are distant, the test will easily detect the difference; a small sample will then suffice to have the desired  $\alpha$  and  $\beta$ . On the other hand, if we want to compare the data with an alternative corresponding to a very small  $\delta$ , more points are needed to obtain satisfactory  $\alpha$  and  $\beta$ . The sample size is a parameter of great importance, since the expensive operations of control survey should be reduced as much as possible.

A mathematical tool that binds these parameters together is the power function of the test. The power of a test is the probability of rejecting the null hypothesis when it is false, and it is a function of the parameters mentioned above.

The fact that the power is function of the sample size follows from the consideration that the statistic of the test, upon which the acceptance or rejection of the hypothesis depends, is more accurate for a bigger sample. A test based on a bigger sample will certainly be more reliable, both in case of acceptance and of rejection of the null hypothesis.

The power function, finally, depends on the location  $\delta$  of the alternative in the sense already mentioned: the more different is the real population with respect to the "null" one, the better will the test be able to detect the difference.

It must be remembered that the evaluation of the power of a test requires the exact specification of the *alternatives* to the null hypothesis, since it is defined as a probability under  $H_a$ . The major difficulty that arises in evaluating the power of statistical tests, especially in the non-parametric case, is that nothing is known about the real form of the population under study, except the random sample. The remaining of the present section discusses a model in which power considerations can be carried out in a reasonable way.

We will suppose to work in the following situation. The coordinates of  $N$  points have been measured with two different techniques; the first one is by photogrammetric restitution or by digitization, which has provided the values  $(X_1, \dots, X_N)$  that are to be tested; the second technique, geodetic survey, guarantees a higher accuracy, and yields the values  $(Y_1, \dots, Y_N)$

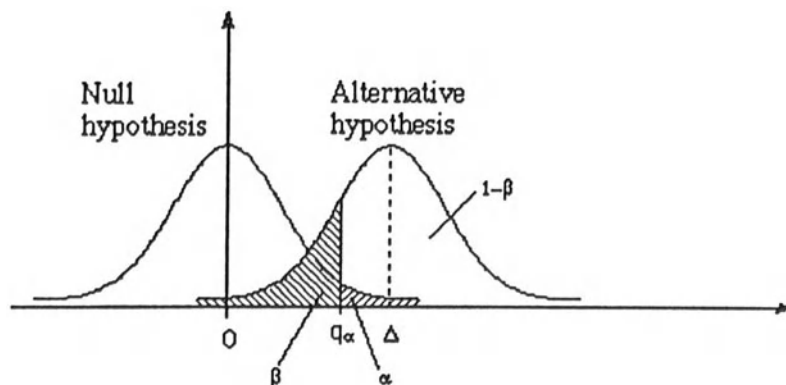


Figure 1: First kind and second kind errors.

used as a comparison. We are interested only in the differences

$$Z_i = Y_i - X_i \quad (1)$$

supposed to be identically distributed with a distribution that we will denote as  $L$ :

$$P(Z_i \leq z) = L(z)$$

The null hypothesis  $H_0$  states that the coordinate values  $X_i$  obtained by photogrammetric restitution are the same as the values  $Y_i$  resulting from alternative high precision control measurements; under  $H_0$ , we expect that the distribution  $L$  of the  $Z_i$  is centered on zero and symmetric (accidental errors give as much positive as negative differences). In case the null hypothesis is false, the values obtained in the two cases are different, say the  $Y$ 's larger than the  $X$ 's, so that the distribution of the  $Z$ 's will be slanted towards positive values and in general no more symmetric.

A simple but important special case is the *shift model* (Lehmann, 1975), which assumes that for some  $\Delta$  we have  $G(z) = G(z - \Delta)$ , where  $G$  denotes a generic distribution. This model is feasible for testing the null hypothesis that the distribution of the  $Z_i$  is symmetric about zero, and corresponds to the assumption that the values produced by the measurement technique to be tested are affected by a purely additive systematic effect: the rejection of the null hypothesis means that the measurement errors add a constant amount and produce no other form of distortion. Note that the only difference between the null and the alternative hypothesis is the position of the center of the distribution, so that the test verifies  $H_0 : \Delta = 0$  against  $H_1 : \Delta \neq 0$ .

A remark about the notation that will be used later: the symbol  $L$  denotes the distribution of the differences  $Z_i$  in the general case, while  $G$  indicates the distribution in the shift model.

## 2.2 The Wilcoxon signed-rank test

In the present section we will present some results (most from Lehmann (1975)) about the power of the main test used in the testing procedure proposed by Crosilla (1992), the Wilcoxon rank-sum test.

As already mentioned, the tests based on the normal distribution, such as "Student's *t*-test", are not always well suited for the comparison of point coordinate values. These tests are designed for data sets following a normal distribution, a situation that is often assumed as reasonable, but not always true. An analysis of the distributional shape of coordinate differences computed as in (1) for several real examples, reveals that departures from normality are frequent, both in the form of asymmetry and in the form of kurtosis (Garlatti, 1990).

Non-parametric tests can be adopted instead, and the Wilcoxon signed-rank test is particularly good in performing the comparison of two populations whose distribution is unknown. This test was introduced in the field of G.I.S. database testing by (Crosilla, 1992).

The Wilcoxon signed-rank test (from here on simply Wilcoxon test) is distribution free, because it bases the comparison on the ranks of the observations. Suppose that two samples  $(X_1, \dots, X_N)$  and  $(Y_1, \dots, Y_N)$  must be compared, as in the situation described above, to check whether the populations from which they were extracted differ significantly from each-other. The differences  $Z_i = X_i - Y_i$  are computed, and each is replaced with its rank: the difference having the smallest absolute value is assigned rank 1, the second smallest rank 2, and so on up to rank  $N$ , assigned to the biggest difference. To each rank  $R_i$  is then given the sign of the corresponding  $Z_i$ . A useful statistic in the comparison of two populations is the sum of the positive ranks

$$V_S = \sum_{i=1}^N R_i^{(+)}$$

$V_S$  tends to have a value near to  $N(N + 1)/2$  if the two populations do not differ, because positive differences will be about as many as negative ones, and their ranks almost equal. On the other hand, if one population is systematically different from the other, there will be more positive than negative ranks (or vice-versa), or positive ranks will all be bigger, so that  $V_S$  will be quite big (or quite small).

A test based on the statistic  $V_S$  can be designed for the null hypothesis that the two populations of the  $X$ 's and of the  $Y$ 's are the same. The hypothesis is accepted if  $V_S$  takes a value near to  $N(N + 1)/2$ , and this is called the Wilcoxon signed-rank test.

The distribution of  $V_S$  under this null hypothesis is known and is called the Wilcoxon signed-rank distribution, whose tables are found in many books of statistics (Lehmann, 1975, for example) together with large sample approximations. The critical values of the Wilcoxon test can be determined from the Wilcoxon signed-rank distribution to obtain an  $\alpha$  probability of first kind error, both for one-sided and for two-sided tests.

Let's turn now to the power of this test.

In the Wilcoxon test, having assumed the shift model, the power as a function of the alternative, that is the probability to reject the null hypothesis under the alternative, is

$$\Pi(\Delta) = P_\Delta(V_s \geq c) \quad (2)$$

where  $V_s$  is the Wilcoxon statistic (sum of positive ranks) and  $c$  is the critical value corresponding to the desired significance level;  $P_\Delta$  indicates that the probability is calculated in the alternative distribution of the shift model.

It is easy to show that  $\Pi(\Delta)$  is a non-decreasing function of  $\Delta$ , as expected (Lehmann, 1975). Unfortunately the exact computation of (2) is quite difficult, since it depends on the distribution of the ranks in case the  $Z_i$  are not symmetric about zero (general alternative hypothesis).

An approximation that avoids these difficulties is applicable in the shift model. Let  $G(z)$  denote the null distribution of the  $Z_i$  and  $G'(z)$  denote the distribution of the sum of two independent variables each with distribution  $G$  ( $G$  is the distribution in the shift model.) The power, which is function of the alternative, becomes in the shift model function of  $\Delta$ . The approximation is given by

$$\Pi(\Delta) \approx \Phi \left[ \frac{N(N - 1)g'(0) + N g(0)}{\sqrt{N(N + 1)(2N + 1)/24}} \Delta - u_\alpha \right] \quad (3)$$

where  $g(0)$  e  $g'(0)$  are the densities of  $G$  and  $G'$  evaluated in zero and  $u_\alpha$  is the  $\alpha$ -th quantile of the standard normal, with  $\alpha$  the significance level. This relation is easy to solve with respect to  $N$  or  $\Delta$ . A heuristic derivation of (3) is found in (Lehmann, 1975).

The quantities  $g(0)$  and  $g'(0)$  required in (3) are still unknown; rather than making assumptions about the parametric family of the distribution  $G$ , we suggest to apply the Bootstrap and to estimate the distribution of the values of interest by the simulated empirical distribution. Bootstrap techniques are discussed in the following section.

Other approaches are present in the literature for the solution of the problem of density estimation. Among these we mention Monte Carlo methods, regression models and generalized likelihoods; some hints on non parametric density estimation are found in (Thompson & Tapia, 1990).

### 3 The Bootstrap

#### 3.1 Introduction

The Bootstrap is a statistical technique recently proposed to measure the accuracy of an estimator (Efron & Tibshirani, 1993); it works as a computer-based simulation from observed data and can be used to produce various kinds of statistical inferences.

The idea upon which the Bootstrap is based is related to some concepts already introduced in statistics long before (for example permutation tests proposed by Fisher in the 1930's). The availability of computational power provided by modern computers has made it possible to develop the Bootstrap algorithm and to study its capabilities.

Suppose a random sample  $\mathbf{x} = (x_1, x_2, \dots, x_n)$  from an unknown probability distribution  $F$  has been observed, and that we wish to estimate a parameter  $\theta = t(F)$  on the base of  $\mathbf{x}$ . This is usually done by applying a certain function (estimator)  $s$  to the points of the sample and obtaining an estimated value  $\hat{\theta} = s(\mathbf{x})$  (as usual  $\hat{\cdot}$  denotes quantities estimated from the sample). The Bootstrap provides estimates of any parameter  $\theta$  in a nearly automatic way together with a measure of their accuracy.

#### 3.2 The empirical distribution

Having observed a random sample of size  $n$ , the *empirical distribution*  $\hat{F}$  is defined as the discrete distribution putting probability  $1/n$  on each of the values  $x_i$ ,  $i = 1, 2, \dots, n$ ; in other words, the empirical probability of each of the  $x_i$  is the proportion of the observed sample having value equal to  $x_i$ .

The empirical distribution is a simple way to estimate the whole unknown distribution  $F$  from which the observed sample is taken. It will be used for making estimations about the population: an obvious way to estimate a certain aspect of  $F$  is by using the same aspect of  $\hat{F}$ . This is called the *plug-in principle* and the Bootstrap is an application of it. The plug-in principle fits particularly to situations where the only available information about  $F$  come from the observed random sample and nothing is known about the parametric family of  $F$ .

#### 3.3 The Bootstrap algorithm

Bootstrap methods are based on the concept of *bootstrap sample*. Suppose a random sample  $\mathbf{x} = (x_1, x_2, \dots, x_n)$  has been observed; a bootstrap sample is a random sample of size  $n$  drawn *with replacement* from the population of  $n$  objects  $(x_1, x_2, \dots, x_n)$ . It will be denoted as  $\mathbf{x}^* = (x_1^*, x_2^*, \dots, x_n^*)$ , where the star notation means that the bootstrap data points are not the original data points, but a *resampled* version. The bootstrap data set consists of the values of the original data set some appearing zero times, some appearing once, some appearing twice, and so on.

Corresponding to each bootstrap data set, the application of the function  $s$  to the bootstrap data points yields a *bootstrap replication* of the estimated parameter  $\theta$ :

$$\hat{\theta}^* = s(\mathbf{x}^*)$$

For instance, if  $s(\mathbf{x})$  is the sample mean, then  $s(\mathbf{x}^*)$  is the mean of the bootstrap sample, obtained dividing by  $n$  the sum of the  $x_i^*$ , for  $i = 1, \dots, n$ .

The Bootstrap algorithm works by drawing many independent bootstrap samples, each giving a bootstrap replication of the parameter  $\theta$ . The parameter of the population is estimated as the mean of the bootstrap replications. It is possible to evaluate the accuracy of this estimation,

1. Generate  $B$  independent bootstrap samples, each consisting of  $n$  data values drawn with replacement from  $\mathbf{x}$ .
2. For each bootstrap sample  $b$  compute the replication of the estimate of the parameter

$$\hat{\theta}^*(b) = s(\mathbf{x}^{*b}) \quad b = 1, 2, \dots, B$$

The number  $B$  of bootstrap replications varies from 25–200 for simple parameters, to 1000–2000 for more complex parameters.

3. Estimate the parameter  $\hat{\theta}^*$  and its error  $\hat{s}e_B$  by the quantities

$$\hat{\theta}^* = \frac{1}{B} \sum_{b=1}^B \hat{\theta}^*(b)$$

$$\hat{s}e_B = \left\{ \frac{1}{B-1} \sum_{b=1}^B [\hat{\theta}^*(b) - \hat{\theta}^*]^2 \right\}^{1/2}$$

Figure 2: *Bootstrap algorithm.*

by the computation of the mean square error of the bootstrap replications. Figure 2 shows a schematic description of the bootstrap algorithm.

It is easy to implement the Bootstrap algorithm on a computer: once the  $n$  values of the original data set have been collected, a uniform random generator produces  $n$  integer values  $i_1, i_2, \dots, i_n$  between 1 and  $n$  (each having probability  $1/n$ ). One bootstrap sample is formed by the corresponding elements of  $\mathbf{x}$ :  $x_1^* = x_{i_1}, \dots, x_n^* = x_{i_n}$ ; this procedure is repeated  $B$  times. The number  $B$  of bootstrap replications varies from 25–200 for simple parameters, to 1000–2000 for more complex parameters. Note that this way of proceeding corresponds to a random sampling from the empirical distribution.

The bootstrap method can be applied to the estimation of any kind of parameter: any function can be applied to the bootstrap data points, obtaining a bootstrap replication of some estimate and its standard error.

### 3.4 Application of the Bootstrap

The major difficulty in carrying out power evaluations for statistical tests is the need of knowing the exact distribution of the alternative hypothesis. In formula (3), for instance, we must know the densities  $g$  and  $g'$  of the distribution of the data  $G$  and  $G'$ . It is difficult to find suitable estimators for those densities evaluated in zero, if we don't want to make assumptions about the form of  $G$ . An attempt to the estimation can be made starting from the observed data through the Bootstrap.

The application of the Bootstrap requires an original data set, a random sample drawn from the population. The size of the original data set need not be too big. The number of bootstrap replications suggested is 2000 in case of complicated parameters, such as confidence intervals (Efron & Tibshirani, 1993). The bootstrap samples available from a data set of size  $n$ , that is the distinct sets of  $n$  points drawn with replacement, are  $(2n-1)^n$ . For  $n = 10$  this number amounts to more than 90000; this ensures that even 2000 bootstrap samples are far from being all the distinct possible resamplings of 10 points; pathological data sets, as those consisting of 10 replications of the same point, are unlikely to appear.

When the testing procedure is applied to the metric quality of a digital map, it is necessary

to know some point coordinates both from photogrammetric restitution (and these are of course available) and from control survey. The original sample is then made up of the differences of coordinates of these points.

The unknown parameters are estimated assuming that the differences are distributed according to the empirical distribution produced by the bootstrap from the observed data. The density in zero is calculated as the derivative in zero of the cumulative distribution function, which in turn is calculated from the empirical distribution. We estimate  $G(z)$  as the proportion of the points in a bootstrap sample that are bigger than  $z$ :

$$\text{Prob}_{\hat{G}}(Z < z) = \frac{(\text{number of } x_i^* < z)}{n}$$

The derivative in zero is approximated as

$$\frac{G(\epsilon) - G(-\epsilon)}{2\epsilon}$$

The estimation of  $g(0)$  is carried out producing  $B$  bootstrap samples and counting in each the proportion of points less than  $-\epsilon$  and bigger than  $\epsilon$ . In this way we obtain  $B$  replications of  $g(0)$  and estimate the parameter as the mean over the replications.

The estimation of  $G'$  requires some bigger effort, since we have to produce the empirical distribution of the sum of two independent variables both distributed according to  $G$ . Since  $G$  was estimated by the empirical distribution  $\hat{G}$  which is discrete, one way to do this is to generate two single bootstrap data points (not the bootstrap samples, but the single points) and to add them together:  $n$  summed pairs of values randomly drawn from the original data set give one bootstrap sample. As in the above case, the density is obtained as the derivative of the cumulative distribution, calculated in zero.

This procedure has been verified on random samples of size 20 drawn from a standard normal distribution and from a uniform (rectangular) distribution, for which the densities have been calculated. In both cases the results have been satisfactory and have encouraged the described approach.

## 4 Numerical experiments

The proposed procedure has been experimented on some real data available from the production of a high precision digital map for the Friuli-Venezia Giulia region, in Italy (Crosilla & Feletig, 1993).

The testing of the map begins with the choice of a set of control points, which must be easily identifiable both on the map and on field. We had a set of 60 points located in the southern part of the considered area (about 770 square Km), for which the map was ready at the time of experiment. The coordinates of these points were measured by geodetic techniques, obtaining the reference data set. The set of data to be compared with the reference was made of the coordinates measured on the map for the same points.

The differences were then computed, treating the  $x$  coordinate separately from the  $y$  coordinate; the set of differences has mean and standard deviation of 0.025 m and 0.277 m for the  $x$  coordinate and mean and standard deviation of 0.077 m and 0.272 m for the  $y$  coordinate. Normality tests were applied to the two samples, showing that the  $x$  do not follow a normal distribution, while the  $y$  do.

The Wilcoxon test was then applied. We will now limit our attention to the  $x$  component of the coordinates, for which the usual "t-test" is not applicable.

	$N = 20$	40	60	80	100
$\Delta = .10 \text{ m}$	.618	.871	.961	.989	.997
$.15 \text{ m}$	.899	.994	.999	.999	1.
$.20 \text{ m}$	.935	.999	1.	1.	1.
$.30 \text{ m}$	.999	1.	1.	1.	1.

Table 1: *Power of the Wilcoxon test computed by formula (3) for the data of our numerical example. The power is reported for various shift-hypothesis alternatives and sample sizes.*

We want to test the null hypothesis that the distribution of the differences is centered about zero, where the center of the distribution is the median (more robust than the mean as a location parameter):

$$H_0 : \text{med}(Z) = 0$$

The chosen significance level is the usual  $\alpha = 0.05$ . The result of the Wilcoxon test leads to the acceptance of the null hypothesis. We want to know against which alternative the hypothesis was accepted with a satisfactory value of the probability of second kind error.

The test is carried out against the alternative of

$$H_1 : \text{med}(Z) = \Delta$$

where the value of  $\Delta$  must express a good metric precision, and must give a power not less than 0.90 for the Wilcoxon test.

By application of the power evaluation (3) we want to know what  $\Delta$  guarantees the required power for the available sample size. The quantities  $g(0)$  and  $g'(0)$  were estimated from the available data, that is from the differences of coordinates, and this was done by the bootstrap, following the method described in section 3.4.

From 100 bootstrap replications we estimate the values  $\hat{g}(0) = 1.75$  and  $\hat{g}'(0) = 1.28$ . These values give the power function reported in Table 4. As we can see the power is rather high for small values of the sample size, as can be expected from “clean” data as those used in the experiment. With a sample of size  $N = 60$ , a power of .90 is achieved for an alternative of approximately  $\Delta = .12 \text{ m}$ .

## 5 Final considerations

The procedure which we intend to propose is carried out in the way described by the example in section 4. It will be here described in detail.

First of all the parameter  $\alpha$  is fixed, at the suggested value of .05. Next, the Bootstrap is used to estimate the unknown parameters of relation (3). As pointed out in section 3.4, 20 elements in the original sample are sufficient for the application of the bootstrap algorithm.

There are now two possibilities (but the second one seems preferable):

1. The size of the sample to draw for the test is fixed first; the power function  $\Pi(\Delta)$  is then computed at the purpose of determining what value  $\Delta$  achieves a satisfactory power. That value will be taken as the accuracy of the tested mapping, provided that the null hypothesis is accepted.
2. The desired accuracy  $\Delta$  is fixed as a parameter of the testing procedure that the mapping must pass. The needed sample size for a good power level computed from (3) will then dictate the number of point coordinate values to use in the test.

A satisfactory power level means at least .90.

Apart from the specific kind of test applied, and from the particular way used to compute the power, the most important result of this paper is the new principle that it introduces in data quality testing. A strong suggestion is made for the consideration of power evaluations and of the alternative hypotheses against which the metric data are tested. Besides requesting a testing procedure based on statistical tests, specifications should fix a level for the three parameters  $\alpha$ ,  $N$  and  $\Delta$  considered in this paper, and especially the amount of  $\Delta$ , defining the accuracy. Once this is fixed, power calculations, such as formula (3), dictate the minimum number of points to consider in the testing.

The proposed testing procedure states the metric quality of a map in a clear and reliable way, because it is based on a statistical comparison which is better than the simple satisfaction of a threshold. Furthermore it achieves the important advantage of minimizing the acquisition of point coordinate values by expensive high-precision techniques, since the desired accuracy of the test (that is how a small  $\Delta$  is requested) determines the number of control points needed.

It is to remark, finally, that the procedure can be adopted not only for the testing of the metric quality of a digital map, but in general in the data quality testing of every part of a G.I.S., since the Wilcoxon test and the Bootstrap can consider any kind of data, following any kind of distribution. This was the reason that lead to the choice of non-parametrics: the possibility to adopt a unique method for the quality statement of the Information System.

## References

- Crosilla, Fabio. 1992. *A Chaining Procedure for Testing the Metric Quality of a Numerical Cartography*. Geodetic Meeting Italy Poland, University of Trieste.
- Crosilla, Fabio, & Feletig, R. 1993. Collaudo di cartografia numerica con tecniche statistiche non parametriche. *Bollettino SIFET*, 3/93.
- Efron, Bradley, & Tibshirani, Robert J. 1993. *An Introduction to the Bootstrap*. New York: Chapman & Hall.
- Fritsch, Dieter, & Crosilla, Fabio. 1992. Robust Procedures for GIS Data Homogeneization. *Int. Arch. of Photogrammetry and Remote Sensing*, 29.
- Garlatti, Claudio. 1990. *Su una proposta di normativa per il collaudo informatico di cartografia numerica di precisione ad uso catastale*. Tesi di Laurea in Ingegneria Civile per la Difesa del Suolo e la Pianificazione Territoriale, Università degli Studi di Udine.
- Lehmann, E. L. 1975. *Nonparametrics: Statistical Methods Based on Ranks*. San Francisco: Holden-Day.
- Thompson, James, & Tapia, Richard. 1990. *Nonparametric Function Estimation, Modeling, and Simulation*. Philadelphia: Siam.

# THE EFFECTS OF FUZZY WEIGHT MATRICES ON THE RESULTS OF LEAST SQUARES ADJUSTMENTS

Hansjörg Kutterer  
Geodätisches Institut, Universität Karlsruhe  
Englerstraße 7, D-76128 Karlsruhe, Germany

## ABSTRACT

In practice stochastical models or their representation in form of weight matrices for least squares adjustments are formulated empirically and so they are fuzzy. Uncertain or "fuzzy" weight matrices are considered here not in the statistical context of the fuzzy-function introduced by ZADEH (1965); in contrast, the effects of fuzzy weight matrices on the results of an adjustment are regarded with respect to fixed intervals of uncertainty. Some previous approaches will be discussed. They lead to a simultaneous treatment of all interesting weight matrices by means of interval mathematics. Numerical examples will conclude the considerations.

## 1 INTRODUCTION

Least squares adjustments are executed using prior information about the stochastical behaviour of observation errors. In general this behaviour is not precisely known but it is introduced into the calculus as stochastical model based on experiences. Usually the stochastical model is fixed until inconsistencies concerning the complete model are detected that cannot be explained by gross errors in the observations. But even careful stochastical modeling leaves a remainder of uncertainty - some kind of fuzziness. So there is a legitimate question for the effects of this fuzziness on the results of an adjustment but also on the quantities that are computable without the introduction of real observations like mean errors or redundancy numbers.

In the early sixties, some relevant papers concerning the subject were published. These publications pointed out two principal ways of dealing with the problem. One of them was initiated by LINKWITZ (1960), followed by WOLF (1961) and later on by HAHN/VAN MIERLO (1987) and KUTTERER (1994). All these authors assume that it is not possible to formulate a "true" weight matrix and they ask for the results coming from an adjustment by a (slightly) changed weight matrix. The results of WOLF are of special interest because he uses the matrix identity of SCHUR/FROBENIUS/WOODBURY. This identity will be the starting point for the discussions in the next chapter. HAHN/VAN MIERLO (1987) examine the change of one single weight. This is not of interest for the present discussion. KUTTERER (1994) handles a series expansion of the normal equations matrix with respect to the changes of the weight matrix by means of interval mathematics. The considerations

as they are presented in the submitted paper give a simplification of its derivations and of the presentation of the results in KUTTERER (1994). In all of the works mentioned above the effects on the discussed quantities appear to be of first order. A completely different point of view is introduced by GOTTHARDT (1962) and in the following by ACKERMANN (1963). GOTTHARDT assumes a "true" weight matrix to be given. In that case the correct procedure is to use the variance-propagation-law. GOTTHARDT shows that the change of the variance-covariance matrix (vc-matrix) of the parameters is of second order, if the essential series expansion is carried out with respect to the correct weight matrix. But because in general this matrix is not known, a series expansion with respect to the known but wrong weighting leads to first order effects. However, despite these apparently different approaches, both positions describe the consequences of certain changes of the weight matrix and both lead to formulae to compute the effects of one concrete change of the weight matrix on the interesting quantities of an adjustment, e.g. the estimated parameters and their vc-matrix. Such a concrete change can be seen as a disturbance, but it must not be seen as a fuzziness which can be understood as the totality of all (slight) disturbances. At last a short remark shall be added on KRARUP (1972), who considers the change of the weights by means of functional analysis as a change of the metric of the observation space. This point of view shall not be deepened, because it is not very helpful for getting formulae that are numerically evaluable.

## 2 FORMAL APPROACH

This work is based on adjustments with parameters. A transfer on adjustments with constraints or mixed models can be done in a comparable way. Let  $A$  be the  $(n \times u)$  design-matrix,  $P$  the  $(n \times n)$  weight matrix,  $l$  the  $n$ -dimensional vector of the observation values and  $E_n$  the identity matrix of dimension  $n \times n$ . Objects of examination are the estimated values of the parameters

$$\hat{x} = (A^T P A)^{-1} A^T P l, \quad (2.1)$$

their cofactor-matrix

$$Q_{\hat{x}\hat{x}} = (A^T P A)^{-1}, \quad (2.2)$$

the vector of the residuals

$$v = - (E_n - A (A^T P A)^{-1} A^T) l \quad (2.3)$$

and the projection operator

$$Q_{vv} P = E_n - A (A^T P A)^{-1} A^T P. \quad (2.4)$$

The considerations can easily be transferred to other results or relevant quantities of least squares adjustments.

The fundamental relation for the following derivations is the matrix identity of SCHUR/FROBENIUS/WOODBURY

$$(A - B D C)^{-1} = A^{-1} + A^{-1} B (D^{-1} - C A^{-1} B)^{-1} C A^{-1}. \quad (2.5)$$

The index 0 stands for the initial value and  $\Delta$  represents its change (Example:  $P_0$  initial weight matrix,  $\Delta P$  change of the weights,  $P = P_0 + \Delta P$  changed weight matrix). This leads to

$$\begin{aligned} N^{-1} &= (N_0 + \Delta N)^{-1} = (N_0 - (-A^T \Delta P) E A)^{-1} \\ &= N_0^{-1} + N_0^{-1} (-A^T \Delta P) (E^{-1} - A N_0^{-1} (-A^T \Delta P))^{-1} A N_0^{-1} \end{aligned}$$

as the inverse of the changed normal equations matrix. Finally we obtain

$$Q_{\hat{x}\hat{x}} = N^{-1} = N_0^{-1} - N_0^{-1} A^T \Delta P (E + Q_{110} \Delta P)^{-1} A N_0^{-1}. \quad (2.6)$$

This corresponds to formula (3) in WOLF (1961) with  $Q_{110} := A N_0^{-1} A^T$ . Inserting (2.6) in (2.1) delivers

$$\hat{x} = \hat{x}_0 - N_0^{-1} A^T \Delta P (E + Q_{110} \Delta P)^{-1} v_0, \quad (2.7)$$

(2.3) leads to

$$v = (E + Q_{11} \Delta P)^{-1} v_0 \quad (2.8)$$

and (2.4) becomes

$$Q_{vv} P = (E + Q_{110} \Delta P)^{-1} Q_{vv0} P_0. \quad (2.9)$$

Now the main business is to compute the inverse of  $E + Q_{110} \Delta P$ . According to the submitted paper, a lot of weightings are possible. However, none of them can be called "wrong". That's the reason why the problem shall be solved by determining the range of values. Given a set of weight matrices and a mapping, for example a product of matrices, the task is to determine the set of all results that can be computed by carrying out the mapping for all weight matrices. An efficient treatment is possible using interval mathematics.

### 3 INTERVAL MATHEMATICS

Interval mathematics is a discipline in its own right dealing with intervals as basic quantities. All fundamentals that are necessary for further understanding will be given in this chapter. Basic references are for example MOORE (1966), MOORE (1979) or ALEFELD/HERZBERGER (1983). KUTTERER (1994) gives a short introduction concerning applications in the field of geodesy. He mentions the few references to the use of interval mathematics in geodesy, too. The theory of transferring the characteristics of interval mathematics on a computer is given by KULISCH/MIRANKER (1981).

#### **Definition 3.1**      Real Interval

a) Definition using lower and upper bound

$$[a] = [a_l, a_u] := \{a \mid a_l \leq a \leq a_u, a, a_l, a_u \in \mathbb{R}\}$$

b) Definition using midpoint and radius

$$[a] = \langle a_m, a_r \rangle := \{ a \mid a_m - a_r \leq a \leq a_m + a_r, a, a_m \in \mathbb{R}, a_r \geq 0 \}$$

$a_l$  is called lower bound,  $a_u$  is called upper bound,  $a_m$  midpoint and  $a_r$  radius of the interval  $[a]$ .

The two representations are equivalent and so it is possible to choose the more convenient one for the intended application. The transformation between the two representations is obvious. The set or space of all real intervals will be called  $\text{IRR}$ . Real numbers are identifiable as point intervals (lower bound = upper bound resp. radius = 0). A graphical representation is given in Figure 1.

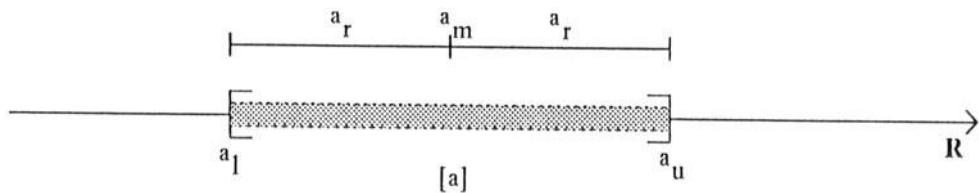


Figure 1: Representation of an interval on the real axis

**Definition 3.2**      Fundamental operations of arithmetic

$$[a] \circ [b] := \{ a \circ b \mid a \in [a], b \in [b]; [a], [b] \in \text{IRR} \} \text{ with } \circ \in \{ +, -, \cdot, / \}$$

and  $0 \notin [b]$ , if  $\circ = /$ .

This means in letters that the result of such fundamental operations between two intervals is the set of the results of the corresponding real operation between all elements of the two intervals. This set is again an interval. The resulting interval can be expressed using the interval bounds, e.g.

$$[a] + [b] = [a_l + b_l, a_u + b_u] \text{ and } [a] - [b] = [a_l - b_u, a_u - b_l]$$

$$\text{resp. } [2,4] + [1,8] = [3,12] \text{ and } [3,5] - [2,7] = [-4,3].$$

For addition and subtraction a representation by midpoint and radius is possible:

$$[a] + [b] = \langle a_m + b_m, a_r + b_r \rangle \text{ und } [a] - [b] = \langle a_m - b_m, a_r + b_r \rangle.$$

It is easy to see that in general  $[a] - [a] \neq [0,0]$ . Subtraction is not inverse to addition. This manifests in increasing interval radii under continued interval operations. Addition and multiplication are commutative and associative, but in general there is no distributivity. However there is a generalization called subdistributivity

$$[a] ([b] + [c]) \subseteq [a] [b] + [a] [c]. \quad (3.1)$$

Furtheron the fundamental operations of arithmetic are **inclusion monotonic**, i.e.

$$[a] \circ [b] \subseteq [c] \circ [d] \quad \forall [a] \subseteq [c] \text{ and } [b] \subseteq [d] \quad \forall [c], [d] \in \mathbb{IR} . \quad (3.2)$$

In fact, inclusion monotonicity holds for all functions of intervals, that are defined according to

$$g([x]) := \{ g(x) \mid x \in [x], [x] \in \mathbb{IR} \} .$$

Example:  $\sin[a] := \{ \sin a \mid a \in [a] \} \Rightarrow \sin[b] \subseteq \sin[a] \quad \forall [b] \subseteq [a]$ .

The operations for vectors of intervals are structurally equal to the real ones, i.e. addition and subtraction are defined by means of the components that are real intervals here. The same holds for matrices of intervals. Let  $\mathbb{IR}^n$  denote the space of the n-dimensional **interval vectors** and  $\mathbb{IR}^m \times \mathbb{IR}^n$  the one of the  $m \times n$ -dimensional **interval matrices**. Addition of interval matrices and multiplication of an interval matrix by an interval are commutative und associative, but the multiplication of interval matrices is in general not associative. This means roughly spoken that the results depend on the succession of the operations.

Finally to this chapter the concept of the **interval extension** is introduced.

### Definition 3.3      **Interval extension**

$f([x_1], [x_2], \dots)$  is called interval extension of the real valued function  $f(x_1, x_2, \dots)$ , if the real quantities  $x_1, x_2, \dots$  are substituted by intervals  $[x_1], [x_2], \dots$  and the real operations and elementary functions are substituted by the ones defined for intervals.

The notions "interval extension" and "result of the evaluation of the interval extension" will further be used synonymously. Only for theoretical reasons it would be useful to distinguish between the notation for the real valued function and the notation for the interval extension and so this will not be done furtheron. The result of the interval extension depends on the actually chosen representation of the function expression, e.g.

$$[x]^2 - [x] \neq [x] ([x] - [1,1]).$$

The factual range of values  $W_f([x])$  is always a subset of the interval extension and in general it is even a proper subset, i.e.

$$W_f([x]) = \{ f(x) \mid x \in [x], [x] \in \mathbb{IR} \} \subseteq f([x]) .$$

## 4      EXACT EVALUATION

Interval mathematics delivers a tool that enables the mathematical formulation of fuzziness in a non-statistical sense. In the present case an empirically chosen initial weighting  $P_0$  shall be supplied with information about fuzziness in terms of an interval matrix  $[\Delta P]$ .

Nevertheless this can also be seen as the midpoint-radius-representation of the set of all possible weight matrices  $[P] = [P_u, P_o]$ , completely detached from the idea of an initial weighting.

Chapter 2 led to the task of computing the inverse of  $E + Q_{110}\Delta P$ . According to this chapter one has to determine the set  $\{ (E + Q_{110}\Delta P)^{-1} \mid \Delta P \in [\Delta P] \}$ , i.e. the set of all possible inverses. In general this is a very difficult problem because the result is not an interval matrix (NEUMAIER, 1990). In comparison to that an inclusion of the factual solution set can relatively easily be given in the form of an interval matrix  $[(E + Q_{110}[\Delta P])^{-1}]$  (KLATTE ET AL., 1991). This can be done using a contractive mapping like

given:  $[M]$

wanted:  $[M^{-1}]$

Iteration rule:

$$[X]^{(k+1)} := ((E - R[M]) [X]^{(k)} + R) \cap [X]^{(k)}$$

Initial value:

$$[X]^{(0)} \supseteq [M^{-1}].$$

The matrix  $R$  is to be seen as a preconditioner for quicker convergence. A possible choice is the inverse of the midpoint matrix of  $[M]$ . But this is not of further interest for the considerations. The PASCAL-extension PASCAL-XSC was conceived for numerical-scientific purposes and so it makes the data-type INTERVAL including all operations and standard functions available. Inclusion monotonicity holds in the presence of a computer arithmetic because of the given directed roundings. This means that the lower bounds are always rounded down and the upper bounds up. A procedure for the numerical computation of an interval inclusion of the set of all inverses is available, too. That's why in the following the inversion of interval matrices is handled as in the real case: it is possible under certain conditions (namely the conditions for real matrices applied on each element of the interval matrix) and so it can be proposed further on.

Now the interval extension of formulae (2.6) - (2.9) can be done. The results are

$$[\hat{x}] = \hat{x}_0 - ((N_0^{-1} A^T) [\Delta P]) [(E + Q_{110}[\Delta P])^{-1}] v_0 \quad (4.1)$$

$$[v] = [(E + Q_{110}[\Delta P])^{-1}] v_0 \quad (4.2)$$

$$[Q_{\hat{x}\hat{x}}] = N_0^{-1} - ((N_0^{-1} A^T) [\Delta P]) [(E + Q_{110}[\Delta P])^{-1}] (A N_0^{-1}) \quad (4.3)$$

$$[Q_{vv}P] = [(E + Q_{110}[\Delta P])^{-1}] (Q_{vv0}P_0). \quad (4.4)$$

The succession of computation has to be noticed in the absence of associativity for the multiplication of interval matrices. It is definite because of the parentheses. If adjustment is used as a means for data analysis, the job is done now. But if one wants to predict the effects of the fuzziness of the stochastical model - a task occurring in the planning phase - it is essential to describe the variations of the parameter vector  $\hat{x}_0$  and of the residual vector  $v_0$  in formulae (4.1) and (4.2). For that an estimation based on intervals for observation values is suitable, because there is always a connection between a certain weighting and a model assumption about the variational behaviour of observation values.

Based on the weights  $P_0$  one can assume for the considerations that are relevant in a practical sense that the observation values will vary at maximum  $k$  times their mean error with e.g.  $k = 2$  or  $k = 3$ . By the use of observation values  $l^*$ , that are consistent with the functional model, intervals for observation values can be formulated. These consistent

observation values are chosen as midpoints and the radii are k times the mean errors, i.e.

$$[l_i] = \langle l_i^*, k \sigma_i \rangle = \langle l_{m_i}, l_{r_i} \rangle = [l_{u_i}, l_{o_i}]. \quad (4.5)$$

The observation interval vector  $[l]$  is obtained by composing all observation intervals to a vector. Actually all possible parameter values caused by the observation data variations are included by

$$[\hat{x}_0] = (N_0^{-1}A^T P_0) [l]. \quad (4.6)$$

However the geometrically correct solution set

$$\{ \hat{x}_0 \mid \hat{x}_0 = (N_0^{-1}A^T P_0) l, l \in [l] \} \quad (4.7)$$

is just a subset of the set given by (4.6). (4.7) describes a convex polyhedron in the parameter space which is not parallel to the directions given by the parameters. (4.6) regarding the used parantheses represents the narrowest interval inclusion of the set denoted by (4.7) in the chosen parameter basis. A few basic knowlegde of linear optimization theory is helpful to verify this assertion. For details see KUTTERER (1994). The same considerations can be carried out for the vector of residuals  $v_0$ . Interval extension leads to

$$[v_0] = - (Q_{vv0} P_0) [l]. \quad (4.8)$$

In the presence of consistent midpoints of the observation intervals the midpoints of the residual intervals are zero. In this case a discussion of the residual intervals simplifies to a discussion of the radii. Inclusion monotonicity (3.2) asserts that (4.6) and (4.8) contain all possible results of an adjustment when the observation data varies in the given intervals. This leads to the two relations

$$[\hat{x}] = ((N_0^{-1}A^T) (P_0 + [\Delta P] [(E + Q_{f10} [\Delta P])^{-1}])) ((Q_{vv0} P_0) [l]) \quad (4.9)$$

$$[v] = [(E + Q_{f10} [\Delta P])^{-1}] (- (Q_{vv0} P_0) [l]), \quad (4.10)$$

that are essential for the planning phase. The succession of computation in the two formulae above was chosen regarding the subdistributivity (3.1). This was necessary because of the missing associativity of the multiplication of interval matrices. KUTTERER (1994) discusses in details the questions arising when observation intervals are formulated. In this meaning the discussions above must be seen as studies on the range of values resp. interval sensitivity analysis of the parameter vector and of the residual vector regarding variations of the observation data.

The explicit inversion of interval matrices is avoidable by using series expansions. KUTTERER (1994) develops the inverse of the normal equations matrix into a Neumann series. Admissible weight changes can be specified based on a convergence criterion for the series expansion. KUTTERER stops the expansion after the linear term and considers the approximation error to accommodate the admissible weight changes to the linearization. The linearized expressions allow a simple interval extension in a conventional programming language like FORTRAN77, for in this case the data-type INTERVAL is not necessary. The result obtained by linearization is close to the inversion based result. This way is transferable on the considerations presented in the submitted paper. A detailed representation will soon be published elsewhere for reasons of space.

## 5 EXAMPLES

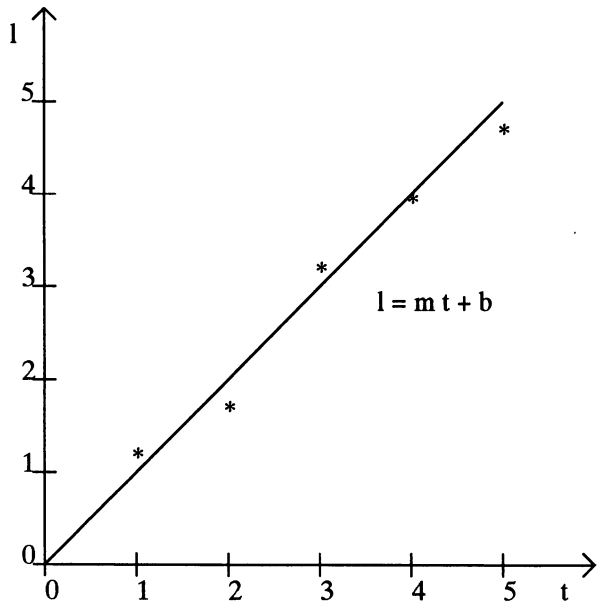


Figure 2: Adjusted straight line - given 6 points

To concretize the considerations two simple examples will be given and discussed. These examples will illustrate the theory and so they will help to understand it. The first one is a straight line computed by means of least squares adjustment. Here a great redundancy can be obtained in a very simple way. The straight line is formulated as  $l + v = m t + b$  with  $l$  observed at position  $t$ ,  $m$  unknown gradient and  $b$  unknown value of the straight line for  $t = 0$  (offset). 6 values are given in equidistant positions. The leftmost one is given at  $t = 0$  and the distance between the positions is 1 so the rightmost position is 5 (see Figure 2). The midpoints represent the bisector of an angle.

The radii for the components of the vector of the observation intervals are equally chosen as 0.01. These radii correspond to the standard deviations of the observations with  $k=1$  (see (4.5)). The fuzziness of the weight matrix is modelled based on fuzzy standard deviations. Here  $\sigma_i = 0.01 = l_r$  for all components and this leads to the intervals  $[0.01 - 10\% * 0.01, 0.01 + 10\% * 0.01] = [0.009, 0.011]$  for the possible standard deviations assuming a fuzziness of 10%. Finally the weight intervals are  $[8264.46.., 12345.67..]$ , if the fuzziness of the weight matrix is restricted to the main diagonal.

Varying the observation values in the intervals  $[l_i - 0.01, l_i + 0.01]$  leads to all possible values for the parameters  $[m] = [0.99486, 1.00514] = <1, 0.00514>$  and  $[b] = [-0.01476, +0.01476] = <0, 0.01476>$  (see (4.6)). Regarding the fuzziness in the weights as it was mentioned above, the parameters will vary in the intervals  $[m] = [0.99281, 1.00719] = <1, 0.00719>$  and  $[b] = [-0.02066, +0.02066] = <0, 0.02066>$  (see (4.9)). That means roughly spoken that all the values in these intervals can be computed by taking the observation values and the weights out of the intervals formulated above. The standard deviations of the computed parameters of the straight line will vary in the intervals  $[\sigma_m] = [0.00202, 0.00264]$  and  $[\sigma_b] = [0.00615, 0.00799]$  (see (4.3)). The behaviour of the residuals and of the redundancy numbers is presented in the following table (the values for 3, 4, 5 are the same as for 2, 1, 0).

It is not surprising that the midpoints of the residual intervals are all zero. But it is interesting that a 10% fuzziness of the standard deviations of the observations causes a 25%-40% fuzziness of the residuals.

value of t	0	1	2
residual (4.8) (no fuzzy weights)	[-0.0143, +0.0143]	[-0.0151, +0.0151]	[-0.0164, +0.0164]
residual (4.10) (fuzzy weights 10%)	[-0.0204, +0.0204]	[-0.0196, +0.0196]	[-0.0205, +0.0205]
redundancy number (4.4)	[0.345, 0.608]	[0.597, 0.813]	[0.741, 0.897]

The next example considers a levelling line consisting of 5 unknown points, starting and ending at known points (see Figure 3). The functional model is a simple because just geometrical one. So the residual equations always are

$v_k + l_k = \Delta h_{ij} = H_j - H_i$ ,  
i.e. the k-th observation is the height difference from Point i to Point j parametrized using the point heights. Because of the two known points the redundancy is always equal to one. Here the interval radii and the standard deviations are chosen in a similar way as in the previous example. The midpoints of the observation intervals shall be all 0 and the heights of the points A and E shall be 0, too. The standard deviation of one height difference by measurement is 1mm and this will hold for the observation interval radii, too. The fuzziness of the standard deviations is again 10% of the original value, namely 0.1mm.

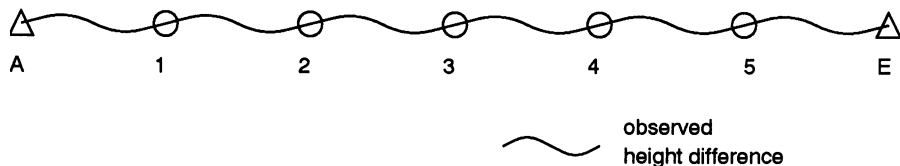


Figure 3: Levelling line - 5 unknown points

The next table gives the resulting fuzziness for the heights of the points 1, 2, ..., 5 as it is effected by least squares adjustment. (Points 4 and 5 behave like 2 and 1). All results are given in [mm].

Point	1	2	3
Height (4.6) (no fuzzy weights)	[-1.7, +1.7]	[-2.7, +2.7]	[-3.0, +3.0]
Height (4.9) (fuzzy weights 10%)	[-2.2, +2.2]	[-3.5, +3.5]	[-3.9, +3.9]
standard deviation of the height (4.3)	[0.8, 1.0]	[1.0, 1.3]	[1.0, 1.4]

Here the fuzziness of the computed point heights is 30% of the factual value, i.e. an amplification of the input by factor 3. A very interesting result concerning the range of the parameters caused by observation intervals is that the standard deviations of the parameters are too optimistic, when all possible values are considered.

## 6 CONCLUSIONS

The consequences of possibly other stochastical models than the initially introduced one were discussed for adjustments with parameters based on studies on the range of values. This is a functional point of view. Interval mathematics proves to be an efficient and compact tool, especially with the object of numerical computations. All of the relevant formulae are transferable on a computer using a higher programming language regarding two main aspects. In the first place the concept of composable data-types should be given connected with an efficient notation based on operators. Secondly the inclusion monotonicity must be ensured in the presence of computer arithmetic. This is reachable by monotonic roundings. The ideas of KULISCH allow a proper transfer of the presented theory on the machine (KULISCH/MIRANKER, 1981). The necessity of describing the effects of fuzzy stochastical models on the results of adjustments is obvious for increasing the quality of subsequent interpretations. There are a lot of possible applications of the given theory in geodesy and so a main task in future research must be their formulation and discussion. ZADEH (1965) gives the ideas of fuzzy sets and fuzzy logic. Between the presented theory and those things there is a difference, because ZADEHs fuzzy numbers additionally allow a rating of uncertainty. This was neither intended nor necessary in the submitted paper. The application of ZADEHs concepts on the objects of the submitted paper is very difficult - especially the inversion of a matrix with fuzzy entries. Nevertheless a future expansion of the presented ideas may use weight matrices containing fuzzy numbers in the meaning of ZADEH, but this will only be useful in connection with a useful motivation and interpretation.

## REFERENCES

- ACKERMANN F. (1963): Ein Beispiel zur Vernachlässigung von Korrelationen bei der Ausgleichung von bedingten Beobachtungen. *ZfV*, **5**, 196-204.
- ALEFELD G. und J. HERZBERGER (1983): Introduction to Interval Computations. New York, Academic Press.
- GOTTHARDT E. (1962): Die Auswirkung unrichtiger Annahmen über Gewichte und Korrelationen auf die Genauigkeit von Ausgleichungen. *ZfV*, **2**, 65-68.
- HAHN M. und J. VAN MIERLO (1987): Die Abhängigkeit der Ausgleichungsergebnisse von der Genauigkeitsänderung einer Beobachtung. *ZfV*, **3**, 105-115.
- KLATTE R., KULISCH U., NEAGA M., RATZ, D. und CH. ULLRICH (1991): PASCAL-XSC. Springer, Berlin Heidelberg New York.
- KRARUP T. (1972): On the Geometry of Adjustment. *ZfV*, **10**, 440-445.
- KULISCH U. und W. L. MIRANKER (1981): Computer Arithmetic in Theory and Practice. Academic Press, New York.
- KUTTERER H. (1994): Intervallmathematische Behandlung endlicher Unschärfen linearer Ausgleichungsmodelle. DGK C, **423**, Munich. (In print)
- LINKWITZ K. (1960): Über den Einfluß verschiedener Gewichtsannahmen auf das Ausgleichungsergebnis bei bedingten Beobachtungen. Part I: *ZfV*, **6**, 179-186, Part II: *ZfV*, **7**, 239-245, Part III: *ZfV*, **9**, 344-354
- MOORE R.E. (1966): Interval Analysis. Prentice Hall, Englewood Cliffs, N.J. .
- MOORE R.E. (1979): Methods and Applications of Interval Analysis. SIAM, Philadelphia.
- NEUMAIER A. (1990): Interval methods for systems of equations. University Press, Cambridge.
- WOLF H. (1961): Der Einfluß von Gewichts-Änderungen auf die Ausgleichungsergebnisse. *ZfV*, **10**, 361-362.
- ZADEH L.A. (1965): Fuzzy Sets. *Information & Control*, **8**, 338-353.

**On Some Alternatives to Kalman Filtering**  
Burkhard Schaffrin  
Dept. of Geodetic Science and Surveying  
The Ohio State University  
1958 Neil Ave., Columbus, Oh 43210-1247, U.S.A.

## Abstract

In a Dynamic Linear Model, the weighted least-squares approach is known to yield the Kalman filter equations. On the other hand, it is also known that any least-squares solution might adversely be affected by undetected model errors. After having previously derived "robust Kalman filters" - which are resistant against multiple scale errors - as one possible remedy, we now develop the so-called "look-ahead filters" which use some of the future observations for the update and can therefore operate only in almost real-time. It will be shown that this new class of filters turns out to be *everywhere superior over Kalman filtering* (in the Mean Square Error sense), and that some of the modified Kalman filters - including Salychev's "wave algorithm" - belong to this class indeed.

## O. Introduction

Since the 1960's, Kalman filtering is the method of choice to evaluate the state of a dynamic system in real-time when observations are being made concurrently. The quality of the Kalman filtered state vector is usually limited by any modelling errors present in the so-called "state equations" - after linearization and discretization - and occasionally in the observation equations. If the latter is not a problem, the observation equations can be used to "control" the impact of possible "biases" in the state equations either by extending the model as in *B. Friedland (1969)*, or by using a more robust filtering technique such as multi-homBLUP, proposed by *B. Schaffrin (1991)*, which is designed to be resistant against multiple scale errors. First results confirming this can be found in *B. Schaffrin (1994)*.

Another possibility consists in adding future observations to determine the state vector at a certain time epoch. Although real-time performance is obviously lost in this case we would argue that this is not always a decisive factor. Unless the system is "highly dynamic", the gain in reliability and certainly the superiority in terms of Mean Square Error comparison makes it a worthwhile venture to develop the so-called "look-ahead filter", particularly so since some of the existing and proven modified Kalman filters belong to this class, including the one introduced by *N. Arent/G. Hckelheim/K.R. Koch (1992)*, but also the "wave algorithm" of *O. Salychev/A. Bykovsky (1991)* which was successfully designed to integrate a geodetic INS (Inertial Navigation System), see e.g. *D. Schröder et al. (1988)*, with satellite data from the Global Positioning System (GPS). We refer to the paper by *O. Salychev/B. Schaffrin (1992)* for first results and to the forthcoming contribution by *Z. Wang/B. Schaffrin/O. Salychev (1995)* on an "adaptive" version of the wave algorithm for Mobile Mapping. The general criterion of MSE-superiority has been extensively used earlier; a detailed description can be found, e.g., in two reports by *H. Toutenburg/B. Schaffrin (1988; 1989)*, though for different applications.

In the following we begin with a review of the Dynamic Linear Model, the basis for Kalman filtering and its variants, including the "dual form" which is also known as "Bayer filter" (*Chapter 1*). Then we shall derive the new class of "look-ahead filters", using an Extended Dynamic Linear Model, in *Chapter 2.1 and 2.2* before we compare it with conventional Kalman filtering (in terms of Mean Square Error) in *Chapter 2.3*. Finally we show in *Chapter 3* how some of the existing modified Kalman filters can nicely be explained as members of the new

class of "look-ahead filters". We conclude this contribution with some outlook on forthcoming investigations.

### 1.1 The Dynamic Linear Model

The *Dynamic Linear Model* consists of n *observation equations* at epoch t=t<sub>1</sub> (say)

$$y_1 = A_{1,n \times m} \cdot x_1 + e_1, \quad e_1 \sim (0, \Sigma_1)$$

with the nx1, vector of observation increments y<sub>1</sub>,

the nxm coefficient matrix A<sub>1</sub>,

the mx1 random vector of unknown states x<sub>1</sub>,

the nx1 vector of observational errors e<sub>1</sub>,

the nxn dispersion matrix Σ<sub>1</sub>=D{e<sub>1</sub>}, supposedly positive-definite;

and a set of m *stochastic constraints*, the so-called "state equations",

$$x_1 = \Phi_{0,m \times m} \cdot x_0 + u_1, \quad u_1 \sim (0, \Theta_1), \quad C\{e_1, u_1\} = 0$$

with the mxm transition matrix Φ<sub>0</sub>,

the mx1 random vector of states x<sub>0</sub> at t=t<sub>0</sub>,

the mx1 vector of system (description) noise u<sub>1</sub>, supposedly uncorrelated with e<sub>1</sub>,

the mxm dispersion matrix Θ<sub>1</sub> = D{u<sub>1</sub>}, supposedly positive -definite.

In addition, we assume some *prior information* on the initial state vector at t=t<sub>0</sub>

$$\tilde{x}_0 = x_0 + e_0^0, \quad e_0^0 \sim (0, \Sigma_0^0), \quad C\{e_0^0, e_1\} = 0, \quad C\{e_0^0, u_1\} = 0,$$

with the mx1 vector of (given) states  $\tilde{x}_0$  at t=t<sub>0</sub>,

the mx1 vector of prior random errors e<sub>0</sub><sup>0</sup>, supposedly uncorrelated with e<sub>1</sub> and u<sub>1</sub>,

the mxm dispersion matrix  $\Sigma_0^0 = D\{e_0^0\}$ , supposedly positive-(semi) definite.

The upper symbol <sup>0</sup> indicates (stochastic) *approximation* while the lower symbol is a running index, starting at t=t<sub>0</sub>. As usually, D denotes *dispersion* and C "covariance".

An *equivalent form* of the Dynamic Linear Model is given by the following two sets of equations, forming a *Random Effects Model*:

$$y_1 = A_1 \cdot x_1 + e_1 = A_1(\Phi_0 x_0 + u_1) + e_1,$$

$$\hat{x}_1 := \Phi_0 \cdot \tilde{x}_0 = x_0 + (\Phi_0 e_0^0 - u_1),$$

$$\begin{bmatrix} e_1 \\ \Phi_0 e_0^0 - u_1 \end{bmatrix} \sim \left( \begin{bmatrix} 0 \\ 0 \end{bmatrix}, \begin{bmatrix} \Sigma_1 & 0 \\ 0 & \Theta_1 + \Phi_0 \Sigma_0^0 \Phi_0^T \end{bmatrix} \right)$$

## 1.2 Least-squares adjustment, best linear prediction and Kalman filtering

The least-squares adjustment for the above model is based on the *target function*

$$\begin{aligned}\phi(e_1, u_1, e_0^0, \lambda_1) := & e_1^T \Sigma_1^{-1} e_1 + u_1^T \Theta_1^{-1} u_1 + (e_0^0)^T (\Sigma_0^0)^{-1} e_0^0 + \\ & + 2\lambda_1^T (e_1 + A_1 u_1 - A_1 \Phi_0 e_0^0 - y_1 + A_1 \Phi_0 \tilde{x}_0)\end{aligned}$$

with the  $n \times 1$  vector  $\lambda_1$  of *Lagrange multipliers*. The variational principle

$$\phi(e_1, u_1, e_0^0, \lambda_1) = \text{stationary}$$

$$e_1, u_1, e_0^0, \lambda_1$$

generates the necessary conditions

$$\begin{bmatrix} \Sigma_1^{-1} & 0 & 0 & I_n \\ 0 & \Theta_1^{-1} & 0 & A_1^T \\ 0 & 0 & (\Sigma_0^0)^{-1} & -\Phi_0^T A_1^T \\ I_n & A_1 & -A_1 \Phi_0 & 0 \end{bmatrix} \begin{bmatrix} \tilde{e}_1 \\ \tilde{u}_1 \\ \tilde{e}_0^0 \\ \hat{\lambda}_1 \end{bmatrix} = \begin{bmatrix} 0 \\ 0 \\ 0 \\ y_1 - A_1 \Phi_0 \tilde{x}_0 \end{bmatrix}$$

which are known as "normal equations". Their solution is given by

$$\begin{bmatrix} \tilde{e}_1 \\ \tilde{u}_1 \\ \tilde{e}_0^0 \end{bmatrix} = \begin{bmatrix} \Sigma_1 \\ \Theta_1 A_1^T \\ -\Sigma_0^0 \Phi_0^T A_1^T \end{bmatrix} [\Sigma_1 + A_1 (\Theta_1 + \Phi_0 \Sigma_0^0 \Phi_0^T) A_1^T]^{-1} (y_1 - A_1 \Phi_0 \tilde{x}_0)$$

which is itself known to represent the *Best Linear Prediction* of  $e_1$ ,  $u_1$ , and  $e_0^0$ . Consequently, we obtain the *Best inhomogeneously Linear Prediction (inhomBLIP)* of  $x_1$ , based on the relation

$$x_1 = \Phi_0 x_0 + u_1 = \tilde{x}_1 + (u_1 - \Phi_0 e_0^0), \quad \tilde{x}_1 := \Phi_0 \tilde{x}_0,$$

in (*weakly*) *unbiased* form through

$$\begin{aligned}\tilde{x}_1 &= \Phi_0 \tilde{x}_0 + (\tilde{u}_1 - \Phi_0 \tilde{e}_0^0) = \tilde{x}_1 + K_1 (y_1 - A_1 \tilde{x}_1) = \tilde{x}_1 + K_1 z_1, \\ K_1 &:= (\Theta_1 + \Phi_0 \Sigma_0^0 \Phi_0^T) A_1^T [\Sigma_1 + A_1 (\Theta_1 + \Phi_0 \Sigma_0^0 \Phi_0^T) A_1^T]^{-1}, \\ z_1 &:= y_1 - A_1 \tilde{x}_1 = y_1 - A_1 \Phi_0 \tilde{x}_0,\end{aligned}$$

where  $K_1$  denotes the  $m \times n$  *Kalman gain matrix*, and  $z_1$  the  $m \times 1$  vector of *innovations*.

The corresponding  $m \times m$  *matrix of mean square prediction errors* results as

$$\begin{aligned}MSPE\{\tilde{x}_1\} &= (I_m - K_1 A_1) (\Theta_1 + \Phi_0 \Sigma_0^0 \Phi_0^T) = \\ &= K_1 \Sigma_1 K_1^T + (I_m - K_1 A_1) (\Theta_1 + \Phi_0 \Sigma_0^0 \Phi_0^T) (I_m - K_1 A_1)^T =: \Sigma_1^0\end{aligned}$$

which, in turn, yields the necessary *prior information* for the following estimation cycle (from  $t_1$  to  $t_2$ ) within the model

$$\begin{aligned} y_2 &= A_2 \cdot x_2 + e_2 = A_2(\Phi_1 x_1 + u_2) + e_2, \\ \hat{x}_2 &:= \Phi_1 \cdot \tilde{x}_1 = x_2 + (\Phi_1 e_1^0 - u_2), \\ \begin{bmatrix} e_2 \\ \Phi_1 e_1^0 - u_2 \end{bmatrix} &\sim \left( \begin{bmatrix} 0 \\ 0 \end{bmatrix}, \begin{bmatrix} \Sigma_2 & : & 0 \\ 0 & : & \Theta_2 + \Phi_1 \Sigma_1^0 \Phi_1^T \end{bmatrix} \right). \end{aligned}$$

The *Kalman filter algorithm* which generates inhomBLIP in each cycle, therefore, computes the matrix  $K_1$ , the vectors  $\hat{x}_1$  and  $z_1$ , from which  $\tilde{x}_1$  and  $\Sigma_1^0$  follow.

Note that the vector  $\hat{x}_1$  would represent the Best Linear Prediction based on the prior information *only*, thus without regarding the information as contained in the observation equations. *This also means that the first observation already leads to some redundancy in the model.*

### 1.3 The dual form of Kalman filtering

While the above form of the *Kalman gain matrix* is most appropriate if the number of observations  $n$  is smaller than the number of states  $m$  ( $n < m$ ), a different form may turn out to be more suitable in the *opposite case* where  $n > m$  holds. Such an alternative algorithm exists indeed and is based on the identity (see Appendix for some fundamental rules)

$$\begin{aligned} K_1 &= (\Theta_1 + \Phi_0 \Sigma_0^0 \Phi_0^T) A_1^T [\Sigma_1 + A_1 (\Theta_1 + \Phi_0 \Sigma_0^0 \Phi_0^T) A_1^T]^{-1} = \\ &= (\Theta_1 + \Phi_0 \Sigma_0^0 \Phi_0^T) A_1^T \Sigma_1^{-1} [I_m + A_1 (\Theta_1 + \Phi_0 \Sigma_0^0 \Phi_0^T) A_1^T \Sigma_1^{-1}]^{-1} = \\ &= [I_m + (\Theta_1 + \Phi_0 \Sigma_0^0 \Phi_0^T) A_1^T \Sigma_1^{-1} A_1]^{-1} (\Theta_1 + \Phi_0 \Sigma_0^0 \Phi_0^T) A_1^T \Sigma_1^{-1} = \\ &= [(\Theta_1 + \Phi_0 \Sigma_0^0 \Phi_0^T)^{-1} + A_1^T \Sigma_1^{-1} A_1]^{-1} A_1^T \Sigma_1^{-1} \end{aligned}$$

provided that the respective matrices are *invertible*. Furtheron, we obtain

$$I_m - K_1 A_1 = [I_m + (\Theta_1 + \Phi_0 \Sigma_0^0 \Phi_0^T) A_1^T \Sigma_1^{-1} A_1]^{-1}$$

and therefore

$$\Sigma_1^0 = (I_m - K_1 A_1) (\Theta_1 + \Phi_0 \Sigma_0^0 \Phi_0^T) = [(\Theta_1 + \Phi_0 \Sigma_0^0 \Phi_0^T)^{-1} + A_1^T \Sigma_1^{-1} A_1]^{-1} = \text{MSPE}\{\tilde{x}_1\}$$

as an immediate result from which follows:

$$\begin{aligned} K_1 &= \Sigma_1^0 A_1^T \Sigma_1^{-1}, \\ \tilde{x}_1 &= \hat{x}_1 + K_1 (y_1 - A_1 \hat{x}_1) \end{aligned}$$

This constitutes, together with  $\hat{x}_1 = \Phi_0 \tilde{x}_0$ , the *dual form of the Kalman filter*, sometimes also called the *Bayes filter*.

Note that  $\tilde{x}_1$  can easily be interpreted as “general weighted arithmetic mean” between  $y_1$  and  $\hat{x}_1$  if we only regard the identity

$$\begin{aligned}\tilde{x}_1 &= \Sigma_1^0 \left[ (\Sigma_1^0)^{-1} \Phi_0 \tilde{x}_0 + A_1^T \Sigma_1^{-1} y_1 - A_1^T \Sigma_1^{-1} A_1 \Phi_0 \tilde{x}_0 \right] = \\ &= \left[ (\Theta_1 + \Phi_0 \Sigma_0^0 \Phi_0^T)^{-1} + A_1^T \Sigma_1^{-1} A_1 \right]^{-1} \cdot \left[ (\Theta_1 + \Phi_0 \Sigma_0^0 \Phi_0^T)^{-1} \hat{x}_1 + A_1^T \Sigma_1^{-1} y_1 \right].\end{aligned}$$

Thus  $\tilde{x}_1$  is the optimal mixture of observational with prior information in the least-squares sense.

For more details, particularly with respect to multiple scale error resistance, we refer to *B. Schaffrin (1991;1994)*.

## 2.1 An Extended Dynamic Linear Model

In this case, let us base our prediction of the state vector  $x_1$  *not only* on the prior information  $\tilde{x}_0$  (and thus  $\hat{x}_1$ ) and the observation vector  $y_1$ , *but also* on the subsequent observation vector  $y_2$ . Therefore the prediction of  $x_1$  takes place only *after* the epoch  $t = t_2$  although we are concerned with the improvement of the state vector at  $t = t_1$ ; the corresponding algorithm thus works in *almost-real-time* only!

$$\begin{aligned}y_1 &= A_1 x_1 + e_1 = A_1 \Phi_0 \tilde{x}_0 + A_1 (u_1 - \Phi_0 e_0^0) + e_1, \\ y_2 &= A_2 x_2 + e_2 = A_2 (\Phi_1 x_1 + u_2) + e_2 = A_2 [\Phi_1 (\Phi_0 \tilde{x}_0 + u_1 - \Phi_0 e_0^0) + u_2] + e_2, \\ \hat{x}_1 &:= \Phi_0 \tilde{x}_0 = x_1 + (\Phi_0 e_0^0 - u_1), \\ \begin{bmatrix} e_1 \\ e_2 \\ u_1 \\ u_2 \\ e_0^0 \end{bmatrix} &\sim \begin{pmatrix} \begin{bmatrix} 0 \\ 0 \\ 0 \\ 0 \\ 0 \end{bmatrix} \\ \begin{bmatrix} \Sigma_1 & 0 & 0 & 0 & 0 \\ 0 & \Sigma_2 & 0 & 0 & 0 \\ 0 & 0 & \Theta_1 & 0 & 0 \\ 0 & 0 & 0 & \Theta_2 & 0 \\ 0 & 0 & 0 & 0 & \Sigma_0^0 \end{bmatrix} \end{pmatrix}\end{aligned}$$

## 2.2 The New “look-ahead” filter

The *least-squares target function* for this model reads

$$\begin{aligned}\phi(e_1, e_2, u_1, u_2, e_0^0, \lambda_1, \lambda_2) &:= \\ &:= e_1^T \Sigma_1^{-1} e_1 + e_2^T \Sigma_2^{-1} e_2 + u_1^T \Theta_1^{-1} u_1 + u_2^T \Theta_2^{-1} u_2 + (e_0^0)^T (\Sigma_0^0)^{-1} e_0^0 + \\ &+ 2\lambda_1^T (e_1 + A_1 u_1 - A_1 \Phi_0 e_0^0 - y_1 + A_1 \Phi_0 \tilde{x}_0) + \\ &+ 2\lambda_2^T (e_2 + A_2 u_2 - A_2 \Phi_1 u_1 - A_2 \Phi_1 \Phi_0 e_0^0 - y_2 + A_2 \Phi_1 \Phi_0 \tilde{x}_0) = \\ &= \text{stationary} \\ &e_1, e_2, u_1, u_2, e_0^0, \lambda_1, \lambda_2\end{aligned}$$

after introducing the two  $n \times 1$  vectors  $\lambda_1$  and  $\lambda_2$  of *Lagrange multipliers*. This variational principle leads to the “normal equations”

$$\begin{bmatrix} \Sigma_1^{-1} & 0 & 0 & 0 & 0 & I_n & 0 \\ 0 & \Sigma_2^{-1} & 0 & 0 & 0 & 0 & I_n \\ 0 & 0 & \Theta_1^{-1} & 0 & 0 & A_1^T & \Phi_1^T A_2^T \\ 0 & 0 & 0 & \Theta_2^{-1} & 0 & 0 & A_2^T \\ 0 & 0 & 0 & 0 & (\Sigma_0^0)^{-1} & -\Phi_0^T A_1^T & -\Phi_0^T \Phi_1^T A_2^T \\ I_n & 0 & A_1 & 0 & -A_1 \Phi_0 & 0 & 0 \\ 0 & I_n & A_2 \Phi_1 & A_2 & -A_2 \Phi_1 \Phi_0 & 0 & 0 \end{bmatrix} \begin{bmatrix} \tilde{\mathbf{e}}_1 \\ \tilde{\mathbf{e}}_2 \\ \tilde{\mathbf{u}}_1 \\ \tilde{\mathbf{u}}_2 \\ \tilde{\mathbf{e}}_0^0 \\ \hat{\lambda}_1 \\ \hat{\lambda}_2 \end{bmatrix} = \begin{bmatrix} 0 \\ 0 \\ 0 \\ 0 \\ 0 \\ y_1 - A_1 \Phi_0 \tilde{x}_0 \\ y_2 - A_2 \Phi_1 \Phi_0 \tilde{x}_0 \end{bmatrix}$$

From the upper part of the “normal equations” we readily obtain

$$\begin{bmatrix} \tilde{\mathbf{e}}_1 \\ \tilde{\mathbf{e}}_2 \\ \tilde{\mathbf{u}}_1 \\ \tilde{\mathbf{u}}_2 \\ \tilde{\mathbf{e}}_0^0 \end{bmatrix} = \begin{bmatrix} -\Sigma_1 & : & 0 \\ 0 & : & -\Sigma_2 \\ -\Theta_1 A_1^T & : & -\Theta_1 \Phi_1^T A_2^T \\ 0 & : & -\Theta_2 A_2^T \\ \Sigma_0^0 \Phi_0^T A_1^T & : & \Sigma_0^0 \Phi_0^T \Phi_1^T A_2^T \end{bmatrix} \begin{bmatrix} \hat{\lambda}_1 \\ \hat{\lambda}_2 \end{bmatrix}$$

while, by means of the lower part, we arrive at

$$\begin{bmatrix} y_1 - A_1 \Phi_0 \tilde{x}_0 \\ y_2 - A_2 \Phi_1 \Phi_0 \tilde{x}_0 \end{bmatrix} = \begin{bmatrix} \tilde{\mathbf{e}}_1 + A_1 \tilde{\mathbf{u}}_1 - A_1 \Phi_0 \tilde{\mathbf{e}}_0^0 \\ \tilde{\mathbf{e}}_2 + A_2 \Phi_1 \tilde{\mathbf{u}}_2 + A_2 \tilde{\mathbf{u}}_2 - A_2 \Phi_1 \Phi_0 \tilde{\mathbf{e}}_0^0 \end{bmatrix} = \\ = - \begin{bmatrix} \Sigma_1 + A_1 (\Theta_1 + \Phi_0 \Sigma_0^0 \Phi_0^T) A_1^T & : & A_1 (\Theta_1 + \Phi_0 \Sigma_0^0 \Phi_0^T) \Phi_1^T A_2^T \\ A_2 \Phi_1 (\Theta_1 + \Phi_0 \Sigma_0^0 \Phi_0^T) A_1^T & : & \Sigma_2 + A_2 [\Theta_2 + \Phi_1 (\Theta_1 + \Phi_0 \Sigma_0^0 \Phi_0^T) \Phi_1^T] A_2^T \end{bmatrix} \begin{bmatrix} \hat{\lambda}_1 \\ \hat{\lambda}_2 \end{bmatrix}$$

which must be solved and inserted to yield the *Best Linear Prediction* of  $e_1, e_2, u_1, u_2$ , and  $e_0^0$ . For this purpose, let us introduce the notation

$$\begin{bmatrix} y_1 - A_1 \Phi_0 \tilde{x}_0 \\ y_2 - A_2 \Phi_1 \Phi_0 \tilde{x}_0 \end{bmatrix} = - \begin{bmatrix} S_{11} & S_{12} \\ S_{12}^T & S_{22} \end{bmatrix} \begin{bmatrix} \hat{\lambda}_1 \\ \hat{\lambda}_2 \end{bmatrix}$$

This leads to the solution

$$-\begin{bmatrix} \hat{\lambda}_1 \\ \hat{\lambda}_2 \end{bmatrix} = \begin{bmatrix} S_{11}^{-1} (y_1 - A_1 \Phi_0 \tilde{x}_0) \\ 0 \end{bmatrix} + \begin{bmatrix} -S_{11}^{-1} S_{12} \\ I_n \end{bmatrix} (S_{22} - S_{12}^T S_{11}^{-1} S_{12})^{-1} [-S_{12}^T S_{11}^{-1}, I_n] \begin{bmatrix} y_1 - A_1 \Phi_0 \tilde{x}_0 \\ y_2 - A_2 \Phi_1 \Phi_0 \tilde{x}_0 \end{bmatrix}$$

and, based on the relations

$$\begin{aligned} \mathbf{x}_1 &= \Phi_0 \mathbf{x}_0 + \mathbf{u}_1 = \Phi_0 \tilde{\mathbf{x}}_0 + (\mathbf{u}_1 - \Phi_0 \mathbf{e}_0^0), \\ \mathbf{x}_2 &= \Phi_1 \mathbf{x}_1 + \mathbf{u}_2 = \Phi_1 \Phi_0 \tilde{\mathbf{x}}_0 + [\mathbf{u}_2 + \Phi_1 (\mathbf{u}_1 - \Phi_0 \mathbf{e}_0^0)], \end{aligned}$$

to the inhomBLIP of  $\mathbf{x}_1$  through

$$\begin{aligned} \tilde{\tilde{\mathbf{x}}}_1 &= \Phi_0 \tilde{\mathbf{x}}_0 + (\tilde{\tilde{\mathbf{u}}}_1 - \Phi_0 \tilde{\mathbf{e}}_0^0) = \hat{\mathbf{x}}_1 + K_1 (y_1 - A_1 \hat{\mathbf{x}}_1) + \\ &+ (I_m - K_1 A_1) (\Theta_1 + \Phi_0 \Sigma_0^0 \Phi_0^T) \Phi_1^T A_2^T \cdot \\ &\cdot [S_{22} - A_2 \Phi_1 K_1 A_1 (\Theta_1 + \Phi_0 \Sigma_0^0 \Phi_0^T) \Phi_1^T A_2^T]^{-1} \cdot \{y_2 - A_2 \Phi_1 [\hat{\mathbf{x}}_1 + K_1 (y_1 - A_1 \hat{\mathbf{x}}_1)]\} = \\ &= \tilde{\mathbf{x}}_1 + \Sigma_1^0 \Phi_1^T A_2^T [\Sigma_2 + A_2 (\Theta_2 + \Phi_1 \Sigma_1^0 \Phi_1^T) A_2^T]^{-1} (y_2 - A_2 \Phi_1 \tilde{\mathbf{x}}_1) \end{aligned}$$

and to the *inhomBLIP* of  $\mathbf{x}_2$  through

$$\tilde{\tilde{\mathbf{x}}}_2 = \Phi_1 \tilde{\tilde{\mathbf{x}}}_1 + \tilde{\tilde{\mathbf{u}}}_2 = \Phi_1 \tilde{\mathbf{x}}_1 + K_2 (y_2 - A_2 \Phi_1 \tilde{\mathbf{x}}_1) = \tilde{\mathbf{x}}_2$$

the latter one being only of formal interest since it will be improved, in turn, using the observations  $y_3$ . We immediately see the *improvement* of  $\tilde{\tilde{\mathbf{x}}}_1$  over  $\tilde{\mathbf{x}}_1$  due to the additional observations  $y_2$  whereas  $\tilde{\tilde{\mathbf{x}}}_2$  results identical to  $\tilde{\mathbf{x}}_2$ . The reason is, of course, that no additional information has been introduced to predict  $\tilde{\tilde{\mathbf{x}}}_2$  if compared with the original Kalman filter solution  $\tilde{\mathbf{x}}_2$ .

### 2.3 Mean square prediction errors - A comparison

A comparison of the respective *matrices of mean square prediction errors* confirms this statement. For we obtain:

$$\begin{aligned} MSPE\{\tilde{\tilde{\mathbf{x}}}_1\} &= D\{\tilde{\tilde{\mathbf{x}}}_1 - \mathbf{x}_1\} = D\{(\tilde{\tilde{\mathbf{x}}}_1 - \hat{\mathbf{x}}_1) - (\mathbf{x}_1 - \hat{\mathbf{x}}_1)\} = \\ &= D\{\tilde{\tilde{\mathbf{u}}}_1 - \Phi_0 \tilde{\mathbf{e}}_0^0\} - C\{\tilde{\tilde{\mathbf{u}}}_1 - \Phi_0 \tilde{\mathbf{e}}_0^0, \mathbf{u}_1 - \Phi_0 \mathbf{e}_0^0\} - \\ &- C\{\mathbf{u}_1 - \Phi_0 \mathbf{e}_0^0, \tilde{\tilde{\mathbf{u}}}_1 - \Phi_0 \tilde{\mathbf{e}}_0^0\} + D\{\mathbf{u}_1 - \Phi_0 \mathbf{e}_0^0\} = \\ &= \dots = \Sigma_1^0 - \Sigma_1^0 \Phi_1^T A_2^T [\Sigma_2 + A_2 (\Theta_2 + \Phi_1 \Sigma_1^0 \Phi_1^T) A_2^T]^{-1} A_2 \Phi_1 \Sigma_1^0 = \\ &= \bar{\Sigma}_1^0 \leq \Sigma_1^0 \end{aligned}$$

in the *Löwner partial ordering* of matrices. In contrast,

$$MSPE\{\tilde{\tilde{\mathbf{x}}}_2\} = D\{\tilde{\tilde{\mathbf{x}}}_2 - \mathbf{x}_2\} = D\{\tilde{\mathbf{x}}_2 - \mathbf{x}_2\} = (I_m - K_2 A_2) \Sigma_1^0 =: \Sigma_2^0$$

is identical to ordinary Kalman filtering, but should be improved as well using the observations  $y_3$  at  $t = t_3$  for the prediction of  $\mathbf{x}_2$  within the following *updated model*:

$$y_3 = A_3 x_3 + e_3 = A_3(\Phi_2 x_2 + u_3) + e_3 = A_3[\Phi_2(\Phi_1 \tilde{x}_1 + u_2 - \Phi_1 e_1^0) + u_3] + e_3,$$

$$\tilde{x}_2 := \Phi_1 \tilde{x}_1 = x_2 + (\Phi_1 e_1^0 - u_2),$$

$$\begin{bmatrix} e_3 \\ u_3 \\ \Phi_1 e_1^0 - u_2 \end{bmatrix} \sim \left( \begin{bmatrix} 0 \\ 0 \\ 0 \end{bmatrix}, \begin{bmatrix} \Sigma_3 & 0 & 0 \\ 0 & \Theta_3 & 0 \\ 0 & 0 & \Theta_2 + \Phi_1 \Sigma_1^0 \Phi_1^T \end{bmatrix} \right)$$

Of course, the observation vector  $y_2$  must *not* appear again since it has been exploited already once to improve the prediction of  $x_1$ . In such a manner, we arrive at a *gliding scheme* where always the observations at the subsequent epoch are taken into account, thereby making this filter algorithm *everywhere superior over Kalman filtering* with respect to Mean Square Error comparison.

A natural generalization to the above extension consists of including the observations of *more than just one* future epoch (here  $t = t_2$ ) in order to further improve the prediction of  $x_1$ . Such an algorithm would still work in *almost-real-time*, depending on the frequency of collecting new data. If set up in a *gliding mode* it, moreover, would produce predictions which are *MSE-superior everywhere* over Kalman filtering as can be proved along similar lines.

A related Bayesian approach may be found in *M. West/P.J. Harrison (1986)*.

### 3.1 Koch's modified Kalman filter

We refer to the recent paper by *N. Arent/G. Hückelheim/K.R. Koch (1992, p. 180)* where a modification of the Kalman filter was introduced which may be easily derived from our extended scheme by setting  $\Theta_2 := 0$ . In this case  $\tilde{\tilde{x}}_1$  can be *transformed* as follows, making use of the matrix identities in the Appendix:

$$\begin{aligned} \tilde{\tilde{x}}_1 &= \tilde{x}_1 + \Sigma_1^0 \Phi_1^T A_2^T [\Sigma_2 + A_2 \Phi_1 \Sigma_1^0 \Phi_1^T A_2^T]^{-1} (y_2 - A_2 \Phi_1 \tilde{x}_1) = \\ &= \tilde{x}_1 + \Sigma_1^0 \Phi_1^T A_2^T \Sigma_2^{-1} [I_m + A_2 \Phi_1 \Sigma_1^0 \Phi_1^T A_2^T \Sigma_2^{-1}]^{-1} (y_2 - A_2 \Phi_1 \tilde{x}_1) = \\ &= \tilde{x}_1 + [I_m + \Sigma_1^0 \Phi_1^T A_2^T \Sigma_2^{-1} A_2 \Phi_1]^{-1} \Sigma_1^0 \Phi_1^T A_2^T \Sigma_2^{-1} (y_2 - A_2 \Phi_1 \tilde{x}_1) = \\ &= [I_m + \Sigma_1^0 \Phi_1^T A_2^T \Sigma_2^{-1} A_2 \Phi_1]^{-1} (\Sigma_1^0 \Phi_1^T A_2^T \Sigma_2^{-1} y_2 + \tilde{x}_1) = \\ &= [\Phi_1^T A_2^T \Sigma_2^{-1} A_2 \Phi_1 + (\Sigma_1^0)^{-1}]^{-1} [\Phi_1^T A_2^T \Sigma_2^{-1} y_2 + (\Sigma_1^0)^{-1} \tilde{x}_1] \end{aligned}$$

which compares nicely with formula (3.21) in the above mentioned paper. Due to the assumption  $\Theta_2 := 0$ , the *matrix of mean square prediction errors* results as

$$\begin{aligned} MSPE\{\tilde{\tilde{x}}_1\} &= \Sigma_1^0 - \Sigma_1^0 \Phi_1^T A_2^T [\Sigma_2 + A_2 \Phi_1 \Sigma_1^0 \Phi_1^T A_2^T]^{-1} A_2 \Phi_1 \Sigma_1^0 = \\ &= \Sigma_1^0 - \Sigma_1^0 [I_m + \Phi_1^T A_2^T \Sigma_2^{-1} A_2 \Phi_1 \Sigma_1^0]^{-1} \Phi_1^T A_2^T \Sigma_2^{-1} A_2 \Phi_1 \Sigma_1^0 = \\ &= [\Phi_1^T A_2^T \Sigma_2^{-1} A_2 \Phi_1 + (\Sigma_1^0)^{-1}]^{-1} \end{aligned}$$

and obviously coincides with the corresponding expression in the quoted paper.

### 3.2 Salychev's wave algorithm

Here we refer to the contributions of *O. Salychev/A. Bykovski (1991)* and *O. Salychev/B. Schaffrin (1992)* where we were able to derive the so-called "wave algorithm" by least-squares methods from the model

$$\begin{aligned} y_1 &= A_1 x_1 + e_1 = A_1 \Phi_0 \tilde{x}_0 + A_1 (C_0 \gamma_0 - \Phi_0 e_0^0) + e_1, \\ y_2 &= A_2 x_2 + e_2 = A_2 \Phi_1 x_1 + e_2 = A_2 \Phi_1 \Phi_0 \tilde{x}_0 + A_2 \Phi_1 (C_0 \gamma_0 - \Phi_0 e_0^0) + e_2, \\ \tilde{x}_1 &:= \Phi_0 \tilde{x}_0 = x_1 + (\Phi_0 e_0^0 - C_0 \gamma_0), \quad o(C_0) = mxl, \quad l = \text{rk } C_0, \\ \begin{bmatrix} e_1 \\ e_2 \\ \Phi_0 e_0^0 \end{bmatrix} &\sim \left( \begin{bmatrix} 0 \\ 0 \\ 0 \end{bmatrix}, \begin{bmatrix} \Sigma_1 & 0 & 0 \\ 0 & \Sigma_2 & 0 \\ 0 & 0 & \Phi_0 \Sigma_0^0 \Phi_0^T \end{bmatrix} \right), \quad 2n > l, \end{aligned}$$

if we restrict ourselves to just two epochs  $t \in \{t_1, t_2\}$ . Note that  $C_0 \gamma_0$  defines the "wave" part with the unknown  $lx1$  vector  $x_0$  of "wave parameters". Compared with the *Extended Dynamic Linear Model*, we have made special choices for the  $\Theta_i$  matrices, namely

$$\begin{aligned} \Theta_2 &:= 0 && \text{(as in Koch's modified approach)} \\ \Theta_1 &:= \lim_{\alpha_1 \rightarrow \infty} \alpha_1 \cdot C_0 C_0^T && \text{for a chosen } mxl \text{ matrix } C_0 \text{ with } \text{rk } C_0 = l \end{aligned}$$

This automatically leads to  $u_2 = 0$  and to  $u_1$  becoming a *non-random* (unknown) vector of fixed parameters which belongs to the range space of  $C_0$  (with probability 1). By this procedure the *redundancy* of the model is decreased by  $l$ ; so we have to make sure that the *inequality*  $2n - l > 0$  holds indeed!

In order to make sure that the redundancy of the resulting model is large enough, usually the observations from *more than two epochs* are collected to derive an estimate for  $\gamma_0$ . In this case, we have to set all the respective  $\Theta_i$  matrices to zero before we introduce a new *impulse vector*  $\gamma_k$  via  $\Theta_{k+1} := \lim_{\alpha_{k+1} \rightarrow \infty} \alpha_{k+1} \cdot C_k C_k^T$ .

The big advantage of this approach is that, under the assumption of *perfect observations*, perfect predictions of the state vector result. This can *never* happen for filter algorithms of Kalman type!

If we now look at our predicted state vector  $\tilde{\tilde{x}}_1$ , due to the assumption  $\Theta_2 := 0$ , we first obtain

$$\tilde{\tilde{x}}_1 = \left[ \Phi_1^T A_2^T \Sigma_2^{-1} A_2 \Phi_1 + (\Sigma_1^0)^{-1} \right]^{-1} \left[ \Phi_1^T A_2^T \Sigma_2^{-1} y_2 + (\Sigma_1^0)^{-1} \tilde{x}_1 \right]$$

as in Koch's modified Kalman filter, but with a *different form* of  $\tilde{x}_1$  because of our special choice for  $\Theta_1$ . Instead of the general expression

$$\begin{aligned}\tilde{x}_1 &= \hat{x}_1 + K_1(y_1 - A_1\hat{x}_1) = \\ &= \left[ (\Theta_1 + \Phi_1 \Sigma_0^0 \Phi_0^T)^{-1} + A_1^T \Sigma_1^{-1} A_1 \right]^{-1} \cdot \left[ (\Theta_1 + \Phi_0 \Sigma_0^0 \Phi_0^T)^{-1} \hat{x}_1 + A_1^T \Sigma_1^{-1} y_1 \right]\end{aligned}$$

we have to take  $\tilde{x}_1$  from the *extended system*

$$\begin{bmatrix} A_1^T \Sigma_1^{-1} A_1 + (\Phi_0 \Sigma_0^0 \Phi_0^T)^{-1} & : & -(\Phi_0 \Sigma_0^0 \Phi_0^T)^{-1} C_0 \\ -C_0^T (\Phi_0 \Sigma_0^0 \Phi_0^T)^{-1} & : & C_0^T (\Phi_0 \Sigma_0^0 \Phi_0^T)^{-1} C_0 \end{bmatrix} \begin{bmatrix} \tilde{x}_1 \\ \hat{\gamma}_0 \end{bmatrix} = \begin{bmatrix} A_1^T \Sigma_1^{-1} y_1 + (\Phi_0 \Sigma_0^0 \Phi_0^T)^{-1} \hat{x}_1 \\ -C_0^T (\Phi_0 \Sigma_0^0 \Phi_0^T)^{-1} \hat{x}_1 \end{bmatrix}$$

which also yields an *estimate*  $\hat{\gamma}_0$  for the impulse vector, provided that the inverses exist.

Similar formulas can readily be derived for the matrix of *mean square prediction errors*  $MSPE\{\tilde{x}_1\}$  and of *mean square estimation errors*  $MSE\{\hat{\gamma}_0\}$ . But this is beyond the scope of this contribution.

#### 4. Outlook

Let us close with a discussion of the question *when exactly* new impulse vectors  $\gamma_k$  should be introduced. Instead of using fixed intervals with a chosen length, a more flexible approach would base this decision on a certain *decision rule*.

Another possibility would be to inspect suitable *test statistics* for the null hypothesis  $H_0: \gamma_k = 0$ . If it is to be rejected with high significance, we should certainly introduce a new vector  $\gamma_k$ ; otherwise it would only increase the computational burden without contributing to an increased accuracy. This idea has been further developed in Z. Wang/B. Schaffrin/O. Salychev (1995). In this context, we like to draw the attention of the reader to the informative paper by J. Nyblom (1986).

#### Acknowledgement:

Part of this research was done while the author was visiting the SFB 228 "High Precision Navigation" on the invitation of E. Grafarend. The comments of two anonymous reviewers are also very much appreciated.

#### References:

- Arent, N., G. Hückelheim and K.R. Koch (1992): Method for obtaining geoid undulations from satellite altimetry data by a quasi-geostrophic model of the sea surface topography, Manus. Geodaet. 17 (1992), 174-185.*
- Friedland, Bernard (1969): Treatment of bias in recursive filtering, IEEE Trans. on Autom. Control AC-14 (1969), 359-367.*
- Nyblom, J. (1986): Testing for deterministic linear trend in time series, J. Amer. Statist. Ass. 81 (1986), 545-549.*
- Salychev, O. and A. Bykovsky (1991): Wave method in processing navigation information in survey systems, Proc. of the IAG Symp. on Kinematic Systems in Geodesy, Surveying and Remote Sensing, Springer: New York, etc. 1991, pp. 238-251.*

*Salychev, O. and B. Schaffrin (1992):* New filter approaches for GPS/INS integration, Proc. of the 6th Intl. Geodetic Symp. on Satellite Positioning, Columbus, Ohio, March 1992, Vol. II, pp. 670-680.

*Schaffrin, B. (1991):* Generating robustified Kalman filters for the integration of GPS and INS, Inst. of Geodesy, University of Stuttgart, Tech. Report No. 15, Sept. 1991.

*Schaffrin, B. (1994):* Quality control for sequential GPS satellite data, Paper prep. for COMPSTAT '94 (11th Symp. on Computat. Statistics), Vienna, Austria, Aug. 1994.

*Schröder, D., Nguyen Chi Thong, S. Wiegner, E. Grafarend and B. Schaffrin (1988):* A comparative study of geodetic inertial systems, Manus. Geodaet. 13 (1988), 224-248.

*Toutenburg, H. and B. Schaffrin (1988):* Biased mixed estimation and related problems, Internal Report, SFB 228 "High Precision Navigation", University of Stuttgart, Dec. 1988.

*Toutenburg, H. and B. Schaffrin (1989):* Investigations concerning the MSE-superiority of several estimates of filter type with applications to the dynamic linear model, Internal Report, SFB 228 "High Precision Navigation", University of Stuttgart, April 1989.

*Wang Zewen, B. Schaffrin and O. Salychev (1995):* A test strategy for the wave algorithm, Mobile Mapping Symp., Columbus, Ohio, May 1995.

*West M. and P.J. Harrison (1986):* Monitoring and adaptation in Bayesian forecasting models, J. Amer. Statist. Assoc. 81 (1986), 741-750.

## Appendix: Some Useful Matrix Identities

(1)  $(AB)^{-1} = B^{-1}A^{-1}$   
whenever the inverses exist.

(2)  $(I + AB)^{-1}A = A(I+BA)^{-1}$   
since  $A(I+BA) = (I + AB)A$ .  
Note that A and B may not be square matrices. For vectors, e.g., we have the special identity:  $(I + ab^T)^{-1}a = a(1 + b^Ta)^{-1}$

(3)  $(A + BDC)^{-1} = A^{-1} - A^{-1}B(D^{-1}+CA^{-1}B)^{-1}CA^{-1}$   
whenever the inverses exist.

(4).  $DC(A+BDC)^{-1} = DCA^{-1}(I + BDCA^{-1}) =$   
 $= DC(I + A^{-1}BDC)^{-1}A^{-1} =$   
 $= D(I+CA^{-1}BD)^{-1}CA^{-1} =$   
 $= (I+DCA^{-1}B)^{-1}DCA^{-1} = (D^{-1}+CA^{-1}B)^{-1}CA^{-1}$   
whenever the inverses exist.

# **CHAOTIC BEHAVIOUR IN GEODETIC SENSORS AND FRACTAL CHARACTERISTICS OF SENSOR NOISE**

Zuofa Li and Klaus-Peter Schwarz  
The University of Calgary, Dept. of Geomatics Engineering  
2500 University Drive, N.W., Calgary, Alberta , CANADA, T2N 1N4

## **Abstract**

Fractal geometry and chaos theory have captured the attention and interest of researchers in various fields of science and engineering. The main reason is that fractals and chaos offer scientists a rich environment for exploring and modelling the complexity of nature. In geodesy, initial research in this field has treated problems in earth surface representation and fractal potential theory. The main purpose of this paper is to show some possible applications to dynamic systems used in geodesy. First, basic concepts of fractals and chaos are briefly introduced. Then, computer simulations for a single axis gyroscopic system are performed, which show chaotic system behaviour in certain regions. Third, the short-term sensor noise of a ring-laser gyro strapdown INS is investigated using generalized Brownian motion. This investigation strongly indicates that such INS sensor errors consist of periodic components caused by dithering and fractional differential noise. A possible explanation for the presence of such noise concludes the paper.

## **1. INTRODUCTION**

In the past ten years, there has been increasing interest among scientists for the new fields of fractal geometry and chaos theory. Much of the motivation comes from the fact that fractal geometry and chaos theory have provided scientists with new tools for exploring and modelling the complexity of nature. More important, however, is the fact that fractal geometry and chaos theory seem to indicate a paradigm shift in how we see our world. This paper will try to answer a few simple questions "What is a fractal?", "What is chaos?", "What is the relationship between them?" and "How can these theories be applied to geodesy?". The motivation for this study grew out of the inertial system research at the U of C. Some unusual error behaviour in inertial systems seemed to call for new methods of modelling these errors. Fractal characterizations gave at least a partial answer to the question.

The paper is organized as follows: In the next section, some basic concepts of fractal geometry and chaos theory will be introduced. A quantitative characterization of fractals and chaos will be given. It provides direct measures for fractal objects and chaotic behaviour of dynamic systems. Computer simulations for a single degree of freedom gyroscopic system in section 3 will introduce the idea of stable and unstable regions and the transition between them. Section 4 will develop the idea of generalized Brownian motion, which will be used to characterize INS sensor noise.

## **2. SOME BASIC CONCEPTS OF FRACTAL GEOMETRY AND CHAOS THEORY**

In this section, we introduce basic concepts of fractal geometry and chaos theory. Reference is made to Mandelbrot (1977 and 1982), Hao (1984), Falconer (1990) and Peitgen et al (1991) for details.

## 2.1 Fractal Geometry

Fractal geometry was developed by Mandelbrot in 1975 starting with a question of interest to geometers and geodesists alike: "How long is the coast of great Britain ?". In his paper, he shows how fractals are used to describe complicated objects which are too irregular to be described by conventional geometry. The word fractal is derived from the Latin fractus, meaning broken (Peitgen et al, 1991). In the real world, there are many fractal objects, such as coast lines, trees, mountains and clouds, etc. Fractal geometry provides a general framework for the study of such irregular objects. Broadly speaking, mathematical and natural shapes whose roughness and fragmentation neither tend to vanish, nor fluctuate up and down, but remains essentially unchanged as one zooms in, is the key area for applying fractal geometry. In this sense, the structure of every piece holds the key to the whole structure (Mandelbrot, 1989). Features of fractal objects are (Falconer, 1990):

- They can usually be defined in a very simple way, often by a recursive formula.
- They have some form of self-similarity, either approximately or statistically.
- They have fine structures, i.e., detail at arbitrarily scales.
- Usually, their fractal dimensions are non-integer (the concept of fractal dimension will be described later on).

In geodesy, Mandelbrot's original question was taken up some years later and fractal geometry was applied to the earth's surface (Patias, 1987) and to the potential field (Sanso, 1987; Li et al, 1991). More recently, fractals have found applications in nonlinear dynamic system theory and this paper shows potential applications in this area.

The following examples of fractals demonstrate the above features.

### **Example 2.1 The middle third Cantor set**

The middle third Cantor set is one of the best known and most easily constructed fractals. It displays many typical fractal characteristics. It is constructed from a unit interval. Let

$$E_0 = [0,1],$$

$$E_1 = [1,1/3] \cup [2/3,1]$$

$$E_2 = [0,1/9] \cup [2/9,1/3] \cup [2/3,7/9] \cup [8/9,1]$$

etc., where  $E_{j+1}$  is obtained by removing the open middle third of each interval in  $E_j$ , see Figure 2.1. Then  $E_j$  consists of  $2^j$  intervals, each of length  $1/3^j$ . The middle third Cantor set is the set  $E = \bigcap_{j=1}^{\infty} E_j$ .

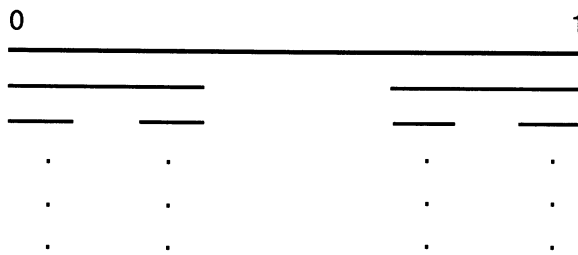


Fig. 2.1. Construction of the middle third Cantor set

### Example 2.2 Random fractals: the curve of fractional Brownian motion.

Fractional Brownian motion is a random process  $X(t)$  with Gaussian increments, described by its variance

$$\text{var}(X(t_1) - X(t_2)) = \sigma^2(t_1 - t_2)^{2H} \quad 0 < H < 1$$

where  $\sigma^2$  is the variance of the Gaussian distribution,  $t$  is time, and  $H$  is the Hurst exponent. When  $H=0.5$ ,  $X(t)$  is Brownian motion (random walk). It has been shown that the graph of  $X(t)$  is a fractal with dimension  $D = 2-H$ . The expressions  $x(r \cdot t) - x(t_0)$  and  $\frac{x(r \cdot t) - x(t_0)}{r^H}$  (where  $r$  is a scale factor) are statistically self-similar, in other words, they

are statistically indistinguishable, and thus they have the same finite dimensional joint distribution function for  $t_0 > 0$  and  $r > 0$  (Peitgen et al, 1991). If  $H$  is not 0.5, the process is called fractional Brownian motion of fractal dimension  $D$ . Figure 2.2 shows graphs of  $x(t)$  for  $2H = 0.5, 1.0$  and  $1.5$  with fractal dimension  $D = 1.75, 1.5$  and  $1.25$ .

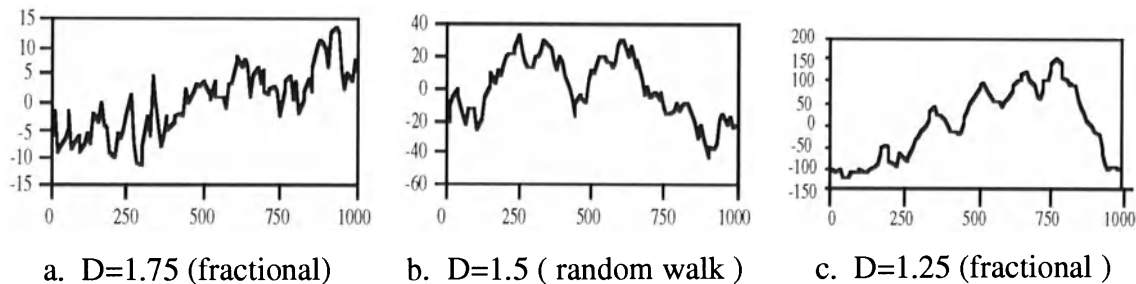


Fig.2.2. Fractional Brownian motion with differential fractal dimension

A property of fractional Brownian motion, which will be used later, is the relationship between  $\beta$ , the Hurst exponent  $H$ , and the fractal dimension  $D$

$$\beta = 2H + 1 = 5 - 2D.$$

where  $\beta$  is defined by the spectral densities

$$S(f) \propto f^{-\beta}.$$

or

$$\text{Amp}(f) \propto f^{-\beta/2}.$$

where  $f$  is the frequency,  $S(f)$  is the power spectral density of  $x(t)$ , which can be defined as

$$S(f) = \lim_{T \rightarrow \infty} \frac{1}{T} \left| \int_T^T x(t) e^{-2\pi j ft} dt \right|^2$$

Turcotte (1992),  $\propto$  is the proportionality sign, and  $\text{Amp}(f)$  is the amplitude spectrum of  $X(t)$ . For a discussion of the relationship between  $\beta$ ,  $H$  and  $D$ , see Turcotte (1992).

The graphs in the above figures are commonly referred to as fractals. Since methods of classical geometry fail in studying these fractals, we need alternative techniques. The main tool for fractal geometry is fractal dimension. Very roughly, the fractal dimension provides a description of how much space a set fills. It is a measure of the irregularities of a set when viewed at very small scales. The fractal dimension contains much information about the geometrical properties of a fractal set.

In order to introduce the concept of fractal dimension, let us look at conventional dimensions first. They are integer dimensions, i.e. a straight line is a 1-dimensional object, a square is a 2-dimensional object and a cube is a 3-dimensional object. For the line, square and cube, there is a power law relation between the number of pieces  $N$  and a given scale  $s$ . This law is

$$N = \frac{1}{s^D}$$

or

$$D = \frac{\log N}{\log \frac{1}{s}}$$

where  $D = 1$  for the line,  $D = 2$  for the square and  $D = 3$  for the cube.

Fractal dimensions are the extension of the above power law for conventional dimensions to integer or non - integer dimensions as follows:

$$D = \lim_{\delta \rightarrow 0} \frac{\log N(\delta)}{\log 1/\delta} \quad (2.1)$$

The above fractal dimension is called the box-counting dimension which is used widely. There are other definitions of fractal dimensions which will not be discussed here in detail.

For the Cantor set,  $\delta=1/3^k$ ,  $N(\delta)=2^k$ ,  $D = \lim_{k \rightarrow \infty} \frac{\log 2^k}{\log 3^k} = \frac{\log 2}{\log 3} = .6309$ . For the

Sierpinsky triangle,  $\delta=1/2^k$ ,  $N(\delta)=8^k$ ,  $D = \lim_{k \rightarrow \infty} \frac{\log 8^k}{\log 3^k} = \frac{\log 8}{\log 3} = 1.8927$ .

For fractional Brownian motion,  $D = 2 - H$  can be derived from the definition (2.1). The derivation can be found in Peitgen et al ( 1991 ).

## 2.2 Basic Concepts of Chaos Theory

The dictionary definition of chaos is ‘the state of complete and thorough disorder and confusion’ (Longman English dictionary). In chaos theory, chaos is used to describe the phenomena related to the occurrence of randomness and unpredictability in completely deterministic nonlinear systems. Chaos theory provides a general framework for the study of such phenomena. Simple deterministic systems can generate random behaviour. The randomness is fundamental, gathering more information does not make it disappear. This fundamental randomness has come to be called chaos Peitgen et al (1991).

To characterize behaviour of systems, the concept of an attractor is used. An attractor is an asymptotic limit of the orbit, the trajectory of a dynamic system, as time approaches infinity. Dynamic systems may have attractors; these are sets which can be considered as “limit sets” for orbits starting with different initial states. An attractor can be a single point or a limit cycle. Sometimes, depending on the control quantity known as the parameter, the attractor becomes a strange attractor. An attractor is called regular if initially close orbits tend to the “same” set, remaining one close to the other. An attractor is called strange if different orbits tend to reproduce the same set in the limit, but diverge from each other during the motion “on” the attractor, no matter how close they were at the beginning. As a rule a regular attractor is a simple smooth set, while a strange attractor has a fractal dimension.

This following two properties characterize chaotic systems:

- Sensitivity: the orbit of the dynamic system exhibits sensitive dependence on the initial condition. This means that a small error in the initial condition will be amplified exponentially with time.

- Fractal: The attractor of the dynamic system is a strange attractor.

The following example shows the above two characteristics of a chaotic system.

### **Example 2.3: Chaos in the Lorenz system**

It is in a famous paper by Lorenz (1963) that a strange attractor appears for the first time. The Lorenz equations can be written as

$$\begin{aligned}\dot{x} &= -\sigma x + \sigma y \\ \dot{y} &= R x - y - x z \\ \dot{z} &= -R z + x y\end{aligned}$$

The numbers  $\sigma$ ,  $R$  and  $B$  are the system's physical parameters, which Lorenz fixed at  $\sigma = 10$ ,  $B = 8/3$ ,  $R = 28$ .

To demonstrate the sensitivity to initial conditions, two trajectories of the system with two different initial conditions  $(x_0, y_0, z_0) = (0, 0, 0)$  and  $(x_{01}, y_{01}, z_{01}) = (0.0001, 0, 0)$  are computed. The two time series, two x-components from two initial conditions, and the difference between them, are plotted in Figure 2.3. The figure clearly illustrates the sensitivity of the system to a small change in  $x$ .

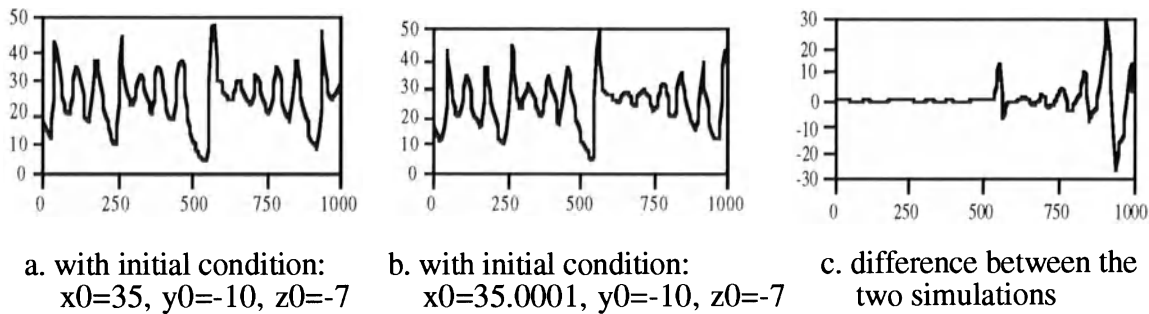


Fig.2.3. Simulation of the Lorenz system

To quantify the two properties of sensitivity and fractals, Ljapunov exponents and fractal dimensions are used. Ljapunov exponents allow a quantitative characterization of sensitivity. For 1D- discrete system  $x_{n+1} = f(x_n)$  the Ljapunov exponent can be written as

$$\lambda(x_0) = \lim_{n \rightarrow 0} \frac{1}{n} \sum_{k=1}^n \ln |f'(x_k)| \quad (2.2)$$

There are many Ljapunov exponents as there are dimensions of a dynamic system. The definition of Ljapunov exponents in two or higher dimensional dynamic systems can be found in Lundqvist (1988).

The Ljapunov exponent characterizes the average logarithmic growth of the relative error per iteration, i.e. the error will be scaled by the factor  $e^\lambda$  (on average) per iteration. Major characteristics of Ljapunov exponents are given in the following without proof, for details see Peitgen et al (1991):

- The dimension of discrete as well as continuous systems determines the number of Ljapunov exponents.
- The system is chaotic if it has one positive Ljapunov exponent.
- If a system of three differential equations has a chaotic attractor, the second Ljapunov exponent is equal to zero.

- The sum of all Ljaponov exponents is negative. It characterizes how fast the area or volume shrinks.
- The Ljapunov exponents are independent of the choice of coordinates.

Applying these rules to the Lorenz system, the three Ljapunov exponents have first to be determined using a formula similar to (2.2), see Tamasz, (1988). They are  $\lambda_1 = 0.9$ ,  $\lambda_2 = 0$  and  $\lambda_3 = -12.8$  respectively. The Lorenz sysyem is therefore chaotic and has a chaotic attractor.

Fractal dimension, described in Section 2.1, can be used for the quantitative characterization of a strange chaotic attractor. For the Lorenz attractor, the fractal dimension is 2.37, which means that the Lorenz attractor is not simply a two dimensional surface but a more complex structure, which occupies more space than that of a 2D surface.

The above methods can be used to determine whether the system is chaotic or not if the system equations are known. However in many cases, especially in natural processes, the system which describes the process is usually not known. The question therefore arises whether measured data can be used to determine, whether the unknown system is chaotic or not? For this purpose, the method of reconstruction of attractors is useful. The question will be further discussed in Section 4.

### 3. CHAOTIC BEHAVIOR IN A SINGLE AXIS GYROSCOPIC SYSTEM

A simulation study of a simple gyroscopic system will be used to illustrate the concept of chaos in a deterministic system. The system equation for a single axis gyroscopic system can be written as follows

$$J\ddot{\theta} + k_1\dot{\theta} + k_2\theta = H\omega_x(\cos\theta - \frac{\omega_z}{\omega_x}\sin\theta) - J\dot{\omega}_y + M \quad (3.1)$$

where the angle  $\theta$  is the system output,  $\omega$  is the system input, i.e. the three dimensional vector of angular velocities,  $J$  is the moment of inertial,  $k_1$  is a damping coefficient,  $k_2$  is the elastic coefficient,  $H$  is the angular momentum and  $M$  is an external torque, which may or may not be a control torque.

Equation (3.1) can be rewritten as

$$\dot{\theta} = \omega \quad (3.2)$$

$$J\dot{\omega} + k_1\omega + k_2\theta = H\omega_x(\cos\theta - \frac{\omega_z}{\omega_x}\sin\theta) - J\dot{\omega}_y + M$$

or

$$\dot{\theta} = \omega \quad (3.3)$$

$$\dot{\omega} + c_1\omega + c_2\theta = c_3 \cdot \omega_x(\cos\theta - c_4\sin\theta) - c_5 ,$$

where

$$c_1 = \frac{k_1}{J}, \quad c_2 = \frac{k_2}{J}, \quad c_3 = \frac{H}{J}, \quad c_4 = \frac{\omega_z}{J\omega_x}, \quad c_5 = \frac{M}{J} .$$

The following computer simulations are based on equation (3.3). The parameters in (3.3) have been chosen as  $J=1$ ,  $c_1 = 1$ ,  $c_2 = 1$ ,  $\omega_y = \omega_z = \dot{\omega}_y = M = 0$ ,  $\omega_x = 1 + 2 \cos 2t$  and  $H$  is a variable. Because of  $M=0$ , this is a free gyroscopic system. Figures 3.1 to 3.4 show the attractor of the system and its sensitivity to the initial conditions for  $H = 1$  (g·cm·sec)

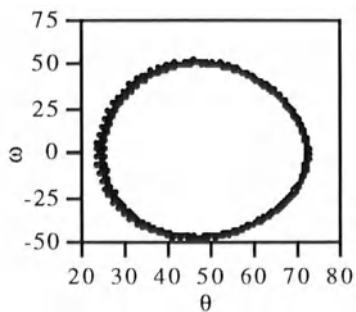


Fig.3.1. The attractor of the single axis gyroscope for  $H = 1$

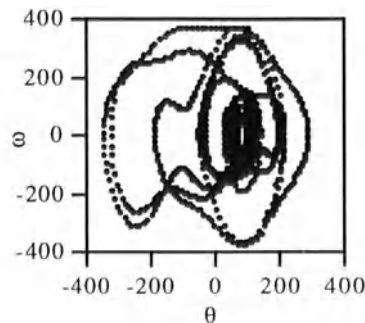
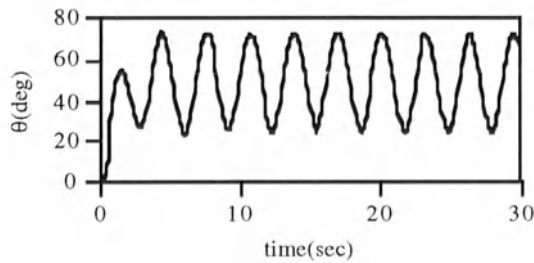
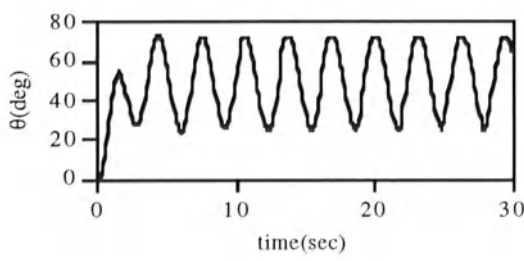


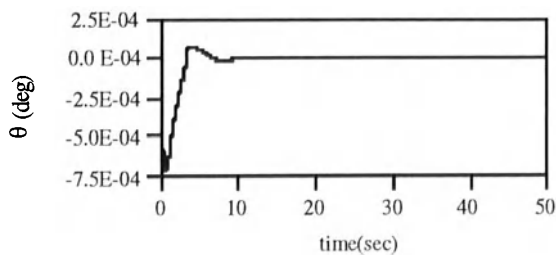
Fig.3.3. The attractor of the single axis gyroscope for  $H = 4$



a. initial condition:  $\theta = 0, \omega = 0$

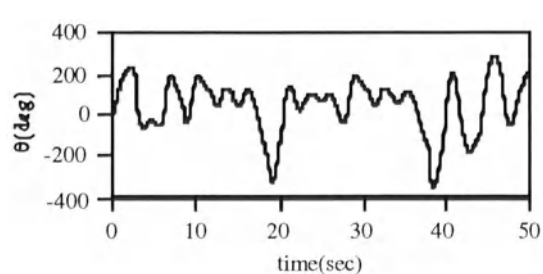


b. initial condition:  
 $\theta = 0.0001, \omega = 0.0001$

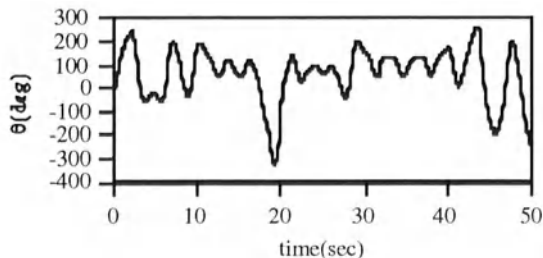


c. difference between the above time series

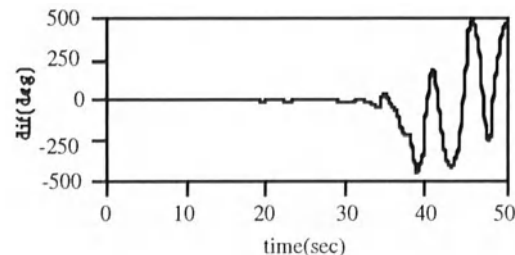
Fig.3.2. The sensitivity of the single axis gyroscopic system to different initial conditions  $H=1$  g·cm·sec



a. initial condition:  $\theta = 0, \omega = 0$



b. initial condition:  
 $\theta = 0.0001, \omega = 0.0001$



c. difference between the above time series

Fig.3.4. The sensitivity of the single axis gyroscopic system to different initial conditions  $H=4$  g·cm·sec

and  $H = 4$  ( $\text{g}\cdot\text{cm}\cdot\text{sec}$ ). These figures strongly indicate that the behavior of the system is stable when  $H = 1$  ( corresponding to a limit cycle ), while the behaviour of the system is chaotic when  $H = 4$ . Further investigation indicates that the transition from order to chaos of the system occurs when  $H$  is around  $2 \text{ g}\cdot\text{cm}\cdot\text{sec}$ . The value of  $H$  is obviously determined by the physical parameters of the gyroscope. It is easy to show that currently manufactured gyros all fall into the stable region. It should also be noted that the system behaviour changes substantially if  $M \neq 0$ . If  $M$  is chosen as a control torque which restricts the nonlinearity of the system, then the system remains stable, even for large  $H$ .

The above results can be related to investigations of pendulum systems done by Arneodo et al (1983), S. Lundqvist (1988), Tomasz (1988). These systems show that chaotic behaviour might occur if the non-linearity is sufficiently strong. In its mathematical structure, the above single axis gyroscopic system can be interpreted as a pendular system.

#### 4. FRACTAL CHARACTERIZATION OF INS SENSOR NOISE

It has been mentioned in Section 2 that in those cases where the system equations are not known, measured data can be used to reconstruct the attractor and in this way obtain information on system behaviour. This is often the case when considering sensor noise which is given as a time series of measured values with random characteristics. The main idea of reconstructing the attractor of a time series is to form a new  $m$ -dimensional time series

$$u(k) = \{ z_k, z_{k+1}, \dots, z_{k+m} \}$$

from a given time series  $z_k = z(kT)$  ( $k=0, 1, 2, \dots$ ), where  $T$  is a time delay, i.e. a multiple of a sampling interval. The new time series will contain information on the attractor of the system. Such a reconstruction procedure can be interpreted as a change of coordinates of an attractor or a projection of the original attractor to a  $m$ -dimensional Euclidean space, for details see Peitgen et al (1991).

Figure 4.1 shows three time series and Figure 4.2 2D reconstruction of their attractors, taken from Peitgen et al (1991). It is difficult to deduce any characteristical difference between the time series themselves. However, one can identify the patterns of these time series from the reconstructions of their attractors. To identify time series characteristics from these attractors, a priori knowledge of typical attractor forms is needed. In this case, attractor (a) characterizes white noise, (b) a deterministic system, and (c) a chaotic system. Thus, the three time series are generated by three very different dynamic systems although they seem to be quite similar.

##### 4.1 Generalized Brownian Motion

Generalized Brownian Motion is defined to be a random process  $X(t)$  such that there exist a frequency  $f_0$  and a parameter  $\beta$  such that for  $f \in [-f_0, f_0]$  the following power law holds:

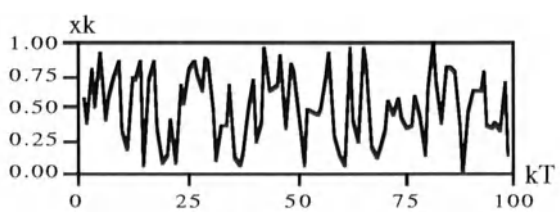
$$S(f) \propto f^{-\beta} \quad (4.1)$$

or

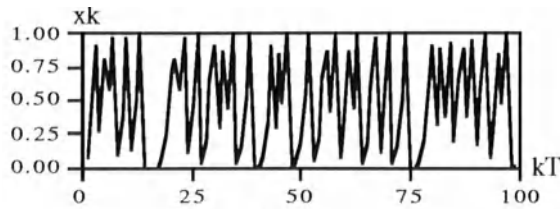
$$\text{Amp}(f) \propto f^{-\beta/2}$$

where  $S(f)$  is the power spectral density of  $X(t)$  and  $\text{Amp}(f)$  is the amplitude spectrum of  $X(t)$ ,  $f$  is the frequency. For fractional Brownian motion, we have  $1 < \beta < 3$ ; for white noise,  $\beta = 0$ . Generalized Brownian motion can be subdivided into two categories:

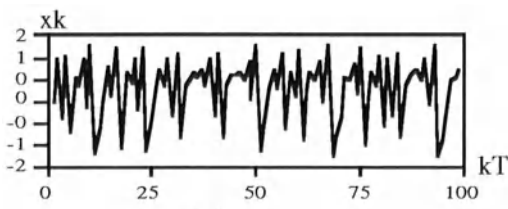
- 1) Fractional integral motion:  $\beta > 0$ .



(a)

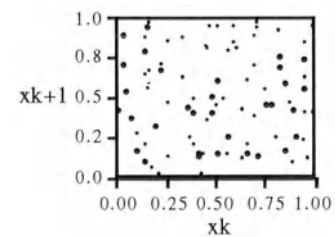


(b)

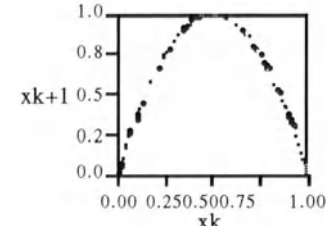


(c)

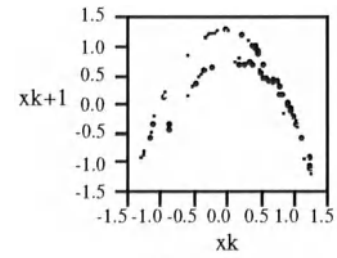
Fig.4.1. Examples of time series



(a)

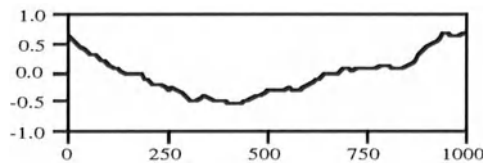


(b)

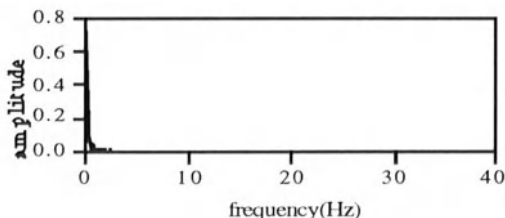


(c)

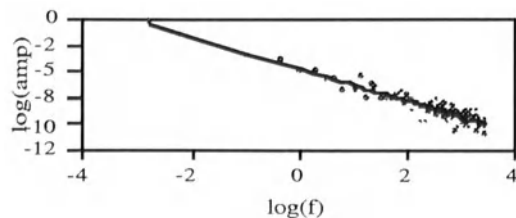
Fig.4.2 Reconstruction of attractors



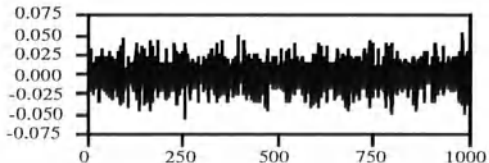
a. time series



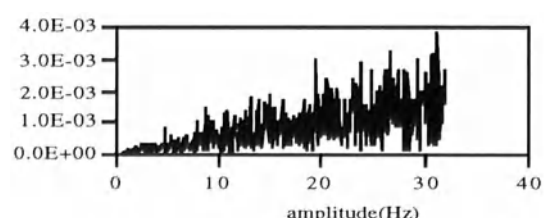
b. amplitude spectrum



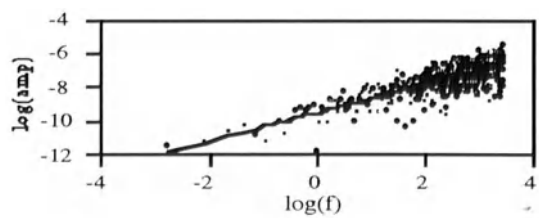
c. log-log diagram for amplitude

Fig.4.3. Fractional integral motion ( $\beta=3$ )

a. time series



b. amplitude spectrum



c. log-log diagram for amplitude

Fig.4.4. Fractional differential motion ( $\beta=-1.72$ )

2) Fractional differential motion:  $\beta < 0$ .

The estimate of  $\beta$  can be obtained from the following formula

$$\beta = -\frac{\log S(f)}{\log f} \quad (4.2a)$$

or

$$\beta = -2 \frac{\log \text{Amp}(f)}{\log f} \quad (4.2b)$$

Figures 4.3 and 4.4 show fractional integral motion and differential motion, their spectra and log - log diagrams for spectra with  $\beta = 3$  and  $\beta = -1.72$ . Figures 4.5 and 4.6 show 2D reconstruction of their attractors. In both cases a white noise sequence has been transformed into the spectral domain and filtered for the given  $\beta$ , then transformed back to the time domain. It is easy to see that the larger  $\beta$  is, the smoother the curve of generalized Brownian motion will be; conversely, the smaller  $\beta$  is, the rougher the curve of generalized Brownian motion will be. It should be noted that the modellings of fractal noise in the standard Kalman filter is restricted to  $\beta=2$  ( Brownian noise with fractal dimension  $D=1.5$  ) and that a modification of the filter is required if the system has fractal noise of dimension  $D \neq 1.5$  ( $\beta \neq 2$ ), for details see Schwarz, et al (1994).

It should be mentioned that the fractal dimension is well defined only for fractional Brownian motion whose paths are continuous functions, i.e.  $1 < \beta < 3$ . Outside that range, e.g. for  $3 < \beta < 4$ , we do not have real functions, but distributions, for which it is not meaningful to speak of dimensions of the plot. However, the parameter  $\beta$  does characterize the smoothness or roughness of the plot, see Figures 4.3 and 4.4.

## 4.2 INS Sensor Noise Analysis

INS sensor noise is usually modelled as either white noise, random walk (Brownian noise) or first-order Markov process. To validate such an assumption, an analysis of sensor noise of the LTN 90/100 INS has been performed. To simplify, the experimental design, the noise has been observed for a stationary system on a stable test bench.

Figures 4.7 and 4.8 show the amplitude spectra before and after eliminating the dithering effect, the log - log diagram for the amplitude after eliminating the dithering effect, and the reconstruction of the attractors before and after eliminating the dithering effect for the x-gyro noise. For the other five sensors, the results are similar. Table 4.1 gives the estimates of  $\beta$  for various sensors after eliminating the dithering effects.

Sensor	x-gyro	y-gyro	z-gyro	x-accel	y-accel	z-accel
$\beta$	-1.72	-1.53	-1.58	-1.73	-1.50	-1.39

Table 4.1. The estimation of  $\beta$  for INS sensors

From Figure 4.7 and Table 4.1, it is easy to see that the sensor noise after elimination of the dithering effect is fractional differential noise. To relate the noise more closely, a new time series was formed using double numerical integration over fractional differential noise for the six sensors. Double integration results are shown in Figures 4.9 and 4.10 for the z-accelerometer, its spectrum and log - log diagram for the spectrum. Similar results are obtained for the other five sensors. Table 4.2 shows the estimated parameters  $\beta$ ,  $H$  and  $D$ , for these time series.

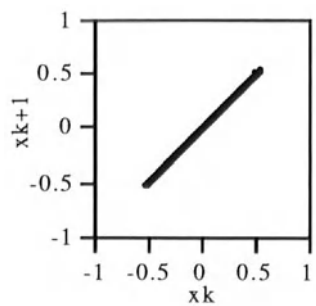


Fig.4.5 Reconstruction of the attractor or fractional integral motion

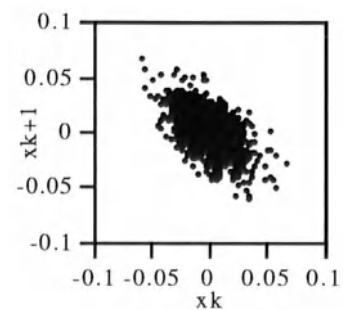


Fig 4.6 Reconstruction of the attractor for fractional differential motion

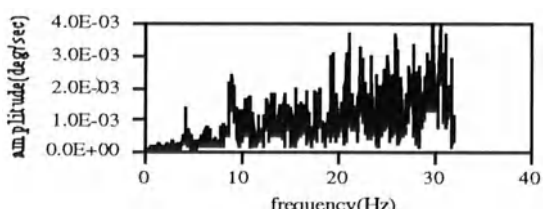
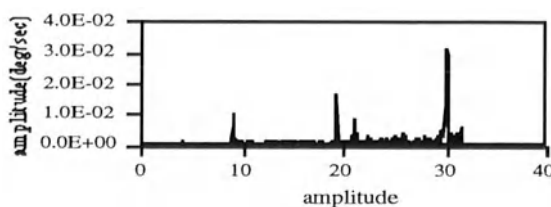


Fig.4.7. Amplitude spectrum of x-gyro

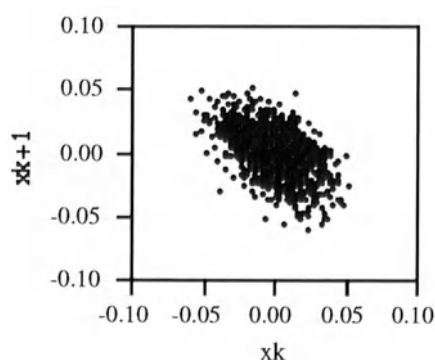


Fig.4.8. Reconstruction of the x-gyro attractor

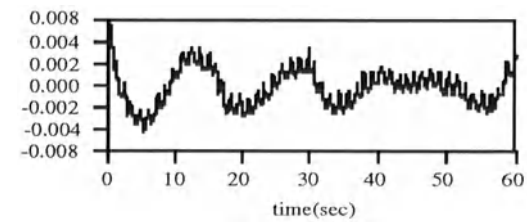


Fig.4.9. The time series and its spectrum generated from z-accelerometer by double integration

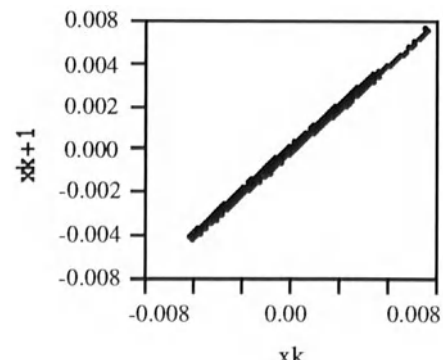


Fig.4.10. Reconstruction of the attractor of the generated time series

sensors	b	H	D
x-gyro	2.09	0.54	1.45
y-gyro	2.14	0.57	1.43
z-gyro	2.21	0.60	1.39
x-accel	2.17	0.58	1.41
y-accel	2.19	0.60	1.40
z-accel	2.33	0.67	1.33

Table. 4.2. Estimated parameters for six time series generated from differential sensor noise using fractional double numerical integration

These results indicate that double integration results in random walk behaviour ( $\beta \sim 2$ ,  $H \sim 0.5$ ) which means that single integration will give white noise ( $\beta \sim 0$ ). The time derivative of white noise is characterized by  $\beta = -2$ . This value is close enough to the empirically determined values given in Table 4.1 ( $-1.4 > \beta > -1.7$ ), to warrant an interpretation based on the assumption that they approximate  $\beta = -2$ . The sensor measurements investigated are the INS approximation of acceleration and angular velocity. They are derived from discrete measurements of velocity increments  $\Delta v$  and angle increments  $\Delta\theta$  which is then differentiated over the time interval  $\Delta t$ . Thus, we have

$$a = \Delta v / \Delta t \text{ and } \omega = \Delta\theta / \Delta t$$

where  $a$  and  $\omega$  are the system output for acceleration and angular velocity. Assuming that the measurement  $v$  and  $\theta$  have errors with white noise characteristics,  $a$  and  $\omega$  would have the characteristics of a white noise time derivative ( $\beta = -2$ ). In that case, the integrated velocity and attitude have white noise errors, while position will show random walk characteristics. It should be noted that correlated noise characteristics, which usually are part of inertial sensor errors, could not be determined from such a short data span.

Comparing Figures 4.8 and 4.10 with Figures 4.6 and 4.5 respectively, it is easy to see that the 2D reconstruction of the attractor for the x-gyro noise has a similar pattern as the fractional differential noise with  $\beta = -1.72$ , and that the noise derived from double integrating the z-accelerometer shows a similar pattern as that of fractional integral noise with  $\beta = 3$ . These comparisons also confirm that the sensor noise after eliminating the dithering effects is fractional differential noise and the derived noise is fractional integral noise.

## 5. CONCLUSIONS

The following conclusions can be drawn from this initial study.

- Chaotic behavior for the single degree of freedom gyroscope has been demonstrated by simulations but is not likely to occur in an actual system.
- The investigation of sensor static noise in the LTN 90/100 INS strongly indicates that it consists of periodic components, caused by dithering, and fractional differential noise. If this noise is an approximation of a white noise derivative, an interpretation in terms of the measurement process can be given.
- The reconstruction of the attractors before and after eliminating dithering effect shows a

distinct pattern for the sensor errors. The information is currently not sufficient to model sensor noise using reconstruction techniques.

**Acknowledgements:** The authors would like to thank the two reviewers for comments on an earlier version of the paper and a number of helpful suggestions. Funding for this research was obtained through an NSERC Operating Grant of the second author.

## References

- Arneodo, A., Coullet, P. and Tresser, C. (1983): On the observation of an uncompleted Cascade in a Raylei-Benard experiment, *Physica* 6D, North-Holland Publishing Company.
- Davaney, R.L. (1990): Chaotic explosions in simple dynamical systems, *The Ubiquity of Chaos* (ed. Saul Krasner), American Association for the Advancement of Science.
- Falconer, K. (1990): *Fractal Geometry: mathematical foundations and applications*, John Wiley & Sons.
- Hao, B.L. (1984): *Chaos*, World Scientific Publishing Co Pte Ltd.
- Li, Z., Li W. and Li, H. (1991): Representation of the Gravitational Potential Generated by Fractal Measures, *Manuscripta Geodaetica*, Vol.19, No.3, pp.129-134..
- Lorenz, E.N. (1963): Deterministic Nonperiodic Flow, *Journal of the Atmosphere, Science*, Vol. 20, No.2, March, 1963.
- Lundqvist, S. (1988): Chaos, order, pattern, fractals - an overview, *Order and Chaos in nonlinear physical systems* (eds. Lundqvist, L., March N.H., and Tosi, M.P.), Plenum Press.
- Mandelbrot, B.B. (1977): *Fractals: form, chance, and dimension*, Freeman, San Francisco.
- Mandelbrot, B.B. (1982): *The Fractal Geometry of Nature*, Freeman, San Francisco.
- Mandelbrot, B.B. (1989): *Fractal Geometry: what is it, and what does it do?*, *Fractals in the Nature Sciences* (Ed. Fleischmann, elat ), Princeton University Press.
- Peitgen, H.O., Jurgens H. and Saupe D. (1992): *Chaos and Fractals - New Frontiers of Science*, Springer-Verlag.
- Patias, P. (1987): Application of Random Field Theory in Mapping Problems, OSU Report No. 378.
- Sanso, F. (1987):Talk on the theoretical foundations of physical geodesy, Contributions to Geodetic Theory and Methodology, IAG Section IV, XIX General Assembly of the IUGG, Vancouver, B.C., Canada, August 9 - 22, 1987.
- Tomasz k. (1988): Chaos in systems with noise, World Scientific Publishing Co Pte Ltd.
- Schertzer, D. and Lovejoy, S. (eds.) (1991): *Non-linear variability in geophysics*, Kluwer Academic Publishes, The Netherlands.
- Schwarz, K.P, Li, Z. and Liu, Z.(1994): Kalman Filtering with Fractal Noise, *Proceedings of the International Symposium on Kinematic Systems in Geodesy, Geomatics and Navigation*, Banff, Canada August 30 - September 2, 1994, pp.155-162.
- Turcotte, D.L. (1992): *Fractal and Chaos in geology and geophysics*, Cambridge University Press.

# **DISCRIMINANT ANALYSIS TO TEST NON-NESTED HYPOTHESES**

**B. Betti**

**Dipartimento di Georisorse e Territorio  
Politecnico di Torino, Turin, Italy**

**M. Crespi**

**Dipartimento di Idraulica, Trasporti e Strade  
Università di Roma "La Sapienza", Rome, Italy**

**F. Sansó**

**Dipartimento di Ingegneria Idraulica, Ambientale e del Rilevamento  
Politecnico di Milano, Milan, Italy**

**D. Sguerso**

**Dipartimento di Ingegneria Civile ed Ambientale  
Università di Trento, Trento, Italy**

## **SUMMARY**

The comparison of different (linear) models, representing different geodetic/geophysic hypotheses, on the light of observational data leads to a testing procedure based on residuals between data and manifolds in general different positions. This topic has already been mentioned in statistical literature as *comparison of non-nested linear models*. The problem is here defined and completely solved by a Bayesian approach.

## **1 - DEFINITION OF THE PROBLEM**

Linear least squares theory is endorsed with a suitable testing theory, particularly for normal variates, allowing to judge on alternative hypotheses. To make it simple, we assume the observation vector  $Y$  is normally distributed in  $R^n$  with covariance matrix  $\sigma_0^2 I$  and its average belongs to one or another linear manifold  $M_A$  or  $M_B$  related to the alternative hypotheses  $H_A$  or  $H_B$ ; moreover, we assume the design

matrices (see (1), (2)) are always of full rank; so, we call *classical* the following two situations, which we know how to handle from the statistical literature:

1.  $M_A \supset M_B$ , i.e. the two manifolds are nested, so that we can express them as:

$$H_A : E\{Y\} = Ax + a \quad \forall x \in R^m \quad (1)$$

$$H_B : E\{Y\} = Ax + a, \quad Cx = c \quad \forall x \in R^m \quad (2)$$

in (2) are included constraints equations  $Cx = c$  just to limit the range of  $x$  in  $R^m$  and therefore defining a manifold  $M_B$  included in  $M_A$ .

2.  $M_A \parallel M_B$ , i.e. the two manifolds are parallel what can be expressed by:

$$H_A : E\{Y\} = Ax + a \quad \forall x \in R^m \quad (3)$$

$$H_B : E\{Y\} = Ax + b \quad \forall x \in R^m \quad (4)$$

In both cases a simple testing procedure is stated basically exploiting the fact that least squares residuals have distributions which do not depend from the theoretical values of the parameters (and, therefore, of the observables  $y = E\{Y\}$ ).

Let us recall shortly the well known reasonings (Koch, 1988) applied in the previous two cases:

1. In the first one (Fig. 1), if we call  $\hat{y}_A$ ,  $\hat{y}_B$  the least squares estimates of  $y$  and  $H_B$  is true, both  $\hat{y}_A$  and  $\hat{y}_B$  are still unbiased estimators of  $y$ , so that  $(\hat{y}_A - \hat{y}_B)$  is still a zero average vector. Then we have:

$$\frac{|U_{AB}|^2}{|U_A|^2} = \frac{|(\hat{y}_A - \hat{y}_B)|^2}{|(Y - \hat{y}_A)|^2} \sim \mathbf{F}_{(m_A - m_B), (n - m_B)} \quad (5)$$

where  $\mathbf{F}$  is a Fisher variate, if, we stress this point, the hypothesis  $H_B$  is true. On the contrary, if  $H_A$  is true, but  $H_B$  is not, the variate (5) is a non-central  $\mathbf{F}$ , i.e. the numerator tends to become significantly larger in the average.

2. In this case (Fig. 2) the two least squares estimates are  $\hat{y}_A$ ,  $\hat{y}_B$  and their difference, due to the parallelism of  $M_A$  and  $M_B$  is a constant vector  $c$ ; as a matter of fact, it is easy to prove that:

$$\begin{aligned} (\hat{y}_A - \hat{y}_B) &= (I - AN^{-1}A^+)(a - b) = \\ &Q(a - b) = c \\ (N = A^+A, \quad Q = I - AN^{-1}A^+) \end{aligned} \quad (6)$$

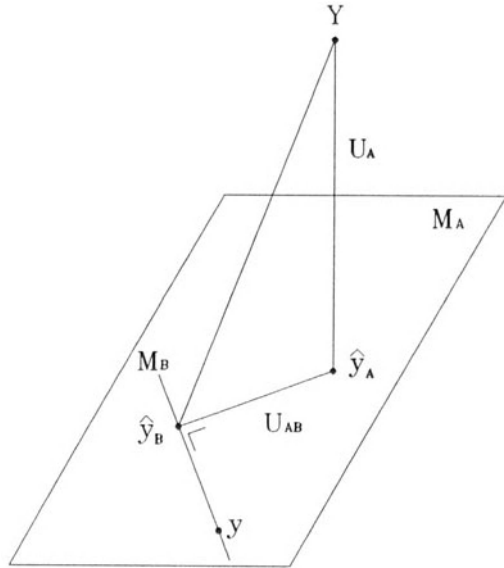


Figure 1: Geometry of the hypotheses testing - 1<sup>st</sup> case

i.e.  $c$  is the projection of  $(a - b)$  on the subspace, orthogonal complement of  $M_A$  and  $M_B$  in  $R^n$ .

The classical *log-likelihood ratio* criterion leads to take into account the variate:

$$\begin{aligned} W &= U_A^+ U_A - U_B^+ U_B \\ (U_A &= Y - \hat{y}_A, \quad U_B = Y - \hat{y}_B) \end{aligned} \tag{7}$$

When  $H_A$  is true we can write:

$$\begin{aligned} U_B &= U_A + c \\ U_A &\sim \mathbf{N}[0, \sigma_0^2 Q] \\ W &\sim \mathbf{N}[-c^+ c, 4\sigma_0^2 c^+ c] \end{aligned}$$

alternatively, if  $H_B$  is true:

$$\begin{aligned} U_A &= U_B - c \\ U_B &\sim \mathbf{N}[0, \sigma_0^2 Q] \\ W &\sim \mathbf{N}[+c^+ c, 4\sigma_0^2 c^+ c] \end{aligned}$$

so that the hypotheses to be tested one against the other are basically:

$$\begin{aligned} H_B : E\{W\} &= c^+ c \\ H_A : E\{W\} &= -c^+ c \end{aligned}$$

and one can adopt, for instance, a decision criterion like:

$$\begin{aligned} W_0 > 0 &\rightarrow \text{accept } H_B \\ W_0 < 0 &\rightarrow \text{accept } H_A \end{aligned}$$

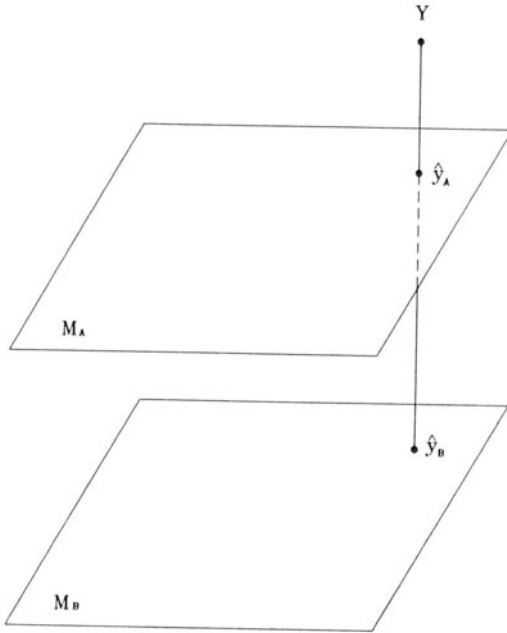


Figure 2: Geometry of the hypotheses testing - 2<sup>nd</sup> case

in this case it is very easy to compute the risks of first and second kind, which result equal since the symmetry of the problem.

Looking more closely at the two *classical* examples, one recognizes that the testing procedure and in particular the possibility of deriving the relevant distributions of our statistics is heavily based on the fact that both the residuals  $U_A$ ,  $U_B$  and their distributions do not depend on the particular theoretical value of  $y$  on  $M_A$  or  $M_B$ .

The situation is completely different if the manifolds  $M_A$  and  $M_B$  are neither nested nor parallel, but they are placed, for example, as shown in Fig. 3; in fact, in this case, if we try to use a statistics like  $W$  defined in (7), we find it impossible to define the exact distribution of this variate without specifying where is the theoretical value of  $y$ . We can write:

$$\begin{aligned} M_A &\equiv \{y = Ax_A + a\} \\ M_B &\equiv \{y = Bx_B + b\} \end{aligned}$$

and:

$$\begin{aligned} U_A &= Y - \hat{y}_A = Q_A(Y - a) \\ (Q_A &= I - AN_A^{-1}A^+) \end{aligned}$$

$$\begin{aligned} U_B &= Y - \hat{y}_B = Q_B(Y - b) \\ (Q_B &= I - BN_B^{-1}B^+) \end{aligned}$$

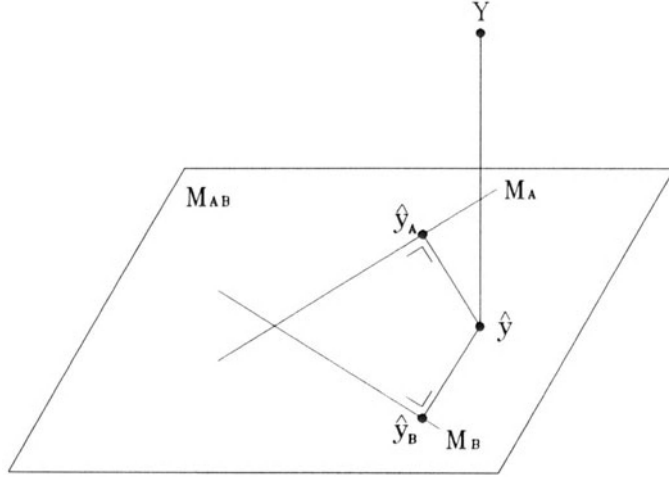


Figure 3: Non-nested manifolds and their linear hull

therefore:

$$\begin{aligned}
 W &= U_A^+ U_A - U_B^+ U_B \\
 &= (Y - a)^+ Q_A (Y - a) - (Y - b)^+ Q_B (Y - b) \\
 &= (Y - a)^+ Q_A (Y - a) - (Y - y)^+ Q_B (Y - y) - \\
 &\quad 2(Y - y)^+ Q_B (y - b) - (y - b)^+ Q_B (y - b)
 \end{aligned}$$

If we assume that  $H_A$  is true, we have:

$$(Y - a)^+ Q_A (Y - a) = (Y - y)^+ Q_A (Y - y)$$

so that, if we call  $m_A$  the dimension of  $M_A$  (in the following we use the notation  $|v|^2$  to denote the improduct  $v^+ Q_{vv} v$ ):

$$E\{|U_A|^2\} = \sigma_0^2 \text{Tr} Q_A = \sigma_0^2 (n - m_A)$$

and similarly:

$$E\{(Y - b)^+ Q_B (Y - b)\} = \sigma_0^2 (n - m_B)$$

while:

$$E\{(Y - y)^+ Q_B (y - b)\} = 0$$

Summarizing and also recalling that hypothesis  $H_A$  is true, we obtain:

$$E\{W\} = \sigma_0^2 (m_B - m_A) - (y - b)^+ Q_B (y - b)$$

what shows clearly that  $E\{W\}$  do depends onto where is exactly located  $y$  on the manifolds  $M_A$ . As a matter of fact, if  $m_B = m_A$  and if  $y$  belongs to the intersection  $M_A \cap M_B$ , so that  $Q_B(y - b) \equiv 0$ , we see that  $E\{W\} = 0$  and the two hypotheses are indistinguishable. On the contrary, if  $y$  is well far away from the crossing  $M_A \cap M_B$ , it is much more likely we are able to discriminate between  $H_A$  and  $H_B$ . Yet, since the problem is not only to choose  $H_A$  or  $H_B$  but also to assign risks of making the wrong decision, we can argue the matter becomes difficult because probabilities like:

$$P\{|U_B| < |U_A| \mid H_A\}$$

depend indeed onto where  $y$  is in  $M_A$ .

This problem is not new in statistics: i.e. we can refer to (Efron, 1984) where an approximate (*Bootstrap*) solution is found. Here we try to follow another approach and we apply the Bayes' theory introducing also as unknown of the problem a parameter  $\pi$  with values  $(0, 1)$  according to whether  $H_A$  or  $H_B$  are to be considered true in a particular experiment; following the Bayes' philosophy, we enter an a priori uniform ignorance into the problem:

$$P(\pi = 0) = P(\pi = 1) = 1/2$$

and we let the data to provide us a posterior distribution:

$$\begin{aligned} p_A &= P(\pi = 1) \\ p_B &= P(\pi = 0) \end{aligned}$$

able to tell us exactly which hypothesis (and how much) is more likely to be true; this will be developed in §2. In §3 it is provided an elementary example just to show how to apply our method to analize different kinematic models for a deforming control network.

## 2 - THE BAYESIAN APPROACH

Our problem is to judge on the likelihood of one of two linear models:

$$y = Ax_A + a \tag{8}$$

$$y = Bx_B + b \tag{9}$$

on the basis of an observation variate  $Y$  for which we assume:

$$Y \sim \mathbf{N}[y, \sigma_0^2 I] \tag{10}$$

Before we get start it is worthwhile to make a remark.

First of all we note that  $M_A$  and  $M_B$  need not have the same dimensions, so that  $x_A$  and  $x_B$  range on different space in general. Second, we observe that if  $M_A \cap M_B$  is again a linear manifold with non-null dimension, the component of  $Y$  along  $M_A \cap M_B$

will not help us in discriminating between the two hypotheses, so this component should be eliminated. Further, if we take the manifold  $M_{AB}$ , the linear hull of  $M_A$  and  $M_B$ , the residual component  $(Y - \hat{y})$  is common to both  $U_A$  and  $U_B$  (Fig. 3) and therefore we also expect this component is unuseful in solving our problem.

Accordingly we see that, given an arbitrary initial situation with models (8),(9) and observation  $Y$ , we can preliminarily reduce our problem going from  $Y$  to  $\hat{y} \in M_{AB}$  and then eliminate all common components of  $M_A$  and  $M_B$ , so to obtain a situation where  $M_A \cap M_B$  is at most a single point (Fig. 3). To tell the truth, the component  $(Y - \hat{y})$  is not useless, since it can provide an estimate of  $\sigma_0^2$ ; in fact:

$$E\{|(Y - \hat{y})|^2\} = \sigma_0^2(n - m_{AB}) \quad (11)$$

where  $m_{AB}$  is the dimension of  $M_{AB}$ . So we will not concentrate any more on the problem of estimating  $\sigma_0^2$  in this paper, but we will assume it is known.

To start we define a new discrete (*head and tail*) variable  $\pi$  which can assume the two values  $(0, 1)$  only and we combine the two models (8),(9) in the following way:

$$y = \pi(Ax_A + a) + (1 - \pi)(Bx_B + b) \quad (12)$$

we stress the fact that now our model is non-linear with two continuous parameters  $x_A$  and  $x_B$  and one discrete parameter  $\pi$ ; this is not new in geodesy, since it was already considered to solve the phase ambiguity problem in GPS theory (Betti, Crespi and Sansó, 1993). The idea is to have the most uninformative prior distribution for the parameters at the beginning, for instance:

$$P(x_A, x_B, \pi) = \begin{cases} 1/2 & \text{if } \pi = 1 \\ 1/2 & \text{if } \pi = 0 \end{cases} \quad (13)$$

to build the likelihood function of the observations and then to derive the posterior distribution of  $(x_A, x_B, \pi)$ ; finally, by integrating over  $x_A, x_B$  we obtain the marginal posterior distribution of  $\pi$ , namely the two numbers:

$$\begin{aligned} p_A &= P(\pi = 1|Y) \\ p_B &= P(\pi = 0|Y) \end{aligned} \quad (14)$$

which is indeed our final goal.

It has to be underlined that (13) is not a real probability distribution since its integral in  $x_A, x_B$  diverges; however, this is typical of Bayes' theory and it only means we derive something which is proportional to the final posterior distribution; in particular we will find numbers proportional to  $p_A, p_B$ , so that we just have to normalize them in order to obtain authentic probabilities.

We can start by forming the joint likelihood:

$$L(Y, x_A, x_B, \pi) = L(Y|x_A, x_B, \pi)p(x_A, x_B, \pi) \quad (15)$$

where:

$$L(Y|x_A, x_B, \pi) = \frac{1}{2\pi^{n/2}\sigma_0^n} \exp\left[-\frac{1}{2\sigma_0^2}|(Y - y)|^2\right] \quad (16)$$

with  $y$  related to  $(x_A, x_B, \pi)$  according to (12).

This two relations (12),(15) can be written also explicitly in a splitted form as:

$$L(Y, x_A, x_B, \pi) = \begin{cases} \frac{1}{2}L_A(Y|x_A) & (\pi = 1) \\ \frac{1}{2}L_B(Y|x_B) & (\pi = 0) \end{cases} \quad (17)$$

with:

$$\begin{aligned} L_A(Y|x_A) &= \frac{1}{(2\pi)^{n/2}\sigma_0^n} \exp\left[-\frac{1}{2\sigma_0^2}|(Y - Ax_A - a)|^2\right] \\ L_B(Y|x_B) &= \frac{1}{(2\pi)^{n/2}\sigma_0^n} \exp\left[-\frac{1}{2\sigma_0^2}|(Y - Bx_B - b)|^2\right] \end{aligned} \quad (18)$$

Let us now define the marginal distribution of the observations  $Y$  as:

$$L(Y) = \frac{1}{2} \int L_A(Y|x_A) dx_A + \frac{1}{2} \int L_B(Y|x_B) dx_B \quad (19)$$

the integrals in (19) are easily computed by using the normalization of gaussian variates and observing that:

$$\begin{aligned} |(Y - Ax_A - a)|^2 &= |(Y - \hat{y}_A)|^2 + |(\hat{y}_A - Ax_A - a)|^2 = \\ &|U_A|^2 + (\hat{x}_A - x_A)^T N_A(\hat{x}_A - x_A) \end{aligned}$$

with:

$$N_A = A^+ A$$

$$\hat{x}_A = N_A^{-1} A^+(Y - a)$$

$$\hat{y}_A = A\hat{x}_A + a$$

as usual; an analogous relation holds for  $|(Y - Bx_B - b)|^2$  too.

So we have:

$$\int L_A(Y|x_A) dx_A = \frac{1}{(2\pi)^{(n-m_A)/2}\sigma_0^{(n-m_A)}\sqrt{\det N_A}} \exp\left[-\frac{1}{2\sigma_0^2}|U_A|^2\right] \quad (20)$$

$$\int L_B(Y|x_B) dx_B = \frac{1}{(2\pi)^{(n-m_B)/2}\sigma_0^{(n-m_B)}\sqrt{\det N_B}} \exp\left[-\frac{1}{2\sigma_0^2}|U_B|^2\right] \quad (21)$$

then, according to Bayes' theorem, we can write:

$$L(Y, x_A, x_B, \pi) = \begin{cases} \frac{L_A(Y|x_A)}{2L(Y)} & (\pi = 1) \\ \frac{L_B(Y|x_B)}{2L(Y)} & (\pi = 0) \end{cases} \quad (22)$$

Let us remark that in (22) the renormalization of the distribution has already been performed.

The last step is now to apply (14), namely:

$$p_A = P(\pi = 1|Y) = \frac{\int L_A(Y|x_A) dx_A}{2L(Y)} \quad (23)$$

$$p_B = P(\pi = 0|Y) = \frac{\int L_B(Y|x_B) dx_B}{2L(Y)} \quad (24)$$

Since, as we have already noticed, we are basically interested in the ratio  $(p_A/p_B)$ , which characterizes our finding because  $p_A + p_B = 1$  has to hold too, we can summarize our result in one formula, i.e.

$$\frac{p_A}{p_B} = \frac{1}{(2\pi)^{(m_B-m_A)/2} \sigma_0^{(m_B-m_A)}} \sqrt{\frac{\det N_B}{\det N_A}} \exp[-\frac{1}{2\sigma_0^2}(|U_A|^2 - |U_B|^2)] \quad (25)$$

This is the basic result of this paragraph and we can observe that it agrees perfectly with what is already known in statistical literature, namely, quoting directly from (Jackson and Matsu'ura, 1985), that *the posterior odds of  $H_A$  versus  $H_B$  is the likelihood ratio multiplied by the prior odds.*

### 3 - AN ELEMENTARY EXAMPLE

We want to show in this paragraph how the theory just recalled is needed when solving problems where different geodetic/geophysical models have to be contrasted one another on the basis of the observational data. We do that by means of an extremely elementary example being perfectly aware that *real world* situations are usually much more complicated. We will come back to this last point in the next paragraph.

So let us imagine that we perform a spirit levelling along a line with four benchmarks for the purpose of controlling its altimetric deformations in time; the redundancy of the observations is provided by time repetitions of three level increments measured at two different epochs and by the following pure kinematic models where:

$$Q_i = \text{height of point } P_i \ (i = 1, 2, 3, 4)$$

$$Q_{i+1} - Q_i = \text{height increment observed at basic epoch } (i = 1, 2, 3)$$

$$Q'_{i+1} - Q'_i = \text{height increment observed at new epoch } (i = 1, 2, 3)$$

$$\delta Q_i = Q'_i - Q_i = \text{height variation between two epochs}$$

(please note that the three  $\delta Q_i$  constitute the components of the  $Y$  vector)

1. First kinematic hypothesis  $H_A$ . This hypothesis (Fig. 4) assumes that, due to particular reasons,  $L$  is raised in its motion against  $R$ ; couple  $(P_1, P_2)$  move parallelly upward while couple  $(P_3, P_4)$  don't move at all, or better move parallelly but we can't see that because we decide to fix the origin of the heights in  $P_4$ , namely  $Q_4 = Q'_4 = 0$ . This is expressed analitically by the model  $M_A$ :

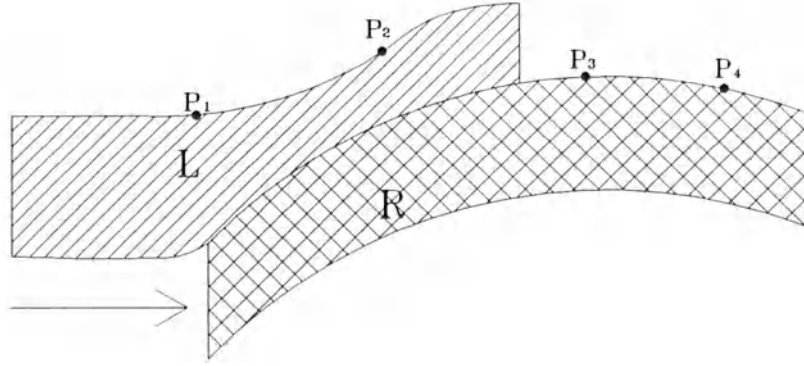


Figure 4: First kinematic hypothesis: the slab  $L$  is moving against the slab  $R$ ;  $R$  doesn't move and  $L$  is uprised

$$\begin{cases} \delta Q_1 = x_A \\ \delta Q_2 = x_A \\ \delta Q_3 = 0 \end{cases} \quad (26)$$

As we see, in this case  $a = 0$ , so that:

$$A = \begin{vmatrix} 1 \\ 1 \\ 0 \end{vmatrix}$$

$$N_A = 2$$

$$Q_A = I - AN_A^{-1}A^+ = \begin{vmatrix} \frac{1}{2} & -\frac{1}{2} & 0 \\ -\frac{1}{2} & \frac{1}{2} & 0 \\ 0 & 0 & 1 \end{vmatrix}$$

$$|U_A|^2 = Y^+ Q_A Y = \frac{1}{2} \delta Q_1^2 + \frac{1}{2} \delta Q_2^2 - \delta Q_1 \delta Q_2 + \delta Q_3^2 \quad (27)$$

2. Second kinematic hypothesis  $H_B$ . In this hypothesis (Fig. 5) there is a basic symmetry so that the couples  $(P_1, P_4)$  and  $(P_2, P_3)$  move upward maintaining their relative heights unchanged; therefore, if we assume again  $Q_4 = Q'_4 = 0$ , we find the model  $M_B$ :

$$\begin{cases} \delta Q_1 = 0 \\ \delta Q_2 = x_B \\ \delta Q_3 = x_B \end{cases} \quad (28)$$

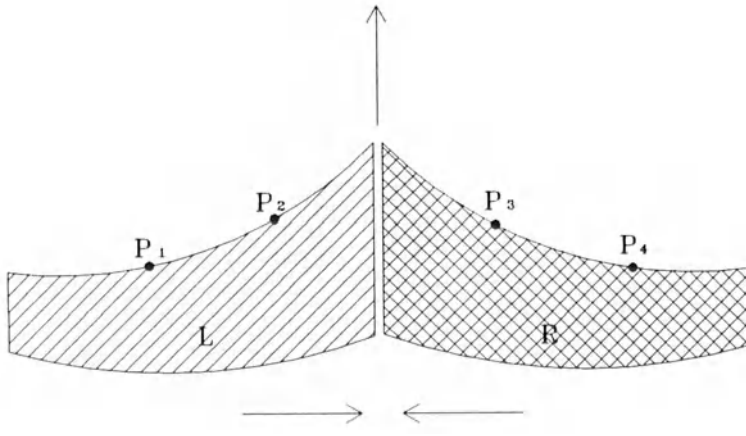


Figure 5: Second kinematic hypothesis: two slabs  $L$  and  $R$  are moving one against the other symmetrically

In this case we have:

$$B = \begin{vmatrix} 0 \\ 1 \\ 1 \end{vmatrix}$$

$$N_B = 2$$

$$Q_B = I - BN_B^{-1}B^+ = \begin{vmatrix} 1 & 0 & 0 \\ 0 & \frac{1}{2} & -\frac{1}{2} \\ 0 & -\frac{1}{2} & \frac{1}{2} \end{vmatrix}$$

$$|U_B|^2 = Y^+ Q_B Y = \delta Q_1^2 + \frac{1}{2}\delta Q_2^2 + \frac{1}{2}\delta Q_3^2 - \delta Q_2 \delta Q_3 \quad (29)$$

The two manifolds  $M_A, M_B$  in the observation space  $(\delta Q_1, \delta Q_2, \delta Q_3)$  are represented in Fig. 6. We observe that, among other simplifications, we have here  $m_A = m_B = 1$ .

Just to illustrate how the method works let us compute the ratio  $p_A/p_B$  assuming 4 different sets of height variations (Tab. 1) and  $\sigma_0 = 0.1\text{cm}$ . In the first two examples the hypothesis  $H_A$  is strongly favoured, while in the others two it is  $H_B$  which is mostly probable. We observe here only that it is not elementary to judge on the posterior distribution by just giving a quick look at the data.

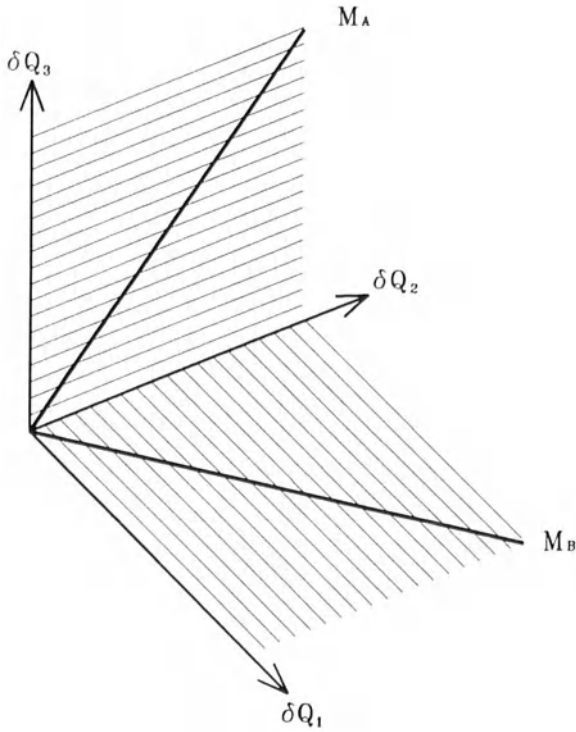


Figure 6: Geometry in the observation space

Example	I	II	III	IV
$\delta Q_1(cm)$	0.8	0.8	0.2	0.2
$\delta Q_2(cm)$	0.6	0.4	0.4	0.6
$\delta Q_3(cm)$	-0.2	0.2	0.4	0.8
$p_A/p_B$	exp 33	exp 27	exp -7	exp -33

Table 1: Examples of height variations and related ratio  $p_A/p_B$

#### 4 - DISCUSSION

The problem stated in the first paragraph has been solved by assuming normality and isotropy of the observations; this can be very easily generalized to anisotropic covariance matrices, which just modify the definition of the metric in the observation space, and even to non-normal variates as long as the functions  $L_A(Y|x_A)$ ,  $L_B(Y|x_B)$  have finite integrals over  $x_A$ ,  $x_B$  respectively. The theory has been applied to an elementary example; what makes this example *too elementary* is not so much the small number of points, the small redundancy or the simplicity of the deterministic (kinematic) model, but rather the simplicity of the stochastic model.

As a matter of fact, it is very unlikely that under one or the other hypothesis the slabs  $L$  and  $R$  would move exactly like rigid bodies. Of course, the largest errors of

models (26), (28) will not be (independent) measuring errors, but model errors due to the fact that they don't take into account for deformations; we are not here thinking about *local* deformations which could be modelled by a white noise with larger  $\sigma_0$ , but rather about global deformations which certainly will display a correlation pattern. It is just the computation of these correlations the difficult matter in applying the theory developed above and it should constitutes the most careful object of study and joint work between geodesists and geofisicists, looking into each specific case to provide the most realistic possible model error.

On the other hand, this difficulty is stressed by many other approaches to geodetic/geophysical inference, like the famous informatic approach (Tarantola, 1987) or more generally by all Bayesian approaches like in (Jackson and Matsu'ura, 1985) or (Betti, Crespi and Sansó, 1993).

*Acknowledgment.* The authors thank very much Mr. O. Evandri (working at the Dipartimento di Idraulica, Trasporti e Strade - Università di Roma "La Sapienza") who drawn all the figures.

## REFERENCES

- Backus G. L. (1971). Inference from inadequate and inaccurate data, *Lectures in Applied Mathematics* n. 14, pp. 1-105.
- Betti B., Crespi M. and Sansó F. (1993). A geometric illustration of ambiguity resolution in GPS theory and a Bayesian approach *Manuscripta Geodaetica* **18**, n. 6, pp. 317-330.
- Cox D. R., Hinkley D. K. (1978). *Theoretical Statistics*. Chapman and Hall, London.
- Efron B. (1984). Comparing non-nested linear models. *Journal of the American Statistical Association* **78**, n. 38b, pp. 791-803.
- Jackson D. D. and Matsu'ura M. (1985). A Bayesian approach to non linear inversion. *Journal of Geophysical Research* **90**, n. B1, pp. 581-591.
- Koch K. R. (1988). *Parameter estimation and hypotheses testing in linear models*. Springer, Berlin Heidelberg New York Tokyo.
- Tarantola A. (1987). *Inverse problem theory*. Elsevier, New York.

# ON STOCHASTIC BOUNDARY CONDITIONS FOR LAPLACE EQUATION

Yu. A. Rozanov  
Steklov Mathematical Institute, Moscow

This report is motivated by some problems in theoretical geodesy (see F. Sansò, [1]) and based on a certain general approach to stochastic boundary conditions for stochastic partial differential equations (see, for example, Yu. Rozanov [2]). For the sake of simplicity, we shall consider the Laplace equation

$$\Delta \xi = 0 \quad (1)$$

in the unit disc  $G = \{(r, \theta) : 0 \leq r < 1\}$  on the plane  $R^2$  with standard polar coordinates  $(r, \theta), 0 \leq r < \infty, 0 \leq \theta < 2\pi$ ; recall that we have for the Laplacian the representation

$$\Delta = \frac{\partial^2}{\partial r^2} + \frac{1}{r} \frac{\partial}{\partial r} + \frac{1}{r^2} \frac{\partial^2}{\partial \theta^2}$$

A problem is to determine a specific solution  $\xi$  by the values it attains, in some way, on the boundary

$$\Gamma = \{(r, \theta) : r = 1, 0 \leq \theta < 2\pi\},$$

when these boundary values are *extremely chaotic*. Having in mind what represents  $\xi$  on  $\Gamma = [0, 2\pi]$ , we admit that it is a random distribution, i.e. a generalized stochastic process, taking values in the space of distributions on  $[0, 2\pi]$ , defined through its “functional coupling”

$$\xi^{(0)} = (\phi, \xi^{(0)}), \phi \in C^\infty([0, 2\pi));$$

the random values  $(\phi, \xi^{(0)})$  are assumed to be meansquare continuous over test functions with respect to a norm

$$E \left\{ (\phi, \xi^{(0)})^2 \right\}^{1/2} \leq C \cdot \|\phi\|_0 \asymp \|\phi\|_0 \asymp \left( \sum_{-\infty}^{\infty} |\tilde{\phi}_n|^2 \right)^{1/2} = \|\phi\|_{L_2}$$

for  $\phi(\theta) = \sum_{-\infty}^{\infty} \tilde{\phi}_n e^{in\theta}$ ,  $0 \leq \theta < 2\pi$ , in the known  $L_2(\Gamma)$ -space. We shall denote  $\underline{W}_2^0(\Gamma)$  a functional class formed with random distributions of this type on  $\Gamma$ . The most chaotic field of boundary values is characterized by a random distribution  $\xi^{(0)}$  with *independent values*  $(\phi, \xi^{(0)})$  for the test functions  $\phi$  with disjoint supports, having  $E\{(\phi, \xi^{(0)})(\psi, \xi^{(0)})\} = 0 \forall \phi, \psi \in C^\infty([0, 2\pi])$ ,  $\phi \cdot \psi \equiv 0$ . Let us note that any random distribution

$$\xi^{(0)} \in \underline{W}_2^0(\Gamma)$$

actually engendres a certain stochastic measure the values of which on any Borel set  $B \subseteq \Gamma$  can be determined as  $(1_B, \xi^{(0)})$  by means of the corresponding indicator-function<sup>1</sup>. One can also apply a notation  $\xi^{(0)}(t) dt$  for "stochastic differential" of this stochastic measure and represent  $\xi^{(0)}$  as a *stochastic integral*

$$(\phi, \xi^{(0)}) = \int_{\Gamma} \phi(t) \xi^{(0)}(t) dt$$

well defined for all  $\phi \in L_2(\Gamma)$ . Let us now turn our attention to the known *Poisson kernel*

$$w(r, \theta, t) = \frac{1}{2\pi} \frac{1 - r^2}{1 - r^2 - 2r \cos(t - \theta)}$$

with  $(r, \theta) \in G$  and  $t \in \Gamma$  on  $\Gamma = [0, 2\pi]$ . We can write symbolically

$$w(r, \theta) = w(r, \theta, t), t \in \Gamma$$

as a harmonic vector-function, i.e. a function of  $(r, \theta) \in G$  which to each fixed  $\bar{r}, \bar{\theta}$  associates a function of  $t$  in the  $L_2(\Gamma)$ -space. We observe that such function can be differentiated with respect to  $r, \theta$ , still obtaining an  $L_2$  function of  $t$ . Hence, for any random distribution  $\xi^{(0)} \in \underline{W}_2^0(\Gamma)$  we can employ the corresponding stochastic integral

$$\xi(r, \theta) = (w, \xi^{(0)}) = \frac{1}{2\pi} \int_0^{2\pi} \frac{1 - r^2}{1 - r^2 - 2r \cos(t - \theta)} \xi^{(0)}(t) dt \quad (2)$$

which determines a harmonic function  $\xi = \xi(r, \theta)$  in the unit disc  $G$ , since for any  $(r, \theta) \in G$ , i.e. for any  $r < 1$ ,

$$\Delta \xi = (\Delta w, \xi^{(0)}) = 0.$$

---

<sup>1</sup>Indeed although  $1_B$  does not belong to  $C^\infty([0, 2\pi])$ , since we can find  $\phi_n \in C^\infty$  and such that  $\phi_n \rightarrow 1_B$  in  $L_2(\Gamma)$ , we have that  $(\phi_n, \xi^{(0)})$  is mean square convergent to a random variable which we can take as definition of  $(1_B, \xi^{(0)})$ .

The behavior of the function  $\xi$  near the boundary  $\Gamma$ , depending on  $\xi^{(0)}$ , typically is extremely chaotic without any point-wise limit values on  $\Gamma$ . Considering its limit behavior, we are to treat  $\xi$  in a generalized sense with suitable test functions. In particular, we can employ as test functions

$$x_\rho = \delta_\rho(r) \times \phi(\theta), \quad \phi \in C^\infty([0, 2\pi)), \quad (3)$$

with delta functions  $\delta_\rho(r)$ ,  $r > 0$ , at  $r = \rho$ . Then, using the representation (2), we receive

$$(x_\rho, \xi) = \int_0^{2\pi} \phi(\theta) \xi(\rho, \theta) d\theta = (\phi_\rho, \xi^{(0)})$$

with  $\phi_\rho(t) = \int_0^{2\pi} \phi(\theta) w(\rho, \theta, t) d\theta$ . It is a well known classical property of the Poisson kernel  $w$  that

$$\lim_{\rho \rightarrow 1} \phi_\rho(t) = \lim_{\rho \rightarrow 1} \int_0^{2\pi} w(\rho, \theta, t) \phi(\theta) d\theta = \phi(t),$$

the limit being uniform in  $t$  for any continuous  $\phi(t)$ . It is also well known that the same limit holds true when  $\phi \in L_2$  and then the convergence of  $\phi_\rho$  to  $\phi$  is also in the same space. Accordingly, following our hypothesis of mean square continuity of  $\xi^{(0)}$  in  $\phi \in L_2$ , we can conclude that  $\lim_{\rho \rightarrow 1} (\phi_\rho, \xi^{(0)}) = (\phi, \xi^{(0)})$  in a mean square sense. Consequently we see that

$$(\phi, \xi^{(0)}) = \lim_{\rho \rightarrow 1} (x_\rho, \xi) \quad (4)$$

represents on the boundary  $\Gamma = [0, 2\pi]$  what seems natural to treat as the corresponding *boundary value* of the generalized function  $\xi$ . According to this, the distribution

$$\xi^{(0)} = (\phi, \xi^{(0)}), \quad \phi \in C^\infty([0, 2\pi]),$$

represents what we would call a *generalized boundary trace* of  $\xi$  on the boundary  $\Gamma$ . Note, that a generalized stochastic harmonic function

$$\xi = \xi(r, \theta), \quad (r, \theta) \in G,$$

- solution of the differential equation (1), admits the representation (2) by means of its boundary trace  $\xi^{(0)} \in W_2^0(\Gamma)$  on  $\Gamma = [0, 2\pi]$  if and only if

$$E \left| \int_0^{2\pi} \phi(\theta) \xi(r, \theta) d\theta \right|^2 \leq C \|\phi\|_{L_2}^2, \quad \phi \in C^\infty([0, 2\pi)) \quad (5)$$

As a matter of fact, in general, there are no other "boundary values" which can be determined by  $\xi$  near the boundary but ones represented by the corresponding distribution  $\xi^{(0)} = (\phi, \xi^{(0)})$ ,  $\phi \in C^\infty([0, 2\pi])$ , in (4). This means that the only "boundary data", we can collect on  $\Gamma$ , actually are with respect to  $\xi^{(0)}$ , so we can only set *boundary conditions* for the solution  $\xi$  of the equation (1) which are of the known *Dirichlet type* with the given boundary trace  $\xi^{(0)}$  on  $\Gamma$ . This situation takes place, in general, as far as  $\xi^{(0)}$  is not better than

$$\xi^{(0)} \in \underline{W}_2^{1/2}(\Gamma). \quad (6)$$

Here the proper *stochastic Sobolev space*  $\underline{W}_2^q(\Gamma)$ ,  $q = 1/2$  for the boundary  $\Gamma = [0, 2\pi]$  is characterized by mean square continuity of  $(\phi, \xi^{(0)})$  over  $\phi \in C^\infty([0, 2\pi])$  with respect to the corresponding norm

$$\|\phi\|_{-q} \asymp \left( \sum_{-\infty}^{\infty} |\tilde{\phi}_n|^2 (1 + |n|)^{-q} \right)^{1/2}$$

for  $\phi(\theta) = \sum_{-\infty}^{\infty} \tilde{\phi}_n e^{in\theta}$ ,  $0 \leq \theta < 2\pi$ . Let us note, that condition (6) exactly describes boundary values of random fields

$$\xi \in \underline{W}_2^1(G) \quad (7)$$

here a stochastic Sobolev space  $\underline{W}_2^p(G)$ ,  $p = 1$ , in  $G$  is characterized by mean square continuity of  $(x, \xi)$  over  $x \in C_0^\infty(G)$  with respect to the corresponding norm

$$\|x\|_{-p} = \left( \int |\tilde{x}(\lambda)|^2 (1 + |\lambda|^2)^{-p} d\lambda \right)^{1/2}$$

defined by means of its Fourier transform  $\tilde{x}$ . In this case we can give the following description of "boundary values". Namely, we have  $\xi \in \underline{W}_2^1(G)$  well defined as generalized function

$$\xi = (x, \xi), x \in X(G) = [C_0^\infty(G)] \quad (8)$$

where the closure of the corresponding test functions space

$$X(G) = \underline{W}_2^{-p}(G), p = 1,$$

is formed with Schwartz distributions which appear as limit of the Schwartz test functions from  $C_0^\infty(G)$  with respect to the norm  $\|x\|_{-p}$ . The *boundary values* of  $\xi$  are then just

$$(x, \xi), x \in X(\Gamma) \quad (9)$$

where  $X(\Gamma) \subseteq X(G)$  represents a subspace of all boundary test functions  $x$ ,  $\text{supp } x \subseteq \Gamma$ , with supports on the boundary  $\Gamma$ . It occurs, that all boundary values in (9) can actually be represented with the distribution  $\xi^{(0)}$  we know about.

The situation is different, for example, when we deal with another stochastic Sobolev space

$$\xi \in \underline{W}_2^2(G); \quad (10)$$

correspondingly we have as boundary value distribution

$$\xi^{(0)} \in \underline{W}_2^{3/2}(\Gamma). \quad (11)$$

Any  $\xi \in \underline{W}_2^2(G)$  is well defined as a generalized function (8) on the corresponding Sobolev space  $X(G) = \underline{W}_2^{-2}(G)$ , and we can employ test functions

$$x_p^{(1)} = -\frac{\partial}{\partial r} \delta_\rho(r) \times \phi(\theta) \in X(G)$$

- see (3). This brings as limit boundary values

$$\lim_{\rho \rightarrow 1} \int_0^{2\pi} \phi(\theta) \xi^{(1)}(\rho, \theta) d\theta = (\phi, \xi^{(1)}), \phi \in C^\infty([0, 2\pi]),$$

which can be taken as the normal derivative of  $\xi$ , i.e.

$$\xi^{(1)}(r, \theta) = \frac{\partial}{\partial r} \xi(r, \theta), (r, \theta) \in G$$

and determine its generalized boundary trace  $\xi^{(1)}$  as the distribution

$$\xi^{(1)} = (\phi, \xi^{(1)}), \phi \in C^\infty([0, 2\pi]),$$

on the boundary  $\Gamma = [0, 2\pi]$ ,

$$\xi^{(1)} \in \underline{W}_2^{1/2}(\Gamma). \quad (12)$$

It occurs that a linear span of  $\xi^{(k)}$ ,  $k = 0, 1$ , represents all boundary values in (9).

In particular, by using the test functions of the type

$$x = \Delta f \in \Delta L_2(G) \subset W_2^{-2}(G) \quad (13)$$

characterized by the condition  $\Delta f = 0$  in  $G$ ,  $f = 0$  outside  $G$ , we get a boundary relations generalizing the well known Green formula and which, taking into account equation (1), gives

$$(x, \xi) = (\Delta f, \xi) = (f^{(1)}, \xi^{(0)}) - (f^{(0)}, \xi^{(1)}) = 0;$$

as we see there exists a relation between the boundary values  $\xi^{(0)}$  and  $\xi^{(1)}$  of  $\xi$ , as a consequence the equation (1).

Hence, the only boundary values  $(x, \xi)$  we can possibly assess by ourselves are those with boundary test functions  $x \in X^+(\Gamma)$  from an appropriate *direct complement* in  $X(\Gamma)$  to the boundary test functions in (13). Namely, we can employ a certain complete system of  $x \in X^+(\Gamma)$  and set *boundary conditions*

$$(x, \xi) = (x, \xi_+), x \in X^+(\Gamma) \quad (14)$$

with an appropriate *stochastic sample*  $\xi_+$  on the boundary  $\Gamma$ . Actually, with this kind of  $X^+(\Gamma)$  we have the following *direct sum representation*

$$X(G) = \Delta L_2(G) + X^+(\Gamma) \quad (15)$$

of our test functions space

$$X(G) = [C_0^\infty(G)].$$

Of course, having at our disposal all boundary test functions  $x \in X(\Gamma)$ , we can set boundary conditions of the type (14) for *any*  $X^+(\Gamma) \subseteq X(\Gamma)$ . It occurs that with these arbitrary given stochastic boundary conditions, equation (1) has a unique solution if and only if the representation (15) holds true. Moreover, the very solution can be described with all test functions  $\phi \in C_0^\infty(G)$ , say, as

$$(\phi, \xi) = (x, \xi_+) \quad (16)$$

according to the direct sum decomposition  $\phi = \Delta f + x$  with the corresponding  $f \in L_2(G)$ ,  $x \in X^+(\Gamma)$ , - see Fig. 1, and  $(\Delta f, \xi) = 0$ . For example, in this scheme we can set *stochastic boundary conditions of the Dirichlet type*

$$\xi^{(0)} = \xi_+,$$

actually considered at the very beginning. Similar example would be with *stochastic boundary conditions of the Neuman type*

$$\xi^{(1)} = \xi_+,$$

where  $(1, \xi_+^{(1)}) = 0$ , and moreover

$$(1, \xi^{(0)}) = (1, \xi_+^{(0)}).$$

## Appendix. A filtering problem for boundary data.

Suppose, the given boundary data are represented with

$$(x, \xi) = (x, u) + (x, \eta), x \in X^+(\Gamma),$$

where  $(x, u)$  represents what we are actually looking for and  $(x, \eta)$  describe random deviations with zero mean  $E(x, \eta) = 0$ ,  $E(x, \eta)^2 < \infty$ . Then we are to look for certain *estimates*  $(x, \hat{u})$  for unknown  $(x, u)$ ,  $x \in X^+(\Gamma)$ . For this, we can apply a linear span  $H_0$  of  $(x, \xi)$ ,  $x \in X^+(\Gamma)$ , considered as random variables with zero mean  $E_0(x, \xi) = 0$ . Taking into account that  $u = (x, u)$ ,  $x \in X^+(\Gamma)$ , is to be from a certain functional family  $U$  we can get the *best linear unbiased estimates* with

$$E(x, \hat{u}) = (x, u), E[(x, \hat{u}) - (x, u)]^2 = \min$$

as projections of  $(x, \xi)$  onto a subspace  $H_0(U)$  generated by random variables  $\eta(u) \in H_0$ ,  $u \in U$ , from equation

$$E_0(x, \xi) \eta(u) = (x, u), x \in X^+(\Gamma).$$

Note, that when we don't know the true probability distribution, we can apply here any probability distribution  $H$  with the corresponding expectation  $E_0$  and get so-called *pseudo-best linear unbiased estimates* (see [3]).

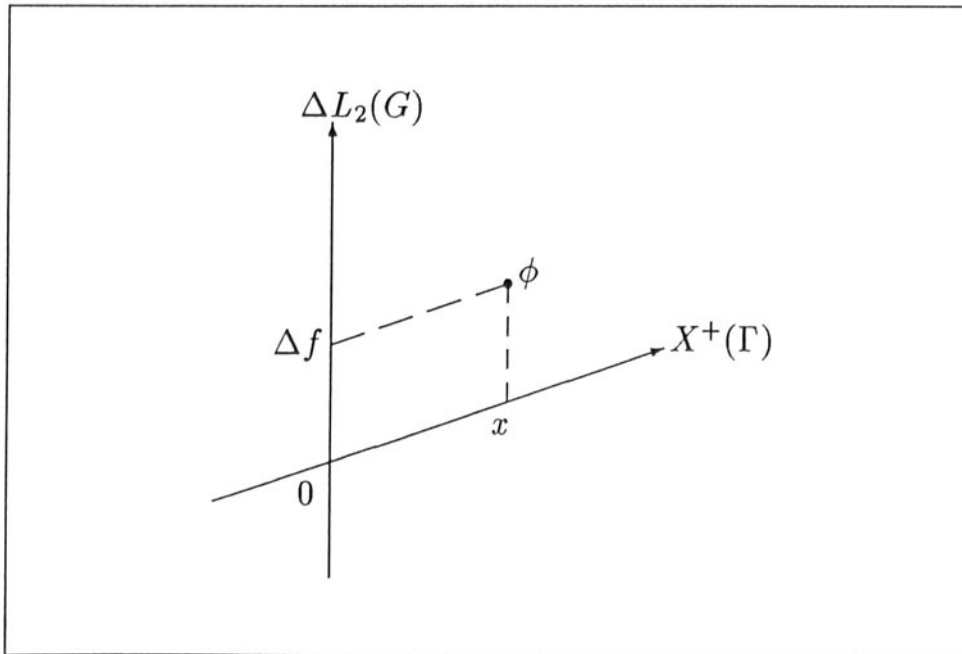


Fig. 1

## References

1. F SANSÒ, *The Wiener integral and overdetermined boundary value problems of physical geodesy*, Manuscripta Geodaetica, 1988, 13, p.p. 75-98.
2. YU. A. ROZANOV, *General boundary value problems for the stochastic partial differential equations*, Proceedings of the Steklov Institute of Mathematics, 200(1991), English trans. by AMS, 1993, Issue 2.
3. YU. A. ROZANOV, *On a new class of estimates*, Multivariate Analysis - II, 1969, p.p. 437-441.

# A SERIES SOLUTION FOR ZAGREBIN'S PROBLEM

Jesús Otero

Instituto de Astronomía y Geodesia. Facultad de Ciencias Matemáticas  
Universidad Complutense. 28040 Madrid

Joan Capdevila

Instituto Geográfico Nacional. Servicio Regional de Cataluña  
Avd. Puerta del Ángel, 42. 08002 Barcelona

**Abstract.** In this paper a series solution for Zagrebin's problem is proposed, based in a sequence of simple Molodensky's type boundary value problems in the domain exterior to the ellipsoid of reference. A sufficient condition is stated for the convergence of this series in terms of the second eccentricity and constants some of them related to properties of the Hölder norms and a Schauder estimate for the simple problem of Molodensky in that domain.

## 1. Introduction

Zagrebin's problem is a boundary problem for the Laplace equation of Robin type arising in Physical Geodesy in the context of the gravimetric determination of the geoid (see, for example, Heiskanen and Moritz 1967, Section 2.13). With the notation usually adopted in Geodesy, the problem is to find a function  $T$  such that

$$\begin{cases} \Delta T = 0 & \text{outside } \Sigma(a,b) \\ \frac{\partial T}{\partial n} - \frac{1}{\gamma} \frac{\partial \gamma}{\partial n} T = -\Delta g & \text{on } \Sigma(a,b) \\ T(\mathbf{x}) = c|\mathbf{x}|^{-1} + O(|\mathbf{x}|^{-3}) & \text{as } |\mathbf{x}| \rightarrow \infty \end{cases} \quad (1.1)$$

where  $T$  is the **anomalous or disturbing potential** (i.e., the difference between the gravity potential of the Earth and a reference or normal gravity potential),  $\gamma$  is the **normal gravity**,  $\Delta g$  is the **gravity anomaly**,  $\Sigma(a,b)$  is an **ellipsoid of revolution** taken as surface of reference with semiaxes  $a$  and  $b$  ( $a>b$ );  $\frac{\partial T}{\partial n} = \langle \nabla T, \mathbf{n} \rangle$  where  $\nabla T$  is the gradient of  $T$ ,  $\mathbf{n}$  is the unit normal to  $\Sigma(a,b)$  pointing to the exterior  $\Sigma^e(a,b)$  and  $\langle \cdot, \cdot \rangle$  denotes the inner product of vectors in  $\mathbb{R}^3$ . The center of the ellipsoid is chosen to be origin of a system of rectangular coordinates, the  $x_3$ -axis being its minor axis.

The condition at infinity means that the harmonic function  $T$  tends to zero and has no component of degree 1 in its spherical harmonic expansion

outside a sufficiently large sphere. If (1.1) has a solution, the restriction of the function  $\frac{1}{\gamma}T$  to  $\Sigma(a, b)$  approximates the distance  $N$  between the geoid and  $\Sigma(a, b)$  along each ellipsoidal normal (*geoid undulation*).

As far as we know, only formal solutions for Zagrebin's problem in terms of series with respect to a small parameter characterizing the deviation of the reference ellipsoid from a sphere are known (see, for example, Molodenskii et al. 1962, and Bjerhammar 1966; for a relatively recent study about the linearized geodetic boundary value problems including a great amount of references see Heck 1991). Following the energy-integral method that L. Hörmander (1976) used in his analysis of the linearized vectorial Molodensky's problem, Otero (1995) has recently stated a uniqueness (and existence) theorem for (1.1).

The main result of this paper is another existence theorem for (1.1) (see Theorem 4.1 in Section 4). The proof is in this case constructive although less explicit with respect to the constants involved than in (Otero, 1995). The main feature of the procedure we shall describe is that Zagrebin's problem is reduced to solve a sequence of "simple Molodensky's problems" (and, therefore, essentially, to solve a sequence of Dirichlet's problems). From now on, we shall use SMP as an abbreviated form to name "Simple Molodensky's Problem".

In Section 2 we propose a series solution for Zagrebin's problem. Section 3 is devoted to analyse some aspects of the SMP. To establish the convergence of the series in Section 2 we shall use Schauder estimates for the SMP, and these are stated using results of Lieberman (1986). These results of Lieberman are valid for regular oblique derivative problems in bounded domains. In our case, these estimates are applicable if we consider the equivalent problem obtained by inversion relative to the unit sphere and Kelvin transform (see Proposition 3.2 and Theorem 3.4).

Throughout this paper we shall use  $C^{k,\alpha}(\bar{\Omega})$  to denote the usual Hölder spaces and  $|\cdot|_{k+\alpha}$  to denote the corresponding norms. For definitions and basic properties of these norms we refer to (Gilbarg and Trudinger, 1983) and to (Hörmander, 1976). By  $\mathcal{H}(\Omega)$  we shall denote the set of all functions harmonic in an open set  $\Omega$  in  $\mathbb{R}^3$ ; if  $\Omega$  is unbounded we shall require regularity at infinity.

Denoting by  $S^2$  the unit sphere in  $\mathbb{R}^3$

$$S^2 = \{\sigma = (\sigma_1, \sigma_2, \sigma_3) \in \mathbb{R}^3 : |\sigma| = (\sigma_1^2 + \sigma_2^2 + \sigma_3^2)^{1/2} = 1\},$$

$d\sigma$  will stand for the (unnormalized) surface measure on  $S^2$ , and we shall simply write  $\int_{\sigma} f(\sigma) d\sigma$  instead of  $\int_{\sigma \in S^2} f(\sigma) d\sigma$  for functions  $f$  defined on  $S^2$ . For points  $\mathbf{x} \in \mathbb{R}^3$  we shall use the abbreviations  $r = |\mathbf{x}|$  and  $\sigma = |\mathbf{x}|^{-1}\mathbf{x}$ . Finally, By  $B_r(\mathbf{y})$  we shall denote the open ball of radius  $r$  centered at  $\mathbf{y}$ .

## 2. A series solution

If we do not take into consideration the rotation of the Earth, the normal gravity potential is a harmonic function outside  $\Sigma(a, b)$  taking a constant value on  $\Sigma(a, b)$ . Then from Bruns' formula (see Heiskanen and Moritz 1967, Eqs. 2-79, 2-80) we have  $\frac{1}{\gamma} \frac{\partial \gamma}{\partial n} = 2H$ , where  $H$  is the *mean curvature* of  $\Sigma(a, b)$ . (Note that in the orientation we have implicitly chosen for  $\Sigma(a, b)$ ,  $H$  is a negative smooth function defined on  $\Sigma(a, b)$ .) The function  $H$  is given by

$$H = -\frac{1}{2} \left[ \frac{1}{\rho} + \frac{1}{\nu} \right]$$

where  $\rho$  and  $\nu$  are the principal radii of curvature of the ellipsoid. As functions of the geodetic latitude  $\phi$ ,  $\rho$  and  $\nu$  are

$$\rho = \frac{a(1+\varepsilon^2)^{1/2}}{(1+\varepsilon^2 \cos^2 \phi)^{3/2}}, \quad \nu = \frac{a(1+\varepsilon^2)^{1/2}}{(1+\varepsilon^2 \cos^2 \phi)^{1/2}}$$

where  $\varepsilon$  is the second eccentricity of  $\Sigma(a, b)$  defined as  $\varepsilon = \frac{(a^2 - b^2)^{1/2}}{b}$ .

The boundary condition in (1.1) is equivalent to

$$\langle \nabla T, \nu \mathbf{n} \rangle + (1+\alpha)T = -\Delta^* g$$

where  $\alpha = \frac{\nu}{\rho} = 1 + \varepsilon^2 \cos^2 \phi$  and  $\Delta^* g = \nu \Delta g$ . On the other hand,  $\nu \mathbf{n}$  can be written as  $\nu \mathbf{n} = \mathbf{x} + \delta \mathbf{x}$ , where  $\mathbf{x} = (x_1, x_2, x_3)$  and  $\delta \mathbf{x} = (0, 0, \varepsilon^2 x_3)$  (see, for example, Heiskanen and Moritz 1967, Eqs. 5-5). Then we obtain

$$\langle \nabla T, \mathbf{x} \rangle + 2T + \varepsilon^2 x_3 \frac{\partial T}{\partial x_3} + \varepsilon^2 \cos^2 \phi T = -\Delta^* g \quad (2.1)$$

Following (Sansò, 1981a) we modify the boundary condition (2.1) in the form

$$\langle \nabla T, \mathbf{x} \rangle + 2T + \varepsilon^2 \left[ x_3 \frac{\partial T}{\partial x_3} + \cos^2 \phi T \right] = -\Delta^* g + \sum_{i=1}^3 a_i A_i$$

where  $A_i(\mathbf{x}) = r^{-2} Y_{1i}(\sigma)$  ( $\mathbf{x} = r\sigma$ ).  $\{Y_{1i}(\sigma) = (3/4\pi)^{1/2} \sigma_i : i=1, 2, 3\}$  is an orthonormal basis for the linear space of spherical harmonics of degree 1, and  $a_i$  are three constants to be determined.

Now the problem is: to find  $T$  and constants  $a_1, a_2, a_3$  such that

$$\begin{cases} \Delta T = 0 & \text{in } \Sigma^e \\ \langle \nabla T, \mathbf{x} \rangle + 2T + \varepsilon^2 \left[ x_3 \frac{\partial T}{\partial x_3} + \cos^2 \phi T \right] = -\Delta^* g + \sum_{i=1}^3 a_i A_i & \text{on } \Sigma \\ T(\mathbf{x}) = c r^{-1} + O(r^{-3}) & \text{as } r \rightarrow \infty . \end{cases} \quad (2.2)$$

(From now on we write  $\Sigma$  instead of  $\Sigma(a, b)$ .)

The idea is to assume for  $T$  and each  $a_i$  an expansion series in powers of  $\varepsilon^2$  in the form

$$T = \sum_{n=0}^{\infty} \varepsilon^{2n} T_n , \quad a_i = \sum_{n=0}^{\infty} \varepsilon^{2n} a_{i,n} \quad (2.3)$$

where  $T_n \in \mathcal{H}(\Sigma^e)$ . A similar assumption is made in (Jorge, 1987) in order to locally study the fixed gravimetric boundary problem in spherical approximation. Closely related ideas are also contained in (Sacerdote and Sansò, 1990), (Sansò, 1981a) and in (Krarup, 1973, Letter IV).

Substituting (2.3) into the boundary condition in (2.2) we formally get,

$$\begin{aligned} \sum_{n=0}^{\infty} \varepsilon^{2n} \left[ \langle \nabla T_n, \mathbf{x} \rangle + 2T_n \right] + \sum_{n=1}^{\infty} \varepsilon^{2n} \left[ x_3 \frac{\partial T_{n-1}}{\partial x_3} + \cos^2 \phi T_{n-1} \right] \\ = -\Delta^* g + \sum_{n=0}^{\infty} \varepsilon^{2n} \left( \sum_{i=1}^3 a_{i,n} A_i \right) . \end{aligned}$$

Comparing coefficients we obtain the following sequence of SMP's

$$\begin{cases} \Delta T_0 = 0 & \text{in } \Sigma^e \\ \langle \nabla T_0, \mathbf{x} \rangle + 2T_0 = -\Delta^* g + \sum_{i=1}^3 a_{i,0} A_i & \text{on } \Sigma \\ T_0(\mathbf{x}) = c_0 r^{-1} + O(r^{-3}) & \text{as } r \rightarrow \infty \end{cases} \quad (2.4a)$$

$$\begin{cases} \Delta T_n = 0 & \text{in } \Sigma^e \\ \langle \nabla T_n, \mathbf{x} \rangle + 2T_n = -x_3 \frac{\partial T_{n-1}}{\partial x_3} - \cos^2 \phi T_{n-1} + \sum_{i=1}^3 a_{i,n} A_i & \text{on } \Sigma \\ T_n(\mathbf{x}) = c_n r^{-1} + O(r^{-3}) & \text{as } r \rightarrow \infty . \end{cases} \quad (2.4b)$$

A sufficient condition for the convergence of the series (2.3) will be stated in Section 4. We previously recall in the next Section a few results on the SMP.

### 3. Some remarks about simple Molodensky's problem

Let  $\omega$  be a  $C^2$  closed surface in  $\mathbb{R}^3$ , *starshaped* with respect to an interior point of the bounded connected component of  $\mathbb{R}^3 - \omega$  that we shall choose as the origin of coordinates  $(0, 0, 0)$ . We shall assume that  $\omega$  has no exceptional points (following Krarup, 1973, by an exceptional point we mean a point where the tangent to  $\omega$  passes through the origin). Let  $\Omega$  be the unbounded connected component of  $\mathbb{R}^3 - \omega$  (the region exterior to  $\omega$ ). T. Krarup (1973) posed the SMP as follows: given  $f \in C^0(\omega)$ , to find  $u \in \mathcal{H}(\Omega) \cap C^1(\bar{\Omega})$  such that  $\langle \nabla u, \mathbf{x} \rangle + 2u = f$  on  $\omega$ . We reformulate the SMP in the following slightly generalized sense: given  $f \in C^0(\omega)$ , to find  $u \in \mathcal{H}(\Omega) \cap C^0(\bar{\Omega})$  such that  $\langle \nabla u, \mathbf{x} \rangle \in C^0(\bar{\Omega})$  and  $\langle \nabla u, \mathbf{x} \rangle + 2u = f$  on  $\omega$ .

Given a function  $f$  defined and continuous on  $\omega$ , we shall denote by  $F$  the function in  $\mathcal{H}(\Omega) \cap C^0(\bar{\Omega})$  such that  $F=f$  on  $\omega$ . This function exists and it is unique under the above conditions (see, for example, Dautray and Lions, 1990).

Although not explicitly stated in (Krarup, 1973, Letter I), we believe that the following Theorem is due to Krarup,

**Theorem 3.1** (Krarup). (i) If  $f=0$ , the solution of the SMP is  $u(\mathbf{x})=r^{-2}Y_1(\sigma)$ , where  $Y_1$  is any spherical harmonic of degree 1. (ii) The non-homogeneous SMP is solvable if and only if

$$\int_{\sigma} F(R\sigma) Y_{1i}(\sigma) d\sigma = 0 \quad \forall i \in \{1, 2, 3\} \quad (3.1)$$

for some  $R > \max_{\mathbf{x} \in \omega} r(\mathbf{x})$ . Furthermore, if (3.1) holds, the solutions of the SMP are the functions

$$u(\mathbf{x}) = cr^{-1} + r^{-2}Y_1(\sigma) - r^{-2} \int_r^{\infty} sF'(s\sigma) ds \quad \mathbf{x} \in \bar{\Omega} \quad (3.2)$$

where  $c = \lim_{r \rightarrow \infty} rF(\mathbf{x})$  and  $F'(\mathbf{x}) = F(\mathbf{x}) - cr^{-1}$ .

*Remarks.* 1. The SMP has also been studied under weaker regularity assumptions in (Sansò, 1981b) and in (Sacerdote and Sansò, 1983).  
 2. The compatibility conditions (3.1) show that the SMP is not always solvable for arbitrary continuous boundary values. This of course agrees with the general Fredholm alternative theory: the index of a regular oblique derivative problem is zero, and since the number of independent

solutions of the homogeneous SMP is three, then the SMP has a solution precisely when three linear forms on  $f$  vanish. If  $G(\mathbf{x}, \mathbf{y})$  is Green's function for  $\Omega$ , (3.1) may be written as

$$\int_{\sigma} \left[ \int_{\omega} \frac{\partial G}{\partial n_y}(R\sigma, \mathbf{y}) f(\mathbf{y}) dS_y \right] Y_{1j}(\sigma) d\sigma = 0$$

where  $n_y$  is the unit outer normal to  $\omega$  in  $\mathbf{y} \in \omega$  and  $dS$  is the surface element of  $\omega$ .

3. We have uniqueness under the additional asymptotic condition,  $u(\mathbf{x}) = cr^{-1} + O(r^{-3})$  as  $r \rightarrow \infty$ .

It is possible to modify the statement of the SMP in such a way that it always has a solution (see, for example, Sansò 1981a): given  $f \in C^0(\omega)$ , to find  $\tilde{u} \in \mathcal{H}(\Omega) \cap C^0(\bar{\Omega})$  and constants  $a_i$  ( $i=1, 2, 3$ ) such that  $\langle \nabla \tilde{u}, \mathbf{x} \rangle \in C^0(\bar{\Omega})$  and  $\langle \nabla \tilde{u}, \mathbf{x} \rangle + 2\tilde{u} = f + \sum_{i=1}^3 a_i A_i$  on  $\omega$ . In fact, there are unique constants  $a_i$  such that the solution of the problem of Dirichlet

$$\tilde{F} \in \mathcal{H}(\Omega), \quad \tilde{F} = f + \sum_{i=1}^3 a_i A_i \quad \text{on } \omega$$

satisfies the compatibility conditions (3.1). Just it should be noted that

$\tilde{F} = F + \sum_{i=1}^3 a_i A_i$  since  $A_i \in \mathcal{H}(\mathbb{R}^3 - \{0\})$ . Hence,

$$\begin{aligned} \int_{\sigma} \tilde{F}(R\sigma) Y_{1j}(\sigma) d\sigma &= \int_{\sigma} F(R\sigma) Y_{1j}(\sigma) d\sigma + R^{-2} \sum_{i=1}^3 a_i \int_{\sigma} Y_{1i}(\sigma) Y_{1j}(\sigma) d\sigma \\ &= \int_{\sigma} F(R\sigma) Y_{1j}(\sigma) d\sigma + R^{-2} a_j \end{aligned}$$

Therefore, choosing

$$a_i = -R^2 \int_{\sigma} F(R\sigma) Y_{1i}(\sigma) d\sigma \quad (3.3)$$

the function  $\tilde{F}$  satisfies (3.1). The modified solution is then

$$\tilde{u}(\mathbf{x}) = cr^{-1} + r^{-2} Y_1(\sigma) - r^{-2} \int_r^{\infty} s \tilde{F}'(s\sigma) ds$$

where  $\tilde{F}' = \left[ F + \sum_{i=1}^3 a_i A_i \right] - cr^{-1}$  and  $a_i$  are given by (3.3).

In order to make use of some Schauder estimates stated for bounded

domains, we shall now introduce the Kelvin transform of  $u$ . First, let  $i: \mathbb{R}^3 \cup \{\infty\} \rightarrow \mathbb{R}^3 \cup \{\infty\}$  be the inversion of  $\mathbb{R}^3 \cup \{\infty\}$  relative to the unit sphere:

$$i(\mathbf{x}) = \mathbf{x}^* = \begin{cases} \mathbf{x}/|\mathbf{x}|^2 & \text{if } \mathbf{x} \neq 0, \infty \\ 0 & \text{if } \mathbf{x} = \infty \\ \infty & \text{if } \mathbf{x} = 0 \end{cases}.$$

Let  $\Omega^* = i(\Omega \cup \{\infty\})$ .  $\Omega^*$  is a bounded domain, starshaped with respect to the origin and with boundary  $\omega^* = i(\omega)$ . We shall also assume that there are not exceptional points.

Let  $K[u]$  be the Kelvin transform of the function  $u$  given by (3.2), that is to say

$$K[u](\mathbf{x}) = |\mathbf{x}|^{-1}u(\mathbf{x}^*) , \quad \mathbf{x} \in \bar{\Omega}^* - \{0\} , \quad \mathbf{x}^* = i(\mathbf{x}) .$$

(In order to avoid a cumbersome notation we also use  $\mathbf{x}$  to denote points in  $\bar{\Omega}^*$ ). We explicitly have

$$\begin{aligned} K[u](\mathbf{x}) &= c + rY_1(\sigma) - r \int_{r^*}^{\infty} sF'(s\sigma) ds \\ &= c + rY_1(\sigma) - r \int_0^r t^{-3}F'(t^{-1}\sigma) dt \\ &= c + rY_1(\sigma) - r \int_0^r t^{-2}K[F'](t\sigma) dt , \quad \mathbf{x} \in \bar{\Omega}^* - \{0\} \end{aligned}$$

where  $r^* = |\mathbf{x}^*|$  and  $K[F']$  is the Kelvin transform of  $F'$ . (It should be noted that  $K[F'](t\sigma) = O(t^2)$  as  $t \rightarrow 0$ .) We see that  $K[u]$  is well defined at the origin and then  $K[u] \in \mathcal{H}(\Omega^*) \cap C^0(\bar{\Omega}^*)$ . Moreover,

$$\frac{\partial K[u]}{\partial r}(\mathbf{x}) = Y_1(\sigma) - \int_0^r t^{-2}K[F'](t\sigma) dt - r^{-1}K[F'](\mathbf{x})$$

and so

$$r \frac{\partial K[u]}{\partial r} = K[u] - c - K[F'] \quad \text{in } \Omega^* .$$

Hence  $\langle \nabla K[u], \mathbf{x} \rangle \in C^0(\bar{\Omega}^*)$  and

$$K[u] - \langle \nabla K[u], \mathbf{x} \rangle = K[F] \quad \text{on } \omega^* .$$

(Cf. Holota 1981, §3.)

Summing up we have proved the following,

**Proposition 3.2** Let  $f \in C^0(\omega)$  be such that  $F$  satisfies (3.1). Let  $u \in \mathcal{H}(\Omega) \cap C^0(\bar{\Omega})$  be a solution of the SMP. Then  $K[u] \in \mathcal{H}(\Omega^*) \cap C^0(\bar{\Omega}^*)$ ,  $\langle \nabla K[u], \mathbf{x} \rangle \in C^0(\bar{\Omega}^*)$  and  $K[u] - \langle \nabla K[u], \mathbf{x} \rangle = K[F]$  on  $\omega^*$ .

The function  $F$  satisfies (3.1) if and only if  $\nabla K[F](\mathbf{0}) = \mathbf{0}$ . In fact,  $B=B_{1/R}(0)$  is strictly contained in  $\Omega^*$ , and since  $\nabla K[F]$  is also harmonic in  $\Omega^*$  it follows by the mean value and divergence theorems that (see Gilbarg and Trudinger 1983, §2.7)

$$\begin{aligned} D_i K[F](\mathbf{0}) &= (3/4\pi) R^3 \int_B D_i K[F] \, dx = (3/4\pi)^{1/2} R \int_{\sigma} K[F](R^{-1}\sigma) Y_{1i}(\sigma) \, d\sigma \\ &= (3/4\pi)^{1/2} R^2 \int_{\sigma} F(R\sigma) Y_{1i}(\sigma) \, d\sigma , \end{aligned}$$

where  $D_i K[F] = \partial K[F]/\partial x_i$ . For the modified problem, we analogously have

$$K[\tilde{u}](\mathbf{x}) = c + r Y_1(\sigma) - r \int_0^r t^{-2} K[\tilde{F}'](t\sigma) \, dt$$

where

$$K[\tilde{F}'] = K[F] + \sum_{i=1}^3 a_i(r Y_{1i}) - c = K[F] + (3/4\pi)^{1/2} \langle \mathbf{a}, \mathbf{x} \rangle - K[F](\mathbf{0})$$

and,

$$\mathbf{a} = -(4\pi/3)^{1/2} \nabla K[F](\mathbf{0}) .$$

Then

$$K[\tilde{F}'] = (K[F] + \langle -\nabla K[F](\mathbf{0}), \mathbf{x} \rangle) - K[F](\mathbf{0}) ,$$

and the boundary condition for  $K[\tilde{u}]$  is now

$$K[\tilde{u}] - \langle \nabla K[\tilde{u}], \mathbf{x} \rangle = K[F] + \langle -\nabla K[F](\mathbf{0}), \mathbf{x} \rangle \text{ on } \omega^*.$$

By the help of Theorem 3.1, Proposition 3.2 and these previous remarks, we conclude the

**Theorem 3.3** Let  $g$  be continuous on  $\omega^*$ . Then, there is a unique function  $v \in \mathcal{H}(\Omega^*) \cap C^0(\bar{\Omega}^*)$  and a unique vector  $\mathbf{a} \in \mathbb{R}^3$  such that  $\langle \nabla v, \mathbf{x} \rangle \in C^0(\bar{\Omega}^*)$ ,

$$v - \langle \nabla v, \mathbf{x} \rangle = g + \langle \mathbf{a}, \mathbf{x} \rangle \text{ on } \omega^*$$

and  $\nabla v(\mathbf{0}) = \mathbf{0}$ . Explicitly,  $\mathbf{a} = -\nabla G(\mathbf{0})$  and

$$v(\mathbf{x}) = G(\mathbf{0}) - r \int_0^r t^{-2} \left[ \{G(t\sigma) + t\langle \mathbf{a}, \sigma \rangle\} - G(\mathbf{0}) \right] dt$$

where  $G$  is the solution of the problem of Dirichlet with boundary value  $g$  on  $\omega^*$ . (Cf. Sansò 1981a, Theorem 5, and Sansò 1978, §5.)

By results of (Lieberman 1986, Theorem 3 (c) and Remark 2), if in Theorem 3.3  $g \in C^\alpha(\omega^*)$  for some  $\alpha \in (0, 1)$ , then  $v \in C^{1,\alpha}(\bar{\Omega}^*)$ . In addition, from (Lieberman 1986, Corollary to Theorem 2), there is a constant  $C$  such that

$$|v|_{1+\alpha} \leq C \left\{ |g + \langle \mathbf{a}, \mathbf{x} \rangle|_{\alpha, \omega^*} + |v|_0 \right\} . \quad (3.4)$$

For the constants  $\mathbf{a} = (a_i)$  and the zero norm of  $v$  we have the following estimates,

**Lemma 3.4** (i)  $|a_i| \leq \frac{3}{d(0, \omega^*)} |g|_{0, \omega^*}$ , where  $d(0, \omega^*) = \text{dist}(0, \omega^*)$ .

(ii) There exists a constant  $C'$  such that  $|v|_0 \leq C' |g|_{0, \omega^*}$ .

**Proof.** From the interior estimates of derivatives of harmonic functions (Gilbarg and Trudinger 1983, Theorem 2.11), we have

$$|a_i| \leq \frac{3}{d(0, \omega^*)} \sup_{\Omega^*} |G| = \frac{3}{d(0, \omega^*)} |G|_0 ,$$

and since  $|G|_0 = |g|_{0, \omega^*}$ , we may conclude (i).

Let  $\varepsilon > 0$  be such that  $B_\varepsilon(\mathbf{0})$  is strictly contained in  $\Omega^*$ . We consider the two possibilities: (a)  $\mathbf{x} \in \bar{B}_\varepsilon(\mathbf{0})$ ; (b)  $\mathbf{x} \in \Omega_\varepsilon = \{\mathbf{x} \in \Omega^* : r > \varepsilon\}$ . In case (a), by Taylor's theorem for any  $t \in (0, r)$  there is a  $t' \in (0, t)$  such that

$$v(\mathbf{x}) = G(\mathbf{0}) - r \frac{1}{2!} \int_0^r \sum_{i,j} D_{ij} G(t'\sigma) \sigma_i \sigma_j dt$$

where  $D_{ij} G = \partial^2 G / \partial x_i \partial x_j$ . The interior estimates for the second order derivatives of  $G$  (Gilbarg and Trudinger 1983, Theorem 2.10) imply after some computations,

$$|v(\mathbf{x})| \leq \left( 1 + 162 \frac{\varepsilon^2}{d_0 d_\varepsilon} \right) |g|_{0, \omega^*}$$

where  $d_\varepsilon = \text{dist}(\bar{B}_\varepsilon(0), \omega^*) = d_0 - \varepsilon$  and  $d_0 = d(0, \omega^*)$ .

In case (b) we may write

$$v(x) = G(0) - r \int_0^\varepsilon t^{-2} \varphi_x(t) dt - r \int_\varepsilon^r t^{-2} \varphi_x(t) dt$$

where  $\varphi_x(t) = G(t\sigma) + t\langle a, \sigma \rangle - G(0)$ . For the first two terms we obtain in a similar manner

$$\left| G(0) - r \int_0^\varepsilon t^{-2} \varphi_x(t) dt \right| \leq \left( 1 + 162 M \frac{\varepsilon}{d_0 d_\varepsilon} \right) |g|_{0, \omega^*}$$

where  $M = \sup_{x \in \omega^*} r(x)$ .

For the last term we have,

$$\begin{aligned} \left| r \int_\varepsilon^r t^{-2} \varphi_x(t) dt \right| &\leq r |g|_{0, \omega^*} \int_\varepsilon^r (2t^{-2} + \frac{3}{d_0} t^{-1}) dt \\ &= \left[ 2 \left( \frac{r}{\varepsilon} - 1 \right) + \frac{3}{d_0} r (\ln r - \ln \varepsilon) \right] |g|_{0, \omega^*} \\ &\leq \left[ 2 \left( \frac{M}{\varepsilon} - 1 \right) + \frac{3}{d_0} M \ln \left( \frac{M}{\varepsilon} \right) \right] |g|_{0, \omega^*}. \end{aligned}$$

We then have for any point  $x \in \Omega^*$  the inequality

$$|v(x)| \leq \left[ 1 + 162M \frac{\varepsilon}{d_0 d_\varepsilon} 2 \left( \frac{M}{\varepsilon} - 1 \right) + \frac{3}{d_0} M \ln \left( \frac{M}{\varepsilon} \right) \right] |g|_{0, \omega^*}$$

and hence for  $|v|_0$ .

If, in particular, we choose  $\varepsilon = \frac{d_0}{2}$ , we get (ii) with

$$C' = (166 + 3 \ln 2) D + 3D \ln D - 1$$

where  $D = \frac{M}{d_0}$ .  $\square$

Introducing the estimates of Lemma 3.4 into (3.4) we get for  $v$  the estimate

$$|v|_{1+\alpha} \leq K |g|_{\alpha, \omega^*} \quad (3.5)$$

where

$$K = C \left[ 1 + \frac{3}{d_0} |\mathbf{x}|_{\alpha, \omega}^* + C' \right] .$$

#### 4. An existence theorem

In order to give a sufficient condition for the convergence of the series (2.3), we shall consider the equivalent boundary value problems to (2.4a, b) for the function  $K[T_n]$  in the domain bounded by  $\iota(\Sigma) = \Sigma^*$ . For simplicity we shall write  $v_n$  instead of  $K[T_n]$ , and by  $\Omega^*$  we shall denote the domain interior to  $\Sigma^*$ .

Simple computations lead to the following sequence of boundary problems:

$$\begin{cases} \Delta v_0 = 0 & \text{in } \Omega^* \\ v_0 - \langle \nabla v_0, \mathbf{x} \rangle = g + \langle \mathbf{a}_0, \mathbf{x} \rangle & \text{on } \Sigma^* \\ \nabla v_0(0) = 0 & \end{cases} \quad (4.1a)$$

and for  $n > 0$ ,

$$\begin{cases} \Delta v_n = 0 & \text{in } \Omega^* \\ v_n - \langle \nabla v_n, \mathbf{x} \rangle = -\gamma v_{n-1} - \langle \nabla v_{n-1}, \beta \rangle + \langle \mathbf{a}_n, \mathbf{x} \rangle & \text{on } \Sigma^* \\ \nabla v_n(0) = 0 & \end{cases} \quad (4.1b)$$

where  $g = -r^{-1} \Delta^* g$ ,  $\gamma = \cos^2 \phi - r^{-2} x_3^2$ ,  $\beta = \beta_1 + \beta_2$  where  $\beta_1 = -2r^{-2} x_3^2 \mathbf{x}$  and  $\beta_2 = (0, 0, x_3)$ , and  $\mathbf{a}_0 = (a_{1,0})$ ,  $\mathbf{a}_n = (a_{1,n})$ .

If  $g \in C^\alpha(\Sigma^*)$ , then  $v_n \in C^{1,\alpha}(\bar{\Omega}^*)$  for any  $n \geq 0$ . On the other hand, from basic properties of the Hölder norms we get

$$\begin{aligned} |\gamma v_n + \langle \nabla v_n, \beta \rangle|_{\alpha, \Sigma^*} &\leq |\gamma v_n|_{\alpha, \Sigma^*} + |\langle \nabla v_n, \beta \rangle|_{\alpha, \Sigma^*} \\ &\leq C_* \{ |\gamma|_{0, \Sigma^*} |v_n|_{\alpha, \Sigma^*} + |\gamma|_{\alpha, \Sigma^*} |v_n|_{0, \Sigma^*} \} + \sum_{i=1}^3 |\beta_i D_i v_n|_{\alpha, \Sigma^*} \\ &\leq C_* C_\gamma |v_n|_{\alpha, \Sigma^*} + \sum_{i=1}^3 \left[ C_* \{ |D_i v_n|_{0, \Sigma^*} |\beta_i|_{\alpha, \Sigma^*} + |D_i v_n|_{\alpha, \Sigma^*} |\beta_i|_{0, \Sigma^*} \} \right] \\ &\leq C_* C_\gamma |v_n|_\alpha + C_* C_\beta |v_n|_{1+\alpha} \end{aligned}$$

where  $C_\gamma = |\gamma|_{0, \Sigma^*} + |\gamma|_{\alpha, \Sigma^*}$  and  $C_\beta = |\beta|_{0, \Sigma^*} + |\beta|_{\alpha, \Sigma^*}$ .

In addition there is a constant  $Z$  such that

$$|v_n|_\alpha \leq Z |v_n|_{1+\alpha} ,$$

and we conclude

$$|\gamma v_n + \langle \nabla v_n, \beta \rangle|_{\alpha, \Sigma^*} \leq C_*(C_\gamma Z + C_\beta) |v_n|_{1+\alpha} \quad (4.2)$$

for any  $n \geq 0$ . Therefore, from (4.2) and (3.5) we have for  $n \geq 1$

$$\begin{aligned} |v_n|_{1+\alpha} &\leq KC_* (C_\gamma Z + C_\beta) |v_{n-1}|_{1+\alpha} \\ &\leq K^2 C_*^2 (C_\gamma Z + C_\beta)^2 |v_{n-2}|_{1+\alpha} \\ &\quad \dots \quad \dots \\ &\leq K^n C_*^n (C_\gamma Z + C_\beta)^n |v_0|_{1+\alpha} \\ &\leq K^{n+1} C_*^n (C_\gamma Z + C_\beta)^n |g|_{\alpha, \Sigma^*} , \end{aligned} \quad (4.3)$$

since  $|v_0|_{1+\alpha} \leq K|g|_{\alpha, \Sigma^*}$ .

For the constants  $a_{i,n}$  ( $n \geq 1$ ), since  $d(0, \Sigma^*) = a^{-1}$  we obtain

$$\begin{aligned} |a_{i,n}| &\leq 3aC_{\gamma\beta} |v_{n-1}|_{1+\alpha} \\ &\leq 3aC_{\gamma\beta} KC_* (C_\gamma Z + C_\beta) |v_{n-2}|_{1+\alpha} \\ &\quad \dots \quad \dots \\ &\leq 3aC_{\gamma\beta} K^{n-1} C_*^{n-1} (C_\gamma Z + C_\beta)^{n-1} |v_0|_{1+\alpha} \\ &\leq 3aC_{\gamma\beta} K^{n-1} C_*^{n-1} (C_\gamma Z + C_\beta)^{n-1} |g|_{\alpha, \Sigma^*} \\ &= 3aC_{\gamma\beta} C_*^{-1} (C_\gamma Z + C_\beta)^{-1} K^n C_*^n (C_\gamma Z + C_\beta)^n |g|_{\alpha, \Sigma^*} , \end{aligned} \quad (4.4)$$

where  $C_{\gamma\beta} = |\gamma|_{0, \Sigma^*} + |\beta|_{0, \Sigma^*}$ .

**Theorem 4.1** Let  $g \in C^\alpha(\Sigma^*)$ . Let  $v_n \in C^{1,\alpha}(\bar{\Omega}^*)$  and  $a_{i,n} \in \mathbb{R}$  be the sequences defined by (4.1a), (4.1b). If

$$\epsilon^2 KC_* (C_\gamma Z + C_\beta) < 1 ,$$

then the series  $\sum_{n=0}^{\infty} \epsilon^{2n} v_n$  and  $\sum_{n=0}^{\infty} \epsilon^{2n} a_{i,n}$  are absolutely convergent in  $C^{1,\alpha}(\bar{\Omega}^*)$  and  $\mathbb{R}$  respectively (and therefore convergent).

Moreover,  $v = \sum_{n=0}^{\infty} \epsilon^{2n} v_n \in \mathcal{H}(\Omega^*) \cap C^{1,\alpha}(\bar{\Omega}^*)$ ,  $\nabla v(0)=0$  and

$$v - \langle \nabla v, \mathbf{x} \rangle + \epsilon^2 [\gamma v + \langle \nabla v, \beta \rangle] = g + \sum_{i=1}^3 a_i x_i \quad \text{on } \Sigma^* \quad (4.5)$$

where  $a_i = \sum_{n=0}^{\infty} \epsilon^{2n} a_{i,n}$ .

**Proof.** The first part is quite clear, since from (4.3) and (4.4) we have

$$\begin{aligned} \epsilon^{2n} |v_n|_{1+\alpha} &\leq K |g|_{\alpha, \Sigma^*} \kappa^n \\ \epsilon^{2n} |a_{i,n}| &\leq 3aC_{\gamma\beta} C_*^{-1} (C_\gamma Z + C_\beta)^{-1} |g|_{\alpha, \Sigma^*} \kappa^n \end{aligned}$$

where  $\kappa = \epsilon^2 K C_* (C_\gamma Z + C_\beta) < 1$ . Hence  $\sum_{n=0}^{\infty} \epsilon^{2n} v_n$  and  $\sum_{n=0}^{\infty} \epsilon^{2n} a_{i,n}$  are absolutely convergent, and

$$\begin{aligned} \left| v = \sum_{n=0}^{\infty} \epsilon^{2n} v_n \right|_{1+\alpha} &\leq \sum_{n=0}^{\infty} \epsilon^{2n} |v_n|_{1+\alpha} < \infty , \\ \left| a_i = \sum_{n=0}^{\infty} \epsilon^{2n} a_{i,n} \right| &\leq \sum_{n=0}^{\infty} \epsilon^{2n} |a_{i,n}| < \infty . \end{aligned}$$

In particular,  $\left| \sum_{n=0}^N \epsilon^{2n} v_n - v \right|_0 \rightarrow 0$  as  $N \rightarrow \infty$ , and since the limit of a uniformly convergence sequence of harmonic functions is harmonic (see, for example, Gilbarg and Trudinger 1983, Theorem 2.8), then  $v \in \mathcal{H}(\Omega^*)$ . For any  $n \geq 0$   $\nabla v_n(0) = 0$ , so that  $\nabla v(0) = \sum_{n=0}^{\infty} \epsilon^{2n} \nabla v_n(0) = 0$ . We finally get (4.5) just noting that

$$S_{v,N} - \langle \nabla S_{v,N}, \mathbf{x} \rangle = g - \epsilon^2 [\gamma S_{v,N} + \langle \nabla S_{v,N}, \beta \rangle] + \sum_{i=1}^3 S_{i,N} x_i \quad \text{on } \Sigma^*$$

where  $S_{v,N} = \sum_{n=0}^N \epsilon^{2n} v_n$  and  $S_{i,N} = \sum_{n=0}^N \epsilon^{2n} a_{i,n}$ .  $\square$

## REFERENCES

Bjerhammar, A. (1966) *On the determination of the shape of the geoid and the shape of the earth from ellipsoidal surface of reference*, Bull. Geod., 81, 235-264.

Dautray, R. and Lions, J-L. (1990) Mathematical analysis and numerical methods for science and technology, Vol.1, Springer-Verlag, Berlin/Heidelberg/New York.

Gilbarg, D. and Trudinger, N.S. (1983) Elliptic partial differential equations of second order, 2nd. Ed., Springer-Verlag, Berlin/Heidelberg/ New York/ Tokyo.

Heck, B. (1991) *On the linearized boundary value problems of physical geodesy*, Dept. of Geod. Sci. Rep. 407, Ohio State Univ., Columbus.

Heiskanen, W.A. and Moritz, H. (1967) Physical Geodesy, W.H. Freeman and Co., San Francisco/Londres.

Holota, P. (1981) *Direct methods for geodetic boundary problems*, Proceedings 4th. Int. Symp. "Geodesy and Physics of the Earth", Veröff. d. Zentr. Inst. f. Phys. d. Erde, Nr. 63, 2, Potsdam, 215-230.

Hörmander, L. (1976) *The boundary problems of physical geodesy*, Arch. Rational Mech. Anal., 62, 1-52.

Jorge, M.C. (1987) *Local existence of the solution to a nonlinear inverse problem in gravitation*, Quart. Appl. Math., 45 (2), 287-292.

Krarup, T. (1973) *Letters on Molodensky's problem*, Unpublished manuscript.

Lieberman, G.M. (1986) *Intermediate Schauder estimates for oblique derivative problems*, Arch. Rational Mech. Anal., 93 (2), 129-134

Molodenskii, M. S., Eremeev, V. F. and Yurkina, M. I. (1962) Methods for study of the external gravitational field and figure of the earth, Transl. from Russian (1960), Israel Program for Scientific Translations, Jerusalem.

Otero, J. (1995) Unpublished manuscript, in preparation. (Tentative title: *A uniqueness theorem for Zagrebin's problem*.)

Sacerdote, F. and Sansò, F. (1983) *The current situation in the linear problem of Molodenskii*, Atti. Accad. Naz. Lincei Cl. Sci. Fis. Mat. Natur. Rend. Lincei (8) 75, 119-126.

Sacerdote, F. and Sansò, F. (1990) *On the analysis of the fixed-boundary gravimetric boundary-value problem*, Proceedings II Hotine-Marussi Symposium, Pisa, 507-516

Sansò, F. (1978) *The local solvability of Molodensky's problem in gravity space*, Man. Geod., 3, 157-227.

Sansò, F. (1981a) *Recent advances in the theory of the geodetic boundary value problem*, Rev. Geophys. Space Phys., 19, 437-449.

Sansò, F. (1981b) *The point on the simple Molodensky's problem*, Atti. Accad. Naz. Lincei Cl. Sci. Fis. Mat. Natur. Rend. Lincei (8) 71, 87-94.

# Solution of the geodetic boundary value problem in spectral form

M.S.Petrovskaya

Institute of Theoretical Astronomy,  
Naberezhnaya Kutuzova 10, St. Petersburg, 191187, Russia

**Summary.** Proceeding from the earlier constructed solution of the scalar free boundary value problem (BVP) for the Earth's potential, several kinds of new formulas are presented for the spectral characteristics of the geopotential. An explicit analytical formula is derived for a geopotential harmonic coefficient as a function of the surface gravity anomaly, Earth's figure ellipticity and terrain topography. Then several basic linear relations are constructed, as well, between the whole set of the harmonic coefficients and gravity anomaly data. These relations can be applied for constructing BVP spectral solution by collocation technique. They can be also used for solving an inverse problem, i.e. the determination of the gravity anomaly on the basis of a known geopotential model.

A procedure for evaluating the geopotential harmonic coefficients on the base of surface gravity data was first elaborated by Zhongolovich (1956). Since then, a great progress has been made in the development of analytical methods and numerical techniques for solving this problem. They are discussed, in particular, in (Molodensky et al. 1962), (Heiskanen and Moritz 1979), (Forsberg and Tscherning 1981), (Jekeli 1981), (Tscherning 1981), (Pellinen 1982), (Hajela 1984), (Rapp 1984), (Wenzel 1985), (Cruz 1986), (Rapp and Cruz 1986 a,b), (Pavlis 1988), (Sjoeberg 1988, 1989), (Heck 1990), (Rapp and Pavlis 1990), (Wang 1990). Because the present paper deals only with analytical relations between basic geodetic quantities, within the frames of the continuous boundary value problem, we have not mentioned a great number of papers in which advanced numerical procedures were elaborated for practical realization of theoretical concepts.

When evaluating the Earth's potential harmonic coefficients from gravity data, two principal approaches exist. One of them aims at deriving an integral expression or an explicit analytical formula for a harmonic coefficient as a solution of an exterior boundary value problem (BVP) for the geopotential. In the alternative procedure, certain basic linear relations are constructed, between the unknowns and gravity data, which are solved by collocation techniques. The problem is complicated on account of the non-spherical terrain surface which makes it necessary to refine a simple solution for the spherical approximation by correction terms induced by the Earth's figure ellipticity and surface topography. It can be noted, however, that some of the known procedures for deriving such correction terms suffer from certain preliminary assumptions for the Earth's density distribution or additional information on the potential functions, besides the gravity anomaly (Heiskanen and Moritz 1979).

In the present paper new formulas are presented for the Earth's potential coefficients, corresponding to the two different approaches mentioned above. When deriving them, no problem of up/downward gravity reduction (or formal analytical continuation) from the terrain surface is performed, by means of Taylor series in particular. No problem

of the solid harmonic series application for the geopotential at the Earth's surface (or the reference ellipsoid) is involved either. The correction terms arise in a "natural" way, proceeding from the strict solution of the scalar free boundary value problem which was derived earlier (Petrovskaya 1994 a,b). This solution was based on the presentation of the Earth's potential in the form of the generalized potential proposed by Brovar (1964 a). The latter has an advantage, as compared with other known forms of the surface potentials, in particular the single layer potential used by Molodensky (Molodensky et al. 1962). This Brovar's potential has a weak (logarithmic) singularity of the integral kernel (which can be removed after rotating the reference set) and therefore essentially simplifies the procedure of BVP solving.

Several kinds of formulas for determination of the geopotential harmonic coefficients will be provided below. First, an explicit analytical formula will be derived for a harmonic coefficient in terms of the gravity anomaly harmonic coefficients, with due regard for the ellipticity and surface topography. Then three basic linear relations will be constructed between the whole set of the geopotential coefficients and observed gravity data. They can be used for deriving observation equations for evaluating the geopotential coefficients from surface gravity data. One of them is especially convenient for solving the inverse problem, i.e. the determination of the gravity anomaly, unknown in some regions, on the base of a geopotential model derived, in particular, from satellite gradiometry observations.

Let us consider the disturbing potential  $T = V - U$ , where  $V$  is the Earth's gravitational potential and  $U$  is the potential of the normal ellipsoid. The latter is chosen in the standard way:  $U_0$  (on the ellipsoid surface) equals  $V_0$  (at the initial point); the ellipsoid mass equals the Earth's one; the mass centers coincide with the origin of the reference set. Then the expansion of potential  $T$  in spherical functions does not contain the zero and first degree harmonics. On and outside the sphere  $\Sigma_0$  of radius  $R_0$ , enveloping the Earth (Brillouin sphere), the disturbing potential  $T$  is presented as the following series of the solid spherical harmonics:

$$T(r, \theta, \lambda) = \frac{kM}{r} \sum_{n=2}^{\infty} \sum_{m=-n}^n \left(\frac{R_0}{r}\right)^n \bar{C}_{n,m} \bar{Y}_{n,m}(\theta, \lambda), \quad (1)$$

$$\bar{Y}_{n,m}(\theta, \lambda) = \bar{P}_{n,|m|}(\cos \theta) \begin{cases} \cos m\lambda, & m \geq 0, \\ \sin m\lambda, & m < 0. \end{cases} \quad (2)$$

Here  $kM$  is the gravitational constant multiplied by the Earth's mass;  $r, \theta, \lambda$  are the geocentric distance, polar angle and longitude of a point  $P$  under consideration;  $\bar{P}_{n,m}$  are fully normalized Legendre functions. By  $\bar{C}_{n,m}$  the corresponding fully normalized harmonic coefficients are denoted. As the normalizing factor, the radius  $R_0$  of the enveloping sphere  $\Sigma_0$  is chosen and not the generally used major semi-axis of the reference ellipsoid, since it essentially simplifies the formulas at the rigorous consideration of the problem. The even zonal harmonic coefficients are equal to the differences between those for the Earth's gravitational potential  $V$  and the corresponding coefficients of the normal potential  $U$ . We shall call  $\bar{C}_{n,m}$  simply the geopotential harmonic coefficients.

The expansions of  $T$  and  $\Delta g$  at the terrain surface can have the zero and first degree harmonics, as opposed to their expansions on / outside enveloping sphere  $\sigma_0$ .

The global gravity anomaly data (obtained directly at the Earth's surface and / or evaluated by satellite observations) is presented as the spherical harmonic series:

$$\begin{aligned}\Delta g &= \sum_{n=0}^{\infty} \Delta g_n, \\ \Delta g_n &= \sum_{m=-n}^n \bar{A}_{n,m} \bar{Y}_{n,m}(\theta, \lambda).\end{aligned}\tag{3}$$

In the spherical approximation, the coefficients in (1) and (3) are related as follows

$$\frac{kM}{a^2} \bar{C}_{n,m} = \frac{\bar{A}_{n,m}}{n-1}, \quad n = 2, 3, \dots\tag{4}$$

where  $a$  is the major semi-axis of the normal ellipsoid.

In the same approximation, the geopotential harmonic coefficients can be also evaluated by the well-known linear relation:

$$\frac{kM}{a^2} \sum_{n=2}^{\infty} \sum_{m=-n}^n (n-1) \bar{C}_{n,m} \bar{Y}_{n,m}(\theta, \lambda) = \Delta g.\tag{5}$$

This relation is convenient for combined treatment of satellite and gravimetric observations.

The formulas of spherical approximation, (4), (5), will be properly refined below for the effect of the Earth's ellipticity and surface topography.

Earlier (Petrovskaya 1994 a,b), starting from Brovar's (1964 a) generalized potential, a new formula was derived for the geopotential, corresponding to the refined boundary value condition for the normal field ellipticity. It has the form of the disturbed Stokes integral, valid both at the Earth's surface and outside it. At the chosen parameters of the normal ellipsoid and the reference set, the potential  $T$  on the enveloping sphere  $\Sigma_0$ , can be presented as

$$T = \frac{a}{4\pi} \int_{\sigma_1} \Delta G S(\psi) d\sigma_1,\tag{6}$$

where

$$\Delta G = \Delta g \left(1 + \frac{\delta a}{a}\right) - (h_1 - h_0) \frac{\partial \Delta g}{\partial h_1} + K + e^2 L,\tag{7}$$

$$K = \frac{1}{8\pi} \int_{\sigma_2} \nu^{(2)} \left(\frac{h_2 - h_1}{l_{12}}\right)^2 \frac{d\sigma_2}{\rho_{12}},\tag{8}$$

$$L = (2 - 3 \cos^2 \theta_1) \sum_{n=2}^{\infty} \frac{\Delta g_n}{n-1} - \sin \theta_1 \cos \theta_1 \frac{\partial}{\partial \theta_1} \sum_{n=2}^{\infty} \frac{\Delta g_n}{n-1},\tag{9}$$

$$\rho_{12} = 2 \sin \frac{\psi_{12}}{2}, \quad \delta a = R_0 - a.\tag{10}$$

Here the following notations were used:  $e$  = first eccentricity of the reference ellipsoid;  $\sigma_1$  and  $\sigma_2$  mean the unit spheres which replace (after transformations) the telluroid;  $\theta_1 =$

polar angle of a current point  $P_1$  on the telluroid, projected on sphere  $\sigma_1$ ;  $\psi$  = angular distance between a fixed point  $P_0$  on sphere  $\Sigma_0$  and  $P_1$ ;  $\psi_{12}$  = angular distance between current points  $P_1$  and  $P_2$  projected on spheres  $\sigma_1$  and  $\sigma_2$ . By  $h_0, h_1$  and  $h_2$  are designated the heights of points  $P_0, P_1$  and  $P_2$  above the inner sphere  $\Sigma$  of radius  $R = b = a(1 - \frac{1}{2}e^2)$  where  $b$  is the minor semi-axis of the reference ellipsoid.

Function  $\Delta G$  represents a disturbed gravity anomaly (with respect to  $\Delta g$ );  $\nu^{(2)}$  is the generalized density  $\nu$  in the spherical approximation, corresponding to integration sphere  $\sigma_2$ . The physical meaning of the generalized density is (Petrovskaya 1994 a):

$$\nu = -2a \frac{\partial \Delta g}{\partial h} - 3\Delta g, \quad (11)$$

where  $\partial \Delta g / \partial h$  is the vertical derivative of  $\Delta g$  in the spherical approximation:

$$\frac{\partial \Delta g}{\partial h} = -\frac{1}{a} \sum_{n=2}^{\infty} (n+2) \Delta g_n. \quad (11^*)$$

The kernel of the integral (6) is Stokes' function which can be expanded as follows

$$S(\psi) = \sum_{n=2}^{\infty} \frac{2n+1}{n-1} P_n(\cos \psi), \quad (12)$$

with  $P_n(\cos \psi)$  being Legendre polynomials.

Let us simplify formulas (6)-(10) by retaining the terms of only the first order with respect to small quantities, which is sufficient for practical applications.

We have

$$h_0 = \frac{1}{2}ae^2 + \delta a, \quad h_k = \frac{1}{2}ae^2 \sin^2 \theta_k + H_k, \quad k = 1, 2, \quad (13)$$

where  $H_1$  and  $H_2$  are the normal heights of  $P_1$  and  $P_2$  which will be further referred, for simplicity, as the topographic heights.

Consider the integral (8). By the application of simple (but rather cumbersome) transformations, similar to the ones performed in (Petrovskaya 1994 a, Sec. 3), this integral, at the accepted approximation, can be presented as

$$K = \frac{1}{2}\nu^{(1)} \left( \frac{\partial H_1}{\partial l_1} \right)^2 \sin \frac{\psi_0}{2}. \quad (14)$$

The error of this approximation of function (8) is a quantity of a higher order of smallness.

In (14)  $\psi_0$  means the radius of a small "cap"  $\sigma_0$  with the center at  $P_1$  and  $\nu^{(1)}$  is the mean value of function (11) over  $\sigma_0$ . When choosing the size of  $\sigma_0$  one can take into account that the contemporary "extended" geopotential models are constructed on the base of observations averaged over rectangular blocks of size  $0.5^0 \times 0.5^0$ . The expression  $(\partial H_1 / \partial l_1)^2$  represents the mean value of the derivative, squared, of the topographic height over all the directions  $l_1$  at point  $P_1$  (averaging over the azimuth). This expression is approximately equal to  $\sin^2 \beta_1$  where  $\beta_1$  is the mean terrain inclination in point  $P_1$ . It can be noted, however, that  $\sin^2 \beta_1$  does not enter explicitly the solution (6)-(10).

In connection with the emergence of terms, depending on the inclination  $\beta_1$ , the following remark is appropriate. In any approach to the solution of BVP (at least by surface integrals or the formal analytical continuation) the inclination is involved, in some way. In particular, Molodensky solution (Molodensky et al. 1962) contains  $\tan^2 \beta_1$ , which "spoils" the convergence of the iteration procedure and demands essential smoothing the terrain surface, as opposed to the present solution, dependent on  $\sin^2 \beta_1$ . The same is true for Brovar solution (Brovar 1964 b, pp. 171-172) and Moritz gradient solution (Moritz 1980) since they are equivalent to the Molodensky one (ibid., Sec. 46). Thus the absence of terms in a solution, dependent on the inclination, can only mean that the corresponding terms are simply omitted in the accepted approximation.

The disturbed anomaly (7) can be transformed to a form of an unique expansion in harmonics (3) with constant coefficients if one uses formulas for spherical function transformations, provided, for instance, in (Moritz 1980, (III.500), (III.530)), just in the same way as was performed in (Cruz 1986). As a result, the following formula can be derived from (1)-(3) and (6)-(14) for the "disturbed" harmonic coefficient:

$$\begin{aligned} \frac{kM}{a^2} \bar{C}_{n,m} &= \left[ \frac{1}{n-1} - \frac{n}{n-1} \frac{\delta a}{a} - e^2 q_{nm} \right] \bar{A}_{n,m} - \\ &- e^2 u_{nm} p_{nm} \bar{A}_{n-2,m} - e^2 v_{nm} r_{nm} \bar{A}_{n+2,m} + \frac{1}{n-1} \Delta G^t_{n,m}, \quad n = 2, 3, \dots \end{aligned} \quad (15)$$

Here

$$\Delta G^t_{n,m} = \frac{1}{4\pi} \int_{\sigma} \Delta G^t \bar{Y}_{n,m}(\theta, \lambda) d\sigma. \quad (15^*)$$

In (15) constants  $\bar{A}_{n,m}$  are the harmonic coefficients of  $\Delta g$ , presented in (3);  $\sigma$  is the unit sphere. By  $\Delta G^t$  the topographic correction for the gravity anomaly  $\Delta g$  is designated. With the use of (7)-(14), (11\*) and formulas from (Petrovskaya 1994 a) this correction can be expressed as

$$\Delta G^t = -a \frac{\partial \Delta g}{\partial H_1} \left[ \frac{H_1}{a} + \sin^2 \beta_1 \sin \frac{\psi_0}{2} \right] - \frac{3}{2} \Delta g \sin^2 \beta_1 \sin \frac{\psi_0}{2} \quad (16)$$

or, in another form,

$$\Delta G^t = G \left[ \frac{H_1}{a \sin \psi_0} + \frac{1}{2} \sin^2 \beta_1 \right] + \frac{3}{2} \frac{H_1}{a} \Delta g. \quad (16^*)$$

Here

$$G = \Delta g - \sum_{n=2}^{\infty} c_n(\psi_0) \Delta g_n. \quad (17)$$

Constants  $c_n(\psi_0)$  can be evaluated by the recurrence relation

$$\begin{aligned} c_n &= 2c_{n-1} - c_{n-2} - 2t^2(1-t^2)^{1/2} \frac{(2n-1)}{n(n-1)} P_{n-1,1}(\cos \psi_0), \\ c_0 &= 1-t, \quad c_1 = 1-3t+2t^3, \quad t = \sin \frac{\psi_0}{2}, \quad n = 2, 3, \dots \end{aligned} \quad (18)$$

It should be noted that the right hand side of (16 \*) is finite for any small  $\psi_0$ , according to the derivation of this formula in (ibid). From numerical estimates follows that for  $\psi_0 \geq 0.5^0$  one has  $|c_n| \leq 1$ . Therefore the series in (17) converges not worse than the expansion (3) for  $\Delta g$ , as opposed to series (11 \*) whose terms are, by the order,  $n$  times larger than for series in (3) and (17). In connection with the rapid convergence of series (17), the following remark is also appropriate. The high degree harmonics are not "lost" anyway in the corresponding expression for  $\partial\Delta g/\partial H_1$  since they are contained in the "observable"  $\Delta g$  in (17).

It can be noted that in (16), for  $\psi_0 \approx 0.5^0$ , the quantity  $\sin^2 \beta_1 \sin(\psi_0/2)$  can even exceed the "principal" correction term  $H_1/a$ , in mountain regions. Therefore, the corresponding additional terms in (16) and (16 \*) should be taken into account.

Formula (15) depends also on the constants ( $n = 2, 3, \dots$ ):

$$\begin{aligned} p_{nm} &= \frac{(n-k)(n-k-1)(n^2-n+2)}{2(n-1)(2n-3)(2n-1)(n-3)}, \quad n = 4, 5, \dots, k = |m|, \\ p_{nm} &= 0, \quad n = 2, 3, \\ q_{nm} &= \frac{n^2-m^2}{4(n-1)^2} + \frac{1}{4(n-1)} - \frac{15}{16} \frac{1}{(n-1)^2} - \frac{7}{16} \frac{(4m^2-1)}{(n-1)^2(2n+3)(2n-1)}, \\ r_{nm} &= \frac{(n^2+3n+4)(n+k+2)(n+k+1)}{2(n^2-1)(2n+3)(2n+5)}, \\ u_{nm}^2 &= \frac{(2n-3)(n+k-1)(n+k)}{(2n+1)(n-k)(n-k-1)}, \\ v_{nm}^2 &= \frac{(2n+5)(n-k+1)(n-k+2)}{(2n+1)(n+k+1)(n+k+2)}. \end{aligned}$$

It can be remarked that these constants remain finite with increasing  $n$ .

The above formulas take into account all the correction terms of order  $e^2$ ,  $\delta a/a$ ,  $H_1/a$  and  $\sin^2 \beta_1$ .

Parallel with the explicit analytical expression (15) for the harmonic coefficients, we can easily derive, from the above formulas, a linear relation between the whole set of  $\bar{C}_{n,m}$  and observational gravity data, depending on the ellipsoid eccentricity and topographic heights. It can serve as a basic relation for constructing observation equations.

Let us present functions (6) and (7) as spherical harmonic series:

$$T = \sum_{n=2}^{\infty} T_n, \quad (19)$$

$$\Delta G = \sum_{n=2}^{\infty} \Delta G_n. \quad (20)$$

Then the substitution of (12) and (20) into (6) gives for the harmonics in (19):

$$T_n = a \frac{\Delta G_n}{n-1}, \quad n = 2, 3, \dots$$

This relation can be rewritten as :

$$\sum_{n=2}^{\infty} (n-1) T_n = a \Delta G.$$

Here  $\Delta G$  is defined in (7)-(14) and the associated formulas.

By comparing (1) for  $r = R_0$  with (19), the latter relation can be presented as follows:

$$\frac{kM}{a^2} \sum_{n=2}^{\infty} \sum_{m=-n}^n (n-1) \bar{C}_{n,m} \bar{Y}_{n,m}(\theta, \lambda) = \overline{\Delta g}, \quad (21)$$

where the "disturbed" anomaly is

$$\overline{\Delta g} = (1 + \frac{\delta a}{a}) \Delta G, \quad \delta a = R_o - a. \quad (22)$$

In (7), (9) and consequently (22), there are the partial derivatives of harmonics  $\Delta g_n$ , multiplied by functions of  $\theta_1$ . These derivatives can be removed and the whole function (22) expressed in terms of spherical functions (2) and  $\Delta g$ . It can be performed with the use of formulas (3) and the spherical approximation relations (11\*) and (4) (applied in the perturbation terms), as well as the spherical function transformations provided in (Moritz 1980, (III. 498)). As a result, the following basic relation is obtained from (21), (22):

$$\frac{kM}{a^2} \sum_{n=2}^{\infty} \sum_{m=-n}^n (n-1) [(1 + f_n) \bar{Y}_{n,m}(\theta, \lambda) + f_{n,m} \bar{Y}_{n+1,m}(\theta, \lambda)] \bar{C}_{n,m} = \Delta g + \Delta G^t. \quad (23)$$

Here

$$\begin{aligned} f_n &= \frac{e^2}{2} \left( n + \frac{2}{n-1} \right) \cos^2 \theta - \frac{2}{n-1} e^2 + n \frac{\delta a}{a}, \\ f_{n,m} &= e^2 \left( 1 + \frac{2}{n-1} \right) \left( 1 - \frac{2}{2n+3} \right)^{1/2} \left( 1 - \frac{m^2}{(n+1)^2} \right)^{1/2} \cos \theta. \end{aligned} \quad (24)$$

The topographic correction  $\Delta G^t$  is presented by (16)-(18) and (16\*).

The potential (6), (7) does not contain the zero and first degree harmonics of the expansion for  $\Delta g$ . Therefore, we assume in (23) and the following relations, by  $\Delta g$ , the quantity  $\Delta g - \Delta g_0 - \Delta g_1$ .

Let us remark the following. The latter term  $e^2 L$  in the disturbed anomaly (7), presented by (9), emerged due to the refinement of the boundary value condition (Petrovskaya 1994 a) for the normal field ellipticity. The corresponding terms in (23), (24), as well as in (15), have the factor  $(n-1)$  in the denominators. It can be readily seen from (24), for instance, that these additional terms have the same order as the principal ellipsoidal correction terms, for low degree harmonics (in particular, for  $n=2, 3$ ). Therefore, the last term in (7) should be really taken into account.

Formula (23) can be also presented in another, more explicit form, if the gravity anomaly derivative, entering the topographic correction (16), is substituted by the series (11\*). It gives, after transformations:

$$\Delta g = \frac{kM}{a^2} \sum_{n=2}^{\infty} \sum_{m=-n}^n (n-1) [(1+f_n^*) \bar{Y}_{n,m}(\theta, \lambda) + f_{n,m} \bar{Y}_{n+1,m}(\theta, \lambda)] \bar{C}_{n,m}, \quad (25)$$

where

$$f_n^* = \frac{e^2}{2} \left( n + \frac{2}{n-1} \right) \cos^2 \theta - \frac{2}{n-1} e^2 + n \frac{\delta a}{a} - (n+2) \frac{H}{a} - (n+\frac{1}{2}) \sin^2 \beta \sin \frac{\psi_0}{2}.$$

The relation (25) is convenient for solving the inverse problem, i.e. the spherical synthesis of the unknown surface gravity anomaly  $\Delta g$ , in a certain region, on the base of a geopotential model derived from satellite observations. In this case formula (25) can be treated as a rigorous downward continuation of the spacial potential in spectral form to the terrain surface, with due regard for the Earth's ellipticity and surface topography.

The left-hand side of (25) depends on  $\cos \theta$ . For performing the spherical analysis (the determination of the geopotential coefficients) it is reasonable to transfer some terms to the other part of the equality. Then, at the accepted approximation, we shall have the following relation:

$$\frac{kM}{a^2} \sum_{n=2}^{\infty} \sum_{m=-n}^n (n-1) \bar{C}_{n,m} \bar{Y}_{n,m} = \Delta g - \sum_{n=2}^{\infty} \sum_{m=-n}^n (f_n^* \bar{A}_{n,m} + f_{n,m}^* \bar{A}_{n-1,m}) \bar{Y}_{n,m}, \quad (26)$$

where

$$f_{n,m}^* = f_{n-1,m}, n = 3, 4, \dots; f_{2,m}^* = 0, f_{n,n}^* = f_{n,-n}^* = 0.$$

The left-hand side of relation (26) represents a "pure" expansion with respect to the orthogonal basis (2), which is important for rigorous application of the mean square procedure, appropriate for a spherical surface. This relation is convenient for simultaneous treatment of surface and satellite data.

Thus, the spectral characteristics of the geopotential can be evaluated from the explicit analytical formula (15) or the basic linear relations (23) (25) and (26), with the supplementary formulas for the quantities involved.

## References

- Brovar V.V. (1964 a) Fundamental harmonic functions with a singularity on the segment and the solution of the exterior boundary value problem. Izv. vyssh. uchebn. zaved. Geodesiya i aerofotos'ema, vyp. 3, pp. 51-61 (in Russian).
- Brovar V.V. (1964 b) On the solutions of Molodensky's boundary value problem. Bulletin Geodesique, Nouvelle Serie, N.72, pp. 167-173.
- Cruz J.Y. (1986) Ellipsoidal corrections to potential coefficients obtained from gravity anomaly data on the ellipsoid. Dept. Geod. Sci., Ohio State Univ., Rep. 371.

- Forsberg R. and Tscherning C.C. (1981) The use of height data in gravity field approximation by collocation. *J. Geophys. Res.*, vol. 86, pp. 7843-7854.
- Hajela D.P. (1984) Optimal estimation of high degree gravity field from global set of  $1^0 \times 1^0$  anomalies to degree and order 250. *Dept. Geod. Sci., Ohio State Univ., Rep.* 358.
- Heck B. (1990) On the linearized boundary value problems of physical geodesy. *Dept. Geod. Sci., Ohio State Univ., Rep.* 407.
- Heiskanen W. A. and Moritz H. (1979) *Physical Geodesy*. Inst. of Physical Geodesy, Technical Univ., Graz, Austria.
- Jekeli C. (1981) The downward continuation to the earth's surface of truncated spherical and ellipsoidal harmonic series of the gravity and height anomaly. *Dept. Geod. Sci., Ohio State Univ., Rep.* 323.
- Molodensky M.S., Eremeev V.F., Yurkina M.I. (1962) Methods for the study of the external gravitational field and figure of the Earth. Israel Program for Scientific Translations. Jerusalem.
- Moritz H. (1980) *Advanced Physical Geodesy*. H. Wichmann Verlag, Karsruhe.
- Pavlis N.K. (1988) Modeling and estimation of a low degree geopotential model from terrestrial gravity data. *Dept. Geod. Sci., Ohio State Univ., Rep.* 386.
- Pellinen L. P. (1982) Effects of the earth's ellipticity on solving geodetic boundary value problem. *Bollettino di Geodesia Scienze Affini*, vol. 41, N. 1, pp. 89-103.
- Petrovskaya M.S. (1994 a) Construction of the solution of the scalar boundary value problem. *Manuscripta Geodaetica*, in press.
- Petrovskaya M.S. (1994 b) Compact formulas for the disturbing potential at the Earth's surface and in exterior space. *Manuscripta Geodaetica*, in press.
- Rapp R. H. (1984) The determination of high degree potential coefficient expansions from the combination of satellite and terrestrial gravity information. *Dept. Geod. Sci., Ohio State Univ., Rep.* 361.
- Rapp R. H. and Cruz J. Y. (1986 a) The representation of the earth's gravitational potential in a spherical harmonic expansion to degree 250. *Dept. Geod. Sci., Ohio State Univ., Rep.* 372.
- Rapp R. H. and Cruz J. Y. (1986 b) Spherical harmonic expansions of the earth's gravitational potential to degree 360 using 30' mean anomalies. *Dept. Geod. Sci., Ohio State Univ., Rep.* 376.
- Rapp R. H. and Pavlis N. K. (1990) The development of geopotential coefficient models to spherical harmonic degree 360. *J. Geophys. Res.*, vol. 95, N.B 13, pp. 21885- 21911.
- Sjoeberg L. E. (1988) A new integral approach to geopotential coefficient determination from terrestrial gravity or satellite altimetry data. *Bull Geod.*, vol. 62, pp. 93-101.
- Sjoeberg L. E. (1989) Integral formulas for geopotential coefficients determination from gravity anomaly versus gravity disturbances. *Bull. Geod.*, vol. 63, pp. 213-221.
- Tscherning C. C. (1981) Comparison of some methods for the detailed representation of the Earth's gravity field. *Reviews. of Geophysics and Space Physics*, vol. 19, pp. 213-221.

- Wang Y. M. (1990) The role of the topography in gravity gradiometer reductions and in the solution of the geodetic boundary value problem using analytical downward continuation. Geod. Dept. , Ohio State Univ., Rep. 405.
- Wenzel H.-G. (1985) Hochaufloesende Kugelfunktionsmodelle fuer das Gravitationspotential der Erde. Wiss. Arb. Fachrichtung Vermess. Univ. Hannover, ISSN 0174-1454, Hannover.
- Zhongolovich I. D. (1956) Determination of the dimensions of the general terrestrial ellipsoid. Inst. Theor. Astron., Trudy, vol. 6, pp. 5-66 (in Russian).

# GRAVITY REDUCTIONS VERSUS APPROXIMATE B.V.P.s.

F.Sanso', G.Sona - DIIAR Politecnico di Milano - Italy

## ABSTRACT

The reduction of gravity data from earth's surface to a reference surface where the proper Geodetic Boundary Value Problem can be solved is a central point in global geopotential modelling, and the analytical downward continuation commonly used, based on a first guess of the gravity field, gives rises to an iterative procedure whose convergence is strongly affected by terrain inclination and roughness. This problem is here formulated as a Dirichlet problem for the earth's surface, whose practical solution is not easy, due to the complexity of the boundary surface, but that is here solved in planar and in spherical approximation. The main result of this paper consists in the proof of a theorem stating that in planar and spherical approximation the first derivative operator is a contraction in the space of the functions continuous up to the boundary  $\Sigma$  (plane or sphere), and therefore the solution of the Dirichlet problem can really be obtained with an iterative procedure that is proved to be convergent. The importance of a good choice of the Taylor point where the first derivative operators are computed is also analysed.

Once that the data have been properly reduced, the corresponding anomalous potential  $T$  can be obtained by a convolution integral on the boundary with the simple Kernel  $1/2\pi l$ , in the planar case, or with the Stokes kernel, in the spherical case.

## 1 INTRODUCTION

One of the classical tasks of physical geodesy is to derive the anomalous potential  $T(x)$  of the gravity field on the surface approximating the actual surface of the earth (the telluroid), by using gravity anomalies  $\Delta g$  and potential (or orthometric heights) as input data (Heiskanen, Moritz, 1990; Rapp, Pavlis, 1990). This problem is usually translated into a Boundary Value Problem (B.V.P.), namely Molodenskii's problem, and its solution leads, via Bruns's relation

$$\zeta = T/\gamma \quad , \quad (1,1)$$

to the necessary correction between normal and ellipsoidal heights nowadays so important after the advent of spatial positioning methods.

Despite many attempts, most of the practical solutions of the Molodenskii's problem rely on a so-called "change of boundary method" (cf. Sanso', 1993), namely on tricks allowing the reduction of our data to a "simple surface" (e.g. a sphere, a plane) and solving B.V.P.s for such a simple geometrical surfaces (Heck, 1991).

Even in the classical solution by series expansion of this problem, what we do is just a repeated application of a spherical solution, giving rise to a series, the convergence of which is conditioned by the inclination and the roughness of the terrain (Moritz, 1973; Holota, 1991).

After all, by "solution of Molodenskii's problem" it is today understood, with some approximation, a solution in which the free air anomalies are simply reduced by truncated analytical downward continuation (Sideris, 1987), the simplest form of which is (cf. Fig. 1.1)

$$\Delta g_\varrho = \Delta g_s - h_\varrho \frac{\partial}{\partial r} \Delta g_s \quad (1.2)$$

$$\Delta g_\varrho = -\frac{\partial T}{\partial r} - \frac{2}{r} T \Big|_\varrho \quad . \quad (1.3)$$

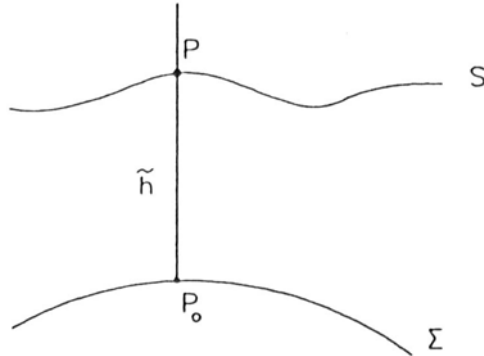


Fig. 1.1. Downward continuation on a spherical boundary.

$s$ = earth's telluroid

$\Sigma$ =reference sphere

Here, as we see, we are adopting a simple spherical approximation in the boundary operator and a first order continuation only.

Sometimes the problem is even reduced to a pure plane approximation formulation (cf. Fig. 1.2) with

$$\Delta g_\varrho = \Delta g_s - h_\varrho \frac{\partial}{\partial z} \Delta g_s \quad (1.4)$$

$$\Delta g_\varrho = -\frac{\partial T}{\partial z} \Big|_\varrho \quad . \quad (1.5)$$

Naturally, we could consider higher order expansions, and we shall shortly comment on them at the end of the paper, though we prefer here to concentrate on the first order only because this is by far the most important case.

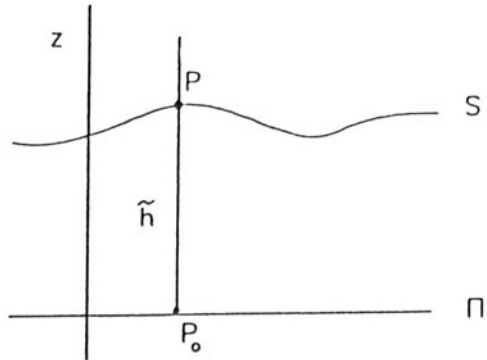


Fig. 1.2. Downward continuation on a reference plane.

$S$ = earth's telluroid

$\Sigma$ =reference plane

Let us first of all remark that, in the plane approximation,  $\Delta g = -\frac{\partial T}{\partial z}$  is a harmonic function in the half space  $z>0$ , as well as that  $r\Delta g = -r\frac{\partial T}{\partial r} - 2T$  is harmonic outside the earth's sphere  $\Sigma$ , when we adopt the spherical approximation.

In both cases therefore we are able to formulate the original problem as a simple Dirichlet problem, i.e. find  $u$  harmonic in space, attaining on  $S$  given values  $f(P)$ , as the corresponding potential  $T$  can always be achieved by a subsequent integration along a vertical line (parallel to  $z$  in plane approximation, in radial direction in spherical approximation).

Yet, even if formulated as a simple Dirichlet problem, the practical solution is far from easy, due to the great complexity of the boundary  $S$ , which mirrors the actual topography of the earth.

So we accept, instead of the original Dirichlet problem, the approximate "change of boundary" formulation:

(a) Plane approximation: find  $u$  harmonic in  $z>0$  and such that

$$u(Q) = f(P) - h_e \frac{\partial u(P)}{\partial z} \quad (1.6)$$

or, since  $P$  and  $Q$  are in biunivocal correspondence and  $f$  is the given datum,

$$u(Q) + h_e \frac{\partial u(P)}{\partial z} = f(P) = G(Q) \quad . \quad (1.7)$$

(b) Spherical approximation: using the radius of the reference sphere as the length unit, find  $u$  harmonic in  $r>1$  such that

$$u(Q) + h_e \frac{\partial u(P)}{\partial r} = f(P) = G(Q) \quad . \quad (1.8)$$

Let us note that in (1.7), (1.8) while Q spans the reference plane, respectively the reference sphere, P spans the telluroid S (of equation  $z = h_Q$ , respectively  $r = 1+h_Q$ ). Equations (1.7), (1.8) therefore imply the contemporary use of boundary and non-boundary functionals of the harmonic function  $u$ ; for this reason, we call the corresponding problems pseudo-boundary value problems.

A typical numerical solution of such problems, for instance in the plane case, is given in geodesy by starting with some model  $u_m$  to compute  $\frac{\partial}{\partial z} u_m(P)$  and then getting a first solution from

$$u_1(Q) = G(Q) - h_e \frac{\partial}{\partial z} u_m(P) ; \quad (1.9)$$

when needed, a better solution is computed by

$$u_2(Q) = G(Q) - h_Q \frac{\partial}{\partial z} u_1(P) \quad (1.10)$$

and so on.

This procedure seems to be a simple iterative solution of (1.7) and it is the main purpose of this paper to show that this iterative scheme is well founded; it is a striking result that a space where the iteration converges is simply the space of continuous functions  $C(\Sigma)$ , contrary to most of the main results of potential theory for which the use of Hölder spaces is mandatory (Miranda, 1970; Sansò, Sacerdote, 1991).

To be definite let us specify from now on that we will denote with  $C(\Sigma)$  the (Banach) space of harmonic functions continuous up to the boundary endowed with the Sup norm.

We just note, closing this paragraph, that once a solution of (a) or (b) is found, the corresponding anomalous potential T can be obtained by a convolution integral on the boundary, either with a simple kernel  $\frac{1}{2\pi} I^{-1} = \frac{1}{2\pi} |\underline{x} - \underline{y}|^{-1}$ , for the case (a), or with the Stokes kernel  $S(\psi_{\underline{x}, \underline{y}})$  for case (b).

## 2 ON THE IMPORTANCE OF THE CHOICE OF THE TAYLOR POINT P

Before deriving the main result of the paper, we want to illustrate how crucial is the choice of the Taylor point P in (1.7), (1.8).

We do that in spherical approximation by using an elementary case in which S is a sphere concentric with  $\Sigma$ , having equation (see Fig. 2.1)

$$r = 1+h \quad h = \bar{h} \text{ constant} \quad (2.1)$$

Then, considering the harmonic expansions of the known and of the unknown term

$$G(Q) = \sum_{nm} G_{nm} Y_{nm}(\sigma_\varrho) \quad , \quad (2.2)$$

$$u(P) = \sum_{nm} u_{nm} \frac{1}{r_P^{n+1}} Y_{nm}(P) \quad , \quad (2.3)$$

the solution of (1,8) becomes

$$\left[ 1 - \frac{\bar{h}(n+1)}{r_P^{n+2}} \right] u_{nm} = G_{nm} \quad . \quad (2.4)$$

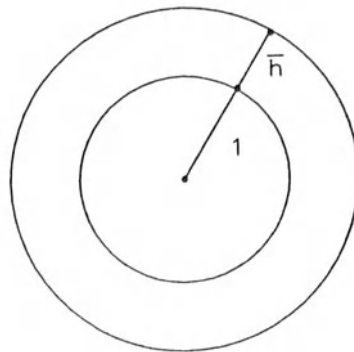


Fig. 2.1. The example of analytical continuation with two spheres.

Since  $r_P = 1 + \bar{h}$ , we see that

$$\frac{\bar{h}}{1 + \bar{h}} < 1 \quad (2.5)$$

and that

$$\max_{\bar{h}} \frac{\bar{h}(n+1)}{(1+\bar{h})^{n+2}} < \frac{1}{\left(1 + \frac{1}{n}\right)^n} < \frac{1}{2} \quad (n \geq 1) \quad . \quad (2.6)$$

Accordingly, equation (2.4) is unconditionally solvable and  $u$  is a well defined function with the same regularity as  $G$ .

On the contrary, we can observe that if we defined a B.V.P. taking  $Q$  as the Taylor point, i.e.

$$u(Q) + h_Q \frac{\partial u(Q)}{\partial r} = G(Q) \quad (h_Q = \bar{h}) \quad , \quad (2.7)$$

we would have obtained the spectral relation

$$\left[ 1 - (n+1)\bar{h} \right] u_{nm} = G_{nm} \quad ; \quad (2.8)$$

this relation shows that existence and uniqueness of the solution of the problem are no more guaranteed, though, when a solution exists, it happens to be more regular than G.

This counterexample has been useful to us in deciding to treat always problems with the Taylor point P on the external surface.

### 3 THE MAIN RESULT

We can state the main result of the paper in the form of a theorem:

Theorem 3.1 : the operators

$$(a) \quad h_o \frac{\partial}{\partial z} u(P) ; \quad P \equiv (x, y, h(x, y)) \quad (3.1)$$

$$(b) \quad h_o \frac{\partial}{\partial r} u(P) ; \quad P \equiv (\varphi, \lambda, 1 + h(\varphi, \lambda)) \quad (3.2)$$

are contractions, i.e. they can have operator norm smaller than 1 in the space  $C(\Sigma)$  of harmonic functions continuous up to the boundary  $\Sigma$ , endowed with norm

$$\|u\| = \sup_{Q \in \Sigma} |u(Q)| . \quad (3.3)$$

Remark 3.1: As it is known,  $C(\Sigma)$  is as a matter of fact a Banach space, as a consequence of the maximum principle.

Remark 3.2 : Another immediate consequence of the maximum principle is that an operator like  $h \frac{\partial}{\partial z}|_h$  is bounded in  $C(\Sigma)$ , for any  $\Sigma$  with bounded curvature; in fact for small h

$$\frac{\partial}{\partial z} u(P) = \frac{1}{\frac{4}{3}\pi h^3} \int_B \frac{\partial}{\partial z} u(P') dB_{P'} = \frac{1}{\frac{4}{3}\pi h^3} \left\{ \int_{S^+} u(P') dx dy - \int_{S^-} u(P') dx dy \right\}$$

with  $S^+, S^-$  the upper and lower hemisphere (cf. Fig. 3.1).

Since  $|u(P)| \leq \|u\|$  and  $S^+, S^-$  project onto a circle of radius h on the x,y plane, we find

$$\left| h \frac{\partial u}{\partial z} \right| \leq \frac{3}{2} \|u\| , \quad (3.4)$$

which is certainly correct but not sufficiently tight for our purposes.

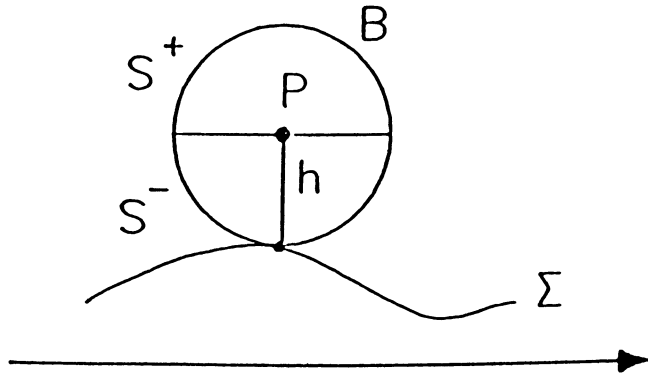


Fig. 3.1. Integration on upper and lower hemisphere

Let us now pass to prove (a). By using the explicit representation

$$u(z, \underline{\xi}) = \frac{1}{2\pi} \int \frac{z}{[\underline{\xi} - \underline{\eta}]^{\frac{3}{2}} + z^2} u(\underline{\eta}) d_2 \underline{\eta} \quad (3.5)$$

( $\underline{\xi}, \underline{\eta}$  are vectors on the x,y plane), one gets directly, with  $\rho = |\underline{\xi} - \underline{\eta}|$  and  $\rho = sz$ ,

$$\left| z \frac{\partial}{\partial z} u(z, \underline{\xi}) \right| = \frac{1}{2\pi} \left| \int \frac{z(\rho^2 - 2z^2)}{[\rho^2 + z^2]^{\frac{3}{2}}} u(\underline{\eta}) d_2 \underline{\eta} \right| \leq \|u\| \int_0^{+\infty} \frac{|s^2 - 2|}{[s^2 + 1]^{\frac{3}{2}}} s ds = \frac{4}{3\sqrt{3}} \|u\| . \quad (3.6)$$

Since the second term of (3.6) is constant, we see that the operator norm of  $z \frac{\partial}{\partial z}$ , computed on any surface  $z = h(x, y)$ , satisfies the inequality

$$\left\| z \frac{\partial}{\partial z} \right\| \leq \frac{4}{3\sqrt{3}} < 1 ,$$

so that this operator is a contraction in  $C(\Sigma)$ .

We can now consider (b). Following a similar line, we start from the Poisson representation

$$u(r, \sigma) = \frac{(r^2 - 1)}{4\pi} \int \frac{u(\omega)}{[r^2 + 1 - 2r \cos \psi]_{\sigma \omega}^{\frac{3}{2}}} d\omega \quad (3.7)$$

to obtain

$$\left| h \frac{\partial u}{\partial r} \right| \leq \frac{h}{4\pi} \int_{\sigma} \frac{|5r - r^3 - (r^2 + 3) \cos \psi|}{[r^2 + 1 - 2r \cos \psi]^{\frac{3}{2}}} |u(\omega)| d\omega . \quad (3.8)$$

Using in (3.8) the spherical surface element

$$d\omega = \sin\psi d\psi d\alpha ,$$

we see that

$$\left| h \frac{\partial u}{\partial r} \right| \leq \|u\| \frac{h}{2} \int_0^\pi \frac{|5r - r^3 - (r^2 + 3)\cos\psi|}{[r^2 + 1 - 2r\cos\psi]^{\frac{3}{2}}} \sin\psi d\psi ; \quad (3.9)$$

with the substitutions

$$\begin{aligned} \cos\psi &= 1 - h^2\tau , \quad h = r - 1 , \\ a &= h^2 + 2h + 4 , \quad b = h + 4 , \end{aligned}$$

we recognise that

$$\left\| h \frac{\partial u}{\partial r} \right\| < \frac{\|u\|}{2} \int_0^{+\infty} \frac{|a\tau - b|}{[1 + 2a\tau]^{\frac{3}{2}}} d\tau = K(h) \|u\| = \frac{1}{2r^2} \left\{ \frac{rb}{3} - \frac{a}{3} + \frac{2a\sqrt{a}}{3(2rb+a)^{1/2}} \right\} \|u\|. \quad (3.10)$$

With some further algebra, we find for  $K(h)$  the exact expression

$$K(h) = \frac{1}{2(h^2 + 2h + 1)} \left\{ h + \frac{2(h^2 + 2h + 4)^{1/2}}{3\sqrt{3}(h+2)} \right\} \quad (3.11)$$

and it is not difficult to prove that  $K(h) < 1$  for every  $h \geq 0$  and in particular

$$K(0) = \frac{4}{3\sqrt{3}} , \quad (3.12)$$

coinciding with the planar estimate, as it had to be.

So, also for the spherical case, the pseudo-boundary operator (3.2) is a contraction in  $C(\Sigma)$ . Therefore, Theorem 3.1 is completely proved and by standard theorems on contractions we can draw the following conclusions:

- 1) there is one and only one solution in  $C(\Sigma)$  of pseudo-B.V.P.'s (1.7), (1.8);
- 2) the solution can be attained as limit of a simple iterative scheme

$$u_{n+1} = G - Bu_n , \quad u_0 = G , \quad (3.13)$$

with  $B$  equal to  $h \frac{\partial}{\partial z}$  or to  $h \frac{\partial}{\partial r}$  depending on the case considered.

Remark 3.3: We conclude the paragraph by observing that once the iterative scheme (3.13) is known to be convergent we can go back to the original problem and write it directly in terms of the anomalous potential:

(a) In the plane case, we had  $u = -\frac{\partial T}{\partial z}$ , so

$$-\frac{\partial T_{n+1}(\xi, 0)}{\partial z} = G + h(\xi) \frac{\partial^2 T_n(\xi, h(\xi))}{\partial z^2} \quad (3.14)$$

which convoluted with the plane Stokes operator

$$(S \cdot u)(\xi) = \frac{1}{2\pi} \int \frac{1}{|\xi - \eta|} u(\eta) d_2 \eta \quad (3.15)$$

gives

$$T_{n+1}(\xi, 0) = S\{G\} + S \left\{ h \frac{\partial^2 T_n}{\partial z^2} \right\} ; \quad (3.16)$$

To continue the iteration, it is necessary to know the vertical derivatives of  $T$  at height  $h$ ; this is achieved by noting that the kernel  $(2\pi |\xi - \eta|)^{-1}$  is continued harmonically in space by  $(2\pi [\rho^2 + z^2])^{-1}$ , with  $\rho = |\xi - \eta|$ , and that, whatever is  $u$ ,

$$h \frac{\partial^2}{\partial z^2} (Su)(\xi, z) \Big|_{z=h} = \frac{h}{2\pi} \int \frac{2h^2 - \rho^2}{[\rho^2 + h^2]^{5/2}} u(\eta, 0) d_2 \eta . \quad (3.17)$$

A warning is necessary here. Although (3.16) with (3.17) supply a closed iteration scheme that could be started from  $T_0 = S\{G\}$ , what we have proved up to now is not sufficient to claim its convergence; in fact the convergence in  $C(\Sigma)$  of  $-\frac{\partial T_n}{\partial z}$  does not imply a similar convergence for  $T_n$ .

However it is easy to see that if both  $G(\xi)$ ,  $h(\xi)$  have compact support then, the same being true for  $-\frac{\partial T_n}{\partial z}$ , we can in fact guarantee the uniform convergence of (3.16). This hypothesis is in fact not too restrictive and is usually accepted.

(b) Also for the spherical case, the iteration can be expressed in terms of  $T$  recalling that

$$u = r \Delta g = -r \frac{\partial T}{\partial r} - 2T . \quad (3.18)$$

By using this relation, the iterative scheme becomes

$$-\frac{\partial T_{n+1}}{\partial r} - 2T_{n+1} = G + 3h \frac{\partial T_n}{\partial r} \Big|_{r=1+h} + h(1+h) \frac{\partial^2 T_n}{\partial r^2} \Big|_{r=1+h} \quad (3.19)$$

i.e. if we use the Stokes operator  $S$  (Heiskanen and Moritz, 1990)

$$T_{n+1} = S\{G\} + S\left\{3h \frac{\partial T_n}{\partial r}\Big|_{r=1+h}\right\} + S\left\{h(1+h) \frac{\partial^2 T_n}{\partial r^2}\Big|_{r=1+h}\right\} . \quad (3.20)$$

As we see, in order to continue the iteration we need to compute  $-\frac{\partial T_n}{\partial r}$ ,  $-\frac{\partial^2 T_n}{\partial r^2}$  at height  $h$ , which can be done with the help of the relations

$$\frac{\partial}{\partial r} S\{u\} = \Pi u - \frac{2}{r} S\{u\} , \quad (3.21)$$

$$\frac{\partial^2}{\partial r^2} S\{u\} = \left( \frac{\partial}{\partial r} \Pi \right) u + \frac{6}{r^2} S\{u\} - \frac{2}{r} \Pi u , \quad (3.22)$$

where  $\Pi$  is the Poisson operator with kernel given in (3.7) and  $\frac{\partial}{\partial r} \Pi$  is the radial derivative of  $\Pi$ , i.e. the operator with kernel

$$\frac{\partial}{\partial r} \Pi \approx \frac{1}{4\pi} \frac{5r - r^3 - (r^2 + 3)\cos\psi}{[r^2 + 1 - 2r\cos\psi]^{5/2}} ;$$

relations (3.21), (3.22) hold throughout the space.

In the spherical case, the convergence of  $\{T_n\}$  in  $C(\Sigma)$  is guaranteed without further restrictions.

## 4 DISCUSSION

The idea of the paper is that practical implementations of solutions of Molodenskii's problem are in fact solutions of approximate pseudo-boundary value problems where the boundary is changed to a simple surface and a suitable pseudo-boundary operator provides the necessary downward continuation.

The case of first order downward continuation is completely analysed here; one could however ask what would be the characteristics of a problem with higher order terms.

For instance with second order downward continuation between two spheres, like the example discussed in §2, one would get the solution, analogous to (2.4),

$$\left[ 1 - \frac{\bar{h}(n+1)}{r_P^{n+2}} + \frac{1}{2} \frac{\bar{h}^2(n+1)(n+2)}{r_P^{n+3}} \right] u_{nm} = G_{nm} , \quad (4.1)$$

which is indeed unconditionally solvable.

It is interesting here to notice that, in this case, even taking the Taylor point P on the internal sphere ( $r_P=1$ ), we would obtain conversion coefficients

$$\left[1 - (n+1)\bar{h} + \frac{1}{2}(n+1)(n+2)\bar{h}^2\right] > \frac{1}{2} + \frac{1}{2}\left[1 - (n+1)\bar{h}\right]^2$$

which are unconditionally positive too, showing that  $u$  always exists and is even significantly more regular than  $G$ .

So this case seems to be worthwhile of further investigation.

Another point of interest would be to generalise this analysis to an ellipsoidal geometry, because the use of the ellipsoid as reference surface is nowadays necessary to produce high degree, highly accurate, global solutions.

## References

- Heck, B. (1991) On the linearized boundary value problems of physical geodesy, Report N.407, Department of Geodetic Science and Surveying, Ohio State University.
- Heiskanen, W.A. and Moritz, H. (1990) Physical Geodesy , Reprint Institute of Physical Geodesy, Technical University, Graz, Austria.
- Holota, P. (1991) On the iteration solution of the geodetic boundary value problem and some model refinements, Contribution to Geodetic Theory and Methodology, XX General Assembly of IUGG, IAG-Sec. IV, Vienna, Politecnico di Milano, pp. 31-60.
- Miranda, C. (1970) Partial Differential Equations of elliptic type, Springer Verlag.
- Moritz, H. (1973), On the convergence of Molodensky's series, Anno XXXII, Bollettino di Geodesia e Scienze Affini, N.3, pp. 125-144.
- Rapp, H.R., and Pavlis, N.K. (1990) The Development and Analysis of Geopotential Coefficients Models to Spherical Harmonic Degree 360 , Journal of Geophysical Research, Vol.95, N.B13, pp 21,885-21,911.
- Sanso', F. (1993) Theory of Geodetic B.V.P.s Applied to the Analysis of Altimetric Data, in Lecture Notes in Earth Science N.50, 'Satellite Altimetry in Geodesy and Oceanography', Springer Verlag.
- Sanso', F. and Sacerdote, F. (1991) The Boundary Value Problems in Geodesy in Proceedings of the Geodetic Day in Honour of Antonio Marussi, Roma, October 9th, Acc.Naz.Lincei.
- Sideris, M.G. (1987) Spectral Methods for the Numerical Solution of Molodenskii's problem , Ph.D. Dissertation, Department of Surveying Engineering, University of Calgary, Alberta.

# CLASSICAL METHODS FOR NON-SPHERICAL BOUNDARY PROBLEMS IN PHYSICAL GEODESY

Petr Holota

Research Institute of Geodesy, Topography and Cartography  
250 66 Zdiby 98, Praha-východ, Czech Republic

## INTRODUCTION

We will discuss a boundary problem at an ellipsoid of revolution and show how the Green's function method can be used in this case. We believe that the solution will also demonstrate some principles associated with the use of the Green's function method for non-spherical boundary problems in general. Similarly as in (Roach, 1986) and (Holota, 1993) our idea is to replace the Green's function associated with a non-spherical boundary problem by a kernel associated with a simpler problem at a simpler boundary which lies close to the given boundary. However, the use of an approximate kernel will cause extra terms to appear in the representation of the solution to the original problem. These terms will give rise to an integral equation for the solution sought. As an alternative recall the work by Ostach (1982), where the Green's function was constructed for an ellipsoidal boundary directly.

Suppose that we have a system of geodetic coordinates  $H, B, L$  related to a reference ellipsoid of revolution of semimajor axis  $a$  and numerical eccentricity  $e$ . The general point of geodetic coordinates  $H, B, L$  has the following rectangular Cartesian coordinates:

$$x_1 = (N + H) \cos B \cos L, \quad x_2 = (N + H) \cos B \sin L, \quad x_3 = [(1 - e^2)N + H] \sin B, \quad (1)$$

where  $N = a(1 - e^2 \sin^2 B)^{-1/2}$  is the principal radius of curvature of our ellipsoid in the direction of the prime vertical. For the point  $\mathbf{x} = (x_1, x_2, x_3)$  we put  $|\mathbf{x}| = (\sum_{i=1}^3 x_i^2)^{1/2}$ .

Our aim is to find  $T$  which is regular at infinity and such that

$$\Delta T = 0 \quad \text{for } H > 0, \quad \frac{\partial T}{\partial H} + \frac{2}{a}(1 + e^2 \cos^2 B)T = f \quad \text{for } H = 0 \quad (2)$$

and  $\Delta$  denoting the Laplace operator. The problem above is often used as a starting point for investigations of the so-called ellipsoidal effects in the determination of the disturbing potential, see e.g. (Moritz, 1980, eqs. III.508 and III.524) or (Cruz, 1986). Here, however, we will not write explicitly how  $f$  can be obtained from input potential and gravity anomalies. We just note that, apart from the telluroid's topography above the ellipsoid, the structure of (2) is close to a linear version of the so-called scalar boundary problem of physical geodesy, cf. (Sacerdote and Sansò, 1986) or (Heck, 1991).

Following our intention to apply an approximate kernel for solution of (2), we first briefly recall (as our "simpler" problem) the famous Stokes problem at a sphere of radius  $R$ :

$$\Delta T = 0 \quad \text{for } |\mathbf{x}| > R, \quad \frac{\partial T}{\partial |\mathbf{x}|} + \frac{2}{R}T = f \quad \text{for } |\mathbf{x}| = R, \quad (3)$$

$$T = \frac{c}{|\mathbf{x}|} + O(|\mathbf{x}|^{-3}) \quad \text{for } \mathbf{x} \rightarrow \infty, \quad (4)$$

where  $c$  is a constant. Thus, clearly,  $T$  does not contain first degree harmonic components  $v_i = x_i/|\mathbf{x}|^3$ ,  $i = 1, 2, 3$ . We easily deduce that  $f$  has to satisfy certain conditions in order

that (3) has a solution. Indeed, multiplying the first eq. in (3) by a function  $v$  that is defined for  $|\mathbf{x}| > R$  and sufficiently regular at infinity and integrating this product over  $\{\mathbf{x}, |\mathbf{x}| > R\}$ , we obtain  $\int_{|\mathbf{x}| > R} v \Delta T d\mathbf{x} = 0$ . Moreover, using Green's identity and the second eq. in (3), we get

$$\int_{|\mathbf{x}|=R} \left( \frac{\partial v}{\partial |\mathbf{x}|} + \frac{2}{R} v \right) T dS - \int_{|\mathbf{x}|=R} f v dS + \int_{|\mathbf{x}| > R} T \Delta v d\mathbf{x} = 0. \quad (5)$$

Here we can see that  $\int_{|\mathbf{x}|=R} f v dS = 0$  for  $\Delta v = 0$ ,  $|\mathbf{x}| > R$ , and  $(\partial v / \partial |\mathbf{x}|) + (2/R)v = 0$ ,  $|\mathbf{x}| = R$ . It can be easily verified that the only non-trivial solutions of this boundary problem are the first degree harmonics  $v_i$ ,  $i = 1, 2, 3$ . In consequence the following conditions

$$\int_{|\mathbf{x}|=R} f v_i dS = 0, \quad i = 1, 2, 3, \quad (6)$$

have to be met by  $f$ . In addition let us suppose that (6) are met. Let  $T$  be a solution of (3) and  $a_i$ ,  $i = 1, 2, 3$ , be arbitrary constants then also  $T^* = \sum_{i=1}^3 a_i v_i + T$  is a solution of (3), as one can easily verify. (The reasoning above reflects the well-known Fredholm alternative.) The freedom in the determination of  $T$  is then eliminated by the asymptotic condition (4).

## THE GREEN'S FUNCTION

Following (Holota, 1984) and the general principles in constructing Green's functions, we start with the fundamental solution  $J = |\mathbf{x} - \mathbf{y}|^{-1}$  of the Laplace equation. For  $|\mathbf{y}| < |\mathbf{x}|$  we have  $J = \sum_{n=0}^{\infty} (|\mathbf{y}|^n / |\mathbf{x}|^{n+1}) P_n(\cos \psi)$ , where  $P_n$  is the usual Legendre polynomial of degree  $n$  and  $\psi$  is the angle between the placement vectors  $\mathbf{x}$  and  $\mathbf{y}$ . For  $|\mathbf{y}| = R$  we put  $F = (\partial J / \partial |\mathbf{y}|) + (2/R)J = F_1 + F_{sum}$ , where

$$F_1 = \frac{3}{|\mathbf{x}|^2} P_1(\cos \psi) \quad \text{and} \quad F_{sum} = \frac{1}{R^2} \sum_{n=0, n \neq 1}^{\infty} (n+2) \left( \frac{R}{|\mathbf{x}|} \right)^{n+1} P_n(\cos \psi). \quad (7)$$

In the next step we will look for a function  $H(\mathbf{y})$  such that

$$\Delta H = 0 \quad \text{for} \quad |\mathbf{y}| > R \quad \text{and} \quad (\partial H / \partial |\mathbf{y}|) + (2/R)H = F_{sum} \quad \text{for} \quad |\mathbf{y}| = R. \quad (8)$$

First we have to verify an analogue of (6). Therefore, we put  $u_i = y_i / |\mathbf{y}|^3$ ,  $i = 1, 2, 3$ , and consider the structure of  $F_{sum}$ . We immediately see that  $\int_{|\mathbf{y}|=R} F_{sum} u_i dS = 0$ ,  $i = 1, 2, 3$ , since  $F_{sum}$  does not contain first degree harmonics. In consequence the conditions, which are necessary for (8) to have a solution, are met. The function  $H(\mathbf{y})$  may simply be found as  $H = \sum_{n=0}^{\infty} H_n$ ,  $H_n = (R/|\mathbf{y}|)^{n+1} \bar{H}_n(\mathbf{y}/|\mathbf{y}|)$ , where  $\bar{H}_n$  are surface (Laplace) spherical harmonics. After the insertion into the second equation of (8) we get

$$\bar{H}_n = -(1/R)(n+2)(n-1)^{-1}(R/|\mathbf{x}|)^{n+1} P_n(\cos \psi) \quad (9)$$

except for  $\bar{H}_1 = (a_1 y_1 + a_2 y_2 + a_3 y_3) / |\mathbf{y}|$ , where the coefficients  $a_i$ ,  $i = 1, 2, 3$ , can be chosen arbitrarily. Thus  $H = H_1 + H_{sum}$  with

$$H_1 = R^2 \sum_{i=1}^3 a_i \frac{y_i}{|\mathbf{y}|^3} \quad \text{and} \quad H_{sum} = -\frac{1}{R} \sum_{n=0, n \neq 1}^{\infty} \frac{n+2}{n-1} \left( \frac{R^2}{|\mathbf{x}| |\mathbf{y}|} \right)^{n+1} P_n(\cos \psi). \quad (10)$$

We are now in the position to define for  $|\mathbf{x}| |\mathbf{y}| > R^2$  the function  $G(\mathbf{x}, \mathbf{y}) = J - H$ . Its restriction for  $|\mathbf{y}| = R$  is closely related to the (Pizzetti extended) Stokes function  $S(|\mathbf{x}|, \psi)$

well-known in physical geodesy. Indeed,

$$G(\mathbf{x}, R \frac{\mathbf{y}}{|\mathbf{y}|}) = G(|\mathbf{x}|, \psi) = -\frac{1}{|\mathbf{x}|} + \sum_{i=1}^3 \left( \frac{x_i}{|\mathbf{x}|^3} - \frac{a_i}{R} \right) y_i + \frac{1}{R} S(|\mathbf{x}|, \psi) , \quad (11)$$

where  $S(|\mathbf{x}|, \psi) = \sum_{n=2}^{\infty} (2n+1)(n-1)^{-1} (R/|\mathbf{x}|)^{n+1} P_n(\cos \psi)$ . Therefore,  $G(\mathbf{x}, \mathbf{y})$  was called the Green-Stokes function in (Holota, 1984). Moreover, using the freedom in the choice of  $a_i$ ,  $i = 1, 2, 3$ , and putting  $a_i = Rx_i/|\mathbf{x}|^3$ ,  $i = 1, 2, 3$ , we obtain

$$G(\mathbf{x}, R \frac{\mathbf{y}}{|\mathbf{y}|}) = -\frac{1}{|\mathbf{x}|} + \frac{1}{R} S(|\mathbf{x}|, \psi) \quad \text{and} \quad H_1 = \frac{1}{R} \left( \frac{R^2}{|\mathbf{x}| |\mathbf{y}|} \right)^2 P_1(\cos \psi) . \quad (12)$$

The function  $G(\mathbf{x}, \mathbf{y})$  will enable us to express the solution of (3)–(4) explicitly. The natural point of departure is the (slightly modified) Green's third identity

$$T(\mathbf{x}) = -\frac{1}{4\pi} \int_{|\mathbf{y}|>R} G(\mathbf{x}, \mathbf{y}) \Delta T(\mathbf{y}) d\mathbf{y} - \frac{1}{4\pi} \int_{|\mathbf{y}|=R} \left[ G(\mathbf{x}, \mathbf{y}) \frac{\partial T(\mathbf{y})}{\partial |\mathbf{y}|} - T(\mathbf{y}) \frac{\partial G(\mathbf{x}, \mathbf{y})}{\partial |\mathbf{y}|} \right] d_y S . \quad (13)$$

Because  $T$  should represent the solution of (3), it follows that

$$T(\mathbf{x}) = \frac{1}{4\pi} \int_{|\mathbf{y}|=R} \left[ \frac{\partial G(\mathbf{x}, \mathbf{y})}{\partial |\mathbf{y}|} + \frac{2}{R} G(\mathbf{x}, \mathbf{y}) \right] T(\mathbf{y}) d_y S - \frac{1}{4\pi} \int_{|\mathbf{y}|=R} G(\mathbf{x}, \mathbf{y}) f(\mathbf{y}) d_y S . \quad (14)$$

Moreover, taking into consideration the fact that

$$\frac{\partial G(\mathbf{x}, \mathbf{y})}{\partial |\mathbf{y}|} + \frac{2}{R} G(\mathbf{x}, \mathbf{y}) = \frac{3}{|\mathbf{x}|^2} P_1(\cos \psi) = \frac{3}{R |\mathbf{x}|^3} \sum_{i=1}^3 x_i y_i \quad \text{for} \quad |\mathbf{y}| = R , \quad (15)$$

see (Smeets, 1993), we can immediately write

$$T(\mathbf{x}) = T_1(\mathbf{x}) - \frac{1}{4\pi} \int_{|\mathbf{y}|=R} G(\mathbf{x}, \mathbf{y}) f(\mathbf{y}) d_y S , \quad (16)$$

where  $T_1(\mathbf{x}) = (R/|\mathbf{x}|)^2 \sum_{i=1}^3 c_i x_i / |\mathbf{x}|$  and  $c_i = (3/4\pi R^2) \int_{|\mathbf{y}|=R} (y_i/R) T(\mathbf{y}) d_y S$ ,  $i = 1, 2, 3$ .

Assuming that (6) is met, we saw that (3) can be solved uniquely, but only apart from first degree harmonics. Therefore, we shall solve (3) in a quotient space with zero vector given by a supplementary space spanned by the first degree harmonics  $v_i$ ,  $i = 1, 2, 3$ . Hence

$$T(\mathbf{x}) = -\frac{1}{4\pi} \int_{|\mathbf{y}|=R} G(\mathbf{x}, \mathbf{y}) f(\mathbf{y}) d_y S \quad (17)$$

is also a solution of (3). Recall that this freedom is removed by the asymptotic condition (4). Moreover, it is clear from (12) that  $G(\mathbf{x}, Ry/|\mathbf{y}|)$  does not contain first degree harmonics. As a result the integral on the right hand side of (17) is also free from first degree harmonics.

Finally, considering again the important fact that  $G(\mathbf{x}, Ry/|\mathbf{y}|)$  does not contain first degree harmonics, we can reformulate our problem. In the new formulation we shall look for  $T$  satisfying the asymptotic condition (4) at infinity and such that

$$\Delta T = 0 \quad \text{for} \quad |\mathbf{x}| > R \quad \text{and} \quad (\partial T / \partial |\mathbf{x}|) + (2/R) T = \bar{f} \quad \text{for} \quad |\mathbf{x}| = R , \quad (18)$$

where  $\bar{f} = f + \sum_{i=1}^3 a_i v_i = f + (1/R^3) \sum_{i=1}^3 a_i x_i$  and the constants  $a_i$ ,  $i = 1, 2, 3$ , are chosen so that the conditions  $\int_{|\mathbf{x}|=R} \bar{f} v_i dS = 0$ ,  $i = 1, 2, 3$ , are met. It is important to point out

that the substitution of  $f$  by  $\bar{f}$ , i.e. also the choice of the coefficients  $a_i$ ,  $i = 1, 2, 3$ , does not affect  $T$  given by the explicit formula (17).

## A CLOSED EXPRESSION FOR THE GREEN'S FUNCTION

Our aim is now to find a closed expression for  $G(\mathbf{x}, \mathbf{y})$ , provided that  $|\mathbf{x}||\mathbf{y}| > R^2$ . We start with  $H_{sum}$  and decompose it as follows:  $H_{sum} = (2R/|\mathbf{x}||\mathbf{y}|) - H^* - H^{**}$ , where

$$H^* = \frac{1}{R} \sum_{n=2}^{\infty} \left( \frac{R^2}{|\mathbf{x}||\mathbf{y}|} \right)^{n+1} P_n(\cos \psi) \quad \text{and} \quad H^{**} = \frac{3}{R} \sum_{n=2}^{\infty} \frac{1}{n-1} \left( \frac{R^2}{|\mathbf{x}||\mathbf{y}|} \right)^{n+1} P_n(\cos \psi). \quad (19)$$

Moreover, let  $\bar{\mathbf{x}}$  be an image of  $\mathbf{x}$  given by a transformation of space known as inversion in a sphere, i.e.  $\bar{\mathbf{x}} = (R/|\mathbf{x}|)^2 \mathbf{x}$ ,  $|\mathbf{x}||\bar{\mathbf{x}}| = R^2$ . Approaching now  $H^*$  and assuming that  $|\mathbf{x}| > R$  and  $|\mathbf{y}| \geq R$ , we know that  $|\bar{\mathbf{x}} - \mathbf{y}|^{-1} = (|\mathbf{x}|/R^2) \sum_{n=0}^{\infty} (R^2/|\mathbf{x}||\mathbf{y}|)^{n+1} P_n(\cos \psi)$ . This yields

$$H^* = \frac{R}{|\mathbf{x}|} \frac{1}{|\bar{\mathbf{x}} - \mathbf{y}|} - \frac{R}{|\mathbf{x}||\mathbf{y}|} - \frac{R^3}{|\mathbf{x}|^2 |\mathbf{y}|^2} \cos \psi. \quad (20)$$

Now we try to find a closed expression for  $H^{**}$ . We will write  $H^{**}$  as follows

$$H^{**} = \frac{3}{R} \left( \frac{R^2}{|\mathbf{x}||\mathbf{y}|} \right)^2 \sum_{n=2}^{\infty} \frac{1}{n-1} \left( \frac{R^2}{|\mathbf{x}||\mathbf{y}|} \right)^{n-1} P_n(\cos \psi) = \frac{3R^3}{|\mathbf{x}|^2 |\mathbf{y}|^2} S, \quad (21)$$

where  $S = \sum_{n=2}^{\infty} (n-1)^{-1} z^{n-1} P_n(\cos \psi)$  and  $z = R^2/|\mathbf{x}||\mathbf{y}|$ . Here we easily deduce that

$$\frac{dS}{dz} = \sum_{n=2}^{\infty} z^{n-2} P_n(\cos \psi) = \frac{1}{z^3} \sum_{n=2}^{\infty} z^{n+1} P_n(\cos \psi) = \left( \frac{|\mathbf{x}||\mathbf{y}|}{R^2} \right)^3 R H^*. \quad (22)$$

Hence, in combination with (20),  $dS/dz = -z^{-2} [1 + z \cos \psi - (1 + z^2 - 2z \cos \psi)^{-1/2}]$ . Putting in addition  $I = \int dz/z^2 \sqrt{1+z^2-2z \cos \psi}$ , we have  $S = z^{-1} - \cos \psi \ln z + I + c$ , where  $c$  is an integration constant, which, however, is a function of  $\psi$ . Referring to (Holota, 1994) for the computation of the integral  $I$ , we give just the final result:

$$S = z^{-1} [1 - (1 + z^2 - 2z \cos \psi)^{1/2} - z \cos \psi \ln 2] - \\ - \cos \psi \ln [1 - z \cos \psi + (1 + z^2 - 2z \cos \psi)^{1/2}] + c(\psi), \quad (23)$$

where  $c = c(\psi)$  has to be determined. Putting  $z = 0$ , we immediately see from the series development that  $S_{z=0} = \lim_{z \rightarrow 0} S(z) = 0$ . Simultaneously, from (23) we can easily deduce that  $S_{z=0} = \cos \psi - 2 \cos \psi \ln 2 + c(\psi)$ . Hence  $c(\psi) = -\cos \psi + 2 \cos \psi \ln 2$  and

$$H^{**} = \frac{3R}{|\mathbf{x}||\mathbf{y}|} - \frac{3R|\bar{\mathbf{x}} - \mathbf{y}|}{|\mathbf{x}||\mathbf{y}|^2} - \frac{3R^3 \cos \psi}{|\mathbf{x}|^2 |\mathbf{y}|^2} - \frac{3R^3 \cos \psi}{|\mathbf{x}|^2 |\mathbf{y}|^2} \ln \frac{1}{2} (1 - \frac{R^2 \cos \psi}{|\mathbf{x}||\mathbf{y}|} + \frac{|\bar{\mathbf{x}} - \mathbf{y}|}{|\mathbf{y}|}). \quad (24)$$

Going now back to our original aim and recalling that  $G(\mathbf{x}, \mathbf{y}) = J - H = J - H_1 - H_{sum}$ , for  $|\mathbf{x}||\mathbf{y}| > R^2$ , we now have  $G(\mathbf{x}, \mathbf{y}) = J - (2R/|\mathbf{x}||\mathbf{y}|) - H_1 + H^* + H^{**}$ . Inserting in addition from (12), (20) and (24), we finally arrive at

$$G(\mathbf{x}, \mathbf{y}) = \frac{1}{|\mathbf{x} - \mathbf{y}|} + \frac{R}{|\mathbf{x}|} \frac{1}{|\bar{\mathbf{x}} - \mathbf{y}|} - \frac{3R|\bar{\mathbf{x}} - \mathbf{y}|}{|\mathbf{x}||\mathbf{y}|^2} - \frac{R^3 \cos \psi}{|\mathbf{x}|^2 |\mathbf{y}|^2} \left[ 5 + 3 \ln \frac{1}{2} (1 - \frac{R^2 \cos \psi}{|\mathbf{x}||\mathbf{y}|} + \frac{|\bar{\mathbf{x}} - \mathbf{y}|}{|\mathbf{y}|}) \right] \quad (25)$$

which is the desired closed expression for the Green's function associated with (3)–(4).

## THE PROBLEM AT THE ELLIPSOID AND AN APPROXIMATE KERNEL

We return to our problem (2) at the ellipsoid of revolution and will develop an approximation procedure to preserve the benefits of the Green's function method. In particular we replace the Green's function associated with (2) by the Green's function  $G(\mathbf{x}, \mathbf{y})$  constructed above. However, for reasons which will be clear later we take  $R \leq b = a(1 - e^2)^{1/2}$ . We start again with the (modified) Green's third identity. This time we will write it for  $\Omega_e$  denoting the exterior of our ellipsoid of revolution. Thus

$$T(\mathbf{x}) = -\frac{1}{4\pi} \int_{\Omega_e} G(\mathbf{x}, \mathbf{y}) \Delta T(\mathbf{y}) d\mathbf{y} - \frac{1}{4\pi} \int_{\partial\Omega_e} \left[ G(\mathbf{x}, \mathbf{y}) \frac{\partial T(\mathbf{y})}{\partial n_y} - T(\mathbf{y}) \frac{\partial G(\mathbf{x}, \mathbf{y})}{\partial n_y} \right] d_y S , \quad (26)$$

where  $\partial\Omega_e$  is the boundary of  $\Omega_e$  and  $\partial/\partial n$  means the derivative in the direction of the outer (unit) normal  $\mathbf{n}$  of  $\partial\Omega_e$ . Because  $T$  should represent the solution of (2) it follows that

$$T(\mathbf{x}) = \frac{1}{4\pi} \int_{\partial\Omega_e} Q(\mathbf{x}, \mathbf{y}) T(\mathbf{y}) d_y S - \frac{1}{4\pi} \int_{\partial\Omega_e} G(\mathbf{x}, \mathbf{y}) f(\mathbf{y}) d_y S , \quad (27)$$

where

$$Q(\mathbf{x}, \mathbf{y}) = \frac{\partial G(\mathbf{x}, \mathbf{y})}{\partial n_y} + \frac{2}{a} (1 + e^2 \cos^2 B_y) G(\mathbf{x}, \mathbf{y}) . \quad (28)$$

$\mathbf{x} \in \Omega_e$  and  $\mathbf{y} \in \partial\Omega_e$ , cf. (15). Our problem is to investigate the first integral on the right hand side in (27). The crucial step is to express the normal derivative of  $G$ .

### NORMAL DERIVATIVE OF THE GREEN'S FUNCTION

Taking into consideration that  $G(\mathbf{x}, \mathbf{y}) = G(|\mathbf{x}|, \psi, |\mathbf{y}|)$ , we can compute

$$\frac{\partial G}{\partial n_y} = (\partial G / \partial |\mathbf{y}|)(\partial |\mathbf{y}| / \partial n_y) + (\partial G / \partial \psi)\partial \psi / \partial n_y . \quad (29)$$

Here, obviously  $\partial |\mathbf{y}| / \partial n_y = \langle \mathbf{y}, \mathbf{n}_y \rangle |\mathbf{y}|^{-1}$ , where  $\langle \cdot, \cdot \rangle$  means the scalar product. Similarly, considering that  $\cos \psi = \sum_{i=1}^3 x_i y_i (|\mathbf{x}| |\mathbf{y}|)^{-1}$ , we easily deduce that

$$\partial \psi / \partial n_y = -(\langle \mathbf{x}, \mathbf{n}_y \rangle |\mathbf{x}|^{-1} - \langle \mathbf{y}, \mathbf{n}_y \rangle |\mathbf{y}|^{-1} \cos \psi) |\mathbf{y}|^{-1} \sin^{-1} \psi . \quad (30)$$

Recalling now that  $\mathbf{n}_y \equiv (\cos B_y \cos L_y, \cos B_y \sin L_y, \sin B_y)$  for  $\mathbf{y} \in \partial\Omega_e$ , we have

$$(n_y)_1 = y_1 N_y^{-1} , \quad (n_y)_2 = y_2 N_y^{-1} , \quad (n_y)_3 = y_3 N_y^{-1} + e^2 (1 - e^2)^{-1} y_3 N_y^{-1} \quad (31)$$

in view of (1). In consequence

$$\frac{\partial |\mathbf{y}|}{\partial n_y} = \frac{|\mathbf{y}|}{N_y} \left[ 1 + \frac{e^2}{1 - e^2} \left( \frac{y_3}{|\mathbf{y}|} \right)^2 \right] , \quad \frac{\partial \psi}{\partial n_y} = -\frac{e^2}{1 - e^2} \frac{1}{N_y} \left( \frac{x_3}{|\mathbf{x}|} - \frac{y_3}{|\mathbf{y}|} \cos \psi \right) \frac{y_3}{|\mathbf{y}| \sin \psi} , \quad (32)$$

where  $|\mathbf{y}| = N_y (1 - 2e^2 \sin^2 B_y + e^4 \sin^2 B_y)^{1/2}$ . Moreover, confining ourselves to an accuracy such that terms multiplied by  $e^4$  or by higher powers of  $e$  are neglected, we can write:

$$\partial |\mathbf{y}| / \partial n_y = 1 \quad \text{and} \quad \partial \psi / \partial n_y = -(e^2 / a \sin \psi) (\sin B_x - \sin B_y \cos \psi) \sin B_y . \quad (33)$$

However, we still have to compute  $\partial G / \partial |\mathbf{y}|$  and  $\partial G / \partial \psi$ . Putting

$$G_1 = |\mathbf{x} - \mathbf{y}|^{-1} , \quad G_2 = (R / |\mathbf{x}|) |\bar{\mathbf{x}} - \mathbf{y}|^{-1} , \quad G_3 = -(3R / |\mathbf{x}| |\mathbf{y}|^2) |\bar{\mathbf{x}} - \mathbf{y}| , \quad (34)$$

$$G_4 = -(R^3/|\mathbf{x}|^2|\mathbf{y}|^2) \cos \psi [5 + 3 \ln(1/2|\mathbf{y}|)(|\mathbf{y}| - |\bar{\mathbf{x}}| \cos \psi + |\bar{\mathbf{x}} - \mathbf{y}|)] , \quad (35)$$

we have  $G = \sum_{i=1}^4 G_i$  in view of (25) and can compute that

$$\frac{\partial G_1}{\partial |\mathbf{y}|} = -\frac{1}{2|\mathbf{y}|} G_1 + \frac{1}{2} \frac{|\mathbf{x}|^2 - |\mathbf{y}|^2}{|\mathbf{y}| |\mathbf{x} - \mathbf{y}|^3} , \quad \frac{\partial G_2}{\partial |\mathbf{y}|} = -\frac{1}{2|\mathbf{y}|} G_2 + \frac{R}{2|\mathbf{x}|} \frac{|\bar{\mathbf{x}}|^2 - |\mathbf{y}|^2}{|\mathbf{y}| |\bar{\mathbf{x}} - \mathbf{y}|^3} , \quad (36)$$

$$\frac{\partial G_3}{\partial |\mathbf{y}|} = -\frac{3}{2|\mathbf{y}|} (G_1 + G_2) + \frac{3}{2|\mathbf{y}|} (G_1 - G_2) + \frac{3R^2 \cos \psi}{|\mathbf{x}| |\mathbf{y}|^2} G_2 - \frac{2}{|\mathbf{y}|} G_3 \quad (37)$$

and

$$\frac{\partial G_4}{\partial |\mathbf{y}|} = -\frac{2}{|\mathbf{y}|} G_4 - \frac{3R^2 \cos \psi}{|\mathbf{x}| |\mathbf{y}|^2} G_2 + \frac{3R^3 \cos \psi}{|\mathbf{x}|^2 |\mathbf{y}|^3} . \quad (38)$$

Thus, summing up, we arrive at

$$\frac{\partial G}{\partial |\mathbf{y}|} = -\frac{2}{|\mathbf{y}|} G + \frac{3}{2|\mathbf{y}|} D + \frac{1}{2} (P_{ext} - \frac{R}{|\mathbf{x}|} P_{int}) + \frac{3R^3 \cos \psi}{|\mathbf{x}|^2 |\mathbf{y}|^3} , \quad (39)$$

where  $D = G_1 - G_2$ ,  $P_{ext} = (|\mathbf{x}|^2 - |\mathbf{y}|^2)/|\mathbf{y}| |\mathbf{x} - \mathbf{y}|^3$  and  $P_{int} = (|\mathbf{y}|^2 - |\bar{\mathbf{x}}|^2)/|\mathbf{y}| |\bar{\mathbf{x}} - \mathbf{y}|^3$ .

*Remark 1.* It is obvious that  $D$  is the Green's function for the Dirichlet problem at the sphere of radius  $R$ . For  $|\mathbf{y}| = R$  we can see that  $P_{ext}$  and  $P_{int}$  turn into the Poisson's kernels associated with the Dirichlet problem for the exterior and the interior of this sphere, respectively, cf. (Kellogg, 1953, Chap. IX, eqs. 8 and 11), (Pick, Pícha and Vyskočil, 1973, eq. D-22.4) or (Roach, 1986, p. 269).

Now we approach derivatives with respect to  $\psi$ . We obtain

$$\frac{\partial G_1}{\partial \psi} = -\frac{|\mathbf{x}| |\mathbf{y}| \sin \psi}{|\mathbf{x} - \mathbf{y}|^3} , \quad \frac{\partial G_2}{\partial \psi} = -\frac{R}{|\mathbf{x}|} \frac{|\bar{\mathbf{x}}| |\mathbf{y}| \sin \psi}{|\bar{\mathbf{x}} - \mathbf{y}|^3} , \quad \frac{\partial G_3}{\partial \psi} = -\frac{3R^2 \sin \psi}{|\mathbf{x}| |\mathbf{y}|} G_2 , \quad (40)$$

$$\frac{\partial G_4}{\partial \psi} = -\frac{\sin \psi}{\cos \psi} G_4 - 3 \left( \frac{R^2}{|\mathbf{x}| |\mathbf{y}|} \right)^2 \left( 1 + \frac{|\bar{\mathbf{x}}| \cos \psi}{|\mathbf{y}| - |\bar{\mathbf{x}}| \cos \psi + |\bar{\mathbf{x}} - \mathbf{y}|} \right) G_2 \sin \psi \cos \psi . \quad (41)$$

### Normal derivative of $G_1(\mathbf{x}, \mathbf{y})$ at the ellipsoid

The case  $\mathbf{x}, \mathbf{y} \in \partial \Omega_e$  will be of special interest. Recalling (29), we easily deduce that

$$\partial G_1 / \partial n_y = \langle \mathbf{x} - \mathbf{y}, \mathbf{n}_y \rangle |\mathbf{x} - \mathbf{y}|^{-3} \quad (42)$$

and that the right hand side of (42) can be interpreted as a weakly singular kernel. Indeed,  $\langle \mathbf{x} - \mathbf{y}, \mathbf{n}_y \rangle = |\mathbf{x} - \mathbf{y}| \cos(\mathbf{x} - \mathbf{y}, \mathbf{n}_y)$  and as is well-known  $|\cos(\mathbf{x} - \mathbf{y}, \mathbf{n}_y)| \leq c |\mathbf{x} - \mathbf{y}|$ , where  $c$  is a constant associated with the geometry of  $\partial \Omega_e$  only, see e.g. (John and Nečas, 1972, §10). This observation makes it possible to follow our accuracy and to neglect terms multiplied by  $e^4$  or by higher powers of  $e$ . In consequence (42) can be written for  $\mathbf{x}, \mathbf{y} \in \partial \Omega_e$  as:

$$\frac{\partial G_1}{\partial n_y} = -\frac{1}{2|\mathbf{y}|} G_1 - \frac{e^2}{16a^2} \frac{(\sin B_x - \sin B_y)^2}{\sin^3(\psi/2)} + \frac{e^2}{4a^2} \frac{\sin^2 B_y}{\sin(\psi/2)} . \quad (43)$$

### Normal derivative of $G_2(\mathbf{x}, \mathbf{y})$ at the ellipsoid

In conformity with (29) we have  $\partial G_2 / \partial n_y = (R/|\mathbf{x}|) \langle \bar{\mathbf{x}} - \mathbf{y}, \mathbf{n}_y \rangle |\bar{\mathbf{x}} - \mathbf{y}|^{-3}$  which is regular in the closure  $\bar{\Omega}_e$  of  $\Omega_e$  (i.e. in  $\bar{\Omega}_e = \Omega_e \cup \partial \Omega_e$ ), possibly apart from the poles  $(0, 0, b)$  and

$(0, 0, -b)$ , where a weak singularity may appear in case of  $R = b$ . We try to express  $\partial G_2 / \partial n_y$  in a similar way as  $\partial G_1 / \partial n_y$ . For this purpose we first will modify it slightly by writing:

$$\partial G_2 / \partial n_y = (R/|\mathbf{x}|)(|\mathbf{x} - \mathbf{y}|/|\bar{\mathbf{x}} - \mathbf{y}|)^3 (\partial G_1 / \partial n_y) - (R/|\mathbf{x}|)|\bar{\mathbf{x}} - \mathbf{x}| \cos(\mathbf{x}, \mathbf{n}_y) |\bar{\mathbf{x}} - \mathbf{y}|^{-3}, \quad (44)$$

where  $|\bar{\mathbf{x}} - \mathbf{y}|^2 = (R/|\mathbf{x}|)^2(|\mathbf{x} - \mathbf{y}|^2 + \varepsilon)$  and  $\varepsilon = R^{-2}(|\mathbf{x}|^2 - R^2)(|\mathbf{y}|^2 - R^2)$ . In particular for  $R = b$  we simply have  $\varepsilon = e^4 a^2 (1 - e^2)^{-1} \cos^2 B_x \cos^2 B_y$ . Going now back to  $\partial G_2 / \partial n_y$ , using (43) and (44), and keeping our accuracy, we finally have for  $\mathbf{x}, \mathbf{y} \in \partial \Omega_e$ :

$$\begin{aligned} \frac{\partial G_2}{\partial n_y} = & -\frac{1}{2|\mathbf{y}|} G_2 - \frac{e^2}{16a^2} p \frac{(\sin B_x - \sin B_y)^2}{\sin^3(\psi/2)} + \frac{e^2}{4a^2} p \frac{\sin^2 B_y}{\sin(\psi/2)} + \\ & + \frac{R}{2|\mathbf{x}|} \frac{|\bar{\mathbf{x}}|^2 - |\mathbf{x}|^2}{|\mathbf{y}| |\bar{\mathbf{x}} - \mathbf{y}|^3} + \frac{R}{|\mathbf{x}|} \frac{|\bar{\mathbf{x}} - \mathbf{x}|}{|\bar{\mathbf{x}} - \mathbf{y}|} [\cos \psi - \cos(\mathbf{x}, \mathbf{n}_y)], \end{aligned} \quad (45)$$

where  $p = (R/|\mathbf{x}|)q^3$  and  $q = |\mathbf{x} - \mathbf{y}| |\bar{\mathbf{x}} - \mathbf{y}|^{-1} = (|\mathbf{x}|/R) |\mathbf{x} - \mathbf{y}| (|\mathbf{x} - \mathbf{y}|^2 + \varepsilon)^{-1/2}$ .

### Normal derivatives of $G_3$ , $G_4$ and $G$ at the ellipsoid

First we approach  $G_3$ . It is a regular function with a regular derivative  $\partial G_3 / \partial n_y$  in  $\bar{\Omega}_e$ . Indeed,  $\partial G_3 / \partial n_y = (6R/|\mathbf{x}||\mathbf{y}|^4) |\bar{\mathbf{x}} - \mathbf{y}| \langle \mathbf{y}, \mathbf{n}_y \rangle + (3R/|\mathbf{x}||\mathbf{y}|^2) (\bar{\mathbf{x}} - \mathbf{y}, \mathbf{n}_y) |\bar{\mathbf{x}} - \mathbf{y}|^{-1}$ . Following (29), (30), (37) and (40), and keeping our accuracy, we obtain that for  $\mathbf{x}, \mathbf{y} \in \partial \Omega_e$ :

$$\begin{aligned} \frac{\partial G_3}{\partial n_y} = & -\frac{3}{2|\mathbf{y}|} (G_1 + G_2) + \frac{3}{2|\mathbf{y}|} D + \frac{3R^2 \cos \psi}{|\mathbf{x}||\mathbf{y}|^2} G_2 - \frac{2}{|\mathbf{y}|} G_3 + \\ & + \frac{3e^2}{2a^2} \left(\frac{R}{a}\right)^3 q \frac{(\sin B_x - \sin B_y \cos \psi)}{\sin(\psi/2)} \sin B_y. \end{aligned} \quad (46)$$

Finally we approach  $G_4$ . It is also a regular function with a regular derivative  $\partial G_4 / \partial n_y$  in  $\bar{\Omega}_e$ . Considering (29), (33), (38) and (41), we obtain for  $\mathbf{x}, \mathbf{y} \in \partial \Omega_e$ :

$$\begin{aligned} \frac{\partial G_4}{\partial n_y} = & -\frac{2}{|\mathbf{y}|} G_4 - \frac{3R^2 \cos \psi}{|\mathbf{x}||\mathbf{y}|^2} G_2 + \frac{e^2}{a^2} \left(\frac{R}{a}\right)^3 \left(5 + 3 \ln \frac{s}{2}\right) (\sin B_x - \sin B_y \cos \psi) \sin B_y + \\ & + \frac{3R^3 \cos \psi}{|\mathbf{x}|^2 |\mathbf{y}|^3} + \frac{3e^2}{2a^2} \left(\frac{R}{a}\right)^5 q \cos \psi \left[1 + \left(\frac{R}{a}\right)^2 \frac{\cos \psi}{s}\right] \frac{\sin B_x - \sin B_y \cos \psi}{\sin(\psi/2)} \sin B_y. \end{aligned} \quad (47)$$

within our accuracy, where  $s = 1 - (R/a)^2 \cos \psi + (2R/a)[(\sin^2(\psi/2) + \delta)]^{1/2}$  and  $\delta = \varepsilon/4a^2$ .

Now, combining (43), (45), (46) and (47), we arrive at

$$\frac{\partial G}{\partial n_y} = -\frac{2}{|\mathbf{y}|} G + \frac{R}{2|\mathbf{x}|} \frac{|\bar{\mathbf{x}}|^2 - |\mathbf{x}|^2}{|\mathbf{y}| |\bar{\mathbf{x}} - \mathbf{y}|^3} + \frac{3R^3 \cos \psi}{|\mathbf{x}|^2 |\mathbf{y}|^3} + \frac{3}{2|\mathbf{y}|} D + \frac{e^2}{a^2} \frac{(1+p)A_1 + A_2}{\sin(\psi/2)}, \quad (48)$$

where

$$A_1 = -\frac{1}{16} \left[ \frac{(\sin B_x - \sin B_y)^2}{\sin^2(\psi/2)} - 4 \sin^2 B_y \right], \quad (49)$$

$$\begin{aligned} A_2 = & \left(\frac{R}{a}\right)^3 \sin \frac{\psi}{2} \left(5 + 3 \ln \frac{s}{2}\right) (\sin B_x - \sin B_y \cos \psi) \sin B_y + \\ & + \frac{3}{2} \left(\frac{R}{a}\right)^3 q \left[1 + \left(\frac{R}{a}\right)^2 \cos \psi + \left(\frac{R}{a}\right)^4 \frac{\cos^2 \psi}{s}\right] (\sin B_x - \sin B_y \cos \psi) \sin B_y \end{aligned} \quad (50)$$

while the last term in (45) was omitted within our accuracy. To complete our analysis of  $\partial G/\partial n_y$  it remains still to estimate the Green's function  $D$  in order to show that in (27) it produces a term which can be ranged under small perturbations.

### ESTIMATES OF THE GREEN'S FUNCTION $D(\mathbf{x}, \mathbf{y})$ .

It is obvious that  $D \geq 0$  since also  $\varepsilon$  is non-negative. At the same time we easily deduce that  $D \leq D_{max}$  for  $\mathbf{x}, \mathbf{y} \in \partial\Omega_e$ , where  $D_{max} = |\mathbf{x} - \mathbf{y}|^{-1} - (|\mathbf{x} - \mathbf{y}|^2 + \varepsilon_{max})^{-1/2}$  and  $\varepsilon_{max} = (a^2 - R^2)^2/R^2 > 0$ . In the sequel, however, we will need an estimate of the integral  $I = (3/4\pi) \int_{\partial\Omega_e} D(\mathbf{x}, \mathbf{y}) |\mathbf{y}|^{-1} d_y S$  in case of  $\mathbf{x}, \mathbf{y} \in \partial\Omega_e$ . We easily deduce that  $I \leq I^*$ , where  $I^* = (3/4\pi b) \int_{\partial\Omega_e} D_{max} d_y S$ , so that in the first place our goal is to estimate  $D_{max}$ . For page limitation, however, we cannot reproduce the detailed computation here. Following (Holota, 1994), we give just the final result:

$$D_{max}(\psi) \leq (1/2a)(1 - e^2)^{-1/2} \sin^{-1}(\psi/2) - [4a^2(1 + k) \sin^2(\psi/2) + \varepsilon_{max}]^{-1/2}, \quad (51)$$

where  $k = 36e^4(1 - e^2)^{-9}$ , i.e.,  $k \approx 0.0016$ , and return to our integral  $I^*$ . We obviously have  $d_y S = |\mathbf{y}|^2 \cos^{-1}(\mathbf{y}, \mathbf{n}_y) d\sigma$ , where  $d\sigma$  denotes the surface element of the unit sphere. In spherical coordinates  $\psi$  (polar distance) and  $\alpha$  (azimuth) with the origin at the projection of  $\mathbf{x}$  on a sphere it is  $d\sigma = \sin \psi d\psi d\alpha$ . Considering in addition eqs. (31), we easily deduce that  $\cos(\mathbf{y}, \mathbf{n}_y) = \langle \mathbf{y}, \mathbf{n}_y \rangle / |\mathbf{y}| \geq (1 - e^2)^{1/2}$ . Hence  $d_y S \leq a^2(1 - e^2)^{-1/2} \sin \psi d\psi d\alpha$  and

$$I^* \leq 3a(1 - e^2)^{-1} \int_0^\pi D_{max}(\psi) \sin(\psi/2) \cos(\psi/2) d\psi. \quad (52)$$

Using (51) and referring to (Holota, 1994), we finally arrive at our desired estimate:

$$I \leq I^* \leq (1/2)(9e^2 + 3k)(1 - e^2)^{-3/2} + (3/2a)\varepsilon_{max}^{1/2}. \quad (53)$$

### REPRESENTATION FORMULA – INTEGRAL EQUATION

The problem which still has to be solved is to find  $T(\mathbf{y})$  in order that eq. (27) would become a real representation formula. For this purpose we will use the (modified) Green's third identity again, but this time for  $\mathbf{x} \in \partial\Omega_e$ . We get the following integral equation for  $T$ :

$$T(\mathbf{x}) - \frac{1}{2\pi} \int_{\partial\Omega_e} Q(\mathbf{x}, \mathbf{y}) T(\mathbf{y}) d_y S = F(\mathbf{x}), \quad F(\mathbf{x}) = -\frac{1}{2\pi} \int_{\partial\Omega_e} G(\mathbf{x}, \mathbf{y}) f(\mathbf{y}) d_y S. \quad (54)$$

The idea of the step above is an analogue of Sec. 11.4 in (Roach, 1986). Related aspects are also in (Svensson, 1991, Lemma 2). Using now (48) and (25), and recalling (28), we easily deduce that:

$$\begin{aligned} Q(\mathbf{x}, \mathbf{y}) &= \frac{3R^3}{|\mathbf{x}|^2 |\mathbf{y}|^3} \cos \psi + \frac{R}{2|\mathbf{x}|} \frac{|\bar{\mathbf{x}}|^2 - |\mathbf{x}|^2}{|\mathbf{y}| |\bar{\mathbf{x}} - \mathbf{y}|^3} + \\ &+ \frac{3}{2|\mathbf{y}|} D(\mathbf{x}, \mathbf{y}) + \frac{e^2}{a} (3 \cos^2 B_y - 1) G(\mathbf{x}, \mathbf{y}) + \frac{e^2}{a^2} \frac{(1 + p) A_1 + A_2}{\sin(\psi/2)}. \end{aligned} \quad (55)$$

In consequence our integral equation attains the following form:

$$\begin{aligned} T(\mathbf{x}) - \frac{3R^3}{2\pi} \sum_{i=1}^3 \frac{x_i}{|\mathbf{x}|^3} \int_{\partial\Omega_e} \frac{y_i}{|\mathbf{y}|^4} T(\mathbf{y}) d_y S - \\ - \frac{R}{4\pi |\mathbf{x}|} (|\bar{\mathbf{x}}|^2 - |\mathbf{x}|^2) \int_{\partial\Omega_e} \frac{1}{|\mathbf{y}| |\bar{\mathbf{x}} - \mathbf{y}|^3} T(\mathbf{y}) d_y S - K T(\mathbf{x}) = F(\mathbf{x}), \end{aligned} \quad (56)$$

where

$$KT(\mathbf{x}) = \frac{3}{4\pi} \int_{\partial\Omega_e} \frac{1}{|\mathbf{y}|} D(\mathbf{x}, \mathbf{y}) T(\mathbf{y}) d_y S + \\ + \frac{e^2}{2\pi a} \int_{\partial\Omega_e} (3 \cos^2 B_y - 1) G(\mathbf{x}, \mathbf{y}) T(\mathbf{y}) d_y S + \frac{e^2}{2\pi a^2} \int_{\partial\Omega_e} \frac{(1+p)A_1 + A_2}{\sin(\psi/2)} T(\mathbf{y}) d_y S . \quad (57)$$

The second term on the left hand side represents traces of first degree harmonics.

In addition, inspecting (56), we can deduce (see also below) that the third term on the left hand side (though regular!) may have a rather large value comparable with  $T(\mathbf{x})$ . We try to reduce its effect. First we recall that

$$\int_{\partial\Omega_e} \frac{\partial G_2}{\partial n_y} d_y S = \frac{R}{|\mathbf{x}|} \int_{\partial\Omega_e} \frac{\partial}{\partial n_y} \left( \frac{1}{|\bar{\mathbf{x}} - \mathbf{y}|} \right) d_y S = -4\pi \frac{R}{|\mathbf{x}|} \quad (58)$$

and that on the right hand side we have (apart from the factor  $R/|\mathbf{x}|$ ) the value of the well-known Gauss integral for  $\bar{\mathbf{x}}$  in the interior of  $\partial\Omega_e$ . Moreover, using (45), (49) and omitting again the last term in (45) within our adopted accuracy, we can write

$$\int_{\partial\Omega_e} \frac{\partial G_2}{\partial n_y} d_y S = -\frac{R}{2|\mathbf{x}|} \int_{\partial\Omega_e} \frac{1}{|\mathbf{y}||\bar{\mathbf{x}} - \mathbf{y}|} d_y S + \frac{e^2}{a^2} \int_{\partial\Omega_e} \frac{pA_1}{\sin(\psi/2)} d_y S + \\ + \frac{R}{2|\mathbf{x}|} (|\bar{\mathbf{x}}|^2 - |\mathbf{x}|^2) \int_{\partial\Omega_e} \frac{1}{|\mathbf{y}||\bar{\mathbf{x}} - \mathbf{y}|^3} d_y S \quad (59)$$

which together with (58) results in

$$\beta(\mathbf{x}) + \frac{e^2}{2\pi a^2} \int_{\partial\Omega_e} \frac{pA_1}{\sin(\psi/2)} d_y S + \frac{R}{4\pi|\mathbf{x}|} (|\bar{\mathbf{x}}|^2 - |\mathbf{x}|^2) \int_{\partial\Omega_e} \frac{1}{|\mathbf{y}||\bar{\mathbf{x}} - \mathbf{y}|^3} d_y S = 0 , \quad (60)$$

with

$$\beta(\mathbf{x}) = \frac{R}{|\mathbf{x}|} \left( 2 - \frac{1}{4\pi} \int_{\partial\Omega_e} \frac{1}{|\mathbf{y}||\bar{\mathbf{x}} - \mathbf{y}|} d_y S \right) . \quad (61)$$

Hence, summing up, we can modify (56) as follows:

$$T(\mathbf{x}) - \frac{3R^3}{2\pi[(1+\beta(\mathbf{x}))]} \sum_{i=1}^3 \frac{x_i}{|\mathbf{x}|^3} \int_{\partial\Omega_e} \frac{y_i}{|\mathbf{y}|^4} T(\mathbf{y}) d_y S - \\ - \frac{R}{4\pi|\mathbf{x}|} \frac{|\bar{\mathbf{x}}|^2 - |\mathbf{x}|^2}{1 + \beta(\mathbf{x})} \int_{\partial\Omega_e} \frac{T(\mathbf{y}) - T(\mathbf{x})}{|\mathbf{y}||\bar{\mathbf{x}} - \mathbf{y}|^3} d_y S - K^* T(\mathbf{x}) = \frac{F(\mathbf{x})}{1 + \beta(\mathbf{x})} , \quad (62)$$

where

$$K^* T(\mathbf{x}) = \frac{1}{1 + \beta(\mathbf{x})} KT(\mathbf{x}) - \frac{e^2}{2\pi a^2[1 + \beta(\mathbf{x})]} T(\mathbf{x}) \int_{\partial\Omega_e} \frac{pA_1}{\sin(\psi/2)} d_y S . \quad (63)$$

Obviously we should express  $\beta(\mathbf{x})$  explicitly. For  $e = 0$  and  $\mathbf{x} \in \partial\Omega_e$  we can easily deduce that  $\beta(\mathbf{x}) = 2 - (1/4\pi R) \int_{|\mathbf{y}|=R} |\mathbf{x} - \mathbf{y}|^{-1} d_y S = 1$ . In consequence for  $e = 0$  formula (62) coincides with (17). For  $e \neq 0$  the computation of  $\beta(\mathbf{x})$  needs a special attention. However, we cannot go in details here.

The effort to derive eqs. (56) and (62) is a preparation for further treatment of our original problem (2) from the introduction, which will be presented in a future paper. Note, however, that the situation here differs from considerations as e.g. in (Holota, 1991, 1992), where the vectorial (astronomical) version of the geodetic boundary problem was discussed.

Indeed, we immediately see that so far we have not associated our original problem with an asymptotic condition of a similar nature as that of (4), though this would be well grounded for a usual disturbing potential in a standard geocentric system of coordinates. What we suppose is just the simple regularity  $T = O(|\mathbf{x}|^{-1})$  at infinity, cf. also (Sacerdote and Sansò, 1986, eqs. 2.2).

**Acknowledgment.** This study has been supported by the Grant Agency of the Czech Republic through Grant No. 205/94/1243. This support is gratefully acknowledged.

## REFERENCES

- Cruz, J.Y. (1986). Ellipsoidal corrections to potential coefficients obtained from gravity anomaly data on the ellipsoid. Report No. 371 from the Dept. of Geod. Sci. and Surv., The Ohio State Univ.
- Heck, B. (1991). On the linearized boundary value problems of physical geodesy. Report No. 407 from the Dept. of Geod. Sci. and Surv., The Ohio State Univ.
- Holota, P. (1984). A new approach to iterations in solving geodetic boundary value problem for real topography. Proc. 5th Int. Symp. Geod. and Phys. of the Earth, Magdeburg, 1984. Veröff. d. Zentralinst. f. Phys. d. Erde, Nr. 81(1985), Teil II, pp. 4-15.
- Holota, P. (1991). On the iteration solution of the geodetic boundary-value problem and some model refinements. Contribution to Geodetic Theory and Methodology. XXth General Assembly of the IUGG, IAG-Sec. IV, Vienna, 1991. Politecnico di Milano, 1991, pp. 31-60; also in: Travaux de l'Association Internationale de Géodésie, Tome 29, Paris 1992, pp. 260-289.
- Holota, P. (1992). Integral representation of the disturbing potential: Effects involved, iteration technique and its convergence. Holota, P. and Vermeer, M. (eds.): Proc. 1st continental workshop on the geoid in Europe, Prague, 1992. Research Inst. of Geod., Topogr. and Cartogr., Prague, in co-operation with IAG-Subcommission for the geoid in Europe, Prague, pp. 402 - 419.
- Holota, P. (1993). The mathematics of gravity field and geoid modelling: Green's function method. Presented at the General Meeting of the IAG, Beijing.
- Holota, P. (1994). Classical methods for non-spherical boundary problems in physical geodesy (A full length version of the paper presented at the III Hotine-Marussi symposium on mathematical geodesy, unpubliushed).
- John, O. and Nečas, J. (1972). Equations of mathematical physics. SPN-publishers, Prague (in Czech).
- Kellogg, O.D. (1953). Foundations of potential theory. Dover Publications, Inc., New York.
- Moritz, H. (1980). Sovremennaya fizicheskaya geodeziya. Nedra Publishers, Moscow, 1983. English original "Advanced Physical Geodesy" published by H. Wichmann Vlg., Karlsruhe and Abacus Press, Tunbridge, Wells Kent.
- Ostach, O.M. (1982). Solution of the Stokes problem for ellipsoidal boundary by means of the Green's function method. Report No. 233 from TsNIIGAiK, Moscow, 1982, pp. 3-20 (in Russian).
- Pick, M., Pícha, J. and Vyskočil, V. (1973). Theory of the Earth's gravitational field. Elsevier, Amsterdam – Academia, Prague.
- Roach, G.F. (1986). Green's functions. Cambridge Univ. Press, Cambridge etc.
- Sacerdote, F. and Sansò, F. (1986). The scalar boundary value problem of physical geodesy. Manuscripta geodaetica, Vol. 11, No. 1, pp. 15–28.
- Smeets, I. (1993). The iterative solution of the linear geodetic boundary-value problem in the second-order approximation with emphasis on topography and global flattening. Manuscripta geodaetica (submitted).
- Svensson, S.L. (1991). The boundary equation approach to the geoid. Rapp, H.R and Sansò, F. (eds.) Determination of the Geoid - Present and Future. Int. Assoc. of Geodesy Symposia 106. Springer-Vlg., New York etc. pp. 357 – 364.

# On a Scalar Fixed Altimetry - Gravimetry Boundary Value Problem

W.Keller  
Geodetic Institute, Stuttgart University  
Keplerstrasse 11, D-70174 Stuttgart, Germany

## 1 Introduction

The existence, uniqueness and computation of a solution of the mixed *Altimetry - Gravimetry BVP* has been under discussion for several years.

The principal difficulty in the theoretical and numerical treatment of this problem is the changing sign in boundary conditions at the continents

$$\left(\frac{1}{2}\varphi - \frac{R}{2} \frac{\partial \varphi}{\partial n}\right)|_{\partial\Omega_2} = 0$$

Here we want to prove the following hypothesis: The changing sign is a consequence of the free boundary at the continents.

Therefore , unconditioned existence and uniqueness can only be achieved by considering the continental part of the surface as fixed. Such a consideration is possible because of the operationality of GPS.

Because of space limitations all proofs are excluded in this paper. For a more detailed discussion, we refer to [Kel].

## 2 Definition of the problem

Let be  $\Gamma$  the surface of the Earth consisting of two part  $\Gamma_1, \Gamma_2$  with  $\Gamma_1 \cup \Gamma_2$  and  $\text{mes}(\Gamma_1 \cap \Gamma_2) = 0$ . On this two parts of the Earths surface  $\Gamma_1$  the continental and  $\Gamma_2$  the oceanic part the following data let be given:

$$N : \Gamma_1 \rightarrow \mathcal{R}^1 , \quad \text{Geoid undulations} \tag{1}$$

$$g : \Gamma_2 \rightarrow \mathcal{R}^1 , \quad \text{modulus of gravitation} \tag{2}$$

What we are looking for is the unknown gravitational potential  $V$  which fulfills:

$$\Delta V(\mathbf{x}) = 0 \quad \mathbf{x} \in \text{ext}\Gamma \quad (3)$$

$$\lim_{|\mathbf{x}| \rightarrow \infty} V(\mathbf{x}) = 0 \quad (4)$$

$$(V - U)|_{\Gamma_1} = \gamma N \quad (5)$$

$$|\nabla V||_{\Gamma_2} = g \quad (6)$$

This

is a **nonlinear scalar fixed mixed BVP**

The first step in the treatment of such a problem is always its linearization

Therefore we choose a normal potential  $U$  and set  $T := V - U$

Consequently, the boundary value problem for the unknown disturbing potential  $T$  is:

$$\Delta T(\mathbf{x}) = 0 \quad \mathbf{x} \in \text{ext}\Gamma \quad (7)$$

$$\lim_{|\mathbf{x}| \rightarrow \infty} T(\mathbf{x}) = 0 \quad (8)$$

$$T|_{\Gamma_1} = \gamma N \quad (9)$$

$$\mathbf{h}^T \nabla T|_{\Gamma_2} = \delta g := g - \gamma \quad (10)$$

where

$$\mathbf{h} := \frac{1}{\gamma} \nabla U \quad (11)$$

This is the **linear scalar fixed mixed external BVP**

### 3 Kelvin transformation

Because it is not convenient to deal with differential equations on unbounded domains we apply a transformation of the external problem into an *equivalent* internal problem defined on a bounded set  $\Omega$ , which results from *Kelvin's* transformation of the Earth's external space.

**Lemma 1** *Let be (applying Einstein's summation convention )*

$$\bar{x}^i = \frac{R^2 x^i}{|\mathbf{x}|^2} \quad (12)$$

$$u(\bar{\mathbf{x}}) := \frac{R}{|\bar{\mathbf{x}}|} T\left(\frac{R^2 \bar{x}^i}{|\bar{\mathbf{x}}|^2}\right) \quad (13)$$

$$f(\bar{\mathbf{x}}) := \frac{R}{|\bar{\mathbf{x}}|} N\left(\frac{R^2 \bar{x}^i}{|\bar{\mathbf{x}}|^2}\right) \cdot \gamma \quad (14)$$

$$g(\bar{\mathbf{x}}) := \delta g\left(\frac{R^2 \bar{x}^i}{|\bar{\mathbf{x}}|^2}\right) \quad (15)$$

$$a(\bar{\mathbf{x}}) := \frac{\bar{h}^i \bar{x}^i}{|\bar{\mathbf{x}}| R} \quad (16)$$

$$\mathbf{b}(\bar{\mathbf{x}}) := \frac{|\bar{\mathbf{x}}|}{R} \bar{h}^i \quad (17)$$

then the following problem

$$\Delta u(\bar{\mathbf{x}}) = 0 \quad \bar{\mathbf{x}} \in \Omega \quad (18)$$

$$\lim_{|\bar{\mathbf{x}}| \rightarrow \infty} u(\bar{\mathbf{x}}) = 0 \quad (19)$$

$$u|_{\partial\Omega_1} = f \quad (20)$$

$$(au + \mathbf{b}^\top \nabla u)|_{\partial\Omega_2} = g \quad (21)$$

has a unique solution if and only if the external problem (7) has a unique solution.

For technical reasons we add a second transformation into an equivalent problem with homogeneous boundary conditions:

**Lemma 2** Let be  $v \in W_2^2(\Omega)$  with  $v|_{\partial\Omega_1} = f$  and  $(av + \mathbf{b}^\top \nabla v)|_{\partial\Omega_2} = g$  in the sense of trace.

Furthermore let be  $d := \Delta v$ .

Then  $u$  is a solution of (18) if and only if for  $\varphi := u - v$  holds:

$$-\Delta \varphi = d \quad (22)$$

$$\varphi|_{\partial\Omega_1} = 0 \quad (23)$$

$$(a\varphi + \mathbf{b}^\top \nabla \varphi)|_{\partial\Omega_2} = 0 \quad (24)$$

This is an **i n t e r n a l** linear fixed mixed BVP with **h o m o g e n e o u s** boundary conditions

## 4 Weak solution

We now want to find a weak solution of the **i n t e r n a l** linear fixed mixed BVP with **h o m o g e n e o u s** boundary conditions. Hereby the oblique derivative  $\mathbf{b}^\top \nabla \varphi$  prevents us from direct application of *Green's theorems*

Consequently, we have to find a transformation of the problem in such a way that *Greens* theorems become applicable.

Let  $\mathbf{n} = (n_1, n_2, n_3)^\top$  be the exterior normal vector to  $\partial\Omega$ . Then we can construct functions  $\rho, a_{12}, a_{13}, a_{23}$  as the solution of a linear system of equations:

**Lemma 3** Suppose that for every  $\mathbf{x} \in \partial\Omega$  the inequality  $\mathbf{b}^\top \mathbf{n} > 0$  holds, then the linear system of equations

$$\begin{pmatrix} \rho b_1 - n_1 \\ \rho b_2 - n_2 \\ \rho b_3 - n_3 \end{pmatrix} = \begin{pmatrix} n_2 & n_3 & 0 \\ -n_1 & 0 & n_3 \\ 0 & -n_1 & -n_2 \end{pmatrix} \begin{pmatrix} a_{12} \\ a_{13} \\ a_{23} \end{pmatrix}$$

has a solution.

With the help of the functions  $\rho, a_{ij}$  suitably and smoothly continued from  $\partial\Omega$  into  $\Omega$  we assign a bilinear form to our mixed problem (22) :

$$\mathcal{A}(\varphi, \psi) := \int_{\Omega} \nabla \varphi^\top \nabla \psi dx \quad (25)$$

$$+ \int_{\Omega} \sum_{i,j=1}^3 \left[ a_{ij} \frac{\partial \varphi}{\partial x_i} \frac{\partial \psi}{\partial x_j} \right] dx \quad (26)$$

$$- \int_{\Omega} \sum_{i \neq j} \frac{\partial a_{ij}}{\partial x_i} \frac{\partial \varphi}{\partial x_j} \psi dx \quad (27)$$

$$+ \int_{\partial\Omega} \rho a \varphi \psi d\sigma, \quad a_{ii} = 0, \quad a_{ij} = -a_{ji} \quad (28)$$

Now we can prove that this bilinear form represents our mixed boundary value problem (22)

**Lemma 4** Let be

$$\varphi \in \tilde{V} := \{u \in C^2(\bar{\Omega}) \mid u|_{\partial\Omega_1} = 0\}$$

Then

$$-\Delta \varphi(\bar{\mathbf{x}}) = d \quad \bar{\mathbf{x}} \in \Omega \quad (29)$$

$$\lim_{|\bar{\mathbf{x}}| \rightarrow \infty} \varphi(\bar{\mathbf{x}}) = 0 \quad (30)$$

$$\varphi|_{\partial\Omega_1} = 0 \quad (31)$$

$$(a\varphi + \mathbf{b}^\top \nabla \varphi)|_{\partial\Omega_2} = 0 \quad (32)$$

if and only if

$$\mathcal{A}(\varphi, \psi) = (d, \psi)_H \quad (33)$$

for any  $\psi \in \tilde{V}$ .

## 5 V coercivity

In this section we will deal with the question under which conditions the variational equations (33) have a solution and whether this solution is unique or ambiguous.

**Lemma 5** *Let be  $V := \{u \in W_2^1(\Omega) \mid u|_{\partial\Omega_1} = 0\}$ . Then the form  $\mathcal{A}$  is  $V$ -coercive on  $V$ .*

The  $V$ -coercivity generates the following alternative

- either the homogeneous variational equation

$$\mathcal{A}(\varphi, \psi) = 0 \quad \psi \in V \tag{34}$$

has only the trivial solution  $\varphi = 0$

- or the inhomogeneous variational equation

$$\mathcal{A}(\varphi, \psi) = (d, \psi) \quad \psi \in V \tag{35}$$

has a solution only for those  $d$  which fulfill  $(d, v)_H = 0$  for all  $v$  with

$$\mathcal{A}(v, \psi) = 0 \quad \psi \in V \tag{36}$$

Therefore it is necessary to investigate the solutions of the homogeneous problem.

## 6 Homogeneous solution

Our goal is to prove that the homogeneous equation can only have the trivial solution. This proof is only possible if the weak solution of the homogeneous equations is *even* solution in the **classical sense** (Regularity of the Domain  $\Omega$  and the coefficients  $a_{ij}$ )

**Lemma 6** *Let  $\varphi \in C^2(\bar{\Omega})$  be a classical solution of the homogeneous variational equations. Then  $\varphi = 0$  holds in  $\Omega$ .*

**Result** If domain  $\Omega$  and boundary values are sufficiently regular the mixed linear altimetry - gravimetry BVP has a unique solution for an arbitrary distribution of land and sea.

## 7 Spherical approximation

Essentially stronger results can be proved for spherical approximation of the problem:  
**spherical approximation:**

$$a(\bar{\mathbf{x}}) = \frac{1}{R} \quad (37)$$

$$\mathbf{b}(\bar{\mathbf{x}}) = \frac{\bar{\mathbf{x}}}{|\bar{\mathbf{x}}|} \quad (38)$$

which leads to the boundary value problem:

$$-\Delta\varphi = d \quad (39)$$

$$\varphi|_{\partial\Omega_1} = 0 \quad (40)$$

$$\left(\frac{1}{R}\varphi + \frac{\partial\varphi}{\partial n}\right)|_{\partial\Omega_2} = 0 \quad (41)$$

The bilinear form representing our spherical approximation is :

$$\begin{aligned} \mathcal{A}(\varphi, \psi) := & \int_{\Omega} \nabla \varphi^T \nabla \psi dx \\ & + \int_{\partial\Omega} \varphi \psi d\sigma \end{aligned}$$

Due to the lack of junior-term in this bilinear form instead of V-coercitivity the much stronger property of V-ellipticity can be proved:

**Lemma 7** *Let be  $V = \{u \in W_2^1(\Omega) \mid u|_{\partial\Omega_1} = 0\}$  . then the bilinear form (42) is V - elliptic.*

Hence, as a consequence of *Lax-Milgram theorem* the mixed linear altimetry - gravimetry problem in spherical approximation has a unique weak solution for an arbitrary distribution of land and sea.

## 8 Conclusions

Considering the continental part of the Earth's surface as fixed the following results can be proved:

- in the sense of the weak solution the problem is normal solvable

- if the boundary and the boundary data are sufficiently regular the problem has a unique solution for an arbitrary distribution of land and sea
- in that case the unique solution is even a solution in the classical sense
- for spherical approximation the unique solution for an arbitrary distribution of land and sea can be proved without any assumption about regularity

## References

- [Arn81] Arnold,K. *Complex evaluation of Gravity Anomalies and Data Obtained from Satellite Altimetry*, Gerlands Beitr. Geophys., **90**(1981), pp. 38 - 42
- [Fic65] Fichera,G. *Linear elliptic differential systems and eigenvalue problems*, Lecture Notes in Mathematics Nr.8, Springer - Verlag Berlin Heidelberg New York 1965
- [Hol83a] Holota,P. *The Altimetry - Gravimetry Boundary Value Problem I: Linearization, Friedrichs' Inequality*,Boll. Geod. e Sci. Aff.,**XLII**(1983), Nr. 1 , pp.14 - 32
- [Hol83a] Holota,P. *The Altimetry - Gravimetry Boundary Value Problem II: Linearization, Weak Solution, V - ellipticity*,Boll. Geod. e Sci. Aff.,**XLII**(1983), Nr. 1, pp 70 - 84
- [Kel] Keller,W.: *On a scalar fixed Altimetry-Gravimetry Boundary Value Problem*, to appear in manuscripta geodaetica
- [Mai86] Mainville,A. *The Altimetry - Gravimetry Problem Using Orthonormal Base Functions*, OSU Report Nr. 373, 1986
- [Sac83] Sacerdote,F.;Sanso',F. *A Contribution to the Analysis of the Altimetry - Gravimetry Problems* Bull. Geod. **57**(1983), pp 183 - 201
- [San93] Sanso',F.: *Theory of Geodetic B.V.P.s Applied to the Analysis of Altimeter Data* in: Rummel,R.;Sanso',F. *Satellite Altimetry in Geodesy and Oceanography* Lecture Notes in Earth Sciences Nr. 50, Springer - Verlag 1993
- [Sve83] Svensson,S.L. *Solution of the Altimetry Gravimetry Problem* , Bull. Geod. **57**(1983), pp 332 - 353
- [Wlo82] Wloka, J.*Partielle Differentialgleichungen* BSB B.G. Teubner Verlagsge-sellschaft , Leipzig 1982

# NON-LINEAR EFFECTS IN THE GEODETIC VERSION OF THE FREE GEODETIC BOUNDARY VALUE PROBLEM BASED ON HIGHER ORDER REFERENCE FIELDS

B. Heck and K. Seitz  
Geodetic Institute  
University of Karlsruhe, D - 76128 Karlsruhe, Germany

## INTRODUCTION

The first step in any evaluation of the Geodetic Boundary Value Problem (GBVP) consists of a linearization of the originally non-linear observation equations, based on a chosen reference potential. Neglecting non-linear terms produces a bias in the observation equations as well as in the derived solution functions. In the following the impact of non-linear terms of second order is considered for the case of the geodetic version of the free GBVP, assuming that the "horizontal" coordinates of the surface points - e.g. the geodetic latitudes  $\varphi_g$  and longitudes  $\lambda$  related to a specific reference ellipsoid - are given, while the "vertical" component of the position vector (e.g. ellipsoidal height  $H$ ) is unknown; occasionally this type of GBVP is denoted as the scalar free GBVP. The most obvious choice of observables consists in using the gravity potential  $W$  and the modulus of gravity  $\Gamma$  as boundary data, balancing the two types of unknowns, namely the external gravity potential and the ellipsoidal heights of the surface points. Theoretical aspects of existence and uniqueness of the geodetic version of the free GBVP have been evaluated by Sacerdote and Sansò (1986) and Otero (1987).

Introducing an analytical model (reference) potential  $w$  and a model surface  $s$  (e.g. via a telluroid mapping), difference quantities such as the potential anomaly  $\Delta c$  and gravity anomaly  $\Delta \gamma$  can be derived from the boundary data. Accordingly, the unknown functions are transformed into the disturbing potential  $\delta w$  and the height anomaly  $\Delta h$ ;  $\delta w$  is harmonic outside the earth's surface  $S$ . The telluroid mapping adapted to the setup of the geodetic version of the free GBVP is Molodensky's definition, relating the points  $P \in S$  to the corresponding telluroid points  $p \in s$  by a projection along the ellipsoidal normal and requiring  $\Delta c = 0$  (Heck, 1989). The relationships between the differenced observables  $\Delta c(p)$ ,  $\Delta \gamma(p)$ , attributed to the telluroid points  $p$ , and the unknowns  $\delta w$ ,  $\Delta h$  are still non-linear.

The non-linear differenced boundary equations can be expanded in Taylor series; expansions including second order terms in  $\delta w$  and  $\Delta h$  have been derived by Heck (1989), Heck and Seitz (1993), and Seitz et al. (1994). Based on a two-step solution of the GBVP in second-order approximation, the incremental terms  $v$  (incremental gravity anomaly),  $\delta u$  (incremental potential) and  $d$  (incremental height anomaly) - induced by the second-order terms neglected in the linearized problem - can be evaluated and added to the linear solution. Obviously the magnitude of these incremental second-order terms strongly depends on the choice of the reference potential. In Heck and Seitz (1993) it has been shown that the incremental terms  $v$ ,  $\delta u$  and  $d$  amount up to  $1 \cdot 10^{-6} \text{ ms}^{-2}$ ,  $0.1 \text{ m}^2\text{s}^{-2}$ , and  $3 \text{ mm}$ , respectively, when a Somigliana-Pizzetti reference field (e.g. GRS 80) is applied in the differencing and linearization process. On the other hand, most of recent practical solutions of the GBVP make intensive use of higher degree reference fields, e.g. spherical harmonic expansions of the potential up to degrees 20 or 36 or even 180. In the following the magnitude of non-linear effects is evaluated, based on spherical harmonic reference fields of degrees 2 to 20. This presentation is restricted to the main results of an extensive numerical analysis reported in Seitz et al. (1994).

## THEORY

The Taylor expansion of the boundary conditions for the differenced quantities  $\Delta c$ ,  $\Delta \gamma$  reads (Heck and Seitz, 1993, Seitz et al., 1994)

$$\begin{aligned}\Delta c &= -\delta w + \Delta w_0 - \langle \gamma, n \rangle \cdot \Delta h + 0_c = 0 \\ \Delta \gamma &= -\frac{1}{\gamma} \cdot \gamma, \text{grad } \delta w + \langle \frac{1}{\gamma} \cdot \gamma, M \cdot n \rangle \cdot \Delta h + 0_\gamma \\ M &= \text{grad grad } w(p),\end{aligned}$$

where  $\gamma = \text{grad } w$  denotes the normal gravity vector,  $n$  the ellipsoidal normal unit vector, and  $0_c$ ,  $0_\gamma$  terms of second (and higher) order. These basic relationships can be split up into a linearized form and non-linear incremental parts using the decomposition

$$\begin{aligned}\delta w &= \delta w^\circ + \delta u \\ \Delta h &= \Delta h^\circ + d;\end{aligned}$$

$\delta w^\circ$ ,  $\Delta h^\circ$  form the solution of the linearized equations

$$\begin{aligned}\Delta c &= -\delta w^\circ + \Delta w_0 - \langle \gamma, n \rangle \cdot \Delta h^\circ = 0 \\ \Delta \gamma &= -\frac{1}{\gamma} \cdot \gamma, \text{grad } \delta w^\circ + \langle \frac{1}{\gamma} \cdot \gamma, M \cdot n \rangle \cdot \Delta h^\circ,\end{aligned}$$

while the increments  $\delta u$ ,  $d$  have to be solved from the second order equations

$$\begin{aligned}0 &= -\delta u - \langle \gamma, n \rangle \cdot d + 0_c \\ 0 &= -\frac{1}{\gamma} \cdot \gamma, \text{grad } \delta u + \langle \frac{1}{\gamma} \cdot \gamma, M \cdot n \rangle \cdot d + 0_\gamma \\ \text{Lap } \delta u &= 0 \text{ outside } s.\end{aligned}$$

Neglecting terms of the order of the earth's flattening in the boundary operator of the second-order equations (but not in the linearized equations), the boundary conditions for the incremental terms read

$$\begin{aligned}\delta u - \bar{\gamma} \cdot d &= -\frac{\bar{\gamma}}{r} \cdot (\Delta h^\circ)^2 - \frac{\partial \delta w^\circ}{\partial r} \cdot \Delta h^\circ \\ -\frac{\partial \delta u}{\partial r} - \frac{2\bar{\gamma}}{r} \cdot d &= \frac{3\bar{\gamma}}{r^2} \cdot (\Delta h^\circ)^2 + \frac{\partial^2 \delta w^\circ}{\partial r^2} \cdot \Delta h^\circ - \\ -\frac{1}{2\bar{\gamma}} \left[ \left( \frac{\partial \delta w^\circ}{r \cdot \partial \varphi} \right)^2 + \left( \frac{\partial \delta w^\circ}{r \cdot \cos \varphi \cdot \partial \lambda} \right)^2 \right],\end{aligned}$$

where  $\bar{\gamma}$  is a global mean value of gravity, e.g.  $\bar{\gamma} = 9.81 \text{ ms}^{-2}$ , and  $r$  can be approximated by the radius of a mean earth sphere, e.g.  $r = R = 6371 \text{ km}$ . The first of these equations can be solved for the incremental height anomaly  $d$  which is composed of two terms

$$\begin{aligned} d &= d_I + d_{II} \\ d_I &:= \frac{\delta u}{\gamma} \\ d_{II} &:= \frac{1}{r}(\Delta h^\circ) + \frac{1}{\gamma} \cdot \frac{\partial \delta w^\circ}{\partial r} \cdot \Delta h^\circ; \end{aligned}$$

the component  $d_I$  describes a vertical shift of the level surfaces due to neglection of non-linear terms in the linear solution of the GBVP. Inserting this expression into the second boundary condition yields the reduced boundary condition for  $\delta u$

$$\begin{aligned} -\frac{\partial \delta u}{\partial r} - \frac{2}{r} \delta u &= v \\ v &:= -\frac{2}{r} 0_c - 0_\gamma \\ &\quad - \frac{\bar{\gamma}}{r^2} \cdot (\Delta h^\circ)^2 + \left( \frac{\partial^2 \delta w^\circ}{\partial r^2} + \frac{2}{r} \cdot \frac{\partial \delta w^\circ}{\partial r} \right) \cdot \Delta h^\circ - \\ &\quad - \frac{1}{2\bar{\gamma}} \left[ \left( \frac{\partial \delta w^\circ}{r \cdot \partial \varphi} \right)^2 + \left( \frac{\partial \delta w^\circ}{r \cdot \cos \varphi \cdot \partial \lambda} \right)^2 \right], \end{aligned}$$

where  $v$  can be interpreted as an incremental gravity anomaly term. From the numerical point of view, the product  $(\partial^2 \delta w^\circ / \partial r^2) \cdot \Delta h^\circ$  is by far the largest term in  $v$ , showing strong variations on the boundary surface.

Since Molodensky's telluroid definition has been applied, the linearized solution for the height anomaly  $\Delta h^\circ$  can be expressed by the approximate relationship

$$\Delta h^\circ \approx \delta w^\circ / \bar{\gamma},$$

which is consistent with the degree of precision aimed at in the calculation of second-order effects. As a consequence, the second-order incremental terms  $v$ ,  $d$ ,  $\delta u$  are quadratic in  $\delta w^\circ$  and its first and second order derivatives. It should be noted that the above formulae hold for an arbitrary selection of the reference potential, for a Somigliana-Pizzetti field as well as for a spherical harmonic expansion of degree  $N_0 \geq 2$ .

## EVALUATION OF SECOND-ORDER TERMS

As soon as the solution  $\delta w^\circ$  of the linearized problem is available, the incremental gravity anomaly  $v$  can be calculated on the boundary surface. Again in consistency with the required precision, we can attribute this boundary data to the surface of a sphere with radius  $R$ . An evaluation of the increments  $v$ ,  $d$ ,  $\delta u$  is achieved in several steps (Heck and Seitz, 1993):

(1) First an analytical approximation of the earth's gravity potential is defined through a

standard earth model based on a spherical expansion of degree  $N$  (e.g. GEM 10C,  $N = 180$ , or OSU 91A,  $N = 360$ ). Choosing a reference (normal) potential in the form of a Somigliana-Pizzetti field (GRS80) or a low-degree harmonic expansion (maximum degree  $N_0$ ), the disturbing potential results from differencing these two fields. For the present investigation the field GEM 10C has been applied, the subset of coefficients up to degree  $N_0 \in \{2, 6, 10, 20\}$  serving for the definition of the reference potential. While the results for  $N_0 = 2$  are similar to the Somigliana-Pizzetti case (Heck and Seitz, 1993), it can be guessed that the magnitude of  $\delta w^\circ$  - and similarly the magnitude of the second-order terms - is reduced for  $N_0 > 2$ . As a consequence of the basic data introduced in this investigation, the resulting signals are band-limited in the frequency domain. The difference harmonic series is assumed to present a sufficient approximation for the linear solution  $\delta w^\circ$  in the framework of the present numerical study.

- (2) The series for  $\delta w^\circ$  is applied for calculating  $v$  at the nodes of a spherical grid. The spherical harmonic coefficients  $v_{nm}^\alpha$ ,  $n = 0, 1, 2, \dots N$ ,  $m = -N, \dots, 0, 1, \dots N$ ,  $\alpha \in \{1, 2\}$  result from a spherical harmonic analysis; the procedure has been described in detail in Heck and Seitz (1993).
- (3) Introducing the simple frequency domain relationship

$$\delta u_{nm}^\alpha = R \cdot v_{nm}^\alpha / (n-1)$$

(Heck and Seitz, 1993), the harmonic coefficients of the incremental potential  $\delta u$  are easily calculated. Grid values of  $\delta u$  then result from spherical harmonic synthesis.

- (4) In a similar way the second-order incremental terms  $d_I$ ,  $d_{II}$ ,  $d$  can be calculated. As a result of this procedure the behaviour of the incremental terms  $v$ ,  $\delta u$ ,  $d$  can be studied in the space domain as well as in the frequency domain.

## RESULTS

Figures 1 and 2 illustrate the non-linear term  $v$  in the reduced boundary condition for  $N_0 = 2$  and  $N_0 = 20$ , respectively. It becomes obvious that the decrease in the order of magnitude is dramatical when the degree of the reference field is increased. The case  $N_0 = 2$  compares well with the case of a Somigliana-Pizzetti reference field (Heck and Seitz, 1993) and shows peak-to-peak maximum variations up to  $0.3 \cdot 10^{-5} \text{ ms}^{-2}$ ; the variations of  $v$  show a strong high-frequency behaviour which could be anticipated due to the linear dependence of  $v$  on the second radial derivative of  $\delta w^\circ$ . Increasing  $N_0$  up to 20 results in a decrease of the maximum peak-to-peak variation to  $0.06 \cdot 10^{-5} \text{ ms}^{-2}$ .

Figures 3 and 4 show the respective behaviour of the incremental gravity potential  $\delta u$ . Due to the damping of higher frequencies, this function contains significant long wavelength components, especially over the continents. The maximum peak-to-peak variation reduces from  $0.15 \text{ m}^2 \text{s}^{-2}$  ( $N_0 = 2$ ) to  $0.04 \text{ m}^2 \text{s}^{-2}$  ( $N_0 = 20$ ). These figures correspond to an incremental second-order variation  $d_I$  in geoidal height of 15 mm and 4 mm, respectively.

Concerning the behaviour of  $d_I$  and  $d_{II}$  the same phenomenon as noted in Heck and Seitz (1993) can be recognized. Since  $d_{II}$  nearly mirrors  $d_I$  and differs mainly in the sign, both components nearly cancel in the sum. As a result, the incremental height anomaly  $d$  shows a long-wavelength behaviour. The maximum peak-to-peak variation reduces from about 4 mm ( $N_0 = 2$ ) to 2 mm ( $N_0 = 20$ ), see figs. 5, 6.

A detailed discussion of the space and frequency domain results for non-linear incremental

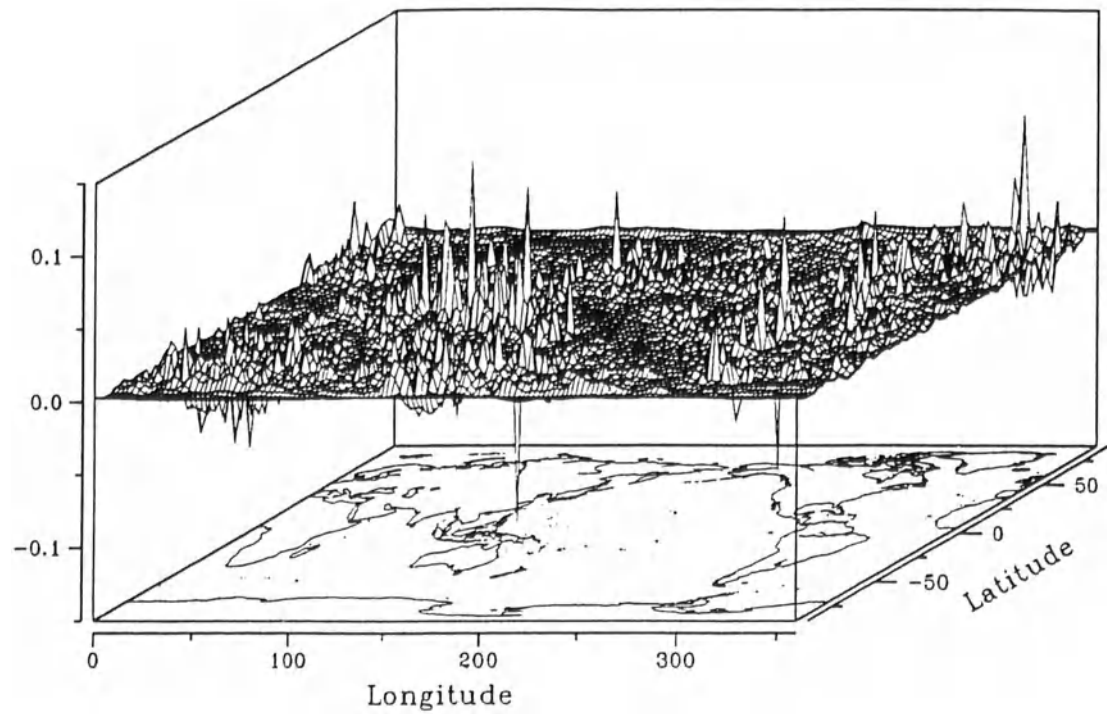


Fig.1. Non-linear incremental term  $v$  [ $10^{-5} \text{ m/s}^2$ ] in the reduced boundary condition  
(GEM 10C,  $N = 180$ ,  $N_0 = 2$ )

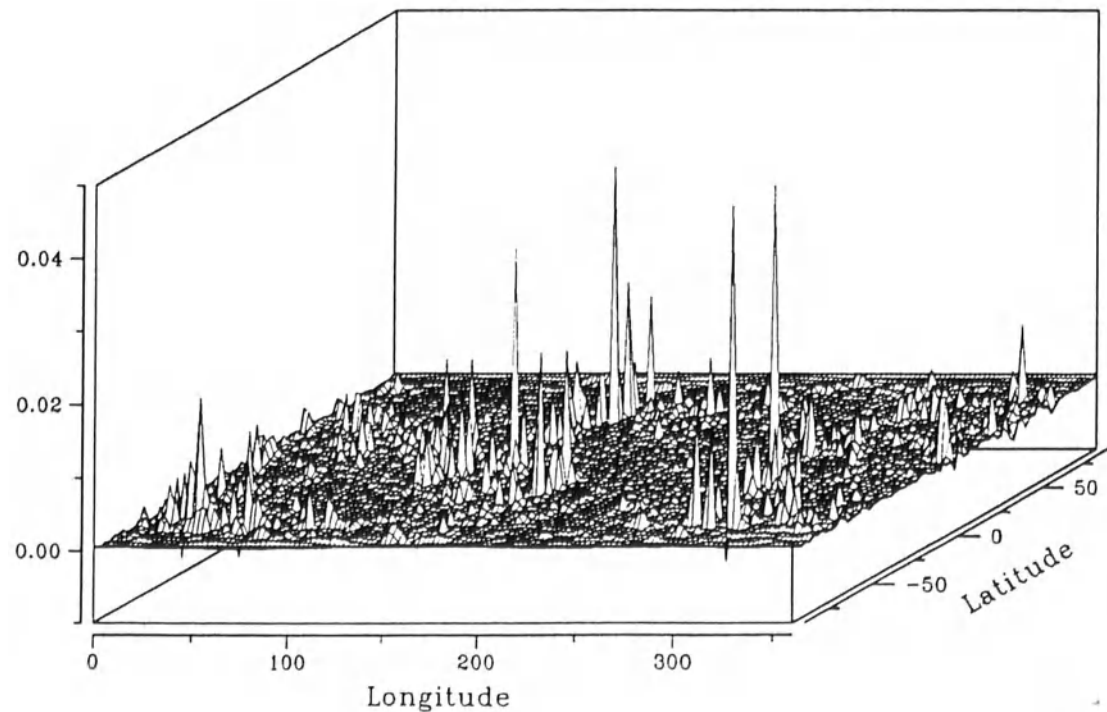


Fig.2. Non-linear incremental term  $v$  [ $10^{-5} \text{ m/s}^2$ ] in the reduced boundary condition  
(GEM 10C,  $N = 180$ ,  $N_0 = 20$ )

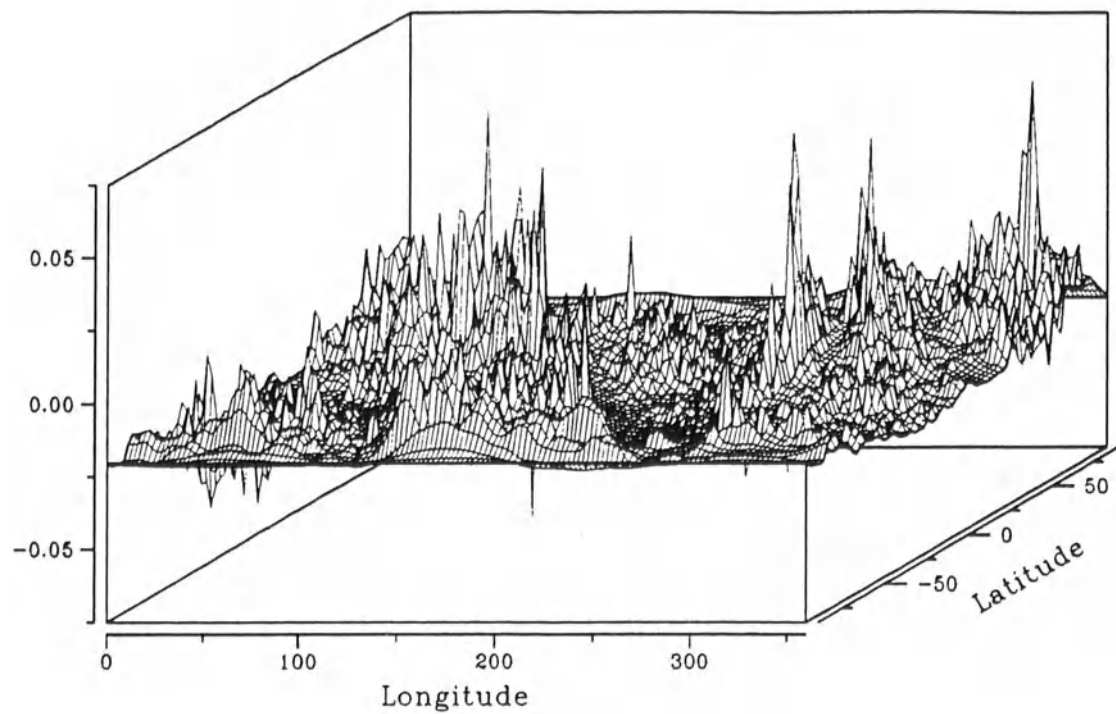


Fig.3. Non-linear incremental term  $\delta u$  [ $m^2/s^2$ ] in the disturbing potential  
(GEM 10C,  $N = 180$ ,  $N_0 = 2$ )

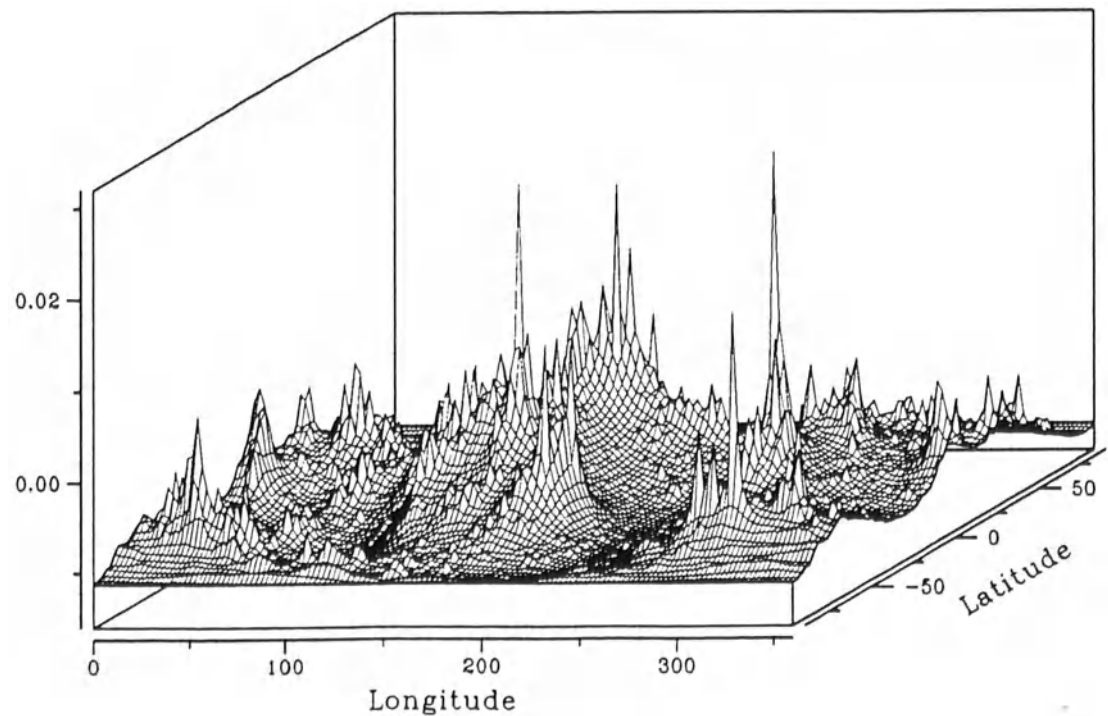


Fig.4. Non-linear incremental term  $\delta u$  [ $m^2/s^2$ ] in the disturbing potential  
(GEM 10C,  $N = 180$ ,  $N_0 = 20$ )

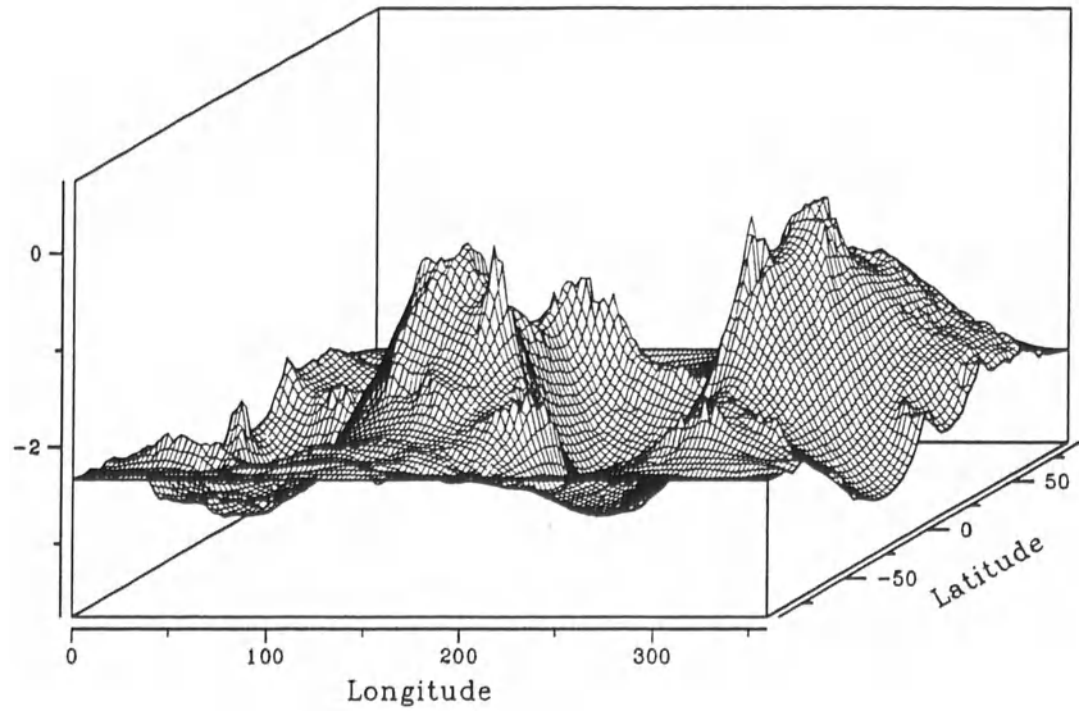


Fig.5. Non-linear incremental term  $d$  [mm] in the height anomaly (GEM 10C,  $N = 180$ ,  $N_0 = 2$ )

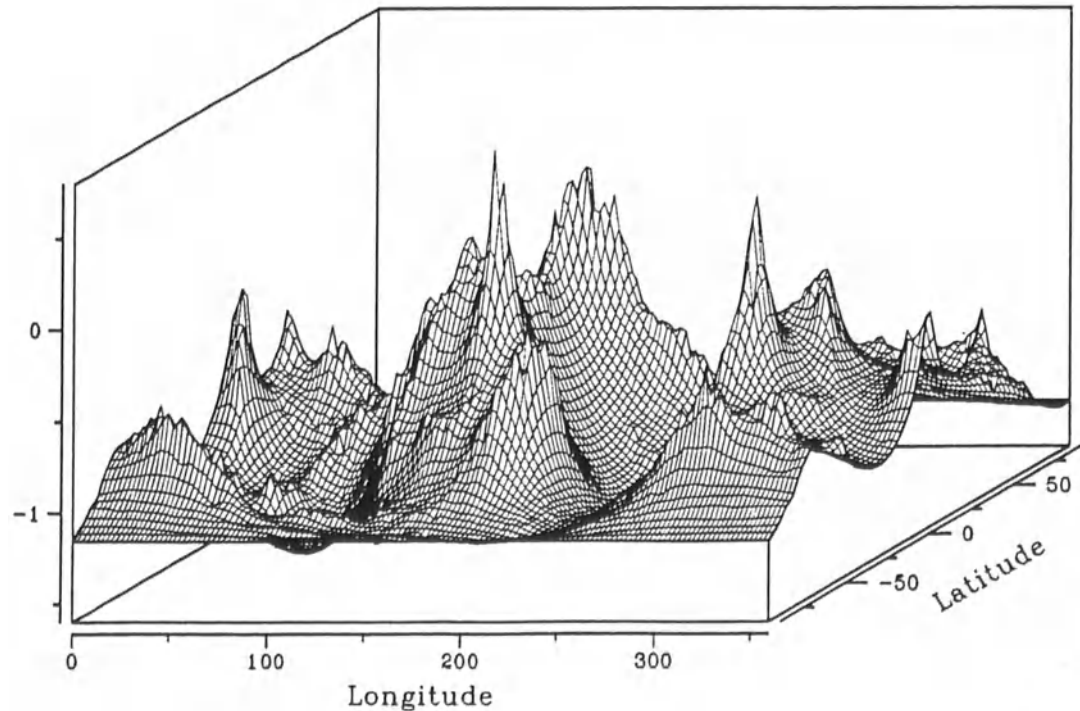


Fig.6. Non-linear incremental term  $d$  [mm] in the height anomaly (GEM 10C,  $N = 180$ ,  $N_0 = 20$ )

effects is contained in Seitz et al. (1994). It should be mentioned that a part of this analysis has been extended by replacing the GEM 10C ( $N = 180$ ) field by the OSU 91A ( $N = 360$ ) gravity field model. The corresponding estimates of non-linear effects increase by using the more detailed representation, but this increase is not drastic. E.g. the maximum peak-to-peak variation in  $v$  increases from  $0.30 \cdot 10^{-5} \text{ ms}^{-2}$  (GEM 10C) to  $0.45 \cdot 10^{-5} \text{ ms}^{-2}$  (OSU 91A), in  $\delta u$  from  $0.15 \text{ m}^2 \text{s}^{-2}$  to  $0.18 \text{ m}^2 \text{s}^{-2}$  when the reference potential is represented by the series terms up to  $N_0 = 2$ . Thus, the order of magnitude of non-linear effects reported above should be correct.

## CONCLUSIONS

The detailed evaluation of non-linear effects in the geodetic version of the free GBVP proves that the effects in the reduced boundary condition, the disturbing potential and the height anomaly are rather small, even when the simple Somigliana-Pizzetti field or a spherical harmonic series up to degree  $N_0 = 2$  is applied as reference potential. Introducing higher degree reference fields produces even smaller impacts of non-linearity, which are mostly negligible in global solutions of the geodetic version of the free GBVP.

It becomes obvious that the strongest variations of the second-order increments  $v$  appear over the continental areas of the earth's surface. As a consequence, local and regional solutions involving integration over small spherical caps might be affected by neglecting non-linear terms much stronger than global solutions. Finally a warning should be given with respect to an extension of these results to other GBVPs: While the fixed GBVP reveals similar properties, it has been shown by Heck and Seitz (1993) that the non-linear terms adopt much larger magnitudes in case of the astronomical variant of Molodensky's problem (vectorial free GBVP); on the other hand it should be stressed that the astronomical version is much less significant from a practical point of view than the geodetic version of the free GBVP.

## REFERENCES

- Heck, B. (1989): A contribution to the scalar free boundary value problem of physical geodesy. *manuscr. geod.*, 14, 87-89.
- Heck, B. and Seitz, K. (1993): Effects of non-linearity in the geodetic boundary value problems. *Deutsche Geodätische Kommission, Reihe A, Heft Nr. 109*, Munich, 74pp.
- Otero, J. (1987): An approach to the scalar boundary value problem of physical geodesy. *manuscr. geod.*, 12, 245-252.
- Sacerdote, F. and Sansò, F. (1986): The scalar boundary value problem of physical geodesy. *manuscr. geod.*, 11, 15-28.
- Seitz, K.; Schramm, B. and Heck, B. (1994): Non-linear effects in the scalar free GBVP based on reference fields of various degrees. *manuscr. geod.*, 19, 327-338.

# **PERTURBATION EXPANSION FOR SOLVING THE FIXED GRAVIMETRIC BOUNDARY VALUE PROBLEM**

**Roland Klees**  
**Faculty of Geodetic Engineering**  
**Delft University of Technology**  
**Thijsseweg 11, 2629 JA Delft**  
**The Netherlands**

## **INTRODUCTION**

One of the most characteristic features of nearly all geodetic boundary value problems is their non-linearity. This property is caused either by our insufficient knowledge of the geometry of the boundary surface or by the boundary condition, which usually is a non-linear functional of the gravitational potential, whereas the partial differential operator is almost linear. All numerical methods, however, which have been considered up to now are restricted to linear boundary value problems (bvp). Therefore, we are faced with mainly three problems:

1. the linearization of the non-linear bvp around an approximate solution,
2. the solution of the related linear bvp, and
3. the construction of a convergent iteration method to solve the non-linear problem by iteration, i.e. by solving a family of related linear problems.

We want to restrict to the third problem, i.e. the construction of a convergent iteration method. This question might be of minor interest for some people since they argue that other error sources are predominant, that one may use a higher degree normal gravity field which makes iteration superfluous, or that because of the numerical effort an iteration might not be reasonable. On the other hand, the density and the accuracy of geodetic boundary data improve permanently and the use of a low degree reference gravity field often simplifies the numerical calculation considerably. Then the question of constructing a convergent iteration method is important. It is true that many iterative methods have been proposed for several geodetic boundary value problems, but only sometimes the convergence of the procedure has been proved.

For the astronomical and the geodetic variant of Molodensky's problem and for the fixed gravimetric bvp some results are known: for the first two problems, the use of a hard implicit function theorem of Moser-Nash type (cf. Hamilton, 1982) allows to solve the nonlinear bvp by iteration of generalized oblique bvp's, a special case of the more general

Poincaré problem. The related iteration method is the so-called Nash iteration, which differs from the well-known Newton method by introducing a smoothing operator in each iteration step (e.g. Schwartz, 1969); however, the construction of a numerically convenient family of smoothing operators is an open question. Therefore, no numerical results are available up to now. For the fixed gravimetric bvp, a "soft" implicit function theorem implies the convergence of a simple Newton method (cf. Zeidler, 1986). In addition, other iteration methods have been proposed by e.g. Bjerhammar and Svensson (1983), Rummel (1988), Heck (1989), Klees (1992); mostly, however, without proving the convergence.

An alternative to using an implicit function theorem is a power series because of its constructive approach. Then, a numerical implementation to approximate the constructed solution is straightforward and does not require any numerical sophistication. In the following we want to construct the power series and want to prove the convergence in classical Hölder spaces using Schauder-type estimates. We will do that for the fixed gravimetric bvp: we want to determine the gravitational potential of the earth, which is harmonic in the external space of the earth, from measurements of the intensity of the field at the earth's surface:

$$\begin{aligned}\Delta V(x) &= 0, \quad x \in B \\ |\text{grad}(V+Z)(x)| &= g(x), \quad x \in \partial B \\ V(x) &= O(|x|^{-1}), \text{ for } |x| \rightarrow \infty\end{aligned}\tag{1}$$

$V$  is the gravitational potential,  $Z$  the centrifugal potential,  $g$  the measured gravity,  $B$  denotes the external space of the earth and  $\partial B$  the earth's surface.

## POWER SERIES EXPANSION

Putting  $V=V_0+T$ , where  $V_0$  is the reference gravitational potential and  $T$  the disturbing potential, we obtain from equation (1), since  $\Delta V_0=0$ :

$$\begin{aligned}\Delta T(x) &= 0, \quad x \in B \\ |\text{grad} T(x)|^2 + 2 \cdot \gamma(x) \cdot \frac{\partial T}{\partial \tau}(x) &= (g^2 - \gamma^2)(x), \quad x \in \partial B \\ T(x) &= O(|x|^{-1}), \text{ for } |x| \rightarrow \infty,\end{aligned}\tag{2}$$

where

$$\begin{aligned}\tau(x) &= \frac{\text{grad}(V_0+Z)}{|\text{grad}(V_0+Z)|}(x), \quad x \in (B \cup \partial B) \quad (\text{oblique direction}) \\ \gamma(x) &= |\text{grad}(V_0+Z)(x)|, \quad x \in (B \cup \partial B) \quad (\text{reference gravity}).\end{aligned}\tag{3}$$

The disturbance potential  $T$  is a small quantity; it can therefore be developed into a series of a small dimensionless parameter  $\epsilon$ :

$$T(x) = \epsilon^1 \cdot T_1(x) + \epsilon^2 \cdot T_2(x) + \dots = \sum_{n=1}^{\infty} \epsilon^n \cdot T_n(x), \quad x \in (B \cup \partial B).\tag{4}$$

After putting (4) into (2) and observing that

$$\left| \sum_{n=1}^{\infty} \epsilon^n \cdot \text{grad } T_n \right|^2 = \sum_{n=1}^{\infty} \epsilon^{n+1} \cdot B_n, \quad B_n := \sum_{s=1}^n \langle \text{grad } T_s, \text{grad } T_{n-s+1} \rangle \quad (5)$$

(Cauchy product formula), we obtain

$$\begin{aligned} \epsilon^1 \cdot \Delta T_1(x) + \epsilon^2 \cdot \Delta T_2(x) + \dots &= 0, \quad x \in B \\ \epsilon^1 \cdot \left( 2\gamma \cdot \frac{\partial T_1}{\partial \tau} \right)(x) + \epsilon^2 \cdot \left( 2\gamma \cdot \frac{\partial T_2}{\partial \tau} + B_1 \right)(x) + \dots &= (g^2 - \gamma^2)(x), \quad x \in \partial B. \end{aligned} \quad (6)$$

Equating equal powers of  $\epsilon$ , we obtain the following sequence of linear boundary value problems (each  $T_i$  is regular at infinity):

$$\begin{aligned} \text{order } \epsilon^1 : \quad \Delta T_1(x) &= 0, \quad x \in B, \quad 2\gamma(x) \cdot \frac{\partial T_1}{\partial \tau}(x) = (g^2 - \gamma^2)(x), \quad x \in \partial B \\ \text{order } \epsilon^2 : \quad \Delta T_2(x) &= 0, \quad x \in B, \quad 2\gamma(x) \cdot \frac{\partial T_2}{\partial \tau}(x) = -B_1(x), \quad x \in \partial B \\ \text{order } \epsilon^3 : \quad \Delta T_3(x) &= 0, \quad x \in B, \quad 2\gamma(x) \cdot \frac{\partial T_3}{\partial \tau}(x) = -B_2(x), \quad x \in \partial B \\ &\vdots \end{aligned} \quad (7)$$

Since the vector field  $\tau$  is oblique to the boundary surface  $\partial B$ , the boundary value problems are oblique boundary value problems. What we have to do now is to prove the convergence of the iterative scheme in some convenient spaces.

## PROOF OF CONVERGENCE

To prove the convergence of the series (4), we first have to choose an appropriate space. We consider the Hölder-spaces  $C^{k+\alpha}(D)$ , where  $k$  is a positive integer,  $0 < \alpha \leq 1$  and  $D$  is a domain in  $\mathbb{R}^3$ . The task is then to prove that for the boundary surface  $\partial B$  from  $C^{1+\alpha}$  and boundary data  $g$  from  $C^{1+\beta}(\Gamma)$ ,  $0 < \beta < \alpha \leq 1$ , the disturbing potential  $T$  is from space  $C^{0+\beta}(D)$ , i.e. that

$$\|T\|_{C^{1+\beta}(D)} \leq \sum_{n=1}^{\infty} \epsilon^n \|T_n\|_{C^{1+\beta}(D)} < \infty \quad (8)$$

The proof consists of 5 steps. First, for every (linear) oblique boundary value problem, we derive an equivalent boundary integral equation. This can be done using e.g. the representation of  $T_n$  as single layer potential with density  $f_n$ :

$$T_n(x) = (Vf_n)(x) = \frac{1}{4\pi} \cdot \int_{y \in \partial B} \frac{f_n(y)}{|x-y|} dB(y) \quad (9)$$

where  $V$  is the single layer operator. Then, we obtain the integral equation:

$$Kf_n(x) := \frac{1}{2} f_n(x) - \frac{1}{4\pi} \cdot \int_{y \in \partial B} k(x, y-x) f_n(y) \cdot dB(y) = b_n(x) \quad (10)$$

with

$$b_n(x) = \begin{cases} \frac{(g^2 - \gamma^2)}{2\gamma}(x), & n=1 \\ -\frac{1}{2\gamma} B_{n-1}(x), & n \geq 2 \end{cases}, \quad k(x, y-x) := \frac{\langle \tau(x), y-x \rangle}{|y-x|^3} \quad (11)$$

The oblique unit vector field  $\tau$  is assumed to be from space  $C^{0+\alpha}$  exactly as the single layer densities  $f_n$ .

The next step consists in the investigation of the properties of the kernel function  $k$  of the integral operator  $K$ . For that we choose a local coordinate system with the origin at  $z \in \partial B$ ; the  $\zeta$ -axis points into the direction of the surface normal at  $z$ ,  $\xi$ -axis and  $\eta$ -axis lie in the tangent plane through  $z$  and define a rectangular right-handed Cartesian coordinate system. It has been proven by Giraud (1934) and Gegelia (1963) that the kernel has then the representation:

$$k(x, y) = k_z(\xi, \eta) = k_{1z}(\xi, \xi - \eta) + k_{2z}(\xi, \eta), \quad (12)$$

and the functions  $k_{1z}$  and  $k_{2z}$  have the properties (see also Kupradze 1979, Klees 1992):

1.  $k_{1z}(\xi, \zeta)$  is homogeneous of degree -2 with respect to  $\zeta$ , and all its derivatives with respect to the cartesian Coordinates of the point  $\zeta$  as a function of  $\xi$  belong to class  $C^{0+\alpha}(S)$  for any  $\zeta$  from  $C(0,1)$ .  $S$  denotes the tangent plane of point  $z$ .
2.  $k_{2z}$  fulfills the following estimates:

$$\begin{aligned} k_{2z} &\text{ is continuous for all pairs } (\xi, \eta) \text{ with } \xi \neq \eta, \\ k_{2z} &= O(|\xi - \eta|^{1+\alpha}), \\ |k_{2z}(\xi, \eta) - k_{2z}(\zeta, \eta)| &\leq C \cdot |\xi - \zeta|^\alpha d_\eta^{-2}(\xi, \zeta), \\ |k_{2z}(\xi, \eta) - k_{2z}(\xi, \zeta)| &\leq C \cdot |\eta - \zeta|^\alpha d_\xi^{-2}(\eta, \zeta), \end{aligned}$$

where  $d_\eta(\xi, \zeta)$  ( $d_\xi(\eta, \zeta)$ ) denotes the distance of the variable  $\eta$  ( $\xi$ ) to the line segment connecting  $\xi$  and  $\zeta$  ( $\eta$  and  $\zeta$ ).

For kernels  $k$  having these properties, it has been proved that the singular integral

$$Af_n := \int_{\partial B} k(x, y) f_n(y) \cdot dy = \lim_{\epsilon \rightarrow 0} \int_{\partial B \setminus S(x, \epsilon)} k(x, y) f_n(y) \cdot dy \quad (13)$$

( $S(x, \epsilon)$  denotes the sphere with centre  $x$  and radius  $\epsilon$ ) exists almost for all  $x$ , and it holds

$$\|Af_n\|_{L^2(\partial B)} \leq C \cdot \|f_n\|_{L^2(\partial B)} \quad (14)$$

(Calderon and Zygmund, 1956). Moreover, any solution  $f_n$  from  $L^2(\partial B)$  of our singular boundary integral equation  $Kf_n = b_n$  belongs for  $b_n$  from  $C^{0+\beta}(\partial B)$ ,  $0 < \beta < \alpha \leq 1$  to class

$C^{0+\beta}(\partial B)$ . In addition, since  $K$  is an invertible operator (i.e. it has a bounded inverse), it holds

$$\|f_n\|_{C^{0+\beta}(\partial B)} \leq C \cdot \|b_n\|_{C^{0+\beta}(\partial B)}. \quad (15)$$

Next, we need some properties of the single layer potential. For  $\partial B$  from  $C^{1+\alpha}$ , single layer density  $f_n$  from  $C^{0+\beta}(\partial B)$ ,  $0 < \beta < \alpha \leq 1$ , we know that the first derivatives of the single layer potential with respect to cartesian coordinates belong to class  $C^{0+\beta}(B)$ , and they are continuously extendible on  $\partial B$  from  $B$ . In addition, it holds

$$\|T_n\|_{C^{1+\beta}(B)} = \|Vf_n\|_{C^{1+\beta}(B)} \leq C \cdot \|f_n\|_{C^{0+\beta}(\partial B)}. \quad (16)$$

Therefore, combining equation (15) and (16), we obtain the estimate:

$$\|T_n\|_{C^{1+\beta}(B)} = \|Vf_n\|_{C^{1+\beta}(B)} \leq C \cdot \|b_n\|_{C^{0+\beta}(\partial B)} < \infty. \quad (17)$$

In addition,  $T_n$  is continuously extendible at each point of  $\partial B$ , and, since  $T_n$  is from  $C^{1+\beta}(B)$ , this extension belongs to class  $C^{1+\beta}(B)$ . Denoting this extension again with  $T_n$ , we can write ( $B = B \cup \partial B$ ):

$$\|T_n\|_{C^{1+\beta}(\bar{B})} = \|Vf_n\|_{C^{1+\beta}(\bar{B})} \leq C \cdot \|b_n\|_{C^{0+\beta}(\partial B)} < \infty. \quad (18)$$

Now, we can apply the results obtained so far to the family of linear boundary value problems given before, and we obtain the estimates:

$$\begin{aligned} \|T_1\|_{C^{1+\beta}(\bar{B})} &\leq K \cdot \frac{\sigma^2 - \gamma^2}{2\gamma} \|b_1\|_{C^{0+\beta}(\partial B)} \\ \|T_n\|_{C^{1+\beta}(\bar{B})} &\leq K \cdot \frac{B_{n-1}}{2\gamma} \|b_{n-1}\|_{C^{0+\beta}(\partial B)} \leq \tilde{K} \cdot \|B_{n-1}\|_{C^{0+\beta}(\partial B)} \\ &\leq 9\tilde{K} \cdot \sum_{s=1}^{n-1} \|T_s\|_{C^{1+\beta}(\bar{B})} \cdot \|T_{n-s}\|_{C^{1+\beta}(B)}, \quad n \geq 2 \end{aligned} \quad (19)$$

with constants  $K = K(\tau, \partial B)$ ,  $\tilde{K} = \tilde{K}(\tau, \partial B)$ , independent on the boundary data.

To complete the proof of the convergence of the series (4) in space  $C^{1+\beta}(B)$ , we construct a convergent majorante. For that we consider the quadratic equation

$$a \cdot x^2 + b \cdot x + c \cdot \epsilon = 0, \quad (20)$$

which has two real solutions if

$$4ac \cdot \epsilon < b^2. \quad (21)$$

Using a binomial expansion we can express any solution in the form

$$x = \sum_{n=1}^{\infty} \epsilon^n \cdot x_n, \quad (22)$$

where the coefficients can be calculated recursively using

$$x_n = -\frac{a}{b} \cdot \sum_{i=1}^{n-1} x_i \cdot x_{n-i}, \quad n \geq 2, \quad x_1 = -\frac{c}{b}. \quad (23)$$

For the proof see Klees (1992). Condition (21) guarantees the convergence of the series (22). To apply this result to our problem we choose

$$a = 9 \cdot \tilde{K}, \quad b = -1, \quad c = K \cdot \left\| \frac{g^2 - \gamma^2}{2\gamma} \right\|_{C^{0+\beta}(\partial B)} \quad (24)$$

and obtain the estimates

$$\begin{aligned} x_1 &\geq \|T_1\|_{C^{1+\beta}(\partial B)}, \\ x_n &\geq \|T_n\|_{C^{1+\beta}(\partial B)}, \quad n \geq 2. \end{aligned} \quad (25)$$

Thus,

$$\sum_{n=1}^{\infty} \epsilon^n \cdot \|T_n\|_{C^{1+\beta}(\bar{B})} \leq \sum_{n=1}^{\infty} \epsilon^n \cdot \|T_n\|_{C^{1+\beta}(\bar{B})} \leq \sum_{n=1}^{\infty} \epsilon^n \cdot x^n < \infty. \quad (26)$$

The condition that the series (4) does converge is now

$$\left\| \frac{g^2 - \gamma^2}{2\gamma} \right\|_{C^{0+\beta}(\partial B)} < \frac{1}{36K \cdot \tilde{K}}, \quad (27)$$

where the constants  $K, \tilde{K}$  have been defined in equation (22). This condition simply means that the reference gravity field has to be chosen such that it is sufficiently close to the actual gravity field, where the closeness is measured in the topology of the space  $C^{0+\beta}(\partial B)$ .

## NUMERICAL RESULTS

To test the iteration scheme (7), we assumed the following scenario: given a spherical boundary surface and a true gravitational field represented by a spherical harmonic expansion up to degree and order 8. As reference gravitational field we used the isotropic part. The test calculations have been performed a) for a non-rotating and b) for a rotating sphere. Then, we have to solve the following family of boundary value problems

$$\begin{aligned} \Delta T_n(x) &= 0, \quad x \in B \\ \frac{\partial T_n}{\partial \tau}(x) &= \frac{1}{2\gamma(x)} \cdot \begin{cases} (g^2 - \gamma^2)(x), & n=1 \\ -B_{n-1}(x), & n \geq 2 \end{cases}, \quad x \in \partial B \\ T_n &= O(|x|^{-1}), \quad \text{for } x \rightarrow \infty \end{aligned} \quad (28)$$

For a non-rotating sphere, the oblique direction field  $\tau$  is normal to the spherical boundary surface, and (28) defines a family of Neumann problems; for a rotating sphere we really have to solve a family of oblique boundary value problems (31) in each iteration step. The results are shown in table 1 for a nonrotating sphere and in table 2 for a rotating sphere.

The rms and maximum errors have been calculated by comparing the solution after each iteration step with the true values calculated at 1891 evenly distributed test points on the

spherical surface. For a nonrotating sphere the potential and the intensity of the field converge very fast. After two iteration steps the relative errors are on the  $10^{-9}$  level. Similar holds for potential of a rotating sphere. For the intensity, however, the results are less satisfactory, and one may argue that there is possibly no convergence of our proposed method; however this is not true. The reason for the apparent problems is that, for keeping the numerics as simple as possible and for studying only linearization errors and not errors that come from solving an oblique boundary value problem, we slightly modified the boundary condition: instead of

$$2 \cdot \langle \text{grad}(V_0 + Z), \text{grad}T_n \rangle = -B_{n-1}, \quad n \geq 2 \quad (29)$$

Table 1. Relative rms and maximum error in potential and intensity for a non-rotating sphere for different iteration counts (eq. (28)) ((x) means  $10^x$ )

iteration count n	gravitational potential V		intensity of the gravitational field	
	rms	max	rms	max
1	2.0 (-6)	2.7 (-6)	1.7 (-6)	5.2 (-6)
2	3.6 (-9)	6.5 (-9)	5.3 (-9)	1.7 (-8)
3	1.8 (-11)	2.9 (-11)	2.0 (-11)	6.8 (-11)
4	7.5 (-14)	1.3 (-13)	9.7 (-14)	3.3 (-13)
5	8.3 (-15)	1.3 (-14)	7.3 (-15)	1.0 (-13)

Table 2. Relative rms and maximum error in potential and intensity for a rotating sphere for different iteration counts (eq. (28))

iteration count n	gravity potential V		intensity of the gravity field	
	rms	max	rms	max
1	2.6 (-6)	3.6 (-6)	3.4 (-6)	6.8 (-6)
2	1.5 (-8)	1.7 (-8)	1.2 (-8)	2.6 (-8)
3	7.2 (-11)	8.1 (-11)	1.4 (-10)	7.4 (-10)
4	3.4 (-13)	3.8 (-13)	1.4 (-10)	7.4 (-10)
5	1.2 (-14)	1.8 (-14)	1.4 (-10)	7.4 (-10)

as theory requires, we implemented the boundary condition

$$2 \cdot \langle \text{grad}V_0, \text{grad}T_n \rangle = -B_{n-1} - 2 \cdot \langle \text{grad}Z, \text{grad}T_{n-1} \rangle, \quad n \geq 2 \quad (30)$$

This minor modification is probably responsible for the slower convergence or even the divergence. However for proving that our method works it is justified to proceed in that way since both the centrifugal potential and the disturbing potential are small quantities compared with the gravitational potential. The local error in the  $n^{\text{th}}$  iteration step is

$$\langle \text{grad}Z, \text{grad}(T_{n-1} - T_n) \rangle; \quad (31)$$

the global errors may be much larger because of accumulation. It may be responsible for the apparent divergence in case of a rotating sphere. The procedure to treat the centrifugal part in this way has first been proposed by Bjerhammar and Svensson (1983) to solve geodetic boundary value problems for a rotating sphere. Whether this is allowed or not is still an open question and no proof of convergence or divergence has been given so far. From a practical point of view it seems to be justified, since the resulting errors are below the  $10^{-9}$  level. We also cannot exclude that rounding-off errors may be responsible for this behaviour.

We compared our method with an iteration procedure that has been proposed by Bjerhammar and Svensson (1983). Here, in each iteration step  $n \geq 1$  the following oblique boundary value problem has to be solved:

$$\begin{aligned} \Delta T_n(x) &= 0, \quad x \in B \\ 2 \cdot \langle \text{grad}(V_0 + Z), \text{grad}T_n \rangle(x) &= (g^2 - \gamma^2)(x) - |\text{grad}T_{n-1}(x)|^2, \quad x \in \partial B \\ T_n(x) &= O(|x|^{-1}), \quad x \rightarrow \infty, \end{aligned} \quad (32)$$

where  $T_0 = 0$ . The results are contained in table 3 and 4.

Here, a similar remark has to be made concerning the way we implemented the algorithm: instead of using the actual boundary condition (cf. (32)), we used the boundary condition

$$\begin{aligned} 2 \cdot \langle \text{grad}V_0, \text{grad}T_n \rangle(x) &= (g^2 - \gamma^2)(x) - |\text{grad}T_{n-1}(x)|^2 \\ &\quad - 2 \cdot \langle \text{grad}Z, \text{grad}T_{n-1} \rangle(x), \quad x \in \partial B \end{aligned} \quad (33)$$

Table 3. Relative rms and maximum error in potential and intensity for a nonrotating sphere for different iteration counts (eq. (32))

iteration count $n$	gravitational potential $V$		intensity of the gravitational field	
	rms	max	rms	max
1	2.0 (-6)	2.7 (-6)	1.7 (-6)	5.2 (-6)
2	3.6 (-9)	6.5 (-9)	5.3 (-9)	1.7 (-8)
3	1.5 (-11)	2.3 (-11)	1.6 (-11)	5.4 (-11)
4	4.0 (-14)	6.9 (-14)	5.2 (-14)	1.8 (-13)
5	5.7 (-16)	1.7 (-15)	2.2 (-16)	1.0 (-13)

Table 4. Relative rms and maximum error in potential and intensity for a rotating sphere for different iteration counts (eq. (32))

iteration count n	gravity potential V		intensity of the gravity field	
	rms	max	rms	max
1	2.6 (-6)	3.7 (-6)	3.4 (-6)	6.8 (-6)
2	1.5 (-8)	1.7 (-8)	1.2 (-8)	2.6 (-8)
3	5.6 (-11)	6.3 (-11)	1.4 (-10)	7.5 (-10)
4	1.8 (-13)	2.0 (-13)	1.3 (-10)	7.4 (-10)
5	1.2 (-15)	3.2 (-15)	1.3 (-10)	7.4 (-10)

When comparing with the power series solution (see table 1 and 2), we observe that both methods give almost identical results; the minor differences are negligible. Unfortunately, the total effort for the iteration (28) is higher than for (32). This is due to the calculation of the right-hand side of the boundary condition in each iteration step: for equation (28), all previously calculated solutions must be available, whereas in (32) only the solution of the last iteration step is needed. Whether this causes a serious problem depends on the number of iterations necessary to fulfil the accuracy requirements.

To get a better impression on the proposed power series method, we consider the simple Newton iteration scheme (we omit the dependency on the boundary x):

$$T_n = T_{n-1} - \phi'(V_0)^{-1}(\phi(V_{n-1}) - g^2), \quad (34)$$

where  $\phi(V)$  denotes the operator of the oblique boundary value problem:

$$\phi(V) = |\text{grad}(V+Z)|^2, \Delta V=0 \quad (35)$$

and  $\phi'(V)^{-1}$  its inverse. Obviously, (34) means nothing else but solving Laplace's equation  $\Delta T_n=0$  with boundary condition

$$2 \cdot \langle \text{grad}(V_0+Z), \text{grad}T_n \rangle = g^2 - \phi(V_{n-1}) + 2 \cdot \langle \text{grad}(V_0+Z), \text{grad}T_{n-1} \rangle. \quad (36)$$

However,

$$\begin{aligned} \phi(V_{n-1}) &= \phi(V_0 + T_{n-1}) = |\text{grad}(V_0 + Z + T_{n-1})|^2 \\ &= \phi(V_0) + 2 \cdot \langle \text{grad}(V_0 + Z), \text{grad}T_{n-1} \rangle + |\text{grad}T_{n-1}|^2. \end{aligned} \quad (37)$$

Putting (37) into (36), we obtain the same boundary condition as in the iteration procedure proposed by Bjerhammar and Svensson (1983). Thus, their method is identical to the simple Newton method. Therefore, we may conclude that the power series behaves like the simple Newton method.

## CONCLUSIONS AND OUTLOOK

The power series expansion is a convenient alternative to the implicit function theorem and the related (simple) Newton iteration scheme. The numerical results seem to prove that this method is equivalent to the simple Newton iteration concerning the speed of convergence. However, further investigations are necessary: other iteration schemes, which have been proposed in the past, should be investigated, e.g. the Newton method and the method proposed by Heck (1989). Besides, the investigations should be extended to the Nash iteration for solving Molodensky's problem(s). In addition, it may be interesting to implement the algorithms for rotating bodies using the actual boundary condition without to approximate the centrifugal potential of the boundary condition. Finally, an extension to higher order reference fields may be of interest.

## REFERENCES

- Bjerhammar, A. and Svensson, L. (1983). On the geodetic boundary value problem for a fixed boundary surface - a satellite approach. *Bulletin Géodésique* 57, 382-393.
- Heck, B. (1989). On the non-linear geodetic boundary value problem for a fixed boundary surface. *Bulletin Géodésique* 63, 57-67.
- Gegelia, T.G. (1963). Some questions of the theory of multidimensional singular integral equations, of the potential theory and of their applications in elasticity (in Russian). Dissertation, Tbil. Math. Inst. of Sci. Acad. of Georgian SSR.
- Giraud, G. (1934). Équations à intégrales principales. Étude suivie d'une application. *Annales Scientifiques de l'Ecole Normale Supérieure, Troisième Serie* 51, 251-372
- Hamilton, R.S. (1982). The inverse function theorem of Nash and Moser. *Bulletin (New Series) of the American Mathematical Society* 7, 65-222.
- Jorge, M.C. (1987): Local existence of the solution to a nonlinear inverse problem in gravitation. *Quarterly of Applied Mathematics*, Vol. XLV, no. 2, 287-292.
- Klees, R. (1992): Loesung des fixen geodaetischen Randwertproblems mit Hilfe der Randelementmethode. German Geodetic Commission, series C, no. 382, Muenchen.
- Kupradze, V.D. (1979). Three-dimensional problems of the mathematical theory of elasticity and thermoelasticity. North-Holland, Amsterdam.
- Rummel, R. (1988). Zur iterativen Loesung der geodaetischen Randwertaufgabe. *Festschrift Rudolf Sigl zum 60. Geburtstag*. German Geodetic Commission, series B, no. 287, 175-181, Muenchen.
- Schwartz, J.T. (1969): Nonlinear functional analysis. Gordon & Breach, New York.
- Zeidler, E. (1986). Nonlinear functional analysis and its application. Vol. I: fixed-point theorems. Springer, New York.

**APPLICATION OF THE CONCEPT OF BIORTHOGONAL SERIES  
TO A SIMULATION OF A GRADIOMETRIC MISSION**  
A.Albertella<sup>(\*)</sup>, F.Migliaccio<sup>(\*\*)</sup>, F.Sansó<sup>(\*)</sup>

(\*) DIIAR - Politecnico di Milano

(\*\*) CNR - IGeS at DIIAR Politecnico di Milano

## 1 Introduction

Over the past 20 years scientists in the fields of oceanography, solid-earth physics and geodesy joined efforts to establish a low-flying gravity field mission in order to obtain an important objective: the resolution of the spatial variations of the gravity field to 100 km half wavelength. Nevertheless, though many concepts were studied (SLALOM, GRAVSAT, GRIM, ARISTOTELES,...) none of the proposed missions has been launched so far and the realisation of an improved gravity field remains an unfulfilled task.

STEP is a mission in the field of fundamental physics: its parameters and payload were not determined for the purpose of a geodesy experiment. But despite this fact, STEP would fly the first gravity gradiometer in space and would produce an excellent high resolution gravity field model.

Regarding the payload, STEP would accomodate on board a set of accelerometers in order to perform several experiments (see Fig.1). As it is well known, differencing the readings of two accelerometers over the distance of their baseline, a first order approximation of a gravity gradient component is derived. In the STEP situation, the G-experiment accelerometers could be used to obtain the  $T_{yy}$  "out-of-plane" component of the gravity tensor with a high accuracy (the intrinsic noise of the gradiometer being better than  $10^{-4}E/\sqrt{Hz}$  for frequencies above  $2 \cdot 10^{-4}Hz$ ).

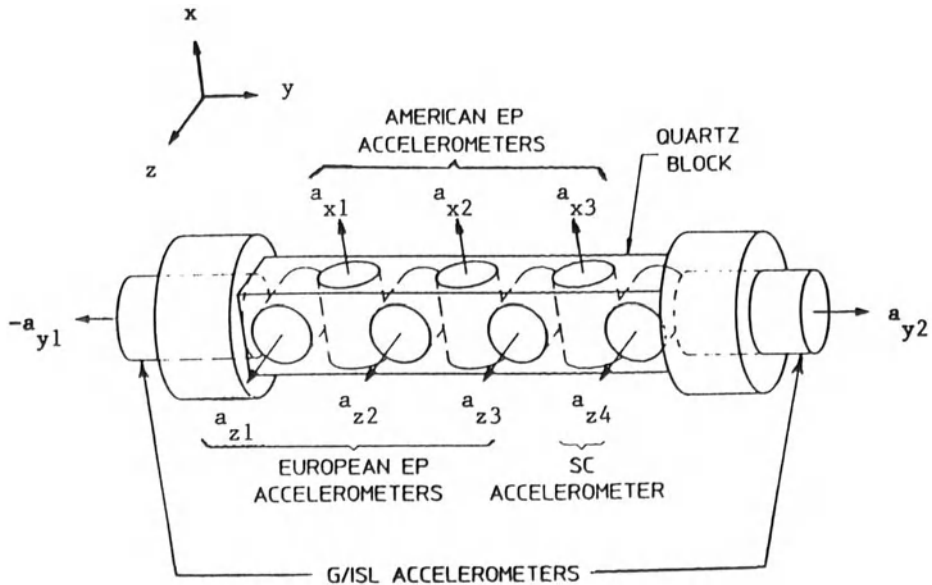


Fig. 1: STEP accelerometers configuration ( $x$  = "along track",  $y$  = "out of plane",  $z$  = "radial"), (ESA-NASA, 1993).

The orbital altitude of STEP would be about 350 km: the low height is fundamental

in any gravity mission, as the gravity signal attenuates exponentially. Other mission parameters include an inclination of  $96^{\circ}.85$  (leaving unsurveyed areas at the poles) and a mission duration of 6 months. Besides, STEP would be drag-free.

Our problem is to recover the coefficients of the power series expansion representing the Earth gravity field, starting from the  $yy$  derivatives of the potential  $T$  observed by means of the STEP gradiometer. Taking advantage from the experiences in the field of gradiometric data treatment gained in the past years while studying simulations of the Aristoteles mission, the Politecnico di Milano group decided to address the problem of processing STEP data by developing its own method and observation equations. Basically, the approach is a “space-wise” one (as opposed to a “time-like” approach). The observations performed by STEP approximately lie on a sphere which has radius equal to the radius of the satellite orbit. Within this frame, the observation equations that must be solved to obtain the model coefficients represent a boundary value problem. Of course it can be handled by means of a “classic” least squares solution. An alternative way of proceeding is to exploit the possibilities of bi-orthogonal series theory.

In this paper we will define the “observables” and the boundary value problem for STEP, write the observation equations and the expressions of the solutions (estimates of the gravity field coefficients) obtained both with the least squares and with the bi-orthogonal series theory.

## 2 Definition of the STEP boundary value problem

The first thing which has to be stated is what we mean by “STEP observable”. In a time frame of six months, the STEP gradiometer would collect 3110401 observations of the  $yy$  component of the Marussi tensor of gravity, at the rate of 1 observation every 5 seconds. The  $yy$  derivative is the one in the out-of-plane direction (where the plane is the one in which the satellite orbit lies). This direction, due to the orbit inclination, does not coincide with the direction of parallels in the terrestrial reference system (cfr. Fig.2).

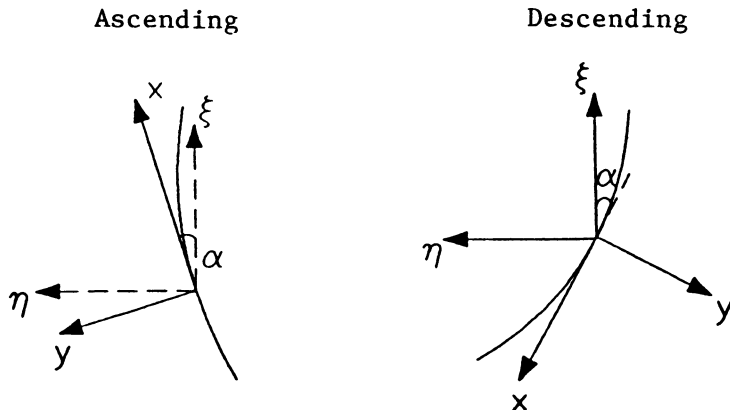


Fig. 2: The orbital  $(x, y)$  and earth  $(\xi, \eta)$  reference systems

The angle between the orbit and the Earth reference systems is represented by  $\alpha$ , and the relation between the second derivatives of  $T$  in the terrestrial reference system and the  $yy$  derivatives are (depending on the fact that the point at which derivatives are computed is taken along an ascending or descending track):

$$\begin{cases} T_{yy}^a = T_{\xi\xi} \sin^2 \alpha - 2T_{\xi\eta} \sin \alpha \cos \alpha + T_{\eta\eta} \cos^2 \alpha \\ T_{yy}^d = T_{\xi\xi} \sin^2 \alpha + 2T_{\xi\eta} \sin \alpha \cos \alpha + T_{\eta\eta} \cos^2 \alpha \end{cases} \quad (1)$$

In our case,  $T_{yy}^a$  and  $T_{yy}^d$  are average values. In fact the sphere at the orbit altitude was divided into a regular (equiangular) grid and to the center point of each block an observed value was assigned representing the average of all the observations performed along ascending ( $T_{yy}^a$ ) and descending ( $T_{yy}^d$ ) arcs in points belonging to that block. Finally, the observable was defined in the following way <sup>1</sup>:

$$D^2 T^o = \frac{T_{yy}^a + T_{yy}^d}{2}. \quad (2)$$

Remembering that the second derivatives along the directions  $\xi$  and  $\eta$  are expressed (in terms of spherical coordinates) in the following way:

$$\begin{cases} T_{\xi\xi} = \frac{1}{r^2} T_{\varphi\varphi} + \frac{1}{r} T_r \\ T_{\eta\eta} = \frac{1}{r^2 \cos^2 \varphi} T_{\lambda\lambda} - \frac{\tan \varphi}{r^2} T_\varphi + \frac{1}{r} T_r. \end{cases} \quad (3)$$

and substituting (3) into (1) the following expression can be found for the observable:

$$D^2 T^o = \left( \frac{1}{r^2} T_{\varphi\varphi} - \frac{1}{r^2 \cos^2 \varphi} T_{\lambda\lambda} + \frac{\tan \varphi}{r^2} T_\varphi \right) \sin^2 \alpha + \frac{1}{r^2 \cos^2 \varphi} T_{\lambda\lambda} - \frac{\tan \varphi}{r^2} T_\varphi + \frac{1}{r} T_r. \quad (4)$$

In (4) the crucial point is to express  $\alpha$  (azimuth of the satellite) as a function of latitude  $\varphi$ ; it is possible to do this by using spherical trigonometry and composing the resulting velocity vectors (see Fig.3).

The expression <sup>2</sup> of  $\sin \alpha$  is:

$$\sin \alpha = \frac{V \frac{\cos i}{\cos \varphi} - wr \cos \varphi}{\sqrt{V^2 + \omega^2 r^2 \cos^2 \varphi - 2Vwr \cos i}} \quad (5)$$

where:

<sup>1</sup>It must be remarked that working with averaged values an important advantage is that the noise level is lowered, but higher frequencies are smoothed.

<sup>2</sup>In the literature (cfr. M.Vermeer, 1990) an expression for the satellite azimuth  $\alpha$  can be found, which is apparently different from (5). However it can be demonstrated that the two expressions are identical.

- $V$  = modulus of the satellite velocity
- $i$  = satellite inclination
- $\omega$  = angular velocity of the Earth
- $r$  = satellite orbit radius.

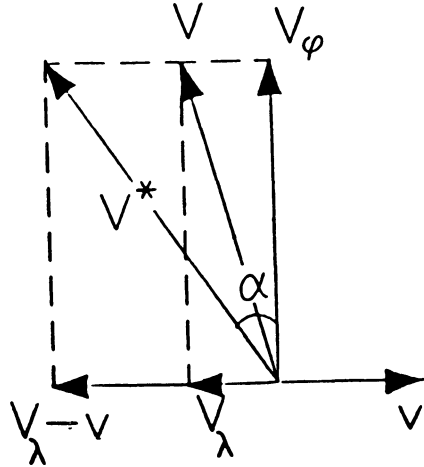


Fig. 3: Definition of the satellite azimuth

Afterwards, the boundary operator  $D^2$  must be applied to the model.  $D^2$  represents the second derivative in the out-of-plane direction, averaged over the block. The gravity field model is expressed (as usual) as a power series expansion in terms of spherical harmonics:

$$T = \sum_{\ell=L_0}^L \sum_{m=-\ell}^{\ell} T_{\ell m} \left(\frac{R}{r}\right)^{\ell+1} Y_{\ell m}(\varphi, \lambda). \quad (6)$$

In (6), not only the expansion must be truncated at a maximum degree  $L$  since obviously only a finite number of coefficients  $T_{\ell m}$  can be determined, but also a minimum degree  $L_0$  was introduced <sup>3</sup>. In fact the lowest degrees harmonics are recovered with a poor accuracy with the use of gradiometric data (especially for order  $m = 0$ ) <sup>4</sup>. Besides when computing the potential coefficients, if the lowest degrees are included in the model the difference between these coefficients and those of the highest degrees is larger than 3 orders of magnitude; as a consequence, if quadrature formulas are used raw numerical errors are introduced in the computations.

<sup>3</sup>Taking advantage from past experiences, we hold that a suitable value for  $L_0$  is close to 10.

<sup>4</sup>In fact in eq.(4) the prevailing term is  $\frac{1}{r^2 \cos^2 \varphi} T_{\lambda \lambda}$  which equals 0 for  $m = 0$ . In this case the terms left are significantly smaller (i.e. carry less information): that's why the resulting estimate of the  $T_{\ell 0}$  coefficients is worse.

Applying  $D^2$  to (6) the following equation is obtained:

$$D^2T = - \sum_{\ell=L_0}^L \sum_{m=-\ell}^{\ell} \frac{1}{R^2} \left(\frac{R}{r}\right)^{\ell+3} T_{\ell m} F_{\ell m}(\varphi) \begin{cases} \cos m\lambda & m \geq 0 \\ \sin |m|\lambda & m < 0 \end{cases} \quad (7)$$

where

$$\begin{aligned} F_{\ell m}(\varphi) &= A_{\ell m}(\varphi) \bar{P}_{\ell m}(\cos \varphi) + B(\varphi) \frac{\partial}{\partial \varphi} \bar{P}_{\ell m}(\cos \varphi) \\ (F_{\ell, -m} &= F_{\ell, m}) \end{aligned} \quad (8)$$

The functions  $F_{\ell m}(\varphi)$  depend not only on the Legendre functions  $\bar{P}_{\ell m}(\cos \varphi)$  and on their derivatives, but also on  $A_{\ell m}(\varphi)$  and  $B(\varphi)$ :

$$A_{\ell m}(\varphi) = (\ell + 1)(\ell + 2) \sin^2 \alpha + \left( \frac{m^2}{\cos^2 \varphi} + \ell + 1 \right) (1 - 2 \sin^2 \alpha) \quad (9)$$

$$B(\varphi) = (1 - 2 \sin^2 \alpha) \tan \varphi \quad (10)$$

It is interesting that  $B(\varphi)$  does not depend on the spherical harmonic degree and order. Besides it can be seen that neither  $A_{\ell m}(\varphi)$  nor  $B(\varphi)$  contain terms oscillating with a frequency increasing with  $\ell$  and  $m$ , though  $A_{\ell m}$  indeed depends on them.

### 3 STEP observation equations

In order to write the STEP observation equations, one has to take into account the way in which the observable was defined, averaging the observations over each block  $B_{kj}$  of the grid, which is identified by means of the coordinates defined in Fig.4.

As a consequence, the observations  $Q_{kj}$  assigned to the point with coordinates  $(\bar{\varphi}_k, \bar{\lambda}_j)$  is obtained by averaging over  $\varphi$  and  $\lambda$  in the following way:

$$Q_{kj} = \frac{1}{A_{kj}} \int_{\varphi_k}^{\varphi_{k+1}} d\varphi \int_{\lambda_j}^{\lambda_{j+1}} D^2T(\varphi, \lambda) d\lambda = \overline{\overline{D^2T}}(\bar{\varphi}_k, \bar{\lambda}_j) \quad (11)$$

where:

$$A_{kj} = \Delta\lambda \cdot \Delta_k = \Delta\lambda \int_{\varphi_k}^{\varphi_{k+1}} \cos \varphi d\varphi = 2\Delta\lambda \cos \bar{\varphi}_k \sin \frac{\Delta\varphi}{2} \quad (12)$$

Of course the real observations contain also the measurement errors  $\nu_{kj}$ , therefore they will be represented by:

$$Q_{kj}^o = Q_{kj} + \nu_{kj}. \quad (13)$$

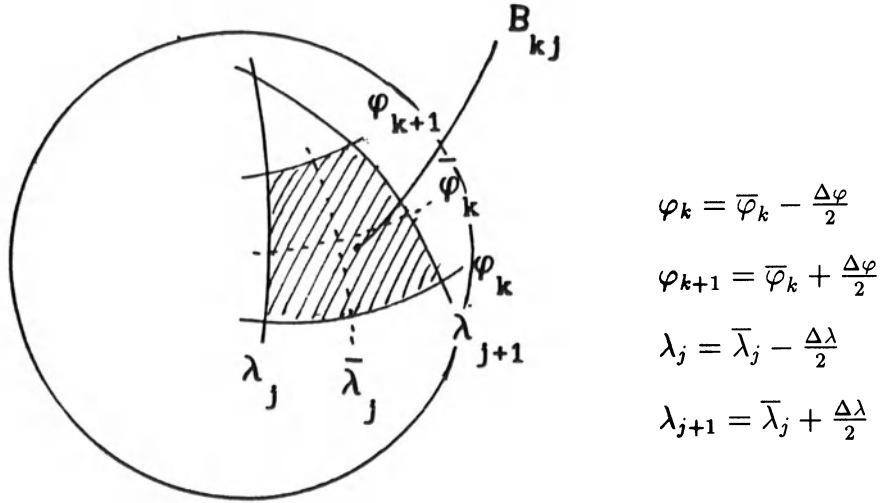


Fig. 4: Definition of the grid block

To write the observation equations to be used in a numerical example, they must be discretized, block averaging the boundary operator defined by (7) over the block  $B_{kj}$ . We start by averaging along a parallel  $\varphi$ :

$$\begin{aligned} \overline{D^2T}(\varphi, \bar{\lambda}_j) &= \frac{1}{\Delta\lambda} \int_{\lambda_j}^{\lambda_{j+1}} D^2T(\varphi, \lambda) d\lambda = \\ &= - \sum_{\ell=L_0}^L \sum_{m=-\ell}^{\ell} \frac{1}{R^2} \left( \frac{R}{r} \right)^{\ell+3} T_{\ell m} q_m F_{\ell m}(\varphi) \begin{Bmatrix} \cos m \bar{\lambda}_j \\ \sin |m| \bar{\lambda}_j \end{Bmatrix} \end{aligned} \quad (14)$$

where:

$$q_m = \begin{cases} \frac{2}{m\Delta\lambda} \sin m \frac{\Delta\lambda}{2} & m \neq 0 \\ 1 & m = 0 \end{cases} \quad (15)$$

Interchanging the summation order and introducing the two symbols:

$$a_{\ell m} \equiv \frac{1}{R^2} \left( \frac{R}{r} \right)^{\ell+3} T_{\ell m} q_m \quad m \geq 0 \quad (16)$$

$$b_{\ell|m|} \equiv \frac{1}{R^2} \left( \frac{R}{r} \right)^{\ell+3} T_{\ell m} q_m \quad m < 0 \quad (17)$$

the equations (14) become:

$$\overline{D^2T}(\varphi, \bar{\lambda}_j) = - \sum_{m=0}^L \left( \sum_{\ell=[m, L_0]}^L a_{\ell m} F_{\ell m}(\varphi) \right) \cos m \bar{\lambda}_j - \sum_{m=1}^L \left( \sum_{\ell=[m, L_0]}^L b_{\ell|m|} F_{\ell m}(\varphi) \right) \sin |m| \bar{\lambda}_j \quad (18)$$

where  $[m, L_0] = \max(m, L_0)$ .

Applying the discrete Fourier transform to (18) and recalling the (discrete) orthogonality relations of sine and cosine functions, we obtain:

$$\sum_{\ell=[m, L_0]}^L a_{\ell m} F_{\ell m}(\varphi) = -\frac{1}{1 + \delta_{m0}} \frac{2}{N} \sum_{j=1}^N \overline{D^2T}(\varphi, \lambda_j) \cos m \bar{\lambda}_j \equiv C_m(\varphi) \quad (19)$$

$$\sum_{\ell=[m, L_0]}^L b_{\ell|m|} F_{\ell m}(\varphi) = -\frac{2}{N} \sum_{j=1}^N \overline{D^2T}(\varphi, \lambda_j) \sin |m| \bar{\lambda}_j \equiv S_m(\varphi) \quad (20)$$

At last, when the average operator along  $\varphi$  is applied to (20) and to (19) the observation equations are obtained in their final discretized form, which means that they can be numerically solved starting from the observations  $Q_{kj}$ :

$$\sum_{\ell=[m, L_0]}^L \begin{pmatrix} a_{\ell m} \\ b_{\ell|m|} \end{pmatrix} F_{\ell m}(\bar{\varphi}_k) = -\frac{1}{1 + \delta_{m0}} \frac{2}{N} \sum_{j=1}^N Q_{kj} \begin{pmatrix} \cos m \bar{\lambda}_j \\ \sin |m| \bar{\lambda}_j \end{pmatrix} = \begin{pmatrix} A_k^{(m)} \\ B_k^{(m)} \end{pmatrix} \quad (21)$$

with  $m = 0, 1, 2, \dots, L$  and

$$\begin{aligned} F_{\ell m}(\bar{\varphi}_k) &= F_{\ell k}^{(m)} = \frac{1}{\Delta_k} \int_{\varphi_k}^{\varphi_{k+1}} F_{\ell m}(\varphi) \cos \varphi d\varphi \simeq \\ &\simeq A_{\ell m}(\bar{\varphi}_k) \frac{1}{\Delta_k} \int_{\varphi_k}^{\varphi_{k+1}} \overline{P}_{\ell m}(\cos \varphi) \cos \varphi d\varphi + \\ &+ \frac{1}{\Delta_k} B(\bar{\varphi}_k) \cos \bar{\varphi}_k [\overline{P}_{\ell m}(\cos \varphi_{k+1}) - \overline{P}_{\ell m}(\cos \varphi_k)] \end{aligned} \quad (22)$$

In eq.(22) an approximation has been carried out. In fact the terms  $A_{\ell m}(\varphi)$  and  $B(\varphi)$  do depend on the latitude, however they are only slowly varying in the integration interval  $[\varphi_k, \varphi_{k+1}]$ , so their values have been considered constant and computed in the central point of the block  $B_{kj}$ .

## 4 Least squares solution

The least squares solution is a straightforward one. The interesting point is how to fix the weight matrix. If one takes (13) as observed quantities, the noise which has to be attached to the  $\begin{pmatrix} A_k^{(m)} \\ B_k^{(m)} \end{pmatrix}$  is represented by:

$$\begin{pmatrix} \nu_{A_k}^{(m)} \\ \nu_{B_k}^{(m)} \end{pmatrix} = -\frac{1}{1 + \delta_{m0}} \frac{2}{N} \sum_{j=1}^N \begin{pmatrix} \cos m \bar{\lambda}_j \\ \sin |m| \bar{\lambda}_j \end{pmatrix} \nu_{kj} \quad (23)$$

where  $\nu_{kj}$  represents the average noise over the block  $B_{kj}$ :

$$\nu_{kj} = \frac{1}{N_{kj}} \sum_{s=1}^{N_{kj}} \nu_{kjs} \quad (24)$$

where  $N_{kj}$  represents the number of observations in each block  $B_{kj}$ .

Under the hypothesis that the noise has the same value  $\sigma_\nu^2$  for each observation, the variance of  $\nu_{kj}$  is:

$$\sigma^2(\nu_{kj}) = \frac{\sigma_\nu^2}{N_{kj}}. \quad (25)$$

Supposing that the data are homogeneously distributed in  $\lambda$  (which has been significantly confirmed by statistical tests with a simulated STEP mission<sup>5</sup>) and that:

$$E\{\nu_{kj}\nu_{mn}\} = 0 \quad \begin{matrix} k \neq m \\ j \neq n \end{matrix} \quad (26)$$

the following expression can be obtained for the covariance of the noise between the sine and cosine components of the solution:

$$E\left\{\begin{pmatrix} \nu_{A_k}^{(m)} \\ \nu_{B_k}^{(m)} \end{pmatrix} \left(\begin{array}{cc} \nu_{A_h}^{(\ell)} & \nu_{B_h}^{(\ell)} \end{array}\right)\right\} = \frac{2\delta_{hk}\sigma_\nu^2}{N(1 + \delta_{m0})^2} \frac{1}{N_k} \begin{pmatrix} 1 + \delta_{m0} & 0 \\ 0 & 1 - \delta_{m0} \end{pmatrix} \delta_{m\ell} \quad (27)$$

Equation (27) shows that, for fixed  $m$ ,  $\nu_{A_k}^{(m)}$  and  $\nu_{B_k}^{(m)}$  are independent and their variances are proportional to  $\frac{1}{N_k}$ . Since:

<sup>5</sup>The simulated data were provided by W.Keller, Stuttgart University.

$$N_k \cong N \rho(\bar{\varphi}_k) 2 \cos \bar{\varphi}_k \sin \frac{\Delta\varphi}{2} \Delta\lambda \quad (28)$$

where  $\rho(\bar{\varphi}_k)$  is the density of observations in a block at latitude  $\bar{\varphi}_k$ :

$$\rho(\bar{\varphi}_k) = \frac{C}{\sqrt{\sin^2 i - \sin^2 \bar{\varphi}_k}} \quad (29)$$

$(C = \text{suitable constant})$

suitable values of the weights are:

$$P_k = \rho(\bar{\varphi}_k) \cos \bar{\varphi}_k. \quad (30)$$

In the end, the l.s. solutions  $\underline{a}^{(m)} = \begin{vmatrix} \vdots \\ a_{\ell m} \\ \vdots \end{vmatrix}$ ,  $\underline{b}^{(m)} = \begin{vmatrix} \vdots \\ b_{\ell|m|} \\ \vdots \end{vmatrix}$  are given by:

$$\begin{cases} \underline{a}^{(m)} = (FPF^+)^{-1} FP(\underline{A}_0^{(m)}) \\ \underline{b}^{(m)} = (FPF^+)^{-1} FP(\underline{B}_0^{(m)}) \end{cases} \quad (31)$$

where  $\underline{A}_0^{(m)}$  and  $\underline{B}_0^{(m)}$  represent the known terms <sup>6</sup>,  $F$  is the matrix containing the elements  $F_{\ell m}(\bar{\varphi}_k)$  (cfr. 22) and  $P$  is the weight matrix (cfr. 30).

The variances  $\sigma_{0m}^2$  (corresponding to each solution) are equal for every  $m$ , except for the case  $m = 0$ , for which  $\sigma_{00}^2$  is half the value of the variance obtained for the other orders  $m \neq 0$  (cfr. eq. (27)).

## 5 Bi-orthogonal series approach and solution

We will now present an alternative approach to the determination of the gravity model: starting from the boundary value problem defined for STEP, the geopotential coefficients can be directly computed from the observations by means of a suitable bi-orthogonal series (cfr. Brovelli and Sansó (1990) and Brovelli and Migliaccio (1993)).

Let us start again from eq.(20) and (19). In the bi-orthogonal series approach, if for example the  $C_m(\varphi)$  should be “exactly” known, the problem would be to find  $\psi_{jm}(\varphi)$  functions such that:

$$\int_{-\frac{\pi}{2}}^{\frac{\pi}{2}} F_{\ell m}(\varphi) \psi_{jm}(\varphi) \cos \varphi d\varphi = \delta_{\ell j} \quad \begin{cases} \ell = [m, L_0], \dots, L \\ j = [m, L_0], \dots, L \end{cases} \quad (32)$$

<sup>6</sup>The index 0 means that these are indeed the “observed” values.

which means that the  $\psi_{jm}(\varphi)$  must be bi-orthogonal to the  $F_{\ell m}(\varphi)$ . Since  $\{F_{\ell m}(\varphi)\}$  is a finite family of functions,  $\psi_{jm}(\varphi)$  is not univocally defined. In fact if for example  $\{\psi_{jm}\}$  is a set bi-orthogonal to  $\{F_{\ell m}\}$  and if  $y$  is perpendicular to the  $\text{Span}_{\ell}\{F_{\ell m}\}$ , then also  $\{\psi_{jm} + y\}$  is bi-orthogonal to  $\{F_{\ell m}\}$ .

A possible criterion which can be applied to fix the  $\psi_{jm}(\varphi)$  is the minimum norm principle. However, we don't know the point values of  $C_m(\varphi)$  and  $S_m(\varphi)$  but only their averages computed over intervals. From (32) the solution would be:

$$\begin{pmatrix} a_{\ell m} \\ b_{\ell|m|} \end{pmatrix} = \int_{-\frac{\pi}{2}}^{\frac{\pi}{2}} \begin{pmatrix} C_m(\varphi) \\ S_m(\varphi) \end{pmatrix} \psi_{\ell m}(\varphi) \cos \varphi d\varphi \quad (33)$$

It is therefore convenient to choose the  $\{\psi_{jm}\}$  in such a way that the scalar products in (33) directly give combinations of the observables.

To this purpose let us define <sup>7</sup>:

$$\psi_{jm}(\varphi) = \sum'_k \Lambda_{jk}^{(m)} \chi_k(\varphi) \quad (34)$$

with  $\chi_k(\varphi)$  characteristic functions:

$$\chi_k(\varphi) = \begin{cases} 1 & \varphi_k \leq \varphi \leq \varphi_{k+1} \\ 0 & \text{elsewhere} \end{cases} \quad (35)$$

(in the summation the intervals with no measures, namely the caps, are skipped).

The simplest minimum norm criterion is the  $L^2$  norm with weights  $\cos \varphi$ :

$$\text{Min} \|\psi_{jm}\|_{L^2}^2 = \text{Min} \sum'_k \Lambda_{jk}^{(m)2} \delta_k \quad (36)$$

(note that  $\int \chi_k(\varphi) \chi_h(\varphi) \cos \varphi d\varphi = \delta_{hk} \Delta_k$  ).

The conditions that must be satisfied by  $\psi_{jm}$  are (cfr. (32)):

$$\langle F_{\ell m}, \psi_{\ell m} \rangle = \delta_{\ell j} \quad j = [m, L_0], \dots, L \quad (37)$$

In matrix notation, (36) and (37) become:

$$\text{Min} \text{ Tr}(\Lambda^{(m)} \Delta \Lambda^{(m)+}) \quad (38)$$

$$M^{(m)} \Lambda^{(m)+} = I^{(m)} \quad (39)$$

<sup>7</sup>The notation  $\sum'_k$  means that the summation is performed only for those  $k$  for which measures exist (polar caps are excluded).

where  $\Delta$  is a diagonal matrix with elements  $\Delta_k$ , and the elements of matrix  $M^{(m)}$  are represented by:

$$M_{\ell k}^{(m)} = \langle F_{\ell m}, \chi_k \rangle = \int_{\varphi_k}^{\varphi_{k+1}} F_{\ell m}(\varphi) \cos \varphi d\varphi \quad (40)$$

After determining the matrix of the Lagrange multipliers:

$$\Lambda^{(m)} = (M^{(m)} \Delta^{-1} M^{(m)+})^{-1} M^{(m)} \Delta^{-1} \quad (41)$$

the solution can be written as:

$$\begin{cases} \underline{a}_{\ell m} = (M^{(m)} \Delta^{-1} M^{(m)+})^{-1} M^{(m)} \Delta^{-1} \underline{A}_0^{(m)} \\ \underline{b}_{\ell m} = (M^{(m)} \Delta^{-1} M^{(m)+})^{-1} M^{(m)} \Delta^{-1} \underline{B}_0^{(m)} \end{cases} \quad (42)$$

If the b.o.s. solution (42) is compared with the l.s. solution (31) their formal identity can be clearly seen. The matrix  $F$  is equivalent to  $M^{(m)}$ . In (42)  $\Delta^{-1}$  plays the role of a weight matrix, but it must be kept in mind that the values of its elements are not weights in a statistical sense.

Finally, we would like to draw some remarks:

- from a conceptual point of view the STEP problem is a very complicated boundary value problem with the  $yy$  derivatives directed along the equator on the equatorial plane and along meridians close to the polar caps; however the observation equations (4) can be handled when block averaged;
- the solutions achieved with both approaches (least squares and bi-orthogonal series) are very close to one another;
- also in a spacewise approach a finite sum of spherical harmonics can be determined, even without polar caps, as it happens in the timewise approach.

## References

M.Brovelli, F.Migliaccio (1993): "The direct estimation of the potential coefficients by biorthogonal sequences". Lectures Notes in Earth Sciences (Sansó and Rummel eds.). Satellite Altimetry in Geodesy and Oceanography. Vol.50, pp.421-441. Springer-Verlag Berlin Heidelberg.

M.Brovelli, F.Sansó (1990): "Gradiometry: the study of the  $V_{yy}$  component in the BVP approach". Manuscripta Geodaetica n.15, pp.240-248.

ESA-NASA (1993): "STEP: Report on the phase A study", SCI(93)4.

F.Migliaccio (1993): "Il progetto STEP: l'utilizzo geodetico". Atti del 12º Convegno GNGTS. Roma.

F.Migliaccio, F.Sacerdote, F.Sansó (1989): "The boundary value problem approach to the data reduction for a spaceborne gradiometer mission". General Meeting IAG, Edinburg, Aug. 3-12.

F.Migliaccio, F.Sansó (1989): "Data processing for the Aristoteles mission". Proc. of the Italian Workshop on "The European Solid-Earth Mission Aristoteles". Trevi, May 30-31.

R.Rummel (1986): "Satellite gradiometry". Lectures Notes in Earth Sciences (H.Sünkel ed.). Mathematical and Numerical Techniques in Physical Geodesy. Vol.50, pp.317-363. Springer-Verlag Berlin Heidelberg.

R.Rummel, M.Van Gelderen, R.Koop, E.Schrama, F.Sansó, M.Brovelli, F.Migliaccio, F.Sacerdote (1993): "Spherical harmonic analysis of satellite gradiometry". Netherlands Geodetic Commission Publications on Geodesy, New Series, Number 39, Delft, The Netherlands.

M.Vermeer (1990): "Observable quantities in satellite gradiometry". Bulletin Geodesique. Vol.64 n.4, pp.347-361.

# LOCAL GEOID ACCURACIES FROM DIFFERENT KINDS OF DATA

A. Albertella, F. Sacerdote

Dipartimento I.I.A.R. - Politecnico di Milano

## ABSTRACT

*Evaluation techniques related to the theory of boundary-value problems with stochastic boundary conditions described by Wiener measures are used to compare the expected accuracies of the geoid obtained from gravity anomalies and from deflections of the vertical, with the current density and precision of individual measurements. Analytical computations are carried out under very simplified assumptions on the distribution of data, initially making the hypothesis of a global data coverage; an outlook at a local computation technique using plane approximation shows that the order of magnitude of the comparative results is essentially unchanged. In both cases, with the current measurement accuracies and densities for deflections of the vertical and gravity anomalies, the latter are shown to yield better accuracies in geoid undulation estimates.*

## INTRODUCTION

In recent times new techniques have been developed for efficient geoid computation starting from different kinds of data localized in a region and from global models of the disturbing potential (Schwarz et al., 1990; Sideris and Forsberg, 1991; Barzaghi and Bottoni, 1993). The use of FFT enables to process a large amount of data; powerful procedures have been devised to evaluate the terrain effect, even in regions with very rough topography.

The most commonly used data are gravity anomalies, together with orthometric heights; computation techniques based on Molodensky's approach have been developed in last years. On the other hand, for geoid computations in mountainous countries, like Switzerland and Austria, the use of vertical deflections has been chosen, due to the very high quality and unusual density of available data sets (Moritz, 1983; Elmiger and Gurtner, 1983; Sünkel et al, 1987). A discussion has been raised in the eighties on advantages and drawbacks of different approaches of local geoid computations, and light has been thrown above all on practical aspects (Kearsley et al., 1985; Tziavos et al., 1992). Previously, a comparison of the accuracies that could be obtained using collocation with different kinds of data, densities and precisions had been presented by (Tscherning, 1975).

On a more theoretical ground, the use of computation techniques based on a continuous description of data, with measurement errors mathematically represented by Wiener measures, allows comparisons of the errors in the determination of the geoid starting from different kinds of data, taking account of the accuracy of individual measurements and of their typical denseness, as found in actually available data sets or in realistic campaign projects. It must be pointed out that this procedure takes account only of the statistical properties of the measurement noise, treated as a generalization of white noise to a continuous set of measurement points; the statistical description of the variation of the observable field is not considered.

For a first rough evaluation, very simplified assumptions can be adopted: data reduced to an equipotential surface and uniformly distributed. In this case, computations can be carried out analytically. Some examples, illustrated in the following sections, show how the formalism of Wiener measures can be used.

## COMPARISON OF ACCURACY LEVELS FOR GLOBAL DATA COVERAGE

In the case of uniform data coverage all over the earth, the computation is very simple. Gravity anomaly data are described by a Wiener measure

$$\mu_{\Delta g}^0(d\sigma) = \Delta g d\sigma + \mu_{\Delta g}^W(d\sigma) \quad (1)$$

that fulfils the properties

$$E\{\mu_{\Delta g}^W(d\sigma)\} = 0 ; \quad E\{\mu_{\Delta g}^W(d\sigma_Q)\mu_{\Delta g}^W(d\sigma_{Q'})\} = \sigma_{\Delta g}^{(W)2}\delta(Q' - Q)d\sigma_Q d\sigma_{Q'} \quad (2)$$

Hence Stokes's formula can be expressed in the form

$$N(P) = \frac{R}{4\pi\gamma} \int_{\Sigma} S(\psi_{PQ})\mu_{\Delta g}^0(d\sigma_Q) \quad (3)$$

where  $\Sigma$  is the unit sphere. Consequently, the expression for the error is

$$\epsilon_N(P) = \frac{R}{4\pi\gamma} \int_{\Sigma} S(\psi_{PQ})\mu_{\Delta g}^W(d\sigma_Q) \quad (4)$$

that leads to the formal expression for the error variance

$$E\{\epsilon_N^2(P)\} = \frac{R^2\sigma_{\Delta g}^{(W)2}}{16\pi^2\gamma^2} \int_{\Sigma} S^2(\psi_{PQ})d\sigma_Q \quad (5)$$

Yet, the integral in (5) diverges, due to the singularity of  $S$  for  $\psi = 0$ . This is a consequence of the fact that the operator introduced in (3), to obtain an estimate of point values of  $N$  from a Wiener measure, is not sufficiently regularizing to make  $N$  continuous. In order to overcome this difficulty, values of  $N$  averaged over small areas may be considered:

$$\bar{N}^{(\psi)}(P) = \frac{1}{\mu(C_\psi)} \int_{C_\psi} N(P') ds_{P'} \quad (6)$$

where  $C_\psi$  is a spherical cap with amplitude  $\psi$ , centred at  $P$ . The corresponding error is

$$\bar{\epsilon}_N^{(\psi)}(P) = \frac{1}{\mu(C_\psi)} \int_{C_\psi} \epsilon_N(P') ds_{P'} = \frac{1}{\mu(C_\psi)} \frac{R}{4\pi\gamma} \int_{C_\psi} ds_{P'} \int_{\Sigma} S(\psi_{P'Q}) \mu_{\Delta_g}^W(d\sigma_Q) \quad (7)$$

and the expression of its variance is

$$E\{\bar{\epsilon}_N^{(\psi)}(P)\}^2 = \frac{1}{\mu^2(C_\psi)} \frac{R^2}{16\pi^2\gamma^2} \sigma_{\Delta_g}^{(W)2} \int_{C_\psi} ds_{P'} \int_{C_\psi} ds_{P''} \int_{\Sigma} S(\psi_{P'Q}) S(\psi_{P''Q}) d\sigma_Q \quad (8)$$

The integral in (8) can be explicitly computed, making use of the harmonic expansion of Stokes's function,  $S(\psi) = \sum_2^\infty \frac{2n+1}{n-1} P_n(\cos \psi)$  and of the definition of the eigenvalues  $\beta_n$  of the average operator over caps:  $\mu(C_\psi)^{-1} \int_{C_\psi} Y_{nm}(\sigma) d\sigma = \beta_n Y_{nm}(\sigma_C)$  ( $\sigma_C$ =centre of the cap). Indeed

$$\begin{aligned} & \int_{C_\psi} ds_{P'} \int_{C_\psi} ds_{P''} \int_{\Sigma} S(\psi_{P'Q}) S(\psi_{P''Q}) d\sigma_Q = \\ &= \int_{\Sigma} d\sigma_Q \int_{C_\psi} ds_{P'} S(\psi_{P'Q}) \int_{C_\psi} ds_{P''} S(\psi_{P''Q}) = \\ &= \int_{\Sigma} d\sigma_Q \int_{C_\psi} ds_{P'} \sum_2^\infty \frac{2n+1}{n-1} P_n(\cos \psi_{P'Q}) \int_{C_\psi} ds_{P''} \sum_2^\infty \frac{2n'+1}{n'-1} P_n(\cos \psi_{P''Q}) = \\ &= \int_{\Sigma} d\sigma_Q \mu^2(C_\psi) \sum \frac{2n+1}{n-1} \frac{2n'+1}{n'+1} \beta_n(\psi) \beta_{n'}(\psi) P_n(\cos \psi_{PQ}) P_{n'}(\cos \psi_{PQ}) = \\ &= \mu^2(C_\psi) \sum \frac{2n+1}{n-1} \frac{2n'+1}{n'+1} \beta_n(\psi) \beta_{n'}(\psi) \int_{\Sigma} d\sigma_Q P_n(\cos \psi_{PQ}) P_{n'}(\cos \psi_{PQ}) = \\ &= \mu^2(C_\psi) \sum \left(\frac{2n+1}{n-1}\right)^2 \beta_n^2(\psi) \frac{4\pi}{2n+1} \end{aligned} \quad (9)$$

The series in the last term converges; a short proof is presented in the appendix. Its sum cannot be computed analytically, but, as the coefficients  $\beta_n$  can be easily computed by recursion formulas, it is not difficult to give an approximate evaluation numerically.

Inserting (9) into (8), one obtains

$$E\{\bar{\epsilon}_N^{(\psi)}(P)\}^2 = \frac{R^2}{4\pi\gamma^2} \sigma_{\Delta_g}^{(W)2} \sum \frac{2n+1}{(n-1)^2} \beta_n^2(\psi) \quad (10)$$

It is remarkable that this value depends on  $\psi$  and grows for decreasing  $\psi$ , as can be deduced from the behaviour of the coefficients  $\beta_n$ . For practical computations a reasonable choice is to average over small regions, say with  $\psi \simeq 0^\circ.1$ , where generally small variations of  $N$  are expected.

As for the numerical value of  $\sigma_{\Delta g}^{(W)2}$ , the relation between this quantity and the variance of individual measurements has to be briefly recalled. The Wiener measure  $\mu^{(W)}$  is in a sense the limit for  $N \rightarrow \infty$  of the quantity

$$\mu^{(W;N)}(A) = \sum_{P_i \in A} \nu_i \mu_i$$

where  $\nu_i$  represent the noise of individual measurements and  $\mu_i$  are the Euclidean measures of domains  $T_i \subset A$  containing just one point  $P_i$ . For a constant measurement density  $\mu_i = \mu_{TOT}/N \equiv \mu$  is independent of  $i$ . Hence

$$E\{\mu^{(W;N)2}(A)\} = \mu^2 N(A) \sigma_\nu^2 = \frac{\mu_{TOT}}{N} \mu(A) \sigma_\nu^2 \quad (11)$$

On the other hand, by (2),  $E\{\mu^{(W)2}(A)\} = \sigma^{(W)2} \mu(A)$ .

As the continuum formulation is introduced to describe a situation of very dense, but actually discrete data, the constants introduced in this formulation must reflect the values corresponding to the actual accuracy of the individual measurements and their total number. Therefore it is reasonable to assume  $\sigma^{(W)2} = \sigma_\nu^2 (\mu_{TOT}/N)$ .

A similar procedure may be adopted if vertical deflections are assumed to be used as data. The two components  $\xi, \eta$  of the deflection of the vertical are expressed as tangential derivatives of the disturbing potential:

$$\begin{pmatrix} \xi \\ \eta \end{pmatrix} = \frac{1}{\gamma R} \nabla_\sigma T \quad ; \quad \nabla_\sigma = \begin{pmatrix} \partial/\partial\phi \\ \frac{1}{\cos\phi} \partial/\partial\lambda \end{pmatrix} \quad (12)$$

correspondingly a two-dimensional Wiener measure may be defined:

$$\mu_{DV}^{(0)}(d\sigma) = \frac{1}{\gamma R} \nabla_\sigma T d\sigma + \mu_{DV}^{(W)}(d\sigma) \quad (13)$$

with covariance

$$E\{\mu_{DV}^{(W)}(d\sigma_Q) \mu_{DV}^{(W)T}(d\sigma_{Q'})\} = \sigma_{DV}^{(W)2} \cdot I \cdot \delta(Q - Q') d\sigma_Q d\sigma_{Q'} \quad (14)$$

It has to be remarked that, if both components of the deflection of the vertical are assumed to be simultaneously known everywhere and used as boundary conditions for a boundary-value problem, they are indeed redundant, so that the BVP has to be treated as overdetermined. Furthermore, such data are consistent with the introduction of an arbitrary additive constant in the disturbing potential on the boundary; hence, the zero-degree harmonic component of the solution is left undetermined.

Following (Sansò 1988), one looks for an estimate of the disturbing potential of the form

$$\hat{T}(P) = \int_{\Sigma} \beta(P, Q) \cdot \mu_{DV}^{(0)}(d\sigma_Q) \quad (15)$$

that minimizes the variance

$$E\left\{ \left| \int_{\Sigma} \beta(P, Q) \cdot \mu_{DV}^{(W)}(d\sigma_Q) \right|^2 \right\} = \sigma_{DV}^{(W)2} \int_{\Sigma} |\beta(P, Q)|^2 d\sigma_Q \quad (16)$$

under the *unbiasedness condition*

$$\hat{T}(P) = \frac{1}{\gamma R} \int_{\Sigma} \beta(P, Q) \cdot \nabla_{\sigma} \hat{T}(Q) d\sigma_Q \quad (17)$$

It is well-known that the constrained minimum is attained by introducing a Lagrange multiplier  $\lambda(P, Q)$  and carrying out a free minimization of the function

$$\frac{1}{2} \sigma_{DV}^{(W)2} \int_{\Sigma} |\beta(P, Q)|^2 d\sigma_Q - \frac{1}{\gamma R} \int_{\Sigma} \beta(P, Q) \cdot \nabla_{\sigma_Q} \lambda(P, Q) d\sigma_Q \quad (18)$$

with respect to  $\beta(P, Q)$ . The result is

$$\beta(P, Q) = \frac{1}{\sigma_{DV}^{(W)2} \gamma R} \nabla_{\sigma_Q} \lambda(P, Q) \quad (19)$$

Inserting (19) into the unbiasedness condition, one obtains

$$\frac{1}{\sigma_{DV}^{(W)2} \gamma^2 R^2} \nabla_{\sigma_Q}^2 \lambda(P, Q) = \delta(P - Q) \quad (20)$$

whose solution for  $\lambda$ , expressed in terms of spherical harmonics, can be formally expressed as

$$\begin{aligned} \lambda(P, Q) &= -\sigma_{DV}^{(W)2} \frac{\gamma^2 R^2}{4\pi} \sum \frac{Y_{nm}(P) Y_{nm}(Q)}{n(n+1)} = \\ &= -\sigma_{DV}^{(W)2} \frac{\gamma^2 R^2}{4\pi} \sum \frac{2n+1}{n(n+1)} P_n(\cos \psi_{PQ}) \end{aligned} \quad (21)$$

Yet, in this case too, the result is not sufficiently regular to yield an acceptable solution; therefore, in order to obtain an estimate of the uncertainty level, again averaged values have to be considered. The error on the geoid undulation, averaged over a small cap, has the expression

$$\bar{\epsilon}_N^{(\psi)}(P) = \frac{1}{\gamma \mu(C_\psi)} \int_{C_\psi(P)} ds_{P'} \int_{\Sigma} \beta(P', Q) \cdot \mu_{DV}^{(W)}(d\sigma_Q) \quad (22)$$

and consequently

$$E\{\bar{\epsilon}_N^{(\psi)2}(P)\} = \frac{1}{\gamma^2 \mu^2(C_\psi)} \sigma_{DV}^{(W)2} \int_{C_\psi(P)} ds_{P'} \int_{C_\psi(P)} ds_{P''} \int_{\Sigma} \beta(P', Q) \cdot \beta(P'', Q) d\sigma_Q \quad (23)$$

Using equation (19) for  $\beta$ , with  $\lambda$  expressed by (21), one obtains

$$E\{\bar{\epsilon}_N^{(\psi)2}(P)\} = \frac{1}{\mu^2(C_\psi)} \sigma_{DV}^{(W)2} \frac{R^2}{(4\pi)^2} \int_{C_\psi(P)} ds_{P'} \int_{C_\psi(P)} ds_{P''} \cdot \\ \cdot \sum \frac{2n+1}{n(n+1)} \frac{2n'+1}{n'(n'+1)} \int_{\Sigma} \nabla_{\sigma} P_n(\cos \psi_{P'Q}) \cdot \nabla_{\sigma} P_{n'}(\cos \psi_{P''Q}) d\sigma_Q \quad (24)$$

The last integral can be transformed in the following way:

$$\begin{aligned} & \int_{\Sigma} \nabla_{\sigma} P_n(\cos \psi_{P'Q}) \cdot \nabla_{\sigma} P_{n'}(\cos \psi_{P''Q}) d\sigma_Q = \\ &= - \int_{\Sigma} P_n(\cos \psi_{P'Q}) \nabla_{\sigma}^2 P_{n'}(\cos \psi_{P''Q}) d\sigma_Q = \\ &= n'(n'+1) \sum_{mm'} \frac{Y_{nm}(\sigma_{P'}) Y_{n'm'}(\sigma_{P''})}{(2n+1)(2n'+1)} \int_{\Sigma} Y_{nm}(\sigma_Q) Y_{n'm'}(\sigma_Q) d\sigma_Q = \\ &= 4\pi n(n+1) \sum_m \frac{Y_{nm}(\sigma_{P'}) Y_{nm}(\sigma_{P''})}{(2n+1)^2} \delta_{nn'} \end{aligned} \quad (25)$$

Inserting (25) into (24), one obtains

$$E\{\bar{\epsilon}_N^{(\psi)2}(P)\} = \\ = \frac{\sigma_{DV}^{(W)2} R^2}{4\pi \mu^2(C_\psi)} \int_{C_\psi(P)} ds_{P'} \int_{C_\psi(P)} ds_{P''} \sum_n \frac{1}{n(n+1)} \sum_m Y_{nm}(\sigma_{P'}) Y_{nm}(\sigma_{P''}) = \quad (26) \\ = \sigma_{DV}^{(W)2} \frac{R^2}{4\pi} \sum_n \beta_n^2(\psi) \frac{2n+1}{n(n+1)}$$

Obviously, for the numerical value of  $\sigma_{DV}^{(W)2}$ , the same procedure used for  $\sigma_{\Delta g}^{(W)2}$ , outlined in the sequel of formula (10), may be followed.

For a rough numerical comparison between (10) and (26), consider their ratio, given by

$$\frac{S(\Delta g)}{S(DV)} \frac{1}{\gamma^2} \frac{\sigma_{\Delta g}^{(W)2}}{\sigma_{DV}^{(W)2}} \quad (27)$$

where  $S(\Delta g)$ ,  $S(DV)$  are respectively the sums of the series in (10) and in (26). It is immediately verified that the ratio of the coefficients is such that

$$\left( \frac{2n+1}{(n-1)^2} \right) / \left( \frac{2n+1}{n(n+1)} \right) < 6 \quad (28)$$

and becomes rapidly very close to 1 for increasing  $n$ . A numerical evaluation of the partial sums of the two series with 2000 terms, for values of  $\psi$  close to  $0^\circ.1$ ,  $0^\circ.2$  shows that their ratio is approximately 1.5; if only harmonic components above degree 20 are taken into account, this ratio drops to about 1.05.

For the variances of individual measurements values of  $10^{-8}$  to  $10^{-10} \text{ gal}^2$  for gravity anomalies and  $10^{-11}$  to  $10^{-12} \text{ rad}^2$  for the deflection of the vertical may be adopted; if, in addition, the density of gravity anomaly measurements is assumed to be 10 to 100 times larger than the density of the deflections of the vertical (one per 1 or 10  $\text{km}^2$  versus 1 per 100  $\text{km}^2$ ), the value of the ratio (27) ranges between  $10^{-3}$  and  $10^{-7}$ , the most reasonable values being between  $10^{-4}$  and  $10^{-5}$ . Hence it is proved that, for realistic values of measurement density and accuracy, the resulting accuracy in the geoid undulation estimate is considerably better for measurements of gravity anomaly than of deflections of the vertical. Yet, it has to be pointed out that reduction errors due to a poor knowledge of orthometric heights and terrain densities may spoil gravity anomaly accuracies, whereas they have a less relevant effect on vertical deflections, whose intrinsic accuracy is comparatively worse.

## PLANE APPROXIMATION AND LOCAL ACCURACY ESTIMATES

The developments of the previous section have been carried out under the unrealistic assumption of a global data coverage. A local approach may be set up adopting the planar approximation. In this context the operator that connects gravity anomalies to the disturbing potential is simply the out-of-plane derivative, while the vertical deflection vector is represented by the plane gradient:

$$\Delta g = -\frac{\partial T}{\partial z} \quad ; \quad \boldsymbol{\epsilon} = \frac{1}{\gamma} \nabla_0 T \quad (29)$$

Correspondingly, the planar version of Stokes's formula is given by

$$T(P) = \frac{1}{2\pi} \int \frac{\Delta g(Q)}{r_{PQ}} d\underline{x}_Q \quad (30)$$

Computations similar to the ones of the previous section may be developed starting from the above formulation. Yet, the integration over an infinite plane leads to an unremovable singularity, whereas difficulties in analytical computation arise if the integration domain is kept bounded.

On the other hand, a simple treatment of noise propagation may be carried out in the frequency space. It is well-known (see for instance Barzaghi et al., 1993) that the Fourier transforms of the equations (29) are given by

$$\tilde{\Delta}g(\underline{k}) = k\tilde{T}(\underline{k}) \quad ; \quad \tilde{\epsilon}(\underline{k}) = \frac{i}{\gamma}k\tilde{T}(\underline{k}); \quad (k = |\underline{k}|) \quad (31)$$

Furthermore, if measurements are assumed to be affected by a white noise, it can be proved that the covariance function of their Fourier transform is consistent with a white noise in the frequency space, with the same variance. Consequently, the observation equations can be written as

$$\tilde{\Delta}g(\underline{k}) = k\tilde{T}(\underline{k}) + \tilde{\nu}_{\Delta g}(\underline{k}) \quad (32a)$$

$$\tilde{\epsilon}(\underline{k}) = \frac{i}{\gamma}k\tilde{T}(\underline{k}) + \tilde{\nu}_{\epsilon}(\underline{k}) \quad (32b)$$

where  $\tilde{\nu}_{\Delta g}$ ,  $\tilde{\nu}_{\epsilon}$  have the statistical properties of white noise. Therefore they can be described by Wiener measures in the frequency space, with the variances  $\sigma_{\Delta g}^{(W)2}$ ,  $\sigma_{DV}^{(W)2}$  introduced in the previous section.

A direct evaluation of the uncertainty in the determination of geoid undulation from both kinds of measurements would have to tackle the difficulty arising from the singularity in the variable  $k$ ; yet, a very simple argument leads to a straightforward, though indirect, comparison. Indeed, taking the scalar product of equation (32b) by  $\underline{e} = -ik/k$ , one obtains

$$\gamma\underline{e} \cdot \tilde{\epsilon}(\underline{k}) = k\tilde{T}(\underline{k}) + \gamma\underline{e} \cdot \tilde{\nu}_{\epsilon}(\underline{k}) \quad (33)$$

that looks exactly like (32a), but for the expression of the noise.

Hence, the ratio of the noise variances in (32a) and in (33), that are respectively  $\sigma_{\Delta g}^{(W)2}$  and  $2\gamma\sigma_{DV}^{(W)2}$ , measures the relative accuracy of geoid undulations obtained by the two kinds of measurements. Comparing this ratio with expression (27), it is clear that it is essentially of the same order of magnitude.

## CONCLUDING REMARKS

The computations above developed show how evaluation techniques taken from general procedures used in BVP theory allows rough a-priori estimations of expected accuracies. The examples presented in previous sections, for which estimates of the same order of magnitude could be obtained with simpler evaluation procedures, are intended to illustrate how the method works.

Obviously a detailed analysis of precise geoid computation procedures leads to more accurate error estimates, as illustrated in the geodetic literature. What has to be stressed here is that the introduction of Wiener measures, taking account of density and accuracy of individual measurements, enables to use BVP theory not only to test well-posedness, but also to compare different boundary conditions with respect to the actual feasibility of measurement campaigns. A more refined analysis might enable to study from this point of view more realistic problems; for example, a first task might be the study of the effect of the uncertainty in height measurements on the

determination of geoid undulations, of the effect of imprecise density in reductions, and so on.

## APPENDIX

From the very definition of  $\beta_n$  (immediately above (9)) it follows that  $\beta_n Y_{nm}(\sigma_P)$  ( $\sigma_P$ =centre of  $C_\psi$ ) are the harmonic coefficients of  $\mu(C_\psi)^{-1} \chi_{C_\psi}(\sigma)$ . Hence

$$\mu(C_\psi)^{-1} \chi_{C_\psi}(\sigma) = \sum_{n,m} \beta_n Y_{nm}(\sigma_P) Y_{nm}(\sigma) = \sum_n \beta_n (2n+1) P_n(\cos \psi_{\sigma_P \sigma}) \quad (A1)$$

Taking the  $L^2$ -norm, one obtains

$$\begin{aligned} \mu(C_\psi)^{-1} &\equiv \|\mu(C_\psi)^{-1} \chi_{C_\psi}(\sigma)\|_{L^2}^2 = \\ &= \sum_{nn'} \beta_n \beta_{n'} (2n+1)(2n'+1) \int_{\Sigma} d\sigma P_n(\cos \psi_{\sigma_P \sigma}) P_{n'}(\cos \psi_{\sigma_P \sigma}) = \\ &= 4\pi \sum_n \beta_n^2 (2n+1) \end{aligned} \quad (A2)$$

As the series in (A2) certainly converges, *a fortiori* the series in the last term of (9) converges too.

## REFERENCES

- Barzaghi, R., G. Bottino (1993) - Fast Collocation, Bull. Géod., 67, 119-126.
- Barzaghi, R., A.Fermi, S.Tarantola, F.Sansò (1993) - Spectral Techniques in Inverse Stokes and Overdetermined Problems, Surveys in Geophysics, 14, 461-475.
- Elmiger, H., W. Gurtner (1983) - Astrogeodätische Geoidbestimmung und Lotabweichungsinterpolation in der Schweiz, ETH Zürich, Inst. für Geod. und Photogr., Bericht Nr.74.
- Kearsley, A.H.W., M.G.Sideris, J.Krinski, R.Forsberg, K.P.Schwarz (1985) - White Sands Revisited. A Comparison of Techniques to Predict Deflections of the Vertical, UCSE Reports, 30007.
- Moritz, H. (1983) - Local Geoid Determination in Mountain Regions, OSU Reports of the Department of Geodetic Science and Surveying, The Ohio State University, 352.
- Sansò, F. (1988) - The Wiener Integral and the Overdetermined Boundary Value Problems of Physical Geodesy, Man.Geod., 13, 75-98.
- Schwarz, K.P., M.G.Sideris and R.Forsberg (1990) - The use of FFT techniques in Physical Geodesy, Geophys.J.Int, 100, 485-514.

Sideris, M.G., R.Forsberg (1991) - Review of Geoid Prediction Methods in Mountainous Regions, in Determination of the Geoid, Present and Future (R.H.Rapp and F.Sansò, eds.), IAG Symposia 106, 51-62, Springer-Verlag.

Sünkel, H., N.Bartelme, H.Fuchs, M.Hanafy, W.D.Schuh, M.Wieser (1987) - The Gravity Field in Austria, Proc. of the IAG Symposia, Vancouver, 475-503.

Tscherning, C.C. (1975) - Application of Collocation for the Planning of Gravity Surveys, Bull. Géod., n.116, 183-198.

Tziavos, I.N., M.G.Sideris and K.P.Schwarz (1992) - A Study of the Contributions of Various Gravimetric Data Types on the estimation of Gravity Field Parameters in the Mountains, JGR, 97, B6, 8843-8852.

# ON CALCULATING THE ATTRACTION OF THE TOPOGRAPHIC-ISOSTATIC MASSES

Hussein A. Abd-Elmotaal  
Civil Engineering Department, Faculty of Engineering,  
Minia University, Minia 61111, Egypt

## ABSTRACT

The representation of the topography is usually made by digital height models and digital density models. Therefore, one can produce the so-called digital Moho model by applying a certain isostatic hypothesis. The attraction of the topographic-isostatic masses is derived. Also, the case of distant mass elements is treated. The procedure of calculating the attraction of the topographic masses from a combination of digital models of different grid sizes is widely studied. The limitations of using the formula of the distant mass elements for both the topographic and the isostatic masses, along with their relative errors, are illustrated. The results show that using an artificial very fine digital height model in the neighbourhood of the computational point (about 2.5 km) gives the minimum errors on calculating the attraction of the topographic masses.

## INTRODUCTION

To use the gravity anomalies in the interpolation process they should be small and fluctuating randomly around zero. It is well known that the isostatic anomalies achieve these requirements to a great extent. The attraction of the topographic-isostatic masses is needed to calculate the isostatic anomalies. The topography is usually represented by digital height models and digital density models (DHM and DDM). One can also build up the so-called digital Moho model (DMM) by applying a certain isostatic hypothesis. In case of the Airy-Heiskanen isostatic model, it is very easy to build up the digital Moho model (Heiskanen and Moritz, 1967, pp. 135–136). In case of Vening Meinesz (Vening Meinesz, 1931), one can apply the concept described in (Abd-Elmotaal, 1991, pp. 27–28) to produce the digital Moho model based on the Vening Meinesz hypothesis.

The attraction of the topographic-isostatic masses will be derived. Also, the case of distant mass elements will be treated. The procedure of calculating the attraction of the topographic masses from a combination of digital models of different grid sizes will be widely studied. The limitations of using the formula of the distant mass elements for both the topographic and the isostatic masses will be examined.

## 1 ATTRACTION OF A TOPOGRAPHIC MASS ELEMENT

Let us consider a topographic mass element of a height  $h'$ , density  $\rho$  and bounded by two latitudes ( $\phi_1$  and  $\phi_2$ ) and two longitudes ( $\lambda_1$  and  $\lambda_2$ ); Fig. 1. Consider that the cross section of this element is infinitely small, so that we can write

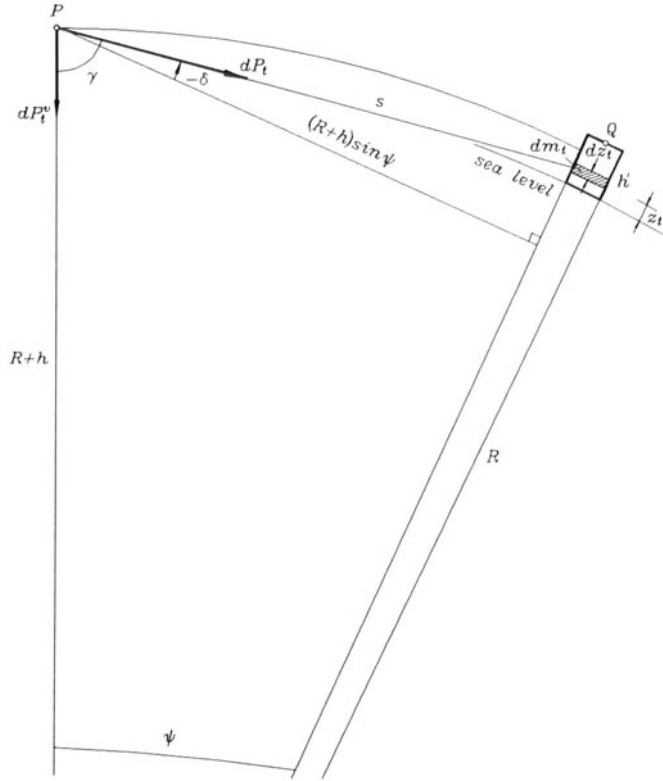


Fig. 1. Attraction of a topographic mass element.

$$d\phi = \phi_2 - \phi_1 \quad \text{and} \quad d\lambda = \lambda_2 - \lambda_1 . \quad (1)$$

The spherical distance  $\psi$  between the center of this topographic mass element  $Q$  and the computational point  $P$  can be given by (Heiskanen and Moritz, 1967, p. 257)

$$\cos \psi = \sin \phi_P \sin \phi_Q + \cos \phi_P \cos \phi_Q \cos(\lambda_Q - \lambda_P) , \quad (2)$$

where  $\phi_Q$  and  $\lambda_Q$  are defined by

$$\phi_Q = \frac{1}{2}(\phi_1 + \phi_2) \quad \text{and} \quad \lambda_Q = \frac{1}{2}(\lambda_1 + \lambda_2) . \quad (3)$$

The mass element  $dm_t$  (cf. Fig. 1) is expressed by

$$dm_t = \rho(R + z_t)^2 \cos \phi_Q d\phi d\lambda dz_t , \quad (4)$$

where  $R$  is the radius of the mean earth's sphere,  $z_t$  is the height (measured from sea level) of the mass element  $dm_t$  and  $dz_t$  is the height of the mass element. The spatial distance  $s$  between the computational point  $P$  and the mass element  $dm_t$  is given by

$$s = (R + z_t) \frac{\sin \psi}{\sin \gamma} = (R + h) \frac{\sin \psi}{\cos \delta} , \quad (5)$$

where  $h$  is the height of the computational point  $P$ . The relation among  $\gamma$ ,  $\delta$  and  $\psi$  is given by (see Fig. 1)

$$\gamma = 90^\circ - \psi - \delta . \quad (6)$$

Let us consider that the mass element  $dm_t$  is infinitely small so that we can apply Newton's gravitational law to get the attraction  $dP_t$  exerted by this mass element at the computational point, that is,

$$dP_t = \frac{Gdm_t}{s^2} , \quad (7)$$

where  $G$  is the gravitational constant. We are interested only on the vertical component  $dP_t^v$  of this attraction, which can be easily expressed as

$$dP_t^v = G\rho \frac{\sin^2\gamma \cos\gamma}{\sin^2\psi} \cos\phi_Q d\phi d\lambda dz_t . \quad (8)$$

Equation (5), using (6), gives

$$z_t = (R + h) \frac{\cos(\psi + \delta)}{\cos\delta} - R . \quad (9)$$

Differentiating this expression, keeping in mind that  $R$ ,  $h$  and  $\psi$  are constants here, gives

$$dz_t = -(R + h) \frac{\sin\psi}{\cos^2\delta} d\delta . \quad (10)$$

Inserting (10) into (8) gives

$$dP_t^v = -G\rho(R + h) \frac{\cos^2(\psi + \delta) \sin(\psi + \delta)}{\cos^2\delta \sin\psi} \cos\phi_Q d\phi d\lambda d\delta . \quad (11)$$

This formula can be easily integrated with respect to  $\delta$  between

$$\delta_o = \arctan \frac{h - 2(R + h) \sin^2 \frac{\psi}{2}}{(R + h) \sin\psi} \quad (12)$$

and

$$\delta_1 = -\arctan \frac{h' - h + 2(R + h) \sin^2 \frac{\psi}{2}}{(R + h) \sin\psi} . \quad (13)$$

By using the standard tables of integrals (Gradshteyn and Ryzhik, 1965, pp. 136–137), one can get the following expression for the vertical attraction  $P_t^v$  at the computational point exerted by the whole topographic mass element of a height  $h'$ :

$$\begin{aligned} P_t^v &= -2G\rho(R + h) \frac{\cos\phi_Q}{\sin\psi} d\phi d\lambda \left\{ \sin\left(\frac{\delta_1}{2} - \frac{\delta_o}{2}\right) \left[ \sin\left(\frac{\delta_1}{2} + \frac{\delta_o}{2}\right) \cos\psi \cdot \right. \right. \\ &\quad \cdot \left. \left[ 1 - \sin^2\psi (4 - \sec\delta_1 \sec\delta_o) \right] + \cos\left(\frac{\delta_1}{2} + \frac{\delta_o}{2}\right) \sin\psi (3 - 4 \sin^2\psi) \right] - \\ &\quad \left. - \sin\psi \left(1 - \frac{3}{2} \sin^2\psi\right) \ln\left(\tan\left(\frac{\pi}{4} + \frac{\delta_1}{2}\right) \tan\left(\frac{\pi}{4} - \frac{\delta_o}{2}\right)\right) \right\} . \end{aligned} \quad (14)$$

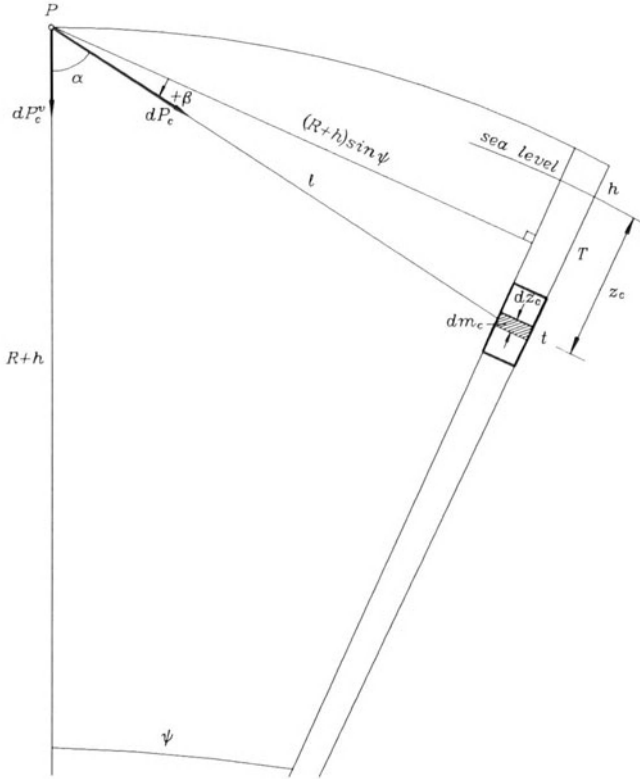


Fig. 2. Attraction of a compensating mass element.

## 2 ATTRACTION OF A COMPENSATING MASS ELEMENT

Let us consider a compensating mass element of a depth  $t$  (measured from the normal crustal thickness  $T$ , see Fig. 2), density  $\Delta\rho$  and bounded by two latitudes ( $\phi_1$  and  $\phi_2$ ) and two longitudes ( $\lambda_1$  and  $\lambda_2$ ). The mass element  $dm_c$  (see Fig. 2) is expressed by

$$dm_c = \Delta\rho(R - z_c)^2 \cos \phi_Q d\phi d\lambda dz_c , \quad (15)$$

where  $z_c$  is the depth (measured from sea level) of the mass element  $dm_c$  and  $dz_c$  is the height of the mass element. The spatial distance  $\ell$  between the computational point  $P$  and the mass element  $dm_c$  is given by

$$\ell = (R - z_c) \frac{\sin \psi}{\sin \alpha} = (R + h) \frac{\sin \psi}{\cos \beta} . \quad (16)$$

The relation among  $\alpha$ ,  $\beta$  and  $\psi$  is given by (see Fig. 2)

$$\beta = 90^\circ - \psi - \alpha . \quad (17)$$

Let us consider again that the mass element  $dm_c$  is infinitely small so that we can apply Newton's gravitational law to get the attraction  $dP_c$  exerted by this mass element at the computational point, that is,

$$dP_c = \frac{Gdm_c}{\ell^2} . \quad (18)$$

Again, we are interested only on the vertical component  $dP_c^v$  of this attraction, which can be easily expressed as

$$dP_c^v = G\Delta\rho \frac{\sin^2\alpha \cos\alpha}{\sin^2\psi} \cos\phi_Q d\phi d\lambda dz_c . \quad (19)$$

Substituting (17) into (16) gives

$$z_c = R - (R + h) \frac{\cos(\psi + \beta)}{\cos\beta} . \quad (20)$$

Differentiating this expression, keeping in mind that  $R$ ,  $h$  and  $\psi$  are constants here, gives

$$dz_c = (R + h) \frac{\sin\psi}{\cos^2\beta} d\beta . \quad (21)$$

Inserting (21) into (19) gives

$$dP_c^v = G\Delta\rho (R + h) \frac{\cos^2(\psi + \beta) \sin(\psi + \beta)}{\cos^2\beta \sin\psi} \cos\phi_Q d\phi d\lambda d\beta . \quad (22)$$

This formula can be easily integrated with respect to  $\beta$  between

$$\beta_0 = \arctan \frac{(T + h) - 2(R + h) \sin^2 \frac{\psi}{2}}{(R + h) \sin\psi} \quad (23)$$

and

$$\beta_1 = \arctan \frac{(H + h) - 2(R + h) \sin^2 \frac{\psi}{2}}{(R + h) \sin\psi} . \quad (24)$$

By using the standard tables of integrals (Gradshteyn and Ryzhik, 1965, pp. 136–137), one can get the following expression for the vertical attraction  $P_c^v$  at the computational point exerted by the whole compensating mass element of a depth  $t$ :

$$\begin{aligned} P_c^v = & 2G\Delta\rho (R + h) \frac{\cos\phi_Q}{\sin\psi} d\phi d\lambda \left\{ \sin\left(\frac{\beta_1}{2} - \frac{\beta_0}{2}\right) \left[ \sin\left(\frac{\beta_1}{2} + \frac{\beta_0}{2}\right) \cos\psi \cdot \right. \right. \\ & \cdot \left[ 1 - \sin^2\psi (4 - \sec\beta_1 \sec\beta_0) \right] + \cos\left(\frac{\beta_1}{2} + \frac{\beta_0}{2}\right) \sin\psi (3 - 4 \sin^2\psi) \left. \right] - \\ & - \sin\psi (1 - \frac{3}{2} \sin^2\psi) \ln\left(\tan\left(\frac{\pi}{4} + \frac{\beta_1}{2}\right) \tan\left(\frac{\pi}{4} - \frac{\beta_0}{2}\right)\right) \left. \right\} . \end{aligned} \quad (25)$$

### 3 DISTANT MASS ELEMENTS

If the mass element is fairly far from the computational point, it is convenient to approximate it as a point mass. Applying this principle, one can derive the following formula for the attraction  $P_t^v$  of the whole topographic mass element as follows:

$$P_t^v = G\rho h' \frac{\cos^2(\psi + \delta) \sin(\psi + \delta)}{\sin^2\psi} \cos \phi_Q d\phi d\lambda , \quad (26)$$

where

$$\delta = \arctan \frac{h - \frac{1}{2}h' - 2(R + h) \sin^2 \frac{\psi}{2}}{(R + h) \sin \psi} . \quad (27)$$

Similarly, one can get the following formula for the attraction  $P_c^v$  of the whole compensating mass element as follows:

$$P_c^v = G\Delta\rho(H - T) \frac{\cos^2(\psi + \beta) \sin(\psi + \beta)}{\sin^2\psi} \cos \phi_Q d\phi d\lambda , \quad (28)$$

where

$$\beta = \arctan \frac{\frac{1}{2}(H + T) + h - 2(R + h) \sin^2 \frac{\psi}{2}}{(R + h) \sin \psi} . \quad (29)$$

The limitations of using (26) and (28) will be given in secs. 6.1 and 6.2, respectively.

### 4 ATTRACTION OF THE TOPOGRAPHIC-ISOSTATIC MASSES

The total attraction of the topographic masses  $A_t$  can be defined as

$$A_t = \int_{\phi=0}^{\pi} \int_{\lambda=0}^{2\pi} P_t^v . \quad (30)$$

Similarly, the total attraction of the compensating masses  $A_c$  can be defined as

$$A_c = \int_{\phi=0}^{\pi} \int_{\lambda=0}^{2\pi} P_c^v . \quad (31)$$

Neither the topography nor the Moho depths are defined as a continuous function of the position on the earth's sphere. Therefore, the integration in (30) and (31) will be replaced by a numerical integration and  $d\phi$ ,  $d\lambda$  will be replaced by  $\Delta\phi$ ,  $\Delta\lambda$  which represent the grid size of the used digital models in the latitude and longitude directions, respectively.

Making the summation over the whole earth is a very hard task. Normally, one calculates the attraction of the topographic-isostatic masses using formulas such as (30) and (31) for a certain reference window. Since the earth models, such as those of OSU, contain implicitly the effect of the topographic masses and their compensation, one can calculate the attraction of the topographic-isostatic masses outside the reference window using the harmonic coefficients of such earth models after removing the effect of the reference window from the harmonic coefficients. The reader who may be interested in the details of calculating the harmonic coefficients of a certain reference window is kindly invited to refer to (Hanafy, 1987, pp. 78-81).

## 5 PROCEDURE OF CALCULATING THE ATTRACTION OF THE TOPOGRAPHIC MASSES

Let us consider a large flat area of a constant height  $h$  and a constant density  $\rho = 2.67 \text{ g/cm}^3$ . We will calculate the attraction of the topographic masses within a radius of 167 km (which represents the outer radius of the Hayford zone  $O$ ) around the computational point. Let us consider that we have a coarse grid DHM with  $90'' \times 90''$  size covers the whole area. Within a certain radius  $r_f$  around the computational point, we will calculate the attraction of the topographic masses using a fine grid DHM with different sizes. Table 1 gives the attraction of the topographic masses using different  $r_f$  and different fine grid DHM sizes. Here  $A_{pl}$  stands for the attraction of the exact spherical Bouguer plate calculated by equation (2-6) in (Kühtreiber et al., 1989).

Table 1. Attraction of the topographic masses using coarse and fine grid DHM ( $h = 1000 \text{ m}$ ).

fine grid size	$r_f$ (km)	$A_t$			$A_{pl} - A_t$ (mgal)
		coarse grid (mgal)	fine grid (mgal)	total (mgal)	
$30'' \times 30''$	2.5	18.27	68.10	86.37	26.64
$30'' \times 30''$	7.5	7.32	80.17	87.49	25.52
$15'' \times 15''$	2.5	18.27	80.66	98.93	14.08
$15'' \times 15''$	7.5	7.32	92.87	100.19	12.82
$6'' \times 6''$	2.5	18.27	88.28	106.55	6.46
$6'' \times 6''$	7.5	7.32	100.52	107.84	5.17
$1'' \times 1''$	2.5	18.27	92.52	110.79	2.22
$1'' \times 1''$	7.5	7.32	104.77	112.09	0.92

It is clear from Table 1 that the neighbourhood topographic elements within a radius of 2.5 km around the computational point gives the main effect on  $A_t$ . Also, using finer grid sizes gives smaller errors expressed by the term  $A_{pl} - A_t$ . Therefore, we will calculate the attraction of the topographic elements within a radius of 2.5 km from a very fine grid DHM with  $1'' \times 1''$  size. In practical application, this very fine grid is only artificial. For example, if your fine DHM has  $15'' \times 15''$  size, then every topographic element will be divided to 225 elements of  $1'' \times 1''$  size having the same  $h$  as the main topographic element. Table 2 gives the attraction of the topographic masses using coarse, fine and very fine DHM. It shows that using this technique to calculate  $A_t$  gives the minimum errors. Also, using different fine grid DHM sizes gives nearly the same results.

Finally, Table 3 gives the recommended radius  $r_f$  of using the fine DHM of different topographic heights  $h$ . Here we have used a  $15'' \times 15''$  fine DHM grid size.

## 6 LIMITS OF USING THE POINT MASS FORMULAS

### 6.1 For The Topographic Masses

Table 4 gives the radius  $s_{pt}$  and the error resulted from using the point mass formula (26) instead of the exact formula (14) after that radius to calculate the attraction of

Table 2. Attraction of the topographic masses using coarse, fine and very fine grid DHM ( $h = 1000$  m).

fine grid size	$r_f$ (km)	$A_t$				$A_{pl} - A_t$ (mgal)
		coarse grid (mgal)	fine grid (mgal)	very fine grid (mgal)	total (mgal)	
$30'' \times 30''$	5	10.33	8.93	92.52	111.78	1.23
$30'' \times 30''$	7.5	7.32	12.07	92.52	111.91	1.10
$15'' \times 15''$	5	10.33	9.05	92.52	111.90	1.11
$15'' \times 15''$	7.5	7.32	12.21	92.52	112.05	0.96
$6'' \times 6''$	5	10.33	9.08	92.52	111.93	1.08
$6'' \times 6''$	7.5	7.32	12.24	92.52	112.08	0.93

Table 3. Recommended radius of using the fine DHM. The used DHM grid size is  $15'' \times 15''$ .

$h$ (m)	1000	2000	3000	4000
$r_f$ (km)	5	7.5	10	10
$A_{pl} - A_t$ (mgal)	1.11	1.24	1.30	1.50

the topographic masses within a radius of 167 km around the computational point. Table 4 shows that the errors are practically zero.

Table 4. Limits of using the point mass formula to calculate  $A_t$ .

$h$ (m)	1000	2000	3000	4000
$s_{pt}$ (km)	10	20	30	40
error (mgal)	0.007	0.015	0.021	0.029

## 6.2 For The Compensating Masses

Figure 3 illustrates the relative error of calculating the attraction of the compensating mass element using the point mass formula (28) instead of the exact formula (25) for different values of  $h$ . The height of the computational point is assumed to be zero. The DMM is created on the basis of the Airy-Heiskanen isostatic model. The used density contrast  $\Delta\rho$  is 0.4 g/cm<sup>3</sup> and the normal crustal thickness  $T$  is 30 km. Figure 3 shows that after a spherical distance of about 300 km from the computational point, the relative error in all cases does not reach 0.3%. It should be noted that several tests were carried out using different heights of the computational point and they give the same behaviour with, more or less, the same relative errors.

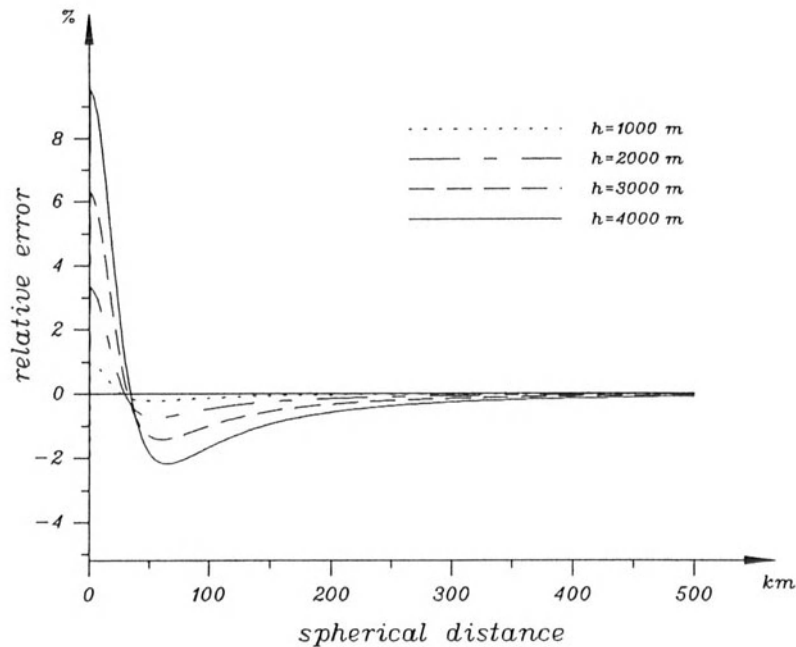


Fig. 3. Relative error of calculating  $A_c$  from the point mass formula.

## 7 CONCLUSION

Calculating the attraction of the topographic masses using coarse, fine and very fine DHM gives the minimum errors on  $A_t$ . The very fine DHM should be used for a radius of about 2.5 km around the computational point. The point mass formula can be used after a relatively short radius giving practically the same results.

After a spherical distance of about 300 km from the computational point, the point mass formula can be used giving a relative error in calculating the attraction of the compensating mass element in the order of 0.3% only.

## REFERENCES

- Abd-Elmotaal, H. (1991) Gravity Anomalies Based on the Vening Meinesz Isostatic Model and Their Statistical Behaviour, *Mitteilungen der geodätischen Institute der Technischen Universität Graz*, **72**.
- Gradshteyn, I.S. and Ryzhik, I.M. (1965) *Table of Integrals, Series, and Products*, 4th ed., Academic Press, New York, London.
- Hanafy, M.S. (1987) Gravity Field Data Reduction Using Height, Density and Moho Information, Ph.D. Dissertation, Graz University of Technology.
- Heiskanen, W.A. and Moritz, H. (1967) *Physical Geodesy*, Freeman, San Francisco.
- Kühtreiber, N., Kraiger, G. and Meurers, B. (1989) Pilotstudien für eine neue Bouguer Karte von Österreich, *Österreichische Beiträge zu Meteorologie und Geophysik*, **2**, 51–72.
- Vening Meinesz, F.A. (1931) Une Nouvelle Méthode pour la Réduction Isostatique Régionale de L'intensité de la Pesanteur, *Bulletin Géodésique*, **29**, 33–51.

# THE FAST HARTLEY TRANSFORM APPLIED TO THE IBERIAN GEOID CALCULATION

M.J. Sevilla and G.Rodríguez-Velasco

Instituto de Astronomía y Geodesia (UCM-CSIC)

Facultad de CC. Matemáticas, Universidad Complutense, 28040 Madrid SPAIN

## ABSTRACT

For the Iberian Peninsula ( $-10.5 < \lambda < 5.5$ ,  $35 < \phi < 45$ ) a quasigeoid solution has been computed using a global geopotential model, a digital terrain model and point gravity anomalies. The Fast Hartley Transform (FHT) technique has been used in the computations. The effect of topographic masses is taken into account by a residual terrain model (RTM) reduction using a 1000x1000 m DTM in the area. The region was divided into two sub-areas with a common part. Some experiments were performed in order to test the results obtained in each individual sub-area and also in a global calculation for all of the region. Then one solution was calculated at 80692 points in a regular grid covering the region and referred to the GRS80. Results are presented in a contour map.

## 1. INTRODUCTION

The first determination of a gravimetric geoid in the Iberian Peninsula area was made last year (Sevilla, 1994). The geoid (quasigeoid) solution was computed based on the following data types: a) a geopotential model, namely the OSU91A spherical harmonic coefficients set, b) a set of 110948 point free-air gravity anomalies covering the Iberian Peninsula and the surrounding regions and c) a 1000x1000 meters digital terrain model for Spain and the ETOPO5U for the rest of the area.

The method used in the computations was Stokes' integral in convolution form. The input data were gridded gravity anomalies. To evaluate the integral, the Fast Hartley Transform (FHT) technique was applied (Bracewell, 1986; Li and Sideris 1992; Tziavos, 1993a,b). To compute height anomalies, discrete spectra of the kernel function is used. 100 % zero-padding was appended around the signal matrix in order to avoid circular convolution effects. The main advantages of the FHT are that the FHT is faster than the FFT (Fast Fourier Transform) and it only needs the half of the computer memory with respect to the FFT (see, e.g., Tziavos, 1993a).

The following tasks were of special interest in this study. The first was to compute absolute geoidal heights in a dense grid ( $2.4' \times 3'$ ) in the area . The second was to investigate the differences obtained using the FHT procedure in the overlapping zones, where different data sets have been used.

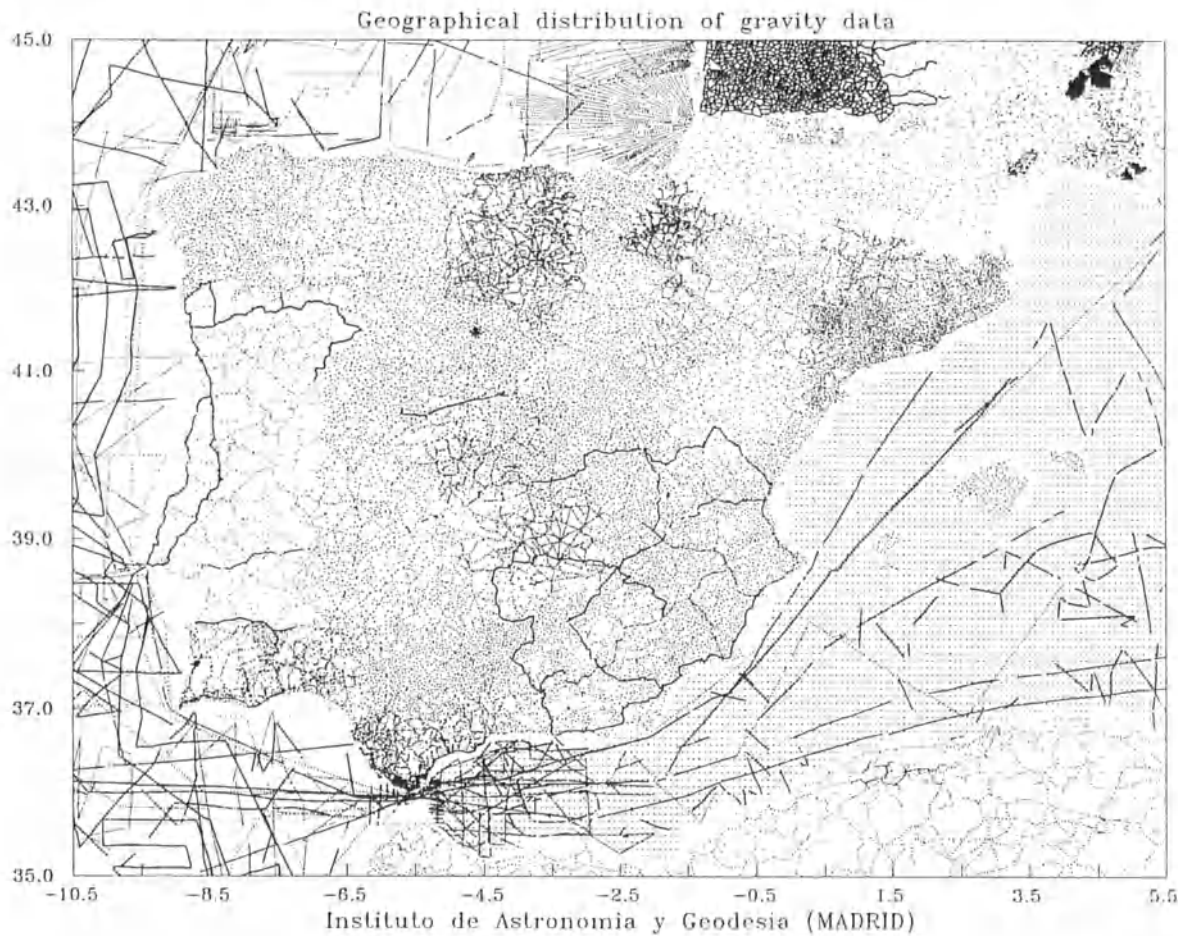


**Fig.1. Geographical distribution of data points**

## **2. DATA TYPES AND PREPROCESSING**

### **Gravity anomalies**

A number of 110948 point free-air gravity anomalies in the area ( $-10.5 < \lambda < 5.5$ ,  $35 < \phi < 45$ ) were used in the geoid computation and transformed to the GRS80 reference system. This data came from different sources. All data sets have been checked carefully and validated for gross errors by applying different procedures (Sevilla et al., 1991).

Figure 1 shows the geographical distribution of the available gravity data. Figure 2a shows an histogram of free-air gravity anomalies.

### **Geopotential Model**

The geopotential model OSU91A (Rapp et al, 1991) complete to degree and order 360 has been used to obtain the reduced free-air gravity anomalies. Thus, the long wavelength part of the Earth's gravity field is removed from the gravity anomalies. This model fits well to the anomalous gravity field of the area (Sevilla, 1994)(see Table 1).

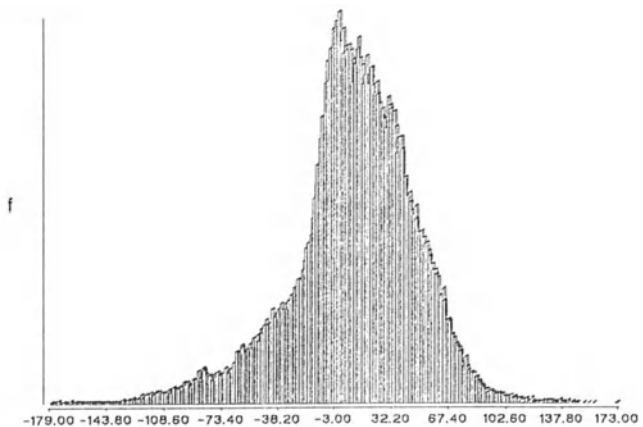


Fig.2a. Histogram of free-air gravity anomalies

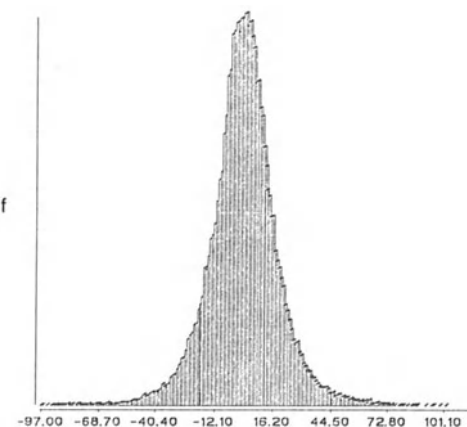


Fig.2b. Histogram of reduced anomalies

### Topographic model

A digital terrain model (MDT200) is available for Spain with spacing 200x200 m. This model was provided by the *Instituto Geográfico Nacional* (Garcia et al. 1992). It was complemented by the ETOPO5U (a global topographic model) in the areas outside the Spanish territory. From these two models a new model covering the whole area with 1000x1000 meters spacing has been produced. Thus, it was possible to make the terrain reduction without finding faults in the data (Sevilla and Rodríguez-Velasco, 1994).

**Topographic correction.** The topography was taken into account by a residual model reduction (Forsberg, 1984, Fosberg and Tscherning, 1981). This means that the effect of the short wavelength variations from a reference surface was computed instead of the effect of the entire topography.

Table 1. Statistics of reduced gravity data in the Iberian Peninsula area

	Mean	S.D.	Minimum	Maximum	Range
Latitude	40.460	3.07	35.000	45.000	10.000
Longitude	-2.888	4.38	-10.500	5.500	16.000
Height	-35.09	1041.9	-5070.0	2950.1	8020.1
Free air	4.00	38.96	-180.10	186.00	366.10
Free air-OSU91A	-4.42	21.98	-117.25	208.19	325.44
F.air-OSU91-rtm	0.64	15.41	-74.68	221.35	296.03

The statistics of the completely reduced gravity anomalies is summarized in Table 1. These anomalies have been used for validation purposes and 1159 gross errors have been detected. Figure 2b shows an histogram of these reduced anomalies (free-air minus OSU91A minus rtm). If we compare the Figures 2a and 2b, we can see that the gravity anomalies have less dispersion after the removal of the topographic effects, also the mean value show a significant reduction.

### 3. GEOID COMPUTATION METHOD

Heights anomalies have been determined for the Iberian Peninsula using the classical remove-restore technique. The predicted height anomalies are obtained by the formula

$$\zeta = \zeta_1 + \zeta_2 + \zeta_3$$

where  $\zeta_1$  is the contribution from the spherical harmonic model OSU91A used,  $\zeta_2$  is the contribution from a residual terrain model (RTM) and  $\zeta_3$  is the contribution from the terrestrial gravity field observations: free-air anomalies after the removal of effect of the global geopotential model and the RTM.

The  $\zeta_3$  component has been computed by Stokes' integral. The integral formula was evaluated by the FHT technique applied to gridded data. The spectral computation by FHT is based on a flat-earth approximation. Thus, Stokes' integral formula may be written as a 2D-convolution in the form

$$\zeta(x, y) = \frac{1}{2\pi\gamma} \Delta g(x, y) * l_N(x, y)$$

where  $\Delta g(x, y)$  are the completely reduced anomalies. The convolution of the kernel function  $l_N(x, y)$  with the data  $\Delta g(x, y)$  is easier done in the frequency domain. Using the FHT:

$$H(u, v) = \int_{-\infty}^{\infty} \int_{-\infty}^{\infty} h(x, y) \text{cas}(ux) \text{cas}(vy) dx dy = H(h(x, y))$$

being  $\text{cas}x = \cos x + \sin x$ , and its inverse

$$h(x, y) = \frac{1}{4\pi^2} \int_{-\infty}^{\infty} \int_{-\infty}^{\infty} H(u, v) \text{cas}(ux) \text{cas}(vy) du dv = H^{-1}(H(u, v))$$

we have (Tziavos, 1993a)

$$\zeta(x, y) = \frac{1}{2\pi\gamma} H^{-1} [\Delta G(u, v) L_N(u, v)]$$

Here  $H^{-1}$  denotes the inverse Hartley Transform,  $(u, v)$  are the frequencies and  $\Delta G(u, v)$  and  $L_N(u, v)$  the Hartley Transforms of  $\Delta g(x, y)$  and  $l_N(x, y)$  respectively.

For the FHT computations, data should be gridded -as in other methods involving transformations- so that they are equidistant. In the FHT, data length should be an integer power of two (Bracewell, 1986). For these reasons, data were distributed in a 2.3'x3' grid for the region (-10.5< $\lambda$ <5.5, 35< $\phi$ <45), to grid the data we use weighted means with a power equal 3. According to this selection we have equal area blocks in the middle of

the region. This is not necessary for the FHT application, but it will be useful for future interpolations of the results.

In order to study the effect of the extension of our test areas on the results obtained by the FHT, the gravimetric solution was performed in two overlapping areas in the west and east parts of the region. Each one yield a grid with spacing of 4.354 kilometres in the x and y directions. The limits of the west and east areas are: West area,  $35^\circ < \phi < 45^\circ$ ,  $-10.5^\circ < \lambda < 2.5^\circ$ ; East area:  $35^\circ < \phi < 45^\circ$ ,  $-7.54^\circ < \lambda < 5.5^\circ$ .

To reduce the spectral leakage due to the periodicity of the discrete transformation and the effect of the circular convolution on our computations we extended each gravity matrix into 256x256. This was done by appending zeros around the gravity anomalies, i.e., a 100% zero padding was used distributed in both parts. Also, we have used discrete spectra of the kernel function that is more efficient than the analytical one in geoid calculations. In these circumstances the results from FHT and from numerical integration are absolutely identical. In the computations we have used a Fortran program kindly offered by Ilias Tziavos (Tziavos, 1993a).

As it was said, the two grids have a common block between the meridians of longitudes  $-7.5431$  and  $2.5510$  degrees. The height anomaly differences obtained in this common block are kept between  $-2.5$  m and  $1.5$  m. These differences are kept under 1 meter in an inner zone limited by the meridians of longitudes  $-3.7196$  and  $-1.23253$  degrees. Here the common points are equally distant from the east and west edges of the whole region.

The distribution of the absolute values of differences by ranks can be seen in Table 2. Figure 3 shows the isolines of these differences. The distribution of the points with differences greater than 1 meter are in the black zones. They mainly correspond to the borders of the overlapping area. The remaining geoid height differences in the overlapping area may be attributed to the lack of the gravity data around the evaluation point at the borders of each test area when performing the two separate geoid solutions.

The good agreement between the solutions in the central part confirms that many of the differences are due to the edge effects, and also, to the bad quality of the topographic correction made using ETOPO5U (see the distribution of bad zones in the sea and Portugal, where a good digital terrain model was not available). Thus, the final solution was constructed joining the results that we suppose are more reliable. That is, the east and west solutions were merged taking the arithmetic average only in the inner overlapping

Table 2. Distribution of W-E differences

Range	Number of points
0	349
From 0 to 0.5	27462
From 0.5 to 1.0	14805
From 1.0 to 2.0	7846
From 2.0 to 2.5	226

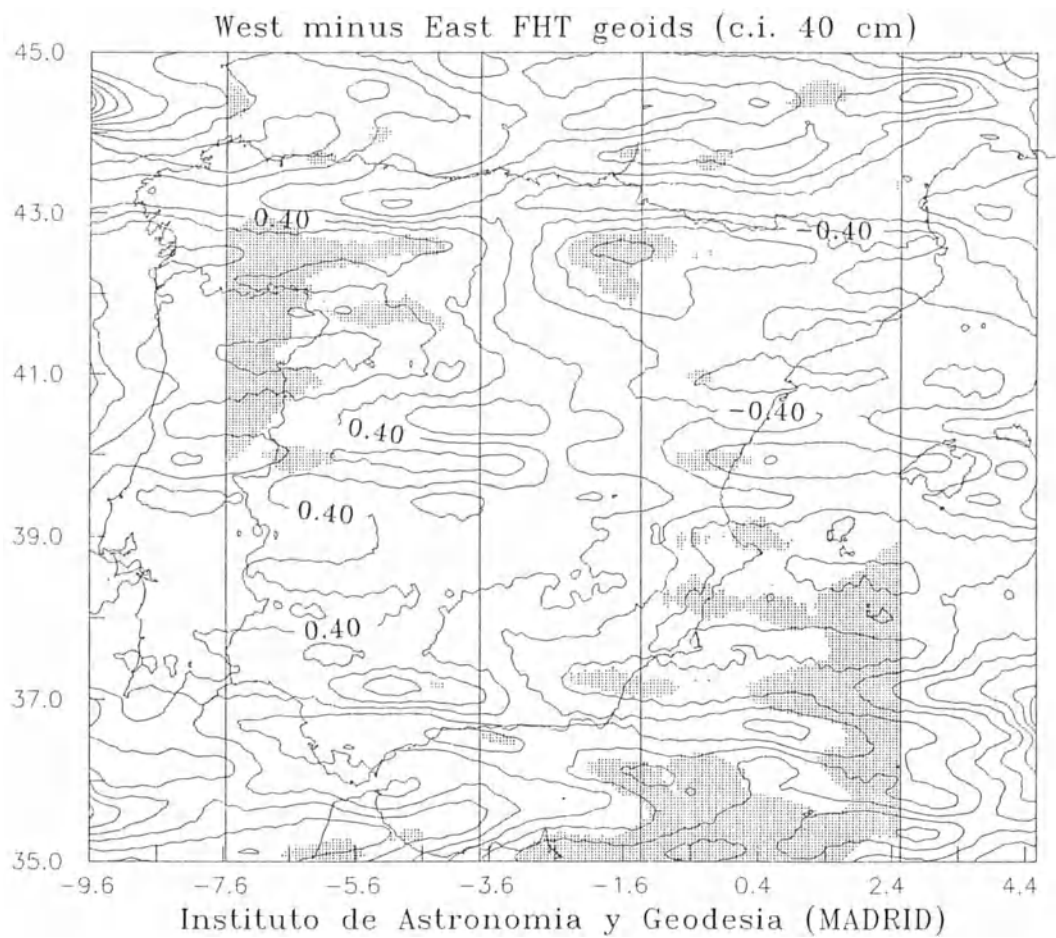


**Fig.3. West minus East FHT Geoids (contour interval 40 cm)**

area. The statistics of the final height anomalies computed for the Iberian Peninsula area are shown in Table 3. The Iberian Geoid 1994 is shown in Figure 4.

**Table 3. Statistics of the IBERIAN GEOID 1994**

	Points	Mean	S.D.	Minimum	Maximum	Range	Zeros
Model	80384	49.95	3.72	36.95	57.48	20.53	0
RTM	80384	0.02	0.16	-1.06	1.08	2.14	2853
FHT	80384	1.63	1.62	-2.93	6.38	9.31	57
Geoid	80384	52.39	4.31	39.24	62.54	23.30	0

#### **4. GLOBAL GEOID COMPUTATION**

As stated before, our objective is to compare the results obtained by FHT using different data sets in the same zone. The compared geoids were:

1. *Geoid A*; it is the geoid computed in two zones of 256x256 points with some overlapping. In the middle of such an overlapping zone, we averaged the two obtained values. The final result is a grid of 256x314=80384 points with a spacing of 0°.0392156862 in latitude and 0°.0509803921 in longitude.
2. *Geoid B*; it is a second geoid. It has also been computed by the FHT technique. It is extended over the same zone as the geoid A, but the number of points and the grid spacing are different (geoid has been computed on 256x256=65536 points and the intervals are 0.°0392156862 in latitude and 0.°062745098 in longitude).

Table 4 shows the statistics of these results.

### **Comparison between Geoid A and B**

It was not possible to make a direct comparison between both of the geoids because spacing in longitude was different. Therefore, the comparison was made over two grids -which were obtained by a bicubic spline from the two previous results on the same points. These two grids, namely InterA and InterB, are compared in Table 5. Differences ranks are classified in table 6. We can deduce that FHT method is more sensitive to the data sampling if a good topographic model has not been used.

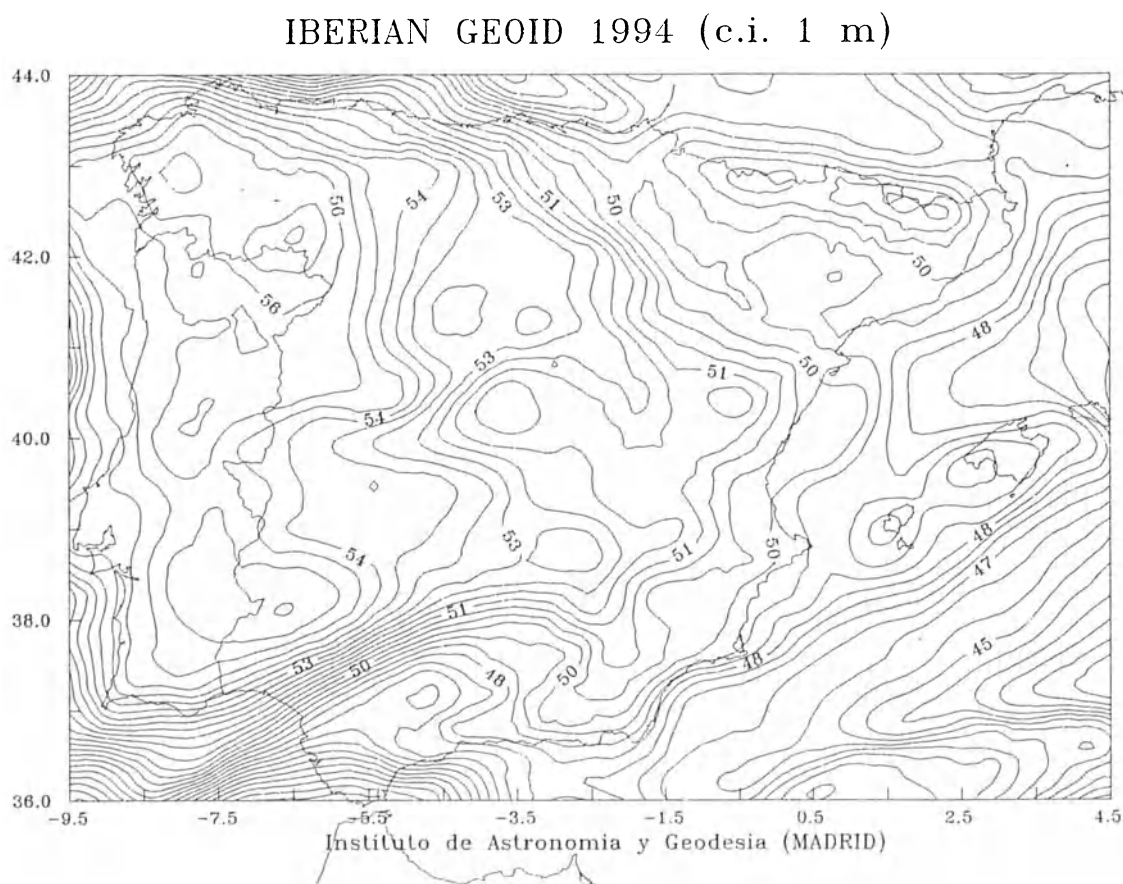


Fig.4. IBERIAN GEOID 1994 (contour interval 1 m)

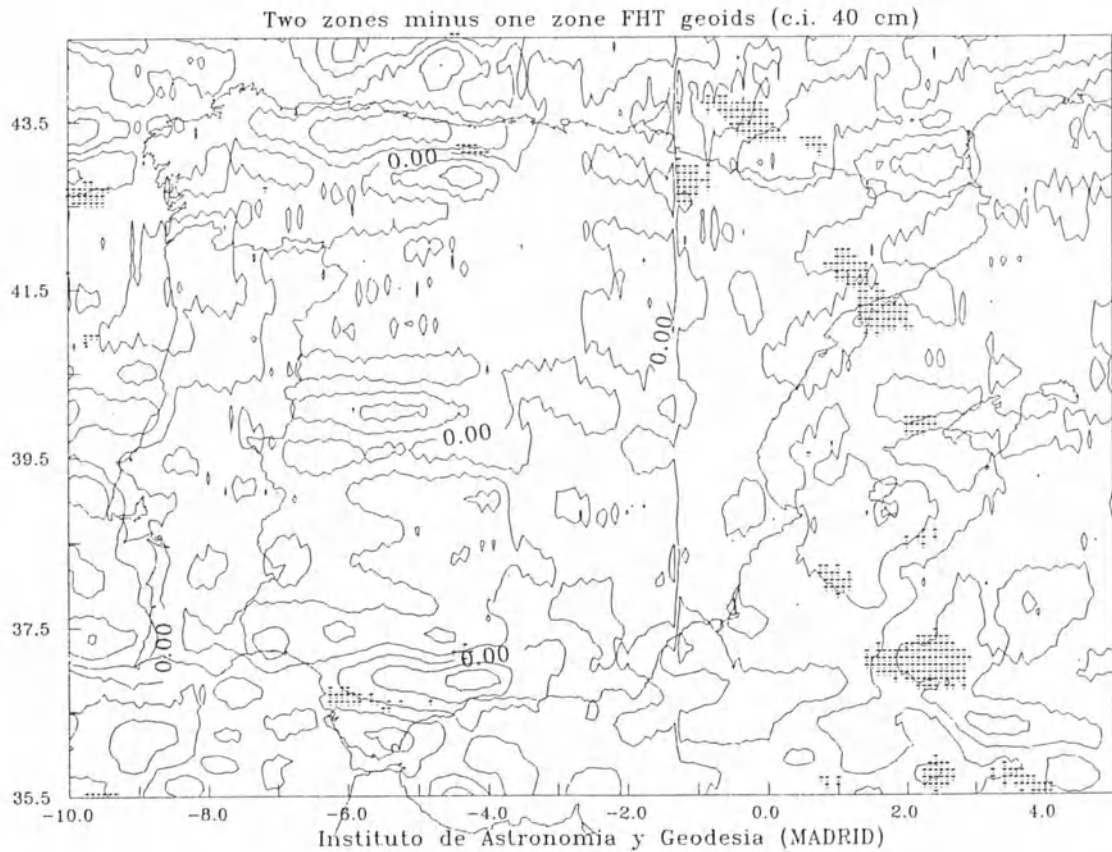


Fig.5. Differences between the two geoids. Dark zones correspond to large differences

Table 4. Statistics of the obtained geoids

Name	N.Points	Mean	S.D.	Minimum	Maximin
Geoid A	80384	52.39	4.31	39.24	62.54
Geoid B	65536	52.14	4.31	38.70	62.22

## 5. CONCLUSIONS

The FHT has been used efficiently for height anomaly computations using discrete spectra for the kernel function and 100 % zero-padding to reduce the effect of circular convolution. Comparisons between FHT results in the overlapping areas show large differences at the borders. Therefore, there is a substantial correlation with the data used in the computations. This can be seen by comparing the results obtained with those derived when using only one zone.

Table 5. Comparison between geoids

	N.Points	Mean	S.D.	Minimum	Maximin
InterA	19729	53.075	4.032	39.586	62.489
InterB	19729	52.820	4.038	39.639	62.218
Diff A-B	19729	0.255	0.425	-1.234	1.581

Table 6. Difference classification by ranks

Range	Number of points
Zero numbers 0	148
From 0 to 0.5	12631
From 0.5 to 1.0	6498
From 1.0 to 1.58	452

Further investigation is needed in order to improve the topographic model and to control the results with external sources as G.P.S. and collocation methods. These works are in progress.

The geoid solution in the Iberian Peninsula could be further improved after using the FHT on the sphere using also 100% zero-padding and discrete spectra for the gravity data.

*Acknowledgment.* This work is a contribution to the GEOMED project sponsored by the European Community contract no. sc1\*-ct92-0808 and by the project CE93-0001 of the Spanish DGICYT. We gratefully acknowledge the support of Professor Ilias N. Tziavos, who has provided the main software package, and also the Institutions who have provided the data.

## REFERENCES

- Bracewell, R.N. (1986). *The Hartley transform*. Oxford Univ. Press.
- Forsberg, R. (1984). A study of terrain reductions, density anomalies and geophysical inversion methods in gravity field modelling. *Dept. of Geodetic Science and Surveying* 355, Ohio State Univ., Columbus.
- Forsberg, R. and Tscherning, C.C. (1981). The use of Height data in gravity field approximation by collocation. *JGR, Vol 86 B9*, pp 7843-7854.
- García Asensio, L., J.J.Lumbreiras, G.Martín y C.Heras (1992). La altimetría en el SIG

- del IGN: Modelos digitales del terreno. *Nota Técnica de Geodesia NTG 5*. IGN Madrid.
- Li, Y.C. and Sideris, M.G. (1992). The fast Hartley transform and its application in Physical Geodesy. *Manuscripta geodaetica* 17, pp 381-387.
- Rapp, R.H., Y.M.Wang and N.K.Paulis (1991). The Ohio State 1991 Geopotential and Sea Surface Topography Harmonic Coefficient Models. *Dept. of Geod. Sci. Rep. 410*. Ohio State Univ., Columbus.
- Sevilla, M.J., A.J. Gil and F.Sansó (1991). The gravimetric geoid in Spain: first results. *Determination of the geoid. Present and future*. R.H.Rapp and F.Sansó (eds.), IAG Symp. 106, pp 276-285. Springer-Verlag.
- Sevilla, M.J. (1994). Regional quasigeoid determination in the Iberian Peninsula. *Mare Nostrum* 4, (Ed. by D. Arabelos and I.N. Tziavos) pp 65-75. Thessaloniki.
- Sevilla, M.J., y Rodríguez-Velasco, G. (1994). Digital terrain model for Spain. *Mare Nostrum* 4, (Ed. by D. Arabelos and I.N. Tziavos) pp 19-31. Thessaloniki.
- Tziavos, I.N. (1993a). Numerical Considerations of FFT Methods in Gravity Field Modelling. *Wissenschaftliche Arbeiten der F.V. n.188*. Univ. Hannover. Hannover.
- Tziavos, I.N. (1993b). Gravity Field modelling using the Fast Hartley Transform. Proc. Session G3 EGS XVIII General Assembly, pp 46-53. Wiesbaden.

# THE IMPACT OF THE GRAVITATIONAL POTENTIAL OF TOPOGRAPHIC AND ISOSTATICALLY ADJUSTED MASSES ON THE GEOID

J. Engels, E. Grafarend, P. Sorcik  
Geodätisches Institut, Universität Stuttgart  
Keplerstraße 11, D-70174 Stuttgart, Germany

## Summary

Topographic masses above a geodetic reference surface generate a *topographic potential* which is computed. In addition these masses load the inner ones leading to an *isostatic compensation*. Here we compute in addition its *isostatic potential* by an advanced slice technique which confirms uniformly convergent series expansions. The gradient of the topographic-isostatic potential leads to an estimate of deflections of the vertical. In particular, we present *geoid undulations* numerically generated by the topographic and isostatic potential based upon a compiled data set of the Moho discontinuity.

The interested reader is referred to a detailed elaboration, which is submitted to *Surveys in Geophysics* (Kluwer Academic Publishers, Netherlands).

# THE TOPOGRAPHIC POTENTIAL WITH RESPECT TO THE REFERENCE ELLIPSOID

Martin Feistritzer  
Geodätisches Institut, Universität Stuttgart  
Keplerstraße 11, D-70174 Stuttgart, Germany

## ABSTRACT

The masses between the topographic surface and a reference surface which approximates the mean sea surface of the earth, i.e. the geoid, are called topographic masses and the potential they create in a certain point under consideration is called topographic potential. Also it is well known that an ellipsoid of revolution is a very good analytic approximation of the geoid and a slightly better one than a sphere. Therefore such an ellipsoid is chosen here as a reference surface.

The idea to derive the analytical formulas for the topographic potential in an exact form by means of a rigorous integral representation was already applied by (Graffarend and Engels, 1993) to a sphere as a reference surface. The technique they used slices the topographic masses into infinitesimal spherical shells with no global, but with interrupted support. Here we present the same idea applied to an ellipsoidal reference surface.

Though the reference surface is an ellipsoid of revolution it is convenient to apply spherical coordinates. Their big advantage is the separability of the threedimensional Laplacean in contrast to geodetic coordinates (Graffarend, 1988). That makes it possible to expand the kernel of the Newton-Integral, which is the formal solution of the topographic potential, into a series of solid spherical harmonics. Then the integration with respect to the radial component can be done very easily with the single drawback that both the upper and the lower limit of integration are functions of latitude and longitude. But that is only a minor problem since the integrals with respect to the surface coordinates must be discretized for numerical evaluation anyway.

By applying spherical coordinates and having an ellipsoidal reference surface one has to distinguish between four different cases depending on the position of the point under consideration and the location of the topographic masses with respect to the sphere of convergency containing this point. After comparison of the four cases one sees that only three different types of integrals occur in all solutions. With the introduction of Heaviside-functions (Walter, 1974) we can summarize the four cases and end up with a sum of six integrals, two of each type. This result is very suitable for numerical evaluation because it keeps the series truncations to a minimum.

In order to compare this solution with already existing solutions an additional series expansion of the radial component must be applied. The reason for this is the fact that all six integrals have only interrupted support and not a global one as the existing solutions have. By introducing this series expansion we get a sum of seven integrals with one integral that has global support and corresponds to the classical solutions.

The other six integrals still depend on Heaviside-functions. Hence they have only interrupted support and can be regarded as correctional terms to the classical solution.

Both solutions are rigorous integral representations of the topographic potential in an exact form as long as numerical analysis is not taken into account. The main advantage of the solution with the global integral is that it is directly comparable to classical solutions whereas the advantage of the first solution is definitely the numerical evaluation because of the minimum of series truncations.

The interested reader is referred to a complete and detailed elaboration of the above given presentation in the Ph.D. thesis of the author which will be published in the near future.

## REFERENCES

- Graffarend, E. (1988). The geometry of the earth's surface and the corresponding function space of the terrestrial gravitational field. In: Festschrift Rudolf Sigl zum 60. Geburtstag, DGK Reihe B, Nr. 287, pp. 76 – 94.
- Graffarend, E. and J. Engels (1993). The gravitational field of topographic-isostatic masses and the hypothesis of mass condensation. Surveys in Geophysics 140, pp. 495 – 524.
- Walter, W. (1974). Einführung in die Theorie der Distributionen, Bibliographisches Institut, Mannheim – Wien – Zürich.

# ON THE APPLICATION OF WAVELETS IN GEODESY

Franz Barthelmes, Ludwig Ballani, Roland Klees<sup>1</sup>

GeoForschungsZentrum Potsdam (GFZ)

Department: "Recent Kinematics and Dynamics of the Earth"  
Telegrafenberg A17, D-14473 Potsdam

## INTRODUCTION

Today, about 10 years after wavelets become popular, more than 20 wavelet-books and a lot of introductory- and overview-papers testify to the rapid development of theory and practice in this field. Nevertheless applications in geodesy hardly exist. Having in mind the spirit of the Hotine - Marussi - Symposium: to build bridges between new mathematical theories and methods on the one hand and the geodetic research and practice on the other, we want to stimulate and encourage you to check whether wavelets might be helpful in solving your problems, and to make your own experiences with wavelets (see also: Benciolini 1994). Our aim is to give an impression what wavelets are and what wavelets are good for in geodesy. To give you an access to the extensive literature we recommend the electronic Wavelet Digest available by e-mail address: *wavelet@math.scarolina.edu*<sup>2</sup> and the wavelet literature survey by (Pittner, Schneider and Ueberhuber 1993). Since most of the papers are hardly readable (at least for non-mathematicians) - we want to mention e.g. the books (Chui 1992), (Daubechies 1992), (Kaiser 1993), (Meyer 1993) and especially the well-understandable introductory papers (Vidaković and Müller 1993) and (Bultheel 1993).

## WHAT ARE WAVELETS ?

Wavelets are functions and the word 'wavelet' or 'small wave' suggests the function has to be well localized. As the sine and cosine in Fourier analysis

$$f(x) = \sum_n a_n e^{inx}$$

wavelets are used as base functions in representing other functions

$$f(x) = \sum_{j,k} c_{j,k} \psi_{j,k}(x)$$

---

<sup>1</sup>since July 1, 1994 at Faculty of Geodetic Engineering, Delft University of Technology, Thijsseweg 11, The Netherlands

<sup>2</sup>sending a mail with the text 'help' will give you more information

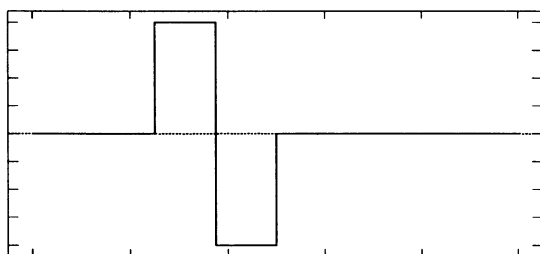
Once the type of the wavelet  $\psi(x)$  has been chosen (often called the Mother wavelet), one can make a basis  $\psi_{n,k}(x)$  by scaling and shifting the Mother Wavelet discretely which for computational efficiency are often chosen to be powers of two.

$$\left\{ \psi_{n,k}(x) = 2^{\frac{n}{2}} \psi(2^n x - k), \quad n, k \in \mathbb{Z} \right\}$$

The corresponding continuous expression, which we will not consider further, is

$$\left\{ \psi_{a,b}(x) = \frac{1}{\sqrt{|a|}} \psi\left(\frac{x-b}{a}\right), \quad a > 0, b \in \mathbb{R} \right\}$$

E.g. the simplest wavelet is the Haar wavelet (Fig. 1).



$$H_{n,k}(x) = 2^{\frac{n}{2}} H(2^n x - k)$$

with

$$H(x) = \begin{cases} 1 & , \quad 0 \leq x < \frac{1}{2} \\ -1 & , \quad \frac{1}{2} \leq x < 1 \\ 0 & , \quad \text{otherwise} \end{cases}$$

Figure 1: One of the Haar wavelets  $H_{n,k}(x)$

In comparison with Fourier analysis or Fourier transform, the result of the Wavelet analysis or Wavelet transform lies somewhere between the x-domain and the frequency domain. Fig. 2 illustrates this property. The Dirac delta ‘function’ is extremely local in the x-domain and is supported on the whole real axis in the frequency domain. On the other hand the sine and cosine functions are extremely local in the frequency domain and supported on the whole axis in the x-domain. Wavelets, however, are local in the x-domain *and* in the frequency domain, nevertheless they could not be ‘arbitrary local’ in both domains. That is similar to Heisenbergs uncertainty principle in quantum physics: the smaller the support in the x-domain the larger it is in the frequency domain and conversely. This property is important in choosing the type of the wavelet for various applications.

## MULTIRESOLUTION ANALYSIS

To go a little step into wavelet theory (but only a very little), multiresolution analysis seems to be a good access to wavelets. It consists in breaking up the Hilbert space of square-integrable functions  $L_2(\mathbb{R})$  in a sequence of nested subspaces  $V_i$  with the following properties (1-5):

$$\dots \subset V_{-2} \subset V_{-1} \subset V_0 \subset V_1 \subset V_2 \subset \dots \quad (1)$$

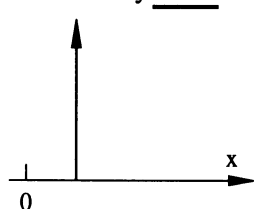
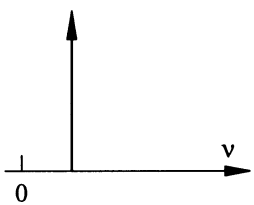
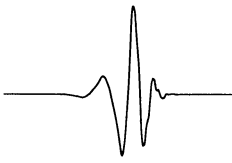
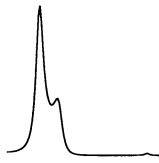
Basis Functions	x-domain	frequency domain
Dirac delta function $\delta(x)$ $f(x) = \int f(u) \delta(x-u) du$	extremely local 	supported on the whole real axis 
$\sin(x)$ $\cos(x)$ $f(x) = \frac{1}{\sqrt{2\pi}} \int \hat{f}(v) e^{ivx} dv$	supported on the whole real axis 	extremely local 
most interesting Wavelets (e.g. Daub-family) (orthogonal)	local compactly supported 	local 

Figure 2: Wavelets between x-domain and frequency domain

$$\bigcup_{n=-\infty}^{+\infty} V_n \text{ is dense in } L_2 \text{ and } \bigcap_{n=-\infty}^{+\infty} V_n = \{0\} \quad (2)$$

$$f(x) \in V_n \Leftrightarrow f(2x) \in V_{n+1}, \quad n \in \mathbf{Z} \quad (\text{scaling}) \quad (3)$$

$$f(x) \in V_0 \Leftrightarrow f(x - k) \in V_0, \quad k \in \mathbf{Z} \quad (\text{shifting}) \quad (4)$$

A scaling function  $\phi \in V_0$  exists such that

$$\{\phi(x - n), \quad x \in \mathbb{R}, \quad n \in \mathbf{Z}\} \text{ is a basis of } V_0 \quad (5)$$

Then, any  $f \in V_0$  can be written as linear combination of the basis  $\phi(x - n)$

$$f(x) = \sum_n a_n \phi(x - n), \quad (a_n) \in l_2 \quad (6)$$

with  $\phi(x)$  being often called the **Father Function**.

But how can the Father Function be characterized? As it is an element of  $V_0$  the stretched function of the next scale  $\phi(x/2)$  also lies in the same space and can be expanded within this space, which results in the so-called **Dilation Equation**

$$\phi\left(\frac{x}{2}\right) = \sum_n c_n \phi(x - n)$$

$$\phi(x) = \sum_n c_n \phi(2x - n) \quad (7)$$

The so-called filter coefficients  $\{c_n\}$  characterize the Father Function, i.e. for given coefficients  $\{c_n\}$  the Dilation Equation can be solved and the solution is the Father Function belonging to these filter coefficients. One possibility to solve the Dilation Equation is e.g. by iteration starting with the box function.

But where are the wavelets? The decisive step is to look at the orthogonal complement  $W_n$  of the nested space  $V_n$  in  $V_{n+1}$

$$V_{n+1} = V_n \oplus W_n \quad (8)$$

Obviously these spaces are not nested but orthogonal

$$W_j \perp W_i, \quad i \neq j \quad (9)$$

$$V_0 \oplus \sum_{k=0}^n W_k = \bigoplus_{-\infty}^n W_k = V_{n+1} \quad \text{and} \quad \bigoplus_{-\infty}^{+\infty} W_k = L_2 \quad (10)$$

Now the important fact is: It can be proved that the solution of the Dilation Equation, the Father Function  $\phi(x)$ , can be used to construct the **Mother Wavelet**  $\psi(x)$

$$\psi(x) = \sum_n (-1)^n c_{1-n} \phi(2x - n) \in V_1 \quad (11)$$

and - by scaling and shifting it - the family of wavelets

$$\psi_{n,k}(x) = 2^{\frac{n}{2}} \psi(2^n x - k), \quad n, k \in \mathbb{Z} \quad (12)$$

with the result that  $\{\psi_{n,k}(x), k \in \mathbb{Z}\}$  forms an orthogonal basis of  $W_n$ , and with (10)  $\{\psi_{n,k}(x), n, k \in \mathbb{Z}\}$  forms an orthogonal basis of  $L_2$ .

## ORTHONORMAL, COMPACTLY SUPPORTED WAVELETS

Now the question arises: Do wavelets exist which are orthogonal *and* compactly supported? Such wavelets would be the most interesting ones, especially in numerics since they can be described by a finite number of filter coefficients. The answer is ‘yes’: Daubechies (1988) introduced a family of new functions: orthogonal wavelets having compact support. Each Mother Wavelet is described by an even number of coefficients and it is very interesting that the simplest one, the Daub2-Mother Wavelet, turned out to be the well-known Haar wavelet. The higher the number of filter coefficients the larger is the support of the wavelet and the smoother it becomes. But the smoother the wavelet, the more localized the spectrum becomes. Fig. 3 shows 3 examples of Daub-wavelets and their spectra.

Similar to the Fast Fourier Transform a (fast) Discrete Wavelet Transform (DWT) exists using only the filter coefficients, i.e. an analytical expression of the Mother wavelet is not necessary. We cannot go into detail (see e.g. Bultheel (1993) and Press et al (1992)) but give you an impression on a DWT. Fig. 4 shows the first 16 Daub4

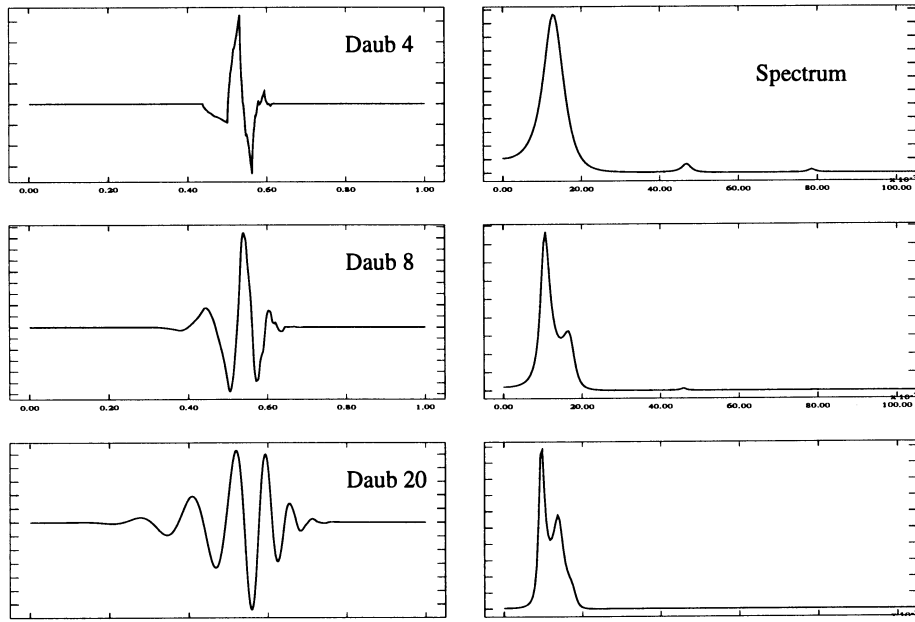


Figure 3: 3 Examples of Daub-wavelets and their spectra

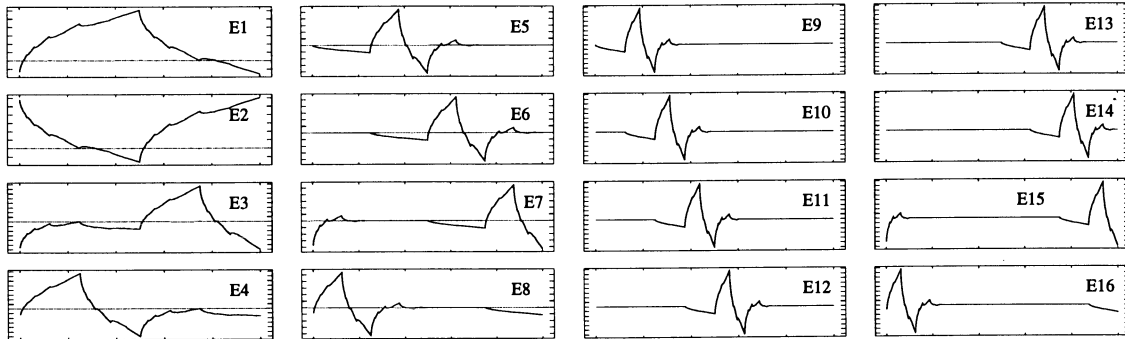


Figure 4: The first 16 Daub4 basis functions of the Discrete Wavelet Transform

base functions of the DWT. Fig. 5 shows the result of a DWT i.e. the wavelet coefficients of the input data (do not confuse filter coefficients with wavelet coefficients!). The magnitudes of the coefficients are arranged according to the resolution they represent. On the left hand side at each resolution level one of the base functions of this level is drawn. Two pieces of sine functions of different wavelengths have been used as input data - drawn at the bottom of the figure. One can see that the coefficients carry information on both, frequency and localization ('time').

Fig. 6 shows the DWT of the x-component of the polar motion time series over 79 years. Compared to Fig. 5, the mean wavelengths (i.e. periods of the resolution levels) are given additionally. The significant wavelengths contained in the data are transformed into the 0.6-year and the 1.2-year resolution level (remember that the wavelet spectra are not sharp), which corresponds to the yearly period, the Chandler period and the half-year period. The magnitudes of the wavelet coefficients show the

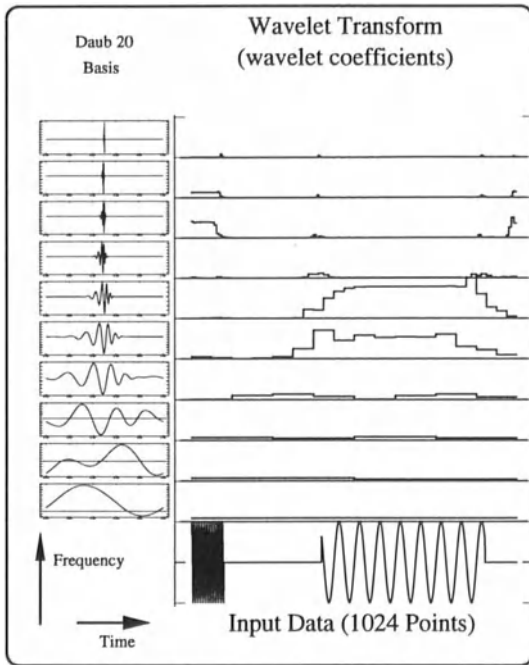


Figure 5: DWT of a function be made up of 2 pieces of the sine function

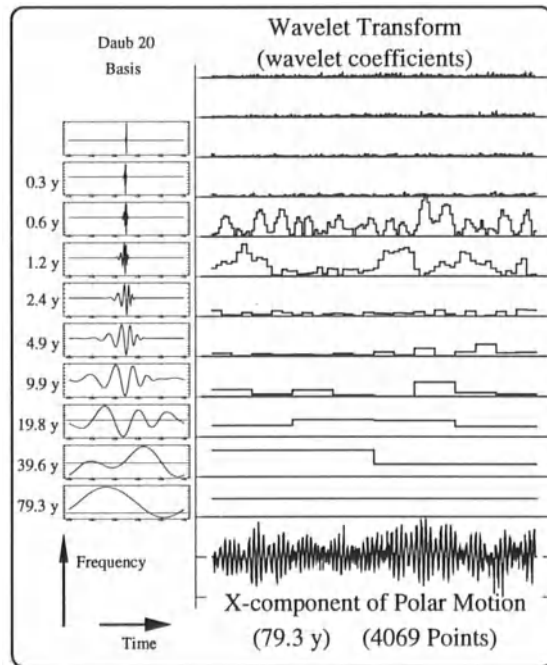


Figure 6: DWT of the x-component of the polar motion

time variation of the amplitudes of the polar motion at different resolution levels. We do not want to interpret this picture from the physical point of view here - but only want to demonstrate, what can be done with wavelets.

## THRESHOLDING AND FILTERING

The idea of the truncated wavelet approximation or thresholding consists in setting equal to zero all those wavelet coefficients that are smaller than a given threshold

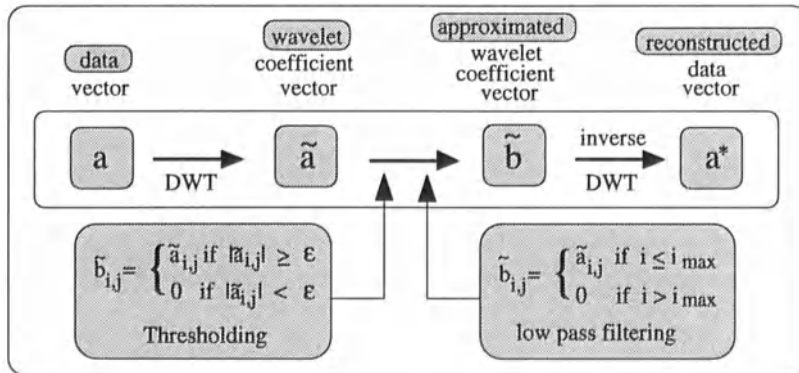


Figure 7: Thresholding and filtering procedure

before the inverse transform is applied (see Fig. 7). The objective mainly consists in removing noise or in some sense unimportant parts of the signal. The data can also be filtered, very similar to thresholding, by neglecting the coefficients of certain

resolution levels before the inverse transform. With other words: The signal is reconstructed using only the coefficients of the interesting resolution level(s) (see Fig. 7). Fig. 8 shows as an example the raw polar motion data, the thresholded curve and the difference. The lower part is a stretching of the marked detail of the upper one. In this example the thresholding procedure mainly cuts the coefficients of the four

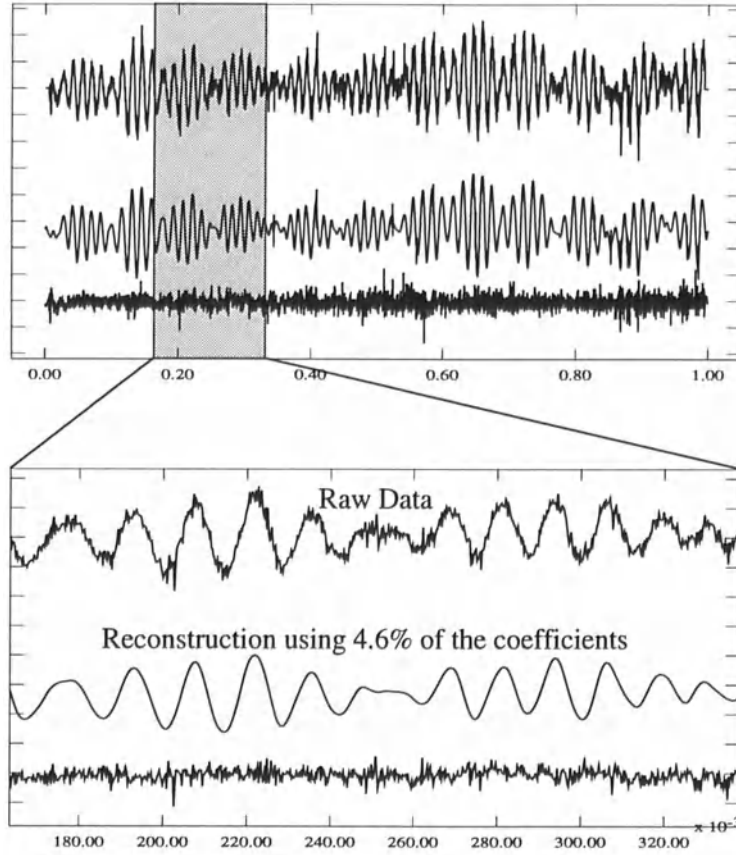


Figure 8: x-component of the pole position before and after thresholding the DWT

highest resolution levels (cf. Fig. 6) and results in data smoothing.

The example in Fig. 9, the approximation of the PREM density function, demonstrates the high efficiency of the thresholding technique in approximating data or functions (especially if they are discontinuous) using Daubechies' wavelet base functions.

An advantageous and widespread (2-dimensional) application of wavelets is image compression by thresholding. The example in Fig. 10 demonstrates how a digital terrain model of the Earth can be compressed (approximated) using wavelets. We used a real  $5' \times 5'$  model of the area  $0^\circ < \lambda < 170.66^\circ$  and  $0^\circ < \vartheta < 85.33^\circ$  consisting of  $(2048 \times 1024)$  points and containing the highest mountains and the deepest trenches of Asia. The maximum relative percentage error after thresholding is drawn over the number of used coefficients (as percentage of the total number). The two pictures on the right hand side are step-by-step vertical stretchings of the marked details of their left neighbour. It is obvious that only a few wavelet coefficients (the first ones,

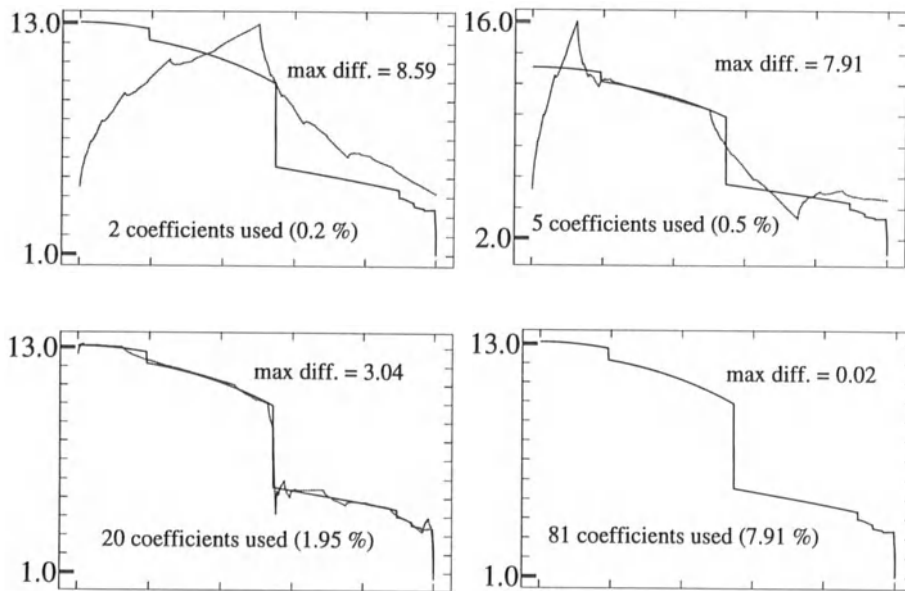


Figure 9: Truncated wavelet approximation of the PREM-model  
(1024 Points) Basis: Daub4

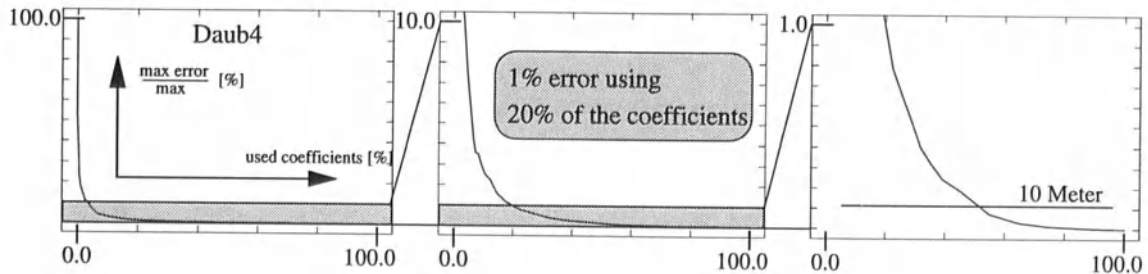


Figure 10: Accuracy of truncated DWT of a  $5' \times 5'$  digital terrain model

if they are arranged by magnitude) carry nearly the whole information about the topography.

## SOLVING LARGE LINEAR SYSTEMS OF EQUATIONS

Wavelets may be used to solve large dense linear systems. The basic idea is that a dense matrix may have an approximate sparse representation in a wavelet basis obtained by thresholding its elements by magnitude against a small fraction of the magnitude of the largest element. In other words, to solve  $Ax = b$  with a dense matrix  $A$  we first wavelet-transform the operator  $A$  and the right hand side  $b$  by  $A_w = WAW^T$ ,  $b_w = Wb$  where  $W$  represents the discrete wavelet transform. Then, we approximately solve the wavelet-transformed system  $A_w x_w = b_w$  using instead of  $A_w$  its thresholded variant  $\hat{A}_w$ , which shows a typical sparsity structure, and finally, we transform it back by the inverse wavelet transform:  $x = W^T \hat{x}_w + \delta$ . The error  $\delta$  of

the procedure depends on the properties of  $A$  and  $W$  and the chosen threshold factor.

The cost of the discrete wavelet transform is  $O(N^2 \cdot \log(N))$ , and the cost of applying the compressed form to an arbitrary vector is typically  $O(N \cdot \log(N))$ , where  $N$  is the dimension of the linear system. That is why wavelet bases are attractive for iterative algorithms in which matrix-vector multiplication with an unchanging matrix are the dominating time factor.

As an example, a typical integral operator that compresses well into wavelets has arbitrary elements near to its main diagonal, but becomes smooth away from the diagonal. That holds for many operators in Physical Geodesy and also for some interpolation methods. Fig. 11 shows a graphical representation of the original and Fig. 12 that of the wavelet-transformed matrix. The original matrix comes from the

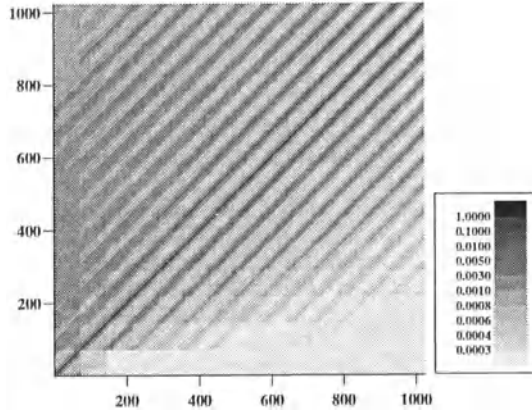


Figure 11: The magnitudes of the elements of the matrix ( $1024 \times 1024$ )

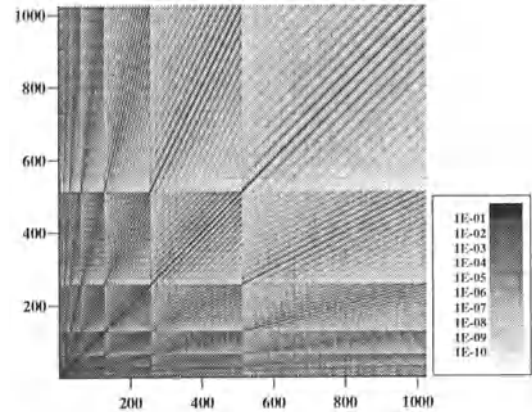


Figure 12: The magnitudes of the elements of the matrix after DWT

discretization of a weakly singular integral operator of the second kind associated to the Neumann problem on an ellipsoidal surface. The number of non-negligible elements in a matrix like that scales only as  $N$ , the dimension of the matrix. As a rough rule of thumb it is about  $10 \cdot N \cdot \log(1/\epsilon)$ , where  $\epsilon$  is the threshold factor, e.g.  $10^{-6}$ . Table 1 shows the compression factor, i.e. the ratio of the number of entries greater than the threshold before the discrete wavelet transform has been applied with respect to that after the transform, for linear systems of different size.

Now, various numerical schemes can be used to solve sparse linear systems of this ‘hierarchically band diagonal’ form, e.g. Schultz’s (or Hotelling’s) method, conjugate gradient method, or generalized minimum residual method. Especially equation solvers that take advantage of the many zero entries in the thresholded matrix are suitable. In this way we are able to solve dense nonsymmetric linear systems in  $O(N^2 \cdot \log(N))$  operations instead of  $O(N^3)$  operations using sparse techniques. However, test calculations have shown that this method does not always work, but is highly dependent on the kind of problem. Poor results have been obtained e.g. for linear systems coming from a least squares approach to gravity field determination

Table 1: Thresholded wavelet-transformed linear systems; threshold factor  $\epsilon = 10^{-6}$

$N$	$A$ elements	$\hat{A}_w$ elements	compr. factor	type of wavelet
256	65536	17832	3.7	Daub4
		15232	4.3	Daub12
		14949	4.4	Daub20
512	262144	30509	8.6	Daub12
1024	1048576	58748	17.8	Daub12
2048	4194304	112831	37.2	Daub12

Table 2: Solution errors of the linear systems after thresholding (Daub4  $N = 1024$ )

thresh. factor $\epsilon$	max. solution error $\delta$	saving of memory (%)
$10^{-10}$	$6.2 \cdot 10^{-12}$	1.6
$10^{-8}$	$2.6 \cdot 10^{-7}$	21.4
$10^{-6}$	$5.3 \cdot 10^{-5}$	63.4
$10^{-4}$	$5.0 \cdot 10^{-3}$	90.7

using satellite measurements. In addition, if the threshold factor is chosen too large it may happen that the condition of the thresholded matrix becomes so bad that the solution time using iterative equation solvers increases or it might happen that the matrix will no longer be positive definite.

Besides reducing the computational cost of matrix-vector multiplication, wavelet transforms may also be used to reduce the memory requirements. Table 2 shows the maximum error  $\delta_{max}$  of the solution  $\hat{x} = W^T \hat{x}_w$  and the resulting saving of memory for the linear system.

## REFERENCES

- Bultheel, A. (1993): Learning to swim in a sea of wavelets. Report TW 202. November 1993 Department of Computing Science, K.U. Leuven
- Benciolini, B. (1994): A note on some possible geodetic applications of wavelets. Section IV Bulletin IAG (1-1994)
- Chui, C.K. (1992): An Introduction to Wavelets. Wavelet Analysis and Its Applications Series 1, Academic Press, Boston 1992
- Daubechies, I. (1988): Orthonormal bases of compactly supported wavelets. Comm. Pure Appl. Math., 41 (1988), pp. 909-996
- Daubechies, I. (1992): Ten Lectures on Wavelets. CBMS-NSF Regional Conference Series in Applied Mathematics 61, SIAM Press, Philadelphia 1992
- Kaiser, G. (1993): A Friendly Guide to Wavelets. Birkhäuser Verlag, Basel 1993
- Meyer, Y. (1993): Wavelets, Algorithms & Applications. SIAM, Philadelphia 1993
- Pittner, S.; Schneid J. and Ueberhuber, C.W. (1993): Wavelet Literature Survey. Technical University Vienna, Vienna 1993
- Press, W.H.; Teukolsky, S.A.; Vetterling, W.T.; Flannery, B.P. (1992): Numerical Recipes in Fortran, The Art of Scientific Computing. Second Edition, Cambridge University Press, Cambridge 1992
- Vidaković, B and Müller P. (1993): Wavelets for Kids - A Tutorial Introduction. Preprint, Institute of Statistics and Decision Sciences, Duke University

# Geodetic Applications of Wavelets: Proposals and Simple Numerical Experiments

Laszlo Battha<sup>1</sup>, Battista Benciolini<sup>2</sup>, Paolo Zatelli<sup>2</sup>

## 0. Introduction

The aim of this paper is to treat at a review level some topics of the theory of wavelets that are relevant for some geodetic applications, to further specify some proposals already formulated by one of the authors (1994) and to enforce the proposals by mean of some numerical experiments. The papers about the geodetic applications of wavelets are quite numerous nowadays (see e.g. Barthelmes et al. 1994 and Ballani 1994), therefore it is worthwhile to better specify our present field of interest. Several authors developed efficient numerical algorithms based on the wavelet representation for the computation of linear operators in  $L^2$  (Beylkin et al. 1991, Beylkin 1992, Alpert 1993). The application of these techniques for the computation of linear operators in physical geodesy is investigated in this paper. We only consider operators in planar approximation in order to rely on well established mathematical tools.

Only references to papers on very specific topics have been inserted; for more general topics on the theory of wavelets see e.g. the two books by Daubechies (1992) and Chui (1992) or the two papers by Daubechies (1988) and Jawert and Sweldens (1994).

## 1. Multiresolution Analysis and Wavelet Bases of $L^2(R)$

A multiresolution analysis is a sequence of subspaces of  $L^2(R)$  with the properties

$$\dots \subset V_2 \subset V_1 \subset V_0 \subset V_{-1} \subset V_{-2} \dots \quad (1-1)$$

$$\overline{\bigcup_m V_m} = L^2(R) \quad (1-2)$$

$$\bigcap_m V_m = \{0\} \quad (1-3)$$

$$f(x) \in V_m \iff f(2^m x) \in V_0 \quad (1-4)$$

$$f(x) \in V_0 \iff f(x - n) \in V_0 \text{ for any integer } n \quad (1-5)$$

<sup>1</sup> Geodetic and Geophysical Research Inst. of the Hungarian Academy of Science – Csatkay U. 6-8 – H-9401 Sopron – Hungary

<sup>2</sup> Dipartimento di Ingegneria Civile e Ambientale – Università di Trento – Via Mesiano, 77 – I-38050 Trento – Italy

the multiresolution character of the sequence is just related to 1-4. The definition of the multiresolution analysis is the first step for the definition of a base of wavelets. We also require the existence of a function  $\phi(x)$  such that the sequence:  $\phi_{0,n}(x) = \phi(x - n)$  is an orthonormal base of  $V_0$ . The sequence (indexed by  $n$ ):

$$\phi_{m,n}(x) = 2^{-m/2} \phi(2^{-m}x - n) \quad (1-6)$$

is therefore a base of  $V_m$ . The relations

$$V_{m-1} = V_m \oplus W_m \text{ and } W_m \perp V_m \quad (1-7)$$

define the orthogonal complement  $W_m$  of  $V_m$  in  $V_{m-1}$ . As a consequence of all these definitions we have:

$$L^2(R) = \bigoplus_m W_m \quad (1-8)$$

so that the construction of a base for each of the subspaces  $W_m$  results in the construction of the base for the whole space  $L^2(R)$ . The subspaces  $\{W_m\}$  exhibit the same scaling property of  $\{V_m\}$ :

$$f(x) \in W_m \iff f(2^m x) \in W_0 \quad (1-9)$$

and a function  $\psi(x)$  exists such that its dilated and translated versions:

$$\psi_{m,n}(x) = 2^{-m/2} \psi(2^{-m}x - n) \quad (1-10)$$

form, for fixed  $m$  and running  $n$ , an orthonormal base of  $W_m$ . The functions  $\psi_{m,n}(x)$  constitute therefore a wavelet orthonormal base of  $L^2(R)$ .

The existence of  $\phi(x)$ , named the scaling function or “the father of wavelets”, and the existence of  $\psi(x)$ , “the mother of wavelets”, are simply postulated in the preceding treatment. To prove that  $\phi(x)$  and  $\psi(x)$  really exist and to study their properties (support, regularity) essentially means to analyse the existence and the properties of the solutions of the two-scale difference equation

$$\phi(x) = \sqrt{2} \sum_n h_n \phi(2x - n) \quad (1-11)$$

where:

$$h_n = \langle \phi, \phi_{-1,n} \rangle \quad (2-12)$$

and

$$\sum_n h_n^2 = 1 \quad (1-13)$$

(the base functions are normalised). The equation 1-11 can be easily obtained if we note that  $\phi \in V_0 \subset V_{-1}$  and that  $\phi_{-1,n} = \sqrt{2}\phi(2x - n)$  is an orthonormal

base of  $V_{-1}$ . The use of Fourier transform techniques finally yields, after some computations, the expression for  $\psi$ :

$$\psi(x) = \sqrt{2} \sum_n (-1)^{n-1} h_{-n-1} \phi(2x - n) \quad (1-14)$$

which links together the functions  $\psi$  and  $\phi$ . The equation (1-11) has been studied in detail and in a more general form by Daubechies and Lagaris (1991) and by other authors. The important point here is to note that the choice of the coefficients  $h_n$  completely characterises both  $\phi(x)$  and  $\psi(x)$ . It is also very important to remember that the computation of the wavelet analysis and synthesis is performed with the Mallat algorithm using just the coefficient  $h_n$ ; the explicit evaluation of the functions  $\phi(x)$  and  $\psi(x)$  is not required.

## 2. Multiresolution Analysis and Wavelet Bases of $L^2(R^N)$

The construction of a base of wavelets for functions of 2 or more variables can be done in several ways. We mention here three different techniques. The tensor product of 1D wavelet bases can be used to construct a multidimensional base: the obvious disadvantage is the combination of wavelets of different resolution (or scale) in different directions. The tensor product of the 1D nested spaces  $V_n$  defined in (1-1)...(1-5) results in the construction of a multidimensional base of wavelets where each element of the base has the same scale in all the different directions. Finally it must be mentioned that the construction of non separable wavelet bases for  $L^2(R^2)$  has been performed by Cohen and Daubechies (1993). The second construction will be emphasised hereafter because it is particularly important for the wavelet representation of operators.

The following relations define the sequence of nested subspaces  $\mathbf{V}_m$  of  $L^2(R^2)$  and the sequence of their complements  $\mathbf{W}_m$ :

$$\mathbf{V}_m = \overset{x}{V}_m \otimes \overset{y}{V}_m \quad (2-1)$$

$$\mathbf{V}_{m-1} = \mathbf{V}_m \oplus \mathbf{W}_m \text{ and } \mathbf{W}_m \perp \mathbf{V}_m \quad (2-2)$$

with properties that are the obvious generalisation of (1-1)-(1-5). (We have denoted by  $\overset{x}{V}_m$  and  $\overset{y}{V}_m$  the spaces of functions of  $x$  and  $y$ .) Now the explicit form of  $\mathbf{W}_m$  can be obtained because we have:

$$\begin{aligned} \mathbf{V}_{m-1} &= \overset{x}{V}_{m-1} \otimes \overset{y}{V}_{m-1} = \\ &= (\overset{x}{V}_m \oplus \overset{y}{V}_m) \otimes (\overset{x}{V}_m \oplus \overset{y}{V}_m) = \\ &= (\overset{x}{V}_m \otimes \overset{y}{V}_m) \oplus (\overset{x}{V}_m \otimes \overset{y}{W}_m) \oplus (\overset{x}{W}_m \otimes \overset{y}{V}_m) \oplus (\overset{x}{W}_m \otimes \overset{y}{W}_m) = \\ &= \mathbf{V}_m \oplus \mathbf{W}_m \quad (2-3) \end{aligned}$$

and from this expression the space  $\mathbf{W}_m$  is defined in term of combinations of spaces of functions of 1 variable. Therefore it results that the set

$$\{\phi_{m,n_x}(x)\psi_{m,n_y}(y) ; \psi_{m,n_x}(x)\psi_{m,n_y}(y) ; \psi_{m,n_x}(x)\phi_{m,n_y}(y)\} \quad (2-4)$$

(for fixed  $m$  and running  $n_x, n_y$ ) is a complete orthonormal base of  $\mathbf{W}_m$  and it is a base of  $L^2(R^2)$  if all the indices run from  $-\infty$  to  $+\infty$ . Please note that in all the functions of (2-4) the scale factor  $m$  is always the same for both  $x$  and  $y$ , but the two translations  $n_x$  and  $n_y$  are independent. The generalisation of this construction to  $N > 2$  dimensions is straightforward. The only important point is to compute the number of different mother functions used in the construction of the base. This number is  $2^N - 1$ .

### 3. A Rational Indexing Scheme for a Multidimensional Wavelet Base

The construction of a base of wavelets for functions of  $R^N$  can be obtained as an obvious generalisation of the procedure of the previous paragraph, but it is necessary to define a rational indexing scheme to denote the various elements of the base. This scheme, that is useful for the development of well structured software that implements the multi-dimensional analysis and synthesis, is realised by the following definitions:

$\mathbf{x} = [x_1, x_2, \dots, x_N]$  is a vector in  $R^N$

$\mathbf{n} = [n_1, n_2, \dots, n_N]$  is a multi integer

$$\alpha_l(x) = \begin{cases} \phi(x), & \text{for } l = 0 \\ \psi(x), & \text{for } l = 1 \end{cases}$$

$$\alpha_{m,n,l}(x) = 2^{-m/2} \alpha_l(2^{-m}x - n)$$

$$\mathbf{k} = \sum_{i=1}^N k_i 2^{(i-1)}$$

where  $k_i$  is 0 or 1, therefore  $\mathbf{k}$  is a number between 0 and  $2^N - 1$ , the  $k_i$  are the digit of the binary representation of  $\mathbf{k}$ . Let us simply remember that  $\{\alpha_{m,n,0}(x), n = -\infty \dots + \infty\}$  is a base of  $V_m$ ,  $\{\alpha_{m,n,1}(x), m, n = -\infty \dots + \infty\}$  is a base of  $L^2(R)$ . Now we define:

$$A_{m,\mathbf{n},\mathbf{k}}(\mathbf{x}) = \prod_{i=1}^N \alpha_{m,n_i,k_i}(x_i) \quad (3-1)$$

And therefore the set  $\{A_{m,\mathbf{n},0}(\mathbf{x}), m \text{ fixed}\}$  is a base of  $\mathbf{V}_m$ , and the set  $\{A_{m,\mathbf{n},\mathbf{k}}(\mathbf{x}), \mathbf{k} = 1 \dots 2^N - 1\}$  is a base of  $L^2(R^N)$ .

An even more complete notation (which is admittedly quite heavy, but useful) is the following:

$$A_{m,\mathbf{n},\mathbf{k}}^{(N)}(\mathbf{x}) = \prod_{i=1}^N \alpha_{m,n_i,k_i}(x_i) \quad (3-2)$$

where the dimension of the argument of  $A$  is shown explicitly. This allows to write:

$$A_{m,\underline{n},\underline{k}}^{(2N)}(\underline{x}) = \prod_{i=1}^2 A_{m,n_i,k_i}^N(\mathbf{x}_i) \quad (3-3)$$

where the argument  $\underline{x}$  and the multi-index  $\underline{n}$  are split into two components of  $N$  elements, and the integer  $\underline{k}$  is represented in base  $2^N$  by the digits  $k_i$ .

#### 4. Wavelet Representation of Operators

The wavelet representation of linear operators has proved to be a convenient tool for practical numerical computations. In a paper of Beylkin et al. (1991) two different representations of operators are discussed: they are named the standard and the non-standard form of the operator; further details and developments on the same topic are also in Beylkin (1992). The two mentioned forms are briefly described here, we neglect all the mathematical details but we comment about the differences of the two forms. These differences are relevant both from the theoretical and from the computational point of view. Consider a linear integral operator :

$$g(x) = \langle K(y, x), f(y) \rangle_y \quad (4-1)$$

where the kernel  $K$  can be considered as a function of  $L^2(R^2)$  (more general operators are considered in the two mentioned papers). If we consider the development of the kernel into a base of wavelets obtained by the tensor product of the bases of functions of  $x$  and functions of  $y$  we have the standard form of the wavelet representation of the operator. If  $K$  is developed using the base described by (2-4) we obtain the non-standard form of the operator that exhibits more convenient numerical properties (again: all this is detailed in the two mentioned papers). The non-standard form of the operator is described hereafter. The kernel  $K(x, y)$  can be written as

$$K(x, y) = \sum_m \sum_{n_x} \sum_{n_y} \left( a_{m, n_x, n_y} \phi_{m, n_x}(x) \psi_{m, n_y}(y) + b_{m, n_x, n_y} \psi_{m, n_x}(x) \psi_{m, n_y}(y) + c_{m, n_x, n_y} \psi_{m, n_x}(x) \phi_{m, n_y}(y) \right) \quad (4-2)$$

therefore the numerical computation of the operator (4-1) is realised (after discretisation and truncation) by the matrix-vector multiplication

$$\mathbf{g} = \mathbf{K}\mathbf{f} \quad (4-3)$$

where the entries of the matrix  $\mathbf{K}$  are the coefficients  $a, b, c$  of (4-2), the entries of the vector  $\mathbf{f}$  are of the form  $\langle \psi_{m, n}(y), f(y) \rangle$  or  $\langle \phi_{m, n}(y), f(y) \rangle$  and the function  $g$  is reconstructed from the entries of  $\mathbf{g}$  in term of a series of functions of  $\psi$  and  $\phi$  type. Some remarks are now necessary.

The main advantage of the described way of computing the operator (4-1) is the sparsity of the matrix  $\mathbf{K}$ , furthermore the coefficients  $a, b, c$  can be computed with efficient techniques. Note that the sparsity of  $\mathbf{K}$  is of numerical nature: there are a lot of non vanishing but practically negligible entries.

The entries of the vector  $\mathbf{f}$  are not the coefficients of the development of  $f$  in a base of wavelets because of the presence of the terms related to the  $\phi_{m,n}$  functions and the same is obviously true for  $\mathbf{g}$  and  $g$ . The vectors  $\mathbf{f}$  and  $\mathbf{g}$  are therefore redundant representations of the corresponding functions, the meaning (and the usefulness) of this redundancy will be clear in a moment.

If the index  $m$  is selected as the dominating index in the ordering of all the considered arrays the matrix  $\mathbf{K}$  is block-diagonal. In other words the computation of the entries of  $\mathbf{g}$  from the entries of  $\mathbf{f}$  is performed level by level. Nothing similar happens if the standard form of the operator is used: all the different resolution levels of the representations of  $f$  and  $g$  are mixed together. This is not a contradiction : with the standard form of the operator we use the coefficients of a true development of the functions  $f$  and  $g$  with respect to a base of wavelets; with the non-standard form of the operator we handle redundant representations of the same functions. This representation (although ordered by the scale index  $m$ ) is not properly stratified into levels of defined resolution because the spaces  $W_m$  are mutually orthogonal, but the spaces  $V_m$  are nested one into the other.

The redundancy of the vectors that represent the involved functions do not create any problem from the point of view of the computation: a slightly modified Mallat algorithm can compute  $\mathbf{f}$  from a sampled version of  $f$  and reconstruct  $g$  from  $\mathbf{g}$ . The representation of an operator in term of wavelet expansion of its kernel is not limited to operators acting on functions of one variable: the multidimensional case is more complicated from the point of view of the practical implementation, but it is conceptually equivalent. If the argument of the functions  $f$  and  $g$  are  $N$ -dimensional vectors, the kernel is a function of two vector variables or of  $2N$  scalar variables. The notation defined in (3-1), but using  $2N$  instead of  $N$ , can be used to put into evidence the dependence of the kernel on the single scalar arguments; the notation defined in (3-3) can be used to put into evidence the dependence on the two vector arguments.

## 5. Numerical Tests With an Operator Relevant for Geodesy

We will now treat the case of the potential generated in the 3D space by a planar single layer. This potential is represented by:

$$T(x_P, y_P, z) = \iint (z^2 + (x_P - x_Q)^2 + (y_P - y_Q)^2)^{-\frac{1}{2}} \rho(x_Q, y_Q) dx_Q dy_Q$$

The numerical test has been done in the following way. The variable  $z$  is treated as a constant. The sampled density function and the sampled potential function are represented by  $M^2$  values over a regular square grid ordered in a vector. The grid step is conventionally fixed equal to 1. The kernel of the transformation is therefore represented by a matrix with a quite particular structure due to the ordering of

the data and to the character of the operator which is a convolution operator. The matrix that represents the non-standard form of the operator has been computed using a wavelet base described in Daubechies (1988). The number of elements above and below a fixed threshold ( $= 0.01$ ) have been counted and their norms have been computed. If the operator is compressed neglecting the entries below the threshold we have a compression rate represented by the ratio ( $\mu$ ) between the retained and the total number of coefficients. The ratio ( $\nu$ ) between the norms of the neglected part and the complete matrix gives an idea of the obtained approximation. The results of some numerical tests are reported in the following table. The pattern of the elements above two different thresholds and for two different submatrices are shown in figures 1 and 2 ( the highest resolution level is plotted).

Test number	base used	$z$	$M$	$\mu$	$\nu$
1	DAUB4	2.	128	0.066	$0.33 * 10^{-4}$
2	DAUB4	1.	128	0.068	$0.36 * 10^{-4}$
3	DAUB4	0.2	128	0.068	$0.36 * 10^{-4}$
4	DAUB4	0.01	128	0.070	$0.25 * 10^{-4}$
5	DAUB8	2.	128	0.101	$0.45 * 10^{-4}$
6	DAUB8	1.	128	0.092	$0.44 * 10^{-4}$
7	DAUB8	0.12	128	0.103	$0.43 * 10^{-4}$
8	DAUB4	2.	256	0.025	$0.25 * 10^{-4}$
9	DAUB4	1.	256	0.025	$0.25 * 10^{-4}$
10	DAUB4	0.2	256	0.025	$0.23 * 10^{-4}$
11	DAUB4	0.01	256	0.025	$0.20 * 10^{-4}$

A comparison between tests 1, 2, 3, and 4 shows that the compression rate and the approximation index do not really depend on the smoothness of the kernel near the origin. Tests 5, 6 and 7 show that it is not convenient to chose a base of smoother elements, because the wider support deteriorates the compression rate. Finally tests 8, 9, 10 and 11 show that a better compression rate can be obtained for larger matrices. The pattern of the significant elements illustrated in the two figures is quite regular, therefore a compact storage of the compressed matrices is possible.

## 6. Conclusions and Perspectives

The results that have been described in the preceding paragraph clearly demonstrates the potential of the method of wavelet expansion for the compression of integral operators. The application of the method to real data is presently under development.

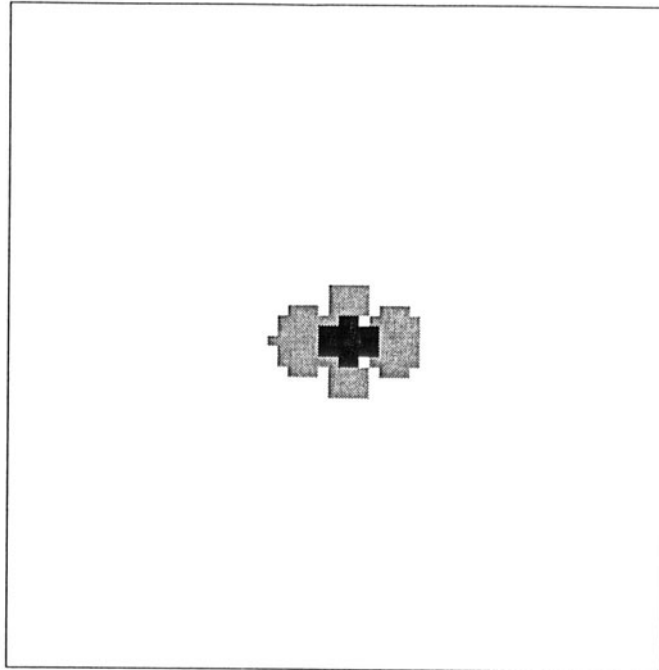


Figure 1: Numerical test number 1; Submatrix corresponding to the base element with  $k = 1 = 20001$ ; black pixels correspond to matrix elements  $> 10^{-2}$ ; grey pixels correspond to matrix elements  $> 10^{-3}$ .

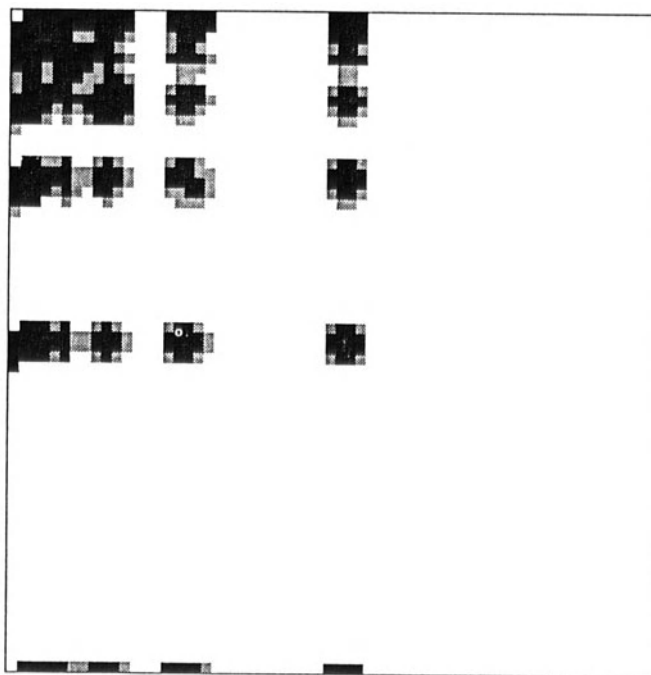


Figure 2: Numerical test number 1; Submatrix corresponding to the base element with  $k = 15 = 21111$ ; black pixels correspond to matrix elements  $> 10^{-2}$ ; grey pixels correspond to matrix elements  $> 10^{-3}$ .

## References

1. ALPERT B. K., *A Class of Bases in  $L^2$  for the sparse representation of Integral Operators*, SIAM J. Math. Anal. **24-1** (1993), 246-262.
2. BALLANI L., *Solving the Inverse Gravimetric Problem: on the Benefit of Wavelets*, presented at the III Hotine-Marussi Symposium (1994).
3. BARTHELMES L., L. BALLANI, R. KLEES, *On the Application of Wavelets in Geodesy*, presented at the III Hotine-Marussi Symposium (1994).
4. BEYLIN G., *On the Representation of Operators in Bases of Compactly Supported Wavelets*, SIAM J. Numer. Anal. **6-6** (1992), 1716-1740.
5. BEYLIN G., COIFMAN R., ROCHLIN V., *Fast Wavelet Transform and Numerical Algorithms I*, Communications on Pure and Applied Mathematics **XLIV - 2** (1991), 141-183.
6. BENCIOLINI B., *A Note on Some Possible Geodetic Applications of Wavelets*, IAG Section IV Bulletin Vol.2 N.1 (1994), 17-22.
7. CHUI C. K., *An Introduction to Wavelets*, Academic Press, Inc., 1992, (ISBN 0-12-174584-8).
8. COHEN A., DAUBECHIES I., *Nonseparable Bidimensional Wavelets Bases*, Revista Metemática Iberoamericana **9-1** (1993a), 51-137.
9. DAUBECHIES I., *Orthonormal bases of Compactly Supported Wavelets*, Communications on Pure and Applied Mathematics **XLI-7** (1988), 909-996.
10. DAUBECHIES INGRID, *Ten Lectures on Wavelets*, SIAM - Philadelphia, 1992, (ISBN 0-89871-274-2).
11. DAUBECHIES I., LAGARIAS J. C., *Two-Scale Difference Equation. I. Existence and Global Regularity of Solutions*, SIAM J. on Mathematical Analysis **22-5** (1991), 1388-1410.
12. JAWERT BJÖRN AND SWELDENS WIM, *An Overview of Wavelet Based Multiresolution Analyses*, SIAM Review **36-3** (1994), 377-412.

\* \* \*

# HOW ACCURATELY DO WE KNOW THE MARINE GEOID IN SHALLOW WATER REGIONS ?

M. Metzner<sup>1,2</sup>, S. Dick<sup>3</sup>, E. W. Grafarend<sup>1</sup>, M. Stawarz<sup>4</sup>

<sup>1</sup>Geodätisches Institut der Universität Stuttgart,  
Keplerstr. 11, 70174 Stuttgart, Germany

present affiliation: <sup>2</sup>Zentrum für Meeres- und Klimaforschung,  
Institut für Meereskunde der Universität Hamburg,  
Tropowitzstr. 7, 22529 Hamburg, Germany

<sup>3</sup>Bundesamt für Seeschiffahrt und Hydrographie (BSH),  
Bernhard-Nocht-Str. 78, 20305 Hamburg, Germany

<sup>4</sup>GKSS Forschungszentrum Geesthacht GmbH,  
Max-Planck-Straße, 21502 Geesthacht, Germany

## ABSTRACT

Radar altimeter (RA) data of the three day orbit and the first three successive cycles of the 35 day repeat orbit of the first European Remote Sensing Satellite (ERS-1) are analysed with an iterative collinear method. The investigation areas are the North Sea, the Baltic Sea and the Indonesian waters. The collinear method is based on the comparison of environmentally corrected RA-data with simulated corresponding water levels of regionally adapted circulation models along individual subsatellite passes. Since the geoid is space rather than time depending, systematic height differences between simulated water levels and altimetric sea surface heights from multiple repeats at nearly the same geographical position are related to uncertainties of the local geoid. The resulting geoid corrections for shallow water regions, e.g. water depth  $\leq 200$  m, relative to the GRIM4-C2 geoid model of the German Processing and Archiving Facility (D-PAF) is  $\pm 1\text{-}2$  m. However, over steep slopes of the sea bottom topography the geoid corrections exceed even  $\pm 16$  m, e.g. in the sea area of the Sunda trench. The comparison of the recalculated geoid heights with those of the gravity model of the Ohio State University (OSU91A) shows good agreement. However, there are still geoid differences of  $\pm 2$  m with local differences of  $\pm 6$  m for the Indonesian waters which will be investigated further.

## INTRODUCTION

In the past earth gravity models have been developed with different wavelengths like OSU91A (Rapp et al., 1987), GEM-T1 (Marsh et al., 1988), GEM-T2 (Marsh et al., 1990), GFZ93A (Bosch and Gruber, 1991), GRIM4-C2 (Schwintzer et al., 1992), etc. In conjunction with oceanographic studies a high precision geoid is demanded for reference purposes. The geoid is an equipotential surface and there-

fore necessary for the calculation of absolute oceanographic parameters like sea surface velocities, transport rates or heat fluxes. Due to the highly variable nature of our climate, the yearly mean value of dynamic topography varies from one year to another one, for instance. Since 70 % of the globe is covered by water an oceanographic approach is demonstrated for retrieving the marine geoid by separating the time dependent from the time independent part of the ocean surface. Since the dynamic topography is the difference between the sea surface above a reference ellipsoid and the geoid height we propose to analyse environmentally corrected instantaneous sea surface heights along-track with corresponding water levels obtained with numerical circulation models.

When combining different data sets a verification of each single data set is necessary for the evaluation of the final result. For the simulated water levels the verification of the result for each forcing term like the tidally induced water level changes as well as the integrated effect of wind and tidal forcing is possible. Furthermore, the two-dimensionality of simulated water levels and altimetric data is a great advantage for studying ocean areas.

## THEORETICAL BACKGROUND

### Altimetric sea surface heights

The processing of RA-data involves several steps like the extraction of certain study areas, cleaning and interpolating. The altimetric data of the geophysical data record of ERS-1 processed by the French Processing and Archiving Facility (F-PAF) have been analysed. After passing a quality control (Metzner et al., 1994) the altimetric instantanoeus sea surface heights ( $H_{corr}$ ) have been calculated according to Cheney et al. (1987) as follows:

$$H_{alt} = H_O - H_A \quad (1a)$$

$$H_{corr} = H_{alt} - H_{LT} - H_{ET} - H_{OT} - H_{Geo} \\ - H_D - H_{WET} - H_I - EMBIAS - INVBAR \quad (1b)$$

with the correction parameters (IFREMER/CERSAT, 1994):

$H_{alt}$	:	uncorrected sea surface height
$H_O$	:	orbit height
$H_A$	:	altitude corrected for instrumental errors
$H_{ET}$	:	earth tide
$H_{OT}$	:	ocean tide
$H_{LT}$	:	loading tide
$H_{Geo}$	:	geoid height
$H_D$	:	dry troposphere
$H_{WET}$	:	wet troposphere (1)
$H_I$	:	ionosphere
$EMBIAS$	:	electromagnetic bias ( $\approx 0.02 * SWH$ )
$SWH$	:	significant wave height
$INVBAR$	:	inverse barometric effect

For our studies the ocean tide is not eliminated because the simulated water levels are resulting from tidal and wind induced forcing. Due to regional differences in the determination of the EM Bias (Glazman et al., 1994) a polynomial with a leading factor of  $c \approx 0.02 * H_{1/3}$  was taken for the global uniform calculation (IFREMER/CERSAT, 1994).

The observation equation (1b) is not free of errors but represent the actual height of the sea surface along-track in a realistic approach. The main error source is the determination of the orbit height. Because of the small geographical extension of the study areas the application of a zero order polynomial is sufficient to correct for the orbit uncertainty as a first approximation.

During the three day repeat cycle of ERS-1 the ocean variability of the multiply corrected altimetric sea surface heights was  $\approx 20$  cm.

### Simulated water levels

Deviations of the sea surface from an equipotential surface, e.g. the geoid, result from the dynamics and density distribution of the water column. Besides earth gravitation and rotation, it is above all the bottom topography, the wind and air pressure as well as riverine inputs that determine the dynamics of the ocean and certainly the shelf region with water depths  $\leq 200$  m. For the North Sea/Baltic Sea a hydrodynamic-numerical circulation model has been developed at the Bundesamt für Seeschiffahrt und Hydrographie (BSH, formerly Deutsches Hydrographisches Institut - DHI). The model has been working operationally for about 15 years and has been improved continuously within different projects (Backhaus, 1980; Backhaus and Maier-Reimer, 1983; Soetje and Brockmann, 1983; Müller-Navara and Mittelstaedt, 1987; Dick and Soetje, 1990; Kleine, 1994).

The circulation of the water is described by the equations of motion, the equation of continuity, the equation of state and the budget equations for temperature and salinity. After vertical integration over a layer of thickness  $h$  and various simplifications (e.g. Boussinesq approximation), the equations for the east and north components of velocity in spherical coordinates read:

$$\begin{aligned} \frac{\partial u}{\partial t} + \frac{u}{R \cos \varphi} \frac{\partial u}{\partial \lambda} + \frac{v}{R} \frac{\partial u}{\partial \varphi} - \frac{\tan \varphi}{R} u v = & 2 \omega \sin \varphi v - \frac{1}{\rho} \frac{1}{R \cos \varphi} \frac{\partial p}{\partial \lambda} \\ & - \frac{1}{R \cos^2 \varphi} \frac{\partial}{\partial \lambda} (\cos \varphi \overline{u' u'}) + \\ & - \frac{1}{R \cos^2 \varphi} \frac{\partial}{\partial \varphi} (\cos^2 \varphi \overline{u' v'}) + \frac{\Delta \tau_\lambda}{h} \quad (2a) \end{aligned}$$

$$\begin{aligned} \frac{\partial v}{\partial t} + \frac{u}{R \cos \varphi} \frac{\partial v}{\partial \lambda} + \frac{v}{R} \frac{\partial v}{\partial \varphi} + \frac{\tan \varphi}{R} u u = & -2 \omega \sin \varphi u - \frac{1}{\rho} \frac{1}{R} \frac{\partial p}{\partial \varphi} \\ & - \frac{1}{R \cos \varphi} \frac{\partial}{\partial \lambda} (\overline{v' u'}) + \\ & - \frac{1}{R \cos \varphi} \frac{\partial}{\partial \varphi} (\cos \varphi \overline{v' v'}) + \frac{\Delta \tau_\varphi}{h} \quad (2b) \end{aligned}$$

with

- $u, v$  : components of current in  $\lambda$  and  $\varphi$  direction
- $p$  : water pressure
- $h$  : thickness of model layer
- $R$  : radius of the earth
- $t$  : time
- $\lambda, \varphi$  : geographical longitude and latitude, respectively
- $\Omega$  : angular velocity of the earth
- $\varrho$  : density of sea water
- $\Delta\tau$  : difference of stress terms at the surface and bottom of the model layer

The current components are split into a term of the mean current ( $u, v$ ) and a term of perturbation ( $u', v'$ ) which represent the turbulent fluctuations of the water motion. The expressions  $\overline{u'u'}$ ,  $\overline{v'v'}$ ,  $\overline{u'v'}$  are horizontal stress terms and are parameterized in terms of the mean current (closure model):

$$-\overline{u'u'} = A_h \cdot \left( \frac{1}{R \cos \varphi} \frac{\partial u}{\partial \lambda} - \frac{1}{R} \frac{\partial v}{\partial \varphi} - \frac{\tan \varphi}{R} v \right) \quad (3a)$$

$$-\overline{u'v'} = A_h \cdot \left( \frac{1}{R \cos \varphi} \frac{\partial v}{\partial \lambda} + \frac{1}{R} \frac{\partial u}{\partial \varphi} - \frac{\tan \varphi}{R} u \right) \quad (3b)$$

$$-\overline{v'v'} = -A_h \cdot \left( \frac{1}{R \cos \varphi} \frac{\partial u}{\partial \lambda} - \frac{1}{R} \frac{\partial v}{\partial \varphi} - \frac{\tan \varphi}{R} v \right) \quad (3c)$$

with  $A_h$  the horizontal eddy viscosity coefficient.

To calculate the shear stress at the sea surface and at the sea bottom, a quadratic law from boundary layer theory is used. The dimensionless coefficients are the wind drag and bottom friction coefficient, respectively. At the sea surface it reads:

$$\tau_{\lambda_s} = \frac{\varrho_{air}}{\varrho_{water}} C_D \cdot W_\lambda \sqrt{W_\lambda^2 + W_\varphi^2} \quad (4a)$$

$$\tau_{\varphi_s} = \frac{\varrho_{air}}{\varrho_{water}} C_D \cdot W_\varphi \sqrt{W_\lambda^2 + W_\varphi^2} \quad (4b)$$

with the wind drag coefficient  $C_D = (0.7 + 0.09 \sqrt{W_\lambda^2 + W_\varphi^2}) \cdot 10^{-3}$ ;  $W_\lambda$  and  $W_\varphi$  the components of surface wind and  $\varrho_{air}$ ,  $\varrho_{water}$  the density of air and sea water, respectively.

At the sea bottom it reads:

$$\tau_{\lambda_b} = r \cdot u \sqrt{u^2 + v^2} \quad (5a)$$

$$\tau_{\varphi_b} = r \cdot v \sqrt{u^2 + v^2} \quad (5b)$$

with the bottom friction coefficient  $r = 0.0025$ .

Inside the water column the following equations apply:

$$\tau_\lambda = A_v \frac{\partial u}{\partial z} \quad (6a)$$

$$\tau_\varphi = A_v \frac{\partial v}{\partial z} \quad (6b)$$

with  $A_v$  the vertical eddy viscosity coefficient, and  $z$  the vertical coordinate.

For the vertical dimension hydrostatics is assumed and therefore, the equation of motion for the vertical current component can be transformed into an equation for the vertical pressure distribution:

$$p(z) = p_{air} + g \varrho \zeta + g \int_z^0 \varrho(z) dz \quad (7)$$

with  $p_{air}$  the atmospheric pressure,  $\zeta$  the water elevation, and  $g$  the gravity acceleration.

The equation of continuity reflects the conservation of mass. This equation is used to calculate the water level by taking into account the kinematic boundary conditions at the sea surface and at the sea bottom, respectively:

$$\frac{1}{R \cos \varphi} \cdot \frac{\partial(h \cdot u)}{\partial \lambda} + \frac{1}{R \cos \varphi} \cdot \frac{\partial(h \cdot v \cdot \cos \varphi)}{\partial \varphi} + \Delta w = 0 \quad (8)$$

with  $\Delta w$  the difference of the vertical current component at the top and the bottom of the model layer  $h$ .

The equation of state describes the connection between water density  $\varrho$ , water temperature  $T$ , salinity  $S$  and water pressure  $p$  (UNESCO, 1981; Gill, 1982):

$$\varrho = \varrho(S, T, p) \quad (9)$$

For a complete description of shallow water dynamics, the budget equations for water temperature  $T$  and salinity  $S$  are required. The budget equation for the water temperature reads:

$$\begin{aligned} \frac{\partial T}{\partial t} + \frac{u}{R \cos \varphi} \frac{\partial T}{\partial \lambda} + \frac{v}{R} \frac{\partial T}{\partial \varphi} + w \frac{\partial T}{\partial z} &= \frac{1}{R^2 \cos^2 \varphi} \frac{\partial}{\partial \lambda} \left( K_h \frac{\partial T}{\partial \lambda} \right) \\ &+ \frac{1}{R^2 \cos \varphi} \frac{\partial}{\partial \varphi} \left( \cos \varphi K_h \frac{\partial T}{\partial \varphi} \right) \\ &+ \frac{\partial}{\partial z} \left( K_v \frac{\partial T}{\partial z} \right) \end{aligned} \quad (10)$$

with  $K_h, K_v$  the horizontal and vertical diffusion coefficient, respectively.

Similarly for the salinity  $S$ , the equation reads:

$$\begin{aligned} \frac{\partial S}{\partial t} + \frac{u}{R \cos \varphi} \frac{\partial S}{\partial \lambda} + \frac{v}{R} \frac{\partial S}{\partial \varphi} + w \frac{\partial S}{\partial z} &= \frac{1}{R^2 \cos^2 \varphi} \frac{\partial}{\partial \lambda} \left( K_h \frac{\partial S}{\partial \lambda} \right) \\ &+ \frac{1}{R^2 \cos \varphi} \frac{\partial}{\partial \varphi} \left( \cos \varphi K_h \frac{\partial S}{\partial \varphi} \right) \\ &+ \frac{\partial}{\partial z} \left( K_v \frac{\partial S}{\partial z} \right) \end{aligned} \quad (11)$$

Because sea surface slopes are mainly created by external forces, for the Indonesian waters the density gradients in the water column are neglected as a first approximation, i.e. the water density is regarded as constant. This is also consistent with the definition of the geoid. However, the regional hydrodynamic numerical barotropic circulation model accounts for the main oceanographic processes.

These equations were discretised by means of the method of finite differences and solved on a discrete grid. The advantage of applying a semi-implicit formulation of the numerical scheme is that the time step does not have to satisfy the Courant-Friedrichs-Lowy criterion for stability purposes.

The applied two models differ only slightly, however, with respect to their tidal forcing, baroclinicity, grid spacing and bathymetric data. Due to the extension of the investigated areas and due to the computing time and storage capacity there are limits for the resolution of such models. The North Sea/Baltic Sea model is a system of three interactive coupled models with staggered grids of different horizontal resolutions. The coarse grid has a spatial resolution of about 22 km, the fine grid of about 11 km and the coastal model (black box) has a resolution of about 1.85 km. The big crosses denote the meteorological mesh. The horizontal distance between grid points for the Indonesian waters is  $10' \times 10'$  in each direction. The model domains with their grids are shown in Figure 1.

For each grid point of the two models the bathymetry is prescribed. Therefore, the sea bottom topography for the North Sea/Baltic Sea has been digitized at the BSH. For the Indonesian waters the bathymetric data of the Technical University of Graz, Austria, is used (Wieser, 1987).

The equations for the current velocities and the sea surface elevation are integrated forward in time.

At the open boundaries the water elevations are prescribed by calculation of harmonic constants for selected partial tidal constituents, which equals the summation of tidal constituents as follows:

$$\zeta(x, y, t) = \zeta_0(x, y) + \sum_{\nu=1}^n \left( j \cdot A(x, y) \cdot \cos(\sigma t + (V_0 + v) - P(x, y)) \right)_\nu \quad (12)$$

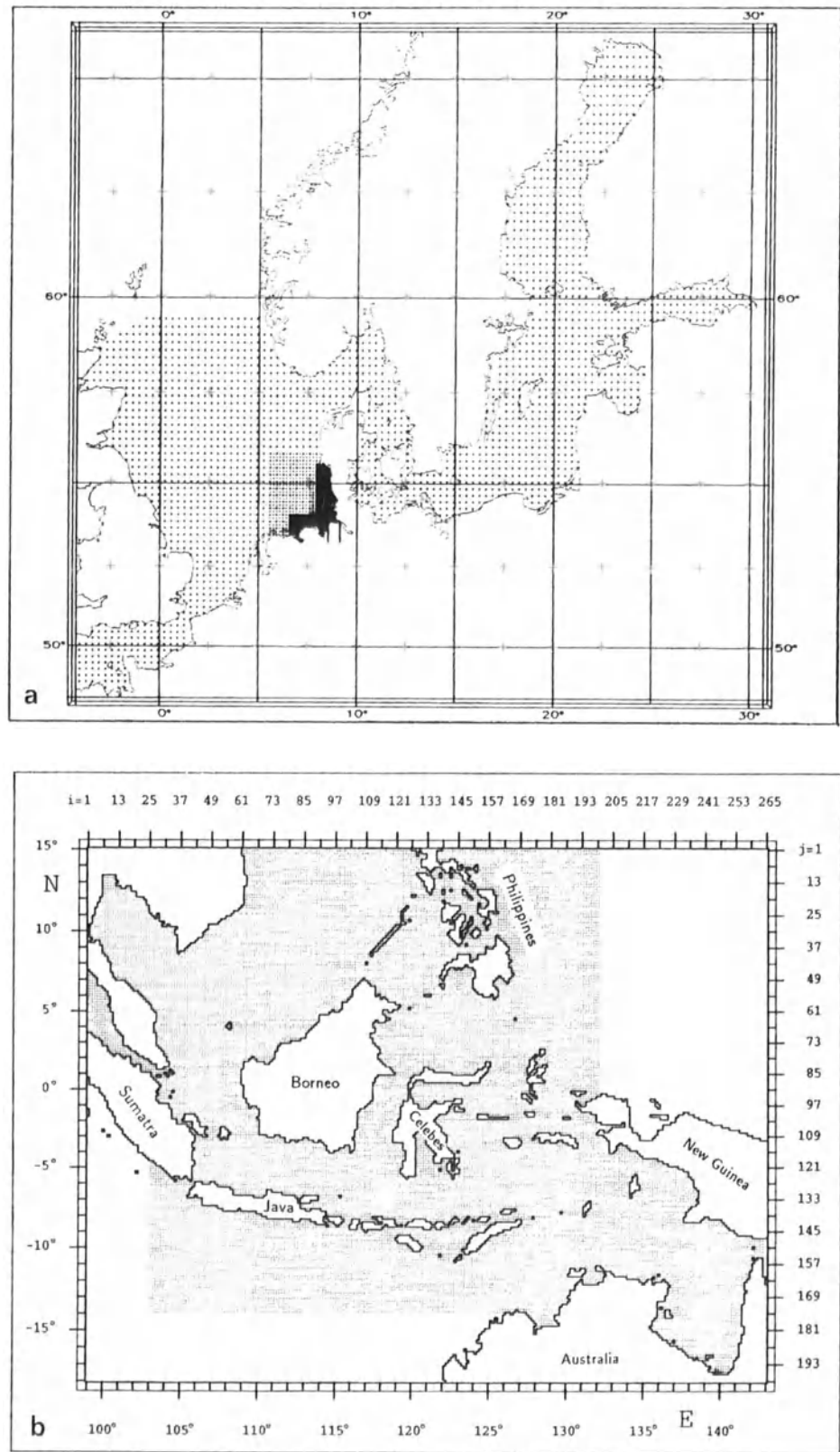


Fig. 1. Model domain of a) the North Sea and Baltic Sea area as well as of b) the Indonesian waters with the calculation mesh.

with

$\zeta(x, y, t)$	: water elevation at time t
$\zeta_0(x, y)$	: mean water level, dependent of sea chart zero (should be the minimum water depth at that point)
$\nu$	: number of partial tide
$A(x, y)$	: amplitude of partial tide
$P(x, y)$	: phase of partial tide
$\sigma$	: angular velocity of partial tide
$V_0$	: astronomical phase lag
$j$	: correction for amplitude
$v$	: correction for phase

For the North Sea/Baltic Sea model 14 constituents and for the Indonesian waters eight tidal constituents have been taken into consideration.

To solve the equation system boundary conditions have to be applied. No transport through closed boundaries is allowed. The horizontal transport through the open boundaries is barotropically adjusted. Initially the current velocity and the water elevation are set to zero.

The driving force at the sea surface is the wind stress and the air pressure. Even in tropical sea areas it is not sufficient to force the circulation model with monthly mean values. High frequency wind data like six hourly wind fields weighted in time and space are necessary to achieve realistic results. As an example, wind fields for the Indonesian waters averaged for July 1992 and for three successive days between 26.-28.07.1992, 12:00 UTC, during the northeast (NE) monsoon are shown in Figure 2.

## Verification

To evaluate the accuracy of the altimetric and simulated sea surface heights a verification against independent data, e.g. tide gauge data, has to be performed. To avoid aliasing due to the sampling rate of the altimeter and to account for the wind and tidal sea surface elevation temporal highly resolved data like hourly ones are needed.

For the Baltic Sea the direct comparison of simulated water levels with corresponding tide gauge data of 10 Scandinavian tide gauge stations for the period between 01.08.-31.12.1991 resulted in a mean root mean square (*RMS*) difference of 11.33 cm (Metzner et al., 1994). This number can be interpreted as the accuracy of the recalculated marine geoid of the Baltic Sea, because the corrected altimetric sea surface heights are adjusted to the simulated water levels.

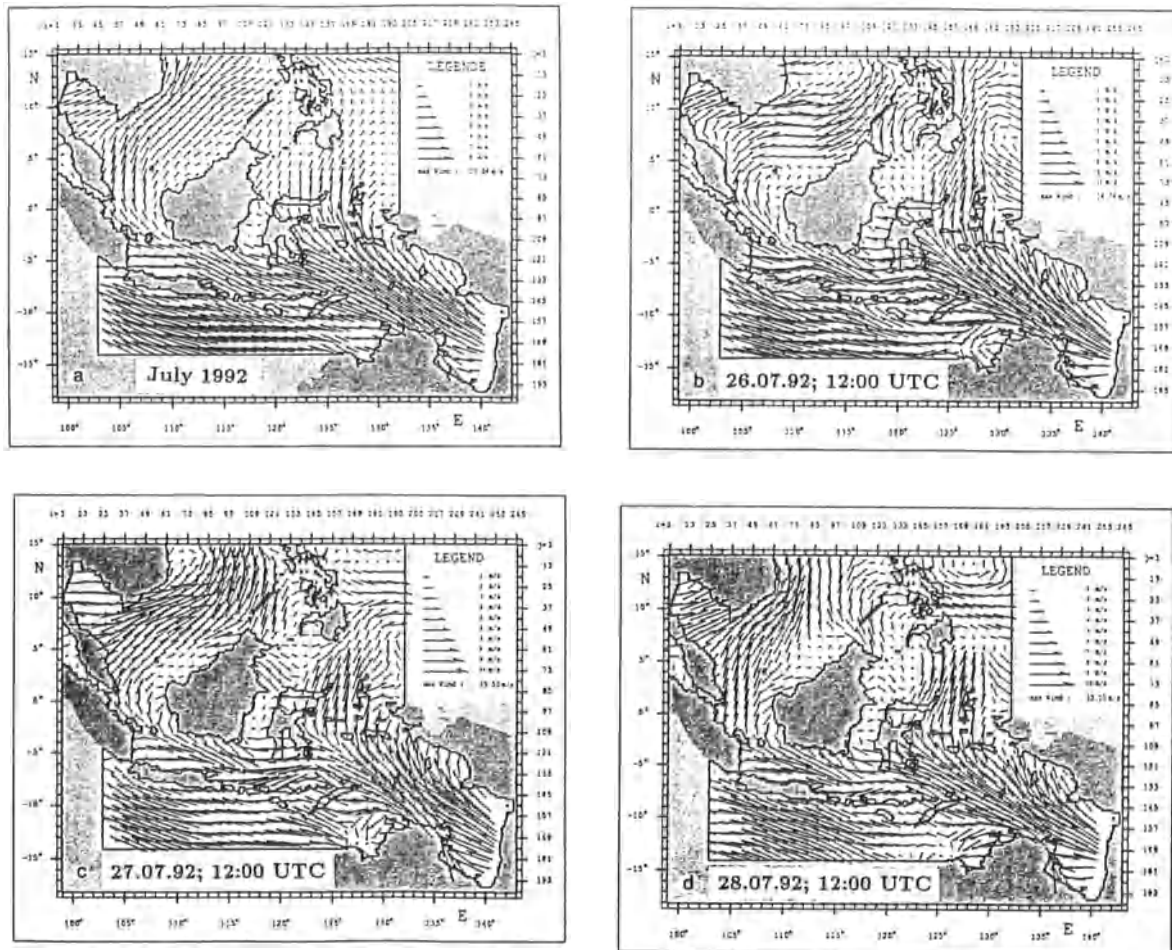


Fig. 2. Wind fields for the sea area of the Indonesian waters from the European Center of Medium Weather forecast (ECMWF) in Reading, U.K.; a) monthly averaged wind field for July 1992, b) synoptic wind field for the 26th July 1992, 12:00 UTC; c) synoptic wind field for the 27th July 1992, 12:00 UTC; d) synoptic wind field for the 28th July 1992, 12:00 UTC.

However, for the Indonesian waters the verification was performed only with predicted high and low waters for selected geographical positions, because hourly tide gauge data were not available. Therefore, a verification of the simulated water levels for the Indonesian waters accounting only for tidal effects was carried out by regression analysis. For this purpose, amplitudes and phases of four tidal constituents  $M_2$ ,  $S_2$ ,  $K_1$  and  $O_1$  calculated by the circulation model have been compared with corresponding tabulated tidal data (Admiralty Tide Tables, 1992). The regression coefficients for the tidal amplitudes and for the tidal phases vary between 0.92-0.94 and 0.80-0.91, respectively. However, the correlation coefficients for certain sea areas like the Banda Sea were only  $M_2\ Amp=0.89$  and  $M_2\ P_{ha}=0.68$ .

The simulated two dimensional time depending water levels are the link to the corrected altimetric sea surface heights.

## Iterative collinear method

Two data sets of sea surface heights have been calculated, namely the altimetric heights and the simulated water levels. Due to the physics of the circulation model these two heights should represent the same ocean dynamics which is reflected in the sea surface heights. However, after collocation of the simulated water levels and the environmentally corrected altimetric sea surface heights systematic differences showed up (Stawarz, 1994; Stawarz and Metzner, 1994). After minimising these differences in the altimetric measurements from the simulated reference water levels for each track individually a residual orbit error has been removed by:

$$H_{CT_i} = H_{C_i} - \left( \frac{1}{N} \sum_{i=1}^N H_{C_i} - \frac{1}{N} \sum_{i=1}^N H_{Mod_i} \right) \quad (13)$$

with

- $i$  : number of data points along-track
- $H_{C_i}$  : single environmentally corrected altimeter measurement along-track
- $H_{Mod_i}$  : single simulated water level along-track
- $H_{CT_i}$  : altimeter data corrected for orbit uncertainty

Due to a missing absolute reference level for both, the altimetric and the simulated data, a vertical datum was determined by averaging the single along track height data (second and third term on right-hand side of (13)). Already accounting for the radial orbit error by applying a zero order polynomial a residual orbit error was eliminated by applying Equation (13).

Having applied the orbit correction for single repeated profiles the altimetric data still exhibited systematic height differences. Due to the amount of repeats of one sub-satellite pass those differences are interpreted as geoid uncertainties. The differences were arithmetically averaged for regular spaced intervals along-track and the geoid corrections for each interval ( $\bar{H}_{Gcorr_j}$ ) were calculated as follows:

$$\bar{H}_{Gcorr_j} = \frac{1}{L} \sum_{m=1}^L \left( \frac{1}{N_j} \sum_{i=1}^{N_j} (H_{CT_i} - H_{Mod_i}) \right) \quad (14)$$

with  $L$  the number of repeats and  $j$  the index of the intervals. The geoid corrections have been added to the given first guess geoid GRIM4-C2 ( $H_{G_i}$ ):

$$H_{GN_i} = H_{G_i} + \bar{H}_{Gcorr_j} \quad (15)$$

The resulting recalculated geoid undulations have a spatial resolution according to the altimetric data distribution along-track and the horizontal resolution of the applied model.

## RESULTS

As an example of the results two profiles are presented in Figures 3 and 4; one for the Baltic Sea during the three day repeat cycle, and one for the Indonesian waters during the 35 day repeat cycle, respectively.

The position of the analysed descending sub-satellite pass of the Baltic Sea is shown in Fig. (3c). After applying the iterative collinear method the resulting geoid corrections (stars) vary between  $\pm 1.60$  m and are presented in Fig. (3a) (right y-axis). Having added the along-track geoid corrections to the corresponding long wavelength geoid undulations of the GRIM4-C2 gravity model (crossed circles) the resulting geoid heights (triangles) show small scale geoid undulations and are also presented in Fig. (3a). For verification of the recalculated geoid undulations, corresponding geoid heights of the Ohio State University gravity model (OSU91A) have been calculated and are shown in Fig. (3b) along with the sea bottom topography profile. The slope and the magnitude of the two geoid profiles agree very well, also the horizontal scales of the geoid undulations. However, at the outer ends of the profiles there are discrepancies of  $\pm 2$  m with a turning point at about  $60^\circ$  N. Knowing about the land uplift effect due to melting ice in the northern hemisphere this might be an indication of isostatic balance.

An overview of the Indonesian waters with the position of the analysed descending sub-satellite track is shown in Fig. (4a). The long wavelength geoid undulation of the GRIM4-C2 gravity model along with the resulting geoid corrections and the recalculated geoid profile is presented in Fig. (4b). The geoid corrections vary between -14 m and +6 m. After applying the track and geoid corrections the *RMS* difference between the altimetric heights and the simulated water levels was about 60 cm. Adding the geoid corrections to the GRIM4-C2 geoid heights the resulting geoid profile shows small scale structures with horizontal scales  $< 100$  km.

The verification of the recalculated geoid profile (triangle) with the corresponding profile of the OSU91A geoid heights (crossed circles) shows good agreement and the curves are presented in Fig. (4c) along with the bathymetric profile. The largest discrepancy between the two geoid profiles are at the turning points of the curves. The deviations vary between -2.223 m and 1.910 m, while the overall difference between the two mean geoid heights along-track is only 9 cm. Due to the large range of the geoid undulations from 30 m - 66 m the differences between the two geoid profiles are presented in Fig. (4d).

## DISCUSSION

According to the multiple repeats during 14.08.-09.12.91 and 14.04.-28.07.92 and because the geoid is space rather than time dependent, systematic height differences between two corresponding sea surface heights at nearly the same geographical position are related to uncertainties of the local geoid.

A weak point in the analysis of the altimeter data could be the simple bias correction for the orbit inaccuracy. If there had been a tilt effect in the altimeter data it would consequently have been revealed in a tilted orbit correction which is

recalculated geoid profile in the Baltic Sea  
 period: 14.08.91 - 09.12.91; repeat cycle: 3 day  
 number of averaged tracks: 27

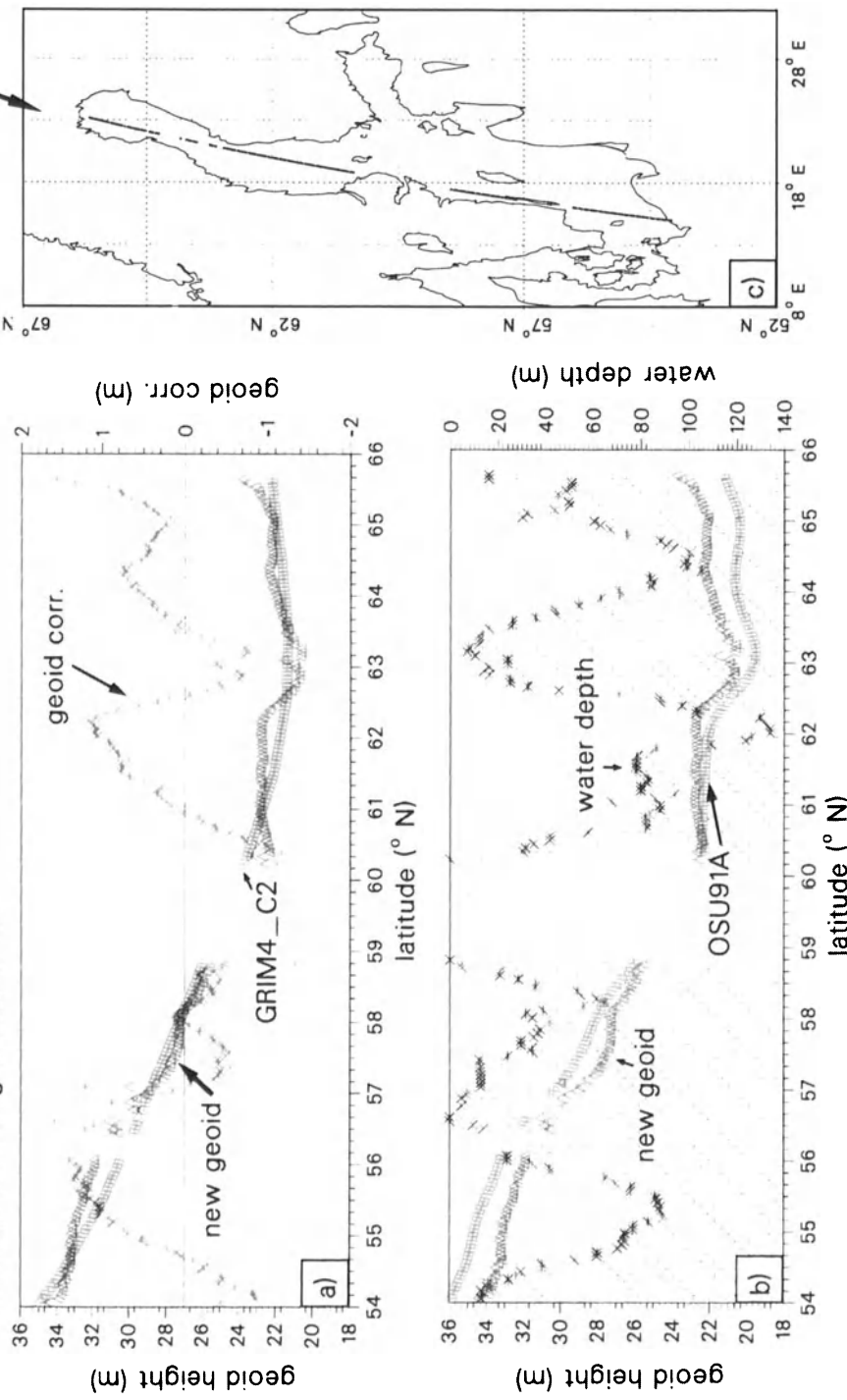


Fig. 3. Analysed sub-satellite track of the Baltic Sea during the three day repeat cycle of ERS-1, a) geoid heights of the GRIM4-C2 gravity model along-track (crossed circles), geoid corrections obtained with the iterative collinear method (stars), and recalculated geoid profile (triangles), b) recalculated geoid profile along-track (triangles), geoid heights of the OSU91A gravity model (crossed circles), and corresponding bathymetric profile, c) geographical overview of the Baltic Sea with location of the analysed ERS-1 sub-satellite pass against latitude.

# recalculated geoid profile of the Indonesian waters

repeat cycle: 35 days

period: 14.04. - 28.07.92

number of averaged tracks: 3

OSU91A - new (m)

$$\begin{array}{ll} H_{\min}: & -2.223 \\ H_{\text{OSU91A}}: & 54.216 \end{array} \quad \begin{array}{ll} H_{\max}: & 1.910 \\ H_{\text{new}}: & 54.303 \end{array}$$

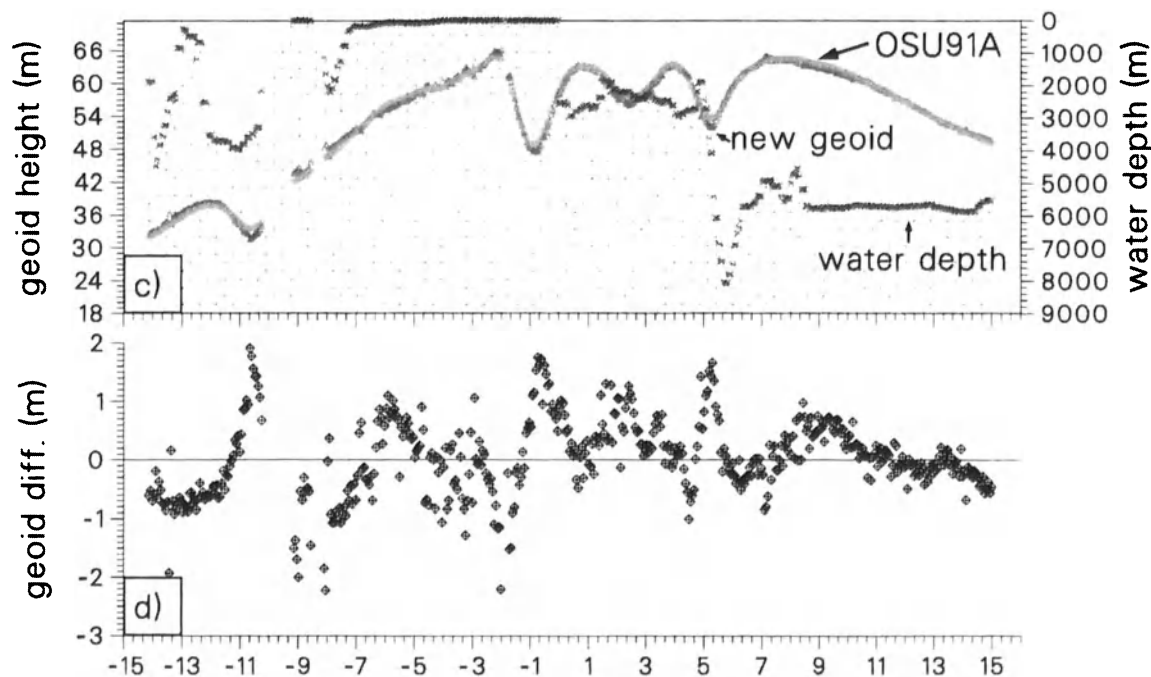
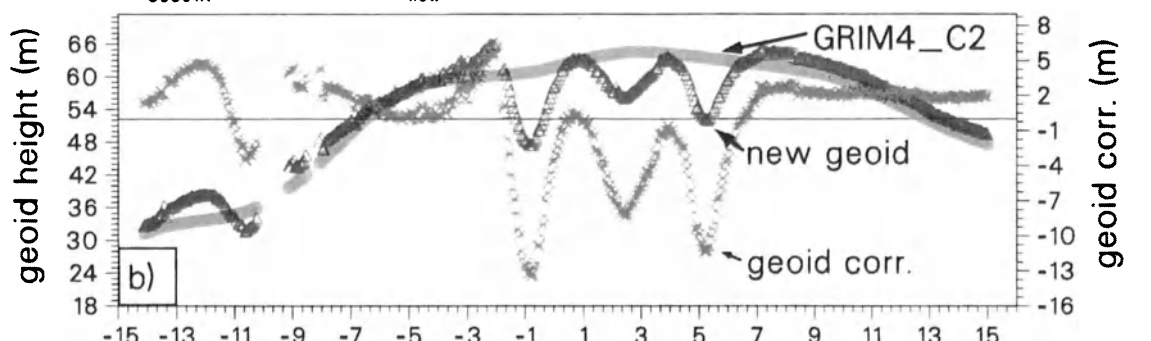
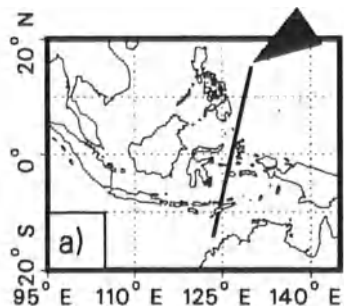


Fig. 4. Analysed sub-satellite track of the Indonesian waters during the 35 day repeat cycle of ERS-1, a) geographical overview of the Indonesian waters with location of the analysed ERS-1 sub-satellite pass, b) geoid heights of the GRIM4-C2 gravity model along-track (crossed circles), geoid corrections obtained with the iterative collinear method (stars), and recalculated geoid profile (triangles), c) recalculated geoid profile along-track (triangles), geoid heights of the OSU91A gravity model (crossed circles), and corresponding bathymetric profile, d) height differences between the recalculated geoid profile and the OSU91A geoid profile against latitude.

not the case. Furthermore, the iterative collinear method was applied to both study areas in the same way. A tilt effect was not observed for the Indonesian waters.

Summarizing the results we can conclude, that geoid corrections for shallow water regions, e.g. water depths  $\leq 200$  m, relative to the GRIM4-C2 geoid model is  $\pm 1\text{-}2$  m. However, over steep slopes of the sea bottom topography the geoid corrections exceed even  $\pm 16$  m, e.g. in the sea area of the Sunda trench.

The comparison of the recalculated geoid heights with those from OSU91A shows good agreement. The *RMS* values are within the range of those given by Rapp (1993). The difference to Rapp (1993) is the independence of the two data sets of geoid heights due to the method. However, there are regional discrepancies of  $\pm 2$  m. One reason for those height differences could be the precision of the bathymetric data as an input for the circulation model, especially for the Indonesian waters where the data of the Technical University of Graz (TUG87) have been used. On the other hand there are still errors in the gravity models due to heterogeneous distribution of gravity data. Furthermore, the circulation models should also account for waves and swell when calculating sea surface heights. Another reason could be the different dimensions of the reference ellipsoids used for OSU91A and the RA-data of ERS-1.

The integration of sea gravity data can perhaps give the final confirmation for the quality assessment of the two independently retrieved geoid undulations. It would be useful to have two-dimensional distribution of marine gravity anomalies in conjunction to the two-dimensional distribution of altimetric and simulated sea surface heights.

**Acknowledgments.** We thank the European Space Agency (ESA) for making available the radar altimeter data of the first European Remote Sensing Satellite (ERS-1). We thank Dr. U. Seiler and Mrs. H. Langenberg for correcting the manuscript. For technical assistance we thank B. Witassek. The work was financially supported by the German Research Foundation (DFG) during the project d3-4. Due to the support of Prof. W. Zahel parts of the study concerning the Indonesian waters was financed during the DFG project SFB 318 *Klimarelevante Prozesse im System Ozean-Atmosphäre*.

## REFERENCES

- Admiralty Tide Tables and Tidal Stream Tables (1992). Pacific Ocean and seas, Vol. 3, published by the *Hydrographer of the Navy*, Crown Copyright, 483 pp.
- Backhaus, J. O. (1980). Simulation von Bewegungsvorgängen in der Deutschen Bucht, *Deutsche Hydrographische Zeitschrift*, Ergänzungsheft Reihe B, Nr. 15, 56 pp.
- Backhaus, J. O., and E. Maier-Reimer (1983). On seasonal circulation patterns in the North Sea, in: *North Sea Dynamics*, Ed. by J. Sündermann and W. Lenz, Springer-Verlag Berlin Heidelberg, 63-84.

- Bosch, W., and Gruber, Th. (1991). Altimetry based geoid determination at the German Processing and Archiving Facility within the ERS-1 project, in: *Determination of the Geoid - Present and Future*, International Association of Geodesy Symposia, No. 106, Ed.: R. H. Rapp and F. Sans'o, Springer-Verlag, 75-85.
- Cheney, R. E., Douglas, B. C., Agreen, R. W., Porter, D. L., and Doyle, N. S. (1987). GEOSAT altimeter geophysical data record user handbook, *NOAA Technical Memorandum*, NOS NGS 46, 28 pp.
- Dick, S., and Soetje, K. Ch. (1990). Ein operationelles Ölausbreitungsmodell für die Deutsche Bucht, *Deutsche Hydrographische Zeitschrift*, Ergänzungsheft Reihe A, Nr. 16, 43 pp.
- Gill, A. E. (1982). *Atmosphere-Ocean Dynamics*, *International Geophysics Series*, Vol. 30, Academic Press., 662 pp.
- Glazman, R. E., Greysukh, A., and Zlotnicki, V. (1994). Evaluating models of sea state bias in satellite altimetry, *J. Geophys. Res.*, 99(C6), 12,581-12,591.
- IFREMER/CERSAT (1994). Altimeter products user manual, *C1-EX-MUT-A21-01-CN*, issue 2, revision 6, 40 pp.
- Kleine, E. (1994). Das operationelle Modell des BSH für Nordsee und Ostsee - Konzeption und Übersicht, (*unpublished manuscript*), Bundesamt für Seeschiffahrt und Hydrographie (BSH), Hamburg, November 1994, 126 pp.
- Marsh, J. G., Koblinsky C. J., Lerch, F. J., Klosko, S. M., and Robbins, J. W. (1988). A new gravitational model for the earth from satellite tracking data: GEM-T1, *J. Geophys. Res.*, 93(B6), 6169-6215.
- Marsh, J. G. et al. (1990). The GEM-T2 gravitational model, *J. Geophys. Res.*, 95(B13), 22,043-22,071.
- Metzner, M., Grafarend, E. W., and Dick, S. (1994). The suitability of ERS-1 radar-altimeter data for oceanographic and geodetic applications for the Baltic Sea, *Proceedings of the Second ERS-1 Symposium*, Hamburg, Germany, ESA SP-361, Vol. 1, 591-596.
- Mihardja, D. K. (1991). Energy and momentum budget of the tides in Indonesian waters, *Berichte aus dem Zentrum für Meeres- und Klimaforschung der Universität Hamburg*, No. 14, 183 pp.
- Müller-Navara, S., and Mittelstaedt, E. (1987). Schadstoffausbreitung und Schadstoffbelastung in der Nordsee - Eine Modellstudie, *Deutsche Hydrographische Zeitschrift*, Ergänzungsheft Reihe B, Nr. 18, 51 pp.
- Rapp, R. H. (1993). Geoid undulation accuracy, *IEEE Transactions on Geoscience and Remote Sensing*, Vol. 31, No. 2, 365-370.
- Rapp, R. H., Wang, Y. M., and Pavlis, N. K. (1991). The Ohio State 1991 geopotential and sea surface topography harmonic coefficient model, *The Ohio State University Report*, No. 410, Department of Geodetic Science and Surveying, 94 pp.

- Schwintzer, P.; Reigber, C.; Barth, W.; Massmann, F.-H., Raimondo, J. C., Gerste, M.; Bode, A.; Li, H.; Biancale, R.; Balmino, G.; Moynod, B.; Lemoine, J. M.; Marty, J. C.; Barlier, F., and Boudon, Y. (1992). GRIM4 - Globale Erdgeschwerefeldmodelle, *Zeitschrift für Vermessungswesen*, Nr. 117, 227-247.
- Soetje, K. C., and Brockmann, Ch. (1983). An operational numerical model of the North Sea and the German Bight, in: *North Sea Dynamics*, Ed.: J. Sündermann and W. Lenz, Springer-Verlag Berlin Heidelberg, 95-107.
- Stawarz, M. (1994). Bestimmung von Geoidkorrekturen der südostasiatischen Gewässer aus simulierten und altimetrischen Meeresoberflächenhöhen, *Diploma thesis*, Universität Hamburg, Fachbereich Geowissenschaften, 104 pp.
- Stawarz, M., and Metzner, M. (1994). Altimetric geoid of the Indonesian waters derived from ERS-1 radar altimeter data, to be published in the *Proceedings of the INSMAP'94*, 19-23 September 1994, Hannover, Germany, 12 pp.
- UNESCO (1981). Tenth report on the joint panel on oceanographic tables and standards, *Technical papers in marine science*, No. 36, 24 pp.
- Wieser, M. (1987). Das globale digitale Höhenmodell TUG87, *Interner Bericht des Instituts für Theoretische Geodäsie*, Abteilung für Mathematische und Datenverarbeitende Geodäsie der Technischen Universität Graz, Österreich, 4 pp.

# Rank deficiency of altimetry-gravimetry SST determination

R. Barzaghi, M.A. Brovelli, F. Sansó

DIIAR Politecnico di Milano - Italy

## 1 Introduction to the problem

In modelling the global gravity field of the earth an important step forward has been done by using altimetric observations. Yet the observational functional of altimetry as such is not a pure functional of the anomalous field  $T$  only but rather it involves other quantities like the stationary sea surface topography,  $t$ , and the (time dependent) radial orbital correction  $\xi$  which we consider as a parametric curve in time. Well known spectral analyses [2], [9] have shown that only few coefficients of the gravity field can give rise to a significant signal  $\xi$ , so  $\xi$  can be modelled empirically by a relatively small number of parameters, for instance by 8 parameters per arc as in [5].

On the other hand the time variation of the sea surface due to tides is assumed here to be known and eliminated from the data. Indeed this is sensible on large oceans only, since in closed seas like the Mediterranean, such models are not yet established with sufficient accuracy; on the other hand these seas are usually covered by gravimetric observations, exactly as the other land areas, so we will consider them as part of the lands.

So we can delineate the problem of finding a global model from altimetric/gravimetric data first of all in the following way; divided the planet surface into a land  $L$  and a sea part  $S$ , we assume that on  $L$  we know the gravity anomalies  $\Delta g$ , while on  $S$  we know  $N - t - \xi$ , ( $N$  being the geoid undulation and  $t$  the sea surface topography); so we can say that

$$\begin{cases} \Delta g|_L = G \\ T - \gamma t - \gamma \xi|_S = H \end{cases} \quad (1)$$

where  $\xi = \xi(\alpha, \text{time})$ <sup>1</sup>: here we collect in the vector  $\alpha$  all the parameters used to represent the radial orbital error. This shows indeed that there is a rank deficiency problem in the cross-over adjustment which has already been treated in literature. The purpose here is to find a harmonic  $T$  satisfying these relations as well as  $t$  and  $\xi$ . For the purpose of the present analysis we can assume that all our data have been reduced so that the surface of the earth is simply approximated by a sphere of radius equal to  $R$ , the mean radius of the earth.

It is obvious that as far as  $t$  is completely arbitrary, the second of (1) can always be

---

<sup>1</sup>Please remark that since  $\xi$  is also function of time the second of (1) is not yet a true boundary relation since at the same point but at different times  $\xi$  can attain different values as it happens in cross over adjustment.

manipulated to provide any  $H$ , even when  $\xi$  is put equal to zero. For this reason it was considered convenient to parametrize  $t$  by a small number of coefficients also taking into account that for physical reasons  $t$  has to be a smooth function. This shows that (1) must in any way be complemented by other information. This is usually taken to be a set of coefficients  $T_{\ell m}$  ( $|m| \leq \ell; 2 \leq \ell \leq N$ ) which is derived from satellite tracking data only, i.e. by an independent source of information; so to (1) we add

$$T_{\ell m} = \bar{T}_{\ell m} \quad |m| \leq \ell, \quad \ell \leq N \quad (2)$$

Naturally when we say that  $t$  is smooth we are purposely expressing a not very precise concept; we should better say that there might be a physically meaningful information in  $t$ , down to  $\sim 100$  km wavelength but unfortunately for the moment we don't have a number of coefficients  $T_{\ell m}$  (derived from satellite to only data) sufficient to close the gap between data and derived resolution of  $t$ .

Suggested by the above conditions, it has been considered convenient to parametrize  $t$  too as <sup>2</sup>

$$t = \sum_{\ell,m=0}^N t_{\ell m} Y_{\ell m}(\sigma) \quad (3)$$

So the problem now becomes to find  $T$  harmonic outside the earth's sphere and coefficients  $t_{\ell m}$  as well as parameters  $\underline{\alpha}$ , used to model  $\xi$ , so that (1) and (2) are satisfied. The first question is where do we get the information to determine  $\underline{\alpha}$ ?

As always in l.s. theory we can think of decreasing the number of observation equations by eliminating part of the parameters; this is exactly what is done in cross-over adjustment where the stationary part,  $T - \gamma t$ , is eliminated between two crossing arcs, thus remaining with a system in the pure unknowns  $\underline{\alpha}$ . As it is known this system, [1], [6], provides an estimate  $\hat{\alpha}$  by imposing some constraints, while contemporarily there is a "free surface"  $f(\sigma)$  which is not absolutely detected by the cross-overs themselves: then by using this we arrive at the equivalent formulation

$$T - \gamma t - \gamma f(\sigma) = H + \gamma \xi(\hat{\alpha}) + \gamma f(\sigma) ; \quad (4)$$

here the left hand side is what is eliminated in the cross-over equations and therefore remains undetermined. It should be noticed that now the right hand side of (4) does not anymore depend on time so that it can be rewritten in the form of a boundary relation, by introducing orbit corrected heights  $\bar{H} = H + \gamma \xi(\hat{\alpha})$ , as

$$T - \gamma t - \gamma f(\sigma) = \bar{H} . \quad (5)$$

<sup>2</sup>Pointing to the fact that  $\{Y_{\ell m}\}$  is a non orthogonal set on the ocean area only, other parametrizations, in particular with orthogonal families, have been proposed, as in [4]; however as we shall see at the end of the paper we believe that the main problem here is not the lack of orthogonality.

It is interesting to observe that  $\gamma t + \gamma f(\sigma) = s$  is a unique signal from which in general it is impossible to disentangle the two components unless we put constraints on  $t$  ( $f$  is already constrained to belong to a certain space of functions), or we use some a-priori spectral information.

Yet since we are not here so much interested in the trade off between free surface of the cross-over adjustment and sea surface topography, but rather in the unique identifiability of the global potential  $T$  together with the SST, we will consider from here on the signal

$$s = \gamma t + \gamma f(\sigma)$$

as a function to be determined from the relations

$$\begin{cases} \Delta g|_L = G \\ T - s|_S = \bar{H} \end{cases} \quad (6)$$

together with

$$T_{\ell m} = \bar{T}_{\ell m}, \quad (\ell \leq N). \quad (7)$$

In particular we want to know whether the problem (6), (7) has rank deficiency, i.e. whether there is a function  $T \neq 0$  harmonic in space and an  $s \neq 0$  such that

$$\begin{cases} \Delta g(T)|_L = -\frac{\partial T}{\partial r} - \frac{2}{r}T|_L = 0 \\ T - s|_S = 0 \end{cases}$$

$$T_{\ell m} = 0 \quad (\ell \leq N). \quad (8)$$

We will prove in this paper that this problem has no rank deficiency if  $s$  is constrained to belong to the subspace of the harmonics up to degree  $N$ , but it has indeed rank deficiency if we give to  $s$  more freedom.

A discussion on the meaning of this result and some advices on the parametrization of the SST are given in the last paragraph.

## 2 A full rank theorem for the constrained SST problem

We want to prove that the problem (8) together with the constraint

$$s = \sum_{\ell,m=0}^N s_{\ell m} Y_{\ell m} \quad (9)$$

has the unique solution

$$T \equiv 0 , \quad s \equiv 0 \quad (s_{\ell m} = 0) \quad (10)$$

To be more precise we shall prove the following:

**Theorem 2.1:** the problem (8) with  $s$  constrained by (9) has only the trivial solution  $T \equiv 0, s \equiv 0$  assuming that  $T$  is so regular that  $T \in H^{\frac{1}{2}}(\sigma)$ <sup>3</sup>.

Under this hypothesis in fact  $\Delta g \in H^{\frac{1}{2}}(\sigma)$  and the following quadratic form can be meaningfully computed

$$\frac{1}{4\pi} \int_{\sigma} \Delta g T d\sigma = \sum_{\ell=0}^{+\infty} \frac{(\ell-1)}{R} T_{\ell m}^2 ; \quad (12)$$

noting that  $T_{\ell m} = 0$  for  $\ell \leq N$  by (8) and that  $\Delta g|_L = 0$ , and  $T|_S = s$ , we can write

$$\begin{aligned} \sum_{\ell=N+1}^{+\infty} \frac{\ell-1}{R} T_{\ell m}^2 &= \frac{1}{4\pi} \int_S \Delta g T d\sigma = \frac{1}{4\pi} \int_S \Delta g s d\sigma = \\ &= \sum_{\ell,m=0}^N s_{\ell m} \frac{1}{4\pi} \int_S \Delta g Y_{\ell m} d\sigma . \end{aligned} \quad (13)$$

On the other hand, for  $\ell \leq N$ ,

$$\frac{1}{4\pi} \int_S \Delta g Y_{\ell m} d\sigma = \frac{1}{4\pi} \int_{\sigma} \Delta g Y_{\ell m} d\sigma = \frac{(\ell-1)}{R} T_{\ell m} = 0$$

so that (13) writes

$$\sum_{\ell=N+1}^{+\infty} \frac{\ell-1}{R} T_{\ell m}^2 = \sum_{\ell,m=0}^N s_{\ell m} \frac{\ell-1}{R} T_{\ell m} = 0 \quad (14)$$

which implies  $T_{\ell m} = 0$  also for  $\ell \geq N + 1$ , i.e.

$$T \equiv 0 . \quad (15)$$

<sup>3</sup>This basically means that the following norm of  $T$  is finite (cfr. [8]):

$$\frac{1}{4\pi} \int T \left( -\frac{\partial}{\partial r} T \right) d\sigma = \sum (l+1)^2 T_{lm}^2 \leq \infty \quad (11)$$

But then

$$s = \sum_{\ell,m}^N s_{\ell,m} Y_{\ell m}(\sigma) \equiv 0 \quad \sigma \in S$$

and since  $\{Y_{\ell m}, \ell \leq N\}$  is a set of linear independent functions on any set of the sphere  $\sigma$ , with positive area, we see that

$$s_{\ell m} = 0 \quad , \quad \ell \leq N \quad (16)$$

too.

In other words the problem (8) with the constraint (9) admits only one solution  $(T, s)$  if we assume that  $T \in H^{\frac{1}{2}}(\sigma)$ .

### 3 The rank deficiency of the unconstrained SST problem

We want to prove that if we don't constrain the SST to any subspace, the problem (8) has a general solution parametrized by an arbitrary function  $\tilde{s}$  orthogonal in  $L^2(S)$  to  $Y_{\ell m}$  ( $\ell \leq N$ ); for any such  $\tilde{s}$  there exist suitable corresponding  $\hat{T}(\tilde{s})$  and  $\hat{s}(\tilde{s})$  which are solutions of (8) and viceversa any solution of (8) has this form.

Before proceeding in our proof we need to recall a theorem on the solution of the altimetry/gravimetry problem for the sphere (cf. [Sansó]);

**Theorem 3.1:** given any  $w \in H^{\frac{1}{2}}(\sigma)$  and  $G \in H^{\frac{1}{2}}(\sigma)$  there exists one and only one  $T \in H^{\frac{1}{2}}(\sigma)$  and a constant  $a$  such that

$$\begin{cases} T|_S = w|_S + a \\ \Delta g(T)|_L = G|_L \end{cases} \quad T_{00} = \frac{1}{4\pi} \int T d\sigma = 0 \quad (17)$$

According to this theorem the following function  $\tilde{T}$  is well defined; let us take any  $\tilde{s} \in H^{\frac{1}{2}}(S)$ , defined as the restriction to  $S$  of functions of  $H^{\frac{1}{2}}(\sigma)$ , then we define  $\tilde{T}, \tilde{a}$  as the solution of

$$\begin{cases} \tilde{T}|_S = \tilde{s} + \tilde{a} \\ \Delta g(\tilde{T})|_L = 0 \end{cases}$$

$$\tilde{T}_{00} = 0 \quad . \quad (18)$$

In particular in what follows we will consider  $\tilde{s}$  ranging on the orthogonal complement in  $L^2(S)$  to  $\text{Span } \{Y_{\ell m}, \ell \leq N\}$ , i.e.  $\tilde{s}$  such that

$$\int_S \tilde{s} Y_{\ell m} d\sigma \equiv 0 \quad , \quad \ell \leq N \quad . \quad (19)$$

Corresponding to any such  $\tilde{s}$  we have suitable  $\tilde{T}, \tilde{a}$  satisfying (18).

Now we are ready to prove the following:

**Theorem 3.2:**

- 1) for any  $\tilde{s} \in H^{\frac{1}{2}}(S)$  satisfying (19) there is a  $\hat{T} = \tilde{T} + \delta T$  and a  $\hat{s} = \tilde{s} + \delta s$ , with  $\delta T, \delta s$  linearly and continuously dependent on  $\tilde{s}$ ,  $\delta s = \sum_{\ell, m=0}^N \delta s_{\ell m} Y_{\ell m}$ , such that  $(\hat{T}, \hat{s})$  is a solution of (8);
- 2) any solution  $(T, s)$  can be written in the form  $\hat{T}, \hat{s}$ , with  $\tilde{s}$  the projection of  $s$  onto the  $L^2$ -orthogonal complement of  $\text{Span } \{Y_{\ell m}, \ell \leq N\}$ .

- If  $\hat{T}, \hat{s}$  has to satisfy (8) one must have, for given  $\tilde{s}$ ,

$$\begin{cases} \hat{T}|_S + \delta T|_S = \tilde{s} + \delta s \\ \Delta g(\tilde{T})|_L + \Delta g(\delta T)|_L = 0 \\ \tilde{T}_{\ell m} + \delta T_{\ell m} = 0 \quad , \quad \ell \leq N \end{cases} \quad (20)$$

which, in the light of (18), implies

$$\begin{cases} \delta T|_S = \delta s - \tilde{a} = (\delta s_{00} - \tilde{a}) + \sum_{\ell, m=1}^N \delta s_{\ell m} Y_{\ell m} \\ \Delta g(\delta T)|_L = 0 \\ \delta T_{\ell m} = -\tilde{T}_{\ell m} \quad , \quad \ell \leq N \end{cases} \quad (21)$$

with

$$\tilde{T}_{\ell m} = \frac{1}{4\pi} \int \tilde{T} Y_{\ell m} d\sigma$$

given because  $\tilde{T}$  is fixed when  $\tilde{s}$  is given.

Let us note that some of the  $\tilde{T}_{\ell m}$  could be zero, as it is certainly  $\tilde{T}_{00}$  because of (18), but some may not; so in general the solution of (21) is not zero. The problem here is to show that whatever are the given  $\tilde{T}_{\ell m}$  we can find the corresponding

$$\delta \tilde{s}_{\ell m} = \begin{cases} \delta s_{00} - \tilde{a} \\ \delta s_{\ell m} \end{cases} \quad (1 \leq \ell \leq N)$$

This however is simple, because if we consider the inverse problem, namely to determine  $\delta T_{\ell,m}$ , given  $\delta \tilde{s}_{\ell,m}$ , in such a way that

$$\begin{cases} \delta T |_S = \sum_{\ell,m=0}^N \delta \tilde{s}_{\ell m} Y_{\ell m} \\ \Delta g(\delta T) |_L = 0 \end{cases}, \quad (22)$$

$$\delta T_{\ell m} = \frac{1}{4\pi} \int \delta T Y_{\ell m} d\sigma , \quad (23)$$

we see that this problem has always a solution and the  $\delta T_{\ell m}$  so determined will be linear homogeneous functions of  $\delta \tilde{s}_{\ell m}$ , i.e.

$$\delta T_{\ell m} = \sum_{jk} A_{\ell m}^{jk} \delta \tilde{s}_{jk} . \quad (24)$$

Now the linear transformation  $A$  goes from  $R^{(N+1)^2}$  into  $R^{(N+1)^2}$  and we have just proved, by **Theorem 2.1**, that if  $A(\delta \tilde{s}) = (\delta T) = 0$  then  $(\delta \tilde{s}_{\ell m}) = 0$ , which shows that  $A$  is also onto, as it was to be proved.

So (21) has always a solution  $\delta T, \delta \tilde{s}$  and correspondingly

$$\hat{T} = \tilde{T} + \delta T , \quad \hat{s} = \tilde{s} + \delta s = \tilde{s} + \delta \tilde{s} + \tilde{a} \quad (25)$$

is a solution of (8).

- Let  $(T, s)$  be a solution of (8) with  $T, s \in H^{\frac{1}{2}}(\sigma)$ . Then the projection of  $s$  onto the  $L^2(S)$ -orthogonal complement of  $\text{Span}\{Y_{\ell m}, \ell \leq N\}$  is uniquely defined and we call it  $\tilde{s}$ ; accordingly we have

$$s = \tilde{s} + s_0$$

with  $s_0 \in \text{Span}\{Y_{\ell m}, \ell \leq N\}$ . Now let us call  $(\hat{T}, \hat{s})$  the solution of (8) constructed from  $\tilde{s}$  according to the part 1 of this theorem; we have

$$\begin{cases} (T - \hat{T}) |_S = s - \hat{s} = s_0 - \delta s \\ \Delta g(T - \hat{T}) = 0 \end{cases}$$

$$(T_{\ell m} - \hat{T}_{\ell m}) = 0 \quad , \quad \ell \leq N \quad ; \quad (26)$$

since

$$s_0 - \delta s = \sum_{\ell=0}^N a_{\ell m} Y_{\ell m}$$

for some  $a_{\ell m}$ , (26) falls under the hypotheses of **Theorem 2.1**, showing that

$$T - \hat{T} \equiv 0 \quad \text{and} \quad s_0 = \delta s \equiv 0 \quad (27)$$

which implies also

$$s = \tilde{s} + s_0 = \tilde{s} + \delta s = \hat{s} \quad , \quad (28)$$

as it was to be proved.

Relations (27), (28) show that the whole null space of (8) is swept by constructing all the solutions of type 1. of Theorem 3.2.

The rank deficiency problem in the unconstrained case is thus completely solved; we will discuss its meaning in the next paragraph.

## 4 A counterexample; discussion

Looking at Theorem 2.1 and Theorem 3.2 one immediately tends to say that naturally in our problem the coefficients  $T_{\ell m} (\ell \leq N)$  derived from an independent source have been introduced exactly to be able to determine with some "resolution" the SST, and this indeed happens with a perfect balance between the number of  $T_{\ell m}$  and the number of coefficients  $s_{\ell m}$  which are determinable; the conclusion seems to be only that the situation is clear and to improve the knowledge of the SST we must only improve our "independent" knowledge of the gravity field provided by the coefficients  $\bar{T}_{\ell m}$ . This point of view is certainly true in general and having more independent information on the gravity field is one of the main targets of the geodetic community nowadays. Yet even considering the information actually available we can at least make some warning and may be improve the actual results.

In fact it is at least important to understand that the way in which spherical harmonics "resolve" a function on the sphere is very peculiar. In particular one should not think that a function orthogonal to  $\text{Span } \{Y_{\ell m}, \ell \leq N\}$  has to display only features with length shorter than  $\frac{\pi}{N}$  (in radius); here you can find a counterexample. Indeed what we will show is perfectly known to anybody working with spherical harmonics and it can be even guessed from a simple drawing of their behaviour on the sphere; so what we provide here is the translation of this intuition in rigorous terms, adapted to the present problem.

**Example 4.1** Assume the ocean part of the sphere,  $S$ , to include a spherical belt on the equator with

$$B \left\{ \begin{array}{l} -\Delta \leq \lambda \leq \Delta \\ -\alpha \leq \phi \leq \alpha \end{array} \right.$$

then there is a function in  $H^{\frac{1}{2}}(S)$  which is different from zero in all of  $B$  and is orthogonal to  $Y_{\ell m}, \ell \leq N$  for any fixed  $N$ .

Let us define smooth functions  $C_\delta(\lambda), C_\alpha(\phi)$  as in Fig. 4.1 with conveniently small values for the parameter  $\epsilon$ ; and let us put

$$\begin{aligned} \tilde{s} &= C_\Delta(\lambda)C_\alpha(\phi)h(\phi) & (\phi, \lambda) \in B \\ \tilde{s} &= 0 & \text{on the rest of } S \end{aligned} \tag{29}$$

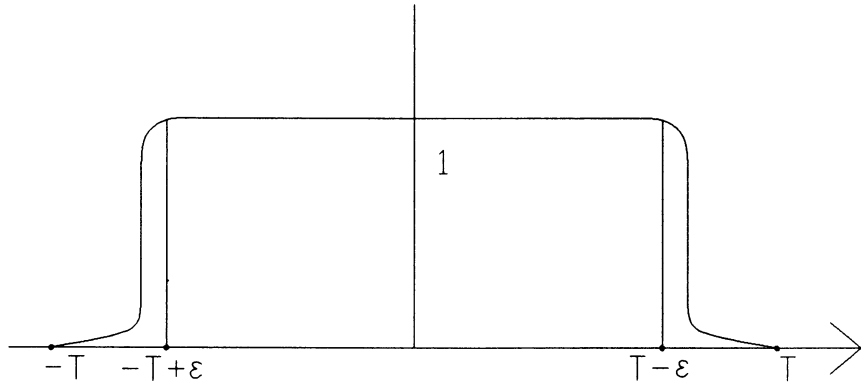


Fig. 4.1 The smoother  $C_T(t)$

Since  $C_\Delta C_\alpha$  are smooth functions,  $s \in H^{\frac{1}{2}}(\sigma)$  (and is even more regular) if  $h \in H^{\frac{1}{2}}(\sigma)$  or is more regular than that.

Now consider the function of  $\phi$  only  $\bar{P}_{N+1,0}$  and the manifold  $H_0 = \text{Span} \{C_\alpha(\phi)\bar{P}_{\ell,m}(\phi), \ell \leq N\}$  in the space of  $L^2$  functions of  $\varphi$ , with weight  $\cos \phi$ . We have  $\bar{P}_{N+1,0} \notin H_0$ ; in fact  $\bar{P}_{N+1,0}$  is a trigonometric polynomial of maximum degree  $N + 1$  and such a polynomial is linearly independent on any interval (e.g. on  $[-\alpha + \epsilon, \alpha - \epsilon]$  where  $C_\alpha = 1$ ) from polynomials of lower degrees. Then, defined the orthogonal projector  $\Pi$  on the complement of  $H_0$ , there is a non-zero function

$$h = \Pi \bar{P}_{N+1,0} \quad (30)$$

which we claim that can be used in (29). In fact note that by definition of  $\Pi$ , for  $j \leq N$

$$\langle h, C_\alpha \bar{P}_{jk} \rangle_{\cos \phi} = \int_{-\alpha}^{\alpha} h C_\alpha(\phi) \bar{P}_{jk}(\phi) \cos \phi d\phi = 0 \quad (31)$$

which implies indeed that

$$\begin{aligned} \langle C_\Delta(\lambda) C_\alpha(\lambda) h, Y_{ik} \rangle &= \int_S C_\Delta(\lambda) C_\alpha(\lambda) h Y_{ik}(\phi, \lambda) \cos \phi d\phi d\lambda = \\ &= \int_{-\Delta}^{\Delta} d\lambda C_\Delta(\lambda) \left\{ \begin{array}{l} \cos k\lambda \\ \sin k\lambda \end{array} \right\} \cdot \int_{-\alpha}^{\alpha} d\phi \cos \phi C_\alpha(\phi) h \bar{P}_{jk}(\phi) = 0 \quad \forall j, k \leq N \end{aligned} \quad (32)$$

So that  $\tilde{s}$ , given by (29), is a function of the type we were looking for.

Let us observe that corresponding to this  $\tilde{s}$  there are a  $\hat{T}$  and a  $\delta s(\tilde{s})$  such that  $\hat{T}, \hat{S} + \delta s$  are solution of our homogeneous problem, i.e. are not detectable by altimetry and the knowledge of the coefficients  $\{T_{\ell m}, \ell \leq N\}$  only.

In particular  $\delta s$  must have to be of the form  $\sum_{\ell, m=0}^N \delta s_{\ell m} Y_{\ell m}$  and it is also orthogonal to  $\tilde{s}$  in  $L^2(S)$ , what implies that (remember that  $\tilde{s}$  is zero outside  $B$ )

$$\int_B \tilde{s} \delta s dS = 0 ; \quad (33)$$

consequently, although we don't know the precise shape of  $\delta s$ , we can say that it is not such as to "kill"  $\tilde{s}$  on  $B$  because, in view of (33),

$$\int_B s^2 dS = \int_B \tilde{s}^2 dS + \int_B \delta s^2 dS$$

showing that the power of  $s$  in  $B$  is even higher than that of  $\tilde{s}$  in the same area.

What this counterexample shows in particular is that there are functions with elongated features which are orthogonal to the basis of spherical harmonics up to some degree  $N$  and corresponding to which we find non-zero solutions of the posed problem; since these functions resemble very much oceanic currents, we must be concerned about this phenomenon. In fact what is shown here is that an oceanic feature displaying high frequency variations in a transversal direction, but being constant along another direction can very well affect

lower degree coefficients through  $\delta s, \hat{T}$ ; in this sense this is an aliasing phenomenon, namely a power transfer from high to low frequencies due to a mismodelling.

As we can see this effect is not so much related to the non-orthogonality of  $Y_{\ell m}$  in  $L^2(S)$ , which is rather causing a loss of stability when  $N$  increases (cfr. [8], [4]); on the contrary what plays a role here is the peculiar shape of  $Y_{\ell m}$  which can have a strong variability in  $\phi$  but not in  $\lambda$  or viceversa; our conclusion would be that it might be worthwhile to try to model the SST by regionalized functions, like harmonic splines or wavelets, although a firm base to do so, would be to prove for such functions a theorem similar to Theorem 2.1, which doesn't appear to be a simple task.

## References

- [1] R. Barzaghi, M. Brovelli, F. Sansó *Altimetry Rank Deficiency in Crossover Adjustment. Determination of the Geoid, Present and Future*, IAG Symposium n.106, Springer-Verlag, 1991.
- [2] T. Engelin *Radial orbit error reduction and sea surface topography determination using satellite altimetry*. O.S.U. Report n. 377, Columbus 1987.
- [3] C. Hwang *Spectral analysis using orthonormal functions with a case study on the Sea surface topography*. Geophysical Journal International n. 115, 1993.
- [4] R.H.Rapp, Wang Y.M. *Geoid Undulation Differences between Geopotential Models*. Surveys in Geophysics, Vol. 14, Nos 4-5, 1993.
- [5] R.H. Rapp *Altimeter data in estimating global gravity models*. In Satellite Altimetry in Geodesy and Oceanography. Lecture Notes in Earth Sciences n. 50, Springer-Verlag, 1993.
- [6] R. Rummel *Principle of Satellite Altimetry and elimination of radial orbit errors*. In Satellite Altimetry in Geodesy and Oceanography. Lecture Notes in Earth Sciences n. 50, Springer-Verlag, 1993.
- [7] F. Sacerdote, F. Sansó *Further remarks on the altimetry-gravimetry problems*. Bull. Geod., n. 1, 1987.
- [8] F. Sansó *Theory of geodetic B.V.P. applied to the analysis of altimetric data*. In Satellite Altimetry in Geodesy and Oceanography. Lecture Notes in Earth Sciences n. 50, Springer-Verlag, 1993.
- [9] C.A. Wagner *Radial variations of satellite orbit due to geopotential errors; implications for satellite altimetry*. Journal Geophysical Research, 90, 1985.
- [10] C. Wunsch *Physics of the ocean circulation*. In Satellite Altimetry in Geodesy and Oceanography. Lecture Notes in Earth Sciences n. 50, Springer-Verlag, 1993.

## LIST OF PARTICIPANTS

**Abd-Elmotaal Hussein**, Civil Engineering Department, Faculty of Engineering, Minia University, Minia, Egypt (ph. +20-86-322083, fax +20-2-2918059 or +20-86-326243)

**Albertella Alberta**, Dipartimento di Ingegneria Idraulica, Ambientale e del Rilevamento, Politecnico di Milano, Piazza Leonardo da Vinci 32, I-20133 Milano, Italy (ph. +39-2-2399.6504, fax +39-2-2399.6530)

**Ballani Ludwig**, Geoforschungs Zentrum, Telegrafenberg A17, D-14473 Potsdam, Germany (ph. +49-331-288-1142, fax +49-331-288-1111, e-mail BAL@GFZ-POTSDAM.DE)

**Barriot Jean-Pierre**, Dept. Geodesie Terrestre et Planetaire, GRGS/CNES, 18 Avenue E. Belin, F-31055 Toulouse Cedex, France (ph. +33-61332894, fax +33-61253098, e-mail barriot@mfp.cnes.fr)

**Barthelmes Franz**, Geoforschungs Zentrum, Telegrafenberg A17, D-14473 Potsdam, Germany (ph. +49-331-288-1143, fax +49-331-288-1111)

**Barzaghi Riccardo**, Dipartimento di Ingegneria Idraulica, Ambientale e del Rilevamento, Politecnico di Milano, Piazza Leonardo da Vinci 32, I-20133 Milano, Italy (ph. +39-2-2399.6528, fax +39-2-2399.6530)

**Battha Laszlo**, Geodetic & Geophysical Research Institute of the Hungarian Academy of Sciences, Csatkai U. 6-8, H-9401 Sopron, Hungary (ph. +36-99-314290, fax +36-99-313267, e-mail h625bat@ella.hu)

**Bayerlein Wolfgang**, Geodaetisches Institut, Universitaet Stuttgart, Keplerstrasse 11, D-70174 Stuttgart, Germany (fax +49-711-1213297)

**Benciolini Battista**, Dipartimento di Ingegneria Civile e Ambientale, Universita' di Trento, Mesiano di Povo 77, I-38050 Trento, Italy (ph. +39-461-882632 or 881919, fax +39-461-882672)

**Betti Barbara**, Dipartimento di Georisorse e Territorio, Politecnico di Torino, Corso Duca degli Abruzzi 24, I-10129 Torino, Italy (ph. +39-11-5647770, fax +39-11-5647699)

**Borre Kai**, Varstvej 314, DK-9260 Gistrup, Denmark (fax +45-98333216, e-mail borre@i4.auc.dk)

**Capdevila Subirana Joan**, Servicio Regional de Catalunya, Instituto Geografico Nacional, Av. Portal de l'Angel 42-5 A, SP-08071 Barcelona, Spain (ph. +34-3-3027974, fax +34-3-3027974)

**Carpino Mario**, Osservatorio Astronomico di Brera, Via Brera 28, I-20121 Milano, Italy (ph. +39-2-874444, fax +39-2-72001600, e-mail carpino@bach.mi.astro.it)

**Crespi Mattia**, Dipartimento di Idraulica, Trasporti e Strade (Area Topografia), Facolta' di Ingegneria, Universita' di Roma, Via Eudossiana 18, I-00184 Roma, Italy (ph. +39-6-44585105, fax +39-6-4817245)

**Dambeck Johann**, Geodaetisches Institut, Universitaet Stuttgart, Keplerstrasse 11, D-70174 Stuttgart, Germany (fax +49-711-1213297)

**De Santis Angelo**, Istituto Nazionale di Geofisica, Via di Vigna Murata 605, I-00143 Roma, Italy (ph. +39-6-51860327, fax +39-6-5041181)

**Drozyner Andrzej**, Institute of Astronomy, Nicolaus Copernicus University, Chopina 12/18, PL-87-100 Torun, Poland (ph. +48-56-26017, fax +48-56-24602, e-mail drozyner@astri.torun.edu.pl)

**Engels Johannes**, Geodaetisches Institut, Universitaet Stuttgart, Keplerstrasse 11, D-70174 Stuttgart, Germany (fax +49-711-1213297)

**Feistritzer Martin**, Geodaetisches Institut, Universitaet Stuttgart, Keplerstrasse 11, D-70174 Stuttgart, Germany (fax +49-711-1213297)

**Fiani Margherita**, Dipartimento di Idraulica, Trasporti e Strade (Area Topografia), Facolta' di Ingegneria, Universita' di Roma, Via Eudossiana 18, I-00184 Roma, Italy (fax +39-6-4817245)

**Freeden Willi**, University of Kaiserslautern, Laboratory of Technomathematics, Geomathematics Group, Kurt-Schumacher-Str. 26, P.O.Box 3049, D-67653 Kaiserslautern, Germany (ph. +49-631-2052852, fax +49-631-29081, e-mail freeden@mathematik.uni-kl.de)

**Grafarend Erik W.**, Geodaetisches Institut, Universitaet Stuttgart, Keplerstrasse 11, D-70174 Stuttgart, Germany (fax +49-711-1213297)

**Heck Bernhard**, Geodetic Institute, University of Karlsruhe, Englerstrasse 7, D-76128 Karlsruhe, Germany (ph. +49-721-608 3674, fax +49-721-694552, telex 721 166 = UNIKar)

**Heidenreich A.**, Geodaetisches Institut, Universitaet Stuttgart, Keplerstrasse 11, D-70174 Stuttgart, Germany (fax +49-711-1213297)

**Hirsch Milo**, Geodaetisches Institut, Universitaet Stuttgart, Keplerstrasse 11, D-70174 Stuttgart, Germany (ph. +49-711-6856601, fax +49-711-1213297)

**Holota Petr**, Research Institute of Geodesy, Topography and Cartography, 250 66 Zdiby 98, Praha-Vychod, Czech Republic (ph. +42-2-6857907, fax +42-2-6857056, telex 121 726 VDS C, e-mail vugtk@csearn.bitnet or vugtk@earn.cvut.cz)

**Keller Wolfgang**, Geodaetisches Institut, Universitaet Stuttgart, Keplerstrasse 11, D-70174 Stuttgart, Germany (ph. +49-711-1213459, fax +49-711-1213297, e-mail wolke@gi5.bauingenieure.uni.stuttgart.de)

**Klees Roland**, Delft University of Technology, Faculty of Geodetic Engineering, Thijsseweg 11, NL-2629 Ja Delft, The Netherlands (ph. +31-15-785100, fax 0031-15-782348)

**Koop Radboud**, Delft University of Technology, Faculty of Geodetic Engineering, Thijsseweg 11, NL-2629 Ja Delft, The Netherlands (ph. +31-15-784543, fax 0031-15-783711, e-mail koop@tudgvl.tudelft.nl)

**Krarup Torben**, Carinlundsvej 23, DK-8700 Horsens, Denmark (ph. +45-75 622928)

**Krumb Friedhelm**, Geodaetisches Institut, Universitaet Stuttgart, Keplerstrasse 11, D-70174 Stuttgart, Germany (fax +49-711-1213297)

**Kutterer Hansjorg**, Geodetic Institute, University of Karlsruhe, Englerstrasse 7, D-76128 Karlsruhe, Germany (ph. +49-721-6083668, fax +49-721-694552, telex 721 166 = UNIKar, e-mail kutterer@giws4.bau-verm.uni-karlsruhe.de)

**Marana Barbara**, Dipartimento di Ingegneria Idraulica, Ambientale e del Rilevamento, Politecnico di Milano, Piazza Leonardo da Vinci 32, I-20133 Milano, Italy (ph. +39-2-2399.6505, fax +39-2-2399.6530)

**Metzner Margitta**, Zentrum fuer Meeres und Klimaforschung, Institut fuer Meereskunde der Universitaet Hamburg, Tropowitzstr. 7, D-22529 Hamburg, Germany (ph. +49-40-4123.2605, fax +49-40-4123.4644)

**Migliaccio Federica**, Dipartimento di Ingegneria Idraulica, Ambientale e del Rilevamento, Politecnico di Milano, Piazza Leonardo da Vinci 32, I-20133 Milano, Italy (ph. +39-2-2399.6507, fax +39-2-2399.6530)

**Milani Andrea**, Dipartimento di Matematica, Universita' di Pisa, Via Buonarroti 2, I-56127 Pisa, Italy (ph. +39-50-599554, fax +39-50-599524, e-mail milani@dm.unipi.it)

**Morujao Daniela**, Apartado 3104, P-3000 Coimbra, Portugal (ph. +351-39-401098, fax +351-39-32568, e-mail daniela@matuc2.mat.uc.pt)

**Mueller Ivan I.**, The Ohio State University, Department of Geodetic Sciences, 1958 Neil Avenue, Columbus, Ohio 43210, U.S.A. (fax +1-614-2922957, e-mail mueller@mps.ohio-state.edu)

**Novak Pavel**, Geodetic Observatory Pecny, CZ-251 65 Ondrejov 244, Czech Republic (ph. +42-204-85235/6, fax +42-2-6857056, e-mail vugtk@csearn.bitnet or vugtk@earn.cvut.cz)

**Okeke Francis**, Geodaetisches Institut, Universitaet Stuttgart, Keplerstrasse 11, D-70174 Stuttgart, Germany (fax +49-711-1213297)

**Otero Jesus**, Instituto de Astronomia y Geodesia, Facultad de Ciencias Matematicas, Ciudad Universitaria, SP-28040 Madrid, Spain (ph. +34-1-3944591, fax +34-1-3944607)

**Pachelski Wojciech**, Space Research Centre, Polish Academy of Sciences, Bartycka 18a, PL-00716 Warsaw, Poland (ph. +48-22-403766, fax +48-39-121273)

**Petrovskaya Margarita**, Institute of Theoretical Astronomy of Russian Academy of Sciences, 10 Naberezhnaya Kutuzova, St. Petersburg, 191187, Russia (ph. +7-812-2754414, fax +7-812-2727968, telex 121578 ita su, e-mail petrovsk@iipah.spb.su)

**Pillirone Giuseppe**, Istituto di Urbanistica e Pianificazione, Universita' di Udine, Via Larga 42, I-33100 Udine, Italy

**Prati Claudio**, Dipartimento di Elettronica e Informazione, Politecnico di Milano, Piazza Leonardo da Vinci 32, I-20133 Milano, Italy (ph. +39-2-2399.3585, fax +39-2-2399.3413)

**Richter Burghard**, Deutsches Geodaetisches Forschungsinstitut, Abt. I, Marstallplatz 8, D-80539 Muenchen, Germany (ph. +49-89-23031214, fax +49-89-23031240, telex 5 213 550 dgfi d, e-mail MAILER@DGFI.BADW-MUENCHEN.DE)

**Riguzzi Federica**, Istituto Nazionale di Geofisica, Via di Vigna Murata 605, I-00143 Roma, Italy (ph. +39-6-51860266, fax +39-6-5041181, telex 610502 GEOROM, e-mail riguzzi@in8800.cineca.it)

**Rodriguez Velasco Gema**, Instituto de Astronomia y Geodesia, Facultad de Ciencias Matematicas, Ciudad Universitaria, SP-28040 Madrid, Spain (ph. +34-1-3944582, fax +34-1-3944607)

**Roesch Konrad**, Geodaetisches Institut, Universitaet Stuttgart, Keplerstrasse 11, D-70174 Stuttgart, Germany (fax +49-711-1213297)

**Rozanov Youri**, Steklov Mathematical Institute, Vavilova Str. 42, 117333 Moscow, Russia (ph. +7-095-1352291, fax +7-095-1350555, e-mail rozanov@prob.mian.su)

**Sacerdote Fausto**, Dipartimento di Ingegneria Idraulica, Ambientale e del Rilevamento, Politecnico di Milano, Piazza Leonardo da Vinci 32, I-20133 Milano, Italy (ph. +39-2-2399.6509, fax +39-2-2399.6530)

**Salemi Giuseppe**, Dipartimento di Georisorse e Territorio, Universita' degli Studi di Udine, Via Cotonificio 114, I-33100 Udine, Italy (ph. +39-432-558732, fax +39-432-558700)

**Sanso' Fernando**, Dipartimento di Ingegneria Idraulica, Ambientale e del Rilevamento, Politecnico di Milano, Piazza Leonardo da Vinci 32, I-20133 Milano, Italy (ph. +39-2-2399.6504 fax +39-2-2399.6530)

**Schaffrin Burkhard**, Department of Geodetic Science & Surveying, The Ohio State University, 1958 Neil Avenue, Columbus, Ohio 43210-1247, U.S.A. (ph. +1-614-2920502, fax +1-614-2922957)

**Scheinert Mirko**, Geodaetisches Institut, Universitaet Stuttgart, Keplerstrasse 11, D-70174 Stuttgart, Germany (ph. +49-711-6856601, fax +49-711-1213297)

**Schreiner Michael**, University of Kaiserslautern, Laboratory of Technomathematics, Geomathematics Group, Kurt-Schumacher-Str. 26, P.O.Box 3049, D-67653 Kaiserslautern, Germany (ph. +49-631-2053244, fax +49-631-29081, e-mail schreiner@mathematik.uni-kl.de)

**Schwarz Klaus-Peter**, The University of Calgary, Faculty of Engineering, Department of Geomatics Engineering, 2500 University Drive N.W., Calgary, Alberta, T2N 1N4, Canada (ph. +1-403-2205834, fax +1-403-2841980)

**Schwarze Volker S.**, Geodaetisches Institut, Universitaet Stuttgart, Keplerstrasse 11, D-70174 Stuttgart, Germany (ph. +49-711-1213393, fax +49-711-1213297)

**Sevilla de Lerma Miguel J.**, Instituto de Astronomia y Geodesia, Facultad de Ciencias Matematicas, Ciudad Universitaria, SP-28040 Madrid, Spain (ph. +34-1-3944582, fax +34-1-3944607, e-mail maast01@sis.ucm.es)

**Sguerso Domenico**, Dipartimento di Ingegneria Civile e Ambientale, Universita' di Trento, Mesiano di Povo 77, I-38050 Trento, Italy (ph. +39-461-882608 or 881919, fax +39-461-882672)

**Stein Alfred**, Wageningen Agricultural University, P.O.Box 37, NL-6700 AA Wageningen, The Netherlands (ph. +31-8370-82420, fax +31-8370-82419)

**Suenkel Hans**, Department of Mathematical Geodesy and Geoinformatics, Graz University of Technology, Steyrergasse 30, A-8010 Graz, Austria (ph. +43-316-8736346, fax 0043-316-813247, telex 311221 tugrz a)

**Syffus Rainer**, Geodaetisches Institut, Universitaet Stuttgart, Keplerstrasse 11, D-70174 Stuttgart, Germany (fax +49-711-1213297)

**Teunissen Peter J.G.**, Delft University of Technology, Delft Geodetic Computing Centre (LCR), Thijsseweg 11, NL-2629 JA Delft, The Netherlands (ph. +31-15-782558, fax +31-15-783711, telex 38151 butud nl, e-mail lgr@tudguz.tudelft.nl)

**Theiss Dietmar**, Geodaetisches Institut, Universitaet Stuttgart, Keplerstrasse 11, D-70174 Stuttgart, Germany (fax +49-711-1213297)

**Tscherning Carl Christian**, University of Copenhagen, Geophysical Department, Haraldsgade 6, DK-2200 Copenhagen N, Denmark (ph. +45-35320582, fax +45-35822565, e-mail cct@osiris.gfy.xxx.dk)

**Unguendoli Marco**, Istituto di Topografia, Geodesia e Geofisica Mineraria, Facolta' di Ingegneria, Universita' di Bologna, Viale Risorgimento 2, I-40136 Bologna, Italy (ph. +39-51-6443107, fax +39-51-6448073)

**Usai Stefania**, Istituto di Topografia, Geodesia e Geofisica Mineraria, Facolta' di Ingegneria, Universita' di Bologna, Viale Risorgimento 2, I-40136 Bologna, Italy (fax +39-51-6448073)

**Van Gelderen Martin**, Delft University of Technology, Faculty of Geodetic Engineering, Thijsseweg 11, NL-2629 Ja Delft, The Netherlands (ph. +31-15-782562, fax 0031-15-783711, telex butud 38151, e-mail gelderen@tudgv1.tudelft.nl)

**Venuti Giovanna**, Dipartimento di Ingegneria Idraulica, Ambientale e del Rilevamento, Politecnico di Milano, Piazza Leonardo da Vinci 32, I-20133 Milano, Italy (ph. +39-2-2399.6502 fax +39-2-2399.6530)

**Vespe Francesco**, Agenzia Spaziale Italiana, Centro di Geodesia Spaziale,  
C.P. 11, I-75100 Matera, Italy (ph. +39-835-377211, fax +39-835-339005,  
e-mail VESPE@ASIMTO.MT.ASI.IT)

**Wittenburg Ruediger**, TU Bergakademie Freiberg, Institut fuer  
Markscheidewesen und Geodaezie, Agricolastrasse 1, D-09595 Freiberg,  
Germany (ph. +49-3731-512960, fax +49-3731-513581)

**You Rey Jer**, Geodaetisches Institut, Universitaet Stuttgart,  
Keplerstrasse 11, D-70174 Stuttgart, Germany (fax +49-711-1213297)